

Short-Lived Radical
Characterisation: Novel
Radical Trap Synthesis,
Application and
Methodology Development

Peter J. H. Williams

Doctor of Philosophy

University of York

Chemistry

January 2022

Abstract

Radical intermediates play a key role in many chemical processes. However, existing methods for their characterisation have flaws that limit mechanistic and kinetic understanding of these processes, especially for short-lived radicals. A new radical characterisation technique was developed which used novel radical traps, consisting of an allyl group attached to a leaving group, which formed a stable radical upon cleavage. Reaction of a radical with novel radical trap formed a stable radical and non-radical product containing the reactant radical, which was then characterised by conventional techniques, such as NMR spectroscopy and MS. Novel radical trapping was used to successfully detect and characterise a diverse array of short-lived and long-lived radical intermediates across a wide range of radical reactions, including synthetic, biochemical and atmospheric radical reactions, offering valuable mechanistic and kinetic insights. Experiments indicated that novel radical trapping did not lead to false positives, in contrast to most existing short-lived radical characterisation techniques. Full characterisation of an isolated trapped phenylthiyl radical confirmed the trapping mechanism occurred as expected. Novel radical trapping indicated the radical resting state for different substrates in Ru-photocatalysed radical thiol-ene addition and enabled an initiation mechanism to be hypothesised for catalyst-free photoinitiated radical dearomative spirocyclisation. The antioxidant activity of ascorbic acid was probed using aqueous novel radical trapping. Observations from novel radical trapping of gaseous α -pinene ozonolysis offered validation to mechanisms hypothesised but not widely accepted in literature. Detection limits of gaseous $[\text{RO}_2^\bullet]$ using novel radical trapping were estimated to be $>1 \times 10^9$ molec. cm^{-3} (S/N = ~2, 10 min), which would be suitable for some atmospheric field measurements. These investigations demonstrated the viability of novel radical trapping as a tool to investigate any radical reaction. It is hoped that chemists will widely adopt this technique to improve understanding and aid development of reactions involving radical intermediates.

List of contents

Abstract.....	2
List of contents.....	3
List of tables.....	11
List of figures.....	16
List of accompanying material	28
Acknowledgments.....	29
Declaration.....	30
1. Introduction.....	31
1.1. Radical reaction stages and radical stability	31
1.2. Common radical reactions and the potential benefits of applying radical characterisation to them	33
1.2.1. Synthetic radical reactions.....	33
1.2.2. Biological and medicinal chemistry applications.....	35
1.2.3. Atmospheric chemistry	38
1.3. Current radical characterisation techniques	41
1.3.1. Direct radical characterisation techniques	41
1.3.1.1. Electron paramagnetic resonance (EPR) spectroscopy.....	41
1.3.1.2. Chemically induced dynamic nuclear polarization (CIDNP) NMR spectroscopy	43
1.3.1.3. Mass spectrometry (MS)	44
1.3.1.4. Ultraviolet-visible (UV-Vis) and fluorescence spectroscopy	45
1.3.1.5. Overall issues with direct radical characterisation techniques	48
1.3.2. Indirect radical characterisation techniques through radical conversion to a longer-lived species	48
1.3.2.1. Spin traps	48
1.3.2.2. Recombination traps	51
1.3.2.3. Other trapping agents	53
1.3.2.4. Overall issues with existing indirect radical characterisation techniques	53
1.4. Summary	54
2. Proposal.....	55
2.1. Project theory	55
2.2. Previous project work	55
2.3. Project aims.....	57
3. Trap design, synthesis and development	58
3.1. Trap design	58
3.2. Grantham TART	59
3.3. Allyl-TEMPO.....	59

3.3.1. One-step synthesis	59
3.3.2. Two-step synthesis	60
3.4. Amide-functionalised TARTs	61
3.4.1. Design	61
3.4.2. Synthesis	62
3.4.2.1. 2-(Bromomethyl)acrylic acid nucleophilic substitution by TMP and Meisenheimer rearrangement	62
3.4.2.2. 2-(Bromomethyl)acrylic acid UV irradiation with TEMPO•	63
3.4.2.3. Methyl 2-(bromomethyl)acrylate reaction with TEMPO•	64
3.5. TART stability, properties and non-radical reactivity	67
3.5.1. TART stability in long-term storage	67
3.5.2. Free TEMPO• concentration in TART solution	67
3.5.3. TART stability in solution and non-radical reactivity	68
3.5.4. TART properties during MS and calibration curves	70
3.6. Conclusions and future work	71
4. General methodology	74
4.1. Introduction	74
4.2. TART trapping	74
4.3. MS characterisation	75
4.3.1. MS theory and instrumentation	75
4.3.1.1. General principles and instrumentation	75
4.3.1.2. Resolution and the mass analyser	76
4.3.1.3. Ionisation and the ion source	78
4.3.1.4. MS quantification	79
4.3.1.5. Tandem MS	81
4.3.1.6. Chromatography	81
4.3.2. Practical MS characterisation	82
4.3.2.1. Sample preparation	82
4.3.2.2. Spectrometer calibration	83
4.3.2.3. Standard MS spectrum	83
4.3.2.4. Background spectrum	83
4.3.2.5. D ₂ O exchange	84
4.3.2.6. Tandem MS	84
4.3.2.7. HPLC-MS	85
4.3.2.8. HPLC-MS source-waste species removal	86
4.4. Mass spectra analysis	86
4.4.1. Acceptance limits	87
4.4.2. Manual analysis	87

4.4.3. Background removal.....	88
4.4.4. Peak Pick.....	88
4.4.5. Carbon content (C _x) estimation.....	88
4.4.6. Formula Find.....	89
4.4.7. Metal complex structures using Formula Find.....	90
4.5. Summary.....	91
5. Synthetic radical reactions.....	92
5.1. Introduction.....	92
5.2. Thiyl radicals.....	92
5.2.1. Initial results.....	93
5.2.2. Optimisation.....	94
5.2.2.1. TART.....	94
5.2.2.2. Mass spectrometer.....	95
5.2.3. Detailed results.....	96
5.3. Common synthetic radical reactions.....	100
5.3.1. Barton reaction.....	100
5.3.1.1. TART trapping using allyl-TEMPO.....	101
5.3.1.2. TART trapping using CHANT TART.....	102
5.3.2. Hofmann-Löffler-Freytag (HLF) reaction.....	103
5.3.3. Hunsdiecker reaction.....	109
5.3.4. Conclusion.....	110
5.4. Modern reactions.....	111
5.4.1. Radical aromatic aminophosphinylation.....	111
5.4.2. Radical decarboxylative aromatic iodination.....	113
5.5. Conclusions and future work.....	115
6. Photochemistry.....	118
6.1. Introduction.....	118
6.2. Methodology and controls.....	118
6.3. Radical cyanomethylation.....	119
6.4. Radical thiol-ene addition.....	122
6.4.1. Introduction.....	123
6.4.2. Literature replication.....	123
6.4.3. Initial results of TART trapping and reaction condition optimisation.....	124
6.4.4. Controls.....	128
6.4.5. TART-trapped radical isolation.....	130
6.4.6. Kinetics experiments and kinetic modelling.....	132
6.4.7. Effect of different thiols on reaction kinetics.....	137

6.4.8. Effect of different alkenes on reaction kinetics	140
6.4.9. Conclusion	142
6.5. Radical dearomative spirocyclisation	142
6.5.1. Main radical cycle mechanism	143
6.5.2. Initiation mechanism	144
6.5.3. Effects of different thiols on reaction mechanism and kinetics	147
6.6. Conclusions and future work	148
7. Biochemistry	151
7.1. Introduction.....	151
7.2. General mechanistic steps of $\bullet\text{OH}$ -initiated substrate degradation	152
7.2.1. $\text{R}\bullet$ formation through $\bullet\text{OH}$ -initiation	152
7.2.2. $\text{RO}_2\bullet$ formation and degradation	153
7.2.3. $\text{RO}\bullet$ degradation	153
7.2.4. Trapping rates.....	154
7.3. Methodology.....	155
7.4. $\bullet\text{OH}$ and $\text{HO}_2\bullet$ trapping.....	156
7.5. Alcohols.....	158
7.6. Nucleobases.....	163
7.6.1. Introduction	163
7.6.2. Initial results.....	165
7.6.3. Main results	166
7.6.4. Structural isomers.....	168
7.7. Dipeptides	174
7.8. Saccharides.....	179
7.9. Antioxidants.....	181
7.10. Conclusions and future work	185
8. Alkene ozonolysis	187
8.1. Introduction.....	187
8.2. General mechanistic steps of alkene ozonolysis.....	187
8.2.1. Alkene reaction with ozone	187
8.2.2. Other mechanistic steps and differences from radical reactions in solution	188
8.3. Methodology.....	189
8.4. TART ozonolysis	190
8.5. Cyclohexene ozonolysis.....	192
8.6. α -Pinene ozonolysis	195
8.6.1. Initial results.....	195
8.6.2. Optimisation.....	196

8.6.2.1. TART phase	196
8.6.2.2. Functionality of TART, solvent and additives	197
8.6.2.3. TART concentration	198
8.6.2.4. Flow rate and substrate concentration	198
8.6.2.5. Residence time	199
8.6.2.6. Reaction time	199
8.6.3. Detailed results	200
8.6.3.1. Formula Find analysis	201
8.6.3.2. Peak Pick analysis	210
8.6.3.3. D ₂ O.....	213
8.6.3.4. Tandem MS.....	215
8.6.3.5. HPLC-MS	215
8.6.3.6. Oligomeric products and trapped radicals.....	217
8.6.3.7. Kinetic modelling	221
8.6.4. Kinetics experiments.....	223
8.7. Conclusions and future work	224
9. •OH-initiated alkane degradation	227
9.1. Introduction.....	227
9.2. General mechanistic steps of •OH-initiated alkane degradation	227
9.3. •OH-initiated alkane degradation using alkene ozonolysis as an •OH source.....	229
9.3.1. Methodology	229
9.3.2. Initial results.....	231
9.3.3. Optimisation.....	232
9.3.4. Detailed results and controls	233
9.4. •OH-initiated <i>n</i> -nonane degradation, using water photolysis as an •OH source.....	236
9.4.1. Methodology	236
9.4.2. Experimental results	238
9.4.3. Kinetic modelling and detection limit estimation	240
9.5. Conclusions and future work	242
10. Overall conclusions and future work.....	244
11. Experimental.....	247
11.1. General.....	247
11.2. TART synthesis	247
11.2.1. Grantham TART	247
11.2.2. Allyl-TEMPO	249
11.2.2.1. Abandoned one-step synthesis.....	249
11.2.2.2. Two-step synthesis	249

11.2.3. Abandoned 2-(bromomethyl)acrylic acid nucleophilic substitution by TMP and Meisenheimer rearrangement.....	250
11.2.4. Unsuccessful 2-(bromomethyl)acrylic acid UV irradiation	252
11.2.5. Methyl 2-(TEMPOmethyl)acrylate.....	253
11.2.6. 2-(TEMPOmethyl)acrylic acid	254
11.2.7. Standard amide coupling procedure.....	254
11.2.8. CHANT	255
11.2.9. COANT	255
11.2.10. DECANT	256
11.2.11. DANT	257
11.2.12. AGLANT	257
11.2.13. GLANT.....	258
11.2.14. Tabaqui-1.....	259
11.2.15. Tabaqui-2.....	260
11.2.16. BIOANT	261
11.2.17. DEADANT.....	263
11.2.18. TREADANT	263
11.2.19. SILANT	264
11.3. TART properties and stability studies.....	265
11.3.1. Free TEMPO• concentration.....	265
11.3.2. Oxidation and reduction.....	265
11.3.3. Michael addition.....	266
11.3.4. Absorbance of blue LED light (455 nm).....	267
11.3.5. MS calibration curves	267
11.4. Synthetic radical reactions	267
11.4.1. Thiyl radicals.....	267
11.4.1.1. AIBN initiated	267
11.4.1.2. PbO ₂ initiated	267
11.4.2. Barton reaction	267
11.4.3. Hoffman-Löffler-Freytag (HLF) reaction.....	268
11.4.3.1. Precursor synthesis.....	268
11.4.3.2. Trapping reaction	268
11.4.4. Hunsdiecker reaction	268
11.4.4.1. Precursor synthesis.....	268
11.4.4.2. Trapping reaction	269
11.4.5. Radical aromatic aminophosphinylation	269
11.4.6. Radical decarboxylative aromatic iodination.....	269
11.5. Photochemistry.....	270

11.5.1. Radical cyanomethylation	270
11.5.2. Radical thiol-ene addition	270
11.5.2.1. Literature replication.....	270
11.5.2.2. Initial reactions	270
11.5.2.3. Standard procedure	271
11.5.2.4. Optimised reaction	271
11.5.2.5. Controls.....	271
11.5.2.6. TART-trapped radical isolation.....	271
11.5.2.7. Kinetics experiments	272
11.5.2.8. Effect of different thiols on reaction mechanism and kinetics	272
11.5.2.9. Effect of different alkenes on reaction mechanism and kinetics	272
11.5.3. Radical dearomative spirocyclisation.....	273
11.5.3.1. Standard procedure	273
11.5.3.2. Main radical cycle mechanism	273
11.5.3.3. Initiation mechanism	273
11.5.3.4. Effects of different thiols on reaction mechanism and kinetics.....	273
11.6. Biochemistry	273
11.6.1. •OH and HO ₂ • trapping	273
11.6.2. •OH-initiated alcohol degradation	274
11.6.3. Standard procedure	274
11.6.4. •OH-initiated biochemical degradations	274
11.6.5. Antioxidant activity of ascorbic acid	274
11.7. Alkene ozonolysis.....	275
11.7.1. Set-up	275
11.7.2. Standard procedure	275
11.7.3. Optimisation.....	276
11.7.3.1. General	276
11.7.3.2. Solid support synthesis and use in TART trapping of alkene ozonolysis..	276
11.7.4. Estimation of α-pinene dissolution	277
11.7.5. α-Pinene kinetics experiment.....	277
11.8. •OH-initiated alkane degradation	278
11.8.1. Using alkene ozonolysis as an •OH source	278
11.8.1.1. Set-up.....	278
11.8.1.2. Initial results, detailed results and controls	278
11.8.1.3. Optimisation	279
11.8.2. Using water photolysis as an •OH source	279
11.9. MS procedures for TART trapping	280

11.9.1. Characterisation.....	280
11.9.2. Analysis	281
11.9.3. Parameters	281
11.10. Modelling procedures	284
11.10.1. General	284
11.10.2. Radical thiol-ene addition	284
11.10.3. α -Pinene ozonolysis.....	285
11.10.4. \bullet OH-initiated <i>n</i> -nonane degradation.....	285
Commonly used abbreviations.....	287
References.....	289

List of tables

Table 1: Summary of advantages and disadvantages of direct radical characterisation techniques. ✓, ✗ and ~ refer to yes, no and sometimes or somewhat respectively. Symbols refer to general radical detection in the most common setups and do not include more specialised cases or instruments.	48
Table 2: Summary of advantages and disadvantages of indirect radical characterisation techniques. ✓, ✗ and ~ refer to yes, no and sometimes or somewhat respectively. Symbols refer to general radical detection in the most common setups and do not include more specialised cases or instruments.	54
Table 3: Species identified from TART trapping of thiyl radicals, using allyl-TEMPO as TART and a HCT mass spectrometer for MS characterisation (11.4.1.1). Systematic m/z error = -0.2; random m/z error = ± 0.4 ; 100% intensity = 1.92×10^8 absolute count.	94
Table 4: Species identified from TART trapping of thiyl radicals, using AIBN as initiator, Grantham TART or allyl-TEMPO as TART and a HCT mass spectrometer for MS characterisation (11.4.1.1). Systematic m/z error = -0.2; random m/z error = ± 0.4 ; 100% intensity = 1.92×10^8 absolute count.	94
Table 5: Species identified from TART trapping of thiyl radicals, using AIBN as initiator, allyl-TEMPO as TART and HCT or solariX mass spectrometers for MS characterisation (11.4.1.1). HCT: systematic m/z error = -0.2; random m/z error = ± 0.4 ; 100% intensity = 1.92×10^8 absolute count. solariX: systematic m/z error = -0.0004; random m/z error = ± 0.0002 ; 100% intensity = 4.87×10^8 absolute count.	95
Table 6: Species identified from TART trapping of thiyl radicals, using AIBN or PbO_2 as initiator, allyl-TEMPO as TART and MS for characterisation (11.4.1). Systematic m/z error = -0.0004; random m/z error = ± 0.006 ; 100% intensity = 4.87×10^8 absolute count.	97
Table 7: Possible molecular formulae for $[\text{RS-ART+H}]^+$ corresponding peak (observed m/z 243.2146) from TART trapping of thiyl radicals, using PbO_2 as initiator, allyl-TEMPO as TART and MS for characterisation (11.4.1.2). Molecular formulae and unsaturation limits were set to $\text{C}_{0-100}\text{H}_{0-100}\text{N}_{0-5}\text{O}_{0-10}\text{S}_{0-5}\text{Na}_{0-1}\text{K}_{0-1}\text{Pb}_{0-5}$ and 20 respectively. Only one molecular formula had an acceptable difference (typically m/z ± 0.0000 -0.0020) between predicted and observed m/z (black).	98
Table 8: Predicted and observed fraction of different isotopes of two most intense species identified from TART trapping of thiyl radicals, using PbO_2 as initiator, allyl-TEMPO as TART and MS for characterisation (11.4.1.2). Systematic m/z error = -0.0004 random m/z error = ± 0.0003 ; 100% intensity = 5.08×10^7 absolute count.	99
Table 9: Species identified from TART trapping of the Barton reaction, using isopentyl nitrite as substrate, allyl-TEMPO as TART and MS for characterisation (11.4.2). Systematic m/z error = 0.0000; random m/z error = ± 0.0006 ; 100% intensity = 2.08×10^6 absolute count.	101
Table 10: Species identified from TART trapping of the Barton reaction, using isopentyl nitrite as substrate, CHANT as TART and MS for characterisation (11.4.2). Systematic m/z error = -0.0008; random m/z error = ± 0.0005 ; 100% intensity = 3.66×10^9 absolute count.	102
Table 11: Species identified from TART trapping of the HLF reaction, using <i>N</i> -chlorodibutylamine as substrate, CHANT as TART and MS for characterisation (11.4.3). Cl containing species are shown with ^{35}Cl only. Systematic m/z error = 0.0000; random m/z error = ± 0.0009 ; 100% intensity = 2.14×10^9 absolute count.	104
Table 12: Species identified from TART trapping of the Hunsdiecker reaction, using silver octanoate as substrate, CHANT as TART and MS for characterisation (Pos ESI, 11.4.4). Br	

containing species are shown with ⁷⁹ Br only. Systematic <i>m/z</i> error = -0.0002; random <i>m/z</i> error = ±0.0005; 100% intensity = 3.66×10 ⁹ absolute count.....	110
Table 13: Species identified from TART trapping of radical aromatic aminophosphinylation, using 4-methylstyrene, 4-chloroalanine, and DPPO as substrates, allyl-TEMPO as TART and MS for characterisation (11.4.5). Cl containing species are shown with ³⁵ Cl only. Systematic <i>m/z</i> error = -0.0008; random <i>m/z</i> error = ±0.0004; 100% intensity = 6.68×10 ⁶ absolute count.	112
Table 14: Species identified from TART trapping of radical decarboxylative aromatic iodination, using <i>p</i> -anisic acid as substrate, CHANT as TART and MS for characterisation (11.4.6). Systematic <i>m/z</i> error = -0.0001; random <i>m/z</i> error = ±0.0006; 100% intensity = 4.71×10 ⁹ absolute count.	114
Table 15: Species identified from TART trapping of Ru-photocatalysed radical cyanomethylation, using MS for characterisation (11.5.1). Systematic <i>m/z</i> error = -0.0006; random <i>m/z</i> error = ±0.0013; 100% intensity = 1.64×10 ⁹ absolute count.	120
Table 16: Species identified from initial TART trapping of Ru-photocatalysed radical thiol-ene addition under Tyson <i>et al.</i> conditions after 2 h, using benzyl mercaptan and styrene as substrates and MS for characterisation (11.5.2.1). Ru containing species are shown with ¹⁰¹ Ru only. Systematic <i>m/z</i> error = -0.0004; random <i>m/z</i> error = ±0.0011; 100% intensity = 2.27×10 ⁹ absolute count.....	124
Table 17: Species identified from TART trapping of Ru-photocatalysed radical thiol-ene addition under Tyson <i>et al.</i> conditions after 1 h, using thiophenol and styrene as substrates and MS for characterisation (11.5.2.1). Systematic <i>m/z</i> error = 0.0000; random <i>m/z</i> error = ±0.0012; 100% intensity = 9.76×10 ⁹ absolute count.....	126
Table 18: Species identified from TART trapping of Ru-photocatalysed radical thiol-ene addition under standard conditions after 2 h, using different thiols and styrene as substrates and MS for characterisation (11.5.2.4). Systematic <i>m/z</i> error = -0.0004; random <i>m/z</i> error = ±0.0011; 100% intensity = 2.69×10 ⁹ absolute count.....	128
Table 19: Species identified from TART trapping of Ru-photocatalysed radical thiol-ene addition and controls under otherwise standard conditions after 2 h, using benzyl mercaptan and styrene as substrates and MS for characterisation (11.5.2.5). Systematic <i>m/z</i> error = -0.0004; random <i>m/z</i> error = ±0.0007; 100% intensity = 2.69×10 ⁹ absolute count.	129
Table 20: Species identified from TART trapping of Ru-photocatalysed radical thiol-ene addition under standard conditions after 2 h, using different thiols and styrene as substrates and MS for characterisation (11.5.2.8). Systematic <i>m/z</i> error = -0.0004; random <i>m/z</i> error = ±0.0011; 100% intensity = 2.55×10 ⁹ absolute count.....	138
Table 21: Species identified from TART trapping of Ru-photocatalysed radical thiol-ene addition under standard conditions after 24 h, using different thiols and styrene as substrates and MS for characterisation (11.5.2.8). Systematic <i>m/z</i> error = -0.0004; random <i>m/z</i> error = ±0.0006; 100% intensity = 2.55×10 ⁹ absolute count.....	138
Table 22: Species identified from TART trapping of Ru-photocatalysed radical thiol-ene addition under standard conditions after 24 h, using benzyl mercaptan and different alkenes as substrates and MS for characterisation (11.5.2.9). Cl containing species are shown with ³⁵ Cl only. Systematic <i>m/z</i> error = -0.0005; random <i>m/z</i> error = ±0.0012; 100% intensity = 2.11×10 ⁹ absolute count.	141
Table 23: Species identified from TART trapping of photoinitiated radical dearomative spirocyclisation, using 3-methoxythiophenol as substrate (1.6 eq.) and MS for characterisation	

(11.5.3.2). Systematic m/z error = -0.0003; random m/z error = ± 0.0025 ; 100% intensity = 3.66×10^9 absolute count.	144
Table 24: Species identified from TART trapping of radical dearomative spirocyclisation, using different quantities of 3-methoxythiophenol as substrate (0.0-1.6 eq.) and MS for characterisation (11.5.3.3). Systematic m/z error = 0.0000; random m/z error = ± 0.0025 ; 100% intensity = 5.45×10^9 absolute count.	146
Table 25: Species identified from TART trapping of radical dearomative spirocyclisation, using different thiols as substrate (1.6 eq.) and MS for characterisation (11.5.3.4). Systematic m/z error = 0.0000; random m/z error = ± 0.0026 ; 100% intensity = 5.45×10^9 absolute count. .	148
Table 26: Species identified from TART trapping of \bullet OH-initiated methanol degradation, using DEADANT as TART and MS for characterisation (11.6.2). Systematic m/z error = -0.0005; random m/z error = ± 0.0003 ; 100% intensity = 1.14×10^9 absolute count.	158
Table 27: Species identified from TART trapping of \bullet OH-initiated t BuOH degradation, using DEADANT as TART and MS for characterisation (11.6.2). 100% = 1.09×10^9 absolute count. Systematic m/z error = -0.0004; random m/z error = ± 0.0007	161
Table 28: D exchanges observed for MS peaks corresponding to TART-trapped radicals from D_2O exchange of \bullet OH-initiated t BuOH degradation, using DEADANT as TART and MS for characterisation (11.6.4). Systematic m/z error = -0.0004; random m/z error = ± 0.0004 . ..	162
Table 29: Species identified from TART trapping of \bullet OH-initiated thymine degradation, using DANT as TART and MS for characterisation (11.6.4). Systematic m/z error = -0.0004; random m/z error = ± 0.0004 ; 100% intensity = 5.83×10^8 absolute count.	165
Table 30: Species identified from TART trapping of \bullet OH-initiated thymine degradation, using DEADANT as TART and MS for characterisation (11.6.4). Systematic m/z error = -0.0002; random m/z error = ± 0.0005 ; 100% intensity = 1.09×10^9 absolute count.	166
Table 31: D exchanges observed for $[R1/R2-ART+H]^+$ from D_2O exchange of \bullet OH-initiated thymine degradation, using DEADANT as TART and MS for characterisation (11.6.4). Systematic m/z error = -0.0004; random m/z error = ± 0.0002	170
Table 32: D exchanges observed for m/z 315.167 from D_2O exchange of \bullet OH-initiated thymine degradation, using DEADANT as TART and MS for characterisation (11.6.4). Systematic m/z error = -0.0004; random m/z error = ± 0.0004	171
Table 33: D exchanges observed for m/z 331.162 from D_2O exchange of TART trapping of \bullet OH-initiated thymine degradation, using DEADANT as TART and MS for characterisation (11.6.4). Systematic m/z error = -0.0004; random m/z error = ± 0.0002	172
Table 34: Species identified from TART trapping of \bullet OH-initiated dipeptide degradation, using Ac-Gly-Gly-OH and Boc-Gly-Gly-OH as substrates, DEADANT as TART and MS for characterisation (11.6.4). Ac-Gly-Gly-OH: systematic m/z error = 0.0000; random m/z error = ± 0.0006 . Boc-Gly-Gly-OH: systematic m/z error = +0.0002; random m/z error = ± 0.0014 . 100% intensity = 1.09×10^9 absolute count.	176
Table 35: Identified radicals from the most intense MS peaks attributed to monomeric non-fragmented TART-trapped radicals from TART trapping of \bullet OH-initiated glucose degradation, using DEADANT as TART and MS for characterisation (11.6.4). Molecular formula limits were set as $C_{14}H_{0-28}N_{2}O_{1-12}$ and m/z limits 100-500. Unreasonable molecular formulae were eliminated. RCO represents formation of carbonyl from an existing alcohol group, i.e., $R\bullet$ and $R(CO)\bullet$ differ by H_2 . Systematic m/z error = -0.0002; random m/z error = ± 0.0005 ; 100% intensity = 1.09×10^9 absolute count.	180

Table 36: Species identified from TART trapping of •OH-initiated ascorbic acid degradation, using DEADANT as TART and MS for characterisation (11.6.4). Systematic <i>m/z</i> error = -0.0005; random <i>m/z</i> error = ±0.0008; 100% intensity = 1.09×10 ¹⁰ absolute count ^a	183
Table 37: Trapped radicals from •OH-initiated thymine, ascorbic acid and simultaneous thymine and ascorbic acid degradation, using DEADANT as TART and MS for characterisation (11.6.5). T and A species are thymine- (Figure 122) and ascorbic acid-derived (Figure 138) respectively. Systematic <i>m/z</i> error = -0.0005; random <i>m/z</i> error = ±0.0007; 100% intensity = 1.09×10 ¹⁰ absolute count ^a	184
Table 38: Ozonolysis products identified in TART trapping of alkene ozonolysis, using MS for characterisation (11.7.2). Systematic <i>m/z</i> error = -0.0005; random <i>m/z</i> error = ±0.0003; 100% intensity = 3.08×10 ⁹ absolute count.....	191
Table 39: Species identified from TART trapping of cyclohexene ozonolysis, using MS for characterisation (11.7.2). Systematic <i>m/z</i> error = -0.0005; random <i>m/z</i> error = ±0.0005; 100% intensity = 3.08×10 ⁹ absolute count.....	193
Table 40: Species identified from TART trapping of α-pinene ozonolysis, using MS for characterisation (11.7.2). Systematic <i>m/z</i> error = -0.0005; random <i>m/z</i> error = ±0.0013; 100% intensity = 2.01×10 ⁹ absolute count.....	196
Table 41: Species identified from TART trapping of α-pinene ozonolysis, conducted at different substrate flow rates, using MS for characterisation (11.7.3). Systematic <i>m/z</i> error = -0.0005; random <i>m/z</i> error = ±0.0013; 100% intensity = 2.01×10 ⁹ absolute count.....	198
Table 42: Ten most intense peaks believed to correspond to TART-trapped radicals from TART trapping of α-pinene ozonolysis, obtained using the Formula Find programme. Molecular formula limits were set as C ₂₀ H ₀₋₃₈ N ₁ O ₁₋₁₀ Na ₀₋₁ and <i>m/z</i> limits 100-500. Illogical molecular formulae were eliminated.....	202
Table 43: Possible molecular formulae calculated for observed <i>m/z</i> 374.2301, ordered with increasing difference from the observed <i>m/z</i> . Sensible molecular formula limits were set as C ₀₋₄₀ H ₀₋₁₀₀ N ₀₋₂ O ₀₋₂₀ Na ₀₋₁ . Only two molecular formulae had an acceptable difference between predicted and observed <i>m/z</i> (black).....	206
Table 44: Species identified from TART trapping of α-pinene ozonolysis, with three repeats and controls undertaken, using MS for characterisation (11.7.2). Systematic <i>m/z</i> error = -0.0005; random <i>m/z</i> error = ±0.0013; 100% intensity = 2.01×10 ⁹ absolute count.....	211
Table 45: D exchanges observed for MS peaks corresponding to species from D ₂ O exchange of TART trapping of α-pinene ozonolysis, using MS for characterisation (11.7.2). Systematic <i>m/z</i> error = -0.0003; random <i>m/z</i> error = ±0.0010.....	213
Table 46: Ten most intense peaks from TART trapping of α-pinene ozonolysis, obtained using the Formula Find programme. Molecular formula limits were set as C ₁₋₄₀ H ₀₋₁₀₀ N ₀₋₂ O ₀₋₁₅ Na ₀₋₁ and <i>m/z</i> limits 100-1000. Illogical molecular formulae were eliminated.....	217
Table 47: ROOR species identified from TART trapping of α-pinene ozonolysis, using MS for characterisation (11.7.2). Systematic <i>m/z</i> error = -0.0005; random <i>m/z</i> error = ±0.0010; 100% intensity = 2.01×10 ⁹ absolute count. ROOR nomenclature is of the form PR-R', where R and R' are the indexes of the two reactant radicals.....	218
Table 48: Radical-alkene dimer species identified from TART trapping of α-pinene ozonolysis, using MS for characterisation (11.7.2). Systematic <i>m/z</i> error = -0.0005; random <i>m/z</i> error = ±0.0010; 100% intensity = 2.01×10 ⁹ absolute count. Radical-alkene dimer nomenclature is of the form PR-Dim-x, where R is the index of reactant radical species and x is the total oxygen count in the α-pinene unit, including the unit bridge (1-2), new alkene inner ring (0-2) and new alkene alcohol/hydroperoxide (1-2) functionalisation.....	219

Table 49: TART-trapped dimer radicals identified from TART trapping of α -pinene ozonolysis, using MS for characterisation (11.7.2). Systematic m/z error = -0.0005; random m/z error = ± 0.0013 ; 100% intensity = 2.01×10^9 absolute count.....	220
Table 50: Species identified from initial TART trapping of \bullet OH-initiated n -nonane degradation, using alkene ozonolysis as an \bullet OH source and MS for characterisation (11.8.1.2). Systematic m/z error = -0.0005; random m/z error = ± 0.0003 ; 100% intensity = 1.38×10^9 absolute count.	231
Table 51: Species identified from TART trapping of \bullet OH-initiated n -nonane degradation at different concentrations of TART, using alkene ozonolysis as an \bullet OH source and MS for characterisation (11.8.1.3). Systematic m/z error = -0.0003; random m/z error = ± 0.0005 ; 100% intensity = 1.89×10^9 absolute count.....	232
Table 52: Species identified from optimised TART trapping of \bullet OH-initiated n -nonane degradation and controls, using alkene ozonolysis as an \bullet OH source and MS for characterisation (11.8.1.2). No TART control showed no peaks corresponding to those in the table. Systematic m/z error = -0.0005; random m/z error = ± 0.0005 ; 100% intensity = 1.38×10^9 absolute count.....	234
Table 53: HPLC conditions of sample analysis from TART trapping of radical decarboxylative aromatic iodination, using p -anisic acid as substrate, CHANT as TART and HPLC-MS for characterisation (11.4.6). Column = Waters Symmetry. Injection speed = $300 \mu\text{L min}^{-1}$	282
Table 54: HPLC conditions of sample analysis from TART trapping of radical thiol-ene addition, using benzyl mercaptan and styrene as substrates, CHANT as TART and HPLC-MS for characterisation (11.5.2.5). Column = Waters Symmetry. Injection speed = $300 \mu\text{L min}^{-1}$	282
Table 55: HPLC conditions of sample analysis from TART trapping of aqueous \bullet OH-initiated biochemical degradation, using DEADANT as TART and HPLC-MS for characterisation (11.6). Column = Atlantis. Injection speed = $500 \mu\text{L min}^{-1}$	283
Table 56: HPLC conditions of sample analysis from TART trapping of gaseous α -pinene ozonolysis and \bullet OH-initiated n -nonane degradation, using CHANT as TART and HPLC-MS for characterisation (11.7, 11.8.1). Column = Eclipse Plus Phenyl-Hexyl. Injection speed = $300 \mu\text{L min}^{-1}$	283
Table 57: HPLC conditions of sample analysis from TART trapping of gaseous α -pinene ozonolysis and \bullet OH-initiated n -nonane degradation, using water photolysis as an \bullet OH source, DEADANT as TART and HPLC-MS for characterisation (11.8.2). Column = Atlantis. Injection speed = $500 \mu\text{L min}^{-1}$	283

List of figures

Figure 1: General initiation, propagation and termination radical reactions.	32
Figure 2: Five rules for radical stabilisation. ^{1,2}	32
Figure 3: Polystyrene synthesis through radical chain-growth polymerisation, initiated by benzoyl peroxide. ¹⁶	34
Figure 4: Mechanism of photocatalysed radical thiol-ene addition, using photocatalyst [PC]. ¹⁷⁻²¹	34
Figure 5: Ideal formation of H ₂ O from O ₂ and non-ideal formation of O ₂ • from O ₂ , that occurs during oxidative metabolic ATP synthesis. ^{24,25}	35
Figure 6: O ₂ • production from O ₂ by NADPH oxidase in the immune system. ^{27,28}	35
Figure 7: O ₂ • conversion into H ₂ O ₂ by superoxide dismutase (SOD). ³¹	36
Figure 8: H ₂ O ₂ uncontrolled conversion by iron into ROS species •OH and HO ₂ • and control conversion by catalase into harmless products. ³³⁻³⁵	36
Figure 9: •OH reduction into H ₂ O using antioxidant glutathione (GSH) forming glutathione dimer (GSSG) and subsequent glutathione dimer oxidation to reform glutathione, using glutathione reductase. ³⁶⁻³⁸	36
Figure 10: DNA crosslinking between adjacent intrastrand guanine and thymine through their C8 and C9 respectively, which may occur through ROS oxidation. ^{46,47}	37
Figure 11: Proposed mechanism of radical SAM enzyme epimerase PoyD catalysed L-valinamide epimerisation. ⁴⁸	37
Figure 12: Daytime formation of •OH through HONO and ozone photolysis. ⁵¹	38
Figure 13: Early stages of •OH-initiated <i>n</i> -nonane degradation in absence of NO _x , showing formation of radical species R•, RO ₂ • and RO•. RCO represents carbonyl species. ^{50,57}	39
Figure 14: Naturally abundant isoprene, four monoterpenes and monoterpene linalool. ..	39
Figure 15: Example ozonolysis mechanism of 2-methylpent-2-ene in presence of O ₂ , showing formation of Criegee intermediates and subsequent RO ₂ • formation.	41
Figure 16: EPR spectra acquired during photolysis of a TEMPO-functionalised benzofuran. Reprinted and adapted with permission. ⁷⁸ Copyright 2019 Beilstein Journals.....	42
Figure 17: NMR (middle) and CIDNP NMR (lower) spectra of UV-irradiated of 2-phenylacetophenone, indicating benzoyl and benzyl radical formation (upper). Numbers (red) indicate protons responsible for observed signals. Reprinted and adapted with permission. ⁸⁸ Copyright 2010 American Chemical Society.....	43
Figure 18: ESI-MS mass spectrum of TEMPO•. Reprinted and adapted with permission. ⁹⁵ Copyright 2019 Sage Publications.....	44
Figure 19: CI-MS mass spectrum of C ₆ H ₁₁ O ₂ . Reprinted and adapted with permission. ⁹⁸ Copyright 2019 American Chemical Society.....	45
Figure 20: UV-Vis spectra of DPPH after 30 minutes in absence (purple) and presence (yellow) of Vitamin E. Reprinted and adapted with permission. ¹⁰³ Copyright 2017 American Chemical Society.	46
Figure 21: Excitation (black, λ _{em} = 440 nm) and emission (red, λ _{exc} = 241 nm) spectra of dithiadiazolyl radical (pictured). Reprinted and adapted with permission. ¹⁰⁴ Copyright 2018 American Chemical Society.....	46
Figure 22: •OH fluorescence spectrum (λ _{exc} = 266.188 nm). Reprinted and adapted with permission. ¹⁰⁵ Copyright 2004 Springer-Verlag.....	47

Figure 23: Reaction of a short-lived radical (R•) with nitroso (top) and nitrene (bottom) spin traps, forming longer-lived nitroxyl radical spin adducts.	49
Figure 24: EPR spectra of DMPO-trapped SO ₃ •- (left) and SO ₄ •- (right). Reprinted and adapted with permission. ¹¹⁴ Copyright 2018 American Chemical Society.	49
Figure 25: DMPO trapping of SO ₃ •- and SO ₄ •- forming sulfur and oxygen linked nitroxyl radical spin adducts respectively. ¹¹⁴	50
Figure 26: Mass spectrum from LC-MS characterisation of PBN-trapped C ₄ H ₅ O• ([M+H] ⁺ m/z = 248.1661) from tobacco smoke. Reprinted and adapted with permission. ¹²⁴ Copyright 2016 Elsevier.	50
Figure 27: Reaction of a short-lived radical (R•) with a recombination trap (X•), forming a longer-lived non-radical recombination adduct. ¹³³	51
Figure 28: Reaction of a short-lived carbon-centred radical (R•) with a nitroxyl radical recombination trap, forming a longer-lived non-radical recombination adduct.	51
Figure 29: Recombination trapping of <i>N</i> -acetyl-L-tyrosinamide radical by TEMPO•, forming non-radical recombination adduct. ¹³⁸	52
Figure 30: Reaction observed when attempting to trap ^t BuOO• with TEMPO• to form intermediate (centre), however this species was not observed and instead TEMPO• acted catalytically to form ^t BuO• and O ₂ . ¹⁴⁰	52
Figure 31: Formation of radical trapping agent 2,4,6-tri- <i>tert</i> -butylphenoxy radical and subsequent NO ₂ • trapping. ¹⁴¹	53
Figure 32: Salicylic acid and •OH reaction to form example hydroxylated salicylic acid, although a mixture of isomers is produced. ¹⁴⁵⁻¹⁴⁷	53
Figure 33: Reaction between reactant radical (R•) and novel allyl radical trap containing bound leaving group, forming a persistent radical (LG•) and non-radical product, containing trapped reactant radical (R). This non-radical product will then be characterised, allowing reactant radical (R) to be identified. R ¹ , R ² and R ³ will be functionalised to suit the radical system being studied.	55
Figure 34: Four traps designed and synthesised by Grantham (left). All four traps had R ¹ and R ² jointly functionalised as one cycloalkane ring. Grantham traps had the shown general structure (right), where X = CHR or O, R = H or CON(CH ₃) ₂ and n = 1 or 2. ¹⁵²	56
Figure 35: [1,3]-sigmatropic rearrangement of Grantham traps, causing terminal alkene to rearrange to non-terminal alkene. This process occurred readily in solution at RTP. X = CHR or O, R = H or CON(CH ₃) ₂ and n = 1 or 2. ¹⁵²	56
Figure 36: Trapped radicals from 1-dodecanethiol reaction with AIBN or PbO ₂ in presence of Grantham trap, observed by Grantham. ¹⁵²	56
Figure 37: i) TEMPO-Allyl Radical Trap (TART) reaction with radical (R•) to form stable non-radical Radical-Allyl Radically Trapped (R-ART) species, and persistent radical leaving group, TEMPO•. ii) Recombination trapping of radical (R•) with TEMPO• to form R-TEMPO. iii) Trapping of R• with the carbon-centred radical formed following hydrogen atom abstraction (HAA) from TART to form R-TART. TARTs were tuned, by R ¹ , R ² and R ³ functionalisation, to suit radical functionality and reaction conditions.	58
Figure 38: Two-step synthesis to form Grantham TART, performed using a literature procedure (11.2.1). ¹⁵²	59
Figure 39: Allyl-TEMPO one-step synthesis, performed using a literature procedure (11.2.2.1). ¹⁵⁴	59

Figure 40: Allyl-TEMPO two-step synthesis was performed using two literature procedures (11.1.2.2). ^{155,156}	60
Figure 41: Mechanism of the second step of allyl-TEMPO synthesis.....	60
Figure 42: Novel amide-functionalised TARTs.	61
Figure 43: 2-(TMPmethyl)acrylic acid formation from 2-(bromomethyl)acrylic acid, adapted from a literature procedure. ³	62
Figure 44: CHANT formation from 2-(TMPmethyl)acrylic acid. The second step was adapted from a literature procedure. ⁴	62
Figure 45: 2-(TEMPOmethyl)acrylic acid TART formation from 2-(bromomethyl)acrylic acid (11.2.4). The second step was adapted from a literature procedure. ¹⁵⁴	63
Figure 46: TEMPO-polymethacrylates formed from UV irradiation of 2-(iodomethyl)acrylic acid with TEMPO•, where n≥1.....	63
Figure 47: 2-(TEMPOmethyl)acrylic acid TART formation from methyl 2-(bromomethyl)acrylate (11.2.5 and 11.2.6).....	64
Figure 48: CHANT formation from 2-(TEMPOmethyl)acrylic acid (11.2.8).	64
Figure 49: Amide-functionalised TARTs synthesised by amide coupling with 2-(TEMPOmethyl)acrylic acid.	65
Figure 50: EPR spectra recorded for CHANT (1.00 mM, scaled×100, black) and TEMPO• (0.100 mM, orange), indicating CHANT had free TEMPO• content ~0.05mol.% (11.3.1). ...	68
Figure 51: Michael addition of diisopropylamine to CHANT, forming a decay product.	69
Figure 52: Decay of CHANT in presence of diisopropylamine dissolved in CD ₃ OD, monitored using ¹ H NMR spectroscopy (11.3.3).....	70
Figure 53: Calibration curve of intensity of MS peak corresponding to [CHANT+H] ⁺ (<i>m/z</i> 323.270) at different CHANT concentrations (black), showing rapidly decreasing intensity >25 μM due to CHANT fragmentation. The most intensely observed fragment peak (<i>m/z</i> 140.144) appears to correspond to a TMP cation (orange).	71
Figure 54: Five main TARTs used for TART trapping, with CHANT and DEADANT being especially ubiquitous.....	72
Figure 55: Potential TARTs with functionalities which would offer advantages over existing TARTs.....	73
Figure 56: Mass spectrometry (MS). An injected sample contains three analytes. These analytes are ionised in the ion source, then separated according to <i>m/z</i> in the mass analyser, before being detected, producing a mass spectrum.	76
Figure 57: MS peak simulations of [naphthalene+H] ⁺ (blue) and [octanone+H] ⁺ (red) with equal MS intensity. The sum of these two peaks yielded the observed intensity (black). Simulations were performed at three different resolutions (±0.1, ±0.025 and ±0.005). Maximum intensity was set equal for both individual species at all resolutions. Different resolutions yielded different degrees of overlapping.	76
Figure 58: Electrospray ionisation mass spectrometry (ESI-MS). Sample solution is passed through the electrospray needle. High needle voltage causes charged liquid droplet formation. Droplet desolvates until droplet Rayleigh limit is reached. Droplets then undergo Coulomb fission forming smaller stable droplets. This process may repeat itself. Eventually droplets form gaseous ions. Gaseous ions then continue into spectrometer.	79
Figure 59: Thiyl radical formation from thiol using initiator and subsequent radical trapping by TART.....	92

Figure 60: Initial thiyl radical trapping experiment, using 1-dodecanethiol as substrate and AIBN as initiator (11.4.1.1).....	93
Figure 61: Mass spectrum from TART trapping of thiyl radicals, using allyl-TEMPO as TART and a HCT mass spectrometer for MS characterisation (11.4.1.1). The peak corresponding to [allyl-TEMPO+H] ⁺ had the greatest intensity (<i>m/z</i> 198.186, green).....	93
Figure 62: Mass spectrum from TART trapping of thiyl radicals, using AIBN as initiator, allyl-TEMPO as TART and HCT (bottom) and solariX (top) mass spectrometers for MS characterisation (11.4.1.1). A peak at <i>m/z</i> 243.0 appears to correspond to [RS-ART+H] ⁺ (predicted <i>m/z</i> 243.2146) using the HCT mass spectrometer, however the solariX mass spectrometer shows that this peak is mainly due to a peak with <i>m/z</i> 243.2877, disproving presence of RS-ART.....	96
Figure 63: TART trapping of thiyl radicals, using 1-dodecanethiol as substrate, PbO ₂ as initiator and allyl-TEMPO as TART (11.4.1.2).....	96
Figure 64: Initially formed RS-TEMPO adduct (left) from TART trapping of thiyl radicals and subsequent rearrangement to form structural isomer suggested by literature. ^{175,176}	99
Figure 65: Widely accepted mechanism of the Barton reaction for isopentyl nitrite. ^{179,180} ...	100
Figure 66: TART trapping of the Barton reaction, using isopentyl nitrite as substrate (11.4.2).	100
Figure 67: Widely accepted mechanism for <i>N</i> -haloamine HLF reaction, where typically X = Cl or Br. ¹⁸³	103
Figure 68: TART trapping of the HLF reaction, using <i>N</i> -chlorodibutylamine as substrate and CHANT as TART (11.4.3).	103
Figure 69: Total D exchange of [R2-ART+H] ⁺ (top) and [R3-ART+H] ⁺ (bottom), yielding 2D and 3D exchanges respectively.	105
Figure 70: Background corrected mass spectra of TART trapping of the HLF, using <i>N</i> -chlorodibutylamine as substrate and CHANT as TART, MS characterised in protonated (top) and deuterated (bottom) solvent, showing peaks corresponding to R2/R3-ART (blue). 2D exchanges were observed (<i>m/z</i> 295.275), indicating R2-ART.....	105
Figure 71: Tandem mass spectrum performed upon peak corresponding to [R2/R3-ART+Na] ⁺ (green) from TART trapping of the HLF reaction, using <i>N</i> -chlorodibutylamine as substrate and CHANT as TART, yielding suggested fragments. Structures were successfully assigned to most fragments (blue).	106
Figure 72: Tandem mass spectrum of <i>m/z</i> 295.275 peak from TART trapping of the HLF reaction, using <i>N</i> -chlorodibutylamine as substrate and CHANT as TART, yielding fragment peaks. Two fragment peaks could only be assigned to R3-ART corresponding structures (red and blue), indicating R3 was also trapped.	107
Figure 73: HPLC-MS chromatograms of the peak corresponding to [R2/R3-ART+H] ⁺ (<i>m/z</i> 295.275±0.002) and overall chromatogram (inset) detected from TART trapping of the HLF reaction, using <i>N</i> -chlorodibutylamine as substrate and CHANT as TART. A peak corresponding to unreacted CHANT dominated the chromatogram (green), whilst two intense peaks corresponding to [R2/R3-ART+H] ⁺ were also clearly visible (red, blue), with maxima at 13.49 min and 13.62 min respectively. This indicated that [R2/R3-ART+H] ⁺ was composed of at least two species. Further separation was attempted but not achieved.	108
Figure 74: Mass spectrum from TART trapping of the HLF reaction, using <i>N</i> -chlorodibutylamine as substrate and CHANT as TART (11.4.3), showing peaks corresponding to unreacted TART (<i>m/z</i> 323.270, green) and R2/R3-ART (<i>m/z</i> 295.275, blue), recorded using the less high resolution compact mass spectrometer.	109

Figure 75: Proposed mechanism for the Hunsdiecker reaction. ¹⁹³	109
Figure 76: TART trapping of the Hunsdiecker reaction, using silver octanoate as substrate and CHANT as TART (11.4.4).	110
Figure 77: Proposed mechanism for radical aromatic aminophosphinylation. ²⁰⁰	111
Figure 78: TART trapping of radical aromatic aminophosphinylation, using 4-methylstyrene, 4-chloroaniline and DPPO as substrates and allyl-TEMPO as TART (11.4.5).	112
Figure 79: Proposed mechanism for reaction performed by Perry <i>et al.</i> ²⁰¹	114
Figure 80: TART trapping of radical decarboxylative aromatic iodination, using <i>p</i> -anisic acid as substrate and CHANT as TART (11.4.6).	114
Figure 81: HPLC-MS chromatograms of peaks corresponding to [CHANT+H] ⁺ (<i>m/z</i> 323.270±0.002, 9.06 min), [R1-ART+H/Na] ⁺ (<i>m/z</i> 318.171±0.002 and <i>m/z</i> 340.152±0.002, 8.57 min), [R2-ART+H/Na] ⁺ ×100 (<i>m/z</i> 294.035±0.002 and <i>m/z</i> 316.017±0.002, 7.82 min) and [R3-ART+H/Na] ⁺ ×1000 (<i>m/z</i> 274.181±0.002 and <i>m/z</i> 296.163±0.002, 1.53 min) detected from TART trapping of radical decarboxylative aromatic iodination, using <i>p</i> -anisic acid as substrate and CHANT as TART (11.4.6).	115
Figure 82: UV-Vis spectrum of CHANT (10.0 mM) in MeCN. Wavelength of blue LED irradiation (455 nm), used for TART trapping of radical thiol-ene addition, is indicated (blue dashed line).	119
Figure 83: Mechanism of Ru-photocatalysed radical cyanomethylation, using 2-bromoacetophenone as substrate, proposed by Donald <i>et al.</i> ²⁰³	119
Figure 84: TART trapping of Ru-photocatalysed radical cyanomethylation, using 2-bromoacetophenone as substrate and CHANT as TART (11.5.1).	120
Figure 85: Mass spectrum from TART trapping of radical cyanomethylation (11.5.1), showing two most intense sets of peaks corresponding to Ru complexes, with [¹⁰¹ Ru(bpy) ₂ ⁷⁹ Br] ⁺ (<i>m/z</i> 492.960, pink) and [¹⁰¹ Ru(bpy) ₂ ⁷⁹ Br ⁸¹ Br] ⁺ (<i>m/z</i> 573.876, sky blue) highlighted. 100% intensity = 1.64×10 ⁹ absolute count.	121
Figure 86: Mass spectrum from TART trapping of radical cyanomethylation (11.5.1), highlighting peaks corresponding to R1-ART (<i>m/z</i> 308.163, blue) and R4-ART (<i>m/z</i> 248.163, red). 100% intensity = 1.64×10 ⁹ absolute count.	122
Figure 87: Mechanism of Ru-photocatalysed radical thiol-ene addition, proposed by Tyson <i>et al.</i> ²⁰⁵	123
Figure 88: Initial TART trapping of Ru-photocatalysed radical thiol-ene addition, using benzyl mercaptan and styrene as substrates and CHANT as TART (11.5.2.1).	124
Figure 89: Possible mechanisms of thiol initiation, through thiol autoxidation (top) and molecule-assisted homolysis (MAH, bottom).	125
Figure 90: TART trapping of Ru-photocatalysed radical thiol-ene addition, using thiophenol and styrene as substrates and CHANT as TART (11.5.2.1).	126
Figure 91: Side reactions of CHANT-derived structures with thiols (S2). S2 reaction with R1-ART and TART form R1-ART+S2 (top) and TART+S2 (bottom) respectively.....	127
Figure 92: HPLC-MS chromatograms of peaks corresponding to [R1-ART+H/Na] ⁺ (<i>m/z</i> 290.158±0.002 and <i>m/z</i> 312.140±0.002, 20.0 min) and [R2-ART+H/Na] ⁺ (<i>m/z</i> 394.220±0.002 and <i>m/z</i> 416.202±0.002, 24.0 min) detected from TART trapping of radical thiol-ene addition, using benzyl mercaptan and styrene as substrates (11.5.2.3).	130
Figure 93: TART trapping of phenylthiyl radical (11.5.2.6).	131

Figure 94: ¹ H NMR spectrum of TART-trapped phenylthiyl radical (CDCl ₃ , 400 MHz, 298 K, 11.5.2.6).....	131
Figure 95: Calibration curve of intensity of MS peaks corresponding to [CHANT+H] ⁺ (<i>m/z</i> 323.270, black), [R1-ART+H] ⁺ (<i>m/z</i> 276.142, dark blue) and [R1-ART+Na] ⁺ (<i>m/z</i> 298.124, light blue) at different analyte concentrations, where R1-ART is CHANT-trapped phenylthiyl radicals. This indicated CHANT ionised more efficiently than low basicity CHANT-trapped radicals.....	132
Figure 96: Kinetic model of radical thiol-ene addition, with initiation rate, <i>k_i</i> , forward and backward propagation rates, <i>k_p</i> and <i>k_{-p}</i> and forward and backward chain transfer rates, <i>k_{CT}</i> and <i>k_{-CT}</i>	133
Figure 97: Kinetic model of TART trapping of radical thiol-ene addition. Arrows with “=” are included to indicate that trapped radicals R1-ART and R2-ART could undergo subsequent radical thiol-ene addition.	134
Figure 98: Kinetic model produced for TART trapping of radical thiol-ene addition (11.10.2), using thiophenol (orange) and styrene (blue) as substrates and TART (purple), yielding thioether product (yellow). Complete styrene conversion and near 100% product yield were obtained after ~3 h.	134
Figure 99: Kinetic model produced for TART trapping of radical thiol-ene addition (11.10.2), using thiophenol and styrene as substrates and TART (purple), yielding TEMPO• (green), R1-ART (sky blue), R2-TEMPO (grey) and R1-ART+S2 (pink).	135
Figure 100: Intensities of peaks corresponding to species identified in TART trapping of radical thiol-ene addition, using methyl thiosalicylate and styrene as substrate and CHANT as TART (11.5.2.7), showing [TART+H/Na/K] ⁺ (purple), [R1-ART+H/Na/K] ⁺ (sky blue), [R2-ART+H/Na/K] ⁺ ×10 (peach), and [R2-TEMPO+H/Na/K] ⁺ (grey).....	137
Figure 101: Thiols probed in TART trapping of radical thiol-ene addition (11.5.2.8). Literature yields after the indicated reaction time are shown for the associated thioether product of each thiol. ²⁰⁵	138
Figure 102: Alkenes probed in TART trapping of radical thiol-ene addition (11.5.2.9). Literature yields after the indicated reaction time are shown for the associated thioether product of each alkene. ²⁰⁵	140
Figure 103: Mechanism of photoinitiated radical dearomative spirocyclisation for indole-tethered ynone (S1), hypothesised based upon TART trapping observations and independently proposed by Ho <i>et al.</i> ²¹²	143
Figure 104: TART trapping of photoinitiated radical dearomative spirocyclisation, using indole-tethered ynone (S1) and 3-methoxythiophenol as substrates and CHANT as TART (11.5.3.2).	143
Figure 105: Initiation of radical dearomative spirocyclisation via indole-tethered ynone excitation, as suggested by Ho <i>et al.</i> ²¹²	145
Figure 106: Hypothesised initiation mechanism for photoinitiated radical dearomative spirocyclisation.....	145
Figure 107: Radicals formed from HAA abstraction from S1 or DCE in absence of thiol. ..	147
Figure 108: Uncontrolled conversion of H ₂ O ₂ into ROS species •OH and HO ₂ •, catalysed by Fe ²⁺ . Individual equations (top and middle) and overall equation (bottom) are shown. ^{33,34}	151
Figure 109: HAA from an R-H bond, by •OH, to form a radical (R•) and water.	152
Figure 110: •OH addition to alkene, forming β-hydroxyl carbon-centred radical.	152

Figure 111: RO ₂ • formation from R• and subsequent RO ₂ • degradation. O ₂ release is not shown.....	153
Figure 112: Common RO• degradation pathways.	154
Figure 113: Radical reaction with alkenes, used to estimate rate of TART trapping.	155
Figure 114: General TART trapping of •OH-initiated biochemical degradation (11.6.3).	156
Figure 115: TART trapping of •OH and HO ₂ • in Fenton chemistry system, using GLANT as TART (11.6.1).	157
Figure 116: TART trapping of •OH and HO ₂ • in Fenton chemistry system, using DANT as TART (11.6.1).	157
Figure 117: Hypothesised mechanism of aqueous •OH-initiated methanol degradation....	158
Figure 118: TART trapping of •OH-initiated alcohol degradation, using DEADANT as TART (11.6.2).....	158
Figure 119: Non-comprehensive hypothesised reaction scheme for •OH-initiated tBuOH degradation in aqueous solution, only indicating major pathways. i) + •OH, - H ₂ O. ii) + O ₂ . iii) + RH, - R•. iv) + RO ₂ •, - RO•. v) + RO ₂ •, - RCO. vi) + RO ₂ •, - ROH. vii) - •OH. viii) Fragmentation. ix) - HO ₂ •.....	160
Figure 120: 3D or 4D exchanges expected for [R1.1.1-ART+H] ⁺ and [R1.1.3.1-ART+H] ⁺ respectively.	162
Figure 121: Possible radical structures for R(OH)O• and R(OOH)•.....	162
Figure 122: Non-comprehensive •OH-initiated thymine degradation in aqueous solution. Structures and pathway probabilities were obtained or hypothesised using literature sources. ⁴⁵ i) + •OH. ii) + •OH, - H ₂ O. iii) + O ₂ . iv) + RH, - R•. v) + RO ₂ •, - RO•. vi) + RO ₂ •, - RCO. vii) + RO ₂ •, - ROH. viii) - •OH. ix) Fragmentation. x) - HO ₂ •.	164
Figure 123: TART trapping of •OH-initiated thymine degradation (11.6.4).	165
Figure 124: HPLC-MS chromatogram of the peak corresponding to R1/R2-ART (<i>m/z</i> 299.172±0.002), detected from TART trapping of •OH-initiated thymine degradation, using DEADANT as TART (11.6.4). Two peaks dominate (blue and red). Mass spectrum (inset) recorded at time of maximum chromatogram intensity (blue) shows <i>m/z</i> 299.172 cleanly isolated (blue).	168
Figure 125: Tandem mass spectrum of peak corresponding to R1-ART and R2-ART (<i>m/z</i> 299.172, green) with structures suggested for major fragment peaks (blue). Structures are derived from R1-ART, but all peaks could be equally attributed to R2-ART	169
Figure 126: Total D exchange of [R1-ART+H] ⁺ , yielding five D exchanges.	170
Figure 127: Total D exchange of [R1.1.1-ART+H] ⁺ and [R1.1.3.1-ART+H] ⁺ , yielding 5D and 6D exchanges respectively.	170
Figure 128: HPLC-MS chromatogram of the peak corresponding to R1.1.1/R1.1.2-ART (<i>m/z</i> 315.167±0.002), detected from TART trapping of •OH-initiated thymine degradation (11.6.4). Two peaks dominate (blue and red), although other smaller peaks were also observed. Mass spectrum (inset) recorded at time of maximum chromatogram intensity (blue) shows <i>m/z</i> 315.167 cleanly isolated (blue).	171
Figure 129: Three radicals possibly formed during •OH-initiated thymine degradation, with same <i>m/z</i> as RO ₂ • species R1.1/R1.2. These radicals are hydroxylated R1.1.1/R2.1.1 (R(OH)O•, left), hydroperoxylated R1/R2 (R(OOH)•, middle) and dihydroxylated R1/R2 (R(OH) ₂ •, right).....	172

Figure 130: HPLC-MS chromatogram of m/z 331.162±0.002, detected from TART trapping of •OH-initiated thymine degradation, using DEADANT as TART (11.6.4). Four peaks had significantly large intensity (coloured) although other smaller peaks were also observed. Mass spectrum (inset) recorded at time of maximum chromatogram intensity (red) shows m/z 315.167 cleanly isolated (red).....	173
Figure 131: •OH-initiated diglycine degradation in aqueous solution. Structures and pathways were obtained or hypothesised using literature sources. ^{32,218,238} X=1: R ¹ =Ac/Boc, R ² =Gly-OH; X=2: R ¹ =Ac/Boc-Gly, R ² =OH. i) + •OH, - H ₂ O. ii) + O ₂ . iii) + RH, - R•. iv) + RO ₂ •, - RO•. v) + RO ₂ •, - RCO. vi) + RO ₂ •, - ROH. vii) - •OH. viii) Fragmentation. ix) - HO ₂ •.	175
Figure 132: TART trapping of •OH-initiated dipeptide degradation, using Ac-Gly-Gly-OH and Boc-Gly-Gly-OH as substrates and DEADANT as TART (11.6.4).....	176
Figure 133: Possible R-Gly-Gly-OH dimer structure formed during MS. ²³⁹	177
Figure 134: Tandem mass spectrum of [R1:R3-ART+H] ⁺ corresponding peak for Boc-Gly-Gly-OH (m/z 387.224, green) with structures suggested for major fragment peaks (blue). These fragments indicated HAA from Boc-Gly-Gly-OH occurs readily upon the Boc group.....	178
Figure 135: Plausible radicals formed after initial HAA in •OH-initiated glucose degradation.	179
Figure 136: TART trapping of •OH-initiated glucose degradation, using DEADANT as TART (11.6.4).....	179
Figure 137: Example structures possibly produced during from •OH-initiated glucose degradation.	181
Figure 138: •OH-initiated ascorbic acid degradation in aqueous solution. Ascorbate and ascorbic acid dominate at physiological pH (typically pH 7.0-7.4) ²³ and under somewhat acidic conditions (pH 4) respectively. Structures and pathways were obtained or hypothesised using literature sources. ³³ Other reaction pathways, such as HAA from allylic C-H and alcohol O-H, were also possible.	182
Figure 139: TART trapping of •OH-initiated ascorbic acid degradation, using DEADANT as TART (11.6.4).	182
Figure 140: TART trapping of •OH-initiated thymine and ascorbic acid degradation, using DEADANT as TART (11.6.5).	183
Figure 141: Example ozonolysis mechanism of 2-methylpent-2-ene in presence of O ₂ , showing formation of Criegee intermediates and subsequent RO ₂ • formation.	188
Figure 142: General reaction mechanism of alkene ozonolysis. Some reactions may occur either intermolecularly or intramolecularly (blue). O ₂ release is not shown. RCO represents carbonyl species.	189
Figure 143: TART trapping of alkene ozonolysis set-up (11.7.1).....	189
Figure 144: CHANT ozonolysis control experiment (11.7.2).....	190
Figure 145: Non-comprehensive mechanism of cyclohexene ozonolysis. O ₂ release is not shown. RCO represents carbonyl species. Structures and pathways were obtained or hypothesised using literature sources. ²⁴⁸	192
Figure 146: TART trapping of cyclohexene ozonolysis (11.7.2).	192
Figure 147: Background corrected mass spectrum from TART trapping of cyclohexene ozonolysis (11.7.2).....	193

Figure 148: Background corrected mass spectrum from TART trapping of cyclohexene ozonolysis (11.7.2), showing peaks corresponding to R1.1-ART (m/z 334.163, blue) and R1.1.2-ART (m/z 318.168, red).....	194
Figure 149: Radicals and products produced early in α -pinene ozonolysis (8.6.3.1). ⁵⁷ These species are formed through mechanisms which are discussed later (Figure 153 and Figure 154).....	195
Figure 150: TART trapping of α -pinene ozonolysis (11.7.2).	196
Figure 151: Species identified from TART trapping of α -pinene ozonolysis after different reaction times, using MS for characterisation (11.7.3). Species are scaled to show their maximum values at 100% intensity. Systematic m/z error = -0.0006; random m/z error = ± 0.0007	200
Figure 152: Background corrected mass spectrum from TART trapping of α -pinene ozonolysis (11.7.2). 100% intensity = 2.01×10^9 absolute count.	201
Figure 153: Mechanism of α -pinene reaction with ozone, showing formation of Criegee intermediates and subsequent degradation to form RO_2^\bullet . Radicals (red) have molecular formulae $C_{10}H_{15}O_4^\bullet$ and $C_9H_{15}O_3^\bullet$. Structures and pathway probabilities were obtained from the MCM. ⁵⁷	203
Figure 154: Mechanism of reaction of RO_2^\bullet formed following α -pinene reaction with ozone, forming RO^\bullet , and subsequent formation of other RO_2^\bullet . O_2 release is not shown. RCO represents carbonyl species. Radicals (red) have molecular formulae $C_{10}H_{15}O_{3-5}^\bullet$, $C_9H_{15}O_{2-4}^\bullet$ and $C_9H_{13}O_4^\bullet$. Structures and pathway probabilities were obtained from the MCM. ⁵⁷	204
Figure 155: Background corrected mass spectrum from TART trapping of α -pinene ozonolysis (11.7.2), showing peaks corresponding to $[R1.1/R1.2-ART+Na]^+$ (m/z 388.210, blue) and $[R1.1.1/R1.2.1-ART+Na]^+$ (m/z 372.215, red). 100% intensity = 2.01×10^9 absolute count.	205
Figure 156: Mechanism of α -pinene reaction with $^\bullet OH$, showing formation of β -hydroxyl- RO_2^\bullet and subsequent RO^\bullet formation. O_2 release is not shown. RCO represents carbonyl species. Radicals (red) have molecular formulae $C_{10}H_{15}O_{3-4}^\bullet$. Structures and pathway probabilities were obtained from the MCM. ⁵⁷	206
Figure 157: Mechanism of $^\bullet OH$ addition to α -pinene and strained four-membered ring opening to form cycloperoxide- RO_2^\bullet and cycloether- RO_2^\bullet . O_2 release is not shown.	207
Figure 158: α -Pinene reaction with $AcCl$, showing formation of the majority of isolated products involved strained four-membered ring rearrangement. ²⁵⁰	207
Figure 159: Mechanism of $^\bullet OH$ addition to α -pinene, four-membered ring opening and subsequent ring closure to form species including cycloperoxide- RO_2^\bullet and cycloether- RO_2^\bullet . O_2 release is not shown. RCO represents carbonyl species. Radicals (red) have molecular formulae $C_{10}H_{17}O_{2-5}^\bullet$. Structures and pathway probabilities were obtained from Vereecken <i>et al.</i> and Berndt <i>et al.</i> ^{249,252}	208
Figure 160: Mechanism of autooxidation and subsequent ring closure, following $^\bullet OH$ addition to α -pinene and four-membered ring opening, to form species including oxygenated cycloperoxide- RO_2^\bullet and cycloether- RO_2^\bullet . O_2 release is not shown. Radicals (red) have molecular formulae $C_{10}H_{17}O_{2-7}^\bullet$. Structures and pathway probabilities were obtained from Vereecken <i>et al.</i> and Berndt <i>et al.</i> ^{249,252}	209
Figure 161: Mechanism of HAA from α -pinene by $^\bullet OH$ forming RO_2^\bullet and subsequent reactions. O_2 release is not shown. RCO represents carbonyl species. Radicals (red) have molecular formulae $C_{10}H_{15}O_{1-2}^\bullet$. Structures and pathways probabilities were obtained from literature or hypothesised using literature. ^{251,255}	210

Figure 162: Background corrected mass spectra run in protonated (top) and deuterated (bottom) solvent, showing peaks corresponding to R6/R7-ART (blue) detected from D ₂ O exchange of TART trapping of α -pinene ozonolysis (11.7.2).....	214
Figure 163: Tandem mass spectrum of the peak corresponding to R1.1/R1.2-ART (m/z 388.210, blue) from TART trapping of α -pinene ozonolysis, yielding suggested fragment (m/z 220.095, red). Structures are derived from R1.1-ART but could be equally attributed to R1.2-ART	215
Figure 164: HPLC-MS chromatogram and mass spectrum (inset) of peaks corresponding to R1.1/R1.2-ART (m/z 366.228 \pm 0.002 and m/z 388.210 \pm 0.002) from TART trapping of α -pinene ozonolysis (11.7.2). MS source was sent to waste between 13.5-14.0 min, to prevent injection of unreacted TART. Mass spectrum of [R1.1/R1.2-ART+H] ⁺ (blue) is at time of maximum intensity (blue).....	216
Figure 165: General radical-alkene dimer structure formed through radical addition to α -pinene and example dimer (P1.1-Dim-4) formed through radical (R1.1) addition to α -pinene, with the α -pinene unit containing four oxygen atoms (4). Radical-alkene dimer nomenclature is of the form PR-Dim-x, where R is the index of reactant radical species and x is the total oxygen count in the α -pinene unit, including the unit bridge (1-2), new alkene inner ring (0-2) and new alkene alcohol/hydroperoxide (1-2) functionalisation.	218
Figure 166: Background corrected mass spectrum from TART trapping of α -pinene ozonolysis (11.7.2), showing peaks corresponding to CHANT (green) and radical-alkene dimer products (blue).....	220
Figure 167: General trimer structure formed through radical addition to two α -pinene and example trimer (P5.1-Trim-7) formed through radical (R5.1) addition to α -pinene, with the two α -pinene units containing seven oxygen atoms (7). Radical-alkene-alkene trimer nomenclature is of the form PR-Trim-x, where R is the index of reactant radical species and x is the total oxygen count in the two α -pinene units, including the unit bridges (1-2), new alkene inner rings (0-2) and new alkene alcohol/hydroperoxide (1-2) functionalisation.....	221
Figure 168: Simulation of gaseous α -pinene ozonolysis between 0-565 ms residence time (11.10.3). 56.5 ms was the typical residence time used in TART trapping of α -pinene ozonolysis.	222
Figure 169: TART trapping of α -pinene ozonolysis kinetics experiments (11.7.5).....	223
Figure 170: Simulation (line) of TART trapping of α -pinene ozonolysis kinetics experiment over different residence times (tube lengths) and corresponding average experimental MS intensities of corresponding peaks and associated errors (scatter and error bars, 11.7.5). Experimental results were globally scaled to minimise RMSD between simulated and experimental data.	224
Figure 171: General reaction mechanism of \bullet OH-initiated alkane degradation. For longer chain n -alkanes, some reactions may occur either intermolecularly or intramolecularly (blue), where reactants and products are a single species. O ₂ release is not shown. RCO represents carbonyl species.	228
Figure 172: Percentage likelihood of HAA from each carbon environment, estimated using a structure-reactivity relationship by Kwok <i>et al.</i> ²⁵⁷	228
Figure 173: Early stages of \bullet OH-initiated n -nonane degradation in absence of NO _x , showing formation of radical species RO ₂ \bullet , RO \bullet and R(OH)O ₂ \bullet . ^{50,57} RCO represents carbonyl species. Structures and pathway probabilities were obtained from the MCM. ⁵⁷	229
Figure 174: Set-up used for TART trapping of \bullet OH-initiated alkane degradation, using alkene ozonolysis as an \bullet OH source (11.8.1.1).	230

Figure 175: TART trapping of •OH-initiated alkane degradation, using alkene ozonolysis as an •OH source (11.8.1.2).	231
Figure 176: Species identified from TART trapping of •OH-initiated alkane degradation at different reaction times, using alkene ozonolysis as an •OH source and MS for characterisation (11.8.1.3). Species are scaled to show their maximum values at 100% intensity. Systematic <i>m/z</i> error = -0.0003; random <i>m/z</i> error = ±0.0006.....	233
Figure 177: Background corrected mass spectrum from optimised TART trapping of •OH-initiated <i>n</i> -nonane degradation, using alkene ozonolysis as an •OH source (11.8.1.2).....	234
Figure 178: Background corrected mass spectrum from optimised TART trapping of •OH-initiated <i>n</i> -nonane degradation, using alkene ozonolysis as an •OH source (11.8.1.2), showing peaks corresponding to RO ₂ -ART (<i>m/z</i> 348.251, blue) and RO-ART (<i>m/z</i> 332.257, red). 100% intensity = 1.38×10 ⁹ absolute count.....	235
Figure 179: HPLC-MS chromatograms of peaks corresponding to RO ₂ -ART (<i>m/z</i> 326.270±0.002 and <i>m/z</i> 348.251±0.002, top, blue) and RO-ART (<i>m/z</i> 310.275±0.002 and <i>m/z</i> 332.257±0.002, bottom, red) from TART trapping of •OH-initiated <i>n</i> -nonane degradation, using alkene ozonolysis as an •OH source (11.8.1.2). HPLC output was sent to waste between 13.5-14.0 min, to prevent spectrometer contamination by unreacted TART.	236
Figure 180: Set-up used for TART trapping of •OH-initiated alkane degradation, using water photolysis as an •OH source (11.8.2).	237
Figure 181: TART trapping of •OH-initiated <i>n</i> -nonane degradation, using water photolysis as an •OH source.	238
Figure 182: HPLC-MS chromatograms of peaks corresponding to RO-ART (<i>m/z</i> 310.275±0.002 and <i>m/z</i> 332.257±0.002) from TART trapping of •OH-initiated <i>n</i> -nonane degradation, using water photolysis as an •OH source and CHANT as TART, after 10 min, 100 min and with controls (11.8.2). HPLC output was sent to waste between 13.5-14.0 min, to prevent spectrometer contamination by unreacted TART.	238
Figure 183: HPLC-MS mass spectrum at time of maximum intensity of peak corresponding to RO-ART (<i>m/z</i> 310.275±0.002, 14.4 min) corresponding peak (blue) from TART trapping of •OH-initiated <i>n</i> -nonane degradation, using water photolysis as an •OH source, using CHANT as TART, after 100 min (11.8.2).	239
Figure 184: HPLC-MS chromatograms of the peak corresponding to RO-ART (<i>m/z</i> 299.270±0.002) from TART trapping of •OH-initiated <i>n</i> -nonane degradation, using water photolysis as an •OH source and DEADANT as TART, with controls (11.8.2). The five distinct peaks observed in the trapping reaction are believed to correspond to the five possible RO• structural isomers.....	240
Figure 185: Modelling of •OH-initiated <i>n</i> -nonane degradation immediately prior to trapping, showing gaseous [•OH] (blue), [RO ₂ •] (orange), [RO•]×10 ⁸ (yellow) and [R(OH)O ₂ •]×10 ³ (purple).....	241
Figure 186: Cyclic voltammogram of CHANT (1.00 mM), using MeCN as solvent and Bu ₄ NPF ₆ (100 mM) as electrolyte and Pt wire working and counter electrodes and a Ag/AgCl reference electrode.	265
Figure 187: Michael addition of diisopropylamine to CHANT, forming a decay product.	266
Figure 188: Stacked ¹ H NMR spectra of CHANT in presence of diisopropylamine after 0 h (top) and 3 weeks (bottom), showing peaks which decrease in intensity (5r-7r) and new signals corresponding to the decay product (5p-7p).	266
Figure 189: Set-up used for TART trapping of alkene ozonolysis.	275

Figure 190: Set-up used for TART trapping of alkene ozonolysis, using solid supported TART.	277
Figure 191: Set-up used for TART trapping of •OH-initiated alkane degradation, using alkene ozonolysis as an •OH source.	278
Figure 192: Set-up used for TART trapping of •OH-initiated alkane degradation, using water photolysis as an •OH source.	279
Figure 193: Kinetic model of TART trapping of radical thiol-ene addition. Arrows are included to indicate that trapped radicals R1-ART and R2-ART could undergo subsequent radical thiol-ene addition.	284

List of accompanying material

Supporting information is provided separately and referenced throughout this thesis as (SI). This includes, but is not limited to, chemicals used, TART synthesis characterisation spectra, TART trapping optimisation data, additional D₂O exchange, tandem MS and HPLC-MS results from TART trapping experiments and equations used for modelling.

Acknowledgments

The author would like to acknowledge and thank the people who have provided fundamental academic and non-academic support, without which, the completion of this project and thesis would not have been possible.

Firstly, I would like to thank my supervisors Victor Chechik and Andrew Rickard and my independent panel member Ian Fairlamb for their indispensable academic and pastoral support throughout the project.

Thank you to the academic support staff who provided training and guidance with performing experiments and measurements, including: Karl Heaton (MS); Heather Fish (NMR spectroscopy); Graeme McAllister (CHN and laboratory technician); Katie Read (ozone measurements) and Emma Dux (laboratory technician). Especially heartfelt thanks must go to the eternally kind and helpful Ed Bergstrom, who spent countless hours helping me conduct and improve my MS characterisation and was far kinder than I deserved when problems arose.

I would like to thank those who provided assistance with designing and conducting experiments and measurements including: Nikolaos Vagkidis (TART synthesis, MS characterisation and biochemistry); Daniel Guban (TART synthesis and biochemistry); Lucy Butler and Daniel Heenan (TART synthesis); William Swansborough-Aston (TART synthesis and alkene ozonolysis); William Unsworth, James Donald, Hon Ho and Nantachai Imprung (photochemistry); Simaran Patel (biochemistry); Terry Dillon and John Slattery (alkene ozonolysis and $\cdot\text{OH}$ -initiated alkane degradation) and from the University of Leeds: Alexander Brennen, Lavinia Onel, Thomas Speak, Graham Boustead, Dwayne Heard and Paul Seakins ($\cdot\text{OH}$ -initiated alkane degradation). I would also like to thank all members of the Chechik Group for their general guidance and support.

I would like to thank all my friends and family who supported me and put up with me during the last four years. In particular, special thanks must go to the wonderful Margot Abbot and Matthew Brookes who have given me so much joy, provided me with immeasurable amounts of pastoral support, fed me more times than I could count and helped me move house far too many times. Secondly, thank you to Nikolaos Vagkidis for being a fantastic friend and support, both in and out of the laboratory and for putting up with me for two Christmases. Thirdly, thank you to my incredible housemates of three years Jodie Brunt, Kieran Fitzgerald, Lisa Pearson and Stuart Morris, for always looking after me and for all the happy memories we have shared together. Fourthly, I would like to thank my "housemates" of one year Paul Cosme, Vincent Klein and Aaron Poole, for willingly adopting me as a housemate and treating me like part of the family. I would also like to thank my parents Marcus and Carol Williams, for providing me with somewhere to be able to write this thesis and offering me so much support in trying times.

Finally, I would like to give special thanks to my partner and best friend Andreas Heller, who provided so much love, care, support and joy to me during this project. This included listening to me and helping me, providing me with a home and cheering me on when I had to go to the laboratory in the middle of the night.

Declaration

I declare that this thesis is a presentation of original work and I am the sole author. This work has not previously been presented for an award at this, or any other, university. All sources are acknowledged as References.

Grantham TART was originally synthesised and isolated by Andrew Grantham (3.2). This synthesis was later adapted for the Grantham TART synthesis described in this thesis, which was performed by the author (3.2).

DANT was originally synthesised and isolated by Daniel Gugan, using a protocol designed by the author (3.4.2.3). Subsequently, the author also synthesised DANT.

EPR spectra obtained for CHANT, used to estimate free TEMPO• concentration, were recorded and analysed by Victor Chechik (3.5.2).

The adapted procedure for TART trapping of thiyl radicals was originally designed and performed by Andrew Grantham. However, all experiments and results reported in this thesis were performed by the author (5.2).

The set-up used for TART trapping in photochemistry systems was designed by William Unsworth (6.2).

Synthesis of 3-azido-2-methylbut-3-en-2-ol and TART trapping of radical cyanomethylation were conducted by James Donald, with MS characterisation and mass spectra analysis conducted by the author (6.3).

Indole-tethered ynone (S1) used in TART trapping of radical dearomative spirocyclisation was synthesised by Hon Ho. Hon Ho also conducted TART trapping of radical dearomative spirocyclisation experiments, to elucidate the main radical cycle mechanism, with MS characterisation and mass spectra analysis conducted by the author (6.5.1). All subsequent TART trapping of radical dearomative spirocyclisation experiments were performed by the author (6.5.2 and 6.5.3).

N-Acetyl-diglycine and *N*-Boc-diglycine, used in TART trapping of •OH-initiated dipeptide degradation, were synthesised by Nikolaos Vagkidis (7.7).

Mass spectra analysis of TART trapping of •OH-initiated ascorbic acid and thymine-ascorbic acid degradation was originally performed by Daniel Gugan, with experiments and MS characterisation performed by the author (7.9). Additionally, these mass spectra were later reanalysed by the author.

Ionic liquids [C₄min]⁺[Tf₂N]⁻ and [C₄pyrr]⁺[Tf₂N]⁻, used in TART trapping of alkene ozonolysis using TARTs immobilised on solid supports, were obtained from John Slattery (8.6.2.1).

TART trapping of •OH-initiated *n*-nonane degradation experiments, using water photolysis as an •OH source, were performed by Graham Boustead using a system designed by Lavinia Onel, Dwayne Heard and Paul Seakins from The University of Leeds, with MS characterisation and mass spectra analysis performed by the author (9.4).

1. Introduction

Radicals (sometimes called free radicals) are atoms, molecules or ions containing at least one unpaired electron.^{1,2} Radical intermediates play a key role in many chemical processes, such as in synthetic chemistry (e.g., radical polymerisation^{3,4} and photoredox catalysis⁵⁻⁷), biochemistry (e.g., oxidative stress^{8,9}) and atmospheric chemistry (e.g., photochemical oxidation cycles and aerosol formation^{10,11}). Many radicals are highly reactive and therefore very short-lived, with half-lives often less than a second.^{1,2} This makes them difficult to detect, characterise and quantify, since most characterisation techniques require longer acquisition times than a short-lived radical lifetime. Though many direct and indirect radical characterisation techniques exist, all have significant drawbacks, which hinder radical system investigation. Development of better methods for short-lived radical detection, characterisation and quantification could significantly develop the areas of chemistry described above.

This chapter describes general features of radical reactions (1.1), common radical reactions and the potential benefits of applying radical characterisation to them (1.2) and existing direct and indirect radical characterisation techniques (1.3).

1.1. Radical reaction stages and radical stability

Radical reactions can consist of up to three distinct phases: initiation, propagation and termination. Initiation involves formation of radical intermediates from non-radical reagents. The first initiation step usually occurs through bond homolysis or single electron transfer processes, forming two radical intermediates (Figure 1). Initiation reactions which involve formation of high energy radicals usually require an external factor to overcome the associated high activation energy, such as heat, light or a catalyst. This high activation energy ordinarily results in initiation occurring at a significantly slower rate than all other steps in a radical reaction. In radical chain reactions, initiation can involve multiple steps, with the final step yielding radicals which undergo propagation. If many propagation cycles occur from a single initiation, rate of initiation rarely defines the overall rate of reaction.^{1,2}

Propagation only occurs in radical chain reactions and involves continuous regeneration of radical intermediates (Figure 1). Propagation can consist of multiple reversible and irreversible steps. In radical chain reactions, propagation usually occurs rapidly, generating radicals at a much faster rate than initiation. Therefore, the slowest propagation step usually defines the overall rate of reaction.^{1,2} In this case, the radical species preceding this step is known as the radical resting state, as this species is the most concentrated radical present in the reaction cycle.

Termination involves reaction between two radicals to form non-radical products and no radical intermediates, usually through bond formation or single electron transfer processes (Figure 1). As such, termination is usually a low energy process and therefore has a fast rate constant. However, because it is a reaction between two radicals, which are usually present in low concentrations, the absolute reaction rate is normally slow. In radical chain reactions, termination causes propagation to end. Therefore, termination rate determines the number of propagations which occur and hence the efficiency of the reaction. In radical chain reactions, termination rate rarely defines the overall rate of reaction.^{1,2} In this thesis, all radicals in figures are coloured red.

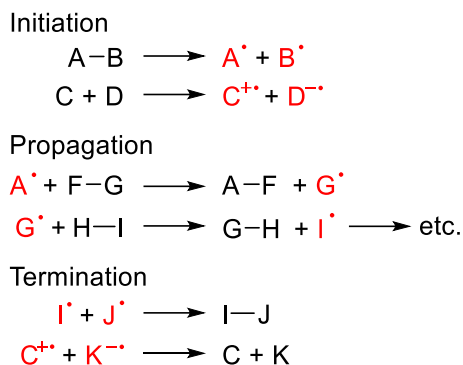


Figure 1: General initiation, propagation and termination radical reactions.

A relatively fast initiation rate can cause high concentrations of intermediate radicals, increasing termination rate. Radical chain reactions with a high termination rate undergo few propagations, causing initiation rate to increasingly define the overall rate of reaction. Therefore, an efficient radical chain reaction has slow initiation, fast propagation and slow termination. Rates of initiation, propagation and termination steps are highly dependent on the internal energy, and hence stability, of reactants, radical intermediates and products. Decreased internal energy of a radical intermediate relative to its reactants and products, increases its stability, resulting in a longer lifetime. Many factors influence the internal energy of a radical intermediate and hence its stability, including^{1,2}:

- Radical atom electronegativity: as radicals are inherently electron-deficient, they are destabilised by increased electronegativity of the radical atom.
- Proximity to the nucleus: radicals are stabilised by increased delocalisation opportunity as size of the radical atom increases.
- Neighbouring electron donating groups: since radicals are inherently electron-deficient, they are stabilised by electron donating neighbouring groups.
- Resonance: radicals are stabilised by increased delocalisation opportunity through p orbital overlap.
- Lone electron pairs on adjacent atoms: as radicals are inherently electron deficient, they are stabilised by partial donation of adjacent lone pairs through p orbital overlap (Figure 2).

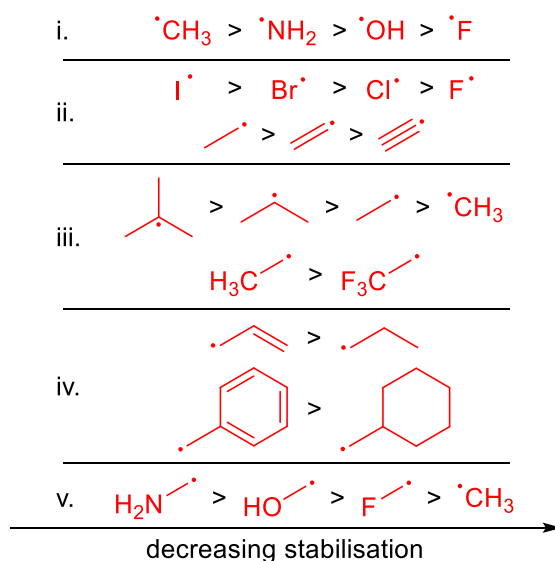


Figure 2: Five rules for radical stabilisation.^{1,2}

Although many radicals are short-lived, persistent radicals have much longer lives, such as triphenylmethyl radical (trityl radical), whilst some radicals are indefinitely stable, such as (2,2,6,6-tetramethylpiperidin-1-yl)oxyl radical (TEMPO•) and molecular oxygen (O₂).^{1,2} TEMPO• is stabilised by radical delocalisation (Figure 2, iv), and partial donation of the adjacent N lone pair (Figure 2, v), through overlapping N and O p orbitals, to form a two-centred three-electron N–O bond. Furthermore, the nitroxyl group lacks β-hydrogen atoms, preventing disproportionation. The inert four methyl groups adjacent to the nitroxyl group provide additional stability through steric protection.¹²

Radical stability strongly influences the mechanisms and kinetics of radical reactions.^{1,2} Short-lived radical detection, characterisation and quantification could be used to better understand radical mechanisms and kinetics. This could significantly develop many areas of chemistry in which radical intermediates are key species, in order to gain mechanism-driven understanding in complex systems and to improve product yields and overall reaction efficiencies. As such, common radical reactions and the potential benefits of applying radical characterisation to them is briefly discussed below.

1.2. Common radical reactions and the potential benefits of applying radical characterisation to them

1.2.1. Synthetic radical reactions

Radical intermediates play a vital role in many synthetic reaction mechanisms, including simple chemical reactions^{13,14}, radical polymerisation^{3,4} and photoredox catalysis⁵⁻⁷.

Early synthetic radical reactions were discovered through serendipity, as chemical mechanisms were generally less well understood at the time. Their mechanisms were later investigated and hypothesised using experimental evidence. More recently however, the perceived importance of mechanistic understanding of radical reactions has increased. Therefore, modern reactions are usually designed based on existing mechanistic knowledge. It is believed that better understanding of radical reaction mechanisms, including initiation and main radical propagation cycles, may aid development of reagents, catalysts and reaction conditions to improve substrate scope, conversion, selectivity, yields and industrial viability.

~45% of industrial polymers are produced through radical polymerisation, including polyethylene, polystyrene and polyvinyl chloride.¹⁵ For alkenes, radical polymerisation first involves initiation through formation of radicals, for example by thermolysis, photolysis or a radical initiator. These radicals react with the alkene double bond in a monomer to form a new carbon-centred polymer radical, initiating the reaction. Propagation or radical chain-growth polymerisation then occurs through sequential alkene monomer addition to the polymer radical. These propagation reactions are highly exothermic and hence occur rapidly. Termination eventually occurs, to form a non-radical polymer species, most commonly through radical-radical cross-coupling with an initiator radical or other polymer radical.^{3,4} An example radical polymerisation reaction is shown below (Figure 3).¹⁶

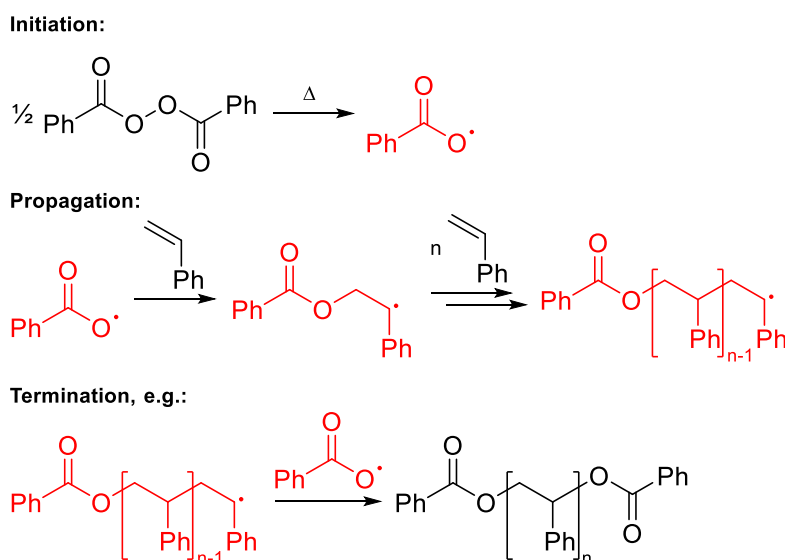


Figure 3: Polystyrene synthesis through radical chain-growth polymerisation, initiated by benzoyl peroxide.¹⁶

Radical polymerisations are generally highly efficient and rapid, as rate of radical addition to alkenes is very fast. Whilst radical polymerisation mechanisms are generally well understood, understanding their kinetics is key to controlling these reactions. For example, very rapid propagation can lead to thermal runaway whilst uncontrolled termination can lead to undesirable polymer chain lengths.^{3,4} Therefore, understanding and controlling kinetics of radical polymerisation leads to desired polymer properties with higher yields.

In recent decades, initiation of radical chains using photoredox catalysts has attracted much attention. Photoredox catalysis has led to the development of a large variety of new bond-forming synthetic methodologies. Photoredox catalysts are excited by light and subsequently catalyse a chemical reaction through single electron transfer processes. Photoredox catalysts are usually transition-metal complexes, organic dyes or semi-conductors, with transition-metal complexes being the most widely used in recent decades.^{6,7}

For example, radical thiol-ene addition, a model click chemistry reaction, commonly uses photoredox catalysts. Thiol-ene addition is a hydrothiolation reaction, involving thiol addition to an alkene double bond to form an anti-Markovnikov thioether.¹⁷⁻²¹ The reaction rose to prominence in recent decades owing to its industrial feasibility, largely due to its usually high yields and stereoselectivity. The reaction is also relatively robust and under certain conditions can even be run in presence of O₂.¹⁸⁻²¹ Furthermore, these properties aid clean and efficient polymer synthesis. The reaction has also proven useful in biosynthesis, such as for fluorescent label functionalisation.²⁰ The general mechanism for photocatalysed radical thiol-ene addition is shown below (Figure 4).¹⁷⁻²¹

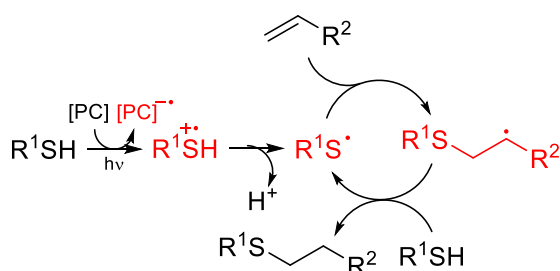


Figure 4: Mechanism of photocatalysed radical thiol-ene addition, using photocatalyst [PC].¹⁷⁻²¹

For photocatalysed radical reactions, better mechanistic and kinetic understanding could allow determination of which step was rate determining for products formed at a slower rate. Mechanistic and kinetic information could be obtained using radical characterisation techniques. This knowledge may inform appropriate improvements for faster product formation and thus improve overall reaction efficiencies.

1.2.2. Biological and medicinal chemistry applications

Radical intermediates play a pivotal role in many biochemical mechanisms, including oxidative metabolism, cell signalling, immunity and some enzymatic processes.

Reactive oxygen species (ROS) are highly reactive species formed from O₂. Many ROS are formed following formation of superoxide O₂^{•-}. In highly acidic conditions, O₂^{•-} exists as hydroperoxyl radicals (HO₂[•], pK_a 4.88)²². However, at physiological pH (typically pH 7.0-7.4²³), unprotonated O₂^{•-} predominates.

O₂^{•-} and other ROS are formed as by-products during oxidative metabolism in most eukaryotic organisms. In these organisms, respiration is performed inside mitochondria. This respiration involves oxidative phosphorylation, which produces adenosine triphosphate (ATP) as a usable energy form. This process utilises an electron transport chain, in which electrons are passed through a series of enzymes, via redox reactions with cofactor transition metal ions. Each sequential enzyme has a greater reduction potential, or affinity for electrons, than the last. This movement of electrons provides energy in order to pump H⁺ from the mitochondrial matrix across the inner membrane to the intermembrane space, generating a proton gradient. These H⁺ pass back across the inner membrane through the enzyme ATP synthase, to generate ATP. The final enzyme in the electron transport chain, cytochrome c oxidase, converts four electrons into H₂O by reaction with O₂ and four H⁺ from the matrix (Figure 5).^{24,25} However, approximately 0.1-2.0% of these reactions do not go to completion and instead, one electron is transferred to O₂, resulting in prematurely released O₂^{•-} by-product (Figure 5).²⁶

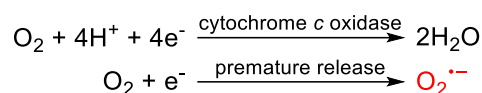


Figure 5: Ideal formation of H₂O from O₂ and non-ideal formation of O₂^{•-} from O₂, that occurs during oxidative metabolic ATP synthesis.^{24,25}

O₂^{•-} and other ROS also play an important role in cell signalling in many organisms. Additionally, O₂^{•-} is purposefully produced by the immune system in many eukaryotic organisms. These ROS work effectively to destroy invading microorganisms. In many eukaryotic organisms, phagocytes encapsulate these microorganisms and bombard them with ROS, destroying them. These phagocytes produce O₂^{•-} using the enzyme nicotinamide adenine dinucleotide phosphate oxidase (NADPH oxidase) (Figure 6).^{27,28}

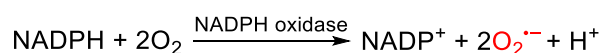


Figure 6: O₂^{•-} production from O₂ by NADPH oxidase in the immune system.^{27,28}

Whilst effective at destroying invading microorganisms, O₂^{•-} and other ROS are also effective at causing cell damage, which can ultimately lead to cell death.²⁹⁻³¹ Cell components particularly at risk include: deoxyribonucleic acid (DNA) and ribonucleic acid (RNA) in nuclei; polyunsaturated fatty acids in lipids; amino acids in proteins and cofactors in enzymes.³² Antioxidants reduce oxidation of cell components by converting ROS into less harmful species, reducing cell damage. Superoxide dismutase (SOD) is an antioxidant enzyme, found in nearly

all organisms, which converts $O_2^{\bullet-}$ into less reactive hydrogen peroxide H_2O_2 (Figure 7).³¹ Highly reactive $O_2^{\bullet-}$ which has neither reacted with an invading microorganism nor been quenched by antioxidants, usually reacts with other nearby cell components, causing cell damage.^{29–31}

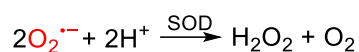


Figure 7: $O_2^{\bullet-}$ conversion into H_2O_2 by superoxide dismutase (SOD).³¹

H_2O_2 is much less reactive than $O_2^{\bullet-}$ and therefore, causes far less cell damage. However, H_2O_2 can form hydroxyl radicals ($\bullet OH$) and HO_2^{\bullet} in presence of transition metal ions, for example Fe^{2+} (Figure 8).^{33,34} Together, $\bullet OH$ and HO_2^{\bullet} are termed HO_x^{\bullet} . $\bullet OH$ is an extremely reactive radical and ROS, and reacts rapidly and non-specifically with almost any biological component.^{30,34} Therefore, nearly all organisms living in O_2 presence contain catalase. Catalase converts H_2O_2 into harmless H_2O and O_2 (Figure 8).³⁵ Unlike superoxide, residual H_2O_2 which has not been safely converted into H_2O by catalase can travel far within a biological system, owing to its lower reactivity. This H_2O_2 can form $\bullet OH$, causing cell damage far away from the H_2O_2 source (Figure 8).^{30,34}

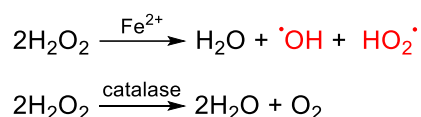


Figure 8: H_2O_2 uncontrolled conversion by iron into ROS species $\bullet OH$ and HO_2^{\bullet} and control conversion by catalase into harmless products.^{33–35}

Common non-enzymatic antioxidant compounds include uric acid, ascorbic acid (vitamin C) and glutathione. In most eukaryotic and some prokaryotic organisms, glutathione has high cellular abundance and is synthesised for its antioxidant properties. The thiol in glutathione (GSH) is highly reductive and reacts readily with many ROS, forming glutathione dimer (GSSG) and simultaneously converting ROS into a less reactive species (Figure 9). This glutathione dimer can be reversibly reduced by glutathione reductase, reforming glutathione antioxidant (Figure 9).^{36–38}

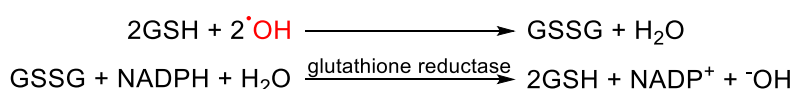


Figure 9: $\bullet OH$ reduction into H_2O using antioxidant glutathione (GSH) forming glutathione dimer (GSSG) and subsequent glutathione dimer oxidation to reform glutathione, using glutathione reductase.^{36–38}

Since radicals, including ROS, are very reactive, production and subsequent destruction of these radicals must be carefully controlled to minimise biological damage. When a biological system fails to control ROS population, known as oxidative stress, cell damage can occur.³⁹ Radical damage to cells is thought to cause many diseases, including Alzheimer's disease, deafness, autism and diabetes.^{40–42} The free radical theory of aging (FRTA) also suggests that the main cause of aging is radical damage to cells.⁴³ Additionally, radical damage to DNA is thought to cause some cancers.⁴⁴ ROS are believed to be able to induce DNA crosslinking, which involves forming a covalent linkage between two nucleotides, either within the same strand (intrastrand) or opposite strand (interstrand). This linkage changes the DNA structure and could cause the cell to behave abnormally, either causing cell death or incorrect DNA replication, which could eventually cause cancer.⁴⁵ DNA crosslinking is believed to occur most commonly between intrastrand guanine and thymine through their C8 and C9 respectively (Figure 10).^{46,47}

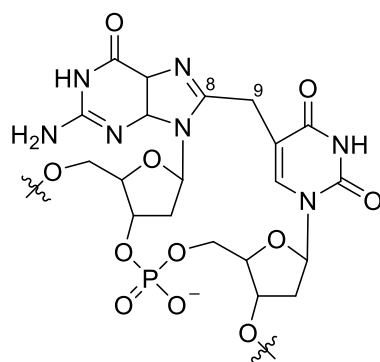


Figure 10: DNA crosslinking between adjacent intrastrand guanine and thymine through their C8 and C9 respectively, which may occur through ROS oxidation.^{46,47}

Consequently, significant medicinal research is concerned with oxidative stress, antioxidants, cell damage and disease. Radical quantification in cells could help determine where and when a biological system is suffering oxidative stress. Furthermore, radical characterisation could allow the site of radical attack and therefore, vulnerable cellular components, to be determined. These pieces of information could be used to treat or prevent further damage to damaged cells and cell components. Furthermore, improved knowledge of areas of biological systems likely to experience oxidative stress and vulnerable cellular components could aid targeted development of antioxidants to reduce this oxidative stress.

Radicals are also observed in some enzymatic mechanisms. Bacterial toxin polytheonamide A utilises novel radical S-adenosyl-L-methionine (SAM) enzymes for post-translational modifications.⁴⁸ Parent *et al.* conducted an *in vitro* mechanistic study of SAM enzyme epimerase PoyD catalysed L-valinamide (L-Val) epimerisation to D-valinamide (D-Val) and proposed its mechanism (Figure 11).⁴⁸

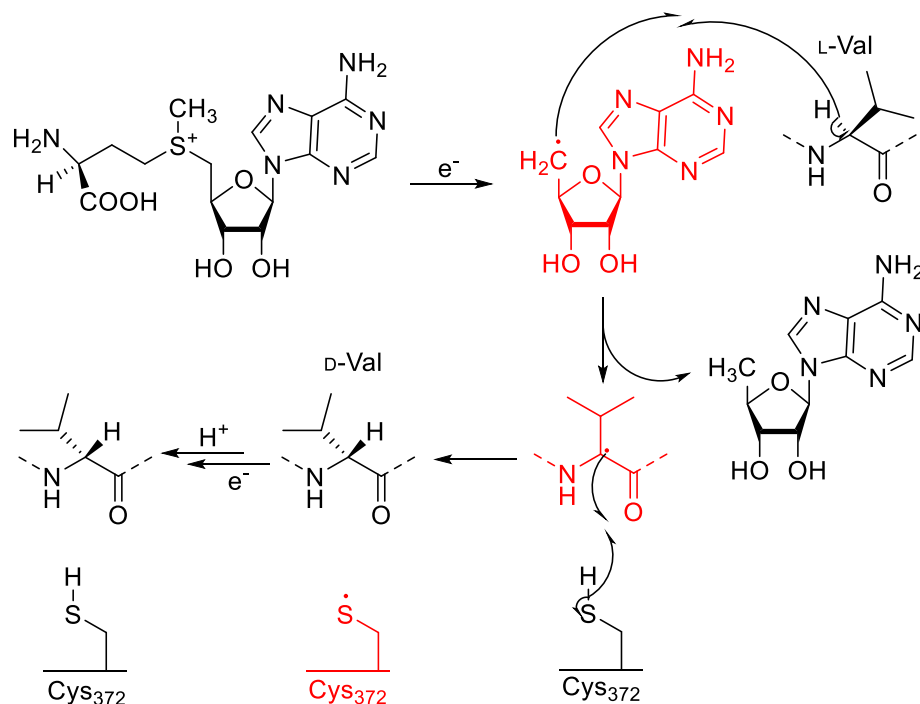


Figure 11: Proposed mechanism of radical SAM enzyme epimerase PoyD catalysed L-valinamide epimerisation.⁴⁸

Improved radical characterisation could aid biochemistry mechanistic studies, informing or validating hypothesised mechanisms and improving understanding of biochemistry mechanisms.

1.2.3. Atmospheric chemistry

Radicals play a key role in the initiation and propagation of atmospheric oxidation cycles of emitted volatile organic compounds (VOCs). These reactions lead to formation of secondary organic aerosol (SOA), photochemical smog and tropospheric ozone, which can significantly influence air quality and climate change and induce environmental damage and negative health effects.^{10,11} In particular, hydroxyl radicals ($\bullet\text{OH}$) are responsible for initiating a large proportion of VOC degradation reactions through oxidation cycles and control the oxidising capacity of the troposphere.^{49,50} In the daytime, $\bullet\text{OH}$ are predominantly generated through the photolysis of nitrous acid (HONO) and ozone photolysis via the reaction of $\text{O}(^1\text{D})$ atoms with water (Figure 12).⁵¹

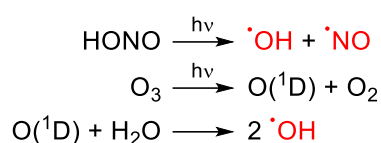


Figure 12: Daytime formation of $\bullet\text{OH}$ through HONO and ozone photolysis.⁵¹

$\bullet\text{OH}$ reaction with VOCs initiates an oxidation cycle which leads to VOC degradation and further radical generation. A relatively simple example is $\bullet\text{OH}$ -initiated alkane degradation. Alkanes are released into the atmosphere biogenically and anthropogenically. Biogenic sources include *Pinus jeffreyi* resin, which contains *n*-heptane⁵² and *Rosa hybrida*, which release *n*-nonane and *n*-decane in their floral fragrances.⁵³ Anthropogenic sources include release of non-combusted alkanes during burning of petrol, diesel and kerosene, such as *n*-nonane and *n*-decane.^{54,55} Oxidative degradation of atmospheric VOCs, including alkanes, is known to contribute to photochemical smog, SOA and tropospheric ozone production. Therefore, their emissions need to be carefully controlled.⁵⁶

In $\bullet\text{OH}$ -initiated alkane degradation, $\bullet\text{OH}$ abstract hydrogen atoms from alkanes to form water and alkyl radicals ($\text{R}\bullet$). In air, these radicals rapidly react with O_2 , forming alkylperoxyl radicals ($\text{RO}_2\bullet$). Reactions of $\text{RO}_2\bullet$ and nitrogen oxides (NO_x) have been found to lead to organic nitrate formation, which are key compounds in photochemical smog.⁵⁶ In absence of NO_x , $\text{RO}_2\bullet$ degrades through self-reaction (Figure 13).^{50,57}

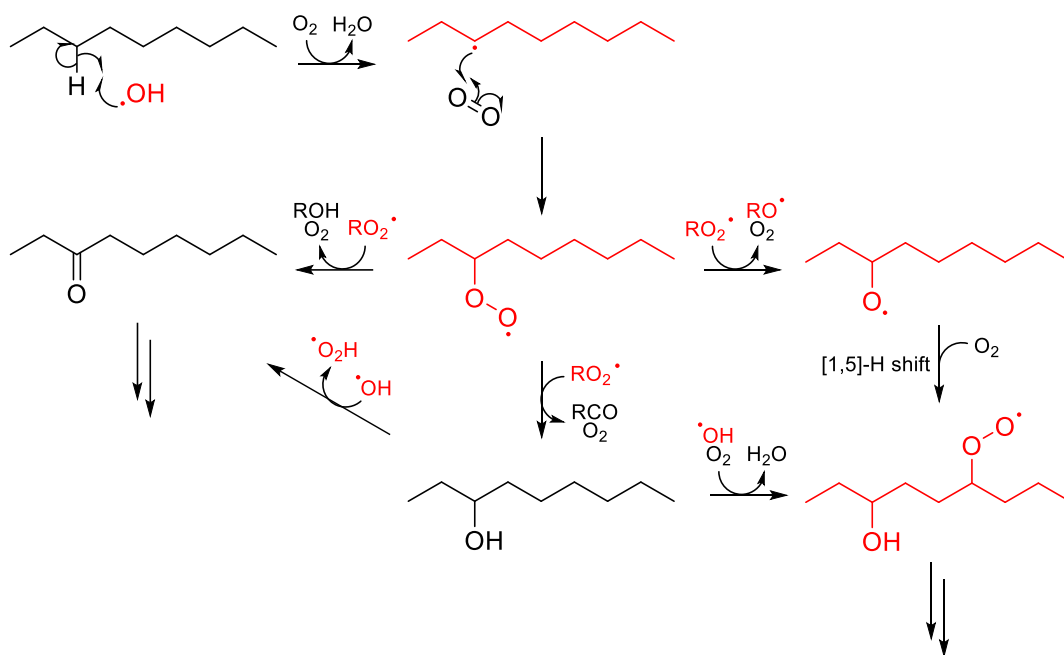


Figure 13: Early stages of $\bullet\text{OH}$ -initiated *n*-nonane degradation in absence of NO_x , showing formation of radical species $\text{R}\bullet$, $\text{RO}_2\bullet$ and $\text{RO}\bullet$. RCO represents carbonyl species.^{50,57}

At night-time, $\bullet\text{OH}$ is predominantly produced as a by-product of alkene ozonolysis.^{58,59} These reactions also occur in the daytime, but are not as significant as photolytic $\bullet\text{OH}$ sources. In particular, atmospheric ozonolysis of biogenic alkenes, especially monoterpenes, is an important non-photolytic contributor to the formation of $\bullet\text{OH}$ and other radicals, as well as SOA.^{58,59}

Terpenes are a large class of diverse compounds found abundantly throughout nature, particularly in plants. These compounds are derived biosynthetically from isopentenyl pyrophosphate (IPP) units. The resultant molecules have structures based upon isoprene units (C_5). Modified terpenes containing additional functional groups are known as terpenoids. Terpenes and terpenoids tend to have strong odours and have multiple biogenic uses in nature, including use as pollinator attractant or herbivore deterrent.⁶⁰ Monoterpenes consist of two isoprene units (C_{10}) and are particularly abundant within plants. Examples include α -pinene and β -pinene (found in pine trees), limonene (found in citrus fruits), myrcene (found in hops) and monoterpenoid linalool (found in lavender) (Figure 14).

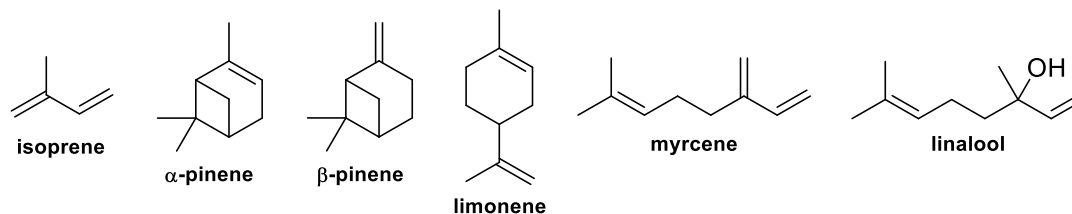


Figure 14: Naturally abundant isoprene, four monoterpenes and monoterpenoid linalool.

Biogenic sources are estimated to be responsible for 760 Tg yr^{-1} VOC emission.⁶¹ This is equivalent to $>70\%$ global VOC emission.⁶² Of these biogenic VOCs (BVOCs), isoprene contributes $\sim 69\%$ whilst monoterpenes contribute $\sim 11\%$. Of this 11%, the greatest contributors are α -pinene ($\sim 34\%$), β -pinene ($\sim 17\%$) and limonene ($\sim 9\%$).⁶¹ These monoterpenes are also widely used as flavourings and fragrances by humans.⁶³ One study reported that each human emitted $170 \mu\text{g h}^{-1}$ monoterpenes, which was mainly attributed to

perfumes.⁶⁴ The high atmospheric abundance of alkenes, including terpenes, coupled with their widespread use in flavourings and fragrances, makes them important VOCs in atmospheric chemistry and indoor and outdoor air quality control.

Atmospheric alkene degradation is predominantly caused by reaction with ozone and especially •OH and nitrate radicals (•NO₃). However, there is strong evidence to suggest significant quantities of •OH which degrade alkenes, are produced as a by-product during alkene ozonolysis. Furthermore, recent measurements predict that alkene ozonolysis provides a missing source of •OH reactivity observed over forested areas.⁵⁸

Alkene ozonolysis is also believed to cause formation of highly oxidised multifunctional (HOM) products. HOMs are of significant interest to atmospheric chemists, as their predicted low volatility could make them excellent nucleators for SOA formation.^{65–67} For HOM classification, a species typically requires at least five or six oxygen atoms.

Alkene ozonolysis is initiated when alkene reacts with ozone in a [3+2] cycloaddition to form a molozonide. This subsequently breaks down into a carbonyl species and an excited zwitterionic carbonyl oxide, known as a Criegee zwitterion (Figure 15). This excited Criegee zwitterion is one of two resonance structures, with the other being an excited α -alkyl-peroxyl biradical, known as a Criegee biradical. Collectively, these two resonance structures are called Criegee intermediates.⁶⁸ Criegee intermediates were first proposed by Rudolf Criegee in the 1950s⁶⁹ and first detected directly in 2008.^{70,71} Recent literature indicates that Criegee intermediates are more zwitterionic in character, with Criegee biradicals being much less stable.⁷² Since Criegee intermediates have significant zwitterionic character, they can exist as E and Z conformers, which have distinctly different reactivities.⁷³ Unsymmetrical alkenes can form two different sets of carbonyls and Criegee intermediates (Figure 15).⁶⁸

Excited Criegee intermediates may either rearrange and rapidly decay into α -radical carbonyl R• species and •OH, via a vinyl hydroperoxide intermediate, or relax to form stabilised Criegee zwitterions, i.e., Criegee intermediates in the ground state (Figure 15). •OH formed during Criegee intermediate degradation can further react with other species. Stabilised Criegee intermediate degrade via non-radical pathways. In presence of air, α -radical carbonyls rapidly react with O₂ to form relatively long-lived RO₂• (Figure 15).

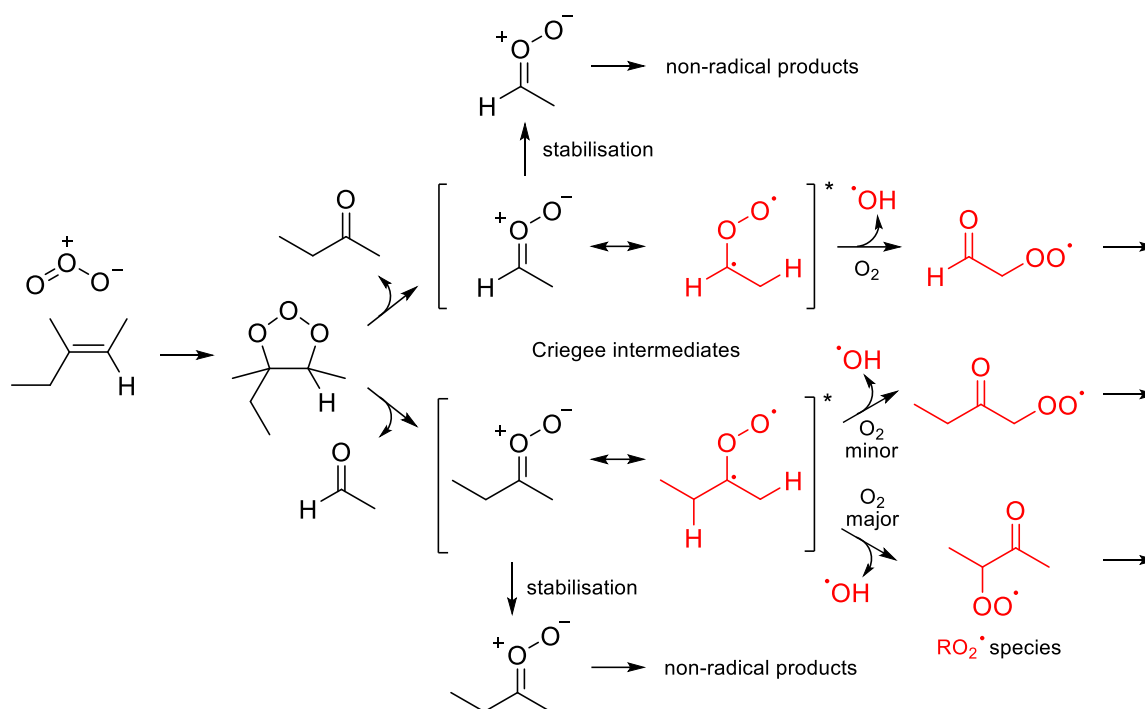


Figure 15: Example ozonolysis mechanism of 2-methylpent-2-ene in presence of O_2 , showing formation of Criegee intermediates and subsequent RO_2^\bullet formation.

Detection, characterisation and quantification of species produced from atmospheric hydrocarbon degradation, and the mechanism by which this occurs, is important for understanding how emission of these chemicals can impact the environment, to what extent VOC emission should be controlled and how atmospheric VOCs and their derivatives can be safely captured or destroyed if required.

1.3. Current radical characterisation techniques

Radical characterisation techniques are frequently used to study radicals in common radical reactions, such as those described above (1.2), to provide mechanistic and kinetic information. Some of the most commonly used radical characterisation techniques are discussed below.

Efficient and highly characteristic direct detection of radicals would offer the simplest and most certain proof of radical identity and hence reactivity. As such, many techniques have been used for direct radical characterisation (1.3.1). Direct radical characterisation has historically been more successful for persistent and stable radicals, as short-lived radicals can usually not be obtained in high concentrations and may decay faster than spectra acquisition time.

1.3.1. Direct radical characterisation techniques

1.3.1.1. Electron paramagnetic resonance (EPR) spectroscopy

Electron paramagnetic resonance (EPR) spectroscopy is arguably the most widely used technique for radical characterisation. EPR spectroscopy detects monochromatic microwaves absorbed when unpaired electrons (radicals) in singly occupied molecular orbitals (SOMOs) are excited from a magnetically aligned state to a magnetically anti-aligned state, relative to a sweeping external magnetic field. Changes in the chemical environment of unpaired electrons shift the external magnetic field at which electron excitation occurs, and thus species can be characterised. Furthermore, coupling between unpaired electrons and nearby nuclear spins creates additional energy states resulting in signal multiplicity.^{74–77} EPR spectroscopy is

analogous to nuclear magnetic resonance (NMR) spectroscopy but characterises electron spin rather than nuclear spin (1.3.1.1.) EPR spectroscopy is well suited to radicals, as all radicals contain at least one unpaired electron, and therefore register a signal.^{75–77} Since EPR spectroscopy exclusively detects unpaired electrons, non-radical products are not detected, significantly cleaning EPR spectra and simplifying analysis. However, this means that radicals and products cannot be detected simultaneously. EPR spectroscopy has been widely used for direct characterisation of long-lived radicals, such as TEMPO•.^{75–79} EPR spectroscopy of TEMPO• produces a triplet signal, due to the interaction between the unpaired electron and the adjacent ¹⁴N nucleus. For example, photolysis of a TEMPO-functionalised benzofuran, designed as an anticancer agent, was monitored using EPR spectroscopy to measure TEMPO• production (Figure 16). This enabled photolysis kinetics, and thus chemical stability, to be determined.⁷⁸

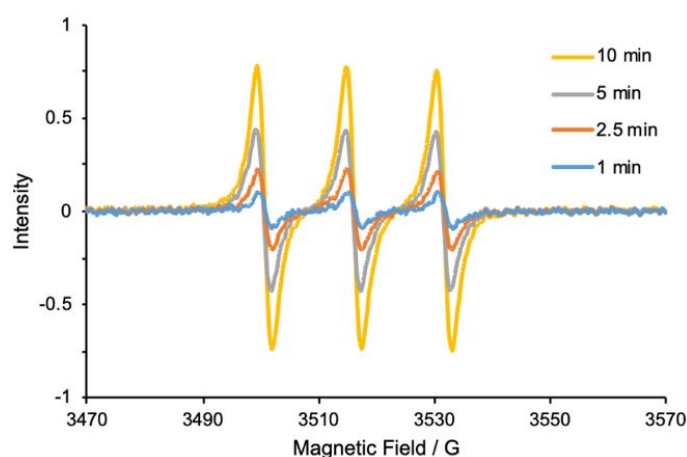


Figure 16: EPR spectra acquired during photolysis of a TEMPO-functionalised benzofuran. Reprinted and adapted with permission.⁷⁸ Copyright 2019 Beilstein Journals.

Matrix isolation EPR spectroscopy, which can be used to detect low concentrations of short-lived radicals by concentrating them in frozen matrices of inert gases, has been used to characterise atmospheric radicals, such as HO₂•, RO₂• and NO₂•, with detection limits ~10⁸ molec. cm⁻³.^{80–82} This has provided mechanistic and kinetic insights into atmospherically relevant VOC degradation (1.2.3).

A significant advantage of EPR spectroscopy is its highly quantitative nature. EPR standards can be used to calibrate EPR spectroscopy intensity, allowing concentration of any radical to be calculated with high accuracy. EPR spectroscopy is non-invasive and can often be performed *in situ*.^{75–77}

However, EPR spectroscopy has several disadvantages which makes directly characterising some radicals challenging. Firstly, it only has moderate sensitivity for liquid phase radical detection (around 1 μM in solution), whilst gaseous radical detection is usually only possible at reduced pressure. Low radical concentration is commonly overcome using spin traps (1.3.2.1).^{77,83,84} Secondly, as EPR spectroscopy is only sensitive to the chemical environment close to the unpaired electron, it provides limited structural information for atoms far from the unpaired electron.^{77,84} This usually makes characterisation and structure elucidation of unknown radical species with complex structures challenging. Thirdly, analysis of EPR spectra is relatively difficult. In complex mixtures, multiple paramagnetic species result in overlapping spectra. This usually requires computational deconvolution to obtain meaningful results, often through spectral simulation.⁷⁷

1.3.1.2. Chemically induced dynamic nuclear polarization (CIDNP) NMR spectroscopy

Chemically induced dynamic nuclear polarisation (CIDNP) NMR spectroscopy is another technique that exclusively detects radicals. CIDNP is an effect detected exclusively for spin-polarised radical pairs in NMR spectroscopy. NMR spectroscopy detects radio waves emitted by nuclear spins when excited by radio waves of fixed frequency, in presence of a fixed external magnetic field. Differences in the chemical environment of nuclear spins, especially the strength of coupling interactions between nuclear and nearby electron spins, yields radio waves of different frequency, and thus species can be characterised. Furthermore, coupling between nearby nuclear spins creates additional energy states resulting in signal multiplicity.⁸⁵⁻⁸⁷ Radicals usually significantly broaden NMR spectra through their paramagnetism, which prevents NMR spectroscopy detection.⁸⁷ However, CIDNP NMR spectroscopy detects enhanced absorption or emission (negative) intensity, for nuclear spins whose excitation is affected by coupling with a radical pair in the triplet state.⁸⁵⁻⁸⁷ This radical pair is usually produced through photoexcitation during spectral acquisition. Chemically induced dynamic electron polarisation (CIDEP) can likewise be detected for this radical pair, using EPR spectroscopy. For example, CIDNP NMR spectroscopy of UV-irradiated 2-phenylacetophenone indicated formation of benzoyl and benzyl radicals, indicating Norrish type I α -cleavage (Figure 17). This offered mechanistic insights into the UV-initiated degradation of 2-phenylacetophenone.⁸⁸

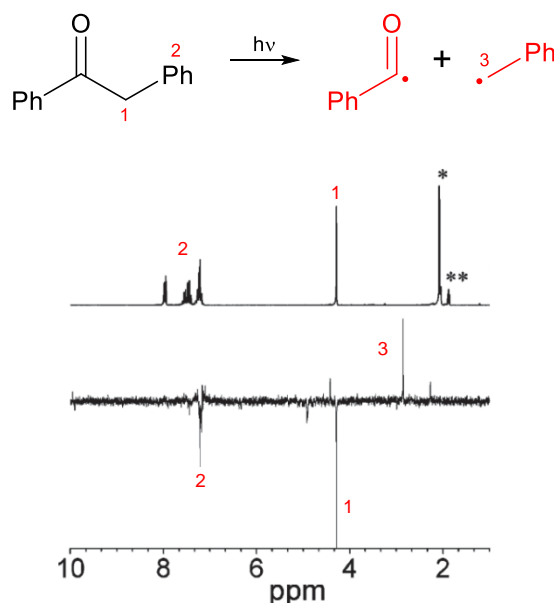


Figure 17: NMR (middle) and CIDNP NMR (lower) spectra of UV-irradiated of 2-phenylacetophenone, indicating benzoyl and benzyl radical formation (upper). Numbers (red) indicate protons responsible for observed signals. Reprinted and adapted with permission.⁸⁸ Copyright 2010 American Chemical Society.

Like other NMR spectroscopic techniques, the main advantage of CIDNP NMR spectroscopy is that it is highly characteristic. It can also be used quantitatively.

The main disadvantage of CIDNP NMR spectroscopy is that it can only be used to detect radical pairs formed through thermolysis or homolysis, significantly limiting its scope. Furthermore, CIDNP NMR spectroscopy must be performed *in situ*, which can make reaction set-up or field measurements complex or unfeasible. Like other NMR spectroscopic techniques, CIDNP NMR spectroscopy has very poor sensitivity and is therefore unsuitable for reactions with low radical concentrations, such as in the gas phase. Finally, CIDNP NMR

spectra analysis can be challenging. In complex mixtures, multiple species can result in overlapping NMR spectra, which produces a complex NMR spectrum. Complex NMR spectrum analysis requires deconvolution to obtain meaningful results, which is time consuming and may be unfeasible. Therefore, CIDNP NMR spectroscopy is usually only suitable for studying simple radical reactions with high radical concentrations.^{85–87}

1.3.1.3. Mass spectrometry (MS)

Mass spectrometry (MS) has been used for direct characterisation of persistent radicals. MS measures the mass to charge ratio (m/z) of charged adducts or charged fragments, formed through ionisation of neutral species and separated based on their m/z ratio, using an electric or magnetic field.^{89–94} MS can detect radicals and non-radicals simultaneously, meaning observed peaks do not necessarily correspond to radical species. However, observation of both types of species means that they can be monitored together. Some persistent radicals have been directly detected using relatively soft electrospray ionisation MS (ESI-MS), for example TEMPO \cdot (Figure 18).⁹⁵

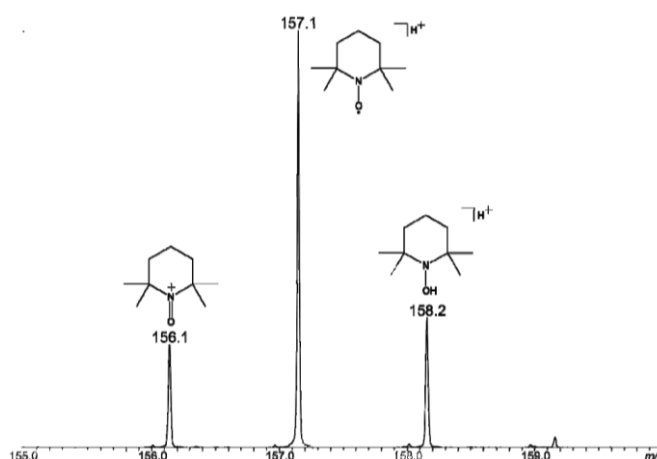


Figure 18: ESI-MS mass spectrum of TEMPO \cdot . Reprinted and adapted with permission.⁹⁵ Copyright 2019 Sage Publications.

The high sensitivity of MS has allowed even gaseous radicals to be observed, with gaseous detection limits $<10^6$ molec. cm^{-3} . For example, chemical ionisation MS (CI-MS) has been used for direct detection of highly-oxygenated low vapour pressure $\text{RO}_2\cdot$, for example in $\text{Cl}\cdot$ -initiated cyclohexane degradation (Figure 19).^{96–99} This has provided mechanistic and kinetic insights into atmospherically relevant hydrocarbon degradation (1.2.3).

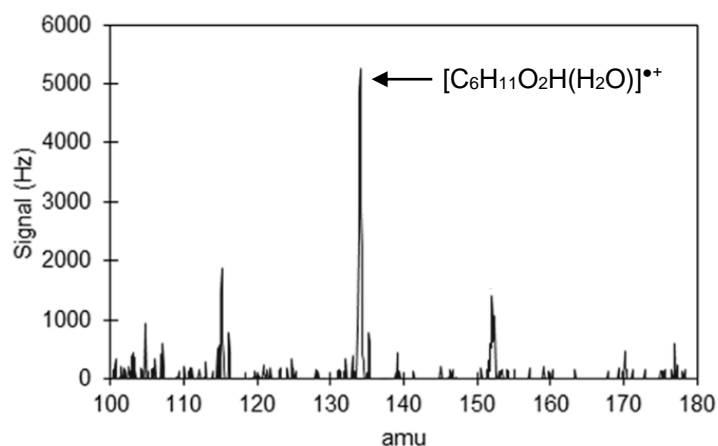


Figure 19: CI-MS mass spectrum of $C_6H_{11}O_2$. Reprinted and adapted with permission.⁹⁸ Copyright 2019 American Chemical Society.

MS is well suited to characterisation of complex mixtures. Mass spectrum peaks can usually be relatively easily attributed to particular molecular formulae and therefore, logical species structures. Additionally, a high resolution mass spectrometer can cleanly separate species with different molecular formulae.^{89–94} MS also has very high sensitivity and can detect picograms of material.¹⁰⁰

The main drawback of MS is that the intensity with which a species is detected is highly dependent on its structure, amongst many other factors. This means that observed radicals are difficult to quantify, whilst other radicals cannot be detected at all. Quality of MS quantification can be increased by calibrating MS for individual species, although even with calibration, accuracy of quantification is highly dependent on other factors and usually cannot be compared between spectrometers. Furthermore, this is not possible for short-lived radicals.^{89–94} Poor short-lived radical stability can be overcome by radical conversion into more stable species (1.3.2). Additionally, MS techniques are invasive and can cause destruction of unstable species, such as short-lived radicals, or alter their nature.^{89–94} This effect can even be observed for persistent radicals, such as TEMPO*, for which soft ionisation ESI-MS can cause formation of non-radical species (Figure 18).⁹⁸

1.3.1.4. Ultraviolet-visible (UV-Vis) and fluorescence spectroscopy

UV-Vis spectroscopy and fluorescence spectroscopy are similar techniques that have both been used for direct radical characterisation. UV-Vis spectroscopy measures the light absorbed when electrons are excited by set wavelengths of ultraviolet-visible light, whilst fluorescence spectroscopy measures the light spectrum emitted when electrons relax, after being excited by a specific wavelength of light (both typically between 200-1000 nm).^{101,102} All radicals contain a singly occupied molecular orbital (SOMO).^{1,2} Excitation of an electron from the next-to-highest occupied molecular orbital to the SOMO absorbs light whilst subsequent relaxation emits light. This relatively low energy gap tends to correspond to wavelengths of visible light and hence, radicals are usually coloured. Radical structure affects the energy of these orbitals and hence affects the corresponding wavelengths of light absorbed and emitted, allowing species to be characterised.

UV-Vis spectroscopy has been performed upon long-lived radical chromophores, for example persistent radical 2,2-diphenyl-1-picrylhydrazyl (DPPH), which is deep violet in solution. DPPH has frequently been used as an antioxidant assay, using UV-Vis spectroscopy for characterisation, with solution typically becoming pale yellow as DPPH is consumed through

radical reaction. For example, DPPH consumption in presence of Vitamin E was monitored using UV-Vis spectroscopy (Figure 20).¹⁰³

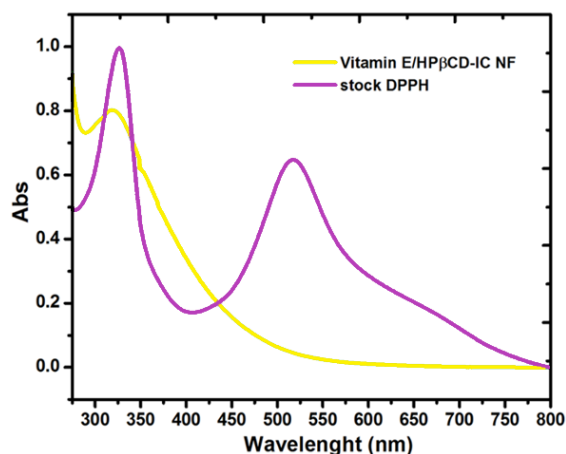


Figure 20: UV-Vis spectra of DPPH after 30 minutes in absence (purple) and presence (yellow) of Vitamin E. Reprinted and adapted with permission.¹⁰³ Copyright 2017 American Chemical Society.

Fluorescence spectroscopy has been performed upon long-lived radical fluorophores, designed as photocatalysts or organic light emitting diodes (OLEDs), for example highly conjugated dithiadiazolyl radicals (Figure 21). These fluorescence spectra were used to determine fluorophore emission wavelengths under photochemistry conditions.¹⁰⁴

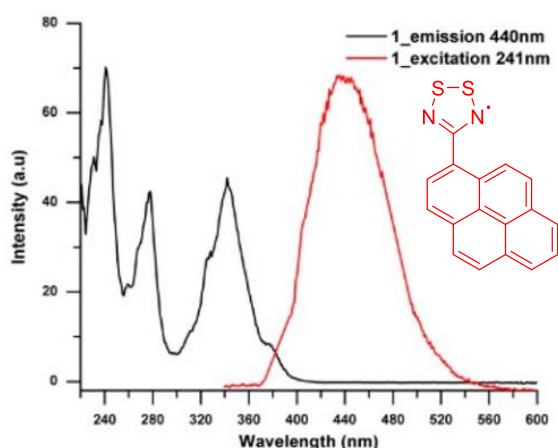


Figure 21: Excitation (black, $\lambda_{em} = 440$ nm) and emission (red, $\lambda_{exc} = 241$ nm) spectra of dithiadiazolyl radical (pictured). Reprinted and adapted with permission.¹⁰⁴ Copyright 2018 American Chemical Society.

Additionally, laser-induced fluorescence (LIF) spectroscopy is a technique used for gaseous radical characterisation, owing to its high irradiance in a narrow wavelength range, which reduces interference from other species. For example, LIF spectroscopy has been widely used to measure $\bullet\text{OH}$ concentration (Figure 22).^{105–108} Such measurements have been used to monitor *in situ* atmospheric $\bullet\text{OH}$ concentration levels, which controls the oxidising capacity of the troposphere, offering mechanistic and kinetic insights into atmospherically relevant reactions (1.2.3).

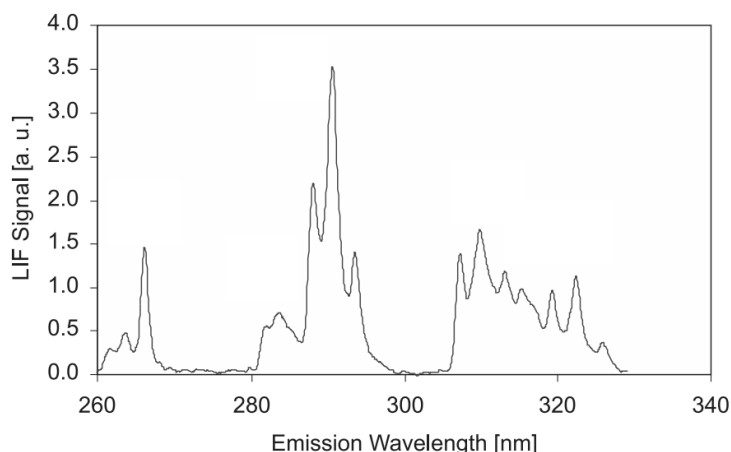


Figure 22: •OH fluorescence spectrum ($\lambda_{\text{exc}} = 266.188 \text{ nm}$). Reprinted and adapted with permission.¹⁰⁵ Copyright 2004 Springer-Verlag.

•OH excitation at 282 nm is optimal for reducing interference from air molecules in absence of ozone or water. As such, 282 nm excitation is commonly used in stratospheric [$\bullet\text{OH}$] measurement, where water concentration is low. Under such conditions, [$\bullet\text{OH}$] detection limits of $<10^5 \text{ molec. cm}^{-3}$ can be achieved.¹⁰⁷ However at this wavelength, when ozone and water are present, considerable amounts of •OH are also generated through photolysis of ambient ozone and subsequent reaction with water, similarly as in the atmosphere (Figure 12). This causes measured [$\bullet\text{OH}$] to be inaccurate.^{106–108}

This issue has been overcome by using longer wavelength excitation under reduced pressure, a technique known as fluorescence assay by gas expansion (FAGE). FAGE typically utilises 308 nm for [$\bullet\text{OH}$] measurement, as ozone absorption cross section is significantly reduced $>290 \text{ nm}$, whilst •OH fluorescence still occurs suitably at this wavelength. The reduced pressure increases the lifetime of •OH whilst reducing interference from air molecules.^{106–108} Calibration can be used to subtract the relatively small amount of •OH produced through ozone photolysis. Using FAGE, [$\bullet\text{OH}$] detection limits of $<10^5 \text{ molec. cm}^{-3}$ can be achieved.^{107,108}

The main advantage of both UV-Vis and fluorescence spectroscopy for direct radical characterisation is that spectral acquisition times are fast, which means that short-lived radicals can be characterised. Additionally, both techniques can be used quantitatively, although each species requires individual calibration.

However, both techniques usually produce broad peaks which often require deconvolution to obtain quantitative data. Like for EPR spectroscopy, complex mixtures usually result in overlapping peaks. However, the broadness of peaks usually observed with UV-Vis and fluorescence spectroscopy makes deconvolution of overlapping peaks very difficult. Quenching further complicates quantification of fluorescence spectra. Additionally, both techniques are poorly diagnostic for radical species structure. This usually makes characterisation and structure elucidation of unknown radicals extremely challenging.^{101,102}

Other techniques have also been used for direct radical characterisation, including infrared (IR) spectroscopy¹⁰⁹; Raman spectroscopy¹¹⁰; differential optical absorption spectroscopy (DOAS)¹¹¹; cavity ring down spectroscopy (CRDS)¹¹² and flash photolysis¹¹³. However, like the above direct radical characterisation techniques, these other techniques have drawbacks which hinder radical study.

1.3.1.5. Overall issues with direct radical characterisation techniques

Direct radical characterisation techniques offer the most certain proof of radical identity. However, all existing direct radical characterisation techniques suffer drawbacks which hinder radical study (Table 1).

A key issue for all these direct radical characterisation techniques is that they are only applicable to specific radicals or reactions. Indeed, most of these techniques are usually not suitable for direct characterisation of short-lived radicals (including EPR spectroscopy and MS). Additionally, many of these techniques are typically impractical for complex mixtures (including EPR, UV-Vis, fluorescence and CIDNP NMR spectroscopy). In addition, most of these techniques are poorly sensitive (including EPR and CIDNP NMR spectroscopy) and are not suitable for detecting radicals with low concentrations. This is commonly the case for short-lived radicals. These limitations hinder the applicability and usefulness of each method.

Many of these techniques are also poorly diagnostic for radical species with complex structures, offering limited structural information for atoms far from the radical centre (including EPR, UV-Vis and fluorescence spectroscopy). This means that the structures of complex radicals must be well-understood to analyse spectra and limits opportunity for analysis of unexpected results. Many of these techniques also require bulky, expensive and niche equipment and are not suitable for field measurements.

Table 1: Summary of advantages and disadvantages of direct radical characterisation techniques. ✓, ✗ and ~ refer to yes, no and sometimes or somewhat respectively. Symbols refer to general radical detection in the most common setups and do not include more specialised cases or instruments.

Technique	Highly sensitive	Highly quantitative	Highly diagnostic for complex radicals	Suitable for short-lived radicals	Suitable for complex mixtures
EPR spectroscopy	~	✓	~	~	~
MS	✓	✗	✓	✗	✓
UV-Vis spectroscopy	~	~	✗	✓	✗
Fluorescence spectroscopy	~	~	✗	✓	✗
CIDNP NMR spectroscopy	✗	✓	✓	✓	~

However, indirect radical characterisation techniques overcome some of these problems by chemically converting radicals to longer-lived radical or non-radical species, usually through reaction with a trapping agent. Many indirect radical characterisation techniques have been developed, using a variety of trapping agents, as discussed below.

1.3.2. Indirect radical characterisation techniques through radical conversion to a longer-lived species

1.3.2.1. Spin traps

Spin trapping is the process in which short-lived radicals are chemically converted into longer-lived radicals using spin traps, which are present in the radical reaction system. Reaction between a short-lived radical and spin trap, for example nitroso or nitrene spin traps, results in a longer-lived radical spin adduct, containing the reactant radical (Figure 23). The resulting

nitroxyl radical spin adducts can be characterised using a variety of techniques but are particularly well suited to EPR spectroscopy, due to their radical nature. The main advantage of spin trapping is that the spin trap can be exposed to radicals until sufficient spin adduct concentration has been accumulated for characterisation, for example by EPR spectroscopy. This overcomes the sensitivity issue suffered by many direct radical characterisation techniques. Additionally, the longer-lived radical overcomes many problems associated with poor stability of short-lived reactant radicals, such as slow acquisition times and difficulty in handling.^{77,83,84}

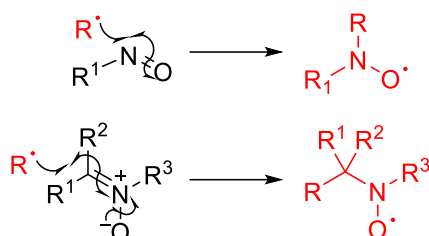


Figure 23: Reaction of a short-lived radical (R^\bullet) with nitroso (top) and nitron (bottom) spin traps, forming longer-lived nitroxyl radical spin adducts.

Most short-lived radicals add quickly and selectively to the double bond in nitrones and nitroso spin traps. Additionally, spin traps can be tailored to suit the radical system being studied. Spin trapping characterisation using EPR spectroscopy is arguably the most well-known and widely used indirect radical characterisation technique, due to its applicability to most liquid and gas phase short-lived radicals.^{77,83}

For example, 5,5-dimethyl-1-pyrroline N-oxide (DMPO) nitron spin trap and EPR spectroscopy have been used for SO_3^\bullet and SO_4^\bullet detection.¹¹⁴ Sulfur oxides are environmentally pervasive and demonstrate high toxicity. It is speculated that their radical forms are principally responsible for their toxicity.¹¹⁵ Radical sulfur oxides can be formed through atmospheric processes. Liquid phase SO_3^\bullet and SO_4^\bullet have been trapped using DMPO and the resulting spin adducts analysed using EPR spectroscopy (Figure 24).¹¹⁴

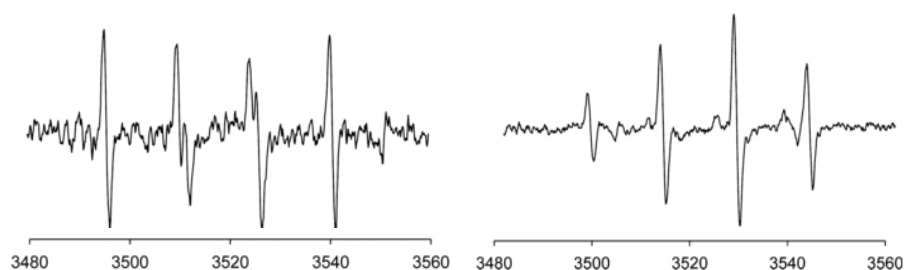


Figure 24: EPR spectra of DMPO-trapped SO_3^\bullet (left) and SO_4^\bullet (right). Reprinted and adapted with permission.¹¹⁴ Copyright 2018 American Chemical Society.

These spectra indicated that SO_3^\bullet and SO_4^\bullet were trapped through their sulfur and oxygen atoms respectively (Figure 25), implying the importance of steric hinderance and electrostatics.¹¹⁴

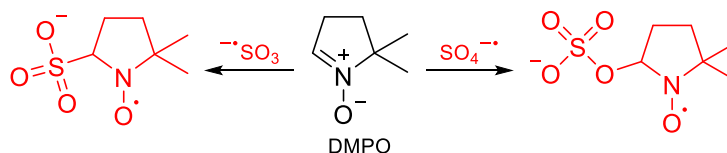


Figure 25: DMPO trapping of $\text{SO}_3^{\bullet-}$ and $\text{SO}_4^{\bullet-}$ forming sulfur and oxygen linked nitroxyl radical spin adducts respectively.¹¹⁴

Many other studies have utilised spin traps to form nitroxyl radical spin adducts, which have been analysed using EPR spectroscopy to successfully quantify and perform limited characterisation of radical species.^{116–118}

A key issue with this method is that although EPR spectroscopy is a moderately sensitive technique, EPR spectra of spin adducts are relatively insensitive to changes in the reactant radical. The further an atom is from the unpaired electron, the less of an effect it will have on EPR spectra. For nitrene and nitroso spin traps, the radical of the resulting nitroxyl radical spin adduct is centred on the oxygen atom, meaning the reactant radical atom closest to the nitroxyl radical group only causes tertiary effects, and subsequent atoms cause even fewer perturbations. Therefore, although this method can be useful for quantification of short-lived radicals, it is poor at their characterisation. Also, other difficulties associated with general EPR spectroscopy are still present, such as difficulties analysing complex spectra (1.3.1.1).^{75–77}

Although spin adducts are usually characterised by EPR spectroscopy, spin adducts have also been detected using other techniques, such as MS.^{119–126} This is possible as the longer-lived radical spin adducts have greater stability than short-lived reactant radicals. For example, liquid chromatography MS (LC-MS) has been used to characterise spin adducts produced when tobacco smoke radicals are trapped by phenyl *tert*-butyl nitrene (PBN) (Figure 26).¹²⁴

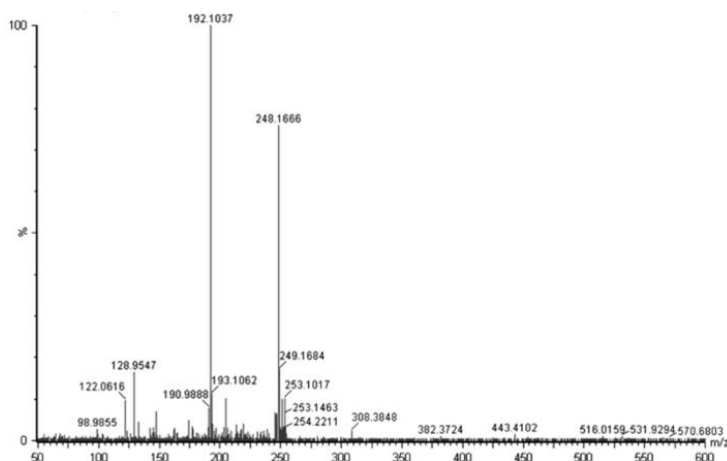


Figure 26: Mass spectrum from LC-MS characterisation of PBN-trapped $\text{C}_4\text{H}_5\text{O}^{\bullet}$ ($[\text{M}+\text{H}]^+$ $m/z = 248.1661$) from tobacco smoke. Reprinted and adapted with permission.¹²⁴ Copyright 2016 Elsevier.

MS and other techniques can provide additional characterisation for spin adducts and thus reactants radicals. These techniques can overcome many of the difficulties associated with EPR spectroscopy, such as being poorly diagnostic.

However, spin trapping has many well-documented drawbacks. The greatest issue with spin trapping is side reactions of non-radical species can lead to artifacts which create false positives. For example, nucleophilic addition of non-radical substrate to a spin trap yields a hydroxylamine. This hydroxylamine can be subsequently oxidised to form the same species produced from radical reaction with a spin trap, creating a false positive. Although methods

exist to detect such artifacts, these suffer from their own limitations.¹²⁷ Additionally, nitrene and nitroso spin traps are not particularly stable and are easily degraded by trace metals.¹²⁸ Spin adducts often have poor stability and therefore short lifetimes, ranging from seconds to hours.^{129–132} This may complicate experimental set-up and field measurements, quantification and prevent sample reanalysis. Additionally, the spin adduct radical prevents characterisation by some commonly used techniques, such as NMR spectroscopy, as discussed previously (1.3.1.1).

1.3.2.2. Recombination traps

Short-lived radicals can be chemically converted into longer-lived non-radical products using persistent radical trapping agents, which are present in the radical system.¹³³ In this work, this process, persistent radical trapping agents and non-radical products are termed recombination trapping, recombination traps and recombination adducts respectively. Reaction between a short-lived radical and recombination trap, results in a longer-lived non-radical recombination adduct, containing the reactant radical (Figure 27). This occurs through radical-radical recombination.¹³³ Recombination adducts are usually stable and can be characterised using many conventional techniques, including MS¹³⁴ and NMR¹³⁵, UV-Vis and fluorescence spectroscopy¹³⁴. This longer-lived non-radical species overcomes many problems associated with poor stability of the short-lived reactant radical, as discussed for spin trapping (1.3.2.1). Additionally, recombination trap can be exposed to radicals until sufficient recombination adduct concentration has been accumulated for characterisation.¹³³ Therefore, recombination trapping is analogous to spin trapping, but utilises a radical trapping agent to generate a non-radical adduct, rather than a non-radical trapping agents to generate a radical adduct (1.3.2.1). Many different recombination traps have been developed.

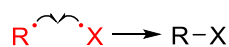


Figure 27: Reaction of a short-lived radical (R•) with a recombination trap (X•), forming a longer-lived non-radical recombination adduct.¹³³

Arguably the most commonly used recombination traps are nitroxyl radicals, such as TEMPO• (Figure 28).

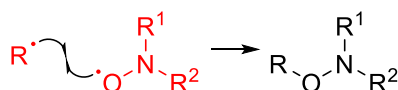


Figure 28: Reaction of a short-lived carbon-centred radical (R•) with a nitroxyl radical recombination trap, forming a longer-lived non-radical recombination adduct.

Reaction between carbon-centred radicals and persistent nitroxyl radicals usually occurs rapidly. Additionally, persistent nitroxyl radicals and their recombination adducts are relatively robust under a range of conditions, usually far more so than spin traps and spin adducts (1.3.2.1). This high stability usually makes experimental set-up and field measurements relatively simple.¹³³ As such, persistent nitroxyl radicals, such as TEMPO•, are routinely used as recombination traps, particularly in synthetic radical reactions, as both starting materials and mechanistic probes.^{134–137} For example, TEMPO• has been used to capture radicals formed in the one electron oxidation of *N*-acetyl-L-tyrosinamide, catalysed by horseradish peroxidase (HRP, Figure 29). Non-radical recombination adduct was characterised using MS, indicating the presence and structure of the intermediate reactant radical.¹³⁸

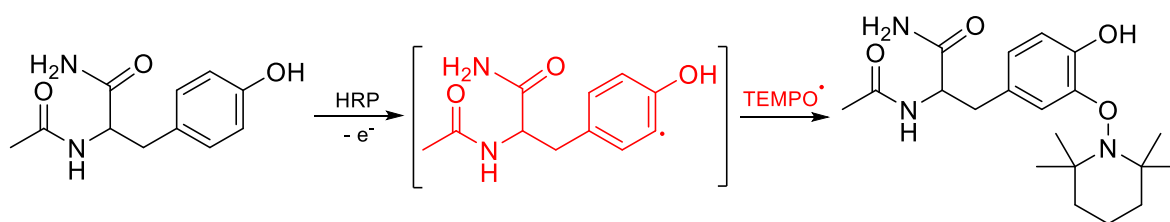


Figure 29: Recombination trapping of *N*-acetyl-L-tyrosinamide radical by TEMPO•, forming non-radical recombination adduct.¹³⁸

A key issue with this method is that persistent nitroxyl radicals do not effectively trap heteroatom-centred radicals which form weak bonds with nitroxyl radical recombination traps, such as oxygen (O–O: ~140 kJ mol⁻¹), nitrogen (N–O: ~200 kJ mol⁻¹) and sulfur (S–O: ~270 kJ mol⁻¹).¹³⁹ This severely limits its applicability. For example, no recombination adducts were detected for recombination trapping of *tert*-butyl peroxy radicals using TEMPO•. Instead, *tert*-butyl oxyl radicals and molecular oxygen were formed and TEMPO• was regenerated. Therefore, TEMPO• acted as a catalyst and not a trapping agent (Figure 30).¹⁴⁰

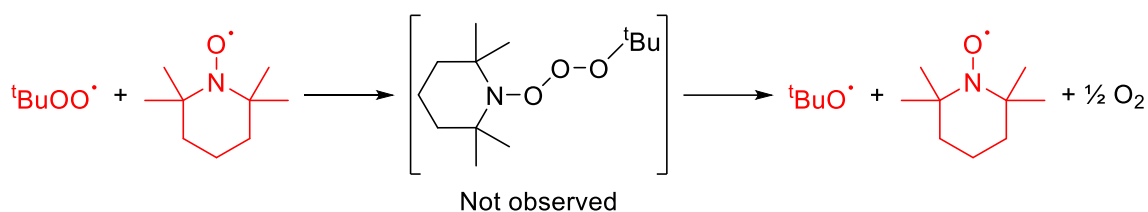


Figure 30: Reaction observed when attempting to trap ^tBuOO• with TEMPO• to form intermediate (centre), however this species was not observed and instead TEMPO• acted catalytically to form ^tBuO• and O₂.¹⁴⁰

This demonstrates that nitroxyl radicals can initiate some radical reactions and this often makes them non-innocent components of reaction mixtures. This can lead to false positives. False positives can also be generated by nitroxyl radical reduction into nitroxide anions, which can undergo nucleophilic reactions to form the same species produced from radical reaction with a recombination trap, creating a false positive, similarly as for spin trapping (1.3.2.1).

Other recombination traps have also been used for indirect radical characterisation. Persistent radical DPPH (1.3.1.4) has frequently been used as a chemical label, as its recombination adducts can be well quantified using UV-Vis spectroscopy (1.3.1.4).¹⁰³ However, DPPH suffers similar issues to nitroxyl radicals, including that it does not react effectively with heteroatom-centered radicals and it can often be a non-innocent component of reaction mixtures, leading to false positives.

2,4,6-Tri-*tert*-butylphenol has also been used as a recombination trap, as it is easily oxidised to long-lived 2,4,6-tri-*tert*-butylphenoxyl radicals, for example by PbO₂ or [Fe(CN)₆]³⁻. These radicals are stabilised through resonance and electron donating *tert*-butyl groups. These radicals can then trap heteroatom-centred radicals, such as oxyl, aminyl and thiyl radicals, through radical-radical recombination.^{141–144} This yields a non-radical stable adduct that can be characterised by conventional techniques. For example, 2,4,6-tri-*tert*-butylphenol has been used to trap NO₂• radicals (Figure 31). The resulting adduct was characterised by its melting point and elemental composition.¹⁴¹

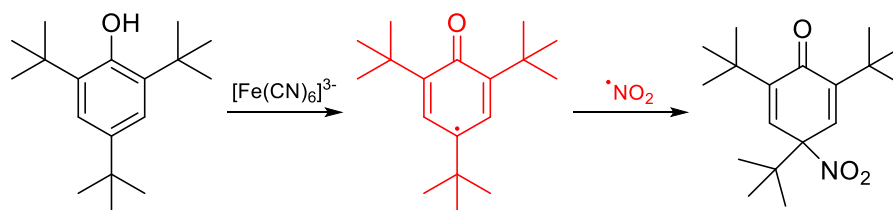


Figure 31: Formation of radical trapping agent 2,4,6-tri-*tert*-butylphenoxy radical and subsequent NO_2^\bullet trapping.¹⁴¹

2,4,6-tri-*tert*-butylphenoxy radicals react much more effectively with heteroatom-centred radicals than nitroxyl radicals and DPPH. However, like other recombination traps, these 2,4,6-tri-*tert*-butylphenoxy radicals can initiate radical reactions, leading to false positives. Furthermore, 2,4,6-tri-*tert*-butylphenol is not easily tunable and has poor water solubility. This limits its applicability, including preventing its use in aqueous solutions.

1.3.2.3. Other trapping agents

Other trapping agents have also been used for short-lived radical conversion into longer-lived products and these products subsequently characterised.

Salicylic acid has been used as a trapping agent. Salicylic acid has been used to trap $\bullet\text{OH}$ in presence of oxygen, to form a mixture of non-radical hydroxylated salicylic acid derivatives, which are then characterised using fluorescence spectroscopy (Figure 32).^{145–147}

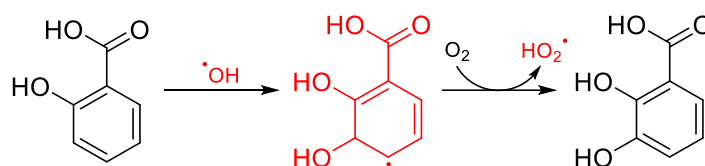


Figure 32: Salicylic acid and $\bullet\text{OH}$ reaction to form example hydroxylated salicylic acid, although a mixture of isomers is produced.^{145–147}

This method suffers many of the disadvantages associated with other trapping agents, such as limited scope and potential for false positives.

1.3.2.4. Overall issues with existing indirect radical characterisation techniques

Indirect radical characterisation techniques overcome some of the drawbacks associated with direct radical characterisation techniques (Table 2).

In particular, trapping agents can be exposed to short-lived radicals, which usually have low concentration, until sufficient longer-lived adduct concentration has been accumulated for characterisation. This overcomes the sensitivity issues associated with many direct radical characterisation techniques. Furthermore, short-lived radicals are converted to longer-lived adducts, allowing more conventional characterisation techniques to be used and easier handling. However, these indirect radical characterisation techniques also entail their own drawbacks (Table 2).

The main issue with these techniques is that they are prone to side reactions, which can lead to false positives. This may reduce validity of experimental results and resulting conclusions. Furthermore, many indirect radical characterisation techniques are only applicable to specific radicals or reactions, limiting their scope. Additionally, some of these techniques yield radical adducts with poor stability, complicating experimental set-up and field measurements and preventing reanalysis.

Table 2: Summary of advantages and disadvantages of indirect radical characterisation techniques. ✓, ✗ and ~ refer to yes, no and sometimes or somewhat respectively. Symbols refer to general radical detection in the most common setups and do not include more specialised cases or instruments.

Trapping agent	Adducts typically stable	Widely applicable	Can lead to false positives	Suitable for EPR spectroscopy	Suitable for other techniques, e.g., MS
Spin traps	✗	✓	✓	✓	~
Recombination traps	✓	✗	✓	✗	✓

1.4. Summary

Existing direct and indirect radical characterisation techniques are invaluable tools for characterising radicals and studying radical reactions. However, all existing techniques have drawbacks which hinder radical system investigation. In particular, no single radical characterisation technique exists which can be used to detect short-lived radicals with low concentration, without the risk of generating false positives. Since radical intermediates are often short-lived and have low concentration, this means there is scope for development of radical characterisation techniques. Development of better methods for short-lived radical detection, characterisation and quantification could significantly develop many areas of chemistry which involve radical intermediates (1.2).

This project involves the design and development of a new radical characterisation technique, which aims to solve many of the drawbacks associated with the existing radical characterisation techniques discussed above (1.3). This new technique will be tested upon a range of radical systems in many areas of chemistry, such as synthetic chemistry, biochemistry and atmospheric chemistry. Specific project aims are discussed in the proposal chapter (2).

2. Proposal

2.1. Project theory

A new method for radical capture, detection and characterisation is proposed. This method will utilise a new class of radical traps, combining ideas from both spin traps (1.3.2.1) and recombination traps (1.3.2.2). These new traps will consist of a leaving group bound to a terminal allyl group, where the leaving group forms a persistent radical upon bond cleavage. Radicals will react with these traps to form a non-radical product and a persistent radical (Figure 33). The radical leaving group is adjacent to the allyl double bond, which allows allylic rearrangement and hence fast and selective addition of radicals, similarly to spin trapping.^{77,83,84} The non-radical product can then be studied by highly sensitive techniques such as MS and NMR spectroscopy, similarly to recombination trapping.^{135,138,148–151} Traps may be functionalised at the allyl or non-terminal alkene position to suit the radical system being studied, for example to contain water-soluble groups for use in biochemistry investigations.

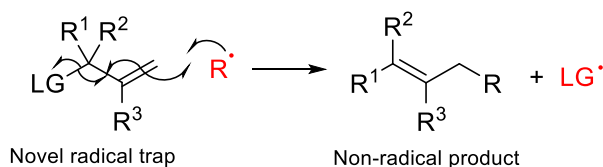


Figure 33: Reaction between reactant radical (R•) and novel allyl radical trap containing bound leaving group, forming a persistent radical (LG•) and non-radical product, containing trapped reactant radical (R). This non-radical product will then be characterised, allowing reactant radical (R) to be identified. R¹, R² and R³ will be functionalised to suit the radical system being studied.

These novel radical traps would have many advantages which overcome some limitations of existing techniques for radical characterisation. Novel radical trapping creates non-radical products which will have significantly greater stability than the reactant short-lived radical intermediates. Characterisation of these non-radical products will allow characterisation of reactant radicals. These non-radical products will likely be significantly more stable than spin-trapped products, which often have short lives (1.3.2.1). Furthermore, these non-radical products can be analysed by conventional and highly characteristic techniques, such as MS and NMR spectroscopy, whereas spin-trapped products often cannot be analysed by such techniques, for example often having poor MS stability and paramagnetically broadened NMR spectra. Novel radical traps should also be reactive to a wide variety of radicals, unlike recombination traps which react poorly with heteroatomic-centred radicals, making novel radical traps more suitable for studying a wide variety of radicals in different systems. Finally, it was hoped that novel radical trapping would not produce false positives. In contrast, recombination traps are usually highly reactive, making them non-innocent components of reaction mixtures, whilst spin traps are prone to side reactions, causing false positives.

This novel radical trapping idea has been previously explored by another PhD student, whose work is built upon in this project.

2.2. Previous project work

This project will build upon previous work from “The Development of Portable Chemosensors for Atmospheric Radicals”, a PhD thesis by Andrew Grantham. Grantham successfully synthesised four novel radical traps. All four traps had the generic novel radical trap structure with R¹ and R² jointly functionalised as one cycloalkane or cycloether ring (Figure 34). These

traps had R¹ and R² functionality as it was believed that otherwise, reactant radicals may abstract allylic hydrogen atoms from the trap, which would cause unwanted side reactions.¹⁵²

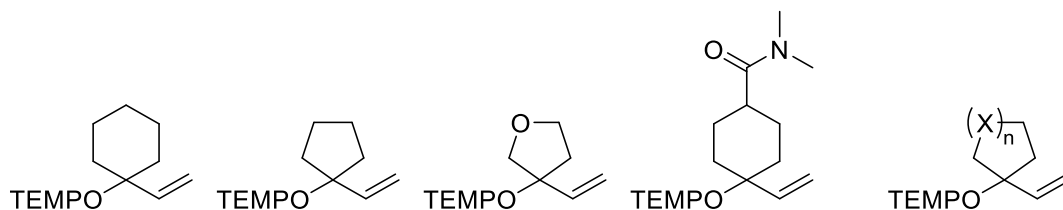


Figure 34: Four traps designed and synthesised by Grantham (left). All four traps had R¹ and R² jointly functionalised as one cycloalkane ring. Grantham traps had the shown general structure (right), where X = CHR or O, R = H or CON(CH₃)₂ and n = 1 or 2.¹⁵²

Grantham had successfully utilised these traps for radical trapping of many different types of radical in many different systems. Grantham used the cyclohexyl trap particularly often in trapping reactions. This was due to its faster and higher yielding synthesis, coupled with its relative inertness. However, whilst hydrogen atom abstraction did not occur from the trap, these traps had a major flaw. Grantham observed that these traps spontaneously isomerised in solution at RTP, to form terminated alkene. Experiments indicated this isomerisation occurred via [1,3]-sigmatropic rearrangement (Figure 35).¹⁵²

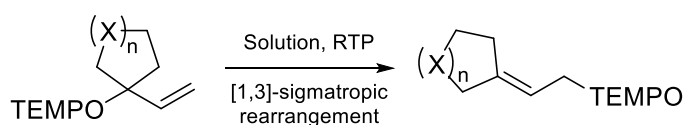


Figure 35: [1,3]-sigmatropic rearrangement of Grantham traps, causing terminal alkene to rearrange to non-terminal alkene. This process occurred readily in solution at RTP. X = CHR or O, R = H or CON(CH₃)₂ and n = 1 or 2.¹⁵²

This isomerisation was detrimental as terminal alkene converted to non-terminal alkene, severely limiting radical access and therefore, reducing trap reactivity with radicals. In solution at RTP, half-life for cyclohexyl Grantham traps was ~3 h. However, by storing trap neat at -20 °C, this half-life could be increased to many months. Therefore, this isomerisation was usually only an issue during trapping reactions, which usually occurred at room temperature and pressure (RTP, 293 K, 101325 Pa) or warmer. Furthermore, this isomerisation meant synthesis had to be done quickly and never yielded pure terminal alkene trap.¹⁵²

Despite these issues, Grantham traps were used to study many liquid and gas phase radical reactions. This involved forming trapped radicals before MS characterisation. MS characterisation was principally undertaken using a Bruker HCT-Ultra ETD II mass spectrometer. Grantham trapped and characterised 1-dodecanethiyl radicals, formed by initiators azobisisobutyronitrile (AIBN) or PbO₂, using Grantham traps. These species originated from non-oxygenated (thiyl), mono-oxygenated (sulfinyl) and di-oxygenated (sulfonyl) 1-dodecanethiyl radicals (Figure 36).¹⁵²

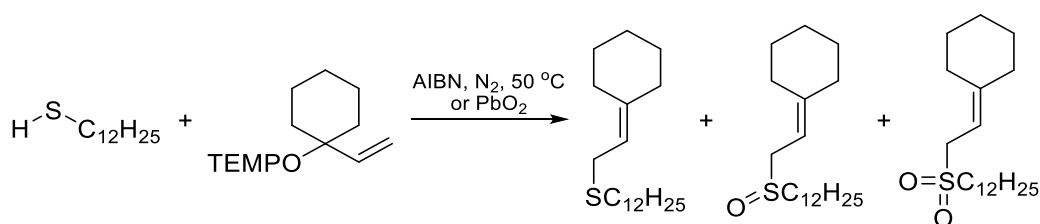


Figure 36: Trapped radicals from 1-dodecanethiyl reaction with AIBN or PbO₂ in presence of Grantham trap, observed by Grantham.¹⁵²

In the gas phase, Grantham trapped and characterised radicals formed during alkene ozonolysis, identifying a great variety of trapped radicals and products. Additionally, Grantham also carried out a detailed analysis of gas phase radicals formed in •OH-initiated *n*-nonane degradation (1.2.3). MS peaks indicated that many radicals were successfully trapped and observed, including RO₂•, R(OH)O₂• and R(CO)O₂•. However formation of other predicted radicals, such as RO•, was not observed.¹⁵²

In this project however, the validity of these results was brought into question, as the Bruker HCT-Ultra ETD II mass spectrometer used had low resolution, making false positives relatively likely (5.2.2.2).

2.3. Project aims

This aim of this project will be to use novel radical trapping to study multiple radical systems. This will first involve developing novel radical traps (3). These traps needed to have several properties to be suitable for trapping radicals. Firstly, they should trap radicals efficiently. Secondly, they should be inert to side reactions and not generate false positives. This will aim to build upon previous work by Grantham, by developing traps which are stable under a wide variety of reaction conditions and do not undergo spontaneous [1,3]-sigmatropic rearrangement (2.2). Thirdly, they should be easy to functionalise to suit a wide variety of radical reactions. For example, study of biochemical reactions will require water-soluble traps. Therefore, this project will aim to synthesise a variety of functionalised traps. This will aim to build upon previous work by Grantham, in which trap functionalisation was hindered by the temperamental synthetic conditions required for Grantham trap formation (2.2). For example, no water-soluble traps were created, meaning Grantham traps were inappropriate for studying biological systems. Further desirable properties were for novel radical traps to be: easily and quickly synthesised; chemically safe; made from cheap starting materials; stable in storage and stable in reaction media.

Once novel radical traps were developed, these would be used to investigate radical systems across many fields of chemistry, including synthetic chemistry, biochemistry and atmospheric chemistry. Such novel radical traps will be used to investigate radical systems of interest which could not be studied using Grantham traps due to their inherently poor stability (2.2), including reactions involving harsh conditions such as high temperature or long reaction times. Additionally, many reactions Grantham investigated will be repeated using the new radical traps and high-resolution MS, to improve upon results obtained by Grantham.

3. Trap design, synthesis and development

3.1. Trap design

Novel radical traps consisted of a leaving group attached to an allyl group (2.1). The leaving group needed to form a persistent radical upon cleavage. It was decided that the leaving group would be (2,2,6,6-tetramethylpiperidin-1-yl)oxyl (TEMPO•). TEMPO• is a ubiquitous, well understood and relatively inert stable radical. This inertness was important, as side reactions would complicate results and analysis. Furthermore, TEMPO• is cheap, readily available and chemically safe. These characteristics made TEMPO• a desirable leaving group for these traps. All novel radical traps synthesised used TEMPO• as their leaving group. However, it is believed that other persistent radicals, such as trityl, may also be effective leaving groups. Other leaving groups were not trialled, as TEMPO• proved suitable in all experiments.

As such, novel radical traps consisted of a TEMPO group bound through its oxygen atom to an allyl group. These novel **TEMPO-Allyl Radical Traps** were termed **TARTs**. TART functionality could be tuned to suit the radical reaction under investigation, at the allyl and non-terminal alkene positions. For example, TART could be functionalised with hydroxyl groups to enable radical trapping in aqueous solutions. TART reaction with radicals (R^\bullet) formed TEMPO• and a non-radical product. This non-radical product consisted of the reactant radical, bound through its radical atom, to the allyl group. These **Radical-Allyl Radically Trapped** species were termed **R-ART**, where R was the name of reactant radical R^\bullet (Figure 37). Similarly, recombination trapping of R^\bullet with TEMPO• was termed R-TEMPO, whilst trapping of R^\bullet with the carbon-centred radical formed following hydrogen atom abstraction (HAA) from TART was termed R-TART (Figure 37). R-TEMPO and R-TART could be formed through non-radical pathways and hence observation of these species would not conclusively indicate a trapped radical.

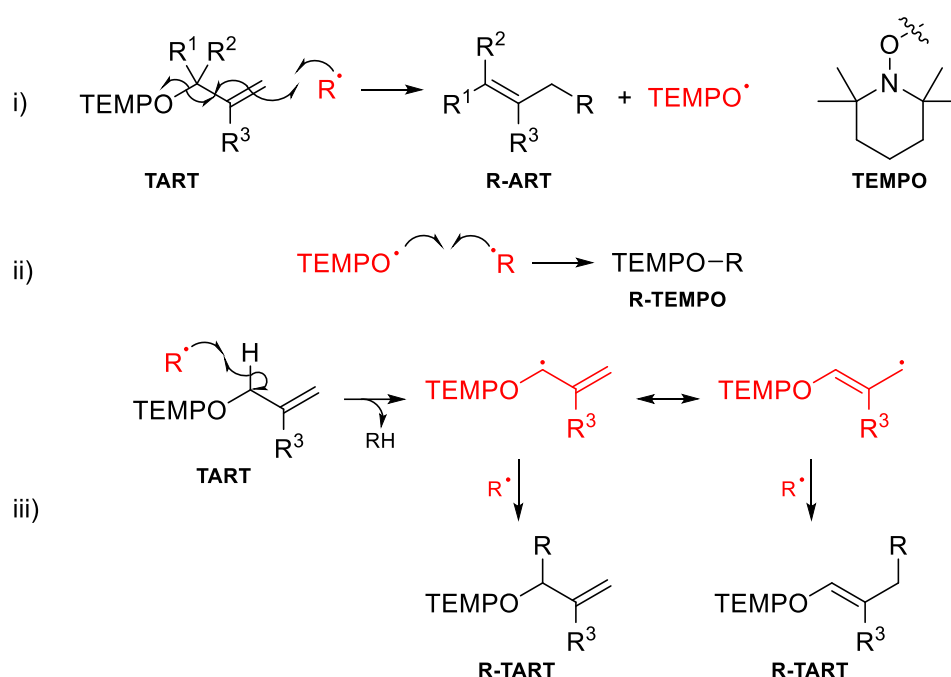


Figure 37: i) TEMPO-Allyl Radical Trap (TART) reaction with radical (R^\bullet) to form stable non-radical Radical-Allyl Radically Trapped (R-ART) species, and persistent radical leaving group, TEMPO•. ii) Recombination trapping of radical (R^\bullet) with TEMPO• to form R-TEMPO. iii) Trapping of R^\bullet with the carbon-centred radical formed following hydrogen atom abstraction (HAA) from TART to form R-TART. TARTs were tuned, by R^1 , R^2 and R^3 functionalisation, to suit radical functionality and reaction conditions.

Four TARTs had previously been synthesised and used for radical trapping by Grantham (2.2).¹⁵² One of these was synthesised by the author using the literature procedure designed by Grantham, so that it could be used for radical trapping if required.¹⁵²

3.2. Grantham TART

Grantham successfully synthesised four TARTs. Grantham principally used the cyclohexyl TART for radical trapping. This cyclohexyl TART was synthesised in a two-step synthesis using the procedure described by Grantham (Figure 38, 11.2.1).¹⁵²

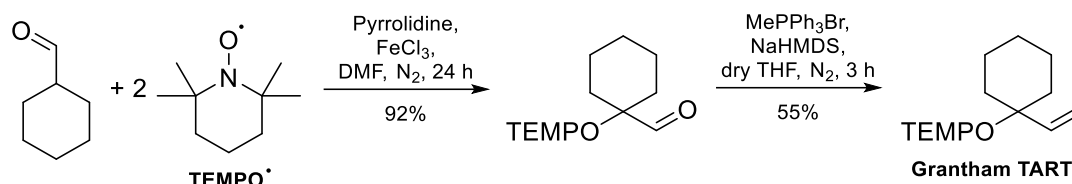


Figure 38: Two-step synthesis to form Grantham TART, performed using a literature procedure (11.2.1).¹⁵²

The first step involved coupling of TEMPO• with cyclohexanecarboxaldehyde, in presence of pyrrolidine and FeCl₃, yielding 92% product (Figure 38, 11.2.1). Pyrrolidine catalyses the reaction by converting cyclohexanecarboxaldehyde into an enamine whilst FeCl₃ catalyses the reaction by forming a TEMPO-metal complex.¹⁵³

The second step involved a Wittig reaction of the product with MePPh₃Br, in presence of sodium bis(trimethylsilyl)amide (NaHMDS), yielding 55% pure Grantham TART, or 51% overall (Figure 38, 11.2.1).

Grantham TART was successfully utilised for radical trapping (5.2.2.1). However, the [1,3]-sigmatropic rearrangement exhibited by Grantham TART restricted its use for radical trapping (2.2). Therefore, alternative TARTs were synthesised, starting with allyl-TEMPO.

3.3. Allyl-TEMPO

Removal of R¹ and R² would mean [1,3]-sigmatropic rearrangement of TARTs would yield the same TART structure. This would prevent TART conversion to a less reactive non-terminal species. Therefore, allyl-TEMPO was synthesised. Allyl-TEMPO would be the simplest possible TART, containing no additional functionality. However, removal of R¹ and R² may have caused side reactions through allylic HAA (2). Therefore, recombination trapping of radicals with the carbon-centred radical formed through allylic HAA (Figure 37), was monitored during radical trapping.

3.3.1. One-step synthesis

Allyl-TEMPO synthesis was first attempted using a single-step literature procedure (Figure 39, 11.2.2.1).¹⁵⁴

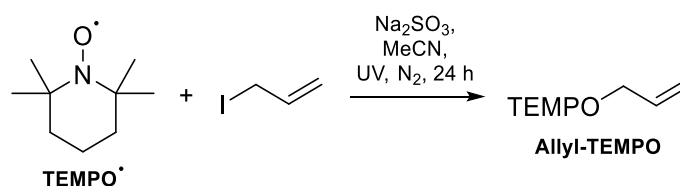


Figure 39: Allyl-TEMPO one-step synthesis, performed using a literature procedure (11.2.2.1).¹⁵⁴

This procedure involved UV-initiated TEMPO• substitution of iodide in allyl iodide, in presence of Na₂SO₃ (Figure 39, 11.2.2.1). UV caused C–I homolysis and the resultant allyl radical was trapped by TEMPO• to yield allyl-TEMPO. NMR spectra indicated that impure product contained high product yield. However, allyl-TEMPO could not be suitably separated from remaining allyl iodide using column chromatography, due to their similar R_f values. Other purification techniques were deemed either impractical or unlikely to successfully separate these two components. Therefore, alternative literature procedures for allyl-TEMPO synthesis were performed.

3.3.2. Two-step synthesis

Allyl-TEMPO was synthesised in a two-step synthesis using literature procedures (Figure 40, 11.2.2.2).^{155,156}

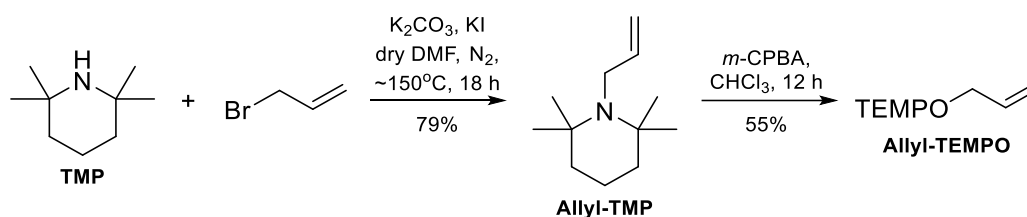


Figure 40: Allyl-TEMPO two-step synthesis was performed using two literature procedures (11.1.2.2).^{155,156}

The first step involved nucleophilic substitution of bromide in allyl bromide, by 2,2,6,6-tetramethylpiperidine (TMP), in presence of K₂CO₃ and KI, yielding 79% pure allyl-TMP (Figure 40, 11.1.2.2). TMP is a non-nucleophilic base and therefore, was difficult to perform nucleophilic substitution with. K₂CO₃ was a strong base added to prevent TMP protonation, which would reduce its nucleophilicity. I⁻ from KI, acted as a nucleophilic catalyst, offering a lower activation barrier. Likewise, high temperature (~150 °C) was required to overcome this activation barrier.

The second step involved N-oxidation of allyl-TMP by *meta*-chloroperbenzoic acid (*m*-CPBA) and subsequent Meisenheimer rearrangement (Figure 41), yielding 55% pure allyl-TEMPO, or 43% overall (Figure 40, 11.1.2.2).⁴

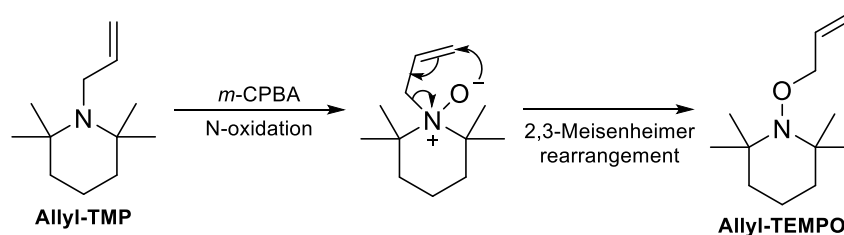


Figure 41: Mechanism of the second step of allyl-TEMPO synthesis.

Allyl-TEMPO was successfully used to trap radicals (5.2, 5.4.1). Observations indicated that trapping via HAA occurred only in small amounts, usually <1% compared to TART trapping. Therefore, allylic HAA was deemed to be an insignificant side reaction, indicating R¹ and R² functionalisation of TARTs was not essential for radical trapping. Nevertheless, R–TART production was still monitored in all trapping reactions.

However, when utilised for TART trapping, allyl-TEMPO had some shortcomings. Firstly, allyl-TEMPO was volatile. This limited its use to liquid phase trapping, as allyl-TEMPO and lightweight allyl-TEMPO-trapped radicals readily evaporated when exposed to a gas stream.

Another issue was that the allyl functionality had poor ionisation efficiency. This meant that radicals with poor ionisation efficiency formed allyl-TEMPO-trapped radicals which also had poor ionisation efficiency, resulting in low MS intensity. This meant allyl-TEMPO could only be used in radical systems where radicals had reasonably high ionisation efficiency (5.3.1.1). Furthermore, quantification of these systems was difficult, as the MS intensity of allyl-TEMPO trapped radicals was highly dependent on radical ionisation efficiency. Finally, allyl-TEMPO could not be easily functionalised, for example, to make water-soluble traps. Therefore, synthesis of alternative TARTs was required.

3.4. Amide-functionalised TARTs

A new class of differently functionalised TARTs were required to minimise problems with existing TARTs, observed for Grantham and allyl-TEMPO TARTs. This novel class of TARTs required careful design considerations.

3.4.1. Design

As for allyl-TEMPO, a [1,3]-sigmatropic rearrangement would be degenerate for an R³ functionalised TART. Therefore, its reactivity with radicals would not be reduced. Ideally, this R³ functionalisation would increase TART reactivity with radicals and hence rate of radical trapping. The new class of TARTs therefore needed to be designed such that they were: low volatility; easily functionalised; relatively inert; solely R³ functionalised and that R³ functionalisation increased TART reactivity with radicals. It was decided that these criteria were most successfully met using R³ amide functionalisation (Figure 42).

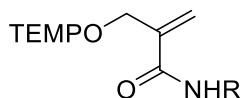


Figure 42: Novel amide-functionalised TARTs.

These TARTs were unlikely to be volatile, due to amide functionalisation having low volatility. Amides are also relatively inert and therefore, new side reactions should have been minimal. Furthermore, radical addition occurs more favourably with α,β -unsaturated carbonyls than alkenes. For example, phenylthiyl radicals react with methyl methacrylate and 2-methyl-1-pentene with rate constants $3.2 \times 10^6 \text{ M}^{-1} \text{ s}^{-1}$ and $2.1 \times 10^4 \text{ M}^{-1} \text{ s}^{-1}$ respectively (296 K).¹⁵⁷ This is because conjugate radical addition, i.e., rearrangement and delocalisation upon radical addition, stabilises the reaction intermediate. This addition would be particularly favourable for electron-rich radicals, although electron-deficient radicals would still add rapidly to such α,β -unsaturated carbonyls. Therefore, rate of radical trapping should be faster for amide-functionalised TARTs than allyl-TEMPO. Increased favourability of TART trapping should also reduce side reactions via allylic HAA.

These amide-functionalised TARTs could be synthesised from an amide coupling reaction between amine and carboxylic acid-functionalised TART. Amide coupling reactions are ubiquitous simple organic transformations, which can be utilised with many different amines. Therefore, amide-functionalised TARTs could be easily functionalised as required. For example, ethanolamine could be utilised to introduce a hydroxyl group, making a water-soluble amide-functionalised TART.

In summary, it was hypothesised that these considerations would make amide-functionalised TARTs superior to Grantham and allyl-TEMPO TARTs. These amide-functionalised TARTs were novel and therefore no literature synthesis existed. Therefore, novel syntheses had to be devised.

3.4.2. Synthesis

3.4.2.1. 2-(Bromomethyl)acrylic acid nucleophilic substitution by TMP and Meisenheimer rearrangement

First, a three-step amide-functionalised TART synthesis was designed. The first two steps were based upon the procedure used for allyl-TEMPO synthesis (3.3.2), whilst the third would be an amide coupling reaction.^{155,156} Nucleophilic substitution was performed before the amide coupling reaction, as it was theorised that bromide would be vulnerable to nucleophilic substitution by the amine used in amide coupling (Figure 43).

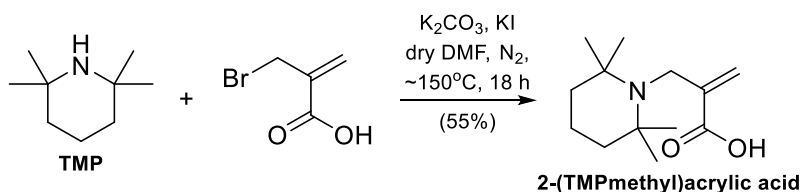


Figure 43: 2-(TMPmethyl)acrylic acid formation from 2-(bromomethyl)acrylic acid, adapted from a literature procedure.³

The first step involved nucleophilic substitution of bromide, in 2-(bromomethyl)acrylic acid, by TMP, under otherwise identical conditions to allyl-TEMPO two-step synthesis, yielding 55% (qNMR) impure 2-(TMPmethyl)acrylic acid. The resultant mixture could not be easily purified by column chromatography, due to similar R_f values for reagents and products. Therefore, this impure mixture was carried into the next step. This step was adapted from a literature procedure.³

Next the N-oxidation and subsequent Meisenheimer rearrangement were performed. This was advantageous as performing the amide coupling last allowed TART functionality to be tuned in a single step. However, N-oxidation of 2-(TMPmethyl)acrylic acid failed. It was hypothesised that the 3° amine may have been protonated by its intramolecular carboxylic acid forming a zwitterion, preventing oxidation. 3° amine protonation could not be prevented using base, as this would interfere with the *m*-CPBA reagent, again causing the reaction to fail. Therefore, the amide coupling was performed before N-oxidation and subsequent Meisenheimer rearrangement, to block the carboxylic acid group (Figure 44, 11.2.3).

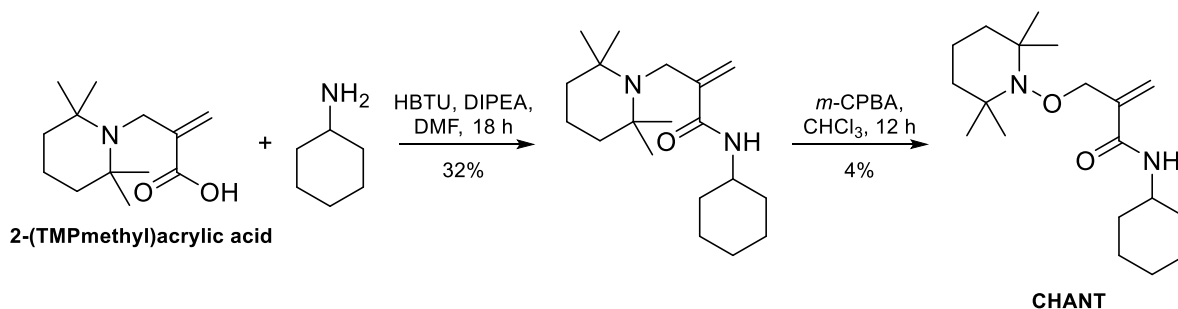


Figure 44: CHANT formation from 2-(TMPmethyl)acrylic acid. The second step was adapted from a literature procedure.⁴

The second step involved amide coupling of cyclohexylamine to 2-(TMPmethyl)acrylic acid, in presence of (2-(1H-benzotriazol-1-yl)-1,1,3,3-tetramethyluronium hexafluorophosphate (HBTU), *N,N*-diisopropylethylamine (DIPEA), yielding 32% pure product (Figure 44, 11.2.3).

The third step involved product N-oxidation by *m*-CPBA and subsequent Meisenheimer rearrangement, under otherwise identical conditions to allyl-TEMPO two-step synthesis, yielding 4% pure CHANT or 1% overall (11.2.3). This final step was adapted from a literature procedure.⁴ This very low 4% final step yield severely limited overall yield and the resulting 1% overall yield was deemed too low for practical use. It was unknown how the poor yield for the final step could be improved. Therefore, an alternate route for amide-functionalised TART synthesis was sought.

3.4.2.2. 2-(Bromomethyl)acrylic acid UV irradiation with TEMPO•

Allyl-TEMPO synthesis had originally been attempted through UV irradiation of allyl iodide with TEMPO•. Although the reaction was high yielding, allyl iodide and allyl-TEMPO could not be separated. However, it was theorised that if the same reaction was performed with different reagents, reagents and products may be separable. Therefore, this reaction was used to form 2-(TEMPOmethyl)acrylic acid (Figure 45, 11.2.4).

2-(Iodomethyl)acrylic acid was not commercially available. Therefore, UV irradiation of 2-(bromomethyl)acrylic acid with TEMPO• was attempted, under otherwise identical conditions to allyl-TEMPO one-step synthesis (3.3.1). This achieved <20% conversion after 24 h. This poor conversion rate was deemed too slow for viable use. Slow conversion rate was likely due to the C–Br bond being stronger than C–I (285 kJ mol⁻¹ compared to 213 kJ mol⁻¹)¹³⁹ and therefore, bond homolysis occurred less readily. Therefore, a Finkelstein reaction was employed to convert 2-(bromomethyl)acrylic acid to 2-(iodomethyl)acrylic acid. 2-(Iodomethyl)acrylic acid was then UV irradiated with TEMPO•, under otherwise identical conditions to allyl-TEMPO one-step synthesis (3.3.1) (Figure 45, 11.2.4).

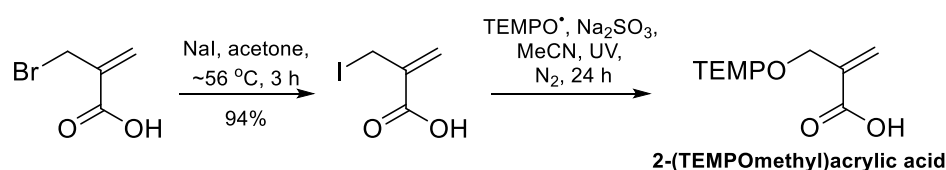


Figure 45: 2-(TEMPOmethyl)acrylic acid TART formation from 2-(bromomethyl)acrylic acid (11.2.4). The second step was adapted from a literature procedure.¹⁵⁴

The first step involved a Finkelstein reaction of 2-(bromomethyl)acrylic acid with NaI, yielding 94% pure 2-(iodomethyl)acrylic acid. The second step involved UV irradiation of 2-(iodomethyl)acrylic acid with TEMPO•, yielding 2-(TEMPOmethyl)acrylic acid (Figure 45, 11.2.4). Conditions were otherwise identical to allyl-TEMPO one-step synthesis (3.3.1). Whilst the desired product was formed, the reaction yielded a complex mixture of TEMPO-polymethacrylates (Figure 46). This second step was adapted from a literature procedure.¹⁵⁴

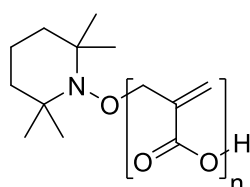


Figure 46: TEMPO-polymethacrylates formed from UV irradiation of 2-(iodomethyl)acrylic acid with TEMPO•, where $n \geq 1$.

It was hypothesised that this polymerisation could be prevented by protecting the carboxylic acid group as an ester, during UV irradiation. These esters would require deprotection prior to

amide coupling. It was decided that 2-(bromomethyl)acrylic acid protection was most easily achieved by starting the entire synthesis with commercially available methyl 2-(bromomethyl)acrylate. This synthesis would be performed similarly as for 2-(bromomethyl)acrylic acid, but with an additional deprotection step, yielding 2-(TEMPOmethyl)acrylic acid.

3.4.2.3. Methyl 2-(bromomethyl)acrylate reaction with TEMPO•

It was originally thought that 2-(TEMPOmethyl)acrylate synthesis would have the same first two steps for as for 2-(TEMPOmethyl)acrylic acid synthesis from 2-(bromomethyl)acrylic acid. However, the first two steps were instead combined, saving time and resources. This combined first step involved UV irradiation of methyl 2-(bromomethyl)acrylate with TEMPO•, in presence of NaI and Na₂SO₃, yielding methyl 2-(TEMPOmethyl)acrylate (Figure 47). It was later discovered that UV irradiation could be replaced by heating the reaction over 48 h, under otherwise identical conditions to UV irradiation conditions above, yielding 93% pure methyl 2-(TEMPOmethyl)acrylate (Figure 47, 11.2.5). This was unexpected, as it was believed that C-I homolysis of methyl 2-(iodomethyl)acrylate required UV. Maximum yield was obtained at 65 °C whilst reflux (~82 °C) resulted in a reduced product yield. The precise mechanism of this transformation is not understood and could involve a combination of nucleophilic and radical reactions. Although methyl 2-(TEMPOmethyl)acrylate was a TART, it was not deemed to have particularly useful functionality.

After methyl 2-(TEMPOmethyl)acrylate formation, deprotection (Figure 47, 11.2.6) and amide coupling reactions were used to synthesise CHANT (Figure 48, 11.2.8), which was previously obtained in a poor yield via a different synthetic route (3.4.2.1).

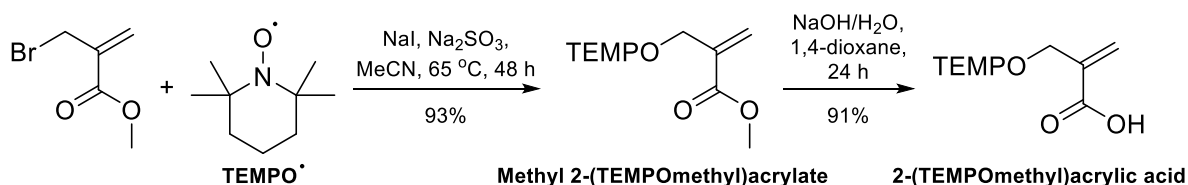


Figure 47: 2-(TEMPOmethyl)acrylic acid TART formation from methyl 2-(bromomethyl)acrylate (11.2.5 and 11.2.6).

This second step involved deprotection of methyl 2-(TEMPOmethyl)acrylate with NaOH, yielding 91% 2-(TEMPOmethyl)acrylic acid (Figure 47, 11.2.6). Although synthesised as an intermediate in the synthesis of amide-functionalised TARTs, 2-(TEMPOmethyl)acrylic acid was a potentially useful TART, due to its carboxylic acid group providing acidic functionality. For example, 2-(TEMPOmethyl)acrylic acid would dissolve readily in basic solution. This could allow it to be used for radical trapping in biochemistry systems conducted in basic solution. Amide-functionalised TARTs were then synthesised through amide coupling with 2-(TEMPOmethyl)acrylic acid (Figure 48, 11.2.8).

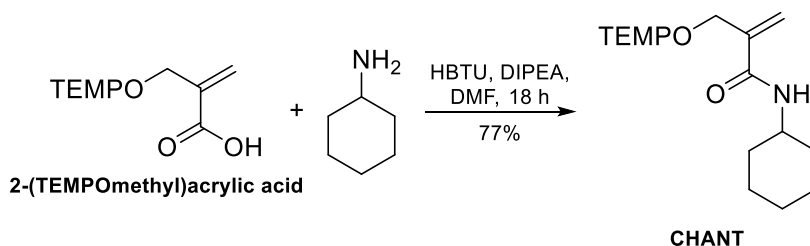


Figure 48: CHANT formation from 2-(TEMPOmethyl)acrylic acid (11.2.8).

This final step involved 2-(TEMPOmethyl)acrylic acid amide coupling to cyclohexylamine, in presence of HBTU and DIPEA, yielding 77% pure CHANT, or 65% overall (Figure 48, 11.2.8). This 65% overall yield was an enormous improvement upon the 1% overall yield previously obtained for CHANT (3.4.2.1) and was deemed acceptable for future use. Further yield optimisation was seen as beyond the scope of the project, as the purpose of the project was not to obtain high TART yields, but to utilise obtained TARTs for radical trapping.

CHANT had been synthesised as an inert, compact, amide-functionalised TART. However, different TART functionalisation was also desired to suit individual radical reaction conditions and to improve methodology. Therefore, different amide-functionalised TARTs were synthesised, each designed with a niche.

As for CHANT, amide-functionalised TART synthesis involved 2-(TEMPOmethyl)acrylic acid amide coupling with the appropriate amine to form the desired amide-functionalised TART. Conditions were otherwise identical to CHANT synthesis from 2-(TEMPOmethyl)acrylic acid (11.2.8). From this, ten amide-functionalised TARTs were synthesised, with yields ranging from 16-77%. Two further TARTs were formed through transformations of these amide-functionalised TARTs, with 32-99% yields (Figure 49).

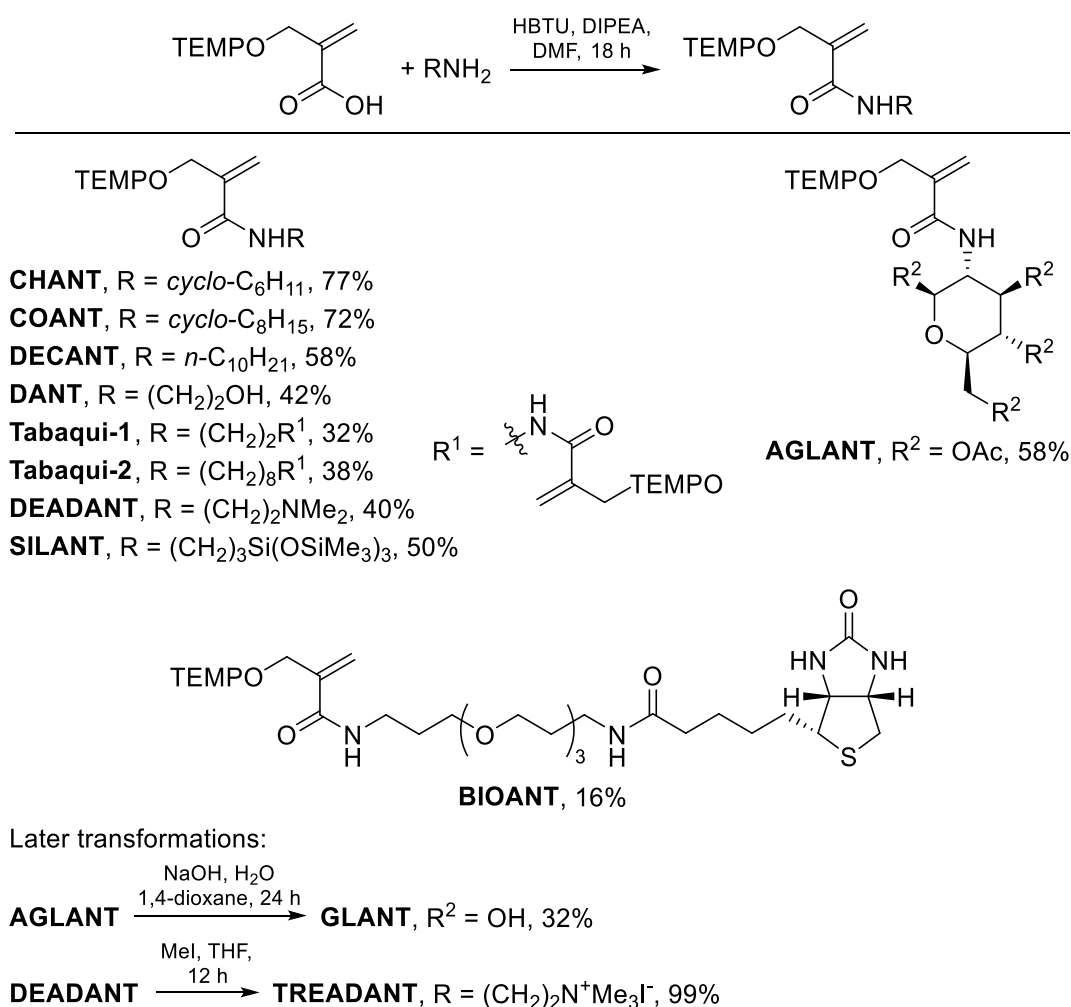


Figure 49: Amide-functionalised TARTs synthesised by amide coupling with 2-(TEMPOmethyl)acrylic acid.

COANT (11.2.9) was chemically very similar to CHANT. However, COANT-trapped radicals had a significant *m/z* difference to CHANT-trapped radicals. This was useful if CHANT-trapped radicals were obscured by nearby dominating non-trapped products. DECANT (11.2.10) was

synthesised for use in TART trapping undertaken in extremely non-polar solvents. However, the need for a less polar TART than CHANT never arose and therefore, DECANT was never used for trapping.

DANT (11.2.11) and GLANT were designed with hydroxyl groups to aid water solubility. Water-soluble TARTs were necessary for studying aqueous radical reactions, such as in biochemistry (7). GLANT was formed from AGLANT (11.2.12), in presence of NaOH (11.2.13). AGLANT was not used in trapping reactions. GLANT was trialled in biochemical radical trapping. However, it was very vulnerable to side reactions, complicating results and analysis. The single hydroxyl group in DANT mitigated this problem, as fewer side reactions were observed whilst water solubility was maintained. However, these side reactions still caused problems and in acidic solution, DEADANT was generally used as alternative, due to it undergoing fewer side reactions. DANT was originally synthesised by Daniel (Dan) Guban, during their Laidlow Undergraduate Research and Leadership Scholarship, mentored by the author.

Tabaqui-1 (11.2.14) and Tabaqui-2 (11.2.15) were designed to increase TART trapping rate. Both TARTs featured two TART groups attached back-to-back. This was hoped to double TART trapping rate for Tabaqui molecules. Tabaqui-1 was synthesised first but found to have poor solubility in many solvents. It was believed that the short amide-amide bridge caused a rigid compact structure, which crystallised very favourably, thereby making redissolution unfavourable. Tabaqui-2 was synthesised to counteract this problem, as it was hypothesised that its longer amide-amide bridge would decrease TART rigidity, making dissolution more favourable. Tabaqui-2 indeed dissolved more easily in solution. However, when Tabaqui-2 was used for radical trapping, it was found that the two TART functional groups created many possible combinations of no TART trapping, single TART trapping or double TART trapping. This considerably increased results and analysis complexity. This increased complexity outweighed potential gain in TART trapping rate and therefore, Tabaqui TARTs were abandoned.

BIOANT (11.2.16) was designed to aid TART-trapped radical purification. TART-trapped radical separation from non-trapped products would have simplified results and analysis. BIOANT and BIOANT-trapped radicals would contain biotin functionality, whereas non-trapped products would not. Species containing biotin functionality could then be separated by using avidin-based enzymes in affinity chromatography to bind biotin containing species. Bound species could then be released and MS characterised as usual. All observed species should be BIOANT-related and therefore, results and analysis would be significantly simplified. This idea was attempted by the University of Copenhagen, using BIOANT synthesised in York.

DEADANT (11.2.17) and TREADANT (11.2.18) were designed to increase MS intensity of TART-trapped radicals. DEADANT-trapped radicals had high basicity, due to 3° amine functionality. Therefore, in presence of weak acid, DEADANT-trapped radicals were protonated. This allowed MS peaks corresponding to DEADANT-trapped radicals to be observed with high intensity. Furthermore, DEADANT dissolved readily in weakly acidic solution. This made it useful for radical biochemistry studies and was used ubiquitously for these studies (7). These highly favourable properties resulted in DEADANT being the second most widely used TART, after CHANT. However, 3° amine functionality made DEADANT-trapped radicals easily oxidised by ozone to N-oxides. This made DEADANT impractical for studying many radical atmospheric chemistry studies, including alkene ozonolysis (8).

TREADANT was synthesised to counteract this problem. This involved nucleophilic substitution of iodide, in MeI, by DEADANT 3° amine yielding TREADANT. Unlike for DEADANT, the 4° ammonium in TREADANT could not be oxidised by ozone. TREADANT-

trapped radicals were likewise observed with high MS intensity, due to their inherent cationic nature. TREADANT also dissolved readily in water, due to its ionic nature. However, TREADANT was unlikely to dissolve in non-polar solvents, limiting its potential usefulness. However, oxidation of the iodide counterion in TREADANT by ozone led to many side reactions, severely complicating results and analysis (8.6.2.2). A possible solution would be to replace the iodide counterion with a non-coordinating and unreactive counterion, such as PF₆⁻. This non-coordinating and unreactive ion should not undergo oxidation by ozone. It was hypothesised that this ion exchange could be easily achieved. However, this was not completed due to time constraints and therefore, should be carried out as future work (0).

SILANT (11.2.19) was designed to give TART-trapped radicals a highly characteristic *m/z* fingerprint. This could be used to unambiguously assign SILANT-related peaks, including TART-trapped radicals. This highly characteristic *m/z* fingerprint meant SILANT was occasionally used as TART, to find elusive TART-trapped radicals.

3.5. TART stability, properties and non-radical reactivity

Before TART trapping could be undertaken, stability of newly synthesised TARTs needed to be determined. As discussed previously, Grantham TARTs isomerised rapidly in solution at RTP, to form non-terminal alkene, which severely limited TART trapping rate (2.2).¹⁵² It was hoped that TART functionalisation at the R³ position, instead of R¹ and R² positions, would remove this issue. This needed to be probed. Furthermore, stability of newly synthesised TARTs in storage (3.5.1) and under radical reaction conditions (3.5.3) needed to be determined. This was to ascertain whether these TARTs were fit for radical trapping in these systems. In particular, it was hoped that TART trapping and subsequent analysis could not lead to false positives (3.5.2 and 3.5.3).

3.5.1. TART stability in long-term storage

Stability of TARTs in long-term storage was investigated, to establish their shelf life. For this, neat CHANT, DEADANT and SILANT TARTs had NMR spectroscopy and MS characterisation performed periodically over six months. TARTs were usually stored neat in the fridge (~5 °C), sealed under air. NMR spectroscopy and MS analysis indicated that CHANT, SILANT and DEADANT purity did not decrease over six months under these conditions. However, DEADANT visibly yellowed over this period. This was presumed to be due to slow N-oxidation formation, a process which occurs commonly for amines. However, this decay was undetectable by NMR spectroscopy and MS and therefore, these three TARTs were assumed to be stable under these storage conditions for six months.

These three TARTs were also characterised over three months, when stored neat on the benchtop at RTP, sealed under air. NMR spectroscopy and MS analysis indicated that purity of these TARTs did not decrease over three months under these conditions. Again however, DEADANT visibly yellowed over this period, likely due to N-oxidation.

This suggested that CHANT, DEADANT and SILANT were stable when stored neat in the fridge and at RTP. Therefore, these TARTs could be synthesised in large quantities, stored for at least six months in the fridge and then used for radical trapping. This contrasted to spin traps, which are generally poorly stable and are easily degraded by trace metals (1.3.2.1).¹²⁸

3.5.2. Free TEMPO• concentration in TART solution

TARTs contained bound TEMPO•, which was released during TART trapping (3.1). Released TEMPO• could then react with radicals through recombination trapping. Therefore, once TART trapping began, TARTs competed with TEMPO• to trap radicals. However, since each TART

trapping reaction released one TEMPO• molecule, TART-trapped radicals should have always outnumbered TEMPO-trapped radicals. However, this may not have been true if free TEMPO• concentration in TART solution was high, for example, due to impurities or if TEMPO was very weakly bound in TARTs and therefore, was released into solution. Furthermore, since TEMPO• terminates radical reactions, if concentration of TEMPO• compared to TART was high, TEMPO• may terminate radical cycles faster than TART trapping could occur. This may have slowed TART trapping and produced low TART-trapped radical yields. Therefore, concentration of TEMPO• compared to TART was investigated. Furthermore, free TEMPO• could initiate radical reactions, potentially making TARTs non-innocent in radical mechanisms.

For this, EPR was conducted to estimate TEMPO• concentration in CHANT/MeCN solution (Figure 50, 11.3.1).

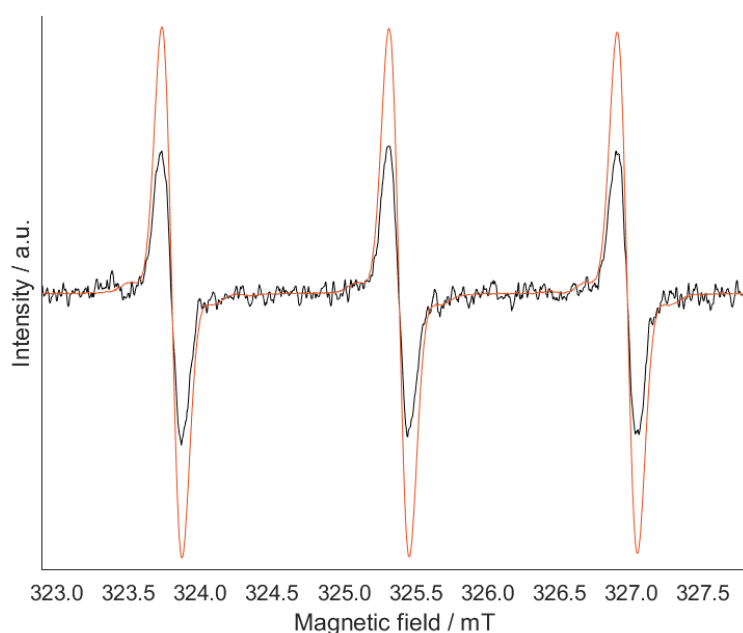


Figure 50: EPR spectra recorded for CHANT (1.00 mM, scaled x100, black) and TEMPO• (0.100 mM, orange), indicating CHANT had free TEMPO• content ~0.05mol.% (11.3.1).

Results indicated that TEMPO• concentration was ~0.05mol.% CHANT concentration in CHANT/MeCN solution. This low TEMPO• content indicated that most TEMPO• was bound in CHANT. This was assumed to be true of all amide-functionalised TARTs. Furthermore, if TEMPO• reacted rapidly with radicals as hypothesised, TEMPO• concentration should remain low compared to TART concentration, throughout TART trapping.

3.5.3. TART stability in solution and non-radical reactivity

TART stability in solution was also investigated. TART stability in CD₃OD and D₂O were of particular concern because the TART alkene group was potentially vulnerable to addition of these polar solvents. Such side reactions would decrease amount of TART available for radical trapping and complicate analysis. A more significant concern was that false positives could occur if solvent addition generated a TART-trapped radical structure through TEMPO• loss, without radicals being present or TART trapping occurring.

For investigation of TART stability in solution, TART dissolved in solvent had NMR spectroscopy performed periodically over three weeks (11.3.3). NMR spectroscopy indicated that purity of CHANT (~10 mM) did not decrease over three weeks at RTP, when dissolved in

CDCl_3 , CD_3CN , CD_3OD or D_2O . These solvents were used because analogues of these solvents were used for most radical reactions to which TART trapping was applied. These data suggested that TARTs were stable when stored in these solvents at RTP. This indicated that TARTs should be suitable for radical trapping in these solvents.

This high stability in solution was an excellent result, particularly for CD_3OD and D_2O . However, TART vulnerability to addition by nucleophiles was still a concern, especially for the potential to generate false positives. Therefore, TART susceptibility to Michael addition by weak bases was explored. CHANT in presence of diisopropylamine (~10 mM CHANT, ~1:5 mol ratio) and dissolved in CD_3OD , showed no detectable decay after 24 h but some decay after three weeks (Figure 52). From NMR spectra (11.3.3), it was believed that diisopropylamine added to the CHANT double bond, without the loss of TEMPO^\bullet (Figure 51). This was because NMR spectra showed decreasing intensity exclusively for peaks corresponding to alkene and allyl hydrogen atoms, whilst new peaks were observed with increasing intensity and hence were assigned to the decay product. Meanwhile, intensity of peaks corresponding to the $4 \times \text{CH}_3$ in the TEMPO moiety did not change, indicating TEMPO^\bullet was not lost.

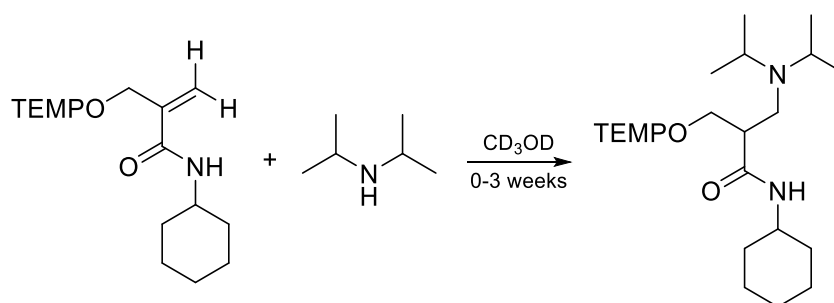


Figure 51: Michael addition of diisopropylamine to CHANT, forming a decay product.

Relative intensities of CHANT and its decay product were mapped over time, indicating ~25% CHANT decay and ~25% decay product yield after three weeks (Figure 52). This showed that CHANT was resistant to polar solvents and fairly resistant to weak nucleophiles but more importantly, indicated that TEMPO^\bullet loss and hence TART trapping, did not occur for non-radicals. Therefore, TART reaction with non-radicals did not lead to false positives. This was assumed to be true for all TARTs. This contrasted to spin trapping and recombination trapping, which can both generate false positives (1.3.2).¹²⁷

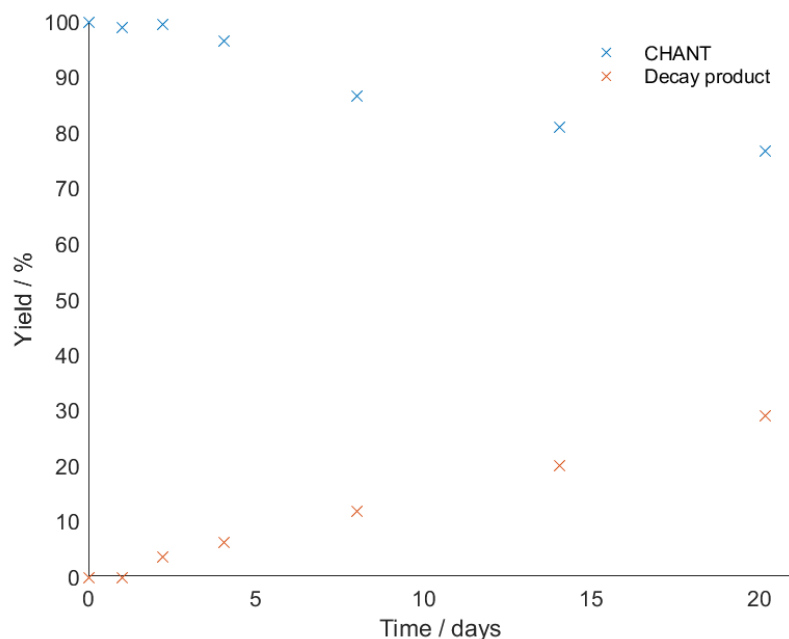


Figure 52: Decay of CHANT in presence of diisopropylamine dissolved in CD₃OD, monitored using ¹H NMR spectroscopy (11.3.3).

Additionally, oxidation and reduction processes of CHANT were investigated using cyclic voltammetry (CV). Cyclic voltammograms showed that CHANT did not undergo any significant oxidative or reductive processes under these conditions (11.3.2). This indicated CHANT was robust under mildly oxidative and reductive conditions.

TARTs were demonstrated to have high stability and react slowly with nucleophiles. However, TARTs also needed to be suitably stable during MS, so that they could be reliably observed. Therefore, mass spectra of TARTs were investigated.

3.5.4. TART properties during MS and calibration curves

MS calibration curves were obtained for CHANT, allowing concentration to be estimated from intensity of CHANT corresponding peaks. This was performed using the mass spectrometer and parameters most routinely used for characterisation of trapping reaction samples (4.3.2) and as such, positive ESI-MS was used for characterisation. MS calibration curves were obtained for CHANT, where CHANT concentration was mapped against MS intensity of [CHANT+H]⁺ (Figure 53).

Mass spectra showed a linear relationship between [CHANT] and MS intensity between ~0.01-1.00 μM and a gently curved relationship between ~1.0-10.0 μM. Therefore, intensity of CHANT corresponding peaks was approximately directly proportional to [CHANT] between ~0.01-10.0 μM. This approximate linearity was assumed true for all TARTs.

However, at concentrations of >25 μM, [CHANT+H]⁺ intensity sharply decreased and fragmentation was observed, with the most intense peak corresponding to a TMP cation (Figure 53). This indicated that at high concentrations, CHANT was unstable in MS. This was assumed to be true for all TARTs. Therefore, TART trapping reactions were not analysed >10.0 μM TART concentration, assuming no TART had reacted.

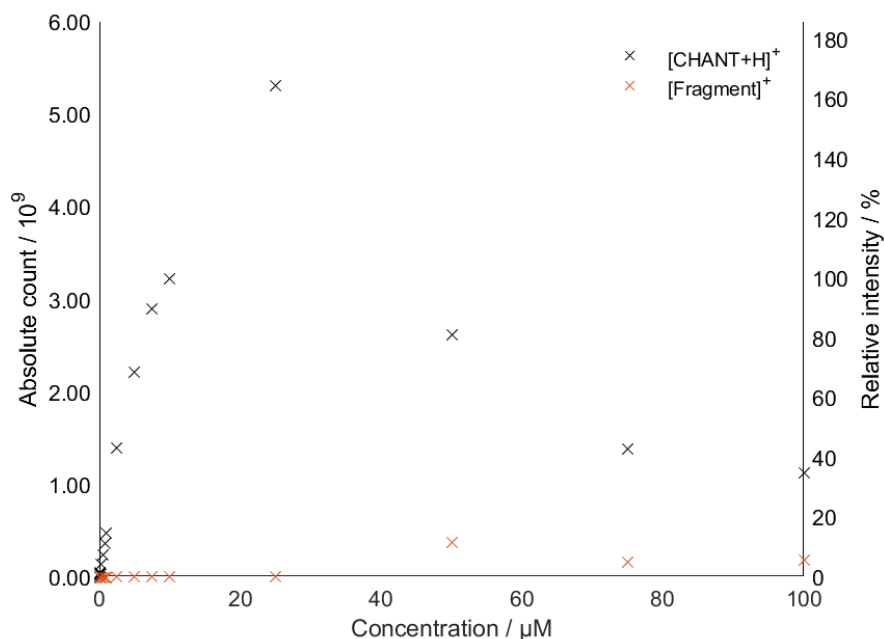


Figure 53: Calibration curve of intensity of MS peak corresponding to [CHANT+H]⁺ (m/z 323.270) at different CHANT concentrations (black), showing rapidly decreasing intensity >25 μM due to CHANT fragmentation. The most intensely observed fragment peak (m/z 140.144) appears to correspond to a TMP cation (orange).

Amide-functionalised TARTs were found to be stable and did not undergo non-radical reactions at a significant reaction rate. Furthermore, amide-functionalised TARTs ionised well and were stable during MS below $\sim 25 \mu\text{M}$. Therefore, amide-functionalised TARTs were trialled as radical traps.

3.6. Conclusions and future work

Novel radical traps consisting of a leaving group attached to an allyl group were synthesised. The leaving group needed to form a persistent radical upon cleavage and hence TEMPO[•] was chosen as the leaving group. Sixteen **TEMPO-Allyl Radical Traps (TARTs)** were successfully synthesised, fourteen of which were novel, with overall yields of 14-93%. These fourteen TARTs all involved the reaction of methyl 2-(bromomethyl)acrylate and TEMPO[•] to form methyl 2-(TEMPOmethyl)acrylate TART with a 93% yield, using a novel synthetic route. Deprotection of methyl 2-(TEMPOmethyl)acrylate afforded 2-(TEMPOmethyl)acrylic acid TART with a 91% yield (85% overall). Subsequent amide coupling with a chosen amine afforded ten other TARTs with yields of 16-77% (14-65% overall). Two further TARTs were formed through transformations of amide-functionalised TARTs.

These TARTs had different functionalities and properties, which allowed them to be used in a wide variety of radical reactions. These different properties included TARTs being: neutral, charged, weakly acidic, weakly basic, volatile, non-volatile, soluble in organic solvents and water soluble. Of these TARTs, five were mainly used for radical trapping, with CHANT and DEADANT being used ubiquitously (Figure 54). This was because CHANT was neutral and robust, whilst DEADANT was soluble in aqueous acidic solution and DEADANT-trapped radicals yielded MS peaks with high intensity.

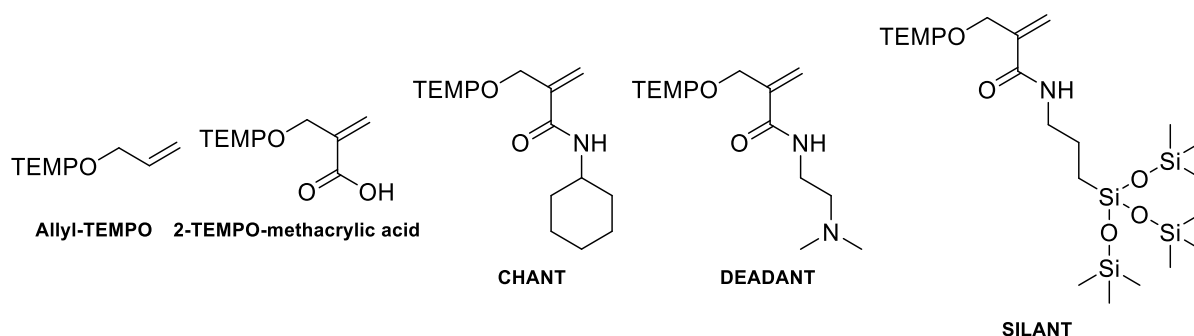


Figure 54: Five main TARTs used for TART trapping, with CHANT and DEADANT being especially ubiquitous.

Stability, properties and non-radical reactivity of amide-functionalised TARTs were then probed. CHANT, DEADANT and SILANT were stable when stored neat and sealed under air in the fridge ($\sim 5\text{ }^{\circ}\text{C}$) for at least six months and at RTP for at least three months. Furthermore, CHANT was found to be stable in solution for at least three weeks. This showed that amide-functionalised TARTs were highly stable and easily stored, making them very practical radical traps. This contrasts to both spin traps, which are generally not very stable, and previously synthesised Grantham TART, which rapidly undergoes [1,3]-sigmatropic rearrangement in solution at RTP (2.2). However, in contrast to Grantham TART, these amide-functionalised TARTs were potentially vulnerable to allylic HAA. As such, allylic HAA from TARTs was monitored in all TART trapping reactions. Alternatively, allylic C–H could have been substituted with a group which would have not been so vulnerable to allylic HAA, such as C–F or N–Me. However, this was not attempted as such substitutions may have caused TARTs to undergo [1,3]-sigmatropic rearrangement, as has been observed previously (2.2).

Experiments also indicated that TARTs did not produce false positives. Firstly, in CHANT, free TEMPO \cdot concentration was low ($\sim 0.05\text{ mol.}\%$), indicating that radical reactions should not be initiated by TARTs. Furthermore, whilst CHANT was shown to slowly undergo Michael addition in presence of weak bases ($\sim 25\%$ CHANT decay over three weeks), this Michael addition did not cause TEMPO \cdot cleavage, unlike TART trapping. Therefore, detection of TART-trapped radicals or **Radical-Allyl Radically Trapped (R-ART)** should only be possible for species formed through reaction of TARTs and radicals. This showed a significant advantage over spin trapping and recombination trapping, which can both generate false positives. Furthermore, MS calibration curves were recorded for CHANT, indicating a linear relationship and an approximately linear relationship between MS intensity and TART concentration, between TART concentrations of $0.01\text{--}1\text{ }\mu\text{M}$ and $0.01\text{--}10\text{ }\mu\text{M}$ respectively. However, it was observed that TARTs were unstable in MS above concentrations of $25\text{ }\mu\text{M}$.

Other amide-functionalised TARTs were conceived which would offer some advantages over existing TARTs (Figure 55). In particular, the formation of an ammonium-functionalised TART was highly desired (Figure 55, left). Most importantly, the TART-trapped radicals this TART would form would be observed with high MS intensity, due to its inherently cationic nature. Furthermore, it would allow DEADANT to be used in presence of ozone without oxidation. Ammonium-functionalised TREADANT was synthesised for this purpose, however oxidation of its iodide counterion by ozone led to many side reactions, severely complicating results and analysis. It was theorised that a PF $_6^-$ counterion could prevent this issue. Such a TART was believed to be easily synthesised from TREADANT reaction with AgPF $_6$ in an organic solvent, forming the desired TART and AgI, which would precipitate from solution, allowing TART purification. Furthermore, it was believed that this new TART would dissolve more easily in organic solution than TREADANT. However, this TART was not synthesised due to time constraints.

Similarly to SILANT, a germanium-functionalised TART (Figure 55, middle) would give TART-trapped radicals a highly characteristic m/z fingerprint, allowing MS peaks corresponding to TART-trapped radicals to be assigned more easily and with greater certainty. A germanium-functionalised TART would produce a more distinctive m/z fingerprint than SILANT, due to its greater number of isotopes which have a more even abundance distribution. However, this germanium-functionalised TART may be more vulnerable to side reactions. Finally, an aromatic-functionalised TART (Figure 55, right) could be used for *in situ* UV-Vis and fluorescence imaging. This could be used to detect areas of high radical reactivity, for example in cells, potentially having applications in biochemistry and medicinal chemistry.

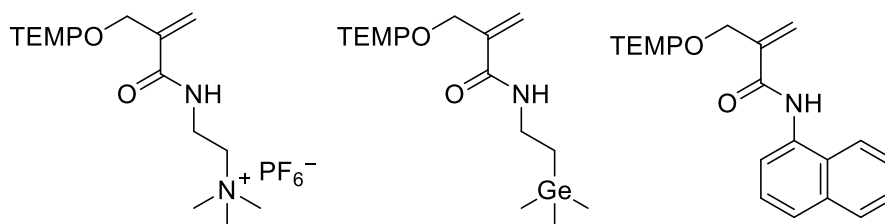


Figure 55: Potential TARTs with functionalities which would offer advantages over existing TARTs.

Once TARTs were synthesised, found to have high stability and proven to not cause false positives through reaction with non-radical species, radical trapping could be undertaken. First however, a methodology for TART trapping, MS characterisation of samples and mass spectra analysis was developed (4).

4. General methodology

4.1. Introduction

Radical intermediates play a key role in many chemical processes (1). In this project, TARTs were used for radical trapping in many fields of chemistry, including: synthetic radical reactions (5); photochemistry (6); biochemistry (7) and atmospheric chemistry (8 and 9). Radicals were investigated across a wide variety of systems, to demonstrate the wide applicability of TART trapping to investigate any radical system. Most importantly, these studies demonstrated the viability of TART trapping, as a tool for all chemists, to investigate any radical reaction. Furthermore, each field required specific methodology development, improving TART trapping methodology for others to use. Additionally, many TART trapping investigations undertaken in this report, have improved scientific understanding of radical reaction mechanisms and kinetics.

TART trapping followed a general methodology, with a more specific methodology developed for each reaction. Generally, TART trapping methodology involved TART trapping and control reactions (4.2), characterisation of samples using MS (4.3) and analysis of obtained mass spectra (4.4). Improvements were made across these three components during the project. The final general methodologies developed for these components are discussed below.

4.2. TART trapping

TART trapping was used to investigate literature-sourced radical reactions. Initially, the procedure for literature-sourced radical reactions was replicated as closely as possible, but with TART incorporated into the system. For liquid phase radical reactions (5-7), this usually involved dissolving TART in the reaction mixture pre-initiation. For gas phase radical reactions (8 and 9), this usually involved bubbling a radical reaction gas stream through a solution containing TART. Workups described in procedures for literature-sourced radical reactions to which TART trapping was applied, were not usually performed, unless the workup: was required for product formation, for example addition of base in Hofmann-Löffler-Freytag (HLF) reaction (5.3.2); physically removed particles which may damage the mass spectrometer, for example filtering out silver bromide particles formed in the Hunsdiecker reaction (5.3.3) or removal of solvents *in vacuo* which were not suitable for ESI-MS, for example DCM removal following the Barton reaction (5.3.1).

For most radical reactions, two experiments were initially run under literature-sourced conditions: a control reaction containing no TART and a trapping reaction containing TART. Aliquots were removed from both reactions pre-initiation and post-reaction and these samples MS characterised (4.3). An unreacted TART standard, with the same initial concentration as was used in the TART trapping reaction, was often MS characterised too. The mass spectra obtained from this MS characterisation were then analysed (4.4). Comparing mass spectra between samples ensured that observation of peaks corresponding to TART-trapped radicals in post-trapping mass spectra, were due to chemical reactions involving TART.

Depending on the results of this analysis and the desired outcomes of the reaction investigation, further TART trapping or control reaction experiments were performed or further MS characterisation upon previously obtained samples was undertaken. Further experiments could have involved performing additional control reactions or reactions which deviated from the literature-sourced conditions. Alternatively, conditions could be altered to optimise conditions for TART trapping or to further investigate the radical reaction, including: substrate structure; substrate concentration; TART structure; TART concentration or environmental reaction conditions.

4.3. MS characterisation

Samples from TART trapping were principally characterised using mass spectrometry (MS). MS was a useful technique for this purpose for many reasons. Firstly, MS is very sensitive, with routine ESI-MS using analyte concentrations of 10^{-5} - 10^{-7} M. However, analyte with concentrations as low as 10^{-14} - 10^{-18} M have been detected.¹⁵⁸ This contrasts with techniques such as NMR spectroscopy, with routine ^1H NMR spectroscopy using analyte concentrations of 10^{-1} - 10^{-3} M.¹⁵⁸ High sensitivity was necessary as many TART-trapped radicals had very low concentrations and therefore, were only observable using highly sensitive techniques. Secondly, MS is a good technique for analysis of complex mixtures. This is because species with different molecular formulae are usually well separated and easily identifiable. This contrasts with techniques such as NMR spectroscopy, IR spectroscopy and GC where complex mixtures usually have overlapping peaks, which makes spectra analysis challenging.

However, MS also has some disadvantages. Firstly, some other techniques offer more structural information, such as NMR spectroscopy. Secondly, MS quantification is very difficult, due to many factors influencing peak intensity, besides species concentrations (4.3.1.4). This contrasts with techniques such as NMR spectroscopy, EPR spectroscopy and GC, which are generally more quantitative techniques.

Thorough understanding of MS theory was required to correctly interpret mass spectra from TART trapping reactions (4.3.1). Practical aspects of MS characterisation of TART trapping samples are discussed below (4.3.2).

4.3.1. MS theory and instrumentation

4.3.1.1. General principles and instrumentation

MS is an analytical technique which measures mass to charge ratio (m/z) of ions. Number or frequency of ions detected is recorded as intensity. MS results are usually presented as a mass spectrum, which plots m/z against intensity. During MS, ions are usually created from neutral species. The sample used can be a gas, liquid or solid. Neutral species in the sample are ionised in an ion source. This ionisation may cause species to simply become charged, or to disintegrate into charged fragments. Extent of fragmentation depends on the MS technique being used. Ionisation eventually causes gaseous ion formation. These gaseous ions are then separated in a mass analyser according to their m/z , for example by subjecting them to an electric or magnetic field. Lighter masses with greater charge are deflected more, whilst heavier masses with lower charge are deflected less. Separated ions are then detected and their m/z and intensity recorded. This produces a mass spectrum (Figure 56).⁸⁹⁻⁹⁴

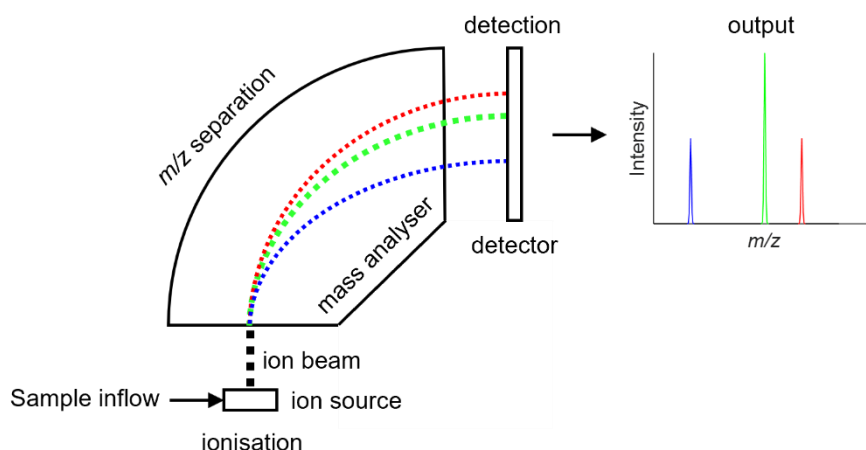


Figure 56: Mass spectrometry (MS). An injected sample contains three analytes. These analytes are ionised in the ion source, then separated according to m/z in the mass analyser, before being detected, producing a mass spectrum.

4.3.1.2. Resolution and the mass analyser

MS performed at higher resolution results in decreased m/z error and narrower MS peaks. This becomes increasingly important as m/z separation between species decreases.^{89–94}

For example, two species with similar m/z , naphthalene and octanone, had their mass spectra simulated (Figure 57). In this example, peaks corresponding to [naphthalene+H]⁺ (m/z 129.0704) and [octanone+H]⁺ (129.1279 m/z), produced through ESI-MS (4.3.1.3), were individually observed with identical intensities. Individual intensities of these two species were then summed to simulate MS characterisation which would be obtained practically. Three simulations were run, each with a different resolution (± 0.1 , ± 0.025 and ± 0.005 m/z).

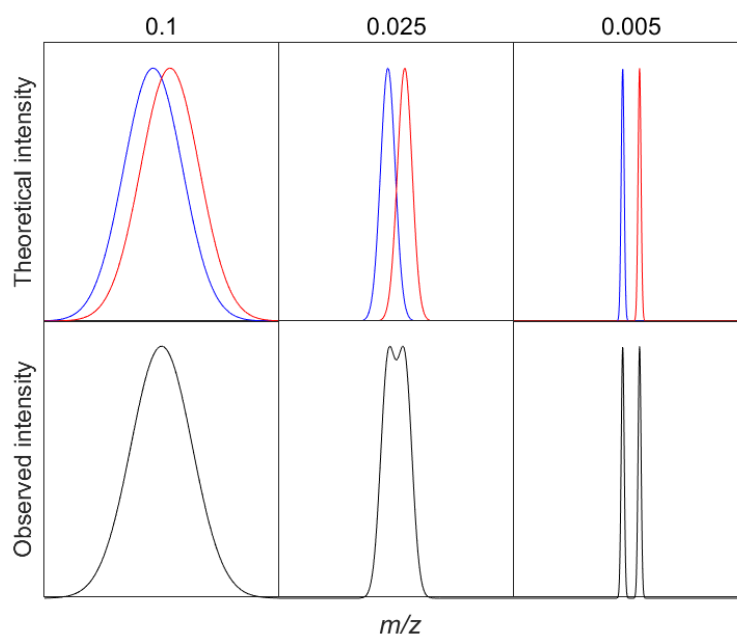


Figure 57: MS peak simulations of [naphthalene+H]⁺ (blue) and [octanone+H]⁺ (red) with equal MS intensity. The sum of these two peaks yielded the observed intensity (black). Simulations were performed at three different resolutions (± 0.1 , ± 0.025 and ± 0.005). Maximum intensity was set equal for both individual species at all resolutions. Different resolutions yielded different degrees of overlapping.

At the lowest resolution ($m/z \pm 0.1$) significant peak overlap was observed, resulting in a single observed MS peak, with m/z 129.0990. This differed from correct values by $m/z \sim 0.029$. At medium resolution ($m/z \pm 0.025$), some peak overlap was observed, resulting in a single observed MS peak with two maxima, with m/z 129.0770 and 129.1210. These differed from correct values by $m/z \sim 0.007$. At high resolution ($m/z \pm 0.005$), no peak overlap was observed, resulting in two observed MS peaks, with m/z 129.0700 and 129.1280. These differed from correct values by $m/z < 0.0005$. Therefore, these m/z were much more accurate than at lower resolution. This shows that as resolution decreases and peak overlap increases, m/z accuracy may decrease.

Higher resolution therefore provides several advantages, especially in complex mixtures. As peak overlap increases, m/z accuracy decreases. This reduces certainty in peak m/z and therefore identity. For example, if two peaks overlap into a signal peak (Figure 57, $m/z \pm 0.1$) it becomes uncertain whether the first species, second species or both species are present and contributing to the peak. This means that each species existence cannot be confirmed.

Also, as m/z precision decreases, peak identity becomes less certain, reducing confidence in peak assignment. This problem becomes more significant when an important unpredicted peak requires assignment. If trying to assign a molecular formula, larger m/z error leads to a greater number of likely species. In the above example, at low resolution, a low accuracy and low precision peak of m/z 129.0990 ± 0.1 was identified (Figure 57, $m/z \pm 0.1$). This could match >20 possible species with sensible molecular formulae (limits set $C_{0-10}H_{0-22}N_{0-5}O_{0-10}$). However, at high resolution, two high accuracy and high precision peaks of m/z 129.0700 ± 0.005 and 129.1280 ± 0.005 , were identified (Figure 57, $m/z \pm 0.1$). These two peaks could respectively match 3 and 2 possible species with sensible molecular formulae (limits set $C_{0-10}H_{0-22}N_{0-5}O_{0-10}$). This smaller number of possible species makes peak assignment easier. Furthermore, the closer m/z values between the peak and its assigned molecular formula, gives greater confidence to the assignment.

Furthermore, as resolution decreases, quantification becomes less reliable. This is because if two peaks combine in a lower resolution system (Figure 57, $m/z \pm 0.1$), it is unknown to what extent each species contributes. Furthermore, unexpected species could significantly increase desired peak intensity, leading to a falsely high intensity.

Therefore, for the complex mixtures produced by TART trapping, high mass spectrometer resolution was ideal. Mass spectrometer resolution is principally determined by the mass analyser used.

The mass analyser separates ions according to their m/z , for example by subjecting them to an electric or magnetic field. A time-of-flight (TOF) mass analyser uses an electric field to accelerate ions. Ions with a greater m/z accelerate more slowly. Therefore, the time taken for these ions to reach the detector is directly related to their m/z . Time taken is calculated by detecting each ion once. Ion trap and Fourier transform ion cyclotron resonance (FT-ICR) mass analysers use an electric field and a magnetic field respectively, to cause ions to oscillate within these fields. The magnetic fields used in FT-ICR-MS cause faster ion oscillation than the electric fields used in ion trap-MS. Ions with a greater m/z oscillate more slowly. Therefore, the cyclotron frequency of these ions is indirectly related to their m/z . Frequency is calculated by detecting each ion many times. Frequency is converted into a function of time using the Fourier Transform.⁸⁹⁻⁹⁴

Resolution is higher for ion trap-MS than TOF-MS, since ions are detected multiple times. However, resolution is higher for FT-ICR-MS than ion trap-MS, as ions are detected more times. In contrast, TOF-MS spectra are recorded more rapidly than ion trap-MS or FT-ICR-MS,

as ions are not detected multiple times. Faster acquisition times may be useful in certain circumstances, such as *in situ* reaction monitoring. Furthermore, a FT-ICR mass spectrometer is larger and more expensive than TOF or ion trap mass spectrometers, due to the large and expensive magnet required.^{89–94}

Therefore, since TART trapping produced complex mixtures, a high-resolution FT-ICR mass spectrometer would be ideal for MS characterisation. Fortunately, the University of York hosts the Centre of Excellence in Mass Spectrometry (CoEMS). This facility houses many different spectrometers and all are available for research purposes. Of these spectrometers, three were used. These were a: Bruker HCT ultra ETD II mass spectrometer (HCT); Bruker compact QTOF mass spectrometer (compact) and Bruker solariX XR FT mass spectrometer (solariX), with the latter being used ubiquitously.

The HCT was a low-resolution mass spectrometer with fast acquisition speeds ($m/z \pm 0.1$ precision, m/z 0.3 mass resolution, m/z 26,000 s^{-1} scan speed). The compact was a higher resolution mass TOF spectrometer ($m/z \pm 0.001$ precision, 30000 resolution, 1-50 Hz scan speed) and was of a type which should be accessible in most well-financed research or industrial chemical institutions. The solariX was a very high-resolution FT-ICR mass spectrometer ($m/z \pm 0.0001$ precision, $>10^7$ maximum resolution, mass accuracy 600 ppb (internal), 1 Hz scan speed) but was of a type unlikely to be found in most well-financed research or industrial chemical institutions. Due to its high resolution, the solariX was used ubiquitously for MS characterisation of TART trapping reactions, being used exclusively for most MS characterisation undertaken.

Whilst the solariX was used ubiquitously for MS characterisation of TART trapping reactions, the HCT and compact were also occasionally used. For most liquid phase synthetic radical reactions, there were relatively few radical structures and radical concentrations were relatively high, resulting in relatively few and highly concentrated TART-trapped radicals. This relatively simple mixture allowed the HCT to be adequate for clearly identifying peaks corresponding to TART-trapped radicals. However, even if the HCT was used for characterisation of TART trapping samples, the solariX was always used additionally to confirm the assignment of analytes. In this report, no mass spectra obtained using the HCT are discussed. Furthermore, the compact could also be used instead of the HCT, due to its high resolution. For most gaseous phase radical reactions, radical concentrations were lower and there were many radical structures, resulting in many TART-trapped radicals with low concentrations. This made the HCT unfit for sample characterisation. However, the compact was sometimes adequate for clearly identifying peaks corresponding to TART-trapped radicals. However, even if the compact was used for TART-trapping sample characterisation, the solariX was always used additionally to confirm the assignment of analytes. Experimental details of how MS characterisation was performed using all three mass spectrometers is detailed in the experimental section (11.9.1).

4.3.1.3. Ionisation and the ion source

The ion source generates ionised species. The ion source ionisation method can be classified as soft or hard. Soft ionisation imparts small quantities of energy into analytes, causing little fragmentation and therefore, mostly resulting in ions containing intact analytes. Therefore, soft ionisation yields m/z of ionised intact analytes. Soft ionisation techniques include electrospray ionisation (ESI), atmospheric-pressure chemical ionisation (APCI) and matrix-assisted laser desorption/ionisation (MALDI). Hard ionisation imparts large quantities of energy into analytes, causing significant fragmentation and therefore, mostly resulting in many fragment ions. Therefore, hard ionisation yields m/z of ionised analyte fragments. Hard ionisation techniques

include electron ionisation (EI). Most ionisation techniques can be used to detect cations (positive mode) or anions (negative mode).^{89–94}

For complex mixtures, soft ionisation is generally more useful. This is because soft ionisation yields far fewer peaks, simplifying complex mixture analysis. Furthermore, hard ionisation of different analytes may result in the same fragment ions, making these analytes more difficult to distinguish.^{89–94} TART trapping produced complex mixtures. Therefore, MS characterisation of TART trapping samples used exclusively soft ionisation, with positive ESI being used ubiquitously.

ESI ionises solvated analytes using an electrospray. An electrospray uses high voltage for formation of highly charged liquid droplets. These highly charged droplets rapidly disperse due to electrostatic repulsion, forming ionic aerosol. This electrostatic repulsion is defined by Coulomb's law. In the aerosol, charged droplets rapidly desolvate, until they reach their Rayleigh limit, i.e., the maximum amount of charge the droplet can hold. At this point, electrostatic repulsion outweighs droplet surface tension, causing the droplet to collapse through Coulomb fission, forming many smaller and more stable droplets. These new droplets may undergo further desolvation and Coulomb fission. Eventually these droplets become sufficiently small and desolvated to form gaseous ions. Usually, these droplets contain a single ionised intact analyte. These species were then separated by electric or magnetic fields, according to their m/z and subsequently detected, as above (Figure 58).^{159–162}

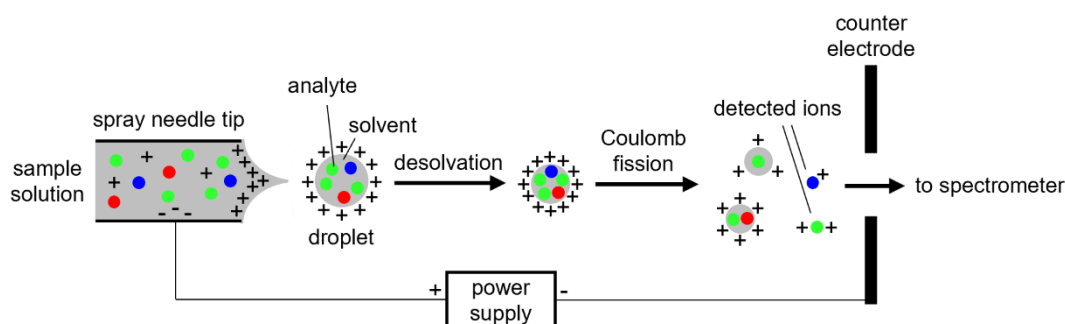


Figure 58: Electro spray ionisation mass spectrometry (ESI-MS). Sample solution is passed through the electrospray needle. High needle voltage causes charged liquid droplet formation. Droplet desolvates until droplet Rayleigh limit is reached. Droplets then undergo Coulomb fission forming smaller stable droplets. This process may repeat itself. Eventually droplets form gaseous ions. Gaseous ions then continue into spectrometer.

ESI requires sample to be dissolved or diluted in solvent. Solvent typically comprises H₂O and a volatile organic solvent, usually MeOH or MeCN. H₂O stabilises ion formation, whilst volatile solvents are used to aid droplet desolvation. Furthermore, these solvents are miscible with each other. Additionally, compounds which increase solution conductivity, such as formic acid or acetic acid, are commonly added to reduce initial droplet size. This reduces desolvation required for droplet Coulomb fission. Additionally, in positive ESI-MS, these weak acids act as a source of protons.^{159–162}

In general, ESI-MS quantification is possible but complicated (4.3.1.4). ESI-MS can be coupled with other techniques to further characterise species. Tandem MS can provide further structural information to analytes (4.3.1.5), whilst chromatography can be used to simplify mass spectra and offer further analyte characterisation (4.3.1.6).

4.3.1.4. MS quantification

Although MS can be a quantitative technique, absolute quantification is usually very challenging. This is because many factors influence the intensity of peaks corresponding to

analytes, including: analyte concentration; analyte ionisation efficiency; concentration of other analytes; solvent composition; cation concentration (including pH) and MS parameters.^{89–94}

In positive ESI-MS, peaks corresponding to neutral analytes are usually observed complexed with cations present in the solvent, most commonly H⁺, Na⁺ or K⁺, creating charged MS adducts [analyte+H]⁺, [analyte+Na]⁺ or [analyte+K]⁺. The solvent system may be selected to contain cations, such as H⁺ in solvent containing formic acid, or cations may leach into the solvent from external sources, such as Na⁺ and K⁺ from glassware. The extent to which an analyte is observed is heavily dependent on its ionisation efficiency. Peaks corresponding to inherently charged analytes are usually detected with high intensity. For neutral analytes, intensities of corresponding peaks are highly dependent on the ionisation efficiency of the analyte. For example, strongly basic analytes, such as 3^o amines, readily form [analyte+H]⁺ complexes and hence, corresponding [analyte+H]⁺ peaks are usually observed with high intensity. In contrast, peaks corresponding to poorly basic analytes, such as alkanes, are usually not observed or observed with low intensity. If peaks corresponding to such species are observed, it is usually most intensely as [analyte+Na]⁺ adducts. This means that the ionisation efficiency of analytes strongly effects the intensity of corresponding peaks. Much research has been undertaken to quantify analyte ionisation efficiency, to improve MS quantification. However, the results of such investigations vastly differ, strongly limiting the universal applicability of such predictions.^{89–94}

Extent of analyte ionisation is highly dependent on concentration of other analytes and cations, as analytes compete for cations with which to form MS adducts. This is especially significant for analytes which ionise with cations which are not in excess, such as leached Na⁺ or K⁺. Therefore, cations are often included in MS solvent, with a source of H⁺ commonly being included in the MS solvent. Chromatography can be used to improve quantification, as it separates analytes, preventing them from competing for cations (4.3.1.6).^{89–94}

MS parameters also affect intensity of peaks corresponding to analytes.^{89–94} For example, ion accumulation time is generally directly related to intensity of peaks corresponding to analytes with greater *m/z*.

However, despite these complications, approximate quantitative interpretations can be made using mass spectra. In the same sample, relative intensities of MS peaks corresponding to analytes with similar structures, similar *m/z* values and forming MS adducts with the same cations, can be used to approximate relative concentrations of these species. For example, for a sample mass spectrum containing two peaks corresponding to [dihexylamine+H]⁺ and [dioctylamine+H]⁺ with equal relative intensities, concentrations of dihexylamine and dioctylamine were assumed to be approximately equal. This approximation was frequently made in this project.

Furthermore, between two different samples, relative intensities of MS peaks corresponding to the same MS adduct for a particular analyte, characterised using the same MS parameters and dissolved in the same solvent, can be used to approximate relative concentrations of analyte between samples. For example, for mass spectra recorded for different aliquots removed after 10 min and 20 min from a reaction mixture in which dihexylamine was consumed, the relative intensity of the peak corresponding to [dihexylamine+H]⁺ observed in a 2:1 ratio was assumed to indicate dihexylamine concentration halved during this time. This approximation was also made frequently in this project.

MS quantification could be improved by making calibration curves for analytes. This involves correlating MS peak intensity with analyte concentration.

4.3.1.5. Tandem MS

Tandem MS can provide further structural information to analytes. Tandem MS involves fragmentation of isolated gaseous ions, yielding new fragment ions. Fragment ion analysis can then indicate fragment ion structure, providing structural information for its parent ion and therefore, its parent analyte. Tandem MS techniques include electron-capture dissociation and (ECD) and collision-induced dissociation (CID).^{163–166} CID was used for tandem MS characterisation of TART trapping samples.

In CID, prior to fragmentation, ions with specific m/z are selected using a multipole, which consists of four parallel metal rods. Ions travel down the multipole between the rods. Only ions of a certain m/z will escape the multipole, with other ions having unstable trajectories and hence colliding with the rods. The selected ions are then accelerated by an applied electric potential, increasing their kinetic energy. An inert collision gas is then introduced, causing these energetic ions to collide with the inert molecules, typically helium, N_2 or argon. These collisions cause some kinetic energy to be converted to internal energy. This internal energy causes ions to undergo bond fission, producing smaller ion fragments.^{163–166} The smaller ion fragments are then detected in the mass analyser.

Additionally, sustained off-resonance irradiation CID (SORI-CID) can be used to further select and fragment ions. This involves multiple CID stages. Short bursts of collision gas and electric field, either applied at resonance frequency (excitation) or off-resonance frequency (relaxation), causes ion excitation, fragmentation and relaxation. This process can be repeated multiple times, yielding many fragmentation stages.^{167,168} SORI-CID can be used much more selectively than CID, however obtained signals are significantly weaker.

4.3.1.6. Chromatography

Chromatography, can be used to separate analytes, simplifying mass spectra, and offer further characterisation to these analytes. Furthermore, separation of analytes reduces the effect of other analytes on the extent of ionisation on target analytes. Chromatography methods include gas chromatography (GC) and high-performance liquid chromatography (HPLC).^{169–171}

HPLC-MS was used for MS characterisation of TART trapping samples. HPLC involves passing pressurised liquid solvent containing sample through a column. The column separates analytes according to their polarity. Once analytes elute from the column, they are injected into the mass spectrometer and are characterised. A chromatogram is then obtained by plotting retention time against MS intensity for each m/z , corresponding to different analytes.^{169–171} HPLC-MS typically uses a reverse phase column and therefore, as analyte polarity increases, retention time inside the column decreases. HPLC-MS uses an appropriate solvent for the MS method. For ESI-MS, solvent used is typically H_2O with MeOH or MeCN. Additionally, formic acid or acetic acid are often added. Eluent typically transitions from higher to lower polarity solvent. This polarity gradient aids elution of less polar analytes from the column.^{169–171}

Although HPLC simplifies mass spectra and offers further characterisation to analytes, HPLC-MS also has some disadvantages. Firstly, HPLC-MS is time consuming to perform and requires significant optimisation, which is also time consuming. Furthermore, some analytes may degrade on the column, due to residual transition metals or other species. Finally, low polarity species may be observed with lower intensity than without HPLC, due to low polarity solvent containing fewer cations. These disadvantages meant that positive ESI-MS without HPLC was initially utilised for characterisation of TART trapping samples, with HPLC-MS only being undertaken if necessary.

4.3.2. Practical MS characterisation

TART trapping samples were analysed near exclusively using positive ESI-MS (4.3.1.3). Negative ESI-MS was occasionally used for characterisation of TART trapping samples when 2-(TEMPOmethyl)acrylic acid was used as TART. This was because 2-(TEMPOmethyl)acrylic acid and its corresponding TART-trapped radicals easily formed anions, due to their weak acidity. However, no TART trapping reactions using 2-(TEMPOmethyl)acrylic acid as TART are discussed in this report and therefore, all presented MS characterisation was performed in positive ion mode. Furthermore, softer positive APCI-MS was occasionally implemented if hypothesised peaks were not observed using positive ESI-MS, for example for peaks corresponding to low-stability organic peroxides. In practice however, APCI-MS only yielded results which were also obtained using ESI-MS and therefore, no APCI-MS results are discussed in this report. Therefore, positive ESI-MS was used exclusively for all presented MS characterisation of TART trapping samples.

Prior to MS characterisation, sample preparation and mass spectrometer calibration were required (4.3.2.1-4.3.2.2).

Many MS techniques were utilised for sample analysis. This was usually to offer further structural information to analytes or to improve obtained characterisation. Standard MS was usually the first MS technique used for sample analysis (4.3.2.3). Standard MS involved performing MS upon sample continuously and directly injected into the mass spectrometer. Standard MS was usually accompanied by background standard MS, to clean spectra and simplify analysis (4.3.2.4). These two techniques were used with all three spectrometers.

Other techniques were used exclusively with the solariX. Further structural information was provided by D₂O exchange or tandem MS characterisation. D₂O exchange analysis yielded number of labile hydrogen atoms in each analyte with an observed MS peak (4.3.2.5). Tandem MS characterisation allowed analyte isolation and fragmentation, yielding further structural information (4.3.2.6). HPLC-MS was used to improve peak isolation, clean spectra and use HPLC to further characterise analytes (4.3.2.7). Furthermore, HPLC-MS source-waste function could be used to remove desired analytes, prior to MS characterisation. In certain cases, this allowed sample concentration to be increased significantly, by removing analytes with a significantly high concentration that they would otherwise have caused spectrometer contamination (4.3.2.8).

4.3.2.1. Sample preparation

Samples which were not in solution first required dissolution. For highly concentrated samples, this was usually in MeCN. MeCN dissolved most species well, was unreactive and contained no labile hydrogen atoms. Samples already in solution, dissolved samples and non-dissolved samples with low concentration, were dissolved or diluted in an appropriate solvent to undertake MS characterisation. TART trapping samples were dissolved or diluted such that, assuming TART did not react, initial unreacted TART concentration was as high as possible, without causing long-term mass spectrometer contamination. This was typically 100 µM for initial unreacted TART concentration. For positive ESI, these samples were usually diluted in 0.1% HCOOH/50% MeCN:50% H₂O (11.9.1).

This solvent system is commonly used for MS sample dilution. 50% MeCN/50% H₂O dissolved or diluted most samples well, whilst HCOOH and H₂O provided H⁺ and Na⁺ for analyte ionisation. Furthermore, H₂O was a good solvent for stabilising cations, encouraging their formation. For negative ESI, these samples were usually dissolved in 50% MeCN/50% H₂O. As

previously, this solvent system dissolved or diluted most samples well. H₂O was a good solvent to aid species anion formation.

4.3.2.2. Spectrometer calibration

Spectrometer calibration was essential to ensure the mass spectrometer used for MS characterisation recorded spectra as accurately and precisely as possible. For this, detected calibrant peaks were calibrated to known calibrant m/z values. Spectrometer calibration was carried out under the same conditions as for sample MS characterisation (11.9.3).

The HCT and compact were routinely calibrated. However, the solariX was calibrated before each use (11.9.1). Calibrant used was CF₃COONa dissolved in 50%MeCN/50%H₂O.

4.3.2.3. Standard MS spectrum

Standard positive ESI-MS was the first MS characterisation performed upon most samples and yielded a standard MS spectrum (11.9.1).

Standard MS involved continual injection of sample solution into the mass spectrometer (2.0 $\mu\text{L min}^{-1}$). Sample injection was continued until MS signal stabilised, monitored by total ion current (TIC) stabilisation (usually ~ 4 min). Once signal stabilised, an average sample mass spectrum was then recorded by averaging 16 mass spectra. TIC was checked to ensure MS signal remained stable. Once sample analysis was complete, sample was washed out using clean solvent (10.0 $\mu\text{L min}^{-1}$, 5 min) and mass spectra inspected to ensure intensities of peaks corresponding to analytes were significantly diminished (11.9.1).

Spectrometer parameters were optimised for MS characterisation of TARTs and TART-trapped radicals (11.9.3). These parameters were optimised to show significant intensity across m/z 100-800, with maximum intensity being observed between m/z 300-400. This was because most studied systems yielded species which produced peaks within m/z 100-800. However, typical species produced peaks within m/z 300-400, hence parameters were optimised to increase intensity of this region. These parameters included: sample injection speed; ion accumulation time; drying gas temperature and number of scans (11.9.3). Spectra were most commonly recorded within m/z 100-1000, although occasionally this was extended to m/z 100-1500, for species with particularly high m/z . The obtained average mass spectrum was then used for sample analysis (11.9.1).

The excellent sensitivity of the solariX caused many low intensity signals to be observed, even in very high purity solvent. These signals likely came from trace solvent impurities and residual spectrometer contamination. Therefore, background signals were removed, to clean and simplify spectra but also to better reflect sample composition.

4.3.2.4. Background spectrum

Prior to sample injection, a background spectrum was taken. This was achieved by continually injecting clean MS solvent (2 $\mu\text{L min}^{-1}$). Injection was continued until MS signal stabilised, as described previously. Once signal stabilised, an average background mass spectrum was then recorded by averaging 16 mass spectra. Before this background spectrum was accepted, it was inspected to ensure intensities of peaks corresponding to analytes were significantly diminished. If sufficiently clean, sample injection was then undertaken.

MS solvent used was the same solvent in which the sample was diluted and all MS parameters and conditions were the same as for sample characterisation (11.9.3). The obtained average background mass spectrum was then used for background removal during analysis (4.4.3).

Standard MS and background mass spectra were recorded for all samples characterised using the solariX. Samples could be further characterised using different MS techniques, such as D₂O exchange (4.3.2.5), tandem MS (4.3.2.6) and HPLC-MS (4.3.2.7).

4.3.2.5. D₂O exchange

D₂O exchange analysis was used to determine the number of labile hydrogen atoms in each analyte corresponding to an observed MS peak. This was achieved by exposing sample to deuterated solvent and observing the mass shifts of peaks, corresponding to the number of deuterium atoms exchanged for each analyte. Equal concentrations of protonated and deuterated analyte were assumed to produce equal corresponding peak intensities.

For this, D₂O exchange was performed very similarly as for standard MS and background spectra, using positive ESI. First, sample was dissolved or diluted in 0.1%DCOOD/50%MeCN:50%D₂O, with D₂O and DCOOD having 99.9 atom % D and 98% atom % D. Sample was then allowed to equilibrate for at least 1 h. Otherwise, background and standard MS spectra were recorded as described previously (4.3.2.3 and 4.3.2.4). The obtained average D₂O sample and background mass spectra were then used for sample analysis. This involved comparing D₂O exchange spectra with sample and background spectra recorded in protonated solvent, as described below.

To simplify calculations, D₂O and DCOOD were assumed to have 100 atom % D and MeCN was assumed to be totally dry. Rapidly exchanged hydrogen atoms (such as in alcohol O–H, amine N–H and ammonium N–H) were assumed to exchange immediately upon exposure to deuterated solvent, at the protonated:deuterated solvent ratio. For example, for CH₃OH weakly dissolved in protonated solvent and then diluted 1:99 in deuterated solvent was assumed to immediately form 1:99 CH₃OH:CH₃OD.

For peaks which corresponded to a single analyte containing a single slowly exchanged hydrogen atom (such as in amide N–H), rate of hydrogen atom exchange could be estimated by comparing the intensity of deuterium shifts observed after D₂O exchange, such as for TARTs. For example, for CHANT weakly dissolved in protonated solvent and then diluted 1:99 in deuterated solvent, with a 0D:1D:2D ratio of 0:1:9, proportion of amide N–H exchange was estimated to be 90.9%, using probability theory. For radicals not containing slowly exchanged hydrogen atoms, proportion of amide N–H exchange calculated for CHANT was also assumed to be true of CHANT-trapped radicals. For example, if rate of amide N–H was calculated to be 90.9% from peaks corresponding to CHANT, for CHANT-trapped radical MS adduct [CH₃O–ART+Na]⁺, 0D→1D was expected to be 90.9%. Likewise, for two species with similar structures, proportion of slow hydrogen atom exchange was assumed to be the same for both species. For example, relative intensities of deuterium shifts observed for peaks corresponding to [thymine+Na]⁺ and [uracil+Na]⁺ were expected to be the same. For >90% full deuterium exchange, this approximation was deemed suitable for making quantitative conclusions, although ideally, samples would have been allowed longer to undergo full deuterium exchange.¹⁷²

4.3.2.6. Tandem MS

Tandem MS characterisation allowed species isolation and fragmentation, yielding further structural information (4.3.1.5).

For this, sample dissolved or diluted in solvent was continually injected into the mass spectrometer. Injection was continued until MS signal stabilised, as for standard MS. Tandem MS was then performed upon peaks of interest. CID was used to select and fragment analytes corresponding to peaks which were very intense compared to nearby peaks. This was used

most commonly to analyse liquid phase TART trapping samples, as these mixtures were less complex and intensities of peaks corresponding to TART-trapped radicals were generally higher. If species could not be suitably selected before CID then SORI-CID was used instead.

SORI-CID was performed upon analytes corresponding to peaks which were similar or lower intensity compared to nearby peaks or analytes which could not be relatively cleanly selected during CID. This was so that nearby peaks could be removed prior to SORI-CID fragmentation, ensuring peak fragments corresponded to the desired parent ion. This was used most commonly to analyse gas phase TART trapping samples, as these mixtures were complex and intensities of peaks corresponding to TART-trapped radicals were low. If SORI-CID could not be used to suitably select or fragment peaks then tandem MS was abandoned. Additionally, SORI-CID was used to further fragment ion fragments formed during CID.

Tandem MS was only performed using positive ESI. Sample was usually dissolved in protonated solvent for tandem MS, although occasionally deuterated solvent was used. Tandem MS was usually most effective on protonated MS adducts, although tandem MS could also be performed upon sodiated MS adducts if no protonated adducts were observed. Tandem MS characterisation often required longer acquisition times, especially for fragmentation of low intensity peaks. Tandem MS parameters utilised the same optimised parameters as standard MS, with the exception of: ion accumulation time; octupole ion selection m/z ; octupole tandem MS CID energy; in-source ion selection m/z ; in-source collision energy and number of scans (11.9.3). Ion accumulation time and number of scans were set depending on the intensity of the selected MS peak. Octupole ion selection m/z and in-source ion selection m/z were set to select the desired MS peak. Octupole tandem MS CID energy and in-source collision energy were set to cause an appropriate amount of fragmentation.

Tandem MS was a challenging technique, particularly for low intensity sodiated MS adducts, with results often being poor.

4.3.2.7. HPLC-MS

HPLC-MS was used to improve peak isolation, clean spectra and use HPLC to further characterise species (4.3.1.6).

Sample dissolved or diluted in protonated solvent was used in HPLC-MS. Before HPLC-MS was performed, MS characterisation parameters had to be optimised. MS method was largely similar to optimised standard MS characterisation parameters (4.3.2.3, 11.9.3). However, instead of several scans being averaged, single scans were taken sequentially, to characterise analytes outputted from the HPLC column more frequently. Furthermore, some MS parameters were changed to suit the fast injection stream speed required by HPLC, including ion accumulation time and drying gas temperature (11.9.3).

In HPLC-MS, sample solution was mixed with HPLC solvent. This mixture was then passed through a column before injection into the mass spectrometer. Analytes were separated in the column, causing MS adducts of these analytes to be detected at different retention times. Sample solution injection needle was washed automatically between each injection. HPLC solvents used were 0.1% HCOOH/H₂O and 0.1% HCOOH/MeCN. Eluent composition changed throughout HPLC-MS run, beginning with high 0.1% HCOOH/H₂O content and ending with high 0.1% HCOOH/MeCN content. HPLC-MS eluent composition and HPLC column were optimised for each sample, such that separation was maximised across a reasonable timeframe (11.9.3).

4.3.2.8. HPLC-MS source-waste species removal

HPLC-MS source-waste function could be used to remove desired species, after HPLC but prior to MS characterisation. In certain cases, this allowed sample concentration to be increased significantly, by removing analytes with high concentration which would otherwise have caused spectrometer contamination. This resulted in some analytes producing MS peaks which were observed with significantly greater intensity. The source-waste function allowed the HPLC stream to be expelled as waste rather than injected into the mass spectrometer.

HPLC-MS source-waste analyte removal involved first performing HPLC-MS characterisation upon a sample dissolved or diluted in solvent (4.3.2.7). This yielded retention time of any highly concentrated analytes. HPLC-MS was then repeated with more concentrated sample. However, the HPLC stream was diverted to waste during the measured retention time windows in which highly concentrated analytes eluted, preventing highly concentrated analytes from entering the mass spectrometer. This prevented mass spectrometer contamination. Outside of these retention time windows, the HPLC stream was injected into the mass spectrometer, allowing other analytes to be MS characterised.

This was used for samples with very high intensity peaks corresponding to a one or two analytes but otherwise low intensity peaks. This was usually used for HPLC-MS characterisation of gas phase TART trapping samples, where low gaseous radical concentrations resulted in high TART concentration but low concentration of TART-trapped radicals. HPLC-MS source-waste function was then used to remove TART from the more concentrated sample, prior to MS characterisation. TART-trapped radicals not expelled as waste during TART removal, were then MS observed, with corresponding peaks usually being observed with increased intensity. This allowed MS observation of peaks corresponding to TART-trapped radicals which were previously undetected.

This technique was very challenging. All highly concentrated species needed to be sent to waste. However, other species would ideally be observed as much as possible, outside of the required waste window. This was made challenging because highly concentrated species retention time varied significantly, up to several minutes. This meant the time window in which the HPLC stream was diverted to waste had to be widened beyond the minimum retention time window. This prevented MS characterisation of other analytes wasted during this time window. Furthermore, occasional mistakes led to severe MS contamination. Therefore, this technique was only used when species were not MS observable through any other technique.

These MS characterisation techniques outputted data, which required analysis to extrapolate meaningful results.

4.4. Mass spectra analysis

MS characterisation generated an enormous quantity of data. Proficient data handling was therefore essential for quickly and efficiently processing these data.

MS characterisation data could be handled manually (4.4.2). However, the enormous quantity of data generated by MS characterisation made manual data handling generally slow and inefficient. Therefore, most data handling was processed through self-written computer programmes. MATLAB was used to write and run all computer programmes, whilst Microsoft Excel was used to input certain data and store outputted results. Many programmes were developed to handle MS characterisation data differently. The most significant programmes are discussed below (4.4.4-4.4.7). However, before data analysis could be undertaken, acceptance limits had to be decided (4.4.1).

All species were searched for as protonated, sodiated and potassiated MS adducts, however only significantly observed MS peaks are discussed. Peaks corresponding to CHANT-trapped radicals and DEADANT-trapped radicals were usually most intensely observed as MS adducts $[R-ART+Na]^+$ and $[R-ART+H]^+$ respectively, depending on the ionisation efficiency of R. Peaks corresponding to R-TEMPO and R-TART were usually most intensely observed as MS adducts $[R-TEMPO+H]^+$ and $[R-TART+H]^+$.

4.4.1. Acceptance limits

Acceptance limits had to be set for all data handling. These acceptance limits were: systematic m/z deviation; random m/z deviation tolerance and noise intensity. These acceptance limits defined whether a peak was deemed valid, by ensuring peaks had m/z acceptably close to their predicted m/z and had intensity significantly greater than noise intensity.

Systematic m/z deviation was the m/z deviation between predicted and observed m/z deviation for TART. In the main region of interest, (usually m/z 300-400), this was typically between m/z -0.0006-0.0000.

Random m/z deviation was the m/z deviation between predicted and observed m/z minus systematic m/z deviation for an individual peak. In the main region of interest, (usually m/z 300-400), this was typically between m/z \sim -0.0000-0.0015. Therefore, random m/z deviation tolerance was typically m/z \pm 0.0008-0.0015. However, if searching for peaks significantly outside the main region of interest, random m/z deviation may be significantly greater and therefore, random m/z deviation tolerance was set wider, typically m/z \pm 0.0015-0.0030, but occasionally m/z \pm 0.0015-0.0050. Random m/z deviation tolerance was usually set such that it included most observed peaks corresponding to hypothesised species.

Finally, noise intensity was the intensity below which signal was considered noise. For a single mass spectrum, this was typically \sim 60000 absolute count. Noise intensity was usually estimated based upon mass spectrum profile observation.

Once acceptance limits were decided upon, spectrum analysis could be undertaken. Manual analysis could be performed without additional programming.

4.4.2. Manual analysis

Mass spectra could be handled manually using Bruker DataAnalysis, a mass spectrum analysis programme. With this, overall mass spectra could be viewed and peak m/z and intensity could be determined. Usually, an overall impression of MS characterisation was obtained by manual observation. However, manual MS analysis was generally slow and therefore, self-made programmes were used for most standard MS analysis. For this, Bruker DataAnalysis was used for converting mass spectra files into text file format, suitable for use in MATLAB programmes.

HPLC-MS mass spectra were usually handled both manually and through self-made programmes. Often, an average HPLC-MS spectrum was obtained manually and converted for programming use, to determine peaks of interest (4.4.4 and 4.4.6). Chromatograms of observed peaks of interest were then obtained manually to find retention time of maximum peaks of interest intensities. Mass spectra in which maximum peaks of interest intensities were observed were then converted for programming.

Although background spectra could be handled manually, background spectra could be subtracted from sample spectra most easily through programming.

4.4.3. Background removal

Before sample MS characterisation was performed, a background spectrum was obtained (4.3.2.4). Background signals were removed during sample analysis processing using the obtained background mass spectrum. Self-made standard MS analysis programmes involved background removal, whilst tandem MS and HPLC-MS usually did not. Peak m/z in all obtained mass spectra were subject to small fluctuations. Therefore, peaks in sample and background spectra did not necessarily align exactly, even if these peaks arose from the same analyte. Therefore, for background removal in analysis programmes, peaks between sample and background spectra within random m/z deviation tolerance of each other were aligned. Programmes then subtracted background peak intensities from corresponding sample peak intensities. If no background peak was observed with random m/z deviation tolerance of a sample peak, intensity of the background signal at the sample peak m/z value was subtracted from the sample peak intensity. Background peak intensities in samples were likely overestimated. This was because in background mass spectra, fewer analytes reduced competition between analytes for cations (4.3.1.4), causing background peak intensities to be greater than in sample spectra. This overestimation increased validity of outputted sample peaks.

Additionally, background removal could be used to subtract sample spectra, in order to compare differences between two different sample spectra. For example, MS characterisation of a no TART control could be subtracted from MS characterisation of a TART trapping sample, yielding only TART related species, including TART-trapped radicals.

4.4.4. Peak Pick

The Peak Pick programme was used to automatically find MS peaks corresponding to hypothesised species in mass spectra of samples (11.9.2). For this, species were hypothesised and inputted into a Microsoft Excel table, along with their predicted m/z when protonated, sodiated and potassiated. Peak Pick then imported these m/z values and screened mass spectra for them. Peaks were only accepted if they satisfied acceptance limits (4.4.1). Observed peak m/z and intensity were then exported into the Microsoft Excel table. Additionally, Peak Pick outputted any peaks above a defined fraction of maximum peak intensity, which had not been inputted into the original Microsoft Excel table. This was to find any intense peaks which had not been hypothesised.

Peak Pick was used to analyse most standard MS and D₂O exchange mass spectra. This radically decreased time required for MS analysis and therefore, increased efficiency. Peak Pick was adapted to include carbon content estimation.

4.4.5. Carbon content (C_x) estimation

Carbon content (C_x) estimation was used to calculate number of carbon atoms in a species, using its corresponding monoisotopic and first ¹³C satellite peaks. This programming aspect was combined with Peak Pick, to output C_x estimation alongside m/z and intensity of observed peaks.

For this, C_x estimation compared the monoisotopic peak corresponding to each hypothesised species with its first ¹³C satellite. ¹²C and ¹³C have isotopic masses 12.0000 g mol⁻¹ and 13.0034 g mol⁻¹, and abundances 98.9% and 1.1% respectively. Therefore, carbon-containing species can contain ¹²C and ¹³C. For lightweight carbon-containing species, probability of containing only ¹²C decreases as number of carbon atoms (n) increases, whilst probability of containing one ¹³C increases. These probabilities are calculated by 0.989^n and

$0.011n \times 0.989^{n-1}$ respectively, resulting in $1 \times ^{13}\text{C}:^{12}\text{C}$ calculated by $0.011n \times 0.989$. Therefore, by comparing the ratio of intensities of peaks corresponding to each hypothesised species and its first ^{13}C satellite, species C_x could be estimated.

If peak C_x estimation was similar to hypothesised species C_x , this further validated that the peak corresponded to the hypothesised species. C_x estimation usually worked well for high intensity peaks but more poorly for low intensity peaks. For example, accuracy of C_x estimation for TARTs decreased with decreasing [TART]. This was because as peak intensity decreased, its relative error increased. Furthermore, for very low intensity monoisotopic peaks, the first ^{13}C satellite was unobserved.

This programme aspect was employed commonly for MS analysis of mass spectra obtained from TART trapping samples. This programme aspect could have been adapted to other elements with multiple abundant isotopes, such as chlorine or bromine. However, it was decided that this would not be particularly useful for several reasons. Firstly, few TART trapping reactions contained such elements. Secondly, of those that did, species usually only contained one or two atoms of these elements. For elements with one isotope vastly more abundant than other, such as sulfur, peak isotopic analogues had low intensity, usually resulting in large atom content estimation error. For elements with many equally abundant isotopes, each isotopic analogue was important and therefore, each isotopic analogue was searched for using Peak Pick.

4.4.6. Formula Find

The Formula Find programme used a reverse strategy to Peak Pick. Whilst Peak Pick aimed to find peaks corresponding to hypothesised species of certain molecular formulae with m/z , Formula Find aimed to find molecular formulae from observed peaks (11.9.2). Species could then be hypothesised for obtained molecular formulae. As for Peak Pick, peaks were only accepted if they satisfied acceptance limits (4.4.1). However, Formula Find was significantly slower than Peak Pick and could yield many more data. Therefore, the Formula Find used additional limits to decrease data quantity. Furthermore, additional limits removed suggestions of unlikely species. These limits were: m/z search range; background proportion tolerance; molecular formulae; unsaturation and species charge.

Firstly, m/z search range limits prevented screening of peaks unlikely to be of interest. Above the main region of interest (usually m/z 300-400), spectra were usually relatively empty and species were less likely to be TART-trapped radicals. Therefore, m/z search range was usually set between m/z 100-500, as required.

Background proportion tolerance was used to remove peaks which appeared relatively intensely in background spectra compared to sample spectra, indicating that these peaks were less likely to be sample related. For this, sample peaks were excluded if the corresponding background peaks had intensity above the fractional proportion tolerance of sample peaks intensity. This was typically set at 0.5. This meant that sample peaks were excluded if the corresponding background peaks had intensity >50% sample peak intensity.

Molecular formulae and unsaturation limits defined what quantities of certain atoms were allowed in species. This produced molecular formulae with plausible atomic compositions for the sample species. C, H, N, O and Na were used exclusively for most systems, with N, O and Na sometimes being excluded for particular samples. Other elements were also included when analytes may plausibly contain them, such as S, Cl and Br. Molecular formulae were typically set with limits $\text{C}_{1-100}\text{H}_{1-100}\text{N}_{0-3}\text{O}_{0-10}\text{Na}_{0-1}$ and unsaturation with limits 0-15, as required. Furthermore, these limits could be used to selectively search for particular types of species.

For example, if DEADANT was used for saturated alkyl radical trapping, all DEADANT-trapped radicals should contain exactly two N, one O and no Na, as all should appear protonated in mass spectra, and two unsaturations. Therefore, setting molecular formulae limits as $C_{1-100}H_{1-100}N_2O$ and two unsaturations yielded only peaks and molecular formulae which could correspond to DEADANT-trapped saturated alkyl radicals. Therefore, using TARTs with ARTs containing elements not found in radicals of interest, made finding TART-trapped radicals using Formula Find significantly easier.

Species charge defined what charges ions could have. This was near-universally set to find singly charged species but was occasionally altered to find more highly charged species.

All these additional limits increased Formula Find speed whilst reducing outputted data quantity, allowing species to be hypothesised more rapidly, using relevant molecular formulae. Additionally, Formula Find outputted whether species corresponding to peaks and their hypothesised molecular formulae had previously been searched for using Peak Pick, again increasing speed of outputted data analysis.

Formula Find was commonly used upon mass spectra obtained from standard MS characterisation, to find species not previously hypothesised. Additionally, Formula Find was used to analyse tandem MS characterisation, with molecular formula limits being set from no molecular formula to equal the parent ion molecular formula. C_x estimation was included in Formula Find to further limit false positive output. However, in reality C_x estimation was seldom used, due to C_x estimation being too unreliable for low intensity peaks. For similar reasons as described for Peak Pick, element content estimation using peak isotopic analogues would not be particularly useful (4.4.5).

Formula Find would likely have been unusable with a significantly lower resolution mass spectrometer, since many other molecular formulae would have fallen with acceptance limits (4.3.1.2 and 4.4.1). This large number of false molecular formulae would have taken too long to exclude to make Formula Find useful.

4.4.7. Metal complex structures using Formula Find

Metal complex structures could also be determined by adapting Formula Find.

Metals present in radical reactions could form charged metal complexes with ligands. These charged metal complexes could be MS characterised. However, in these radical reactions, different ligands could be present. This could result in formation of many different metal complexes. This was further complicated when sample was diluted in MS solvents, as up to three further ligands were available for metal complex formation. Therefore, Formula Find was applied to determine metal complex structure.

For this, Formula Find was used similarly as to previously, including setting additional limits to improve Formula Find analysis efficiency (4.4.7). These limits were: m/z search range; background proportion tolerance; molecular formulae and species charge (4.4.7). However, unlike Formula Find, unsaturation limits were not used. Furthermore, molecular formulae and species charge limits were used differently to Formula Find.

For molecular formulae limits, metal centres and ligands were utilised instead of atoms. Species thought likely to be able to complex to metals were also included. These species could include: initial metal salt, ligands and anions; substrate; additives; solvents and MS solvents. Number of each ligand was set to a maximum coordination number. This number could be decreased for multidentate ligands.

For species charge, overall species charge was not limited. Instead, a metal charge range limit was applied. This would be the likely oxidation states for the metal within radical reaction conditions. Additionally, inputted ligands were also assigned charges. When Formula Find was applied, each possible metal complex would use overall metal complex charge to calculate theoretical m/z .

Formula Find was occasionally used upon standard MS characterisation of radical reactions containing metals, to find metal complexes not previously hypothesised.

4.5. Summary

A general TART trapping, MS characterisation and mass spectra analysis methodology was developed. TART trapping was usually used to investigate literature-sourced radical reactions. Initially, the procedure for literature-sourced radical reactions was replicated as closely as possible, but with TART incorporated into the system. A trapless control was also run, with aliquots removed before and after reactions. Any required workups were then performed before MS characterisation was undertaken.

MS characterisation involved first obtaining a background and standard mass spectrum for all samples. Mass spectra analysis was then undertaken. This typically used the Peak Pick programme to search for hypothesised MS adducts, with manual analysis often conducted as well. Additionally, the Formula Find programme was sometimes employed to suggest molecular formulae corresponding to observed MS peaks, depending on the desired outcome of the radical reaction investigation.

Depending on the results of this analysis and the desired outcomes of the reaction investigation, further TART trapping or control reaction experiments were performed or further MS characterisation upon previously obtained samples was undertaken. Further TART trapping or control reaction experiments involved altering reaction conditions to obtain further mechanistic or kinetic information. Further MS characterisation could include D₂O exchange, tandem MS, HPLC-MS or a combination of these techniques, for example tandem HPLC-MS. Mass spectra from these MS characterisation techniques were typically analysed using: Peak Pick for D₂O exchange; Formula Find for tandem MS and manually for HPLC-MS, with programmes sometimes being employed for HPLC-MS analysis too.

With a protocol developed for TART trapping and MS characterisation, TART trapping was undertaken. TARTs were used for radical trapping in: liquid phase synthetic radical reactions (5); liquid phase photochemistry (6); aqueous biochemistry (7); gaseous alkene ozonolysis (8) and gaseous •OH-initiated alkane degradation (9). Initially, TART trapping was used to investigate synthetic radical reactions (5). This was due to their relative simplicity, high radical flux and widely accepted mechanisms.

5. Synthetic radical reactions

5.1. Introduction

Liquid phase synthetic radical reactions were chosen for initial TART trapping investigations, due to their high radical flux and relative simplicity. Higher radical flux would help generate a higher concentration of trapped radicals, whilst the relative simplicity of these reactions would generate relatively few trapped radical structures. Higher concentration of few trapped radical structures would reduce the sensitivity required for MS detection, making successful observation of TART-trapped radicals more likely. Furthermore, TART trapping undertaken in relatively simple homogenous reaction mixtures would likely be easier to troubleshoot, should TART-trapped radicals not be observed. These attributes were especially advantageous during development of TART trapping and MS characterisation methodology.

Radical characterisation within these reactions should allow structures of intermediate radicals to be determined. This could validate or inform synthetic reaction mechanisms. Additionally, radical quantification could validate or inform reaction kinetics.

TART trapping was first applied to a model thiyl radical system, where radicals were generated using thiol as substrate and an initiator. Grantham also performed TART trapping upon thiyl radicals, using Grantham TARTs (2.2).¹⁵² Thiyl radical TART trapping was performed very early in the project and therefore, little development of TART trapping and MS characterisation methodology had occurred. As such, thiyl radical TART trapping analysis did not benefit from many TART trapping methodology improvements established during the project. Since this thiyl radical TART trapping was designed as a test and not to yield new information about this system, these test experiments were not repeated with methodology improvements.

5.2. Thiyl radicals

Thiyl radicals were generated by hydrogen atom abstraction (HAA) from thiol using an initiator. TART was employed to trap these thiyl radicals (Figure 59).

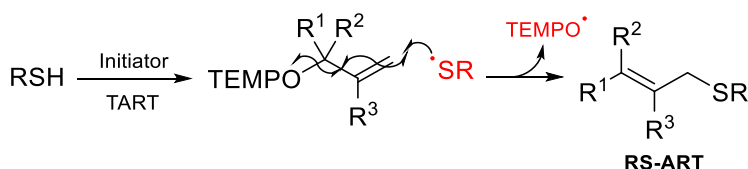


Figure 59: Thiyl radical formation from thiol using initiator and subsequent radical trapping by TART.

1-Dodecanethiol was chosen as reactant because its high boiling point should have ensured that TART-trapped 1-dodecanethiyl radicals also had a high boiling point, regardless of ART identity. Therefore, minimal sample loss should have occurred through evaporation, prior to MS characterisation.

Initially azobisisobutyronitrile (AIBN) was used as initiator at 50 °C. At this temperature, AIBN decomposed to form two isobutyronitrile radicals (IBN[•]) and N₂. These radicals then abstract hydrogen atoms from thiol S–H to form thiyl radicals (RS[•]). 1-Dodecanethiyl radicals can react with O₂ to form sulfinyl radicals (RS(O)[•]) or sulfonyl radicals (RS(O)₂[•]). Therefore, this reaction was performed under N₂, to prevent thiyl radical oxidation.

When TART trapping of thiyl radicals was undertaken, only Grantham TART and allyl-TEMPO TARTs had successfully been synthesised. Since Grantham TART would decay rapidly in solution at 50 °C (2.2), allyl-TEMPO was initially employed to trap thiyl radicals (Figure 60,

11.4.1.1). The sample mixture, containing TART-trapped radicals, was then MS characterised. Initially positive ESI-MS was performed using a Bruker HCT-Ultra ETD II ion trap mass spectrometer (4.3.1.2).

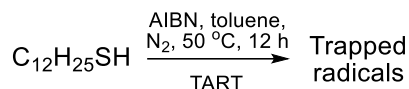


Figure 60: Initial thiyl radical trapping experiment, using 1-dodecanethiol as substrate and AIBN as initiator (11.4.1.1).

Mass spectrum analysis was then undertaken. Initially, this involved manually analysing the spectrum to find MS peaks corresponding to hypothesised species (4.4.2).

5.2.1. Initial results

Initial results indicated that thiyl radicals were successfully TART-trapped using allyl-TEMPO (Figure 61, Table 3, 11.4.1.1). Initially, only peaks corresponding to species relevant to TART trapping were searched for. More detailed investigation was undertaken following system optimisation (5.2.3).

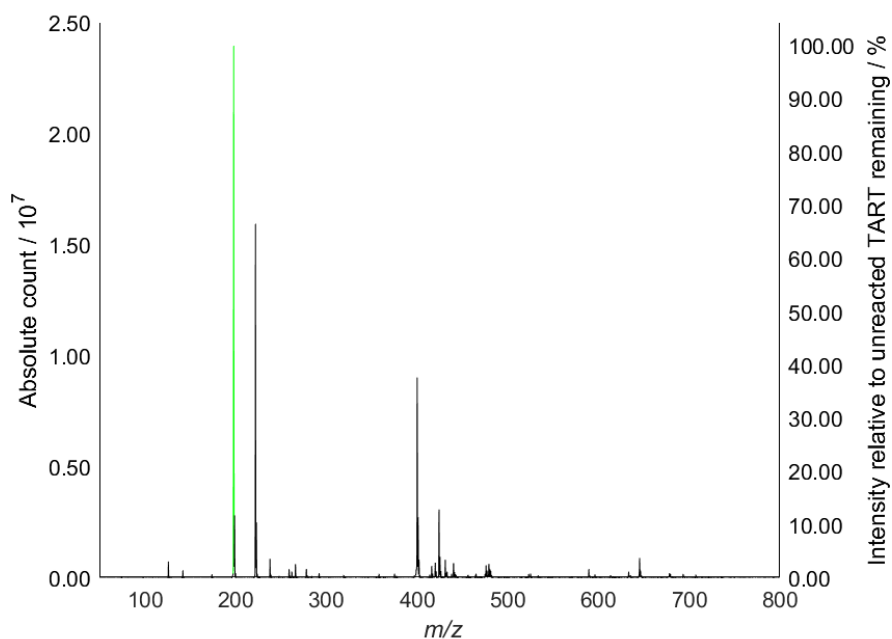


Figure 61: Mass spectrum from TART trapping of thiyl radicals, using allyl-TEMPO as TART and a HCT mass spectrometer for MS characterisation (11.4.1.1). The peak corresponding to [allyl-TEMPO+H]⁺ had the greatest intensity (*m/z* 198.186, green).

Table 3: Species identified from TART trapping of thiyl radicals, using allyl-TEMPO as TART and a HCT mass spectrometer for MS characterisation (11.4.1.1). Systematic m/z error = -0.2; random m/z error = ± 0.4 ; 100% intensity = 1.92×10^8 absolute count.

	Species	Predicted m/z	Intensity relative to unreacted TART / %
TART	[Allyl-TEMPO+H] ⁺	198.2	100
	[Allyl-TEMPO+Na] ⁺	220.2	0.06
Trapped radicals	[RS-ART+H] ⁺	243.2	0.05
	[RS-ART+Na] ⁺	265.2	0.13
	[RS(O)-ART+H] ⁺	259.2	1.71
	[RS(O)-ART+Na] ⁺	281.2	0.06
	[RS(O) ₂ -ART+H] ⁺	275.2	0.02
	[RS(O) ₂ -ART+Na] ⁺	297.2	0

Peaks corresponding to TART-trapped RS[•] (RS-ART) RS(O)[•] (RS(O)-ART) and RS(O)₂[•] (RS(O)₂-ART) were observed. These observations indicated that RS[•] was trapped using allyl-TEMPO and that this species could be detected using MS. This was a good result, as it suggested that TARTs could be used to trap, detect and characterise liquid phase radicals.

Grantham conducted similar thiyl radical trapping experiments but instead utilised Grantham TART. Grantham observed MS peaks corresponding to the equivalent Grantham TART-trapped sulfur-centred radicals.¹⁵² Therefore, these observations agreed with Grantham.

Before more detailed or quantitative analysis was undertaken, optimisation was carried out to identify the best TART (5.2.2.1) and spectrometer (5.2.2.2) for sample MS characterisation.

5.2.2. Optimisation

5.2.2.1. TART

TART trapping of thiyl radicals was undertaken in presence of Grantham TART to prove allyl-TEMPO was a superior TART for investigating this reaction (Table 4, 11.4.1.1).

Table 4: Species identified from TART trapping of thiyl radicals, using AIBN as initiator, Grantham TART or allyl-TEMPO as TART and a HCT mass spectrometer for MS characterisation (11.4.1.1). Systematic m/z error = -0.2; random m/z error = ± 0.4 ; 100% intensity = 1.92×10^8 absolute count.

	Species	Grantham TART		Allyl-TEMPO	
		Predicted m/z	Intensity relative to unreacted allyl-TEMPO / %	Predicted m/z	Intensity relative to unreacted allyl-TEMPO / %
TART	[TART+H] ⁺	266.2	26.97	198.2	100
	[TART+Na] ⁺	288.2	0.01	220.2	0.06
Trapped radicals	[RS-ART+H] ⁺	311.3	0.01	243.2	0.05
	[RS-ART+Na] ⁺	333.3	0.02	265.2	0.13
	[RS(O)-ART+H] ⁺	327.3	0.02	259.2	1.71
	[RS(O)-ART+Na] ⁺	349.3	0.05	281.2	0.06
	[RS(O) ₂ -ART+H] ⁺	343.3	0.30	275.2	0.02
	[RS(O) ₂ -ART+Na] ⁺	365.2	1.20	297.2	0

MS peaks corresponding to TART-trapped sulfur-centred radicals were successfully observed for both TARTs. Peaks corresponding to allyl-TEMPO-trapped sulfur-centred radicals had

significantly greater intensity than peaks corresponding to Grantham TART-trapped sulfur-centred radicals, as predicted. This indicated that rearrangement was more of a hinderance to TART trapping than HAA (3.1). As such, allyl-TEMPO became first choice of TART for studying simple liquid phase synthetic radical reactions, until other TARTs were successfully synthesised.

5.2.2.2. Mass spectrometer

Initially a HCT mass spectrometer had been used for sample MS characterisation. However, this HCT mass spectrometer had relatively poor accuracy and precision. This reduced confidence in obtained results, as discussed previously (4.3.1.2). Therefore, thiy radical TART trapping was repeated, but using the higher accuracy and higher precision solariX mass spectrometer for MS characterisation (4.3.1.2, Table 5). Using this higher accuracy and higher precision mass spectrometer increased confidence in obtained results.

Table 5: Species identified from TART trapping of thiyl radicals, using AIBN as initiator, allyl-TEMPO as TART and HCT or solariX mass spectrometers for MS characterisation (11.4.1.1). HCT: systematic m/z error = -0.2; random m/z error = ± 0.4 ; 100% intensity = 1.92×10^8 absolute count. solariX: systematic m/z error = -0.0004; random m/z error = ± 0.0002 ; 100% intensity = 4.87×10^8 absolute count.

Species	Predicted m/z	HCT		solariX		
		Difference from predicted m/z	Intensity relative to unreacted TART / %	Difference from predicted m/z	Intensity relative to unreacted TART / %	
TART	[Allyl-TEMPO+H] ⁺	198.1858	-0.2	100	-0.0004	100
	[Allyl-TEMPO+Na] ⁺	220.1677	0.1	0.06	-0.0005	0.045
Trapped radicals	[RS-ART+H] ⁺	243.2146	-0.2	0.05	-	0
	[RS-ART+Na] ⁺	265.1966	-0.2	0.13	-	0
	[RS(O)-ART+H] ⁺	259.2096	-0.2	1.71	-0.0005	4.23
	[RS(O)-ART+Na] ⁺	281.1915	-0.1	0.06	-	0
	[RS(O) ₂ -ART+H] ⁺	275.2045	-0.2	0.02	-0.0004	0.015
	[RS(O) ₂ -ART+Na] ⁺	297.1864	-	0	-	0

Differences between predicted and observed m/z for observed species were significantly smaller and fluctuated less using the solariX mass spectrometer compared to the HCT mass spectrometer (typically $< \pm 0.0010$ compared to $< \pm 0.5$). Therefore, the solariX mass spectrometer was much more accurate and precise. This higher accuracy and precision improved confidence in obtained results (4.3.1.2).

Furthermore, many peaks corresponding to predicted species observed by the HCT mass spectrometer were not observed using the solariX mass spectrometer. This was due to the lower resolving power of the HCT mass spectrometer causing other species to contribute to peaks corresponding to predicted species (4.3.1.2). This brought into question the validity of the results reported by Grantham. Grantham had exclusively used the HCT mass spectrometer for thiyl radical trapping experiments (2.2).¹⁵² Concerns as to the HCT mass spectrometer suitability, threatened the validity of these results.

This was particularly significant for RS-ART, for which no corresponding MS peak was observed using the solariX mass spectrometer, indicating that this species was not present in the sample mixture at sufficiently high concentration for detection. Upon solariX mass spectrum inspection, the peak initially observed at m/z 243.0 using the HCT mass spectrometer, appeared to have instead come from a peak observed at m/z 243.288 (Figure 62). Furthermore, this peak seemed to be a $1 \times ^{13}\text{C}$ satellite peak of m/z 242.284, thereby making its correspondence to RS-ART even less plausible.

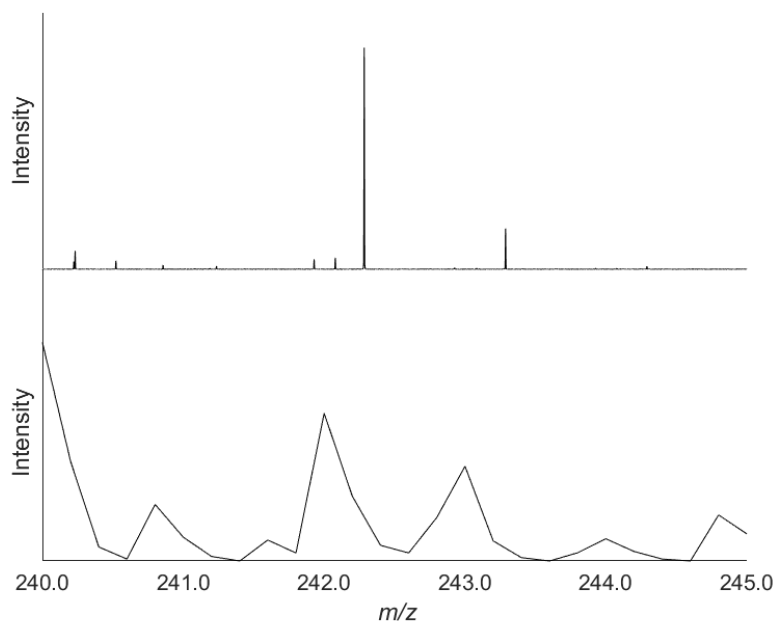


Figure 62: Mass spectrum from TART trapping of thiyl radicals, using AIBN as initiator, allyl-TEMPO as TART and HCT (bottom) and solarix (top) mass spectrometers for MS characterisation (11.4.1.1). A peak at m/z 243.0 appears to correspond to $[RS-ART+H]^+$ (predicted m/z 243.2146) using the HCT mass spectrometer, however the solarix mass spectrometer shows that this peak is mainly due to a peak with m/z 243.2877, disproving presence of RS-ART.

This false positive obtained using the HCT mass spectrometer but not in the solarix mass spectrometer shows the importance of using a high accuracy, high precision and high resolving power mass spectrometer for MS characterisation. Therefore, the solarix mass spectrometer was used in all following studies for MS characterisation of TART trapping samples (4.3.2).

These results indicated that TART-trapped thiyl radical was not present in the system. This was a disappointing result. However, a peak corresponding to TART-trapped sulfinyl radical was observed convincingly. Since the reaction was performed under N_2 , the reason sulfinyl radicals were TART trapped whilst thiyl radicals were not, was uncertain. However, it was decided that further MS analysis should be undertaken, since some positive results were obtained.

5.2.3. Detailed results

Once the TART and mass spectrometer had been chosen for the thiyl radical TART trapping experiment, more detailed MS analysis could be undertaken. First however, PbO_2 was also explored as an initiator for thiyl radical formation, in an attempt to observe TART-trapped thiyl radicals (Figure 63, 11.4.1.2).

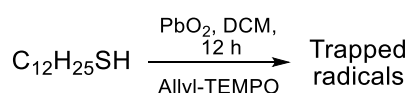


Figure 63: TART trapping of thiyl radicals, using 1-dodecanethiol as substrate, PbO_2 as initiator and allyl-TEMPO as TART (11.4.1.2).

MS characterisation and analysis was then performed and compared to TART trapping of AIBN-initiated thiyl radical formation (Table 6).

Table 6: Species identified from TART trapping of thiyl radicals, using AIBN or PbO₂ as initiator, allyl-TEMPO as TART and MS for characterisation (11.4.1). Systematic m/z error = -0.0004; random m/z error = ± 0.006 ; 100% intensity = 4.87×10^8 absolute count.

	Species	Predicted m/z	Intensity relative to unreacted TART in AIBN sample / %	
			AIBN	PbO ₂
TART	[Allyl-TEMPO+H] ⁺	198.1858	100	10.4
	[Allyl-TEMPO+Na] ⁺	220.1677	0.045	0.085
Reactants	[RSH+H] ⁺	203.1833	0	0
	[RSH+Na] ⁺	225.1653	0	0
	[AIBN+H] ⁺	165.1140	0	0
	[AIBN+Na] ⁺	187.0960	0	0
Trapped radicals	[RS-ART+H] ⁺	243.2146	0	0.016
	[RS-ART+Na] ⁺	265.1966	0	0
	[RS-TEMPO+H] ⁺	358.3143	0.036	0.030
	[RS-TEMPO+Na] ⁺	380.2963	0	0
	[RS-TART+H] ⁺	398.3456	0.018	0.075
	[RS-TART+Na] ⁺	420.3276	0	0
	[RS(O)-ART+H] ⁺	259.2096	4.23	11.9
	[RS(O)-ART+Na] ⁺	281.1915	0	0.022
	[RS(O)-TEMPO+H] ⁺	374.3093	0	0.060
	[RS(O)-TEMPO+Na] ⁺	396.2912	0.021	0.037
	[RS(O)-TART+H] ⁺	414.3406	0.021	0.316
	[RS(O)-TART+Na] ⁺	436.3225	0	0
	[RS(O) ₂ -ART+H] ⁺	275.2045	0.015	0.066
	[RS(O) ₂ -ART+Na] ⁺	297.1864	0	0
	[RS(O) ₂ -TEMPO+H] ⁺	390.3042	0	0
	[RS(O) ₂ -TEMPO+Na] ⁺	412.2861	0.017	0
[RS(O) ₂ -TART+H] ⁺	430.3355	0	0	
[RS(O) ₂ -TART+Na] ⁺	452.3174	0	0	

Importantly, it was noted that particular MS adducts formed for certain types of species. MS peaks corresponding to allyl-TEMPO were observed much more intensely protonated than sodiated. This was hypothesised to be due to its highly basic 3° amine group. This was found to be true for all synthesised TARTs. For identical reasons, TEMPO-trapped radicals and radicals trapped via allylic HAA from TART were also observed most intensely as protonated MS adducts. From here onwards, only protonated MS adducts are shown for TART, TEMPO-trapped radicals and trapped radicals formed via allylic HAA of TART, although sodiation was still monitored. Conversely, TART-trapped radicals did not contain this 3° amine group. This meant that the most likely MS adduct formed was highly dependent on the R-ART structure. From here onwards, both protonated and sodiated MS adducts are shown for TART-trapped radicals, unless they are predicted to be predominantly one MS adduct, such as radicals containing highly basic amine groups.

The MS peak corresponding to [TART+H]⁺ showed significantly lower intensity in presence of PbO₂ than AIBN. This suggested that more TART was consumed in the PbO₂-initiated reaction. In contrast, greater intensities were generally observed for MS peaks corresponding to TART-trapped radicals in the PbO₂-initiated reaction. This matched the lower intensity observed for peaks corresponding to TART in the PbO₂-initiated reaction.

Furthermore, a peak corresponding to TART-trapped thiyl radical (m/z 243.2146) was observed using PbO₂ as initiator using the solarix mass spectrometer. The high accuracy, precision and resolving power of this spectrometer ensured that this peak could

unambiguously be assigned to the molecular formula of TART-trapped thiyl radical (C₁₅H₃₁S). Other possible molecular formulae had *m/z* values outside the solariX *m/z* acceptance limits for this peak (Table 7).

Table 7: Possible molecular formulae for [RS-ART+H]⁺ corresponding peak (observed *m/z* 243.2146) from TART trapping of thiyl radicals, using PbO₂ as initiator, allyl-TEMPO as TART and MS for characterisation (11.4.1.2). Molecular formulae and unsaturation limits were set to C₀₋₁₀₀H₀₋₁₀₀N₀₋₅O₀₋₁₀S₀₋₅Na₀₋₁K₀₋₁Pb₀₋₅ and 20 respectively. Only one molecular formula had an acceptable difference (typically *m/z* ±0.0000-0.0020) between predicted and observed *m/z* (black).

Molecular formula	Difference from observed <i>m/z</i>
C ₁₅ H ₃₁ S	0.0000
C ₁₈ H ₂₇	0.0033
C ₁₂ H ₂₇ N ₄ O	-0.0039

Therefore, TART was successfully used to trap and characterise thiyl radicals, satisfying the experimental aim. However, more information was gathered by further analysing sample MS characterisation.

For both initiators, MS peaks corresponding to RS(O)-ART were observed with greatest intensity of TART-trapped sulfur-centred radicals. Therefore, thiyl radicals potentially reacted faster with O₂ than allyl-TEMPO. Indeed, literature suggests that reaction rate of sulfur-centred radicals with O₂ is diffusion controlled.^{173,174} Alternatively, in PbO₂ presence, PbO₂ may act as an oxidising agent, causing thiyl radical oxygenation. However, thiyl radical formation using AIBN as initiator was performed under N₂. Therefore, O₂ should not have been present in the system. This may have suggested that N₂ purging had not been performed thoroughly enough. However, repeating this experiment especially carefully did not improve experimental results.

An alternative explanation was that RS(O)-ART was more easily ionised than RS-ART. This would make MS peaks corresponding to RS(O)-ART of greater intensity than peaks corresponding to the same concentration of RS-ART. This could mean that sample [RS-ART] was much greater than [RS(O)-ART]. This illustrates a key issue for MS quantification. TARTs which yielded TART-trapped radicals with higher ionisation efficiency, regardless of reactant radical structure, were later synthesised to combat this issue (3.4.2.3). However, this system was not further investigated with these new TARTs, since this thiyl radical TART trapping was designed as a test and not to yield new information about this system.

No reactant corresponding peaks were observed. Thiol was initially in a large excess compared to all other reactants, making it unlikely that no thiol remained. This was likely due to thiol having poor ionisation efficiency, concurring with previous observations.

MS peaks corresponding to TEMPO-trapped radicals (e.g., RS(O)-TEMPO) were generally of low intensity, especially for RS(O)-TEMPO compared to RS(O)-ART. This was expected, since it was believed that TEMPO• would poorly trap sulfur-centred radicals, since the N-O-S bond formed would be weak. However, any RS-TEMPO corresponding peak observation was unexpected. Literature suggested that a rearrangement of the initially formed N-O-S species occurs to form a mono-oxygenated N-S=O species (Figure 64).^{175,176} However, since these two species have identical molecular formulae, standard MS cannot be used to confirm which structural isomers are present. Although, tandem MS may have helped elucidate species structure, this was not attempted.

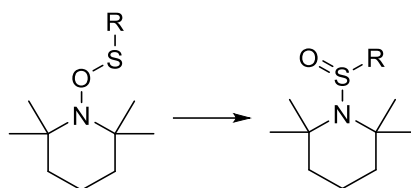


Figure 64: Initially formed RS-TEMPO adduct (left) from TART trapping of thiyl radicals and subsequent rearrangement to form structural isomer suggested by literature.^{175,176}

Allylic HAA from TART and subsequent radical trapping (e.g., RS(O)-TART) was observed (3.1, Figure 37). This was unfortunate as this wasted TART and further complicated mass spectra (3.1). RS-TART and RS(O)₂-TART were observed with similar or greater intensity than RS-ART and RS(O)₂-ART. This may have suggested that allylic HAA occurred faster than TART trapping. However, trapped radicals formed via allylic HAA of TART, were significantly more basic than TART-trapped radicals and therefore, MS intensity of peaks corresponding to these species would likely be significantly greater for trapped radicals formed via allylic HAA of TART. This was somewhat confirmed by RS(O)-ART being of significantly greater intensity than RS(O)-TART. This potentially suggested that in the sample, allylic HAA occurred relatively slowly. However, this was not certain and needed to be monitored in further reactions.

Several satellite peaks were visible for peaks corresponding to TART-trapped radicals formed in PbO₂-initiated thiyl radical formation. For the intensely observed peaks corresponding to [allyl-TEMPO+H]⁺ and [RS(O)-ART+H]⁺, predicted and observed ratio of satellite peaks to their monoisotopic peak correlated well, further validating that these monoisotopic peaks corresponded to these species (Table 8).

Table 8: Predicted and observed fraction of different isotopes of two most intense species identified from TART trapping of thiyl radicals, using PbO₂ as initiator, allyl-TEMPO as TART and MS for characterisation (11.4.1.2). Systematic *m/z* error = -0.0004 random *m/z* error = ±0.0003; 100% intensity = 5.08×10⁷ absolute count.

Species	Formula	Predicted fraction	Observed <i>m/z</i>	Intensity relative to unreacted TART / %	Observed fraction
[TART+H] ⁺	¹² C ₁₂ H ₂₃ NOH	1.000	198.1853	100.00	1.000
	¹² C ₁₁ ¹³ CH ₂₃ NOH	0.133	199.1886	14.55	0.146
	¹² C ₁₀ ¹³ C ₂ H ₂₃ NOH	0.008	200.1919	1.04	0.010
[RS(O)-ART+H] ⁺	¹² C ₁₅ H ₃₀ O ³² SH	1.000	259.2090	114	1.000
	¹² C ₁₄ ¹³ CH ₃₀ O ³² SH	0.162	260.2125	19.3	0.170
	¹² C ₁₅ H ₃₀ O ³⁴ SH	0.045	261.2049	5.52	0.048
	¹² C ₁₃ ¹³ C ₂ H ₃₀ O ³² SH	0.012	261.2159	1.35	0.012
	¹² C ₁₄ ¹³ CH ₃₀ O ³⁴ SH	0.007	262.2082	0.827	0.007
	¹² C ₁₂ ¹³ C ₃ H ₃₀ O ³² SH	0.001	-	-	-

TART was successfully used to trap thiyl radicals and these TART-trapped radicals were then successfully observed using MS characterisation. This proved that liquid phase radicals could be trapped and characterised using TARTs and MS characterisation. This implied that TART trapping could be used to trap, characterise and possibly quantify radicals in simple liquid phase synthetic reactions, potentially validating or informing reaction mechanisms and kinetics. As such, synthetically useful liquid phase radical reactions were explored.

5.3. Common synthetic radical reactions

Initially it was decided to explore well-known and widely used simple liquid phase synthetic radical reactions. These reactions had well-established mechanisms. This high mechanistic certainty was beneficial whilst TART trapping methodology and MS methodology were being established. TART trapping could offer further validation to these reaction mechanisms.

Three common synthetic radical reactions were explored: the Barton reaction (5.3.1), the Hofmann-Löffler-Freytag reaction (5.3.2) and the Hunsdiecker reaction (5.3.3). Initially, all three reaction mechanisms were investigated using allyl-TEMPO, as only Grantham TART and allyl-TEMPO had been successfully synthesised at the time. However, TART trapping using allyl-TEMPO was largely unsuccessful for all three reactions, for example, as shown for the Barton reaction. This was hypothesised to be due to shortcomings of allyl-TEMPO as a radical trap, especially that its allyl ART group provided poor ionisation efficiency, resulting in TART-trapped radicals having low MS intensity (5.3.1.1).

These three radical reactions were reinvestigated once amide-functionalised TARTs were successfully synthesised, principally using CHANT and DEADANT. These investigations were much more successful, with MS peaks corresponding to TART-trapped radicals being observed for all three reactions. These investigations are discussed for the Barton reaction (5.3.1.2) and exclusively shown for the Hofmann-Löffler-Freytag reaction (5.3.2) and the Hunsdiecker reaction (5.3.3).

5.3.1. Barton reaction

The Barton reaction was discovered by Sir Derek Barton in 1960, who mainly used it for synthesis of unnatural steroids.^{177–179} Although this reaction is less commonly utilised today, the Barton reaction demonstrates one of the first examples of C–H activation reactions. The Barton reaction involves alkyl nitrite UV photolysis to form δ -nitroso alcohols. Barton used the kinetic isotope effect to suggest a mechanism for this reaction (Figure 65).¹⁷⁹

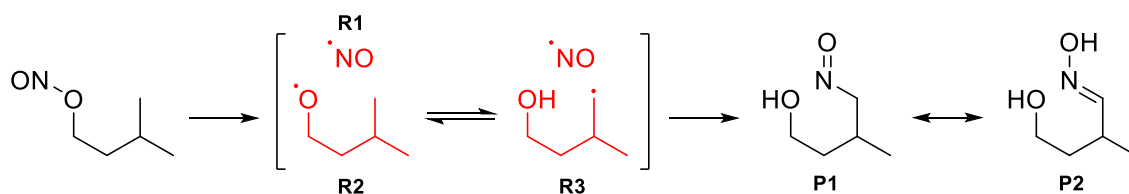


Figure 65: Widely accepted mechanism of the Barton reaction for isopentyl nitrite.^{179,180}

Whilst widely accepted, TART trapping could further validate the Barton reaction mechanism. This would involve TART trapping of R1, R2 and R3 in a Barton reaction and subsequent MS characterisation of these TART-trapped species. Successful MS identification of these TART-trapped radicals would indicate that these radicals were produced during the Barton reaction, hence offering validation to the widely accepted mechanism. Therefore, TART trapping was performed on the Barton reaction, using isopentyl nitrite as substrate (Figure 66, 11.4.2).

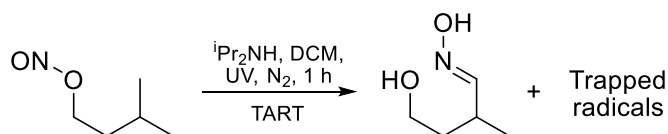


Figure 66: TART trapping of the Barton reaction, using isopentyl nitrite as substrate (11.4.2).

5.3.1.1. TART trapping using allyl-TEMPO

Initially, TART trapping of the Barton reaction was carried out using allyl-TEMPO. For this, a control reaction containing no TART and a trapping reaction containing TART were undertaken. Aliquots were removed from these reaction mixtures pre-initiation and post-reaction and these aliquots MS characterised (Table 9, 11.4.2). R2 and R3 had the same molecular formulae and therefore, all R2/R3 related species could not be distinguished using standard MS.

Table 9: Species identified from TART trapping of the Barton reaction, using isopentyl nitrite as substrate, allyl-TEMPO as TART and MS for characterisation (11.4.2). Systematic m/z error = 0.0000; random m/z error = ± 0.0006 ; 100% intensity = 2.08×10^6 absolute count.

	Species	Predicted m/z	Intensity relative to unreacted TART pre-trapping reaction / %		
			Trapless control	Pre-initiation	Post-trapping
TART	[Allyl-TEMPO+H] ⁺	198.1858	0	100	0
	[R1-ART+H] ⁺	72.0449	0	0	0
	[R1-ART+Na] ⁺	94.0269	0	0	0
	[R1-TART+H] ⁺	227.1759	0	0	3.46
Trapped radicals	[R2/R3-ART+H] ⁺	129.1279	0	0	0
	[R2/R3-ART+Na] ⁺	151.1099	0	0	0
	[R2/R3-TEMPO+H] ⁺	244.2276	0	0	29.5
	[R2/R3-TART+H] ⁺	284.2589	0	0	0

No MS peaks corresponding to TART were observed post-reaction, indicating that TART was totally consumed during the reaction.

However, no MS peaks corresponding to TART-trapped species were observed. This was a disappointing result. However, MS peaks corresponding to R1-ART were outside m/z limits and therefore were undetectable. Likewise, peaks corresponding to R2/R3-ART were at the edge of m/z limits. Therefore, it was theorised that these TART-trapped radicals may have formed but evaporated prior to MS characterisation. Furthermore, both TART-trapped radicals likely had poor ionisation efficiency. Therefore, this reaction would have been better studied using a TART that generated TART-trapped radicals with higher m/z and higher ionisation efficiency.

Whilst no MS peaks corresponding to TART-trapped species were observed, MS peaks corresponding to R2/R3-TEMPO were observed. This implied that TEMPO[•] had trapped R2, R3 or both. These MS peaks were predicted to be exclusively caused by R3-TEMPO, since TEMPO[•] trapping of non-carbon centred radicals is generally unfeasible (1.3.2.2).¹³⁹ Therefore, peaks corresponding to TEMPO-trapped nitrogen-centred, oxygen-centred or halo-centred radicals are generally not shown from here onwards. For TEMPO[•] to react with R3, TEMPO[•] must have been released by TART trapping. This validated that TART trapping had occurred, but that the resulting TART-trapped radicals were unobservable.

Although MS peaks corresponding to R1-TART were observed, this was not proof of TART reaction with [•]NO, as this species could be an artefact.

TART trapping of the Barton reaction using allyl-TEMPO was unsuccessful. This was largely attributed to allyl-TEMPO functionality being inappropriate to form TART-trapped radicals which could be MS characterised. TART trapping of the Barton reaction was later undertaken using CHANT.

5.3.1.2. TART trapping using CHANT TART

TART trapping of the Barton reaction and subsequent MS characterisation was repeated as before (5.3.1.1), but with CHANT being used as TART (Table 10, 11.4.2). As previously, R2 and R3 had the same molecular formulae and therefore, all R2/R3 related species could not be distinguished using standard MS.

Table 10: Species identified from TART trapping of the Barton reaction, using isopentyl nitrite as substrate, CHANT as TART and MS for characterisation (11.4.2). Systematic m/z error = -0.0008; random m/z error = ± 0.0005 ; 100% intensity = 3.66×10^9 absolute count.

	Species	Predicted m/z	Intensity relative to unreacted TART pre-trapping reaction / %		
			Trapless control	Pre-initiation	Post-trapping
TART	[CHANT+H] ⁺	323.2698	0.036	100	43.6
Trapped radicals	[R1-ART+H] ⁺	197.1290	0	0	0
	[R1-ART+Na] ⁺	219.1109	0	0	0
	[R1-TART+H] ⁺	352.2600	0.003	0	0.046
	[R2/R3-ART+H] ⁺	254.2120	0	0	0.026
	[R2/R3-ART+Na] ⁺	276.1939	0	0	0.184
	[R3-TEMPO+H] ⁺	244.2276	0.003	0	0.003
	[R2/R3-TART+H] ⁺	409.3430	0.001	0	0.025

Intensity of MS peaks corresponding to TART approximately halved during the reaction, indicating that approximately half of TART was consumed and therefore that TART reaction had occurred.

Peaks corresponding to R2/R3-ART were observed exclusively post-trapping reaction. This indicated that R2/R3 were present in the trapping reaction and were successfully TART trapped. This agreed with the widely accepted Barton reaction mechanism (Figure 65). This was an excellent result and proved that CHANT was more appropriate for TART trapping in the Barton reaction than allyl-TEMPO. As previously, R2-ART and R3-ART were indistinguishable and therefore, standard MS could not confirm existence of either species.

As previously, MS peaks corresponding to R1-ART were not observed. This was a disappointing result. However, nitroso compounds have notoriously poor stability, due to the high stability of nitric oxide (\bullet NO). R1-ART may have especially poor stability, due to \bullet ART stabilisation through allylic resonance. Therefore, [R1-ART] was likely to be low and hence was not observed. Although MS peaks corresponding to R1-TART were observed, this was not proof of TART reaction with \bullet NO, as this species could be an artefact.

Although standard MS could not be used to determine presence of R2, R3 or both, D₂O exchange or tandem MS may have offered further structural characterisation. At the time, D₂O exchange had not been considered as a useful tool for further structural characterisation. However, tandem MS was employed to try and distinguish whether R2/R3-ART corresponding peaks were due to R2-ART, R3-ART or both. Tandem MS indicated R3-ART presence, whilst R2-ART presence could not be confirmed (SI3.1). D₂O exchange may have enabled R2-ART detection.

TART trapping of the Barton reaction using CHANT was successful and provided evidence to support the widely accepted reaction mechanism proposed by Barton (Figure 65).^{179,180}

5.3.2. Hofmann-Löffler-Freytag (HLF) reaction

The Hofmann-Löffler-Freytag (HLF) reaction was discovered in 1885 by August Wilhelm von Hofmann but was little utilised until Karl Löffler and Curt Freytag increased the reaction scope in 1909.^{181,182} The HLF reaction involves thermal or photochemical decomposition of a *N*-haloamine, in presence of strong acid, to form a cyclic amine. A widely accepted mechanism was later published by Corey *et al.* (Figure 67).¹⁸³ In the propagation cycle, 1,5-HAT is widely reported to be the rate-determining step.^{184–187} It should be noted that numbering of species restarts for each investigated radical reaction, for example, S1, R1 and P1 in the Barton reaction are not necessarily the same species as S1, R1 and P1 in the HLF reaction.

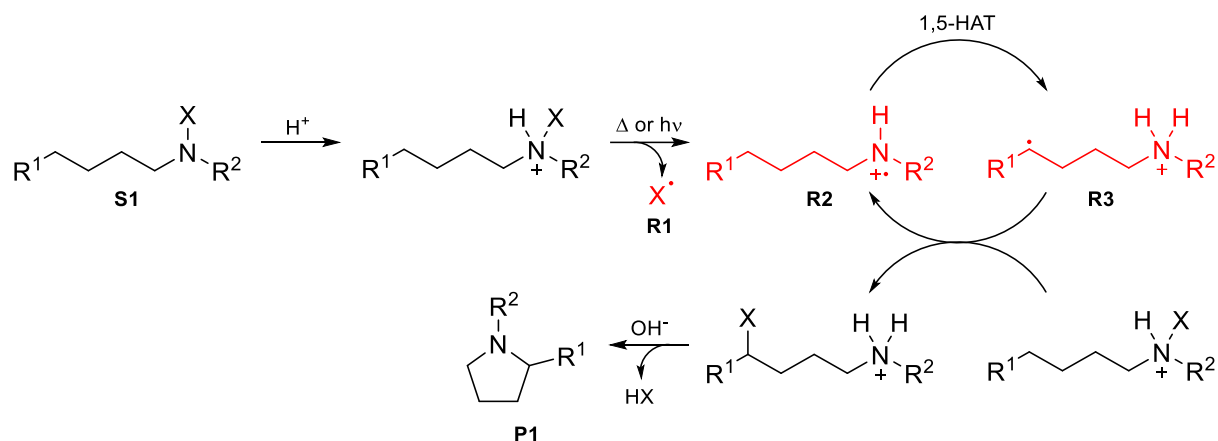


Figure 67: Widely accepted mechanism for *N*-haloamine HLF reaction, where typically X = Cl or Br.¹⁸³

TART trapping was applied to this reaction because of the difficulty in detecting its N-centred radical.^{188,189} As for the Barton reaction, TART trapping was first unsuccessfully performed using allyl-TEMPO, before later being successfully performed using CHANT. For this, a control reaction containing no TART and a trapping reaction containing TART were undertaken, using *N*-chlorodibutylamine as substrate and CHANT as TART (Figure 68). Aliquots were removed from these reaction mixtures pre-initiation and post-reaction and these aliquots MS characterised (Table 11, 11.4.3). R2 and R3 had the same molecular formulae and therefore, all R2/R3 related species could not be distinguished using standard MS.

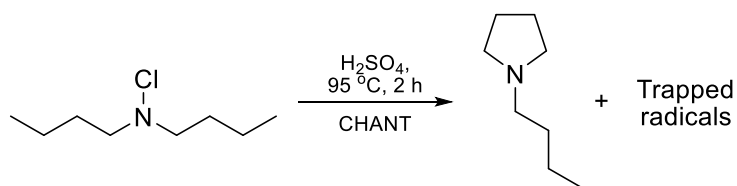


Figure 68: TART trapping of the HLF reaction, using *N*-chlorodibutylamine as substrate and CHANT as TART (11.4.3).

Table 11: Species identified from TART trapping of the HLF reaction, using *N*-chlorodibutylamine as substrate, CHANT as TART and MS for characterisation (11.4.3). Cl containing species are shown with ³⁵Cl only. Systematic *m/z* error = 0.0000; random *m/z* error = ±0.0009; 100% intensity = 2.14×10⁹ absolute count.

	Species	Predicted <i>m/z</i>	Intensity relative to unreacted TART pre-trapping reaction / %		
			Trapless control	Pre-initiation	Post-trapping
TART	[CHANT+H] ⁺	323.2698	0	100	47.2
Products	[<i>N</i> -Butylpyridine+H] ⁺	128.1439	0.003	0	0.157
	[<i>N</i> -Butylpyridine+Na] ⁺	150.1259	0	0	0
Trapped radicals	[R1-ART+H] ⁺	202.0999	0	0	0
	[R1-ART+Na] ⁺	224.0818	0	0	0
	[R1-TART+H] ⁺	357.2309	0	0	0.287
	[R2/R3-ART+H] ⁺	295.2749	0	0	23.8
	[R2/R3-ART+Na] ⁺	317.2569	0	0	0.729
	[R3-TEMPO+H] ⁺	285.2906	0.001	0	0.008
	[R2/R3-TART+H] ⁺	450.4059	0	0	0.021
Side products	[TART+HCl+H] ⁺	359.2465	0.002	0	0
	[TART+HOCl+H] ⁺	375.2414	0.009	0	0.312

Intensity of MS peaks corresponding to TART approximately halved during the trapping reaction, indicating TART trapping had occurred.

MS peaks corresponding to R2/R3-ART were observed exclusively post-trapping reaction, suggesting R2, R3 or both were formed during the HLF reaction. This agreed with the mechanism proposed by Corey *et al.* (Figure 67). Intensity of the [R2/R3-ART+H]⁺ corresponding peak was especially high, with intensity nearly half that of the peak corresponding to [TART+H]⁺. Assuming these two species ionised equally, this indicated that most TART was converted to R2/R3-ART. Since R2/R3-ART had identical molecular formulae, they could not be distinguished using standard MS. These observations indicated that TART and TART-trapped radicals were stable in mild acid and at high temperature. Peaks corresponding to R3-TEMPO were also detected, however with significantly weaker intensity than for R2/R3-ART.

In contrast, no peaks corresponding to R1-ART were detected. This was likely due to low Cl[•] flux, since Cl[•] was only produced during initiation and not during propagation. It was theorised that manipulation of reaction conditions could allow Cl[•] to be trapped, though this was not attempted.

MS peaks corresponding to R1-TART and R2/R3-TART were detected. R1-TART was particularly intensely observed, possibly due to reaction with Cl⁻ ions formed in the reaction. Alternatively, Cl[•] may have been abstracted from *N*-chlorodibutylamine following TART allyl radical formation. Peaks corresponding to R2/R3-TART were observed with significantly weaker intensity than for R2/R3-ART. This suggested that TART trapping was occurring far more readily than allylic HAA from TART, as desired. Radical trapping via allylic HAA from TART was monitored in all trapping reactions, however from here onwards, it is not reported unless deemed particularly significant.

Further investigations were performed to determine whether the peak corresponding to [R2/R3-ART+H]⁺ (*m/z* 295.275) corresponded to [R2-ART+H]⁺ or [R3-ART+H]⁺ or both. [R2-ART+H]⁺ and [R3-ART+H]⁺ would contain two and three labile hydrogen atoms respectively (Figure 69). Therefore, a D₂O exchange was performed to determine number of labile hydrogen atoms associated with each peak (Figure 70).

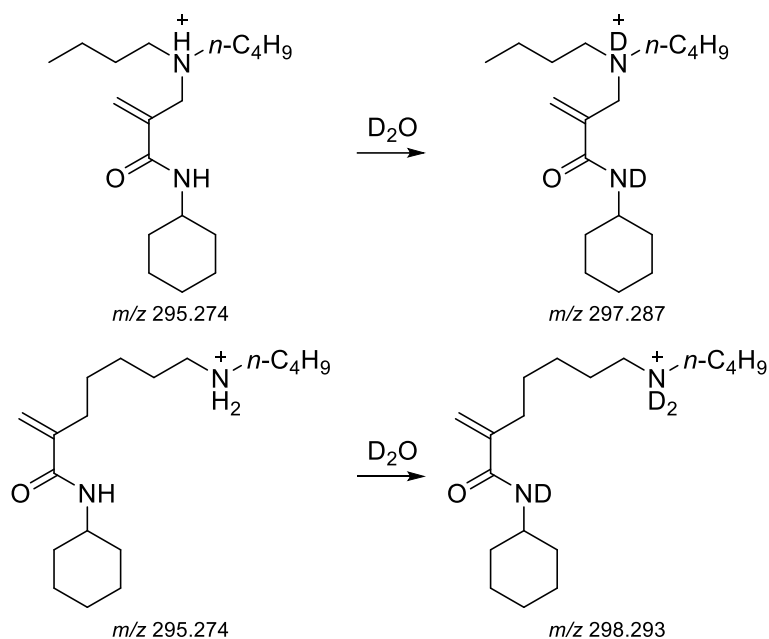


Figure 69: Total D exchange of [R2-ART+H]⁺ (top) and [R3-ART+H]⁺ (bottom), yielding 2D and 3D exchanges respectively.

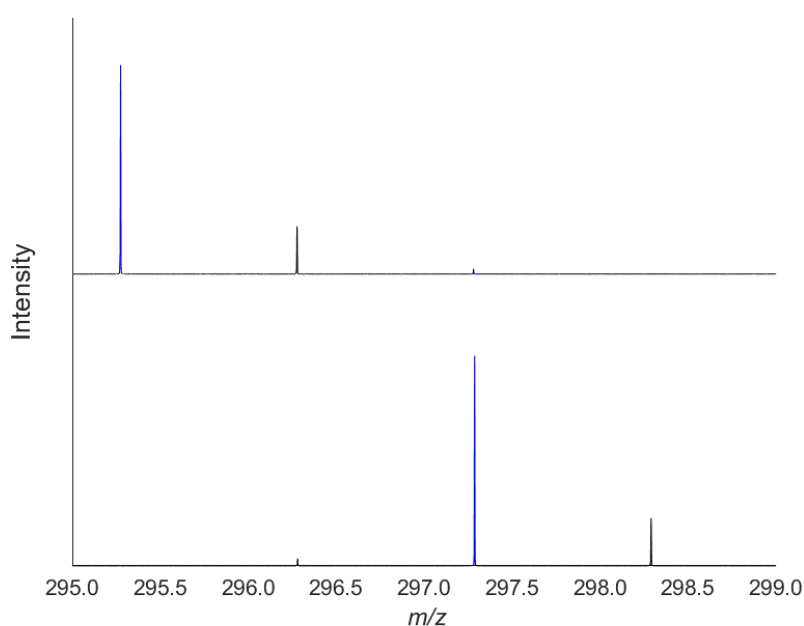


Figure 70: Background corrected mass spectra of TART trapping of the HLF, using *N*-chlorodibutylamine as substrate and CHANT as TART, MS characterised in protonated (top) and deuterated (bottom) solvent, showing peaks corresponding to R2/R3-ART (blue). 2D exchanges were observed (*m/z* 295.275), indicating R2-ART.

The *m/z* 295.275 peak shifted to *m/z* 297.287, corresponding to R2-ART. The peak predicted for deuterated R3-ART at *m/z* 298.294 was dominated by the first ¹³C satellite of the *m/z* 297.287 peak (*m/z* 298.291). Since each R2-ART and R3-ART species were expected to have similar ionisation efficiency, it was concluded that [R2-ART] was much greater than [R3-ART]. Therefore, these data indicated that R2 was produced in reaction mixtures, whilst there was no evidence that R3 was produced. High [R2] to [R3] ratio matched literature evidence that the 1,5-HAT was rate-determining.^{184–187} Further investigations were undertaken

to discover if R3 had also been trapped. Tandem MS was utilised to fragment the m/z 295.275 peak, to provide further structural information (Figure 71, 11.4.3).

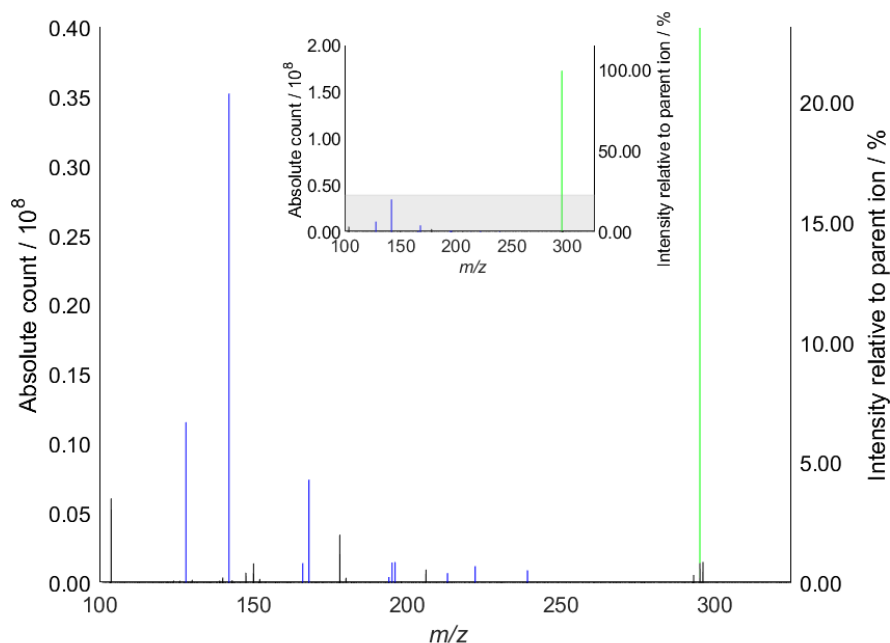


Figure 71: Tandem mass spectrum performed upon peak corresponding to $[R2/R3-ART+Na]^+$ (green) from TART trapping of the HLF reaction, using *N*-chlorodibutylamine as substrate and CHANT as TART, yielding suggested fragments. Structures were successfully assigned to most fragments (blue).

Whilst most peaks could be attributed to either TART-trapped radical, two low-intensity peaks could only be attributed to R3-ART (Figure 72, SI3.2.2). This indicated that R3 was also produced in reaction mixtures, albeit at much lower concentrations than R2. These observations offered validation to the widely accepted mechanism.^{183,190}

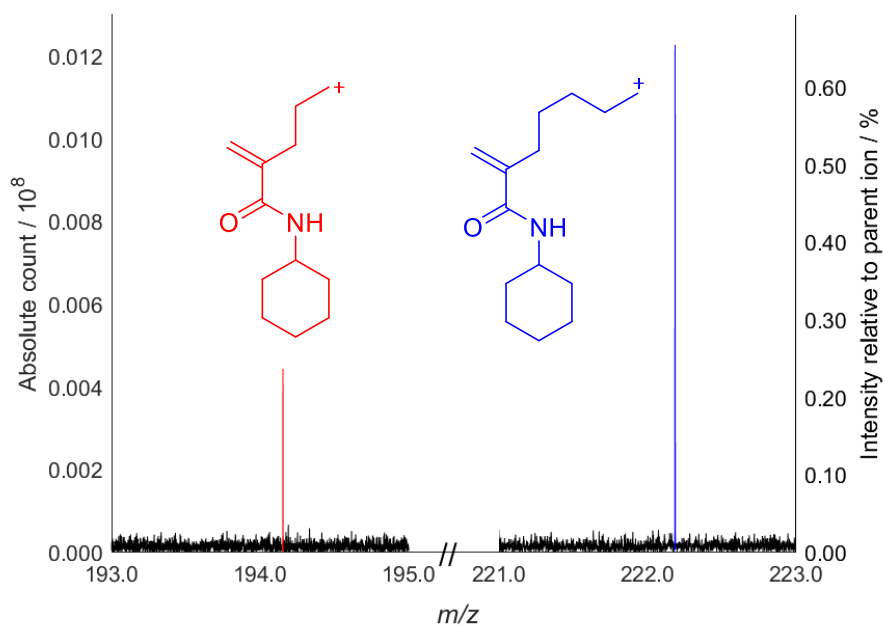


Figure 72: Tandem mass spectrum of m/z 295.275 peak from TART trapping of the HLF reaction, using *N*-chlorodibutylamine as substrate and CHANT as TART, yielding fragment peaks. Two fragment peaks could only be assigned to R3-ART corresponding structures (red and blue), indicating R3 was also trapped.

Further evidence for R3-ART formation was obtained using tandem MS upon deuterated samples. For this, the deuterated R2-ART corresponding peak at m/z 297.287 was fragmented (SI3.2.2). Intensity of the deuterated equivalents of the two fragmentations attributed exclusively to R3-ART (Figure 72, SI3.2.2) were diminished compared to other fragmentations. This suggested that these two fragments were not R2-ART related, which provided further evidence for R3-ART formation.

Furthermore, HPLC-MS was undertaken to further characterise R2-ART and R3-ART. Two intense chromatogram peaks corresponding to R2/R3-ART emerged, with a lower intensity maximum at 13.49 min and a greater intensity maximum at 13.62 min (Figure 73). A third significantly less intense peak was observed at 13.85 min. The two intense peaks were assumed to correspond to R2-ART and R3-ART, with the greater intensity peak (13.62 min) predicted to correspond to R2-ART, based on previously obtained D_2O exchange characterisation (Figure 70). The structure of the species corresponding to the third less intense peak (13.85 min) was unknown.

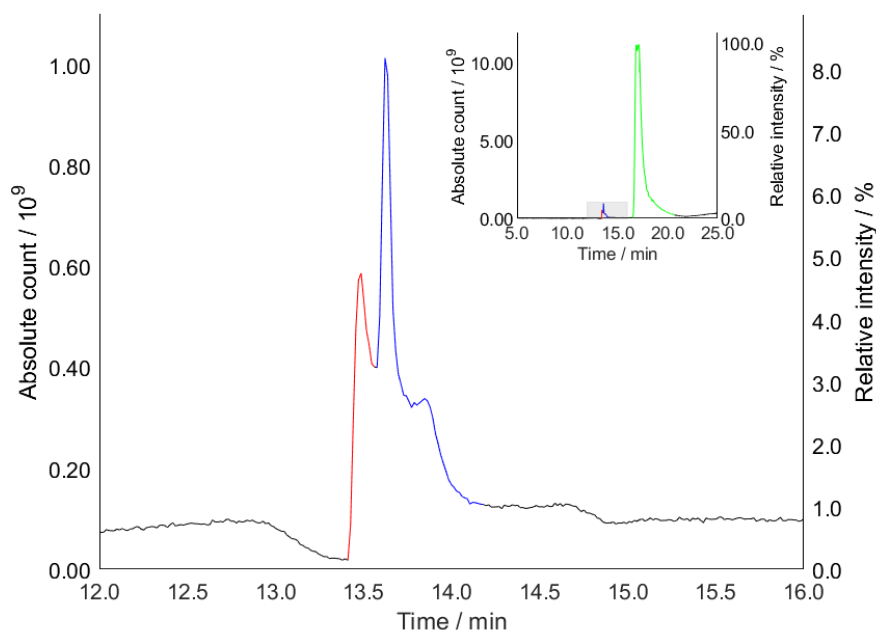


Figure 73: HPLC-MS chromatograms of the peak corresponding to $[R2/R3-ART+H]^+$ (m/z 295.275 \pm 0.002) and overall chromatogram (inset) detected from TART trapping of the HLF reaction, using *N*-chlorodibutylamine as substrate and CHANT as TART. A peak corresponding to unreacted CHANT dominated the chromatogram (green), whilst two intense peaks corresponding to $[R2/R3-ART+H]^+$ were also clearly visible (red, blue), with maxima at 13.49 min and 13.62 min respectively. This indicated that $[R2/R3-ART+H]^+$ was composed of at least two species. Further separation was attempted but not achieved.

Furthermore, tandem HPLC-MS was also undertaken upon the R2/R3-ART corresponding MS peak (m/z 295.275). Intensity of the two fragmentations attributed exclusively to R3-ART (Figure 72, SI3.2.2) were more intense for the first chromatogram peak (13.49 min) compared to the second (13.62 min), whilst other fragmentations were observed with similar intensity for both peaks (SI3.2.2). This suggested that the first peak was due to R3-ART, whilst the second was due to R2-ART. These data provided further evidence that both R2 and R3 were present in the reaction mixture and trapped, offering validation to the widely accepted mechanism.^{183,190} Tandem HPLC-MS of the third smaller peak indicated the corresponding species was similar in character to R2-ART. The relatively high intensity of R2-ART compared to TART, potentially made R2-ART a viable candidate for isolation and further characterisation, for example by NMR spectroscopy. However, this was not attempted.

Standard MS was also performed using the compact mass spectrometer, to show that lower resolution mass spectrometers were also suitable for characterisation of TART-trapped radicals. Peaks corresponding to TART and R2/R3-ART were the most intensely observed peaks in the mass spectrum, as previously (Figure 72).

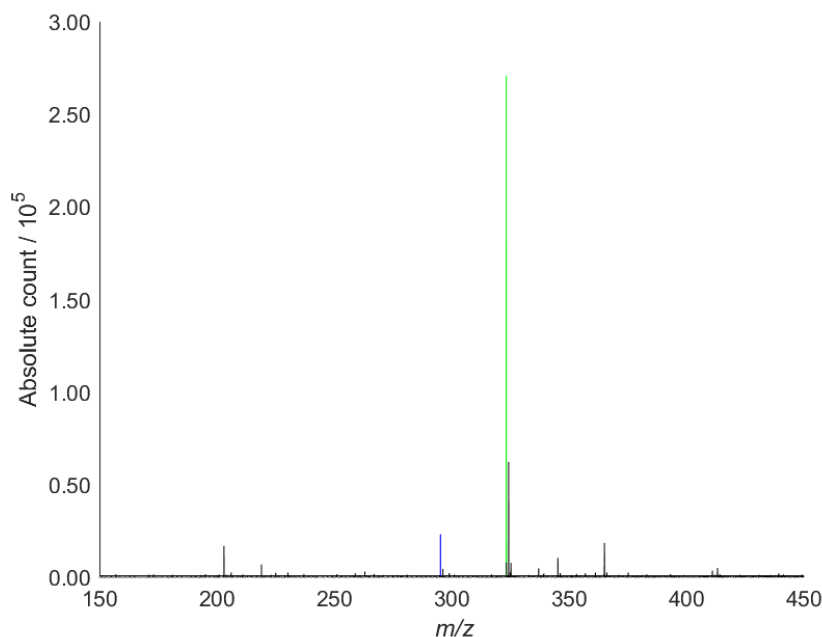


Figure 74: Mass spectrum from TART trapping of the HLF reaction, using *N*-chlorodibutylamine as substrate and CHANT as TART (11.4.3), showing peaks corresponding to unreacted TART (m/z 323.270, green) and R2/R3-ART (m/z 295.275, blue), recorded using the less high resolution compact mass spectrometer.

TART trapping of the HLF reaction using CHANT was successful and provided evidence which supported the widely accepted reaction mechanism proposed by Corey *et al.* (Figure 67) and that the 1,5-HAT step was rate-determining.^{183–187,190} Furthermore, D₂O exchange, tandem MS and HPLC-MS had been used effectively to aid characterisation of two species with identical molecular formulae.

5.3.3. Hunsdiecker reaction

The Hunsdiecker Reaction was discovered by Alexander Borodin in 1861, however was developed into a general method by Cläre and Heinz Hunsdiecker around 1940.^{191,192} The Hunsdiecker Reaction involves silver carboxylate decarboxylation and subsequent alkane bromination. The most widely accepted mechanism is still largely unproven (Figure 75).¹⁹³

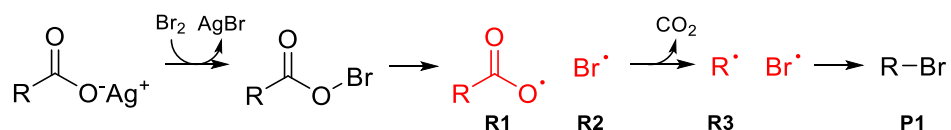


Figure 75: Proposed mechanism for the Hunsdiecker reaction.¹⁹³

Carboxyl radicals generally decarboxylate rapidly, with rate constants between $\sim 10^6$ - 10^9 s⁻¹ (\sim RTP) having been reported.^{194–196} However, carboxyl radicals also react rapidly with alkenes, with rate constants between $\sim 10^7$ - 10^9 M⁻¹ s⁻¹ (\sim RTP) having been reported.^{197–199} Therefore, it was deemed plausible that TARTs could be used to trapped carboxyl radicals, if used at suitably high concentrations.

As for the Barton reaction, TART trapping was first unsuccessfully performed using allyl-TEMPO, before later being successfully performed using CHANT. For this, a control reaction containing no TART and a trapping reaction containing TART (0.1 M, 0.2 eq.) were undertaken, using silver octanoate as substrate and CHANT as TART (Figure 76). Aliquots

were removed from these reaction mixtures pre-initiation and post-reaction and these aliquots MS characterised (Table 12, 11.4.4).

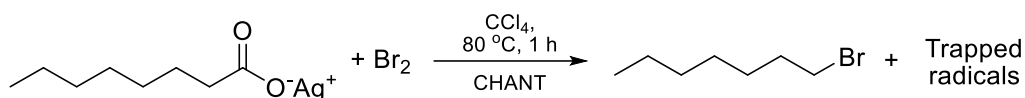


Figure 76: TART trapping of the Hunsdiecker reaction, using silver octanoate as substrate and CHANT as TART (11.4.4).

Table 12: Species identified from TART trapping of the Hunsdiecker reaction, using silver octanoate as substrate, CHANT as TART and MS for characterisation (Pos ESI, 11.4.4). Br containing species are shown with ^{79}Br only. Systematic m/z error = -0.0002; random m/z error = ± 0.0005 ; 100% intensity = 3.66×10^9 absolute count.

Species	Predicted m/z	Intensity relative to unreacted TART standard / %			
		Trapless control	Pre-initiation	Post-trapping	
TART	[CHANT+H] ⁺	323.2698	0.873	0	39.5
Trapped radicals	[R1-ART+H] ⁺	310.2382	0	0	0.001
	[R1-ART+Na] ⁺	332.2202	0.002	0	3.89
	[R2-ART+H] ⁺	246.0493	0	0	0
	[R2-ART+Na] ⁺	268.0313	0	0	0
	[R3-ART+H] ⁺	266.2484	0	0	0
	[R3-ART+Na] ⁺	288.2303	0	0	0
	[R3-TEMPO+H] ⁺	256.2640	0	0	0

CHANT was entirely consumed in the pre-initiation sample. The reason for this was unclear but was presumed to be due to unreacted Br_2 causing TART degradation. Therefore, intensities were set relative to an unreacted TART standard. In the post-trapping reaction, intensity of peaks corresponding to CHANT had decreased to approximately 40% of the unreacted TART standard. This indicated that around 60% TART was consumed during the trapping reaction.

A peak corresponding to R1-ART was observed exclusively post-trapping reaction, indicating that R1 was produced during the reaction. This agreed with the proposed Hunsdiecker mechanism (Figure 75). Alternatively, R1-ART could have been produced through octanoate undergoing Michael addition to TART and subsequent TEMPO⁻ cleavage. However, this was deemed unlikely, as this effect was not observed in control experiments, in which stronger diisopropylamine base was used (3.5.3). No peaks corresponding to R2-ART or R3-ART were observed. For R3-ART, it was hypothesised that efficient R1-ART formation or rapid R2-R3 radical coupling, caused [R3] to be low, preventing significant R3-ART formation. For R2-ART, since each R1 forming reaction also created an R2, if R1-ART was observed then R2-ART should also have been observed. It was hypothesised that R2-R2 radical termination may have occurred efficiently, reducing [R2] concentration. It is possible that R3 could still form product with terminated Br_2 . This was less likely to occur for R1, due to the formed $\text{RCO}_2\text{-O}_2\text{CR}$ terminated products having weak bond strengths. Alternatively, R2-ART may be poorly stable, either not forming or decomposing readily.

TART trapping of the Hunsdiecker reaction using CHANT was successful and had provided some evidence to support the widely accepted reaction mechanism proposed (Figure 75).

5.3.4. Conclusion

TART trapping was successfully used to study three old, well-known and widely used simple liquid phase synthetic radical reactions, using CHANT. Many hypothesised radicals were

successfully TART trapped and MS characterised, offering validation to previously suggested mechanisms and kinetic observations for these reactions. Additionally, this proved the viability of the TART trapping method as a new method for short-lived radical isolation and characterisation. Furthermore, TART trapping methodology and MS methodology were developed.

CHANT had successfully been used for TART trapping in these three reactions. However, early unsuccessful investigations utilised allyl-TEMPO as TART. Allyl-TEMPO was hypothesised to be unsuitable for TART trapping in these reactions because of the low ionisation efficiency of its allyl functionality. Furthermore, highly volatile radicals would also yield volatile allyl-TEMPO-trapped radicals. These would likely evaporate easily and be weakly detected using MS. Therefore, it was theorised that allyl-TEMPO could only be used upon liquid phase synthetic radical reactions which yielded radicals with suitably high ionisation efficiency and low volatility. This was largely untrue for the three previously explored reactions.

Therefore, after TART trapping of common synthetic radical reactions was performed unsuccessfully using allyl-TEMPO, and in absence of a more suitable TART, similar radical reactions which yielded radicals believed to be suitable for study with allyl-TEMPO, were investigated. For this, TART trapping using allyl-TEMPO was performed upon a suitable modern reaction, to investigate its mechanistic aspects (5.4).

5.4. Modern reactions

Contrary to the common synthetic radical reactions (5.3), investigated modern reactions were newer, less well-known and little used. Early reactions were discovered through serendipity, as mechanisms were less well understood at the time. Their mechanisms were later investigated and hypothesised using experimental evidence. In contrast, modern reactions are usually designed based on existing mechanistic knowledge. Therefore, when a modern reaction is published, it is normally accompanied by a hypothesised mechanism. However, this often means that the predicted mechanism is not thoroughly investigated.

Whilst these reactions were less ideal for preliminary investigations, since their mechanisms were not widely proven, there was not believed to be a viable alternative at the time. Therefore, a modern radical aromatic aminophosphinoylation reaction had its mechanism probed using TART trapping with allyl-TEMPO.

5.4.1. Radical aromatic aminophosphinoylation

Wang *et al.* developed a radical aromatic aminophosphinoylation reaction, using different styrenes, anilines and diphenylphosphine oxide (DPPO) as substrates, FeCl₃ as catalyst and ^tBuOOH as initiator, producing 64-87% yields. Wang *et al.* also suggested a mechanism for this reaction (Figure 77), though they did not undertake experiments to validate it.²⁰⁰

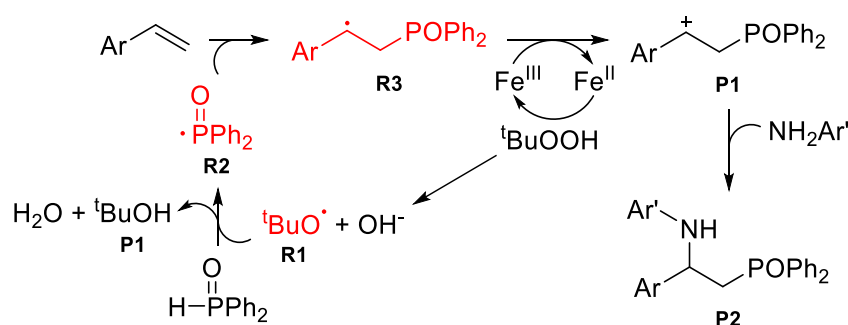


Figure 77: Proposed mechanism for radical aromatic aminophosphinoylation.²⁰⁰

This reaction was designated appropriate for allyl-TEMPO trapping due to the low volatility and relatively high ionisation efficiency of radicals. Therefore, TART trapping of radical aromatic aminophosphinylation was undertaken, using allyl-TEMPO as TART. For this, a trapless control reaction and a trapping reaction containing TART were undertaken, using 4-methylstyrene, 4-chloroaniline and DPPO as substrates (Figure 78). In TART absence, this reaction yielded 83% product.²⁰⁰ Aliquots were removed from these reaction mixtures pre-initiation and post-trapping and these aliquots MS characterised (Table 13, 11.4.5).

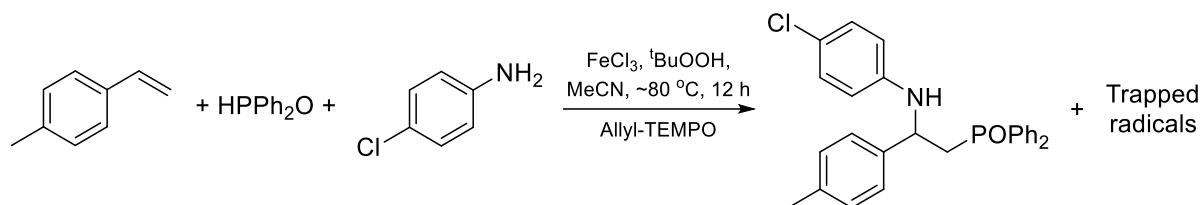
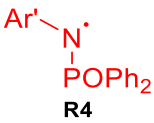


Figure 78: TART trapping of radical aromatic aminophosphinylation, using 4-methylstyrene, 4-chloroaniline and DPPO as substrates and allyl-TEMPO as TART (11.4.5).

Table 13: Species identified from TART trapping of radical aromatic aminophosphinylation, using 4-methylstyrene, 4-chloroaniline, and DPPO as substrates, allyl-TEMPO as TART and MS for characterisation (11.4.5). Cl containing species are shown with ³⁵Cl only. Systematic *m/z* error = -0.0008; random *m/z* error = ±0.0004; 100% intensity = 6.68×10⁶ absolute count.

Species	Predicted <i>m/z</i>	Intensity relative to unreacted TART pre-trapping reaction / %			
		Trapless control	Pre-initiation	Post-trapping	
TART	[Allyl-TEMPO+H] ⁺	198.1858	0	100	34.6
Reactants	[DPPO+H] ⁺	203.0626	8.41	5740	16.8
	[DPPO+Na] ⁺	225.0445	0	33.7	0
Products	[P1] ⁺	319.1252	32200	2080	35300
	[P2+H] ⁺	446.1440	0	0	0
	[P2+Na] ⁺	468.1260	206	0	448
Suggested trapped radicals	[R1-ART+H] ⁺	115.1123	0	0	0
	[R1-ART+Na] ⁺	137.0942	0	0	0.32
	[R2-ART+H] ⁺	243.0939	0	1.78	19.7
	[R2-ART+Na] ⁺	265.0758	0	0	0
	[R2-TEMPO+H] ⁺	358.1936	0	0	0
	[R3-ART+H] ⁺	361.1721	0	0	48.6
	[R3-ART+Na] ⁺	383.1541	0	0	12.1
[R3-TEMPO+H] ⁺	476.2718	0	0	3.35	
Other trapped radical	[R4-ART+H] ⁺	368.0971	0	0	2.93
	 [R4-ART+Na] ⁺	390.0790	0	0	0
Side products	[R3-H+H] ⁺	321.1408	158	0.833	866
	[R3-H+Na] ⁺	343.1228	4.22	0	69.0
	[R3-R2+H] ⁺	521.1799	97.4	0	313
	[R3-R2+Na] ⁺	543.1619	17.9	0	79.4
	[R3-R4+H] ⁺	646.1831	0	0	11.8
	[R3-R4+Na] ⁺	668.1651	14.6	1.15	51.9

	[R4-H+H] ⁺	328.0658	314	538	233
Side products	[R4-H+Na] ⁺	350.0477	0	11.4	0
	[R4-R4+H] ⁺	528.1049	29.0	0	21.2
	[R4-R4+Na] ⁺	550.0868	3.77	0	3.62

MS peaks corresponding to TART decreased to around a third from pre-initiation to post-trapping, which indicated approximately two thirds of TART was consumed during the trapping reaction.

DPPO was the only detectable reactant, with intensity of its MS corresponding peaks being decreased by >99% post-trapping, suggesting >99% DPPO had reacted. The MS peak corresponding to P1 was observed with very high intensity, likely due to P1 being inherently ionised, offering mechanistic validity. MS peaks corresponding to P2 were detected in the trapless control and post-trapping, indicating product could be formed even in TART presence. This theoretically allowed for formation of all hypothesised radicals.

Peaks corresponding to R1-ART, R2-ART and R3-ART were observed exclusively or with much greater intensity post-trapping, compared to other samples. This indicated radicals R1, R2 and R3 were produced during the reaction, offering mechanistic validity. MS peaks corresponding to R2-TEMPO were not detected, likely due to N-O-P bond formation being unfavourable, showing TART trapping superiority over TEMPO• trapping.

Additionally, peaks corresponding to R4-ART were also detected, suggesting a radical R4 was produced during the reaction, which had not previously been hypothesised. This radical species likely formed through R2 reaction with 4-chloroaniline. Additionally multiple side products were also detected. These observations offered potential side radicals and side products formed during radical aromatic aminophosphinylation, potentially explaining the 17% yield loss observed in TART absence.²⁰⁰

Tandem MS was conducted upon MS peaks corresponding to R2-ART and R3-ART, yielding many fragments which sensibly corresponded to the predicted TART-trapped radical structures (SI3.3).

These data gave significant validation to the proposed radical aromatic aminophosphinylation mechanism, which was otherwise largely unproven. It also proved that liquid phase synthetic radical reactions could be studied using TART trapping and hence validated that TART-trapped radicals were not observed for the common synthetic radical reaction, due to allyl-TEMPO being unsuitable for TART trapping in these reactions. Once amide-functionalised TARTs were synthesised, the common synthetic radical reactions were reinvestigated (5.3). Subsequently, TART trapping was applied to a modern decarboxylative aromatic iodination radical reaction using amide-functionalised TARTs (5.4.2). However, in the radical aromatic aminophosphinylation reaction, all hypothesised radicals were observed and hence, this reaction was not reinvestigated using CHANT as TART.

5.4.2. Radical decarboxylative aromatic iodination

Perry *et al.* developed a radical decarboxylative aromatic iodination, using different benzoic acid derivatives and iodine as reactants and K₃PO₄ as base, producing 0-99% yields. Perry *et al.* suggested a possible radical decarboxylation-radical recombination pathway (Figure 79).²⁰¹ This reaction and its suggested mechanism are similar to the Hunsdiecker reaction (5.3.3), but do not require transition metal catalyst.

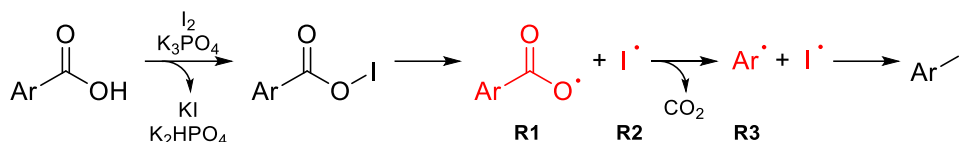


Figure 79: Proposed mechanism for reaction performed by Perry *et al.*²⁰¹

Perry *et al.* later concluded that the mechanism actually occurred through a non-radical concerted decarboxylation-iodination pathway, evidenced using radical clock and DFT experiments.²⁰¹ Nevertheless, it was decided to investigate this reaction using TART trapping, to determine if the previously hypothesised radical mechanism occurs.

Therefore, TART trapping of radical decarboxylative aromatic iodination was undertaken, using CHANT as TART. For this, a control reaction containing no TART and a trapping reaction containing TART were undertaken, using *p*-anisic acid as substrate. In TART absence, Perry *et al.* reported a 93% yield for this reaction.²⁰¹ Samples were removed from these reaction mixtures pre-initiation and post-reaction and these samples MS characterised (Table 14, 11.4.6).

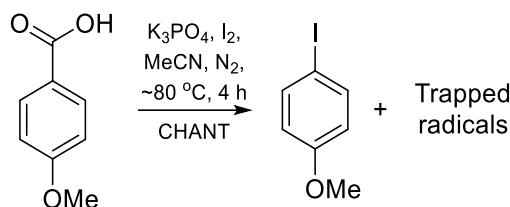


Figure 80: TART trapping of radical decarboxylative aromatic iodination, using *p*-anisic acid as substrate and CHANT as TART (11.4.6).

Table 14: Species identified from TART trapping of radical decarboxylative aromatic iodination, using *p*-anisic acid as substrate, CHANT as TART and MS for characterisation (11.4.6). Systematic *m/z* error = -0.0001; random *m/z* error = ± 0.0006 ; 100% intensity = 4.71×10^9 absolute count.

Species	Predicted <i>m/z</i>	Intensity relative to unreacted TART pre-trapping reaction / %			
		Trapless control	Pre-initiation	Post-trapping	
TART	[CHANT+H] ⁺	323.2698	3.08	100	22.0
	[R1-ART+H] ⁺	318.1705	0	0	4.32
	[R1-ART+Na] ⁺	340.1525	0.018	0.004	3.32
Trapped radicals	[R2-ART+H] ⁺	294.0355	0	0.002	0.013
	[R2-ART+Na] ⁺	316.0174	0	0.009	0.012
	[R3-ART+H] ⁺	274.1807	0	0	0.011
	[R3-ART+Na] ⁺	296.1626	0	0	0
	[R3-TEMPO+H] ⁺	264.1963	0.001	0	0

Intensity of MS peaks corresponding to TART decreased to ~20% from pre-initiation to post-trapping, which implied ~80% TART was consumed during the trapping reaction. No peaks corresponding to reactants or products were observed, likely due to these species having poor ionisation efficiency.

MS peaks corresponding to R1-ART, R2-ART and R3-ART were observed exclusively or with much greater intensity post-trapping, compared to other samples. This indicated radicals R1, R2 and R3 were produced during the reaction, supporting the radical pathway previously hypothesised by Perry *et al.* However, this contradicted Perry *et al.* who concluded that the

mechanism was non-radical. MS peaks corresponding to R3-TEMPO were not detected, showing TART trapping superiority over TEMPO• trapping.

Additional MS characterisation was undertaken to provide further evidence for TART-trapped radical structures. Tandem MS was conducted upon MS peaks corresponding to R1-ART and R3-ART yielding many fragments which sensibly corresponded to the predicted TART-trapped radical structures (SI3.4). Furthermore, HPLC-MS chromatograms indicated a single structure for each TART-trapped radical, as expected (Figure 81, SI3.4).

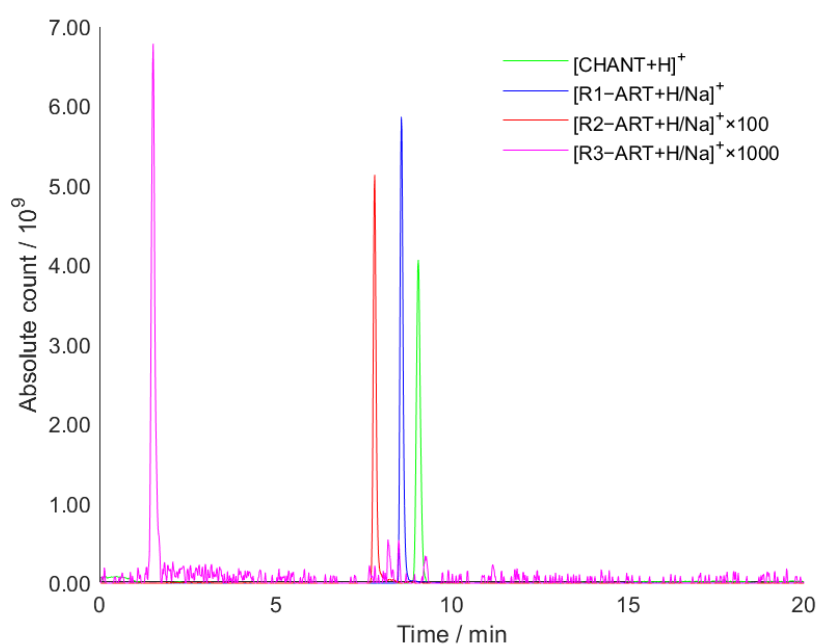


Figure 81: HPLC-MS chromatograms of peaks corresponding to [CHANT+H]⁺ (m/z 323.270±0.002, 9.06 min), [R1-ART+H/Na]⁺ (m/z 318.171±0.002 and m/z 340.152±0.002, 8.57 min), [R2-ART+H/Na]⁺ × 100 (m/z 294.035±0.002 and m/z 316.017±0.002, 7.82 min) and [R3-ART+H/Na]⁺ × 1000 (m/z 274.181±0.002 and m/z 296.163±0.002, 1.53 min) detected from TART trapping of radical decarboxylative aromatic iodination, using *p*-anisic acid as substrate and CHANT as TART (11.4.6).

These observations further supported the hypothesised TART-trapped radical structures. Whilst presence of radicals does not necessarily indicate the reaction proceeds via a radical pathway, it is suggested that the radical pathway previously hypothesised by Perry *et al.* may proceed to at least some extent.

TART trapping was successfully used to study the mechanism of radical decarboxylative aromatic iodination. Many previously hypothesised radicals were successfully TART trapped and MS characterised, offering new mechanistic insights. Additionally, this proved the viability of the TART trapping method as a new method for short-lived radical isolation and characterisation. Further liquid phase synthetic radical reactions were explored, which were photoinitiated (6).

5.5. Conclusions and future work

TART trapping was successfully used to investigate a wide variety of synthetic radical reactions, including well-established reactions, such as the Barton reaction, Hofmann-Löffler-Freytag (HLF) reaction and the Hunsdiecker reaction, and newly developed reactions. From these reactions, many hypothesised radicals were successfully TART trapped and MS characterised. These included carbon-centred and heteroatom-centred radicals, such as

nitrogen-, oxygen-, phosphorus- and sulfur-centred radicals. In contrast, recombination trapping using nitroxyl radicals is usually not suitable for studying heteroatom-centred radicals (1.3.2.2). Results also indicated that TART trapping occurred significantly faster than side reactions of TART involving HAA from allylic C–H.

TART trapping was conducted under a range of conditions including: strong acid at high temperature (95 °C) for 2 h; strong base at high temperature (~80 °C) for 4 h; weak base under UV for 1 h and at high temperature (~80 °C) for 12 h in presence of a metal catalyst. Observations of peaks corresponding to TART-trapped radicals under these conditions showed that TARTs and TART-trapped radicals were stable under fairly harsh conditions. This contrasts to spin traps, which are highly vulnerable to metal catalysts, showing a significant advantage of TART trapping over spin trapping (1.3.2.1).¹²⁸ Furthermore, studying short-lived radicals formed during these reactions, using direct radical characterisation techniques, would have been very challenging, if not impossible, under all these reaction conditions (1.3.1). Therefore, TART trapping offered advantages over all existing radical characterisation techniques, for studying these synthetic radical reactions.

TART trapping results offered validation to hypothesised and widely accepted mechanisms and kinetic observations. For example, TART trapping of the HLF reaction indicated presence of the nitrogen-centred radical (R2) and carbon-centred radical (R3) formed following 1,5-HAT proposed in literature. Furthermore, observations showed that R2 was the radical resting state in the reaction, agreeing with literature that the 1,5-HAT was rate determining.

These investigations proved the viability of TART trapping and MS characterisation as a new method for short-lived radical isolation and characterisation. Furthermore, it showed that TART trapping and MS characterisation could offer mechanistic and kinetic information to synthetic radical reactions. This information could be used to develop and improve such reactions, for example by increasing product yields.

These studies also aided development of TART trapping, MS characterisation and mass spectra analysis methodology. In particular, it was discovered that Grantham TART and allyl-TEMPO were generally inferior to amide-functionalised TARTs for TART trapping. Therefore, from here onwards, TART trapping was only undertaken using amide-functionalised TARTs. Furthermore, investigations showed that using a high-resolution mass spectrometer was essential for complex reaction mixtures. D₂O exchange, tandem MS and HPLC-MS were also used effectively to further characterise TART-trapped radicals.

These TART trapping studies were preliminary and much deeper investigations could be undertaken upon all synthetic radical reactions explored. For all reactions this could include: effect of different substrates; substrate concentration; different TART concentration and functionality; experimental conditions; kinetics investigations; D₂O exchange studies; tandem MS studies and HPLC-MS studies. Kinetic modelling would also allow results to be more fully interpreted, for example to convert intensity of MS peaks corresponding to TART-trapped radicals into relative concentrations of radicals.

D₂O exchange MS characterisation of the Barton reaction could indicate presence of R2-ART, R3-ART or both. This could offer the proposed mechanism further validation.

Furthermore, investigation into the effect of using different substrates in the HLF reaction, could provide kinetic insights. Many studies report that HLF reaction efficiency is highly dependent on *N*-haloamine structure. This is because *N*-haloamine structure determines radical stability and therefore, governs propagation and chain transfer rates.^{184–187} For example, propagation rate would likely be faster for *N*-chloro-*N*-methyl-4-phenylbutylamine than *N*-chloro-*N*-methyl-butylamine, due to aromatic resonance stabilisation of carbon-centred

radical R3. Therefore, changing substrate structure would likely affect concentration of nitrogen-centred radical R2 and carbon-centred radical R3. TART-trapping could be used to monitor [R2] and [R3] via MS intensities of R2-ART and R3-ART. Furthermore, R2-ART may be suitable for isolation and further characterisation, for example by NMR spectroscopy, providing further evidence for R2-ART structure. From this, MS calibration curves could be made for R2-ART, to obtain better quantification of TART trapping in the HLF reaction. Additionally, reaction conditions could be altered to favour R1-ART formation.

TART trapping had offered mechanistic and kinetic information to these synthetic radical reactions. Additionally, TART trapping had been successfully performed in the presence of UV in the Barton reaction. Therefore, TART trapping was applied to photochemical radical reactions (6). In recent years, these reactions have gained a lot of attention (1.2.1) and hence information regarding their mechanisms and kinetics obtained using TART trapping would be of greater interest.

6. Photochemistry

6.1. Introduction

Photochemistry uses light absorption to activate chemical reactions. Photochemistry often employs a photoredox catalyst, which absorbs light and subsequently activates and catalyses a chemical reaction through single electron transfer processes (1.2.1).^{6,7} Historically, photochemistry reactions have been discovered and optimised through empirical findings. Although reaction mechanisms have often been hypothesised, significant proof of hypothesised mechanisms and utilisation of mechanistic understanding for further reaction development are unusual.²⁰²

More recently however, the importance of mechanistic understanding of photochemical reactions has increased. It is believed that better understanding radical reaction mechanisms, including initiation and main radical cycle mechanisms, may help optimise reaction conditions to improve product yields, substrate scope and industrial viability.

It was hypothesised that TART trapping could be used to probe photochemistry mechanisms. A collaboration was sought with Dr. William Unsworth at the University of York to explore TART trapping within such systems. All these reactions used a general methodology (6.2).

First, TART trapping was tested in a Ru-photocatalysed radical cyanomethylation, offering validation to the suggested mechanism (6.3). Once it was discovered that TART trapping could be used to trap and characterise radicals in photocatalytic systems, TART trapping was used to investigate many aspects of a more generic Ru-photocatalysed radical thiol-ene addition (6.4). Using the knowledge gained from TART trapping of this reaction, TART trapping was used to investigate a niche catalyst-free photoinitiated radical dearomative spirocyclisation, which was closely related to radical thiol-ene addition (6.5).

6.2. Methodology and controls

TART trapping in photochemistry systems broadly followed the general methodology for TART trapping (4). Additionally, photochemistry systems used blue LEDs (60 W) for photoinitiation. All trapping reactions used CHANT as TART, due to its high stability in solution and otherwise relatively low chemical reactivity.

Absorbance of ultraviolet-visible light (250-800 nm) by CHANT was measured using ultraviolet-visible (UV-Vis) spectroscopy. This was to ensure CHANT did not absorb light from the blue LEDs (455 nm) used for radical thiol-ene addition photoinitiation, which may have caused CHANT to be non-innocent in the thiol-ene addition radical cycle. The resulting UV-Vis spectrum showed CHANT did not absorb light above 350 nm, ensuring CHANT could not contribute to photoinitiation (Figure 82). As such, TART trapping of photochemical radical reactions was undertaken.

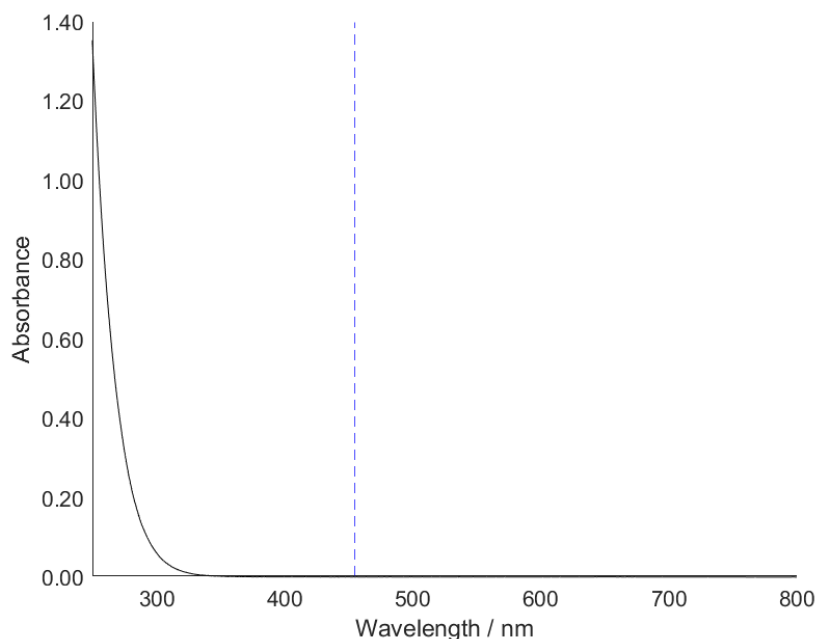


Figure 82: UV-Vis spectrum of CHANT (10.0 mM) in MeCN. Wavelength of blue LED irradiation (455 nm), used for TART trapping of radical thiol-ene addition, is indicated (blue dashed line).

6.3. Radical cyanomethylation

Donald *et al.* developed a general Ru-photocatalysed radical cyanomethylation reaction, using a great variety of compounds and 3-azido-2-methylbut-3-en-2-ol as reactants, $[\text{Ru}(\text{bpy})_3]^{2+}$ as photocatalyst and 2,6-lutidine as base, forming 31 products with ~36-100% yields over 4-24 h. Donald *et al.* also suggested a mechanism for this reaction (Figure 83), though did not undertake experiments to validate this mechanism.²⁰³

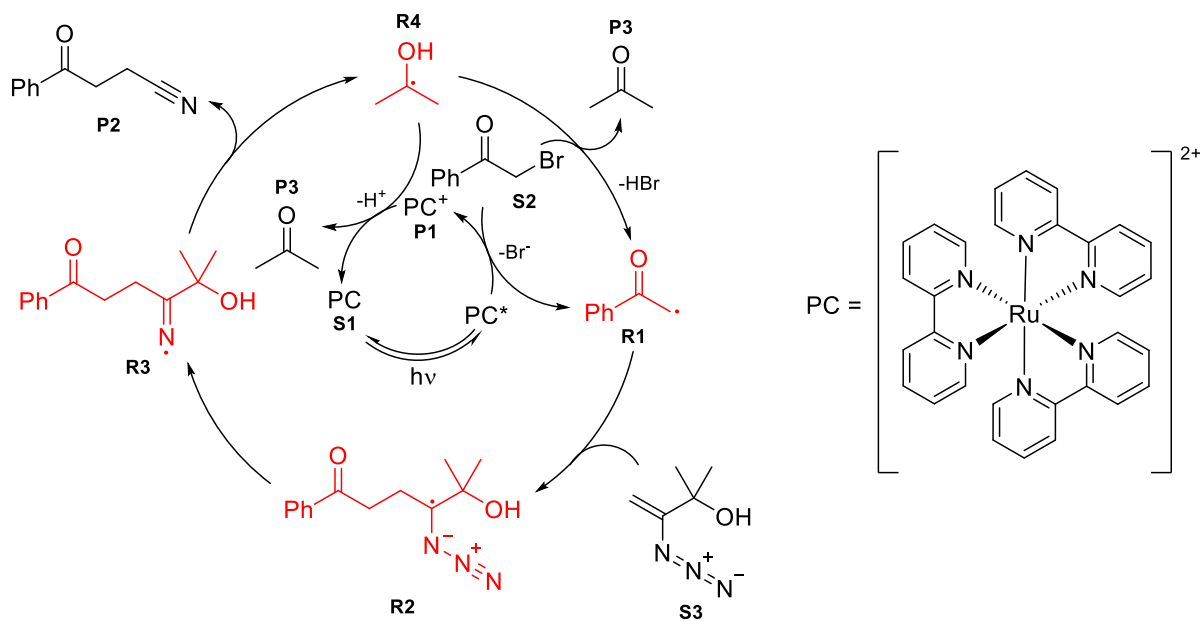


Figure 83: Mechanism of Ru-photocatalysed radical cyanomethylation, using 2-bromoacetophenone as substrate, proposed by Donald *et al.*²⁰³

TART trapping of radical cyanomethylation was undertaken, using CHANT as TART. For this, a control reaction containing no TART and a trapping reaction containing TART were undertaken, using 2-bromoacetophenone as substrate (11.5.1). In TART absence, this reaction yielded 97% product.²⁰⁰ Aliquots were removed from these reaction mixtures pre-initiation and post-trapping and these aliquots MS characterised (Table 15, 11.5.1). Dr. James Donald synthesised the starting materials and performed the trapping reactions and controls. MS characterisation and mass spectra analysis performed by the author.

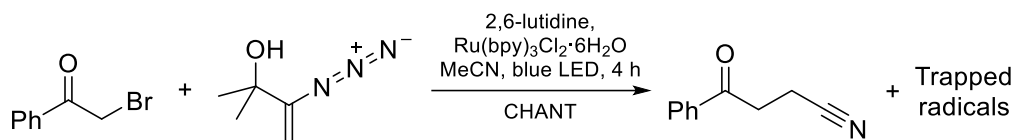


Figure 84: TART trapping of Ru-photocatalysed radical cyanomethylation, using 2-bromoacetophenone as substrate and CHANT as TART (11.5.1).

Table 15: Species identified from TART trapping of Ru-photocatalysed radical cyanomethylation, using MS for characterisation (11.5.1). Systematic m/z error = -0.0006; random m/z error = ± 0.0013 ; 100% intensity = 1.64×10^9 absolute count.

	Species	Predicted m/z	Intensity relative to unreacted TART pre-initiation / %		
			Trapless control	Pre-initiation	Post-trapping
TART	[CHANT+H] ⁺	323.2698	0	100	47.2
Reactants	[S1] ²⁺	285.0553	0.348	4.05	0
	[S2+Na] ⁺	220.9578	0	0	0
	[S3+Na] ⁺	150.0643	0	0	0
Trapped radicals	[R1-ART+Na] ⁺	308.1626	0	0.065	4.40
	[R1-TEMPO+H] ⁺	298.1783	0	0	0.122
	[R2-ART+Na] ⁺	435.2372	0	0	0
	[R2-TEMPO+H] ⁺	425.2528	0	0	0
	[R3-ART+Na] ⁺	407.2311	0	0	0
	[R4-ART+Na] ⁺	248.1626	0	0.025	0.773
	[R4-TEMPO+H] ⁺	238.1783	0	0	0
Products	[P1] ³⁺	190.7087	0	0.043	0
	[P2+Na] ⁺	182.0582	0.024	0.002	0.011
Other products	[¹⁰¹ Ru(bpy) ₂ ³⁵ Cl ⁷⁹ Br] ⁺	527.9290	0.024	0	0.344
	[¹⁰¹ Ru(bpy) ₂ ⁷⁹ Br ⁸¹ Br] ⁺	573.8765	0.350	0	19.9
	[¹⁰¹ Ru(bpy) ₂ ⁷⁹ Br] ⁺	492.9602	11.3	4.42	3.25

Intensity of MS peaks corresponding to CHANT approximately halved from pre-initiation to post-trapping, indicating around half of CHANT was consumed during the trapping reaction.

No peaks corresponding to S2, S3 or P2 were observed, likely due to these species having poor ionisation efficiency. Peaks corresponding to Ru-photocatalyst S1 were observed significantly more intensely pre-initiation compared to other samples, indicating that the catalyst degraded during the reaction. Peaks corresponding to P2 were detected in the trapless control and post-trapping, indicating product could be formed even in TART presence. This theoretically allowed for formation of all hypothesised radicals. Additionally, peaks corresponding to other Ru complexes were observed, indicating catalyst degradation. These complexes were clearly recognisable by their distinctive isotopic profile (Figure 85), allowing their structures to be suggested. Simulation of the expected isotopic distribution patterns of the suggested Ru complexes matched the observed isotopic profiles. [¹⁰¹Ru(bpy)₂⁷⁹Br]⁺ was

likely to be an MS artefact formed from $[^{101}\text{Ru}(\text{bpy})_2\text{Br}^{79}\text{Br}]$, which was chargeless and therefore unobservable using MS. Therefore, $[\text{Ru}(\text{bpy})_2\text{Br}_2]$ and $[\text{Ru}(\text{bpy})_2\text{Br}_2]^+$ were hypothesised to be the two most significant catalyst degradation products. Although these species were unrelated to radical trapping, they did offer some mechanistic insights.

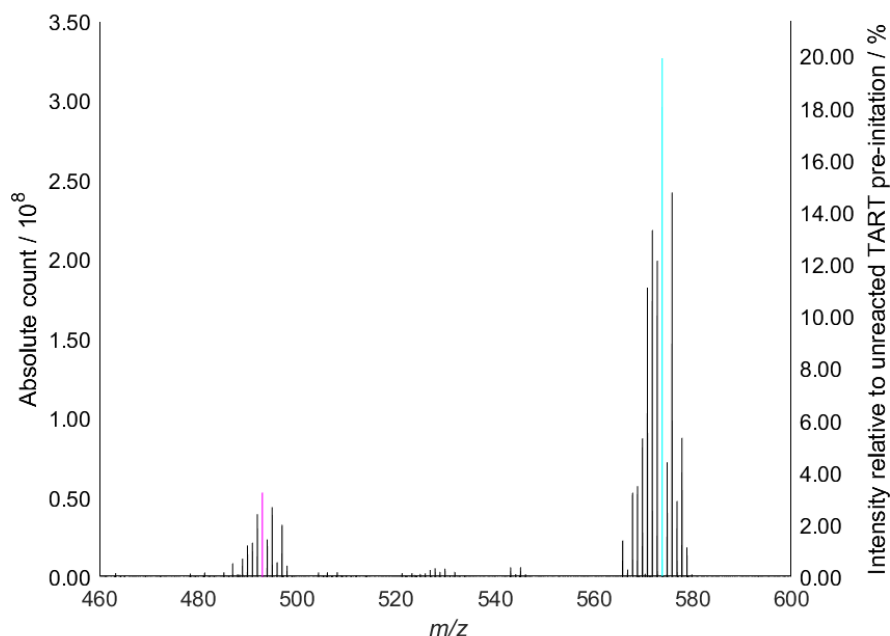


Figure 85: Mass spectrum from TART trapping of radical cyanomethylation (11.5.1), showing two most intense sets of peaks corresponding to Ru complexes, with $[^{101}\text{Ru}(\text{bpy})_2^{79}\text{Br}]^+$ (m/z 492.960, pink) and $[^{101}\text{Ru}(\text{bpy})_2^{79}\text{Br}^{81}\text{Br}]^+$ (m/z 573.876, sky blue) highlighted. 100% intensity = 1.64×10^9 absolute count.

Peaks corresponding to R1-ART and R4-ART were observed exclusively or with much greater intensity post-trapping, compared to other samples. Post-trapping, these peaks were observed with high intensity compared to neighbouring peaks (Figure 86). This indicated radicals R1 and R4 were produced during the reaction, as expected. Furthermore, peaks corresponding to R1-ART were significantly more intense than R4-ART, possibly due to R4 being formed later in the reaction cycle, meaning R4 radical flux would be lower, due to chain termination through trapping. These observations supported the hypothesised mechanism (Figure 83). In contrast, peaks corresponding to R1-TEMPO and R4-TEMPO were observed with significantly lower intensity, showing TART trapping superiority over TEMPO[•] trapping.

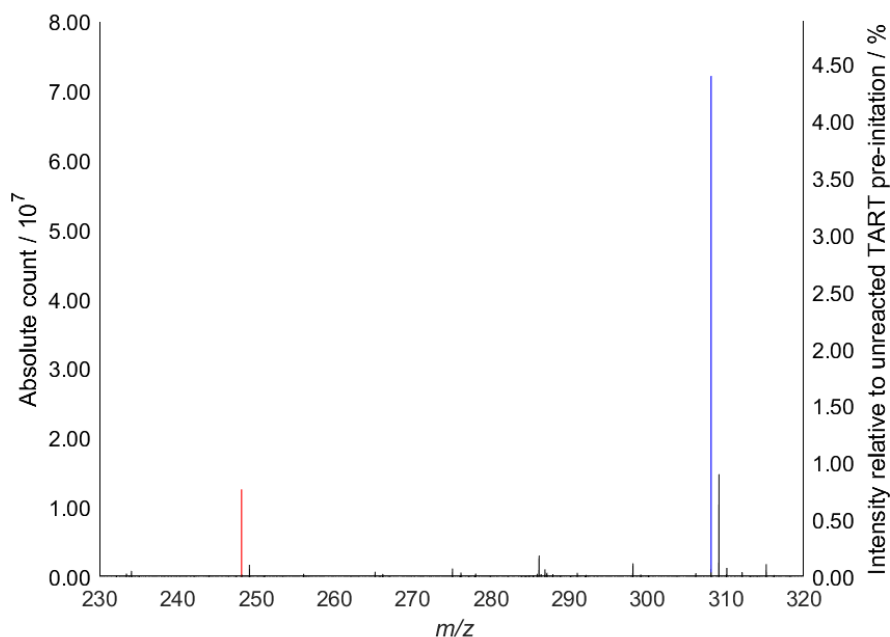


Figure 86: Mass spectrum from TART trapping of radical cyanomethylation (11.5.1), highlighting peaks corresponding to R1-ART (m/z 308.163, blue) and R4-ART (m/z 248.163, red). 100% intensity = 1.64×10^9 absolute count.

Peaks corresponding to trapped R2-ART and R3-ART were not observed. It was hypothesised that the suggested R2 and R3 intramolecular reactions occurred too quickly for trapping to occur. This indicated a limitation of TART trapping, that TART trapping may not be able to detect radicals which undergo fast intramolecular reactions.

Tandem MS was conducted upon $[R1-ART+H]^+$ (m/z 286.181) and $[R4-ART+H]^+$ (m/z 226.181) corresponding peaks, yielding many fragments which sensibly corresponded to the predicted TART-trapped radical structures (SI4.1). Additionally, for $[R4-ART+H]^+$ one fragment peak likely corresponded to dehydration, indicating an alcohol with neighbouring β -hydrogen atom, validating the hypothesised R4 structure.

TART trapping was successfully used to study the mechanism of Ru-photocatalysed radical cyanomethylation. Two previously hypothesised radicals were successfully TART trapped and MS characterised, supporting the suggested mechanism (Figure 83). Products were also MS characterised, which showed that the Ru-photocatalyst degraded during reaction. This demonstrated that products and radicals could be characterised simultaneously, a significant advantage of TART trapping over other radical characterisation methods. These observations proved the viability of the TART trapping method as a new method for short-lived radical isolation and characterisation in photochemistry systems.

6.4. Radical thiol-ene addition

Once it was proven that TART trapping could be used to trap radicals in photochemistry systems in presence of photocatalyst, it was decided that further investigations would be better focused on a more generic and better studied photochemistry reaction. This was because utilising radical trapping, other than for qualitative radical identifying purposes, would be better suited to a more widely studied and understood system. Therefore, a click chemistry Ru-photocatalysed radical thiol-ene addition reaction was investigated.

6.4.1. Introduction

Thiol-ene click chemistry is a hydrothiolation reaction, involving thiol addition to an alkene double bond to form an anti-Markovnikov thioether (1.2.1). The reaction can proceed through a radical addition or Michael addition pathway.^{17,21} The radical addition pathway is typically initiated using light and a photocatalyst. Propagation then occurs through anti-Markovnikov addition of thiyl radical to alkene, forming a carbon-centred radical. Finally, chain transfer occurs through carbon-centred radical abstracting a hydrogen atom intermolecularly from another thiol, forming thioether product and a new thiyl radical, creating a propagation cycle (Figure 87).^{17,21} Structure of substrates determines which propagation step is rate determining.^{18,19,204}

The reaction rose to prominence in recent decades owing to its industrial feasibility, largely due to its usually high yields and stereoselectivity. The reaction is also relatively robust and under certain conditions can even be run in presence of O₂.¹⁸⁻²¹ Furthermore, these properties aid clean and efficient polymer and dendrimer synthesis. The reaction has also proven useful in biosynthesis, such as for fluorescent label functionalisation.²⁰

Tyson *et al.* developed a Ru-photocatalysed radical thiol-ene addition, using different thiols and alkenes as reactants (in a 4:1 ratio) at high concentrations (2.00 M yield limiting concentration) and [Ru(bpz)₃]²⁺ as photocatalyst, forming 21 products with 73-99% yields over 1-26 h. Optimisation was undertaken using benzyl mercaptan and styrene as reactants, achieving 98% product yield after 2 h using 4:1 thiol:alkene. Tyson *et al.* also suggested a mechanism for this reaction (Figure 87), though did not undertake experiments to validate this mechanism.²⁰⁵ This mechanism included initiation from thiol (S2) to thiyl radical (R1), propagation of R1 to carbon-centred radical (R2) via addition to alkene (S3) and chain transfer of R2 to R1 and thioether product (P2), via hydrogen atom abstraction (HAA) of S2. As discussed previously, rate of propagation steps determines the rate of reaction.

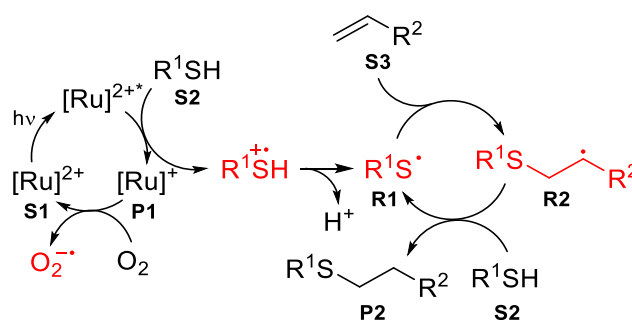


Figure 87: Mechanism of Ru-photocatalysed radical thiol-ene addition, proposed by Tyson *et al.*²⁰⁵

6.4.2. Literature replication

First, replication of these literature results was attempted. This was to ensure the reactants, photocatalyst and light source were suitable for probing this radical thiol-ene addition. For this, benzyl mercaptan and styrene were used as reactants (in a 2:1 ratio), for which Tyson *et al.* reported an 80% yield (11.5.2.1).²⁰⁵ A 2:1 ratio thiol:alkene ratio was used, as it was feared that when TART trapping, a significant excess of thiol would cause TART-trapped radicals to undergo side reactions, as discussed later (6.4.3).

The post-reaction sample was characterised by NMR spectroscopy without work-up or purification (SI4.2.1). Final reactant:product ratio was ~1:0.4, indicating ~30% styrene conversion and ~30% yield. This assumed all styrene was converted to product, which appeared to be the case from NMR spectra. This 30% yield was far below the reported 80%

yield.²⁰⁵ It was believed that conditions had been reproduced as closely as possible and therefore, this exact yield could not be produced with the equipment and reactants available. Since some product had been generated, this yield was deemed acceptable for reaction investigation. As such, TART trapping was undertaken in this system.

6.4.3. Initial results of TART trapping and reaction condition optimisation

TART trapping of the above Ru-photocatalysed radical thiol-ene addition was undertaken, using CHANT as TART, but otherwise replicating literature conditions (Figure 88).²⁰⁵ For this, a control reaction containing no TART and a trapping reaction containing TART were undertaken, using benzyl mercaptan and styrene as reactants (in a 2:1 ratio). Aliquots were removed from these reaction mixtures pre-initiation (no irradiation) and post-trapping and these aliquots MS characterised (Table 16, 11.5.2.1).

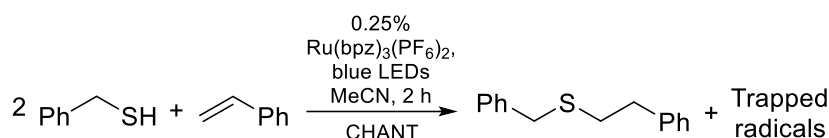


Figure 88: Initial TART trapping of Ru-photocatalysed radical thiol-ene addition, using benzyl mercaptan and styrene as substrates and CHANT as TART (11.5.2.1).

Table 16: Species identified from initial TART trapping of Ru-photocatalysed radical thiol-ene addition under Tyson *et al.* conditions after 2 h, using benzyl mercaptan and styrene as substrates and MS for characterisation (11.5.2.1). Ru containing species are shown with ¹⁰¹Ru only. Systematic *m/z* error = -0.0004; random *m/z* error = ±0.0011; 100% intensity = 2.27×10⁹ absolute count.

	Species	Predicted <i>m/z</i>	Intensity relative to unreacted TART standard / %		
			Trapless control	Pre-initiation	Post-trapping
TART	[CHANT+H] ⁺	323.2698	0.078	70.5	82.5
Reactants	[S1] ²⁺	288.0410	0	0.005	0
	[S2+H] ⁺	125.0425	0	0	0
	[S2+Na] ⁺	147.0244	0	0	0
	[S3+H] ⁺	105.0704	0	0	0
	[S3+Na] ⁺	127.0524	0	0	0
Trapped radicals	[R1-ART+H] ⁺	290.1579	0	0.002	0.071
	[R1-ART+Na] ⁺	312.1398	0	0.025	0.490
	[R1-TEMPO+H] ⁺	280.1735	0	0	0
	[R2-ART+H] ⁺	394.2205	0	0	0.091
	[R2-ART+Na] ⁺	416.2024	0	0	0.090
	[R2-TEMPO+H] ⁺	384.2361	0	0	2.01
Other trapped radicals	[R1-ART+S2+H] ⁺ ^a (thiol-ene addition)	414.1925	0	0	0.003
	[R1-ART+S2+Na] ⁺ ^a (thiol-ene addition)	436.1745	0	0	0.001
Products	[P1] ⁺	576.0821	0	0	0
	[P2+H] ⁺	229.1051	0.035	0	0.042
	[P2+Na] ⁺	251.0870	0.091	0	0.090
Other products	[TART+S2+H] ⁺ ^b (thiol-ene addition)	447.3045	0	0.010	2.57

^aFormed through thiol-ene addition of S2 to R1-ART. ^bFormed through thiol-ene addition of S2 to TART.

Intensity of MS peaks corresponding to CHANT decreased by ~20% post-trapping compared to the unreacted TART standard (Table 16), indicating around ~20% of TART was consumed during the trapping reaction. However, intensity of peaks corresponding to CHANT decreased by ~30% pre-initiation compared to the unreacted TART standard (Table 15). The reason for this was unclear but was presumed to be due to unreacted thiol causing TART degradation, either through radical or non-radical mechanisms.

Peaks corresponding to S2 and S3 were not observed (Table 16), likely due to these species having poor ionisation efficiency. Peaks corresponding to Ru-photocatalyst S1 were observed pre-initiation but not in other samples, indicating that the catalyst degraded during the reaction. Peaks corresponding to P1 were also not observed. Peaks corresponding to reactants and P1 were observed with low intensity for all subsequent radical thiol-ene addition reactions and therefore, are not shown from here onwards. Peaks corresponding to product P2 were observed exclusively post-reaction, in similar amounts in both presence and absence of TART. This theoretically allowed for formation of all hypothesised radicals.

Peaks corresponding to R1-ART and R2-ART were observed exclusively or with much greater intensity post-trapping, compared to other samples. This indicated radicals R1 and R2 were produced during the reaction, as expected, and successfully trapped. Furthermore, peaks corresponding to R1-ART were significantly more intense than R2-ART. Modelling was required to fully interpret these data (6.4.6). These observations supported the hypothesised mechanism (Figure 87). In contrast, peaks corresponding to R1-TEMPO were not observed, likely due to TEMPO• trapping heteroatom-centred radicals poorly, showing TART trapping superiority over TEMPO• trapping. Therefore, peaks corresponding to R1-TEMPO are not shown from here onwards. However, peaks corresponding to R2-TEMPO were observed with much greater intensity post-trapping than R2-ART, likely due to the superior ionisation efficiency of -TEMPO to -ART.

Peaks corresponding to R1-ART were also observed pre-initiation. Trapless optimisation by Tyson *et al.* observed that some product was formed during radical benzyl mercaptan-styrene addition both with and without catalyst when irradiated with compact fluorescent lamp (CFL) light but (82% compared to 19%). Furthermore, the same product yield was achieved for radical thiophenol-styrene addition with and without catalyst (98% compared to 99%). These observations indicated that some radical thiol-ene additions could progress in this system, in absence of certain reaction conditions.²⁰⁵ Literature indicated that concentrated radical thiol-ene addition reactions can self-initiate. This self-initiation can occur through thiol autoxidation or molecule-assisted homolysis (MAH) to form thiyl radicals (Figure 89). Self-initiation occurs especially favourably at high reactant concentrations and for thiols with strongly polarised S-H bonds, such as thiols with electron-withdrawing groups.²⁰⁶ Formed thiyl radicals may then progress through the main radical cycle. Many radical cycles may occur through a single initiation, meaning few self-initiation reactions would be required to form high product yields.

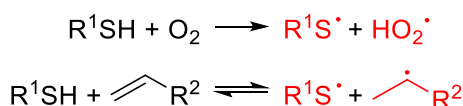


Figure 89: Possible mechanisms of thiol initiation, through thiol autoxidation (top) and molecule-assisted homolysis (MAH, bottom).

Tyson *et al.* used high reactant concentrations in Ru-photocatalysed radical thiol-ene addition, aiding self-initiation. Observation of peaks corresponding to R1-ART from TART trapping of this radical thiol-ene addition in absence of light provided evidence for self-initiation.

Initial experiments showed that TART trapping and MS characterisation could be used to trap and characterise short-lived radicals formed during Ru-photocatalysed radical thiol-ene addition, using benzyl mercaptan and styrene as reactants and CHANT as TART. Next, TART trapping of radical thiophenol-styrene addition was undertaken. This was of particular interest for kinetic study. This was because radical thiophenol-styrene addition was prolific in kinetic literature of radical thiol-ene addition, meaning rate constants were widely obtainable, allowing more reliable kinetic modelling to be undertaken.

TART trapping of Ru-photocatalysed radical thiol-ene addition was undertaken, using CHANT as TART, adapted from literature conditions (Figure 90).²⁰⁵ For this, a control reaction containing no TART and a trapping reaction containing TART were undertaken, using thiophenol and styrene as reactants (in a 2:1 ratio). Aliquots were removed from these reaction mixtures pre-initiation (no irradiation) and post-trapping and these aliquots MS characterised (Table 17, 11.5.2.1).

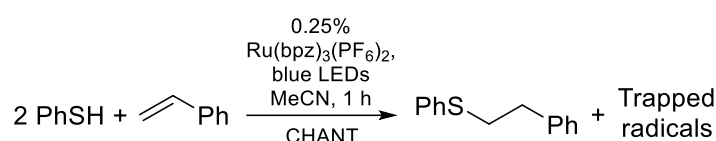


Figure 90: TART trapping of Ru-photocatalysed radical thiol-ene addition, using thiophenol and styrene as substrates and CHANT as TART (11.5.2.1).

Table 17: Species identified from TART trapping of Ru-photocatalysed radical thiol-ene addition under Tyson *et al.* conditions after 1 h, using thiophenol and styrene as substrates and MS for characterisation (11.5.2.1). Systematic m/z error = 0.0000; random m/z error = ± 0.0012 ; 100% intensity = 9.76×10^9 absolute count.

	Species	Predicted m/z	Intensity relative to unreacted TART standard / %		
			Trapless control	Pre-initiation	Post-trapping
TART	[CHANT+H] ⁺	323.2698	0.020	0	0
Trapped radicals	[R1-ART+H] ⁺	276.1422	0.003	0.018	0.023
	[R1-ART+Na] ⁺	298.1241	0.012	0.159	0.120
	[R2-ART+H] ⁺	380.2048	0	0	0.001
	[R2-ART+Na] ⁺	402.1867	0	0	0.004
	[R2-TEMPO+H] ⁺	370.2205	0	2.85	1.54
Other trapped radicals	[R1-ART+S2+Na] ⁺ ^a (thiol-ene addition)	386.1612	0	0.073	1.60
	[R2-ART+S2+Na] ⁺ ^a (thiol-ene addition)	408.1432	0	1.10	5.96
Products	[P2+H] ⁺	215.0894	0.031	0.001	0.004
	[P2+Na] ⁺	237.0714	0.060	0.001	0.004
Other products	[TART+S2+H] ⁺ ^b (thiol-ene addition)	433.2889	0	0.494	1.13

^aFormed through thiol-ene addition of S2 to R1-ART. ^bFormed through thiol-ene addition of S2 to TART.

Peaks corresponding to CHANT indicated that no CHANT was present in either the pre-initiation or post-trapping samples. This was not ideal as without excess TART, TART-trapped radicals were more likely to undergo side reactions with radicals. Furthermore, this reduced kinetic information as to how rapidly the reaction had occurred, since TART could have been totally consumed anytime between 0-60 min.

Peaks corresponding to P2 product were observed in all samples, although most intensely in the trapless control. This was likely because TART trapping hindered product formation, by breaking the radical cycle.

Peaks corresponding to R1-ART and R2-ART were observed near exclusively in TART presence. This indicated radicals R1 and R2 were produced during the reaction, as expected, and successfully trapped. However, peaks corresponding to R1-ART were observed with greater intensity pre-initiation than post-trapping. This indicated that the reaction was self-initiating, as discussed previously. This occurred more efficiently in radical thiophenol-styrene addition than radical benzyl mercaptan-styrene addition, likely due to resonance in thiophenol better stabilising the resultant thiyl radical.

The most intense peak observed post-trapping corresponded to R1-ART+S2, i.e., the product formed through thiol-ene addition of S2 to R1-ART. This thiol-ene addition could occur through a radical or nucleophilic mechanism with either RS^\bullet or RS^- respectively (Figure 91). Likewise, peaks corresponding to TART+S2, i.e., the product formed through thiol-ene addition of S2 to TART, were also observed relatively intensely. However, TART+S2 likely had high ionisation efficiency due to its -TEMPO group, likely making its corresponding peak relatively intense. S2 addition to TART was believed to occur through a nucleophilic mechanism (Figure 91). This was because nucleophilic addition to TARTs was previously observed to result in nucleophilic addition to the alkene without TEMPO $^\bullet$ cleavage (3.5.3). Alternatively, it could be due to radical addition to the other end of the alkene.

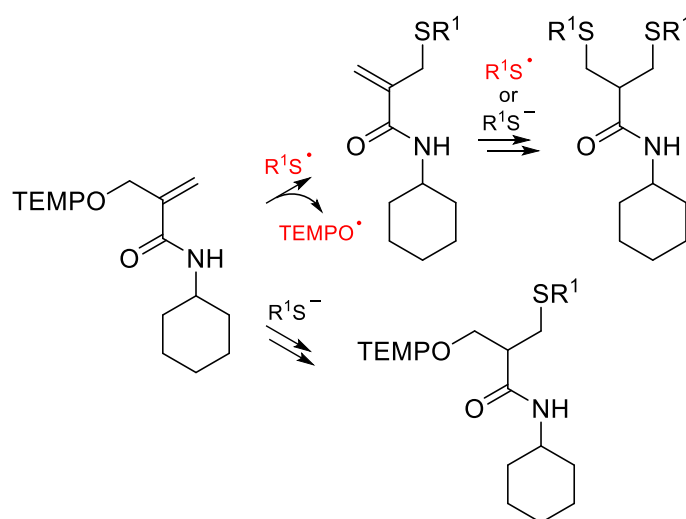


Figure 91: Side reactions of CHANT-derived structures with thiols (S2). S2 reaction with R1-ART and TART form R1-ART+S2 (top) and TART+S2 (bottom) respectively.

These observations indicated that TART was totally consumed and that [R1-ART+S2] was significantly greater than [R1-ART], indicating that after 1 h, the reaction had progressed too far. This was not ideal, as these side reactions complicated mass spectra and reduced intensity of peaks corresponding to TART-trapped radicals. Therefore, the TART trapping of radical thiol-ene addition procedure was altered to reduce the rate of reaction. This was mainly achieved by reducing the concentrations of all reactants by a factor of ten. This would also reduce rate of self-initiation.²⁰⁶ Samples were also diluted immediately upon removal from the reaction mixture and analysed as soon as possible, to reduce the extent to which the reaction occurred. These changes reduced the rate of reaction and therefore allowed better control over reaction progression, significantly improving results (Table 18, 11.5.2.4).

Table 18: Species identified from TART trapping of Ru-photocatalysed radical thiol-ene addition under standard conditions after 2 h, using different thiols and styrene as substrates and MS for characterisation (11.5.2.4). Systematic m/z error = -0.0004; random m/z error = ± 0.0011 ; 100% intensity = 2.69×10^9 absolute count.

Species		Intensity relative to unreacted TART standard / %			
		BnSH pre-initiation	BnSH post-trapping	PhSH pre-initiation	PhSH post-trapping
TART	[CHANT+H] ⁺	71.9	69.7	22.3	20.9
Trapped radicals	[R1-ART+H] ⁺	0	0.014	1.31	1.43
	[R1-ART+Na] ⁺	0.018	0.192	5.19	6.76
	[R2-ART+H] ⁺	0	0.005	0.003	0
	[R2-ART+Na] ⁺	0	0.012	0	0
	[R2-TEMPO+H] ⁺	0	0.277	1.20	3.05
Other trapped radicals	[R1-ART+S2+H] ⁺ (thiol-ene addition)	0	0	0.469	0
	[R2-ART+S2+Na] ⁺ (thiol-ene addition)	0	0	0.247	0.002
Products	[P2+H] ⁺	0	0.017	0	0
	[P2+Na] ⁺	0	0.021	0	0
Other products	[TART+S2+H] ⁺ (thiol-ene addition)	0.060	0.209	2.19	1.74

These data indicated that TART was not totally consumed during trapping, as desired.

Peaks corresponding to R1-ART were observed with significantly greater intensity post-trapping than R1-ART+S2 corresponding peaks. Furthermore, for radical thiophenol-styrene addition, peaks corresponding to R1-ART were observed much more intensely under these diluted conditions than under Tyson *et al.* conditions. These observations indicated that under these conditions, the reaction did not progress to the same extent, making these conditions much more suitable for TART trapping. However, for radical thiophenol-styrene addition, peaks corresponding to TART-trapped radicals were observed with similar intensity both pre-initiation and post-trapping, indicating that self-initiation was still occurring.

From here onwards, these optimised “standard” conditions were applied to all trapping reactions, deviating from Tyson *et al.* conditions. However, whilst Tyson *et al.* conditions were optimised for high product yield, trapping conditions were optimised for suitable kinetic control over reaction progression.²⁰⁵ Whilst not exactly emulating Tyson *et al.* conditions, it was assumed that reaction dilution would not significantly change rate constants, allowing conclusions to be applied to Tyson *et al.* reaction conditions.

Following optimisation of TART trapping conditions, control reactions were undertaken.

6.4.4. Controls

A full set of controls were undertaken for TART trapping of radical thiol-ene addition, to ensure peaks corresponding to TART-trapped radicals were only detected in presence of all reaction conditions necessary for TART-trapped radical formation. TART trapping of radical thiol-ene addition (three repeats) and control reactions were carried out using standard optimised conditions and benzyl mercaptan and styrene as substrates (11.5.2.5). Each control omitted a single condition required for TART-trapped radical formation: no thiol, no alkene, no catalyst, no light, no TART and an unreacted TART standard (set as 100% relative intensity). MS was then used to characterise these reaction mixtures (Table 19).

Table 19: Species identified from TART trapping of Ru-photocatalysed radical thiol-ene addition and controls under otherwise standard conditions after 2 h, using benzyl mercaptan and styrene as substrates and MS for characterisation (11.5.2.5). Systematic m/z error = -0.0004; random m/z error = ± 0.0007 ; 100% intensity = 2.69×10^9 absolute count.

Species	Predicted m/z	Intensity relative to unreacted TART standard / %					Trapping reaction ^a
		No thiol	No alkene	No catalyst	No light	No TART	
[CHANT+H] ⁺	323.2698	74.5	16.3	67.1	74.1	0	97.4 \pm 1.1
[R1-ART+H] ⁺	290.1579	0	0.059	0.004	0.008	0	0.017 \pm 0.001
[R1-ART+Na] ⁺	312.1398	0	0.275	0.035	0.034	0	0.200 \pm 0.005
[R2-ART+H] ⁺	394.2205	0	0	0	0	0	0.031 \pm 0.002
[R2-ART+Na] ⁺	416.2024	0	0	0	0	0	0.015 \pm 0.012
[R2-TEMPO+H] ⁺	384.2361	0	0	0	0	0	0.53 \pm 0.03
[R1-ART+S2+H] ⁺ (thiol-ene addition)	414.1925	0	0	0	0	0	0
[R1-ART+S2+Na] ⁺ (thiol-ene addition)	436.1745	0	0	0	0	0	0
[P2+H] ⁺	229.1051	0	0	0	0	0.029	0.009 \pm 0.001
[P2+Na] ⁺	251.0870	0	0	0	0	0.138	0.018 \pm 0.001
[TART+S2+H] ⁺ (thiol-ene addition)	447.3045	0	0.290	0.020	0.015	0	0.248 \pm 0.013

^aThree repeats undertaken and an average and associated error calculated.

Peaks corresponding to TART were observed in all reactions, except the no TART control, as expected. In general, the errors observed across the three trapping reactions were very low, improving the validity of these intensities.

Peaks corresponding to product P2 were only observed in the no TART control and trapping reactions, as expected. Additionally, these peaks were observed with much greater intensity in absence than presence of TART. This was likely because TART broke the radical cycle, hindering the reaction and therefore producing lower product yields.

Peaks corresponding to R1-ART were not detected in absence of thiol or TART, since these species are both required for R1-ART formation. In contrast, peaks corresponding to R1-ART were observed intensely in absence of alkene and in trapping reactions. The radical thiol-ene addition mechanism shows that alkene was not required for R1-ART formation (Figure 87). Since R1 reacted with alkene, [R1] was higher in absence of alkene and hence maximum intensity was observed for R1-ART corresponding peaks in absence of alkene. Likewise, peaks corresponding to TART indicated that more TART was consumed in absence of alkene than other reactions, likely due to presence of alkene causing reduced [R1], reducing rate of TART trapping of R1 and hence TART consumption. In contrast, peaks corresponding to R1-ART were observed with much lower intensity in absence of catalyst and light. This was logical as although absence of catalyst and light led to significantly less initiation, self-initiation could still occur, causing some R1-ART to be formed. All these observations indicated that R1-ART was formed most efficiently with or without alkene, but in presence of all other trapping reaction conditions, as expected.

Peaks corresponding to R2-ART were only exclusively observed in trapping reactions. Thiol, alkene and TART were all constituents of R2-ART and therefore, R2-ART was not formed in their absence. In absence of catalyst and light, intensities of MS peaks corresponding to R1-ART indicated that the reaction progresses much less efficiently than in the trapping reactions. Therefore, [R2-ART] was likely significantly lower in these controls than in trapping

reactions. Since peaks corresponding to R2-ART were near the MS detection limits in the trapping reactions, R2-ART was likely below the detection limits in these controls.

These observations indicated that TART-trapped radicals were only formed in presence of all necessary conditions, validating the suggested structures and indicating that TART trapping could be used to investigate short-lived radicals formed in radical photochemistry systems. Furthermore, reproducibility of the three trapping reactions was excellent. For example, the peak corresponding to [R1-ART+Na]⁺ was detected with 0.200±0.005%, a percentage error of <3%. This increased confidence in experimental findings. Furthermore, HPLC-MS chromatograms indicated a single structure for each TART-trapped radical, as expected (Figure 92, SI4.2.2).

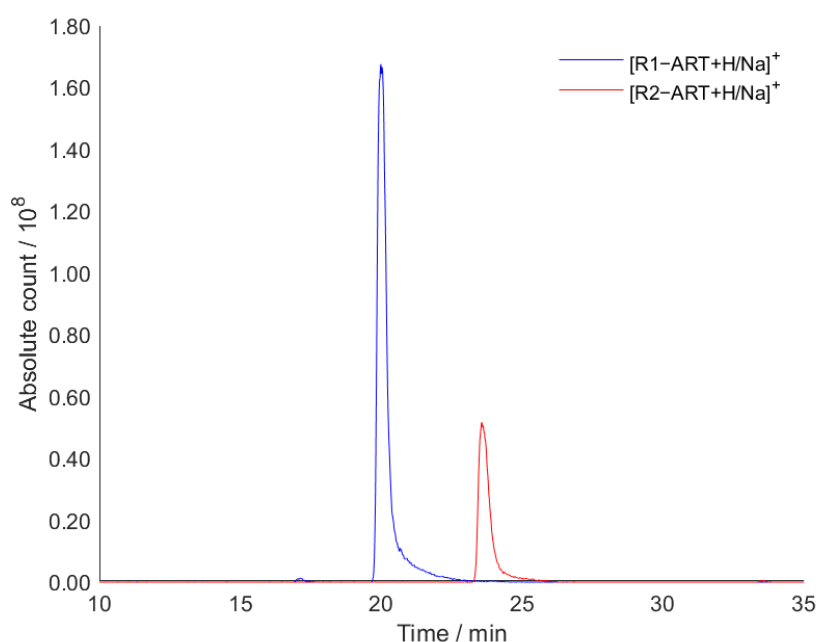


Figure 92: HPLC-MS chromatograms of peaks corresponding to [R1-ART+H/Na]⁺ (m/z 290.158±0.002 and m/z 312.140±0.002, 20.0 min) and [R2-ART+H/Na]⁺ (m/z 394.220±0.002 and m/z 416.202±0.002, 24.0 min) detected from TART trapping of radical thiol-ene addition, using benzyl mercaptan and styrene as substrates (11.5.2.3).

To further validate the suggested structures of TART-trapped radicals, isolation and further characterisation of a TART-trapped radical was attempted.

6.4.5. TART-trapped radical isolation

TART-trapped radical isolation was undertaken using thiophenol as substrate and CHANT as TART, forming R1-ART. Thiophenol was used in preference to benzyl mercaptan, due to its faster rate of reaction with TART and its widespread discussion in kinetic literature of radical thiol-ene addition. Alkene was excluded as this reduced R1-ART formation, as discussed previously (6.4.4). Reaction conditions used closely matched those used by Tyson *et al.*, i.e., using highly concentrated reactants.²⁰⁵ Due to the risk of R1-ART+S2 formation, the reaction was monitored using MS and stopped when maximum intensity of peaks corresponding to R1-ART was observed, totalling 3 h (Figure 93, 11.5.2.6).

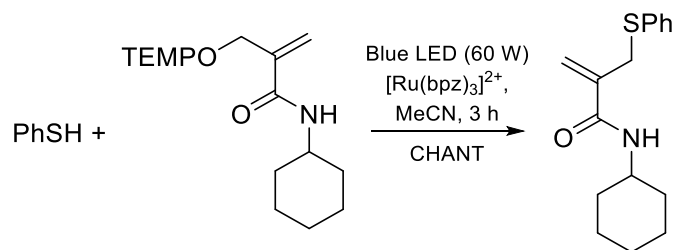


Figure 93: TART trapping of phenylthiyl radical (11.5.2.6).

A 63% isolated yield was obtained for CHANT-trapped R1, with characterisation confirming the suggested structure (11.5.2.6). The ^1H NMR spectrum showed appearance of aromatic signals and loss of $-\text{TEMPO}$ signals, confirming the suggested TART-trapped radical structure (Figure 94).

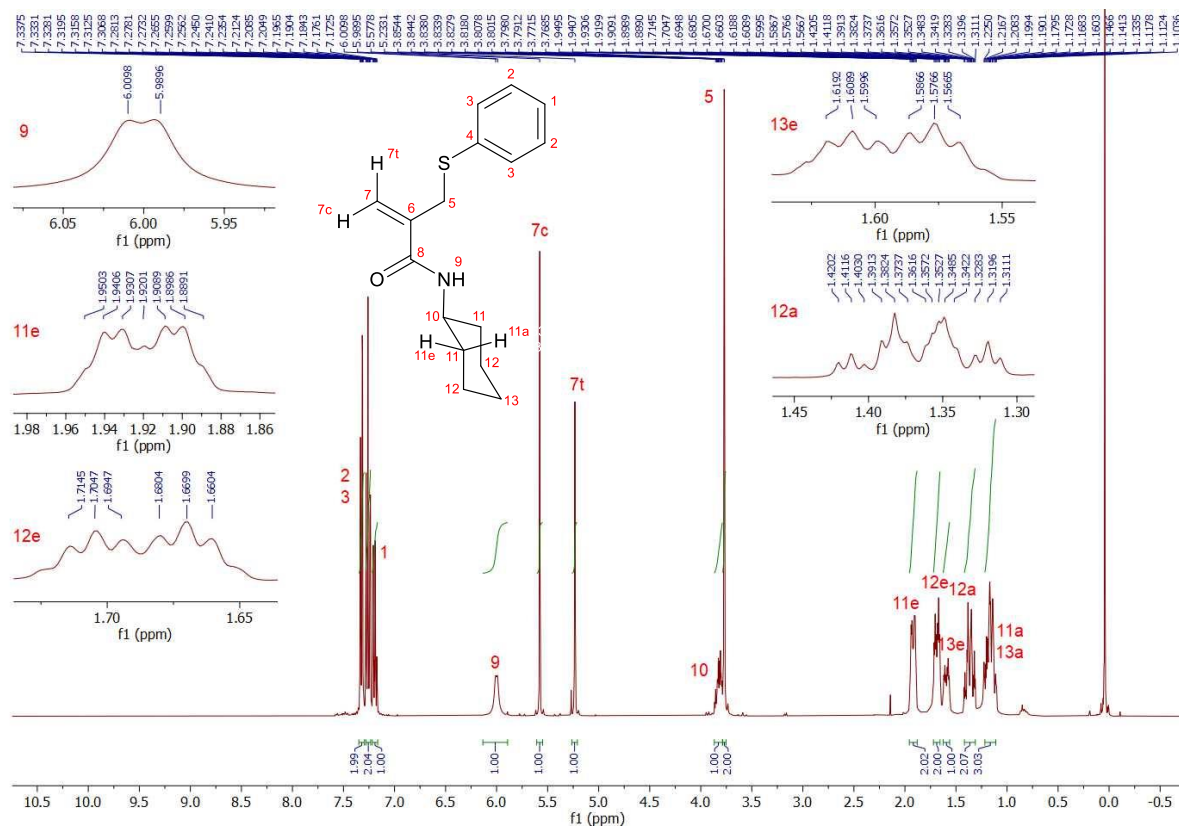


Figure 94: ^1H NMR spectrum of TART-trapped phenylthiyl radical (CDCl_3 , 400 MHz, 298 K, 11.5.2.6).

This was an excellent result, as it confirmed the TART trapping mechanism occurred as expected. Furthermore, it showed that other analytical techniques, besides MS, could be used to characterise TART-trapped radicals.

MS calibration curves were recorded for CHANT and CHANT-trapped R1 (11.5.2.6). This was so that MS intensities of peaks corresponding to these substrates could be correlated to substrate concentration. Substrate concentrations used were in the range of values used in TART trapping of radical thiol-ene addition, after dilution. These calibration curves showed that equally concentrated CHANT and CHANT-trapped R1 were observed with significantly different corresponding peak MS intensities, with intensity of CHANT corresponding peaks being five times greater than intensity of CHANT-trapped R1 corresponding peaks (Figure 95). This indicated CHANT ionised more efficiently than low basicity CHANT-trapped radicals.

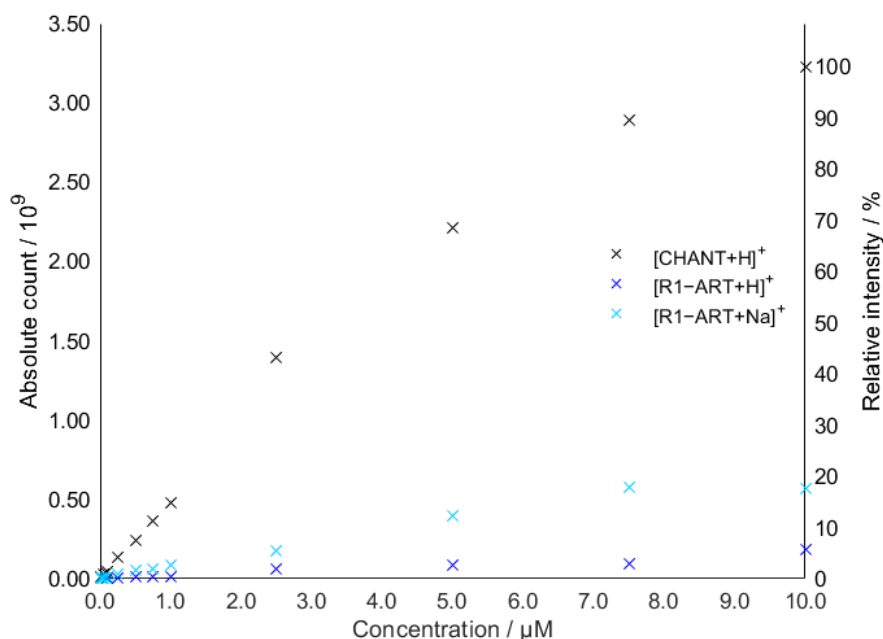


Figure 95: Calibration curve of intensity of MS peaks corresponding to [CHANT+H]⁺ (m/z 323.270, black), [R1-ART+H]⁺ (m/z 276.142, dark blue) and [R1-ART+Na]⁺ (m/z 298.124, light blue) at different analyte concentrations, where R1-ART is CHANT-trapped phenylthiyl radicals. This indicated CHANT ionised more efficiently than low basicity CHANT-trapped radicals.

These calibration curves were used with kinetic experiments and kinetic modelling to relate MS intensity of peaks corresponding to TART and R1-ART to their concentrations in TART trapping of radical thiophenol-ene addition.

6.4.6. Kinetics experiments and kinetic modelling

Radical thiol-ene addition is a relatively simple and highly efficient radical reaction. However, once radical trapping is employed, the mechanism quickly becomes too complex to make well-informed conclusions about reaction kinetics. Therefore, kinetic modelling was used to justify results from TART trapping of radical thiol-ene addition (11.10.2). Kinetics experiments were also undertaken to compare to kinetic modelling. This would inform adjustment of the rate constants used in the kinetic model, as required. This kinetic model would then be used to interpret other results from TART trapping of radical thiol-ene addition, for example, the effect of different substrates on reaction kinetics.

A kinetic model was built and run using the Kintecus chemical simulation programme.²⁰⁷ This model was designed using previous DFT-informed kinetic modelling of radical thiol-ene addition undertaken by Northrop *et al.*²⁰⁴ and Findik *et al.* (298 K).²⁰⁸ who focused upon radical methanethiol-alkene and aromatic thiol-alkene addition respectively (11.10.2). First, the main radical cycle of thiol-ene addition was kinetically modelled. Rate constants for initiation (k_i), propagation (k_p), chain transfer (k_{CT}) and radical-radical termination (k_T) were obtained from Northrop *et al.* and Findik *et al.*, where propagation and chain transfer steps had associated forward and backward (k_{-p} and k_{-CT}) rates (Figure 96).^{204,208}

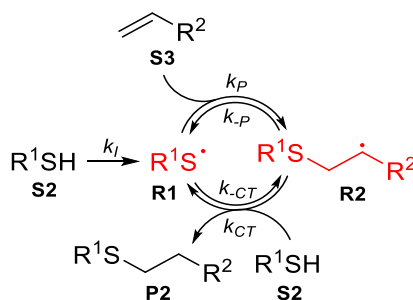


Figure 96: Kinetic model of radical thiol-ene addition, with initiation rate, k_i , forward and backward propagation rates, k_p and k_{-p} and forward and backward chain transfer rates, k_{CT} and k_{-CT} .

Initiation rate constant was unknown for photocatalytic systems. Therefore initiation rate constant was initially set as 10^{-5} s^{-1} , estimated by Northrop *et al.* and Findik *et al.* and later altered to better fit experimental findings.^{204,208} Rate constants of propagation and chain transfer were obtained from Northrop *et al.* and Findik *et al.* for each substrate or estimated from similar substrates.^{204,208} Radical-radical termination rate constant was set as $10^8 \text{ M}^{-1} \text{ s}^{-1}$, as estimated by Northrop *et al.*²⁰⁴

Radical trapping was then included in the model (Figure 97). Trapping by both TART and TEMPO• were included. Trapping was believed to be irreversible. The rate constant of TART trapping of R1 (k_{R1-ART}) was estimated to be equal to forward R1 reaction with methyl methacrylate ($4.35 \times 10^6 \text{ M}^{-1} \text{ s}^{-1}$), calculated by Findik *et al.*²⁰⁸ This compared with a literature-sourced experimental rate constant for the same reaction of $3.2 \times 10^6 \text{ M}^{-1} \text{ s}^{-1}$.¹⁵⁷ TEMPO• reacted poorly with heteroatom-centred radicals and hence TEMPO• trapping of R1 was not modelled. Rate constants of trapping of R2 by TART (k_{R2-ART}) and TEMPO• ($k_{R2-TEMPO}$) were estimated from literature, with rate constants of benzyl radical reaction with methyl acrylate ($450 \text{ M}^{-1} \text{ s}^{-1}$)²⁰⁹ and PhC•HCH₃ reaction with TEMPO• ($1.64 \times 10^8 \text{ M}^{-1} \text{ s}^{-1}$)²¹⁰ being used respectively. This former rate constant was reasonable because although not an exact match, since both the reactant radical and the radical formed were missing an alkyl group, it was estimated that these would stabilise both radicals approximately equally and therefore, a more representative rate constant would be similar. Ideally, calculations would be undertaken to estimate more accurate rate constants, however this was beyond the scope of the project.

Additionally, TART-trapped radicals could undergo further radical thiol-ene addition, as seen experimentally (6.4.3). Rate constants of forward and backward propagation and chain transfer were estimated to be equal to R1 reaction with methyl methacrylate, calculated by Findik *et al.*⁵ Furthermore, the radicals formed could be trapped, for which the same rate constants were assigned as previously. From these reactions, the kinetic model of TART trapping of radical thiol-ene addition was developed (Figure 97).

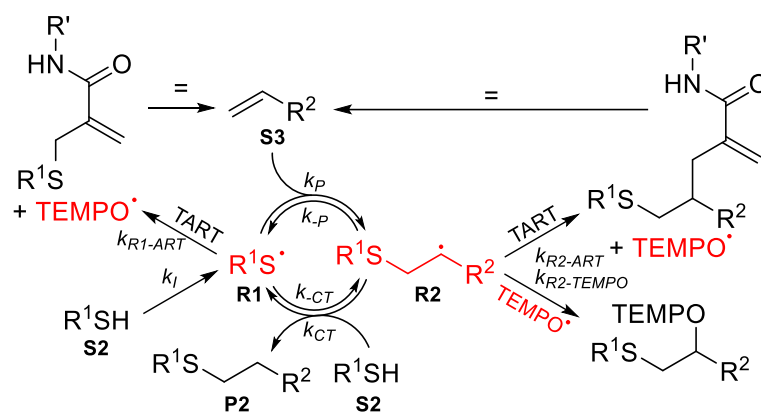


Figure 97: Kinetic model of TART trapping of radical thiol-ene addition. Arrows with “=” are included to indicate that trapped radicals R1-ART and R2-ART could undergo subsequent radical thiol-ene addition.

The model was initially used to simulate TART trapping of radical thiophenol-styrene addition, using experimental concentrations of substrates and TART (Figure 98, 11.5.2.4).

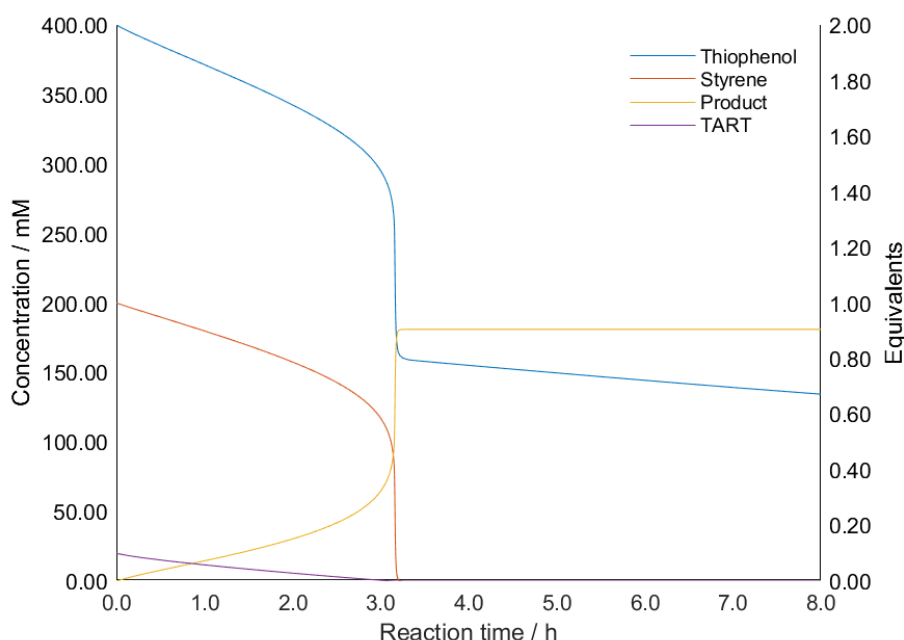


Figure 98: Kinetic model produced for TART trapping of radical thiol-ene addition (11.10.2), using thiophenol (orange) and styrene (blue) as substrates and TART (purple), yielding thioether product (yellow). Complete styrene conversion and near 100% product yield were obtained after ~3 h.

The model predicted that TART was slowly consumed over ~3 h. In contrast, ~50% styrene was slowly consumed over ~3 h, whilst the remaining ~50% was rapidly consumed in the following few minutes, with ~90% product yield obtained overall. This indicated that the reaction occurred significantly slower in TART presence, with modelling indicating that in TART absence, complete styrene conversion and ~100% product yield were obtained after ~1 min. This effect occurred because TART terminated radical propagation cycles, meaning that its presence significantly slowed the overall rate of reaction. However, once TART was mostly consumed, radical thiol-ene addition occurred rapidly. [Thiophenol] after 3 h was ~0.9 eq. and ~0.8 eq. in TART absence and presence respectively. Reduced product yield and greater thiophenol consumption in TART presence, was due to formation of R2-TEMPO, R1-ART formation and R1-ART+S2 formation (Figure 99).

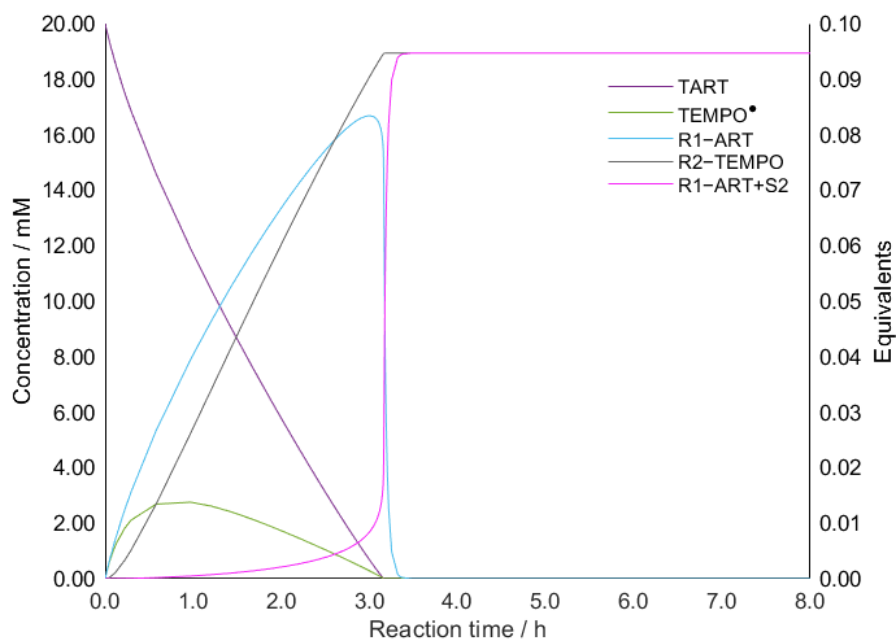


Figure 99: Kinetic model produced for TART trapping of radical thiol-ene addition (11.10.2), using thiophenol and styrene as substrates and TART (purple), yielding TEMPO• (green), R1-ART (sky blue), R2-TEMPO (grey) and R1-ART+S2 (pink).

Modelling indicated that TART was near totally consumed by R1-ART formation, as was observed experimentally (6.4.3). As for styrene, [R1-ART] sharply decreased after ~3 h. As previously, this was because R1-ART rapidly underwent radical thiol-ene addition into R1-ART+S2, once TART was consumed. The computed model predicted minimal formation of R2-ART but much greater formation of R2-TEMPO. The model predicted similar [R1-ART] and [R2-TEMPO] until TART was near totally consumed ~3 h and indeed similar intensities of corresponding MS peaks were observed for both species after 1 h (6.4.3).

It was subsequently decided that each rate constant should be varied individually, to determine to what extent their values influenced species concentrations. Initiation rate constant had the largest effect on species concentrations, significantly affecting all species. This value had only been estimated by Northrop *et al.* and was not specific to any initiation method.⁴ This meant that accuracy of this value was unknown. Furthermore, this initiation rate constant was more significant in radical trapping experiments compared to trapless experiments, as radical trapping resulted in cycle termination, meaning relatively more R1 were formed through initiation than the main radical cycle. This indicated that experimental TART trapping and kinetic modelling could be used to determine initiation rate constants in photochemical reactions. [R1-ART] was little affected by fluctuations of other rate constants. In contrast, [R2-ART] and [R2-TEMPO] were much more susceptible to rate constant changes, particularly to rate constants of the main radical cycle, R1-ART formation and their own formations through R2 trapping.

To inform the model, kinetics experiments were undertaken using standard conditions of TART trapping of radical thiol-ene addition, with aliquots regularly removed and MS characterised over 24 h, using CHANT as TART (11.5.2.7). Rate of TART trapping of radical benzyl mercaptan-styrene addition was deemed too slow for kinetic experiments to be practical. Therefore, kinetics of TART trapping of radical thiophenol-styrene was investigated (11.5.2.7). Additionally, radical methyl thiosalicylate-styrene addition was investigated as it was believed that rate constants should be comparable to radical thiophenol-styrene addition but yielded

greater [R2-ART] (6.4.7). Furthermore, better results were generally obtained for this reaction, possibly due to methyl thiosalicylate-derived TART-trapped radicals having better ionisation efficiency and hence improved MS detection. MS intensities of protonated, sodiated and potassiated MS adducts were summed for each analyte, as these three adducts all indicated analyte concentration and relative efficiencies of protonation, sodiation and potassiation were unknown. The kinetic experimental results for TART-trapping of thiophenol-styrene addition and calibration curves were used to inform the kinetic model.

Intensities of MS peaks corresponding to TART and R1-ART were converted to concentrations using existing calibration curves. These concentrations were then used to calculate a more accurate initiation rate constant. The obtained initiation rate constant was $6.81 \times 10^{-6} \text{ s}^{-1}$, about half that predicted by Northrop *et al.*²⁰⁴

A comparison of the experimentally estimated and simulated [TART] and [R1-ART] using this rate constant showed an approximate but not excellent fit (Figure SI90). Whilst experimental data showed that TART was consumed more rapidly than the simulation suggested, consumption of R1-ART occurred more slowly than the simulation suggested. This potentially indicated that TART was consumed by additional side reactions not modelled in the simulation or that the rate constant for R1-ART consumption was too rapid. It was first hypothesised that radicals may undergo oxidation. However, MS peaks corresponding to oxygenated TART-trapped radicals were observed with relatively low intensity compared to R1-ART and R2-ART, making this unlikely to be a significantly occurring process. It was unknown what other side reactions could occur. Therefore, due to the number of reactions involved and the uncertainties in their rate constants, it was decided that the model was too complex to develop further. Such development would require additional experimentation or calibration curves to convert intensities of MS peaks corresponding to reactants, products or TART-trapped radicals into their respective concentrations. However, since the obtained initiation rate constant was similar to that suggested by Northrop *et al.*, it was decided that this value was suitable for use, although should be treated with caution.²⁰⁴ As such, the developed model was used with an awareness of its potential inaccuracy.

Using these rate constants and in absence of TART, steady state [R1]/[R2] was $\sim 10^6$ (SI4.2.4), meaning R1 was the radical resting state. This factor was significantly large that R1 was near certainly the resting state.

Like for thiophenol-styrene addition, the results of the kinetics experiment conducted for methyl thiosalicylate could not be well modelled, due to the number of reactions with uncertain rate constants. Worse still, the R1-ART calibration curve used for the thiophenol-styrene model, could not be used in the methyl thiosalicylate model because MS peaks corresponding to R1-ART were observed with significantly greater intensity in the methyl thiosalicylate kinetics experiments. Nevertheless, the results of the methyl thiosalicylate experiment had a qualitatively plausible profile (Figure 100). Therefore, it was believed that with appropriate calibration curves or more accurate rate constants, these results could be well modelled.

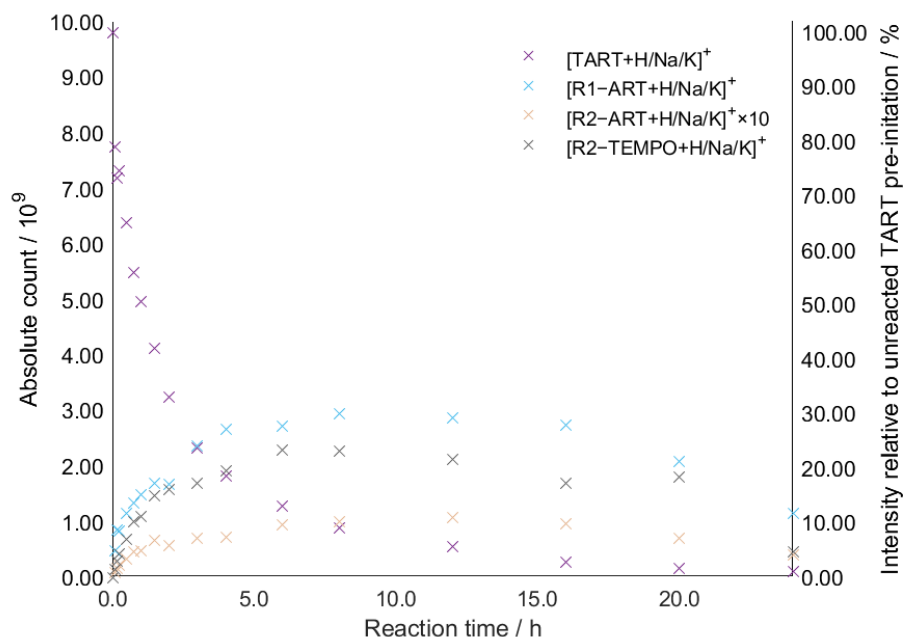


Figure 100: Intensities of peaks corresponding to species identified in TART trapping of radical thiol-ene addition, using methyl thiosalicylate and styrene as substrate and CHANT as TART (11.5.2.7), showing $[TART+H/Na/K]^+$ (purple), $[R1-ART+H/Na/K]^+$ (sky blue), $[R2-ART+H/Na/K]^+ \times 10$ (peach), and $[R2-TEMPO+H/Na/K]^+$ (grey).

Kinetic modelling was developed to aid interpretation of results from TART trapping of radical thiol-ene addition. Therefore, TART trapping of radical thiol-ene addition was used to explore the effects of the thiol (6.4.7) and alkene (6.4.8) on reaction kinetics, with kinetic modelling being used to allow further interpretation of obtained results.

6.4.7. Effect of different thiols on reaction kinetics

Tyson *et al.* tested thiol scope in their system, using styrene as substrate. Whilst obtained yields were high, reaction time varied significantly for different thiols, from 86-98% over 1-20 h.²⁰⁵ For each radical thiol-ene addition, the slower propagation step determines the rate of reaction. The rate constant of each propagation step is dependent on the thiol and alkene structures and hence the slower propagation step can either be the first or second propagation step, causing either R1 or R2 to be the radical resting state respectively. Thus, it was hypothesised that in TART presence, different thiols would incur different intensities of peaks corresponding to trapped radicals. TART trapping results could then be used to inform reaction kinetics, determine the radical resting state and potentially aid development of reaction conditions to improve product yields.

To explore this, TART trapping of radical thiol-ene addition was undertaken, using different thiols and styrene as substrates (Table 20, 11.5.2.8). Four of the six thiols probed were used as reactants by Tyson *et al.*, whilst two additional thiols were probed in order to increase aromatic thiol diversity (Figure 101).

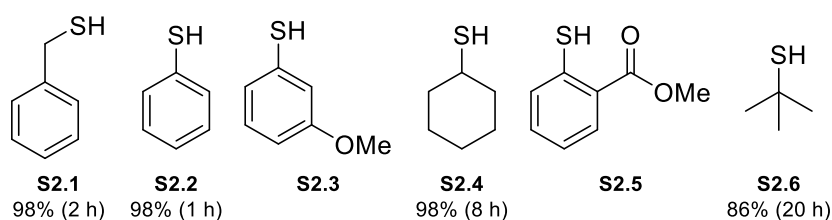


Figure 101: Thiols probed in TART trapping of radical thiol-ene addition (11.5.2.8). Literature yields after the indicated reaction time are shown for the associated thioether product of each thiol.²⁰⁵

Table 20: Species identified from TART trapping of Ru-photocatalysed radical thiol-ene addition under standard conditions after 2 h, using different thiols and styrene as substrates and MS for characterisation (11.5.2.8). Systematic m/z error = -0.0004; random m/z error = ± 0.0011 ; 100% intensity = 2.55×10^9 absolute count.

Thiols S2.		1	2	3	4	5	6
Species		Intensity relative to unreacted TART standard / %					
TART	[CHANT+H] ⁺	69.7	20.9	13.5	58.5	36.3	84.9
Trapped radicals	[R1-ART+H] ⁺	0.014	1.43	1.84	0	1.49	0
	[R1-ART+Na] ⁺	0.192	6.76	9.16	0	13.6	0
	[R2-ART+H] ⁺	0.005	0	0	0	0.016	0
	[R2-ART+Na] ⁺	0.012	0	0	0	0.102	0
	[R2-TEMPO+H] ⁺	0.277	3.05	3.48	0.051	5.70	0.013
Other trapped radicals	[R1-ART+S2+H] ⁺ (thiol-ene addition)	0	0	0	0	0	0
	[R1-ART+S2+Na] ⁺ (thiol-ene addition)	0	0.002	0.004	0	0	0
Products	[P2+H] ⁺	0.017	0	0.011	0	0.014	0
	[P2+Na] ⁺	0.021	0	0.018	0	1.39	0
Other products	[TART+S2+H] ⁺ (thiol-ene addition)	0.209	1.75	2.42	0.009	0.272	0

Results for each thiol differed dramatically depending on their functionality. Peaks corresponding to TART-trapped radicals were not observed for S2.6. Under Tyson *et al.* conditions, 86% product yield was achieved after 20 h, much longer than that required for benzyl mercaptan (98%, 2 h). Therefore, it was likely that after 2 h, little S2.6 conversion had occurred, hence trapped radical concentration was low. Therefore, to increase trapped radical intensity for all thiols, the experiment was repeated for all thiols over 24 h (Table 21, 11.5.2.8).

Table 21: Species identified from TART trapping of Ru-photocatalysed radical thiol-ene addition under standard conditions after 24 h, using different thiols and styrene as substrates and MS for characterisation (11.5.2.8). Systematic m/z error = -0.0004; random m/z error = ± 0.0006 ; 100% intensity = 2.55×10^9 absolute count.

Thiols S2.		1	2	3	4	5	6
Species		Intensity relative to unreacted TART standard / %					
TART	[CHANT+H] ⁺	91.2	0.093	0.016	93.3	1.22	113
Trapped radicals	[R1-ART+H] ⁺	0.029	7.32	0.705	0.083	3.67	0.015
	[R1-ART+Na] ⁺	1.05	12.2	11.6	0.181	22.8	0.051
	[R2-ART+H] ⁺	0.030	0.016	0.013	0.056	0.031	0.095
	[R2-ART+Na] ⁺	0.078	0.011	0.014	0.068	0.126	0.204
	[R2-TEMPO+H] ⁺	2.24	17.9	10.7	1.15	10.8	2.18
Other trapped radicals	[R1-ART+S2+H] ⁺ (thiol-ene addition)	0	0.103	0.043	0	0	0
	[R1-ART+S2+Na] ⁺ (thiol-ene addition)	0	0.089	0.052	0	0.004	0

Products	[P2+H] ⁺	0.004	0.001	0.018	0	0.013	0
	[P2+Na] ⁺	0.017	0.009	0.031	0.008	1.158	0
Other products	[TART+S2+H] ⁺ (thiol-ene addition)	1.56	6.30	3.49	0.285	2.87	0.015
	\sim [R1-ART+X] ⁺ /[R2-ART+X] ⁺ ^a	10.0	726	459	2.14	169	0.219
	Resting state ^b	\sim R2	R1	R1	R2	\sim R1	R2

^aEstimated by ratio of summed intensities of peaks corresponding to protonated (X = H) and sodiated (X = Na) MS adducts. Greater than ratios (>) were determined assuming [R2-ART+X]⁺ was at intensity detection limits (0.002%). ^bDetermined using kinetic modelling (11.10.2).

After 24 h, peaks corresponding to trapped radicals were observed in presence of all thiols, allowing better comparison between experiments.

TART consumption was observed for all species. Intensity of peaks corresponding to TART were weakest and strongest in presence of 3-methoxythiophenol (S2.3) and ^tBuSH (S2.6) respectively, indicating radical TART was consumed the fastest and slowest in presence of 3-methoxythiophenol and ^tBuSH respectively. Peaks corresponding to TART were observed with lower intensity in presence of the three functionalised thiophenols (S2.2, S2.3 and S2.5) than the three alkylthiols (S2.1, S2.4 and S2.6), indicating TART was consumed faster in presence of thiophenols. Indeed, peaks indicated that CHANT was near totally consumed in presence of thiophenols (Table 21), making side reactions more likely. Likewise, peaks corresponding to R1-ART+S2 were observed in these reactions. However, these peaks had weak intensity and therefore, few side reactions had occurred.

Peaks corresponding to R1-ART were observed most intensely in presence of the three thiophenols as previously, with the highest and lowest total R1-ART corresponding peak intensities observed in presence of methyl thiosalicylate (S2.5) and ^tBuSH (S2.6) respectively, with two orders of magnitude difference between these two intensities (Table 21). Indeed, R1-ART corresponding peak intensities were observed at least one order of magnitude greater in presence of thiophenols than alkylthiols. Similarly, peaks corresponding to R2-TEMPO were most intense in presence of thiophenols (Table 21). However, the variation in R2-TEMPO corresponding peak intensities between different thiols was much smaller, with the maximum and minimum being only one order of magnitude apart.

In contrast, the least intense R2-ART corresponding peaks occur in presence of thiophenols S2.3 and S2.2, whilst the most intense R2-ART corresponding peak occurred in presence of ^tBuSH (S2.6, Table 21). This was noteworthy since Tyson *et al.* reported that product formation occurred an order of magnitude slower for ^tBuSH (S2.6) than thiophenol (S2.2).²⁰⁵ Therefore, it was likely that generally, R1-ART and R2-ART were detected more and less intensely in presence of thiophenols than alkylthiols respectively, suggesting that [R1] was relatively higher than [R2] in presence of thiophenols than alkylthiols. [R1-ART+X]⁺/[R2-ART+X]⁺ ratio well demonstrated this conclusion, which was estimated by comparing the ratio of summed MS intensities of peaks corresponding to protonated (X = H) and sodiated (X = Na) MS adducts for or R1-ART and R2-ART (Table 21). [R1-ART+X]⁺/[R2-ART+X]⁺ is broadly proportional to [R1]/[R2]. For example, as [R1-ART+X]⁺/[R2-ART+X]⁺ decreases, R2 becomes relatively more populated and therefore, more likely to be the resting state.

Kinetic modelling was used to predict the resting states in presence of each thiol (11.10.2). For effects of different thiols, all rate constants were kept the same except for rate in which R1 was involved. Reverse rate constants were kept constant and hence, k_P/k_{-P} and k_{CT}/k_{-CT} defined the propagation cycle rate constants. Trapping rate constants were estimated from Northrop *et al.* and Findik *et al.*^{204,208} Initiation and forward propagation rate constants were then reasonably altered by hand until [R1-ART]/[R2-ART] broadly matched the ratio of experimental intensities of MS peaks corresponding to [R1-ART+X]⁺/[R2-ART+X]⁺. TART

was then removed from the simulation, to determine [R1]/[R2] and hence estimate the radical resting state (Table 21, 11.10.2).

Kinetic modelling indicated that in presence of thiophenols, R1 was the resting state, particularly for thiophenol (S2.2), although methyl thiosalicylate (S2.5) was a borderline case. In contrast, in presence of alkylthiols, R2 was the resting state, particularly for ^tBuSH (S2.6), although benzyl mercaptan (S2.1) was a borderline case. For thiophenols, the R1 resting state was attributed to increased R1 stability. Thiyl radical delocalisation into the phenyl ring aided R1 stabilisation, meaning phenylthiyl radicals generally had greater stability than alkylthiyl radicals.²¹¹ However, for methyl thiosalicylate, the *o*-ester group was electron withdrawing, slightly destabilising the phenylthiyl radical compared to thiophenol. This caused it to be a borderline case. Similarly for benzyl mercaptan, the adjacent benzyl group offered additional stabilisation to the alkylthiyl radical and hence caused it to be a borderline case. In presence of the other alkylthiols, R2 was favoured, due to its benzylic stabilisation outweighing the poorly stabilising alkyl groups for R1 stabilisation.

Tandem MS was conducted upon peaks corresponding to trapped radicals in all reactions, to offer further validity to their suggested structures (SI4.2.5). Tandem MS of these peaks yielded fragments which sensibly corresponded to the predicted trapped radical structures.

6.4.8. Effect of different alkenes on reaction kinetics

Tyson *et al.* tested alkene scope whilst utilising benzyl mercaptan as thiol. Whilst obtained yields were high, reaction time varied significantly for different alkenes. For example, the standard styrene reaction reached a 98% yield after 2 h, whilst ethyl *trans*-cinnamate reached a 93% yield after 26 h, with R1 adding to the double bond at the α -carbonyl position and hence R2 being formed at the β -carbonyl position.²⁰⁵ This demonstrates variable reaction rates for different alkenes, affecting radical population throughout the reaction. Thus it was hypothesised that in presence of radical trap, different alkenes would incur different trapped radical intensities. Therefore, like for different thiols, standard radical trapping reaction optimised previously (6.4.2) was undertaken, but using benzyl mercaptan and different alkenes as substrates (Table 22, 11.5.2.9). Six of the fourteen alkenes Tyson *et al.* obtained products for were probed (Figure 102). Furthermore, since TART trapping of benzyl mercaptan-alkene was now understood to occur slowly, aliquots were removed from these reactions periodically over 24 h, so that comparisons between different alkenes could be drawn when TART-trapped radical concentrations were suitably high for MS characterisation. This occurred after 24 h.

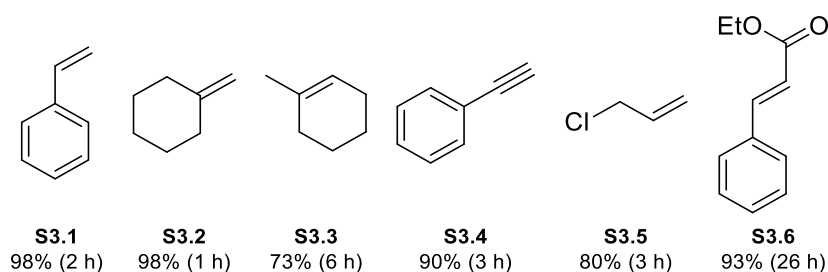


Figure 102: Alkenes probed in TART trapping of radical thiol-ene addition (11.5.2.9). Literature yields after the indicated reaction time are shown for the associated thioether product of each alkene.²⁰⁵

Table 22: Species identified from TART trapping of Ru-photocatalysed radical thiol-ene addition under standard conditions after 24 h, using benzyl mercaptan and different alkenes as substrates and MS for characterisation (11.5.2.9). Cl containing species are shown with ³⁵Cl only. Systematic *m/z* error = -0.0005; random *m/z* error = ±0.0012; 100% intensity = 2.11×10⁹ absolute count.

Alkenes S3.		1	2	3	4	5	6
Species		Intensity relative to unreacted TART standard / %					
TART	[CHANT+H] ⁺	72.2	7.91	9.79	1.50	10.1	7.78
Trapped radicals	[R1-ART+H] ⁺	0.176	0.260	0.139	1.26	0.138	0.400
	[R1-ART+Na] ⁺	1.43	2.45	3.28	7.29	1.19	2.48
	[R1-TEMPO+H] ⁺	0.014	0	0	0.014	0	0
	[R2-ART+H] ⁺	0.317	0	0	0.049	0.006	0
	[R2-ART+Na] ⁺	0.314	0	0	0	0.014	0
	[R2-TEMPO+H] ⁺	5.13	0.008	0.017	0.240	0.044	0.209
Other trapped radicals	[R1-ART+S2+H] ⁺ (thiol-ene addition)	0.005	0.039	0.164	0.217	0.052	0.042
	[R1-ART+S2+Na] ⁺ (thiol-ene addition)	0.010	0.116	0.236	0.800	0.065	0.090
Products	[P2+H] ⁺	0.031	0.008	0	0.015	0	0.061
	[P2+Na] ⁺	0.045	0	0	0.027	0	0.500
Other products	[TART+S2+H] ⁺ (thiol-ene addition)	1.73	3.69	7.43	17.6	4.17	3.78
	~[R1-ART+X] ⁺ /[R2-ART+X] ⁺ ^a	2.54	>1360	>1710	175	68.3	>1440
	Resting state ^b	~R2	R1	R1	~	~R1	R1

^aEstimated by ratio of summed intensities of peaks corresponding to protonated (X = H) and sodiated (X = Na) MS adducts. Greater than ratios (>) were determined assuming [R2-ART+X]⁺ was at intensity detection limits (0.002%). ^bDetermined using kinetic modelling (11.10.2).

TART corresponding peaks were decreased compared to the unreacted TART standard, as expected. However, these results indicated TART was consumed much less significantly with styrene than any other alkene. In contrast, TART was consumed most significantly in presence of phenylacetylene (S3.5).

Peaks corresponding to R1-ART were in all reactions. In contrast, R2-ART corresponding peaks were only observed in presence of S3.1, S3.4 and S3.5. As such, [R1-ART+X]⁺/[R2-ART+X]⁺ was smaller for these three species, indicating R2 is relatively more populated. As previously, kinetic modelling (11.10.2) indicated that in presence of styrene (S3.1), modelling indicated R2 was the resting state, although was a borderline case. For phenylacetylene (S3.5) modelling indicated R1 and R2 were similarly populated and hence no resting state was determined. R2 was destabilised for phenylacetylene compared to styrene, as R2 was centred on a double bond instead of a single bond, meaning the radical was less delocalised, due to the smaller size of the radical atom. All other alkenes had R1 resting states, with allyl chloride (S3.5) being a borderline case. For styrene, R2 was more stabilised than for S3.2, S3.3 and allyl chloride, due to the adjacent phenyl ring offering resonance stabilisation. Allyl chloride was a borderline case, due to the adjacent β-chlorine atom offering some additional stabilisation over β-alkyl groups. Finally, ethyl *trans*-cinnamate was an interesting case. Although modelling clearly indicated R1 was the resting state, R2 was stabilised by the adjacent phenyl ring as for styrene. However, it was theorised that formation of R2 from R1 was relatively unfavourable, due to this causing the conjugated system to be broken and hence R1 was the favoured state.

Tandem MS was conducted upon peaks corresponding to trapped radicals in all reactions, to further validate their suggested structures (S14.2.6). The yielded fragments from tandem MS sensibly corresponded to the predicted trapped radical structures.

6.4.9. Conclusion

TART trapping was used to thoroughly characterise mechanistic and kinetic aspects of a Ru-photocatalysed radical thiol-ene addition. This led to several developments in TART trapping methodology. Initially, thiyl radicals (R1) and carbon-centred radicals (R2) were successfully trapped and MS characterised. Results also indicated that thiophenol-styrene self-initiated without requiring photocatalysis.

In radical thiophenol-styrene addition, phenylthiyl radicals were formed so favourably that by altering experimental conditions, TART-trapped phenylthiyl was successfully isolated in a 63% yield and fully characterised. NMR spectra were consistent with the expected structure of this TART-trapped radical, indicating that the TART trapping mechanism occurred as expected. This isolated TART-trapped radical was used to make MS calibration curves.

These calibration curves were used to quantify concentration of TART-trapped phenylthiyl, formed during kinetics experiments involving TART trapping of radical thiophenol-styrene addition, using its corresponding MS peak intensities. This aided improvement of the kinetic model for this reaction, although a high quality fit could not be obtained.

This model aided interpretation of results from TART trapping of other radical thiol-ene additions, in which different thiols and alkenes were used as substrates. This allowed radical resting states to be assigned to these reactions, in absence of TART. This kinetic information could be used to modify radical thiol-ene addition reactions, to improve product yields.

The knowledge gained from TART trapping of radical thiol-ene addition was applied to a more niche but similar radical dearomative spirocyclisation.

6.5. Radical dearomative spirocyclisation

Ho *et al.* developed a catalyst-free photoinitiated radical dearomative spirocyclisation reaction, using assorted indole-tethered ynones and thiols as substrates, forming 20 products with 36-99% yields over 16 h. A mechanism for the main radical cycle of this reaction was hypothesised and offered validity using observations from TART trapping of this system. Ho *et al.* also independently suggested the same mechanism, which was later published, though without TART trapping validation (Figure 103).²¹²

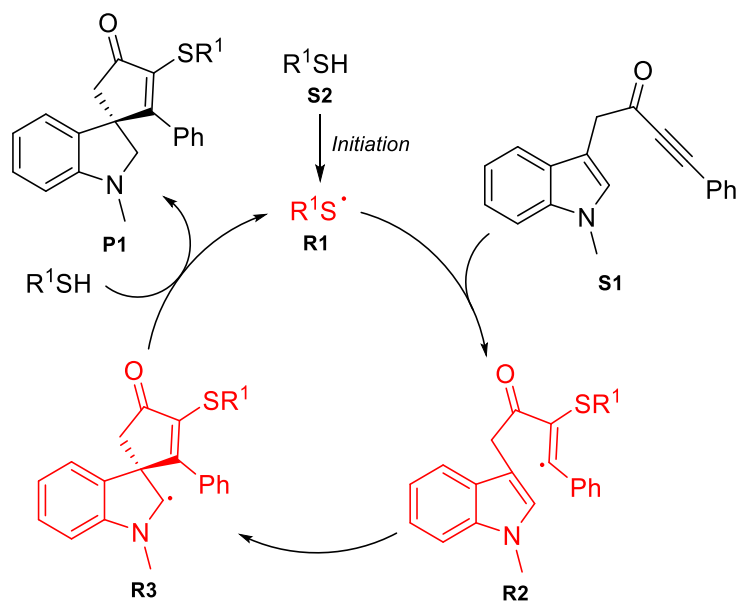


Figure 103: Mechanism of photoinitiated radical dearomative spirocyclisation for indole-tethered ynone (S1), hypothesised based upon TART trapping observations and independently proposed by Ho *et al.*²¹²

TART trapping was used to probe the main radical cycle mechanism (6.5.1), initiation mechanism (6.5.2) and the effects of different thiols on the reaction mechanism and kinetics (6.5.3).

6.5.1. Main radical cycle mechanism

First, the mechanism of the main radical cycle was probed. For this, TART trapping of the photoinitiated radical dearomative spirocyclisation was undertaken, using CHANT as TART, but otherwise replicating literature conditions (Figure 104).²¹² For this, a control reaction containing no TART and a trapping reaction containing TART were undertaken, using an indole-tethered ynone (S1) and 3-methoxythiophenol (S2) as substrates. These reactions and an unreacted TART standard were then MS characterised (Table 23, 11.5.3.2). Hon Ho synthesised the starting materials and performed these initial trapping reactions and controls. MS characterisation and mass spectra analysis performed by the author.

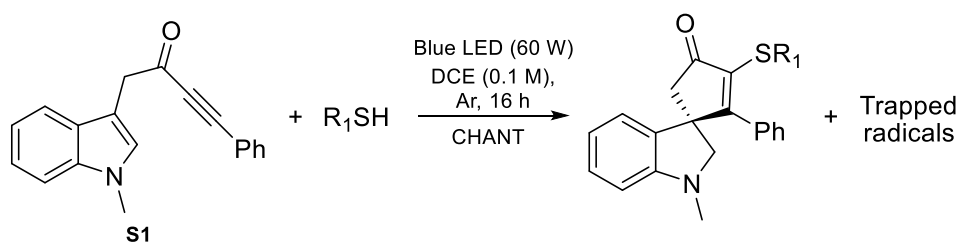


Figure 104: TART trapping of photoinitiated radical dearomative spirocyclisation, using indole-tethered ynone (S1) and 3-methoxythiophenol as substrates and CHANT as TART (11.5.3.2).

Table 23: Species identified from TART trapping of photoinitiated radical dearomative spirocyclisation, using 3-methoxythiophenol as substrate (1.6 eq.) and MS for characterisation (11.5.3.2). Systematic m/z error = -0.0003; random m/z error = ± 0.0025 ; 100% intensity = 3.66×10^9 absolute count.

	Species	Predicted m/z	Intensity relative to unreacted TART standard / %		
			Trapless control	TART standard	Trapping reaction
TART	[CHANT+H] ⁺	323.2698	0	100	33.3
Reactants	[S1+H] ⁺	274.1232	0.002	0	5.58
	[S1+Na] ⁺	296.1051	0.067	0	0.150
Trapped radicals	[R1-ART+H] ⁺	306.1528	0	0	3.83
	[R1-ART+Na] ⁺	328.1347	0	0	18.6
	[R2/R3-ART+H] ⁺	579.2681	0	0	0.005
	[R2/R3-ART+Na] ⁺	601.2501	0	0	0.058
	[R2/R3-TEMPO+H] ⁺	569.2838	0	0	0
Other trapped radicals	[R1-ART+S2+H] ⁺ (thiol-ene addition)	463.2994	0	0	0.612
	[R1-ART+S2+Na] ⁺ (thiol-ene addition)	485.2814	0	0	0.028
Products	[P1+H] ⁺	414.1527	72.4	0	4.56
	[P1+Na] ⁺	436.1347	9.93	0	62.6

Intensity of the MS peak corresponding to CHANT was ~33% in the trapping reaction compared to the unreacted TART standard, indicating around ~67% of TART was consumed during the trapping reaction. Peaks corresponding to S2 were not observed, likely owing to poor ionisation efficiency. Peaks corresponding to S1 were observed significantly more intensely in presence than absence of TART, likely due to TART quenching the radical cycle and hence, S1 was consumed less rapidly. Peaks corresponding to P1 were observed with significant intensity both in presence and absence TART, indicating all radicals formed in absence of TART were available for trapping.

Peaks corresponding to R1-ART and R2/R3-ART were observed exclusively in the trapping reaction. R2 and R3 had the same molecular formula and therefore, R2 and R3-derived species were indistinguishable. However, it was predicted that peaks corresponding to R2/R3-ART were mainly due to R3-ART, as intramolecular cyclisation was predicted to be rapid and hence R2 trapping was unlikely, as observed previously in TART trapping of radical cyanomethylation (6.3). Further characterisation was required to confirm this.

As previously, results indicated that S2 could add to TART-trapped radicals. However, the intensities observed suggested that this had not occurred too significantly, as desired.

No other radicals were observed and hence, the initiation mechanism was still unknown. Therefore, TART trapping was used to try and determine the initiation mechanism.

6.5.2. Initiation mechanism

The initiation mechanism of radical dearomative spirocyclisation was of particular interest, as although the reaction was photoinitiated, it did not require a photocatalyst. This was unusual and consequently, the initiation mechanism was poorly understood. UV-Vis spectra obtained by Ho *et al.* suggested that S1 formed an intramolecular charge transfer complex that could undergo electron transfer upon photoexcitation, forming a zwitterionic diradical (Figure 105).

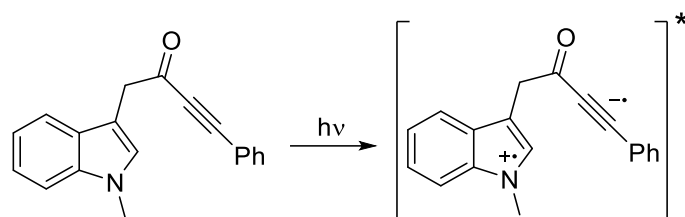


Figure 105: Initiation of radical dearomative spirocyclisation via indole-tethered ynone excitation, as suggested by Ho *et al.*²¹²

This suggested that S2 was not required for initial excitation. Initiation was predicted to be a slow process due to a high activation barrier. However, once R1 was formed through initiation, the radical cycle (Figure 103) was expected to occur at a much faster rate, quickly depleting remaining S1, similarly as for radical thiol-ene addition (6.4.6). This theory assumed radical cycle quenching was low. Therefore, few S1 were expected to be produced during initiation in S2 presence, owing to remaining initiator S1 being quickly depleted in the main radical cycle.

As such, TART trapping of radical dearomative spirocyclisation was undertaken as previously, but with reduced amounts of S2 (11.5.3.3). It was theorised that with less thiol available for reaction, S1 would be more slowly depleted and therefore, would allow more initiation reactions to occur. It was hoped that radicals produced later in this initiation process would be sufficiently trapped to allow MS detection. An initiation mechanism (Figure 106) was suggested for the trapless reaction based upon MS characterisation of TART-trapped radicals from these experiments (Table 24, 11.5.3.3). In this suggested initiation mechanism, photoexcitation of S1 forms a zwitterionic diradical, as described by Ho *et al.*²¹² This zwitterionic diradical and its derivatives react with thiol S2 leading to S1-derived radicals R4/R5 and thiyl radical R1 or undergo charge transfer with another S1 to form S1-derived radical R6. R4-R6 may further react with S2 to form R1 (Figure 106). Formed R1 then undergoes propagation in the main radical cycle (Figure 103).

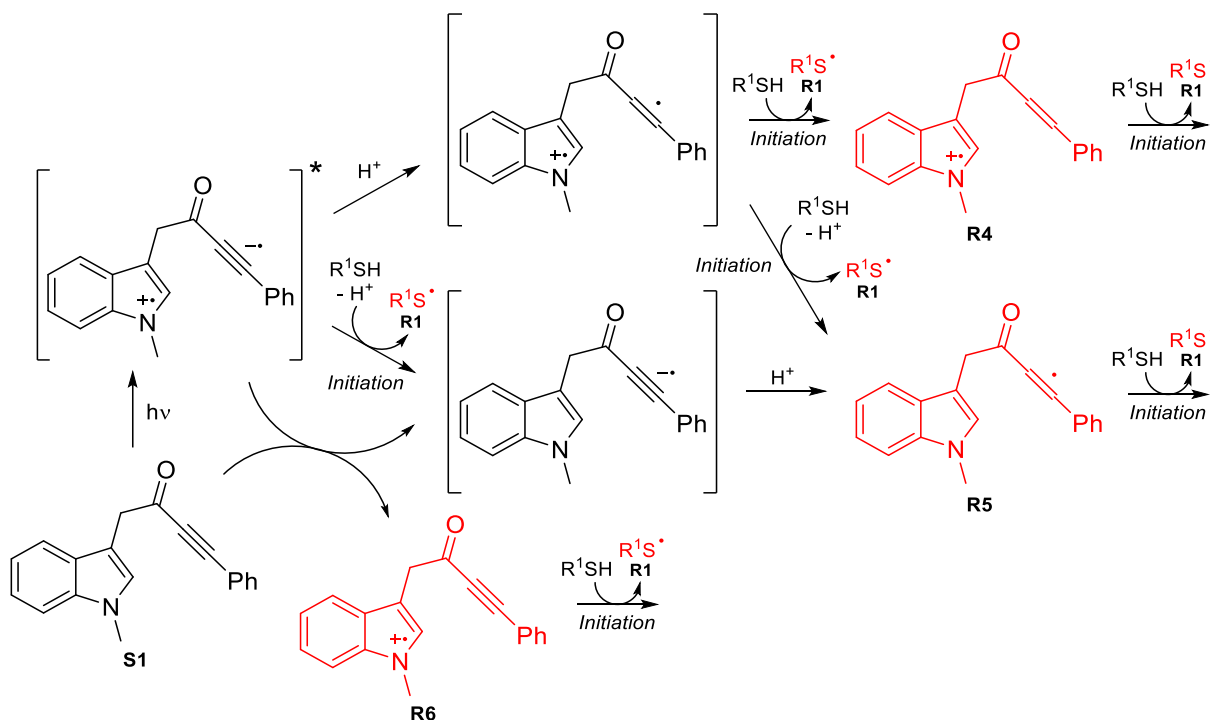


Figure 106: Hypothesised initiation mechanism for photoinitiated radical dearomative spirocyclisation.

Table 24: Species identified from TART trapping of radical dearomative spirocyclisation, using different quantities of 3-methoxythiophenol as substrate (0.0-1.6 eq.) and MS for characterisation (11.5.3.3). Systematic m/z error = 0.0000; random m/z error = ± 0.0025 ; 100% intensity = 5.45×10^9 absolute count.

	Species	Predicted m/z	Intensity relative to unreacted TART in 0.0 eq. /		
			0.0 eq.	0.5 eq.	1.6 eq.
TART	[CHANT+H] ⁺	323.2698	100	0.206	0
Reactants	[S1+H] ⁺	274.1232	3.93	0	0.411
	[S1+Na] ⁺	296.1051	22.6	0.353	0
Trapped main cycle radicals	[R1-ART+H] ⁺	306.1528	0.007	0.054	0.445
	[R1-ART+Na] ⁺	328.1347	0.015	0.139	0.678
	[R2/R3-ART+H] ⁺	579.2681	0	0.072	0.010
	[R2/R3-ART+Na] ⁺	601.2501	0.001	0.784	0.086
	[R2/R3-TEMPO+H] ⁺	569.2838	0	0	0.003
Trapped initiation radicals	[R4-ART] ⁺	441.2542 ^a	0.006	0.002	0
	[R5-ART+H] ⁺	441.2542 ^a	0.006	0.002	0
	[R5-ART+Na] ⁺	463.2361	0.043	0.010	0
	[R5-TEMPO+H] ⁺	431.2698	0.062	0.039	1.07
	[R6-ART] ⁺	439.2385 ^a	0.021	0	0
Other trapped radicals	[R7-ART+H] ⁺	439.2385 ^a	0.021	0	0
	[R7-ART+Na] ⁺	461.2205	0.024	0	0
	[R7-TEMPO+H] ⁺	429.2542	0	0	0
	[R8-ART+H] ⁺	264.0922	0.007	0	0
	[R8-ART+Na] ⁺	286.0741	0.017	0	0
	[R8-TEMPO+H] ⁺	254.1078	0	0	0
Products	[P1+H] ⁺	414.1527	0.021	11.7	19.8
	[P1+Na] ⁺	436.1347	0.057	1.68	11.2

^aOther table entries have predicted species with same m/z .

Peaks corresponding to CHANT decreased significantly with increasing thiol equivalence. This suggested that radical concentrations were much higher in presence of thiol. Intensity of S1 corresponding peaks decreased significantly with increasing thiol equivalence. This suggested that S1 was depleted much faster through the radical cycle than through initiation, as theorised. Likewise, intensity of P1 corresponding peaks increased significantly with increasing thiol equivalence, as expected.

[R4-ART]⁺ and [R5-ART+H]⁺ had the same molecular formula and therefore, were indistinguishable using MS. Peaks corresponding to R4/R5-ART and R6-ART decreased in relative intensity when thiophenol equivalence increased. This was expected as these radicals would react rapidly with thiols leading to further initiation. Furthermore, fewer initiation reactions were expected to occur in thiol presence, due to the increased S1 depletion caused by the faster dominating radical cycle that occurs following R1 formation.

R6 formation involved charge transfer from excited S1. Therefore, this reaction would be expected to proceed in thiol absence. However, for initiation from S1 forming R4/R5, a labile hydrogen atom source was required. Due to its weak S-H bond, thiol was the most likely source of labile hydrogen atoms when present. In thiol absence however, the labile hydrogen atom source was less certain. HAA could have occurred from S1, forming R7 (Figure 107). Alternatively, HAA occurred from dichloroethane (DCE) solvent, forming R8 (Figure 107). MS peaks corresponding to R7-ART and R8-ART were observed exclusively when thiol was absent. Despite the vastly greater quantity of DCE available for HAA than S1, the relatively high activation barrier of HAA from haloalkanes resulted in a lower corresponding peak intensity of R8-ART than R7-ART.⁵⁷

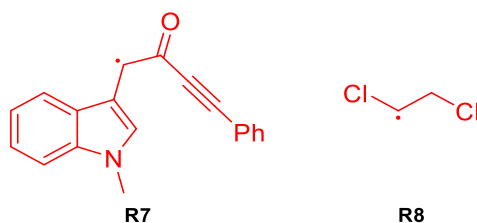


Figure 107: Radicals formed from HAA abstraction from S1 or DCE in absence of thiol.

Peaks corresponding to TART-trapped radicals formed through initiation decreased with varying linearity as thiol equivalence increased. Peaks corresponding to R4/R5 were observed with 0.0 eq. to 0.5 eq. of thiol, whilst peaks corresponding to R6/R7 and R8 were not. This agreed with the suggested initiation mechanism, since formation of R4/R5 occur more efficiently in thiol presence and therefore these initiation routes were accelerated, however this was counteracted by partial S1 depletion caused by faster dominating radical cycle. Conversely charge transfer for R6 formation was not accelerated by thiol presence, but S1 depletion occurred more rapidly, causing decreased R6 formation. Furthermore, HAA by S1 would occur preferentially from thiol to S1 or DCE, causing decreased formation of R7 and R8. Therefore, formation of R6, R7 and R8 decreased more rapidly with increasing thiol equivalence than R4/R5. TART-trapped radicals formed through initiation were not observed with 1.6 eq. thiol, likely due to rapid S1 depletion in the main reaction cycle leaving little S1 for initiation. These observations support the proposed initiation mechanism (Figure 106).

Tandem MS of peaks corresponding to TART-trapped initiation radicals was attempted but their low intensities meant that they could not be suitably isolated.

Intensity of peaks corresponding to R1-ART and R2/R3-ART did not increase linearly compared to each other with increasing thiol equivalence. R1-ART corresponding peak intensity peaked with 1.6 eq. thiol, whereas R2/R3-ART corresponding peak intensity peaked with 0.5 eq. thiol. This was hard to explain without modelling, though this was not undertaken.

6.5.3. Effects of different thiols on reaction mechanism and kinetics

TART trapping of radical thiol-ene addition was used to explore the effects of thiols on reaction kinetics, similarly as was undertaken for radical thiol-ene addition (6.4.7).

Ho *et al.* tested thiol scope in their system, using S1 as substrate and obtaining 37-99% product yields. As previously, TART trapping results could be used to inform reaction kinetics, determine the radical resting state and potentially aid development of reaction conditions to improve product yields.

Therefore, TART trapping of radical dearomative spirocyclisation was undertaken as previously, but with different thiols used as substrate (Table 25, 11.5.3.4). Four thiols used by Ho *et al.* to probe reaction scope were used as thiol substrates. These varied significantly in structure and product yield: 3-methoxythiophenol (S2.3, 94%); cyclohexanethiol (S2.4, 74%); methyl thiosalicylate (S2.5, 54%) and ^tBuSH (S2.6, 37%).²¹²

Table 25: Species identified from TART trapping of radical dearomative spirocyclisation, using different thiols as substrate (1.6 eq.) and MS for characterisation (11.5.3.4). Systematic m/z error = 0.0000; random m/z error = ± 0.0026 ; 100% intensity = 5.45×10^9 absolute count.

Thiol S2.		3	4	5	6
Literature yield ²¹² / %		94	74	54	37
Species		Intensity relative to unreacted TART standard / %			
TART	[CHANT+H] ⁺	0.012	0	0.017	0.013
Reactants	[S1+H] ⁺	0.763	0.492	1.44	0.280
	[S1+Na] ⁺	0.006	0.276	0	0.416
Trapped radicals	[R1-ART+H] ⁺	0.661	0.546	0.980	0.874
	[R1-ART+Na] ⁺	1.01	1.25	3.49	1.41
	[R2/R3-ART+H] ⁺	0.015	0.141	0.013	0.188
	[R2/R3-ART+Na] ⁺	0.127	1.32	0.005	2.00
	[R2/R3-TEMPO+H] ⁺	0	0	0	0
Products	[P1+H] ⁺	29.5	121	61.3	81.7
	[P1+Na] ⁺	16.7	15.7	32.9	7.96
	\sim [R1-ART+X] ⁺ /[R2/R3-ART+X] ⁺ ^a	11.8	1.23	251	1.04

^aEstimated by ratio of summed intensities of peaks corresponding to protonated (X = H) and sodiated (X = Na) MS adducts.

In general, these results showed similar trends to results from TART trapping of radical thiol-styrene addition, using different thiols as substrates.

Results indicated that TART was near totally consumed in all reactions. Likewise, peaks corresponding to products were observed in all reactions. However, results also indicated that a significant quantity of S1 remained, meaning the reactions had not gone to completion.

In general, peaks corresponding to R1-ART were more intense for functionalised thiophenols. This was likely due to increased R1 stability due to aromatic resonance stabilisation. Conversely, peaks corresponding to R2/R3-ART were more intense for alkylthiols. This is likely due to the poorer stability of R1, causing less favourable radical HAA by R3. These observations were similar as for radical thiol-ene addition (6.4.7). However, [R1-ART+X]⁺/[R2/R3-ART+X]⁺ was higher for methyl thiosalicylate (S2.5) than 3-methoxythiophenol (S2.3). The reason for this was not totally understood. However, it was tentatively hypothesised that the greater electron withdrawing effect of methyl thiosalicylate reduces alkene electron density on the carbon-centred radical, stabilising it.

From the obtained [R1-ART+X]⁺/[R2/R3-ART+X]⁺ it was suggested that for thiophenols, the radical resting state was R1, whereas for alkylthiols, the radical resting state was R2, as for radical thiol-ene addition (6.4.7). However, confidently interpreting these ratios required kinetic modelling, which was not attempted.

Tandem MS was conducted upon peaks corresponding to trapped radicals in S2.6 reactions, to offer further validity to their suggested structures (SI4.2.5). Tandem MS of these peaks yielded fragments which sensibly corresponded to the predicted trapped radical structures.

6.6. Conclusions and future work

MS peaks corresponding to TART-trapped carbon-centred and heteroatom-centred radicals were successfully observed in multiple photochemical radical reactions, some of which used transition metal complexes as photocatalysts. In general, spin trapping and nitroxyl radical recombination trapping would have been inappropriate to study such systems, due to spin traps being easily degraded by transition metal catalysts and nitroxyl radical recombination

traps not be able to trap heteroatom-centred radicals (1.3.2).¹²⁸ Direct radical characterisation techniques would also have been inappropriate, due to these reactions being complex and many of the intermediate radicals having low concentration and being short-lived (1.3.1). Therefore, TART trapping offered advantages over existing radical characterisation techniques.

TART trapping offered validation to previously hypothesised main radical cycles. For a Ru-photocatalysed radical thiol-ene addition, TART trapping indicated that thiophenol-styrene addition could self-initiate. By adjusting experimental conditions, a TART-trapped phenylthiyl radical was successfully isolated in a 63% yield and fully characterised, with NMR spectroscopy confirming the hypothesised structure of this TART-trapped radical. This validated that the TART trapping mechanism occurred as hypothesised. Using this TART-trapped radical, MS calibration curves were recorded, allowing concentration of TART-trapped phenylthiyl to be obtained from the MS intensities of its corresponding peaks. This calibration curve was used to improve a kinetic model by relating it to a kinetics experiment in which mass spectra were recorded over time for TART trapping of radical thiophenol-styrene addition. Intensities of peaks corresponding to TART-trapped radicals formed during TART trapping of radical thiol-ene addition, using different thiols and alkenes as substrates, were then used in conjunction with the model, to estimate radical resting states for each reaction. This suggested that TART trapping could be used to inform and potentially measure reaction rate constants. This improved knowledge could be used to improve product yields in trapless reactions, by changing reaction conditions to increase the rate constant of the rate limiting step.

A more niche metal-free photoinitiated radical dearomative spirocyclisation reaction, which was related to radical thiol-ene addition, was also investigated using TART trapping. This allowed a main radical cycle to be proposed. Additionally, by changing reaction conditions, peaks were observed corresponding to TART-trapped radicals formed exclusively through initiation. From these radicals, an initiation mechanism was hypothesised. TART trapping and MS characterisation offered a new technique to decipher such mechanisms. As for thiol-ene addition, TART trapping was then used to observe how different thiols affected the reaction mechanisms and kinetics. This showed that TART trapping could have real applications as a tool to aid mechanistic and kinetic understanding.

In general, the biggest improvement that could be made to these investigations is to make TART trapping and MS characterisation more quantitative. This would allow more meaningful interpretation of results and allow models to be fitted and hence make rate constants more accurate, which would further improve interpretation. This could involve using TARTs or substrate which produce species which are observed with similar intensities regardless of species structure, for example by using an ammonium-functionalised TART. HPLC-MS may also improve quantification, by reducing differences in intensity of MS peaks corresponding to species when in presence of other species. Calibration curves of all significant TART-trapped radicals would also allow their concentration to be calculated from their corresponding MS intensities. Substrates and products were also suitably concentrated that they could be monitored using other techniques, such as NMR spectroscopy, to further inform reaction kinetics. Together, these could allow reaction mechanisms and kinetics to be well modelled. Better understanding of these mechanisms and kinetics could lead to improved product yields, by changing reaction conditions which would increase the rate of the rate limiting step.

Additionally, the radical dearomative spirocyclisation should be modelled, including the suggested initiation steps. If the modelling matched experimental observations, this would offer validation to the suggested initiation mechanism.

Selected synthetic radical reactions, including photochemical radical reactions, had been investigated using TART trapping with MS characterisation. Next, TART trapping was applied to aqueous biochemistry systems, to determine if TART trapping could be used to provide them with mechanistic and kinetic insights (7).

7. Biochemistry

7.1. Introduction

Investigation of radical intermediates produced in biological systems is of great scientific interest, particularly in biochemistry and medicinal chemistry (1.2.2). Unquenched radicals produced as by-products during oxidative metabolism, such as reactive oxygen species (ROS) $O_2^{\bullet-}$ and $\bullet OH$, cause cell damage.^{30,34} This cell damage is thought to induce many diseases, such as cancers, autism and Alzheimer's disease.⁴⁰⁻⁴² Oxidative stress describes when a biological system fails to control ROS concentration (1.2.2).^{30,34}

$\bullet OH$ is widely believed to be the most damaging ROS, due to it reacting extremely rapidly and non-specifically with almost any biological component.^{30,34} $\bullet OH$ and HO_2^{\bullet} are formed during free iron-catalysed degradation of H_2O_2 (Figure 8).^{33,34}

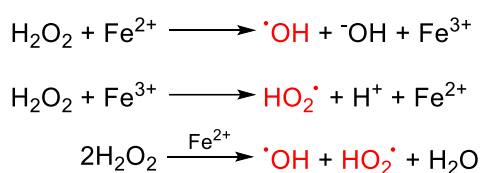


Figure 108: Uncontrolled conversion of H_2O_2 into ROS species $\bullet OH$ and HO_2^{\bullet} , catalysed by Fe^{2+} . Individual equations (top and middle) and overall equation (bottom) are shown.^{33,34}

Though not discussed in further detail, the total mechanism of H_2O_2 degradation by Fe^{2+} is much more complex. Additionally, whilst H_2O_2 reaction with Fe^{2+} is fast, reaction with Fe^{3+} is much slower and hence limits the rate of reaction.

Mildly reactive H_2O_2 , formed in mitochondria as a by-product of oxidative metabolism, can travel far within a biological system, for example, to the cell nucleus. H_2O_2 may then degrade into $\bullet OH$ causing cell damage far from the H_2O_2 source, for example, to DNA in the nucleus. ROS are believed to be able to induce DNA crosslinking, which changes DNA structure and could cause the cell to behave abnormally, either causing cell death or incorrect DNA replication, which could lead to cancer (1.2.2).²¹³⁻²¹⁶ Cell components which are particularly vulnerable to ROS include DNA and proteins.³² Antioxidants, such as ascorbic acid, reduce oxidation of cell components by converting ROS into less harmful species, (1.2.2).^{33,34}

Radical quantification in cells could help determine where and when a biological system is suffering oxidative stress. Furthermore, radical characterisation could allow the site of radical attack and therefore, vulnerable cellular components, to be determined. This information could be used to treat or prevent further damage to damaged cells and cell components. Furthermore, improved knowledge of areas of biological systems likely to experience oxidative stress and vulnerable cellular components could aid development of antioxidants to reduce this oxidative stress (1.2.2). Therefore, TART trapping was used to investigate *in vitro* $\bullet OH$ -initiated substrate degradation of alcohols (7.5), nucleobases (7.6), dipeptides (7.7), saccharides (7.8) and antioxidants (7.9). Nucleobases and dipeptides were investigated as a proxy for key components of DNA and protein macromolecules, as these substrates were much simpler and hence more suitable for initial investigations. Furthermore, MS characterisation would likely be less accurate for high m/z macromolecules, reducing analysis reliability. However, $\bullet OH$ -initiated proxy degradation did not necessarily correspond to $\bullet OH$ -initiated macromolecule degradation. These investigations would determine if TART trapping could be used for studying aqueous biochemistry radical reactions and could offer

these reactions mechanistic and kinetic information. For this, a general methodology was designed for TART trapping of $\bullet\text{OH}$ -initiated biochemical degradation (7.3).

$\bullet\text{OH}$ -initiated biochemical degradation progresses through many possible propagation and termination steps. Principal radicals and products formed are radicals ($\text{R}\bullet$) and for carbon-centred radicals: peroxy radicals ($\text{RO}_2\bullet$); oxyl radicals ($\text{RO}\bullet$); hydroperoxides (ROOH); alcohols (ROH) and carbonyls (RCO). For most biochemicals, these species are produced and destroyed through the same key pathways, as described below.

7.2. General mechanistic steps of $\bullet\text{OH}$ -initiated substrate degradation

7.2.1. $\text{R}\bullet$ formation through $\bullet\text{OH}$ -initiation

$\bullet\text{OH}$ -initiates biochemical degradation by reacting with substrate through the most favourable pathway. Therefore, in species with many different environments, radicals will form more favourably in some locations than others, yielding certain radical structures. $\bullet\text{OH}$ is so reactive that it reacts near immediately once formed, which tends to keep $[\bullet\text{OH}]$ low, with typical rate constants being $10^8\text{-}10^{10} \text{ M}^{-1} \text{ s}^{-1}$ in solution ($\sim\text{RTP}$).²¹⁷ This high reactivity means $\bullet\text{OH}$ generally react with lower selectivity than other radicals, although selectivity is still important. For species not containing unsaturated carbon-carbon bonds, $\bullet\text{OH}$ usually abstracts hydrogen atoms from R-H bonds, to form a new radical $\text{R}\bullet$ and water (Figure 109). Low stability of $\bullet\text{OH}$ and highly favourable formation of water, drive this reaction. Hydrogen atom abstraction (HAA) typically occurs at C-H bonds, but can also occur at other bonds, such as N-H or O-H .²¹⁸

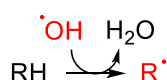


Figure 109: HAA from an R-H bond, by $\bullet\text{OH}$, to form a radical ($\text{R}\bullet$) and water.

HAA from C-H bonds by $\bullet\text{OH}$ typically occurs with rate constants of $10^8\text{-}10^{10} \text{ M}^{-1} \text{ s}^{-1}$ in solution ($\sim\text{RTP}$).^{217,219} HAA by $\bullet\text{OH}$ becomes increasingly favourable as resultant radical stability increases. For example, HAA usually occurs more rapidly from allylic C-H than alkane C-H , due to resonance stabilisation. In addition, HAA occurs faster for 3° C-H than 2° C-H in alkanes. However, HAA may occur more quickly at a 2° carbon-centre than a 3° carbon-centre, due to the former having a greater number of C-H (1.1).

In presence of carbon-carbon unsaturated bonds however, $\bullet\text{OH}$ can instead add to these unsaturated bonds. Proportion of HAA compared to addition is dependent on the stabilities of the resulting intermediate radicals but the two processes are usually competitive. $\bullet\text{OH}$ addition involves $\bullet\text{OH}$ reacting with a double bond to form alcohol β -hydroxyl- $\text{R}\bullet$ and water.²¹⁸ For unsymmetrical alkenes, two different β -hydroxyl carbon-centred radicals may be formed (Figure 110). $\bullet\text{OH}$ addition to alkenes typically occurs with rate constants of $10^9\text{-}10^{10} \text{ M}^{-1} \text{ s}^{-1}$ in solution ($\sim\text{RTP}$).^{217,219}

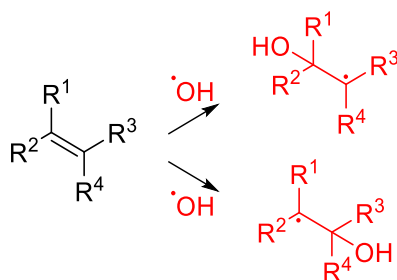


Figure 110: $\bullet\text{OH}$ addition to alkene, forming β -hydroxyl carbon-centred radical.

Carbon-centred radicals, such as those described above, generally have low stability and quickly form peroxy radicals RO_2^\bullet .²¹⁸

7.2.2. RO_2^\bullet formation and degradation

In solution, carbon-centred radicals R^\bullet rapidly react with dissolved O_2 to form peroxy radicals RO_2^\bullet , with rate constants typically being $\sim 10^9 \text{ M}^{-1} \text{ s}^{-1}$ ($\sim \text{RTP}$) in solution (Figure 111).^{220,221} RO_2^\bullet are generally relatively stable and consequently long-lived, degrading in solution with typical rate constants being $10^6\text{-}10^7 \text{ M}^{-1} \text{ s}^{-1}$ ($\sim \text{RTP}$).²²¹ As such, RO_2^\bullet degradation, which is generally slow, usually strongly influences the overall rate of reaction.²¹⁸

RO_2^\bullet typically degrade through $\text{RO}_2^\bullet + \text{RO}_2^\bullet$ reaction, propagating to form two highly unstable oxyl radicals (RO^\bullet), terminating to form alcohol (ROH) and carbonyl (RCO) via a non-radical pathway (known as the Russel Mechanism) or coupling to form peroxide (ROOR), with O_2 being released in all processes (Figure 111). These two RO_2^\bullet species may have different structures, resulting in two potential RO^\bullet and ROH structures, up to two RCO structures, depending on each RO_2^\bullet structure, and one ROOR , for each RO_2^\bullet pair.²¹⁸ Proportion of propagation, termination and coupling depends on RO_2^\bullet structure and resulting radical intermediate and product stabilities. HAA may occur from ROH and RCO , forming new R^\bullet , whilst ROOR can reversibly decay to form RO^\bullet , although this process is usually slow at RTP.²¹⁸ Besides ROOR formation through TART trapping, ROOR product formation was largely ignored, since many possible ROOR structures would significantly complicate analysis.

Alternatively, RO_2^\bullet may undergo reversible intramolecular or intermolecular HAA (Figure 111), forming hydroperoxide ROOH .²¹⁸ If this occurs from an α -hydroxyl- RO_2^\bullet , a highly unstable RO^\bullet is formed, which quickly fragments to form a carbonyl and HO_2^\bullet (7.2.3, Figure 112).²¹⁸ HAA by RO_2^\bullet can also occur with HO_2^\bullet , forming ROOH and O_2 . HAA is significantly slower for RO_2^\bullet than $\bullet\text{OH}$, due to the greater stability of RO_2^\bullet compared to $\bullet\text{OH}$. For example, RO_2^\bullet and $\bullet\text{OH}$ react with $(\text{CH}_3)_2\text{CHOH}$ with rate constants $\sim 10^{-2}$ (303 K) and $\sim 10^9 \text{ M}^{-1} \text{ s}^{-1}$ ($\sim \text{RTP}$) respectively.^{219,222} ROOH can reversibly degrade to form RO^\bullet and $\bullet\text{OH}$, although this process is usually slow at RTP (Figure 111).²¹⁸

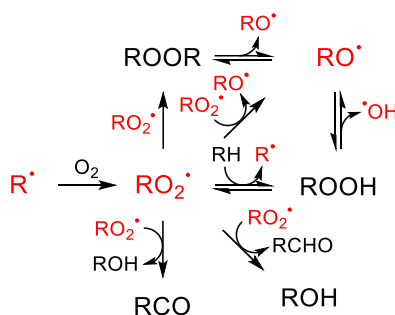


Figure 111: RO_2^\bullet formation from R^\bullet and subsequent RO_2^\bullet degradation. O_2 release is not shown.

Relative proportion of $\text{RO}_2^\bullet + \text{RO}_2^\bullet$ reactions to HAA by RO_2^\bullet is dependent on concentrations of RO_2^\bullet and hydrogen atom donors and stabilities of RO_2^\bullet and resulting intermediate radicals and products. The RO^\bullet species formed through these processes are highly unstable and degrade rapidly.²¹⁸

7.2.3. RO^\bullet degradation

Oxyl radicals RO^\bullet are highly unstable and hence very reactive, with similar reactivity to $\bullet\text{OH}$. As such, RO^\bullet degrade rapidly through many possible paths. RO^\bullet can undergo intramolecular or intermolecular HAA, forming a radical R^\bullet and ROH (Figure 112).²¹⁸

Alternatively, RO• may fragment to form a carbonyl species and new radical R• (Figure 112). This occurs rapidly for α-hydroperoxide-RO•, forming RCO and HO₂•, and carboxyl radical, forming carbon-centred radical R• and CO₂ (Figure 112).²¹⁸ RO• may also undergo radical-radical coupling with RO• to form ROOR (Figure 111).

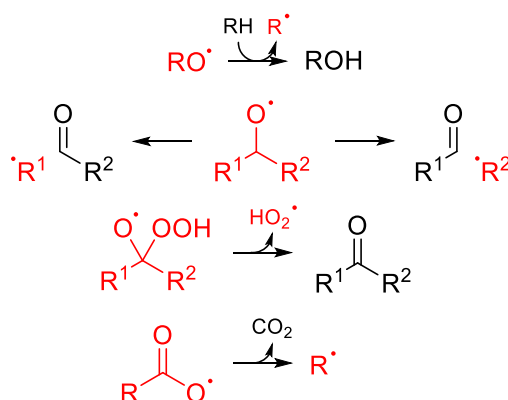


Figure 112: Common RO• degradation pathways.

Relative proportion of HAA by RO•, fragmentation and radical-radical coupling is dependent on concentrations of hydrogen atom donors and stabilities of resulting intermediate radicals and products.

These key •OH-initiated substrate degradation pathways can be used to predict an overall mechanism for a particular substrate. Principal radicals and products formed usually include radicals (R•) and for carbon-centred radicals (R•): peroxy radicals (RO₂•); oxy radicals (RO•); hydroperoxides (ROOH); alcohols (ROH), carbonyls (RCO) and peroxides (ROOR). TART trapping of these systems will involve trapping of R•, RO₂• and RO• and subsequent MS characterisation. Differences in trapping rates of these types of radicals will affect concentrations of TART-trapped radicals. Therefore, quantifying radical concentrations in solution through measuring TART-trapped radical concentration requires consideration of TART trapping rate.

7.2.4. Trapping rates

According to Hammond's postulate, rates of radical reaction are strongly dependent on radical stability. Radical stability is dependent on the radical atom and its surrounding structure (1.1). This also holds true for radical trapping, meaning some radicals are trapped much more efficiently than others, resulting in relatively greater trapped radical concentrations. Subsequent MS characterisation then measures higher intensity for these greater trapped radical concentrations. This was previously observed in photochemistry (6). Therefore, rate of radical trapping must be carefully considered when determining radical concentration from MS intensities of trapped radicals.

Since no literature rate constants were available for TART trapping, rate of TART trapping was estimated using solution phase rate constants for radical addition to alkenes, ideally methacrylates, forming a new carbon-centred R• (Figure 113). These literature reactions were chosen such that their substrates used were as similar as possible to the substrates used experimentally.

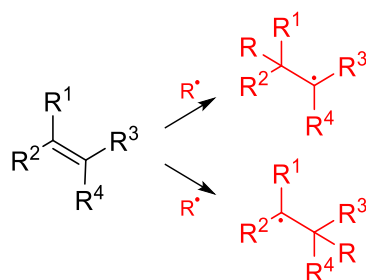


Figure 113: Radical reaction with alkenes, used to estimate rate of TART trapping.

As shown above, $\bullet\text{OH}$ -initiated biochemical degradation yields carbon-centred R^\bullet , RO_2^\bullet and RO^\bullet . R^\bullet stability is dependent on the structure surrounding the radical. For example, $\bullet\text{CH}_3$ and $(\text{CH}_3)_3\text{C}^\bullet$ react with $\text{H}_2\text{C}=\text{C}(\text{CH}_3)_2$ with rate constants $\sim 10^4$ and $\sim 10^3 \text{ M}^{-1} \text{ s}^{-1}$ (298 and 300 K) respectively.^{223,224}

RO_2^\bullet are generally relatively stable, hence RO_2^\bullet addition to alkenes, such as TARTs, is generally slow. R^\bullet are generally less stable, hence R^\bullet addition to alkenes is faster. For example, $(\text{CH}_3)_3\text{C}^\bullet$ reacts with $\text{H}_2\text{C}=\text{C}(\text{H})\text{COOCH}_3$ with rate constant $\sim 10^6 \text{ M}^{-1} \text{ s}^{-1}$ (299 K) whilst $(\text{CH}_3)_3\text{CO}_2^\bullet$ reacts with $\text{H}_2\text{C}=\text{C}(\text{CH}_3)\text{COOCH}_3$ with rate constant $\sim 0.1 \text{ M}^{-1} \text{ s}^{-1}$ (303 K).^{225,226} These alkenes have similar alkene functionality to TARTs. TEMPO^\bullet reacts rapidly with carbon-centred radical R^\bullet , for example $(\text{CH}_3)_3\text{C}^\bullet$ recombination with TEMPO^\bullet occurs with rate constant $\sim 10^9 \text{ M}^{-1} \text{ s}^{-1}$.²¹⁰ This is orders of magnitude faster than R^\bullet reaction with TARTs. In contrast, TEMPO^\bullet does not recombine with RO_2^\bullet , since the N-O-O bond that would be formed would be very weak.

RO^\bullet are poorly stable, hence RO^\bullet addition to alkenes is rapid. As such RO^\bullet react much more efficiently with alkenes. For example, $(\text{CH}_3)_3\text{CO}_2^\bullet$ reacts with $(\text{CH}_3)_2\text{C}=\text{C}(\text{CH}_3)_2$ with rate constant $\sim 10 \text{ M}^{-1} \text{ s}^{-1}$ (393 K) whilst $(\text{CH}_3)_3\text{CO}^\bullet$ reacts with norbornene with rate constant $\sim 10^6 \text{ M}^{-1} \text{ s}^{-1}$ (301 K).^{227,228} TEMPO^\bullet does not recombine with RO^\bullet , since the N-O-O bond that would be formed would be very weak.

Reaction kinetics would ideally be investigated in conjunction with kinetic modelling. However, due to the general lack of rate constants available for $\bullet\text{OH}$ -initiated biochemical degradation pathways, such modelling would be challenging and time consuming and therefore, was not undertaken. However, comparable modelling was undertaken for gaseous systems involving RO_2^\bullet and RO^\bullet (8.6.3.7 and 9.4.3).

Key $\bullet\text{OH}$ -initiated substrate degradation pathways and kinetics, allowed an overall mechanism to be determined for substrates. A broad understanding of trapping rates enabled some quantitative conclusions to be drawn from results of TART trapping of $\bullet\text{OH}$ -initiated substrate degradation. A general methodology was designed for TART trapping of $\bullet\text{OH}$ -initiated biochemical degradation and subsequent MS characterisation.

7.3. Methodology

For TART trapping of $\bullet\text{OH}$ -initiated biochemical degradation, $\bullet\text{OH}$ was generated using Fenton chemistry, which utilised iron-catalysed H_2O_2 degradation to generate $\bullet\text{OH}$ and HO_2^\bullet , as occurs similarly in biological systems (Figure 8).²²⁹ Therefore, this system partially emulated biological conditions. In contrast, an acetic acid/sodium acetate buffer was used to create an acidic system (pH 4), which was below what was usually biologically relevant (pH 7.0-7.4).²³⁰ This was because at biologically relevant pH, Fe^{3+} solubility would be significantly reduced, forming insoluble $\text{Fe}(\text{OH})_3$. Fe^{3+} precipitation would restrict access to Fe^{3+} , causing significant slowing of reaction rate. This is especially significant since the reaction between H_2O_2 and

Fe^{3+} is rate limiting. Therefore, pH was lowered to prevent Fe^{3+} precipitation. At lower pH still, Fe^{2+} coordinates more strongly to water, forming more tightly bound $[\text{Fe}(\text{H}_2\text{O})_6]^{2+}$, which restricts access to Fe^{2+} , reducing the rate of reaction. Therefore an optimal pH 4 was used in the system, as is commonly used in Fenton chemistry.²³¹ Importantly, acetic acid/sodium acetate buffer was also vulnerable to degradation by $\bullet\text{OH}$.

To emulate $\bullet\text{OH}$ -initiated biochemical degradation, the biochemical of interest (1 eq.) was included into the Fenton chemistry system, containing H_2O_2 (10 eq.) and FeSO_4 catalyst (1 eq.). The procedure and conditions used were adapted from literature procedures.^{232–234} For TART trapping of $\bullet\text{OH}$ -initiated biochemical degradation, TART (0.1 eq.) was similarly included in the same system. This was hoped to generate trapped radicals and products of $\bullet\text{OH}$ -initiated biochemical degradations (11.6.3, Figure 114). All $\bullet\text{OH}$ -initiated biochemical degradation reactions were left open to air and stirred rapidly, allowing atmospheric O_2 to immediately replace consumed aqueous O_2 .

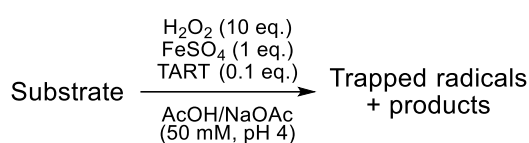


Figure 114: General TART trapping of $\bullet\text{OH}$ -initiated biochemical degradation (11.6.3).

H_2O_2 was significantly in excess of substrate and TART, with a 10 and 100 fold excess respectively. Each H_2O_2 had the potential to form two $\bullet\text{OH}$. Even though side reactions may cause $\bullet\text{OH}$ quenching, it was therefore likely that $\bullet\text{OH}$ was significantly in excess of substrate and TART. This meant that non-radical products formed following $\bullet\text{OH}$ reaction with substrate could be reinitiated by another $\bullet\text{OH}$. This does not well emulate a biological system, in which sites available for attack far exceed the number of $\bullet\text{OH}$ and hence, $\bullet\text{OH}$ are unlikely to react with the same reaction site multiple times. However, these conditions were used to replicate conditions in similar literature investigations.^{232–234}

Initially, only a $\bullet\text{OH}$ -initiated biochemical degradation trapless control and trapping reaction were performed and MS characterised. Peaks exclusively or significantly more intensely observed in the trapping reaction compared to trapless control, were attributed to trap related species, including TART-trapped radicals. However, it was later realised that peaks exclusively or significantly more intensely observed in the trapping reaction, could have corresponded to minor contaminants already present in unreacted TART. Therefore, latterly MS characterisation of unreacted TART standard was undertaken as an additional control.

Whilst all species were able to undergo TART trapping, only carbon-centred radicals could be trapped by TEMPO \bullet , hence TART-trapped and TEMPO-trapped carbon-centred radicals were hypothesised, whilst heteroatom-centred radicals were hypothesised to be exclusively TART trapped.

Before TART trapping was used to investigate $\bullet\text{OH}$ -initiated biochemical degradation, TART trapping was undertaken in the Fenton chemistry system in absence of a biochemical. TART-trapped $\bullet\text{OH}$ and $\text{HO}_2\bullet$ would indicate that the Fenton chemistry system was producing these radicals as desired and that aqueous radicals could be trapped using TARTs.

7.4. $\bullet\text{OH}$ and $\text{HO}_2\bullet$ trapping

Initial TART trapping of $\bullet\text{OH}$ -initiated biochemical degradation studies utilised GLANT as TART. First, GLANT was subjected to $\bullet\text{OH}$ radical attack (Figure 115).

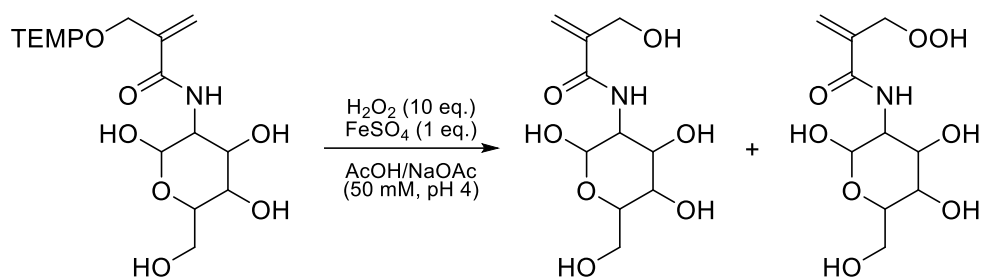


Figure 115: TART trapping of $\bullet\text{OH}$ and $\text{HO}_2\bullet$ in Fenton chemistry system, using GLANT as TART (11.6.1).

In the trapless control, orange particles precipitated whilst in the trapping reaction, no colour change or precipitation occurred. It was theorised that the precipitated particles were a mixture of iron hydroxides. Trapped radicals were characterised using MS (11.6.1).

Peaks corresponding to TART-trapped $\bullet\text{OH}$ radicals were observed albeit with very low relative intensity ($\sim 0.01\%$), whilst no peaks corresponding to $\text{HO}_2\bullet$ were observed. This was surprising, as H_2O_2 was in significant excess. It was theorised that since iron hydroxide precipitation had not occurred, as it had for the trapless control, GLANT had instead chelated most iron, preventing its precipitation. This iron chelation may have reduced the catalytic activity of the iron, which would hamper H_2O_2 degradation and radical formation. Indeed glucose, which has structural similarities to GLANT, has been observed to chelate Fe^{2+} and especially strongly chelate Fe^{3+} .²³⁵ Furthermore, it was hypothesised that GLANT may easily undergo HAA side reactions, due to relatively low energy HAA from its many $\text{C}(\text{OH})\text{-H}$. Therefore, GLANT was deemed unsuitable for Fenton chemistry trapping. Project student Dan Gugan later synthesised new water-soluble trap DANT. DANT would likely complex iron significantly less well than GLANT and be less vulnerable to side reactions and therefore, should have been more suitable for trapping in this system (Figure 116, 11.6.1). Nevertheless, HAA may have still occurred from the allylic C-H and amide N-H .

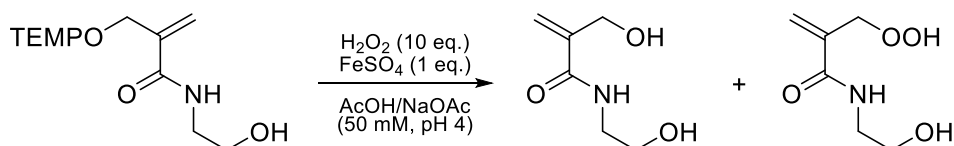


Figure 116: TART trapping of $\bullet\text{OH}$ and $\text{HO}_2\bullet$ in Fenton chemistry system, using DANT as TART (11.6.1).

Iron hydroxide precipitations were observed both with and without DANT presence, indicating DANT was not significantly complexing iron, as desired. However, peaks corresponding to these TART-trapped $\text{HO}_x\bullet$ species were not observed in MS spectra. This was theorised to be due to their poor ionisation efficiency and low m/z , disfavoured MS observation, as had been observed previously in non-aqueous liquid phase experiments (5.3.1.1). However, it was decided that TART trapping of biochemicals subjected to Fenton chemistry should be undertaken, as these trapped radicals may have greater ionisation efficiency and higher m/z , therefore making them more suitable for MS observation.

TART trapping was subsequently used to investigate many $\bullet\text{OH}$ -initiated substrate degradations, including for alcohols (7.5), nucleobases (7.6), dipeptides (7.7), saccharides (7.8) and antioxidants (7.9). Initially DANT was used for TART trapping investigation of $\bullet\text{OH}$ -initiated nucleobase degradation (7.6.2). However, DEADANT was found to perform superiorly to DANT in this system (7.6.3). As such, all subsequent TART trapping investigations of $\bullet\text{OH}$ -initiated biochemical degradation used DEADANT as TART. This included TART trapping of $\bullet\text{OH}$ -initiated alcohol degradation, which was investigated as a

simpler model system, appropriate for testing TART trapping of $\bullet\text{OH}$ -initiated biochemical degradation system, despite its biological irrelevance (7.5). This was especially advantageous, as unlike previous TART trapping experiments, mechanisms of $\bullet\text{OH}$ -initiated biochemical degradations are less finite and therefore, significantly more complex.

7.5. Alcohols

TART trapping was used to investigate $\bullet\text{OH}$ -initiated alcohol degradation. First methanol was used as substrate, due to its very simple structure and hence, relatively simple mechanism of aqueous $\bullet\text{OH}$ -initiated degradation (Figure 117).

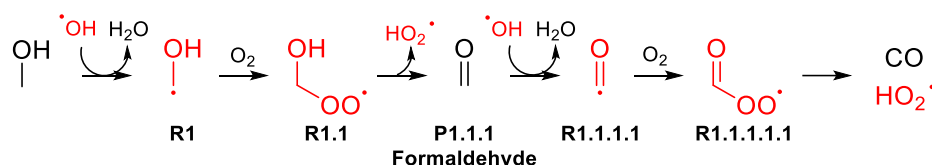


Figure 117: Hypothesised mechanism of aqueous $\bullet\text{OH}$ -initiated methanol degradation.

TART trapping was undertaken in this system, alongside two control reactions excluding trap or substrate, and all were MS characterised (Figure 118, Table 26, 11.6.2). This latter control was usually unnecessary, however it was hypothesised that acetic acid/sodium acetate buffer degradation may lead to some of the same radicals as methanol degradation. Therefore, comparison between the trapping reaction and this control would indicate if and to what extent methanol-derived trapped radicals indeed originated from methanol degradation.

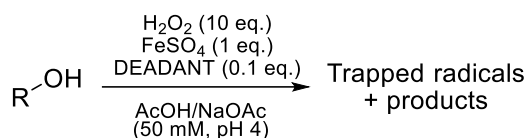


Figure 118: TART trapping of $\bullet\text{OH}$ -initiated alcohol degradation, using DEADANT as TART (11.6.2).

Table 26: Species identified from TART trapping of $\bullet\text{OH}$ -initiated methanol degradation, using DEADANT as TART and MS for characterisation (11.6.2). Systematic m/z error = -0.0005 ; random m/z error = ± 0.0003 ; 100% intensity = 1.14×10^9 absolute count.

	MS species	Predicted m/z	Intensity relative to unreacted TART standard / %		
			No substrate	Trapless control	Trapping reaction
TART	[DEADANT+H] ⁺	312.2651	13.1	0.030	6.53
	[R1-ART+H] ⁺	187.1446	0	0	0.013
	[R1-TEMPO+H] ⁺	188.1650	0	0	0
	[R1.1-ART+H] ⁺	219.1345	0.004	0	0.141
Trapped radicals	[R1.1.1.1-ART+H] ⁺	185.1290	0	0	0
	[R1.1.1.1-TEMPO+H] ⁺	186.1494	0	0	0
	[R1.1.1.1.1-ART+H] ⁺	217.1188	0.090	0	0.385
	[OH-ART+H] ⁺	173.1290	0.018	0	0.018
	[HO ₂ -ART+H] ⁺	189.1239	0	0	0.007

MS peaks corresponding to TART exhibited significantly lower intensity in unreacted TART standard than in the trapping reaction and no substrate control, indicating TART consumption. This likely meant that TART trapping had occurred. Furthermore, TART corresponding peaks were observed with greater intensity in absence of methanol, potentially indicating methanol-derived radicals were more efficiently TART-trapped than $\bullet\text{OH}$ or $\text{HO}_2\bullet$.

Peaks corresponding to TART-trapped methanol-derived radicals were detected exclusively or with significantly greater intensity in the trapping reaction compared to controls, indicating these trapped radicals predominantly originated from $\bullet\text{OH}$ -initiated methanol degradation. Peaks corresponding to TART-trapped radicals were observed, corresponding to radicals including R1 (radical formed during initial HAA) and R1.1 (the subsequently formed $\text{RO}_2\bullet$). This validated the hypothesised radical structures and hence mechanism suggested. Furthermore, peaks corresponding to $\bullet\text{OH}$ and $\text{HO}_2\bullet$ were both observed in the trapping reaction, with OH-ART observed with similar intensity in the no substrate control. These TART-trapped $\text{HO}_x\bullet$ radicals were not observed for DANT, which was attributed to poor ionisation efficiency of DANT-trapped radicals (7.4). However, DEADANT had much better ionisation efficiency, due to its basic 3° amine functionality. This allowed peaks corresponding to $\bullet\text{OH}$ and $\text{HO}_2\bullet$ to be observed. This indicated that DEADANT was more suitable for TART trapping than DANT, as discussed later (7.6.2).

The simplicity of methanol and its degradation mechanism made it a model substrate, suitable for testing the $\bullet\text{OH}$ -initiated biochemical degradation. Next, TART trapping was used to investigate $\bullet\text{OH}$ -initiated *tert*-butanol ($^t\text{BuOH}$) degradation. Whilst being a more complex alcohol than methanol, the nine identical C-H limited the possible $^t\text{BuOH}$ degradation pathways and structural isomers. An $\bullet\text{OH}$ -initiated $^t\text{BuOH}$ degradation mechanism was proposed, based upon known general $\bullet\text{OH}$ -initiated biochemical degradation reaction pathways (Figure 119). As previously, TART trapping was undertaken in this system, alongside two control reactions excluding trap or substrate, and all were MS characterised (Table 27).

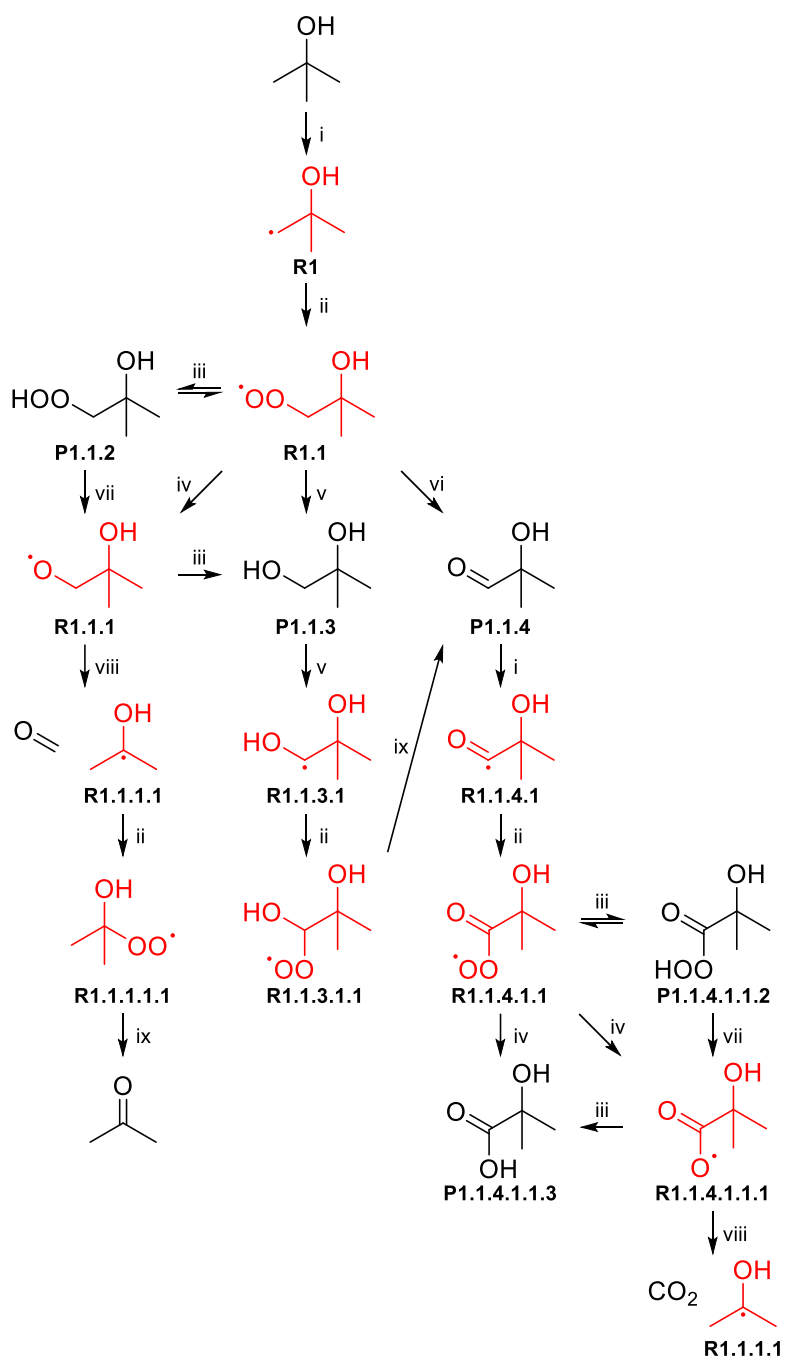


Figure 119: Non-comprehensive hypothesised reaction scheme for $\cdot\text{OH}$ -initiated ${}^t\text{BuOH}$ degradation in aqueous solution, only indicating major pathways. i) + $\cdot\text{OH}$, - H_2O . ii) + O_2 . iii) + RH , - $\text{R}\cdot$. iv) + $\text{RO}_2\cdot$, - $\text{RO}\cdot$. v) + $\text{RO}_2\cdot$, - $\text{RCO}\cdot$. vi) + $\text{RO}_2\cdot$, - ROH . vii) - $\cdot\text{OH}$. viii) Fragmentation. ix) - $\text{HO}_2\cdot$.

Table 27: Species identified from TART trapping of $\bullet\text{OH}$ -initiated $^1\text{BuOH}$ degradation, using DEADANT as TART and MS for characterisation (11.6.2). 100% = 1.09×10^9 absolute count. Systematic m/z error = -0.0004; random m/z error = ± 0.0007 .

	Species	Predicted m/z	Intensity relative to unreacted TART standard / %		
			No substrate	Trapless control	Trapping reaction
TART	[DEADANT+H] ⁺	312.2651	13.1	0.004	3.88
	[R1-ART+H] ⁺	229.1916 ^a	0	0	0.075
	[R1-TEMPO+H] ⁺	230.2120 ^a	0	0	1.73
	[R1.1-ART+H] ⁺	261.1814	0	0	0.209
	[R1.1.1-ART+H] ⁺	245.1865 ^a	0	0	0.129
	[R1.1.1.1-ART+H] ⁺	215.1759	0	0	0
	[R1.1.1.1-TEMPO+H] ⁺	216.1963	0	0	0
	[R1.1.1.1.1-ART+H] ⁺	247.1658	0	0	0.045
Trapped radicals	[R1.1.3.1-ART+H] ⁺	245.1865 ^a	0	0	0.129
	[R1.1.3.1-TEMPO+H] ⁺	246.2069 ^a	0.004	0	0.154
	[R1.1.3.1.1-ART+H] ⁺	277.1764	0	0	0.069
	[R1.1.4.1-ART+H] ⁺	243.1709	0.004	0	0.042
	[R1.1.4.1-TEMPO+H] ⁺	244.1913	0	0	0.092
	[R1.1.4.1.1-ART+H] ⁺	275.1607	0	0	0.054
	[R1.1.4.1.1.1-ART+H] ⁺	259.1658	0.004	0	0.143
	[OH-ART+H] ⁺	173.1290	0.018	0	0.006
	[OH-TEMPO+H] ⁺	174.1494	0.005	0	0.009
		[HO ₂ -ART+H] ⁺	189.1239	0	0
	[HO ₂ -TEMPO+H] ⁺	190.1443	0	0	0

^aOther table entries have predicted species with identical m/z .

As previously, MS peaks corresponding to TART had significantly lower intensity in the unreacted TART standard than in the trapping reaction and no substrate control, likely meaning TART trapping had occurred. TART corresponding peaks were observed with greater intensity in presence of methanol than $^1\text{BuOH}$ (6.53% to 3.88%), potentially indicating $^1\text{BuOH}$ -derived radicals were trapped more efficiently than methanol-derived radicals or that $\bullet\text{OH}$ reacted more efficiently with $^1\text{BuOH}$ than methanol.

Peaks corresponding to nearly all TART-trapped $^1\text{BuOH}$ -derived radicals were detected exclusively or with significantly greater intensity in the trapping reaction compared to controls, indicating these trapped radicals originated from $\bullet\text{OH}$ -initiated $^1\text{BuOH}$ degradation. These observations validated the hypothesised radical structures and hence mechanism suggested.

However, some isomers could not be distinguished using standard MS, such as R1.1.1/R1.1.3.1-ART, since these two species had the same m/z . However, these two species had different numbers of labile hydrogen atoms (Figure 120). Therefore, D₂O exchange was used to assess labile hydrogen atom population (4.3.2.5). The resulting D-shifted peak intensities could be used to indicate relative concentrations of these two species. Unreacted DEADANT contained two labile hydrogen atoms, one quickly exchanged ammonium NH and one slowly exchanged amide NH. Two shifted peaks were observed for unreacted DEADANT which corresponded to one and two D exchanges, with relative intensities 14.7% and 85.3% respectively. From this and inherent solvent D/H ratio of 99.0%, 86.1% of slow D/H amide exchange was calculated to have occurred. This slow D/H amide exchange could be applied to TART-trapped radicals, as they had identical amide functionality to unreacted TART (4.3.2.5). However, since 86.1% was below 90%, quantitative interpretation should be treated with caution (4.3.2.5).

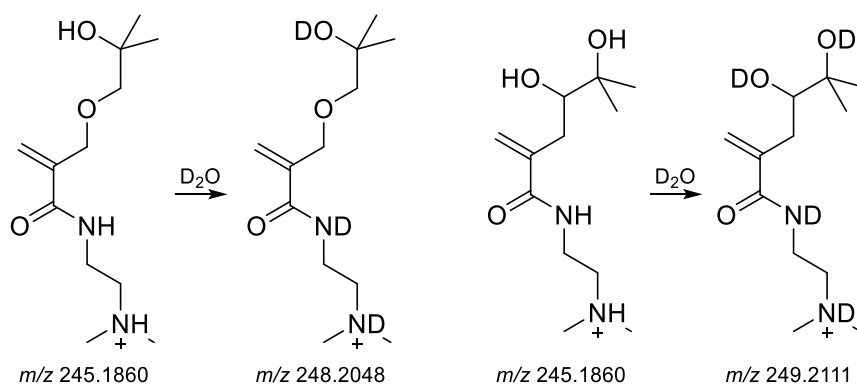


Figure 120: 3D or 4D exchanges expected for [R1.1.1-ART+H]⁺ and [R1.1.3.1-ART+H]⁺ respectively.

Table 28: D exchanges observed for MS peaks corresponding to TART-trapped radicals from D₂O exchange of •OH-initiated tBuOH degradation, using DEADANT as TART and MS for characterisation (11.6.4). Systematic *m/z* error = -0.0004; random *m/z* error = ±0.0004.

	Species	Predicted D shift	Proportion of total intensity of all D-shifted species / %					
			0D	1D	2D	3D	4D	5D
Observed	[DEADANT+H] ⁺	2D	0	14.7	85.3	0	0	0
	[R1-ART+H] ⁺	3D	0	0	2.5	97.5	0	0
	[R1.1-ART+H] ⁺	3D	0	0	4.1	29.9	66.0	0
	[R1.1.1/R1.1.3.1-ART+H] ⁺	3D/4D	0	0	13.2	79.0	7.9	0
Predicted	[2 labile H+H] ⁺	3D	0	0.3	15.3	84.4	0	0
	[3 labile H+H] ⁺	4D	0	0	0.4	16.0	83.5	0
	[4 labile H+H] ⁺	5D	0	0	0	0.6	16.7	82.7

^aSimulated using inherent solvent D/H ratio = 99.0% and calculated D/H amide exchange = 86.1% from DEADANT.

For R1-ART, 3D exchanges were observed, consistent with the suggested R1-ART structure.

For R1.1.1/R1.1.3.1-ART, the observed D exchanges appeared to partially correspond to both 3D and 4D exchanges, as predicted. Simulation indicated that 91% and 9% of species contributing to the protonated peak had three and four labile hydrogen atoms respectively, indicating 91% R1.1.1-ART and 9% R1.1.3.1-ART. Since the exact rate of R1.1.1 and R1.1.3.1 trapping is unknown, it is difficult to estimate concentrations of these radicals.

For R1.1-ART, the observed D exchanges appeared to mainly correspond to 4D exchanges, with 3D exchanges being less intensely observed. Simulation indicated that 21% and 79% of species contributing to the protonated peak had three and four labile hydrogen atoms respectively, indicating 21% RO₂-ART and 79% R(OH)O-ART or R(OOH)-ART. This was perhaps surprising. However, TART-trapping rate of RO₂• was likely to be slow, as discussed previously (7.2.4). No structure corresponding to R(OH)O-ART or R(OOH)-ART was hypothesised in the mechanism. However, such structures were simply assigned to further •OH-initiation of products. For example, R(OH)O• could be formed from HAA from -CH₃ of P1.1.3 by •OH and subsequent RO₂• and RO• formation, whilst R(OOH)• could be formed from HAA from P1.1.2 by •OH (Figure 121). Further analysis was required to determine which of these two species this 4D exchange corresponded to.

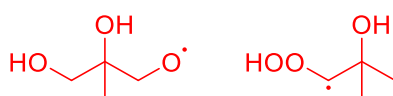


Figure 121: Possible radical structures for R(OH)O• and R(OOH)•.

Tandem MS was undertaken to further characterise and elucidate trapped radical structures. Tandem MS was performed upon peaks corresponding to $[R1-ART+H]^+$ (m/z 229.192), $[R1.1-ART+H]^+$ (m/z 261.181) and $[R1.1.1/R1.1.3.1-ART]^+$ (m/z 245.187). All these tandem MS spectra showed peaks indicating dehydration and dehydration with loss of $NH(CH_3)_2$ (SI5.1). Dehydration indicated an alcohol with neighbouring β -hydrogen atom, whilst loss of $NH(CH_3)_2$ indicated the 1,1-dimethylethylenediamine functionality present in DEADANT-trapped radicals, supporting the suggested structures. However, tandem MS of peak corresponding to $[R1.1-ART+H]^+$ (m/z 261.181), did not yield fragments which confirmed presence of $R(OH)O-ART$ or $R(OOH)-ART$ (SI5.1).

TART trapping was successfully used to investigate model $\bullet OH$ -initiated alcohol degradation, using standard MS characterisation. Additional MS characterisation techniques, D_2O exchange and tandem MS, were used to further elucidate trapped radical structures. These data validated the suggested radical structures and hence hypothesised mechanism. This success indicated TART trapping could be used to investigate more complex and biologically relevant $\bullet OH$ -initiated biochemical degradations. As such, TART trapping was used to investigate $\bullet OH$ -initiated nucleobase degradation.

7.6. Nucleobases

7.6.1. Introduction

DNA oxidation, especially nucleobase oxidation, is believed to be a significant cause of carcinogenesis (1.2.2).^{213–216} Detection, characterisation and quantification of radicals produced during oxidative damage of DNA and subsequent mechanistic understanding of this process could lead to development in cancer prevention and treatment. Therefore, radical trapping was used to investigate $\bullet OH$ -initiated nucleobase degradation as a proxy for key components in $\bullet OH$ -initiated DNA degradation. $\bullet OH$ -initiated nucleobase degradation was a simpler system and hence more suitable for initial investigations, although did not necessarily correspond to $\bullet OH$ -initiated DNA degradation. Once TART trapping was shown to successfully characterise trapped radicals produced in TART trapping of $\bullet OH$ -initiated nucleobase degradation, investigation of $\bullet OH$ -initiated DNA degradation would have been more feasible, although this was not attempted. TART trapping was initially applied to $\bullet OH$ -initiated thymine degradation.

DNA utilises four nucleobases: adenine, thymine, guanine and cytosine. Of these, thymine was chosen as substrate in the TART trapping investigation of $\bullet OH$ -initiated nucleobase degradation, due to it having the highest water solubility (3.82 g L^{-1}).²³⁶ This higher solubility was hoped to aid reproducibility. An $\bullet OH$ -initiated thymine degradation mechanism was proposed, based upon literature and known general $\bullet OH$ -initiated biochemical degradation reaction pathways (Figure 122).^{45,218,237}

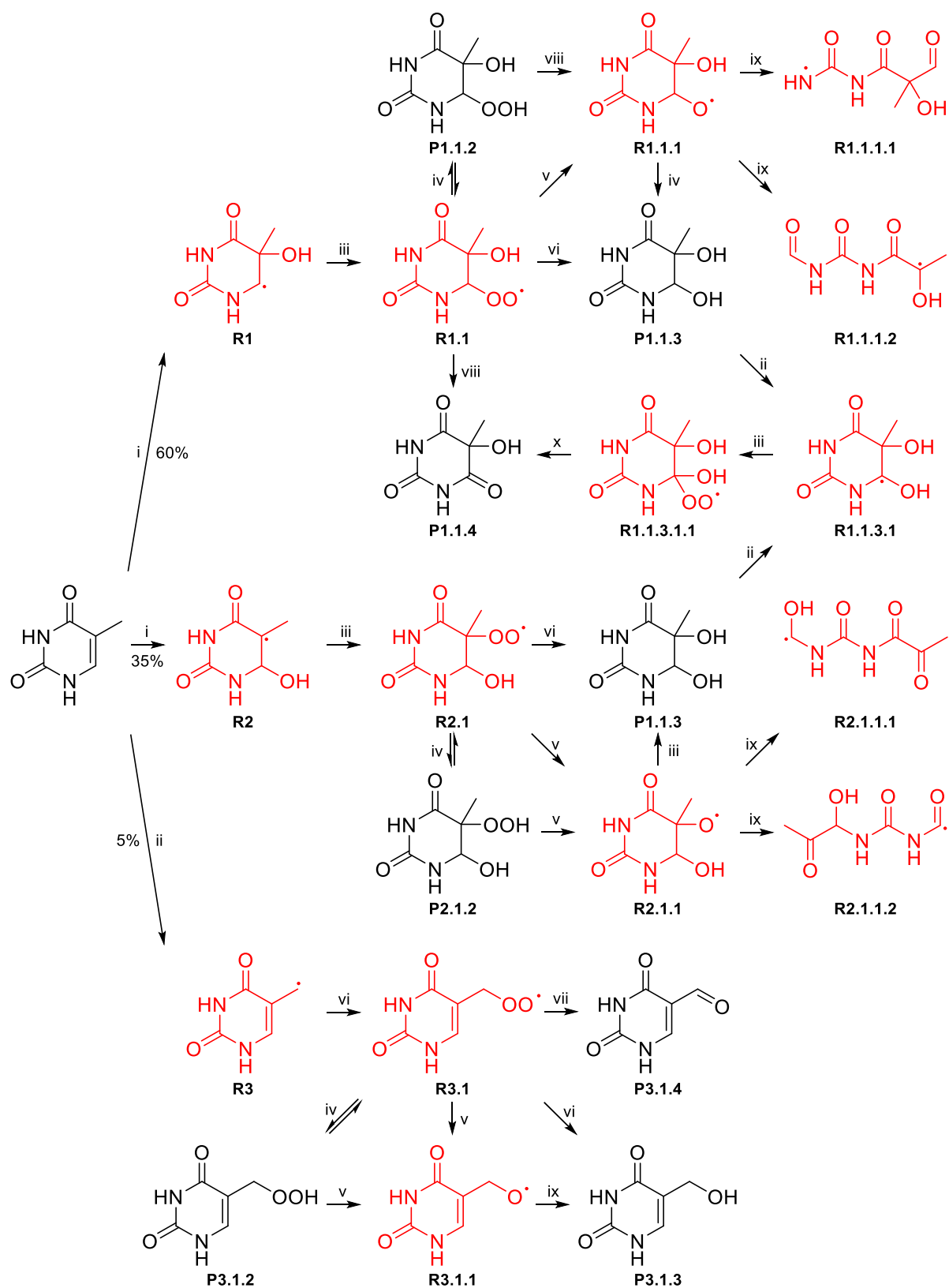


Figure 122: Non-comprehensive $\bullet\text{OH}$ -initiated thymine degradation in aqueous solution. Structures and pathway probabilities were obtained or hypothesised using literature sources.⁴⁵ i) + $\bullet\text{OH}$. ii) + $\bullet\text{OH}$, - H_2O . iii) + O_2 . iv) + RH , - $\text{R}\bullet$. v) + $\text{RO}_2\bullet$, - $\text{RO}\bullet$. vi) + $\text{RO}_2\bullet$, - RCO . vii) + $\text{RO}_2\bullet$, - ROH . viii) - $\bullet\text{OH}$. ix) Fragmentation. x) - $\text{HO}_2\bullet$.

TART trapping was used to investigate the radical intermediates produced in this mechanism.

7.6.2. Initial results

TART trapping of •OH-initiated thymine degradation was initially performed using DANT as TART (Figure 123, 11.6.4). A trapless control was also performed and reaction mixtures characterised using MS (Table 29, 11.6.4).

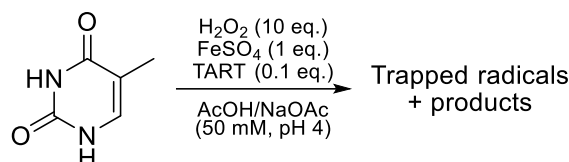


Figure 123: TART trapping of •OH-initiated thymine degradation (11.6.4).

Table 29: Species identified from TART trapping of •OH-initiated thymine degradation, using DANT as TART and MS for characterisation (11.6.4). Systematic m/z error = -0.0004; random m/z error = ± 0.0004 ; 100% intensity = 5.83×10^8 absolute count.

Species		Predicted m/z	Intensity relative to unreacted trap in trapping reaction / %		
			Trapless control	Trapping reaction	
TART	[DANT+H] ⁺	285.2178	0	100	
Reactants	[Thymine+Na] ⁺	149.0327	0.083	0.128	
	[R1/R2-ART+Na] ⁺	294.1066	0	0.304	
Trapped radicals	[R1/R2-TEMPO+H] ⁺	300.1923	0	0.709	
	[R1.1/R2.1-ART+Na] ⁺	326.0964	0	0.016	
	[R1.1.1/R2.1.1-ART+Na] ⁺	310.1015 ^a	0	0	
	[R1.1.1.1/R1.1.1.2-ART+Na] ⁺	310.1015 ^a	0	0	
	[R1.1.1.2-TEMPO+H] ⁺	316.1872 ^a	0	0	
	[R1.1.3.1-ART+Na] ⁺	310.1015 ^a	0	0	
	[R1.1.3.1-TEMPO+H] ⁺	316.1872 ^a	0	0	
	[R1.1.3.1.1-ART+Na] ⁺	342.0913	0	0	
	[R2.1.1.1/R2.1.1.2-ART+Na] ⁺	310.1015 ^a	0	0	
	[R2.1.1.1/R2.1.1.2-TEMPO+H] ⁺	316.1872 ^a	0	0	
	[R3-ART+Na] ⁺	276.0960	0	0	
	[R3-TEMPO+H] ⁺	282.1818	0	0.596	
	[R3.1-ART+Na] ⁺	308.0859	0	0	
	[R3.1.1-ART+Na] ⁺	292.0909	0	0	
	[OH-ART+Na] ⁺	168.0637	0	0.053	
	[HO ₂ -ART+Na] ⁺	184.0586	0	0	
	Products	[P1.1.2/P2.1.2+Na] ⁺	199.0331	0.142	0.029
		[P1.1.3+Na] ⁺	183.0382	0.151	0.026
[P1.1.4+Na] ⁺		181.0225 ^a	0.050	0.015	
[P3.1.2+Na] ⁺		181.0225 ^a	0.050	0.015	
[P3.1.3+Na] ⁺		165.0276	0	0	
[P3.1.4+Na] ⁺		163.0120	0.008	0	

^aOther table entries have predicted species with identical m/z .

As for CHANT and other non-basic reactants (5.3), peaks corresponding to DANT-trapped radicals, reactants and products were not observed or observed exclusively or much more intensely as sodiated MS adducts and hence, are only these adducts are shown.

R1/R2 corresponding peaks were observed with significant intensity exclusively in the trapping reaction. Literature indicated 95% thymine molecules decay via these two species. An R3

corresponding peak, comprising the remaining 5%, was not observed, nor was its successor R3.1, likely due to a low proportion of R3 production. R1.1/R2.1 corresponding peaks were also observed, albeit with lower intensity than their predecessors.

It was theorised that tandem MS may allow structural elucidation of R1.1/R2.1 corresponding peaks. Tandem MS was attempted upon $[R1/R2-ART+H]^+$ and $[R1.1/R2.1-ART+H]^+$ corresponding peaks to elucidate species structure, however high intensity fragments were unobtainable. It was previously established that tandem MS performed upon protonated species is generally more successful than for sodiated species (4.3.2.6). Therefore, a more basic water-soluble trap was suspected to be more useful for tandem MS elucidation of trapped $\bullet OH$ -initiated thymine degradation radicals.

It was theorised that in the acidic system used (pH 4), weakly basic DEADANT radical trap may be protonated and consequently water-soluble. Furthermore, this protonation would reduce N-oxidation through single electron transfer. Use of DEADANT over DANT in $\bullet OH$ -initiated thymine degradation radical trapping offered many potential advantages:

- Peaks corresponding to basic species tended to be observable with greater MS intensity, due to their high protonation affinity compared to lower sodiation affinity of non-basic species. This may have increased MS intensity of peaks corresponding to TART-trapped species relative to other species, possibly making peaks corresponding to R3 and R3.1 observable.
- DEADANT 3^o amine basicity was predicted to mainly govern protonation propensity of TART-trapped radicals and not reactant radical structure. This contrasted to DANT, where the structure of radicals affected TART-trapped radical sodiation propensity. Therefore, quantification of TART-trapped radicals, relative to each other, was likely be more accurate for DEADANT-trapped radicals.
- Useful tandem MS fragmentation occurred more readily for protonated species, allowing better elucidation of trapped radical structure.

7.6.3. Main results

Therefore, TART trapping of $\bullet OH$ -initiated thymine degradation using DEADANT was undertaken (Figure 123). A trapless control was also performed. Reaction mixtures and TART standard were then characterised using MS (Table 30, 11.6.4).

Table 30: Species identified from TART trapping of $\bullet OH$ -initiated thymine degradation, using DEADANT as TART and MS for characterisation (11.6.4). Systematic m/z error = -0.0002; random m/z error = ± 0.0005 ; 100% intensity = 1.09×10^9 absolute count.

	Species	Predicted m/z	Intensity relative to unreacted TART standard / %		
			Trapless control	Standard	Trapping reaction
TART	$[DEADANT+H]^+$	312.2651	0	100	51.4
Reactants	$[Thymine+Na]^+$	149.0327	0.024	0	0.036
	$[R1/R2-ART+H]^+$	299.1719	0	0	1.62
Trapped radicals	$[R1/R2-TEMPO+H]^+$	300.1923	0	0	1.45
	$[R1.1/R2.1-ART+H]^+$	331.1618	0	0	0.456
	$[R1.1.1/R2.1.1-ART+H]^+$	315.1668 ^a	0	0	1.55
	$[R1.1.1.1/R1.1.1.2-ART+H]^+$	315.1668 ^a	0	0	1.55
	$[R1.1.1.2-TEMPO+H]^+$	316.1872 ^a	0	0	0.727
	$[R1.1.3.1-ART+H]^+$	315.1668 ^a	0	0	1.55
	$[R1.1.3.1-TEMPO+H]^+$	316.1872 ^a	0	0	0.727

Trapped radicals	[R1.1.3.1.1-ART+H] ⁺	347.1567	0	0	0.134
	[R2.1.1.1/R2.1.1.2-ART+H] ⁺	315.1668 ^a	0	0	1.55
	[R2.1.1.1/R2.1.1.2-TEMPO+H] ⁺	316.1872 ^a	0	0	0.727
	[R3-ART+H] ⁺	281.1614	0	0	0.033
	[R3-TEMPO+H] ⁺	282.1818	0	0	1.23
	[R3.1-ART+H] ⁺	313.1512	0	0	0.090
	[R3.1.1-ART+H] ⁺	297.1563	0	0	0.032
	[OH-ART+H] ⁺	173.1290	0	0	0.010
Products	[HO ₂ -ART+H] ⁺	189.1239	0	0	0
	[P1.1.2/P2.1.2+Na] ⁺	199.0331	0.042	0	0.025
	[P1.1.3+Na] ⁺	183.0382	0.064	0	0.054
	[P1.1.4+Na] ⁺	181.0225 ^a	0.033	0	0.022
	[P3.1.2+Na] ⁺	181.0225 ^a	0.033	0	0.022
	[P3.1.3+Na] ⁺	165.0276	0.003	0	0.007
	[P3.1.4+Na] ⁺	163.0120	0.007	0	0

^aOther table entries have predicted species with identical *m/z*.

MS peaks corresponding to TART had ~50% intensity compared to unreacted TART standard in the trapping reaction. Thymine corresponding peak had lower intensity in the trapless control than in the trapping reaction, suggesting greater thymine consumption. In contrast, product corresponding peaks generally had greater intensity in the trapless control than in the trapping reaction, suggesting greater product formation. These results indicated that TART had hindered •OH-initiated thymine degradation, as has been similarly observed and discussed for other trapping reactions.

As anticipated, R1/R2 and R1.1/R2.1 corresponding peaks were observed with much greater intensity when DEADANT was used as TART, instead of DANT. Additionally, peaks corresponding to multiple radicals which were previously unobserved, were realised. TART-trapped radicals were observed near-exclusively protonated. Therefore, DEADANT performed superiorly for radical trapping in biochemistry systems and showed that DEADANT was soluble in acidic solution.

Peaks corresponding to all hypothesised thymine-derived radicals were observed exclusively in the trapping reaction, as expected. R1/R2 corresponding peaks were observed the most intensely. This made good sense, as R1/R2 were the earliest radicals formed and therefore, had the highest radical flux of all radicals, allowing the most opportunity for trapping. R3 was also observed exclusively in the trapping reaction, as expected. Relative intensity of [R3-ART+H]⁺ compared to [R1/R2-ART+H]⁺ was ~2:98%, broadly corresponding with the relative intensities of the R3 to R1/R2 routes indicated by literature to be 5:95%.⁴⁵ These differences likely arose from differences in rates of radical consumption and trapping.

R1.1.1/R2.1.1-ART corresponding peaks were also observed with high intensity, whilst R1.1/R2.1-ART corresponding peaks were observed with significantly lower intensity. This was likely due to RO• reacting with TART more efficiently than RO₂•, as discussed previously (7.2.4). Similar intensities of R1/R2-ART and R1.1.1/R2.1.1-ART corresponding peaks may be similarly explained by the relatively low concentrations of RO• compared to R• being counteracted by the relative faster trapping rate of RO• compared to R• (7.2.4). Another possible reason for the R1.1.1/R2.1.1-ART corresponding peak having higher intensity than the R1.1/R2.1-ART corresponding peak was that the former peak was believed to be able to correspond to multiple other radicals including R1.1.1.1/R1.1.1.2-ART and R1.1.3.1-ART, which could also contribute to peak intensity. Modelling was required to fully interpret these data, however this was not attempted.

Most hypothesised radicals had identical molecular formulae but different structural formulae to other radicals. This meant that the corresponding trapped radicals would have identical m/z and therefore could not be distinguished by standard MS. Therefore, further MS techniques were utilised.

7.6.4. Structural isomers

D₂O exchange, tandem and HPLC-MS were used to further elucidate trapped radical structures. D₂O exchange assessed labile hydrogen atom population (4.3.2.5), tandem MS created fragments with m/z values which aided parent ion structure elucidation (4.3.2.6) and HPLC-MS separated and detected species with the same m/z (4.3.2.7).

The R1/R2 corresponding peak (m/z 299.172) was hypothesised to only correspond to R1 and R2, which had similar structures containing the same functional groups. Separation and detection of these two species was achieved using HPLC-MS (Figure 124).

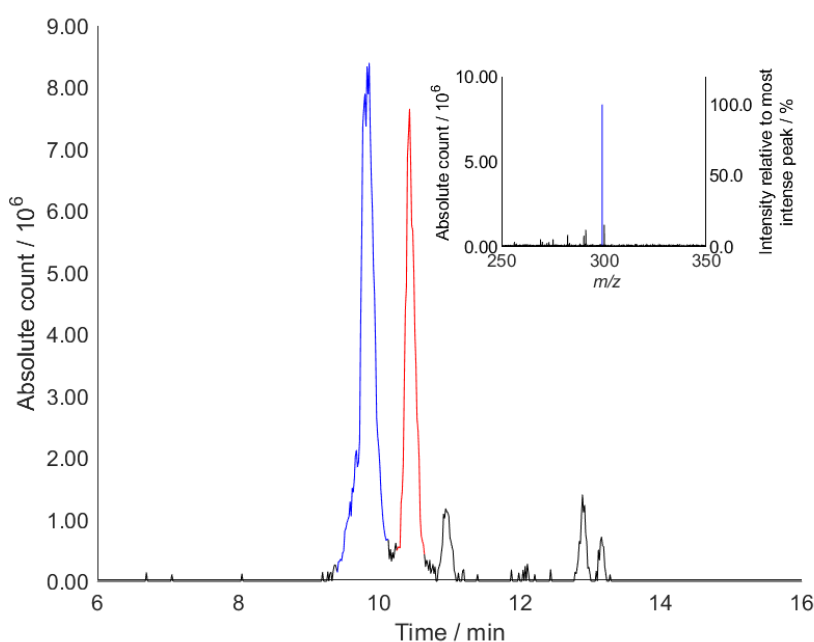


Figure 124: HPLC-MS chromatogram of the peak corresponding to R1/R2-ART (m/z 299.172 \pm 0.002), detected from TART trapping of \bullet OH-initiated thymine degradation, using DEADANT as TART (11.6.4). Two peaks dominate (blue and red). Mass spectrum (inset) recorded at time of maximum chromatogram intensity (blue) shows m/z 299.172 cleanly isolated (blue).

The HPLC-MS chromatogram of the m/z peak corresponding to R1/R2-ART (m/z 299.172) was indeed dominated by two peaks, believed to correspond to R1 and R2. R1-ART and R2-ART were expected to ionise equally, due to their near-identical functionality and identical m/z . This implied that relative intensities of these two chromatogram peaks would approximately correspond to relative concentrations of R1 and R2. Integration of these chromatogram peaks produced relative intensities of 63% (blue) and 37% (red). This may match the relative proportion of R1 (63%) and R2 (37%) production, as indicated by literature.⁴⁵ However, the relative integrations of these chromatogram peaks are significantly similar that without values for radical consumption or trapping, peaks cannot be confidently assigned to each species. Nevertheless, the observation of two different species offered validation to the hypothesised mechanism.

Tandem MS of the peak corresponding to R1-ART and R2-ART (m/z 299.172) was also performed, to further prove the peak corresponded to both species (Figure 125). However, tandem MS did not distinguish between R1-ART and R2-ART. This was because differences between R1-ART and R2-ART structures were located directly on the cyclic ring, but ring fragmentation did not alter m/z , stopping normally useful fragmentations from elucidating structure. Nevertheless, observed peaks supported that these parent ion peaks emanated from TART-trapped radical species. One peak also likely corresponded to dehydration, indicating an alcohol with neighbouring β -hydrogen atom. These data further validated the suggested structures.

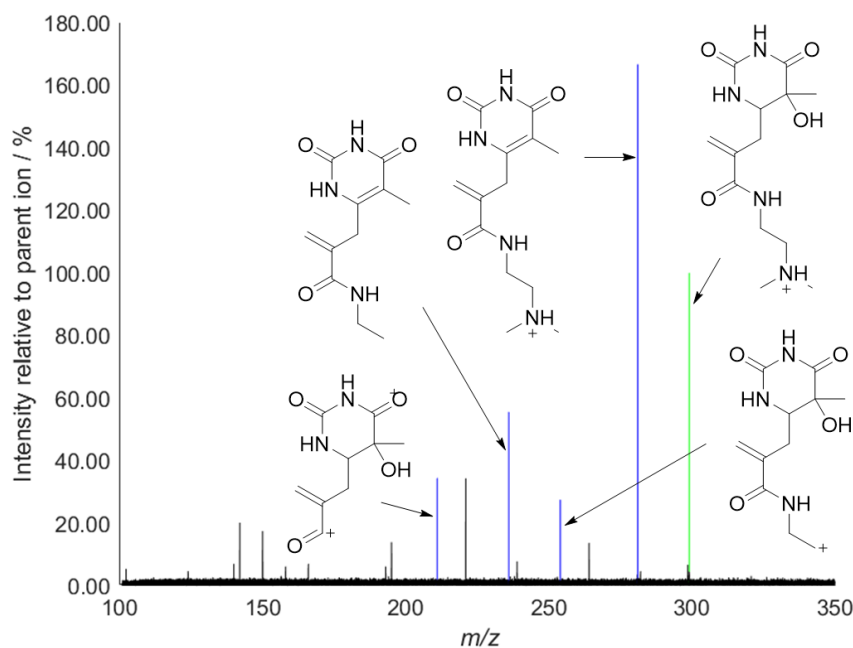


Figure 125: Tandem mass spectrum of peak corresponding to R1-ART and R2-ART (m/z 299.172, green) with structures suggested for major fragment peaks (blue). Structures are derived from R1-ART, but all peaks could be equally attributed to R2-ART.

Although R1-ART and R2-ART could not be distinguished using D_2O exchange, D_2O exchange could offer further validation to their structures. For $[R1-ART+H]^+$ and $[R2-ART+H]^+$, five D exchanges were expected (Figure 126). These were two rapidly exchanged H (in ammonium and hydroxyl groups) and three slowly exchanged H (-ART amide NH and two other amide NH). Assuming that all MS peak corresponding to $[R1-ART+H]^+$ and $[R2-ART+H]^+$ (m/z 299.172) corresponded to only these two species, exchange of slow amide NH present in TART-trapped thymine-derived radicals could be estimated using the observed D shifts (Table 31). This was a reasonable assumption, based upon the hypothesised mechanism and HPLC-MS evidence.

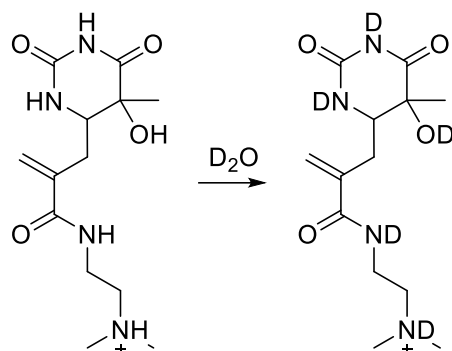


Figure 126: Total D exchange of $[R1-ART+H]^+$, yielding five D exchanges.

Table 31: D exchanges observed for $[R1/R2-ART+H]^+$ from D_2O exchange of $\bullet OH$ -initiated thymine degradation, using DEADANT as TART and MS for characterisation (11.6.4). Systematic m/z error = -0.0004; random m/z error = ± 0.0002 .

D exchange	Predicted m/z	Contribution / %	
		Observed	Simulated ^a
0	299.1719	0	0
1	300.1782	0	0
2	301.1845	0	0.34
3	302.1908	4.13	5.31
4	303.1970	32.43	31.13
5	304.2033	63.07	63.21
6	305.2096	0	0

^aSimulated using inherent solvent D/H ratio = 99.0% and calculated slow D/H exchange = 64.6%.

5D exchanges were observed with greatest intensity as expected, further validating the suggested R1-ART and R2-ART structures. From these data, slow D/H exchange of TART-trapped thymine-derived radicals was calculated to be 86.4%. This slow D/H exchange ratio was used to estimate labile hydrogen atom population of other TART-trapped thymine-derived radicals.

In contrast to R1-ART and R2-ART, the R1.1.1/R2.1.1 corresponding peak (m/z 315.167) was believed to be able to correspond to multiple other species, including R1.1.1.1/R1.1.1.2 and R1.1.3.1. Whilst having the same m/z , the MS adduct of trapped $RO\bullet$, such as $[R1.1.1-ART+H]^+$, would have different numbers of labile hydrogen atoms to the MS adduct of trapped $R(OH)\bullet$, such as $[R1.1.3.1-ART+H]^+$, with five and six respectively (Figure 69). Therefore, D_2O exchange was used to distinguish these species (Table 32).

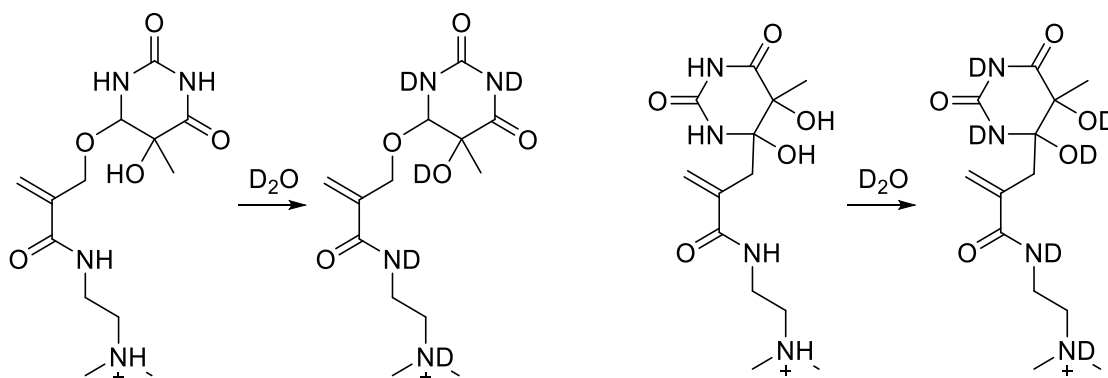


Figure 127: Total D exchange of $[R1.1.1-ART+H]^+$ and $[R1.1.3.1-ART+H]^+$, yielding 5D and 6D exchanges respectively.

Table 32: D exchanges observed for m/z 315.167 from D_2O exchange of $\bullet OH$ -initiated thymine degradation, using DEADANT as TART and MS for characterisation (11.6.4). Systematic m/z error = -0.0004; random m/z error = ± 0.0004 .

D exchange	Predicted m/z	Observed	Contribution / %	
			Simulated 5D exchange ^a	Simulated 6D exchange ^a
0	315.1668	0	0	0
1	316.1731	0	0	0
2	317.1794	0	0.34	0
3	318.1857	2.95	5.31	0.39
4	319.1920	22.01	31.13	5.57
5	320.1982	75.04	63.21	31.45
6	321.2045	0	0	62.58
7	322.2108	0	0	0

^aSimulated using inherent solvent D/H ratio = 99.0% and calculated slow D/H exchange = 64.6% from R1/R2-ART.

The observed D exchanges broadly matched the prediction for 5D exchanges and not 6D. This suggested all trapped radicals were trapped $RO\bullet$, such as R1.1.1-ART and R2.1.1-ART, and not trapped $R(OH)\bullet$. Therefore R1.1.3.1 production could not be validated.

The HPLC-MS chromatogram of m/z 315.167 was dominated by two peaks although, other less intense peaks were also observed (Figure 128). These peaks were believed to correspond to R1.1.1 and R2.1.1, due to these radicals being formed first in the mechanism and hence having a greater radical flux, though this could not be confirmed.

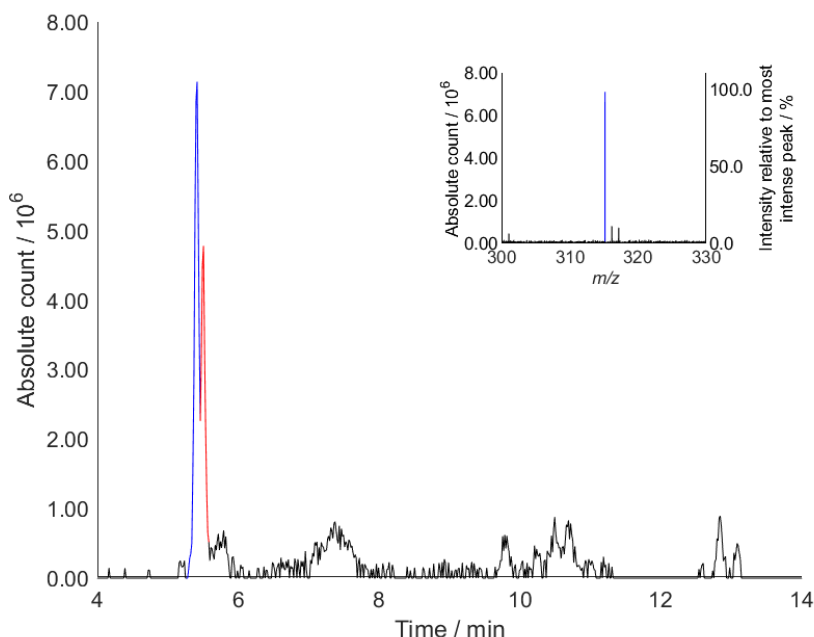


Figure 128: HPLC-MS chromatogram of the peak corresponding to R1.1.1/R1.1.2-ART (m/z 315.167 \pm 0.002), detected from TART trapping of $\bullet OH$ -initiated thymine degradation (11.6.4). Two peaks dominate (blue and red), although other smaller peaks were also observed. Mass spectrum (inset) recorded at time of maximum chromatogram intensity (blue) shows m/z 315.167 clearly isolated (blue).

Non-deconvoluted integration of the two dominant chromatogram peaks produced relative intensities of 62% (blue) and 38% (red). As previously, without further characterisation, these peaks could not be specifically assigned to R1.1.1-ART or R1.1.2-ART. Other peaks could correspond to radicals such as R1.1.1.1/R1.1.1.2 and R2.1.1.1/R2.1.1.2, but this could not be

confirmed. Tandem MS was not performed upon the m/z 315.167 peak but may have aided further structural elucidation.

Like for R1.1.1-ART and R2.1.1-ART, the R1.1/R2.1 corresponding peak (m/z 331.162) was believed to be able to correspond to multiple other species. These species were not shown in the reaction scheme, since they were later stage products but could include $R(OH)O^\bullet$ or $R(OH)_2^\bullet$ species, such as hydroxylated R1.1.1/R2.1.1, hydroperoxylated R1/R2 or dihydroxylated R1/R2 respectively (Figure 129). Whilst having the same m/z , $[RO_2-ART+H]^+$, $[R(OH)O-ART+H]^+$, $[R(OOH)-ART+H]^+$ and $[R(OH)_2-ART+H]^+$ would have five, six, six and seven labile hydrogen atoms respectively. Therefore, D_2O exchange was used to distinguish these species (Table 33).

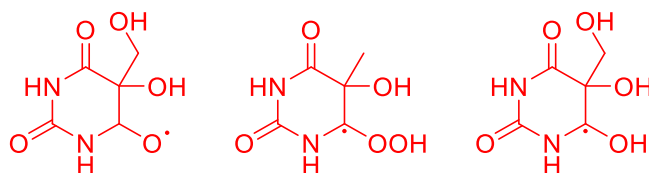


Figure 129: Three radicals possibly formed during $^\bullet OH$ -initiated thymine degradation, with same m/z as RO_2^\bullet species R1.1/R1.2. These radicals are hydroxylated R1.1.1/R2.1.1 ($R(OH)O^\bullet$, left), hydroperoxylated R1/R2 ($R(OOH)^\bullet$, middle) and dihydroxylated R1/R2 ($R(OH)_2^\bullet$, right).

Table 33: D exchanges observed for m/z 331.162 from D_2O exchange of TART trapping of $^\bullet OH$ -initiated thymine degradation, using DEADANT as TART and MS for characterisation (11.6.4). Systematic m/z error = -0.0004; random m/z error = ± 0.0002 .

D exchange	Predicted m/z	Observed	Contribution / %		
			Simulated 5D exchange ^a	Simulated 6D exchange ^a	Simulated 7D exchange ^a
0	331.1618	0	0	0	0
1	332.1680	0	0	0	0
2	333.1743	0	0.34	0	0
3	334.1806	0	5.31	0.39	0.01
4	335.1869	7.93	31.13	5.57	0.20
5	336.1932	33.36	63.21	31.45	3.41
6	337.1994	58.71	0	62.58	25.65
7	338.2057	0	0	0	70.73
8	339.2120	0	0	0	0

^aSimulated using inherent solvent D/H ratio = 99.0% and calculated slow D/H exchange = 64.6% from R1/R2-ART.

The observed D exchanges appeared to partially correspond to both 5D and 6D exchanges. Simulation indicated that 6% and 94% of species contributing to the m/z 331.162 peak had five and six labile hydrogen atoms respectively, indicating 6% RO_2-ART and 94% $R(OH)O-ART$ or $R(OOH)-ART$. This 6% RO_2-ART was expected to be predominantly R1.1/R2.1-ART, since R1.1/R2.1 were the first RO_2^\bullet formed in the suggested mechanism and therefore would have had the highest radical flux and hence, greatest opportunity for trapping. The 94% $R(OH)O-ART$ or $R(OOH)-ART$ was expected to be predominantly hydroxylated R1.1.1/R2.1.1-ART, since literature rate constants indicate that RO^\bullet are trapped much more rapidly than R^\bullet . It was perhaps surprising that the somewhat low intensity peak corresponding to R1.1/R2.1 was mainly caused by species other than R1.1/R2.1. This is predominantly attributed to the relatively slow trapping rate of RO_2^\bullet radicals.

Many peaks were visible in the HPLC-MS chromatogram of m/z 331.162 but four peaks were significantly greater intensity than the others (Figure 130).

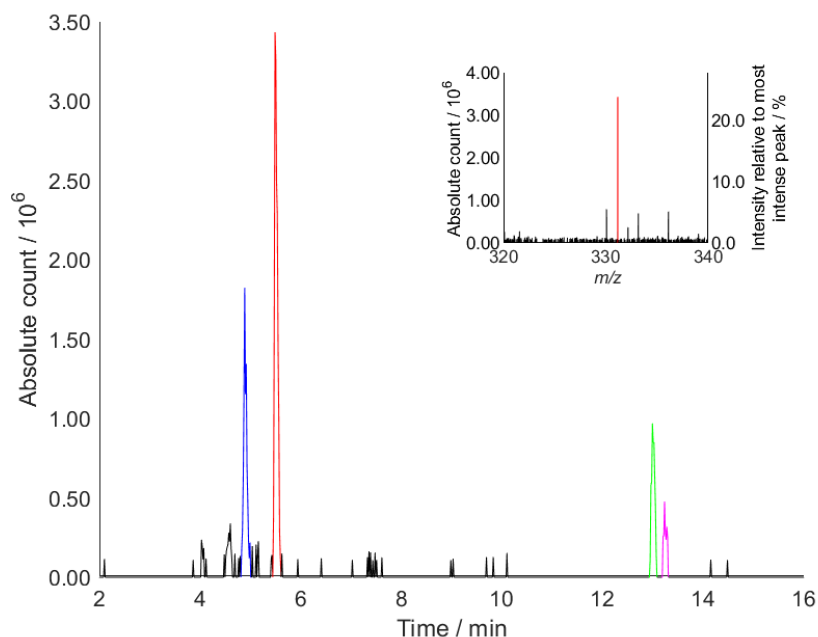


Figure 130: HPLC-MS chromatogram of m/z 331.162±0.002, detected from TART trapping of \bullet OH-initiated thymine degradation, using DEADANT as TART (11.6.4). Four peaks had significantly large intensity (coloured) although other smaller peaks were also observed. Mass spectrum (inset) recorded at time of maximum chromatogram intensity (red) shows m/z 315.167 cleanly isolated (red).

These four peaks could be separated into two groups, with the two most and two least intense peaks eluting at ~5 mins and ~13 mins respectively. Peaks eluting at similar times likely had similar functionality, whilst the two groups had different functionality. Integration of the four peaks produced relative intensities of 26% (blue), 51% (red), 16% (green) and 7% (pink) or in their groups, total relative intensities of 77% (earlier, blue, red) and 23% (later, green, pink). These broadly matched the D₂O exchange data for m/z 331.162, with relative intensities of 6D and 5D exchanges being 94% and 6% respectively. This suggested the earlier and later chromatogram peaks corresponded to hydroxylated R1.1.1/R2.1.1 and R1.1/R2.1 respectively. For R1.1/R2.1, relative intensities of the two peaks were 71% (green) and 29% (pink), whilst for hydroxylated R1.1.1/R2.1.1, relative intensities of the two peaks were 34% (blue) and 66% (red). As previously, these peaks could not be specifically assigned to any TART-trapped radicals without further characterisation.

Therefore, tandem MS was undertaken to elucidate these structures of hydroxylated R.1.1.1/R2.1.1-ART (SI5.2). However, all obtained peaks could correspond to any of the four species and therefore, no further structural elucidation was achieved. Nevertheless, observed peaks supported that these parent ion peaks emanated from TART-trapped radical species, with loss of NH(CH₃)₂ indicating the 1,1-dimethylethylenediamine functionality present in DEADANT-trapped radicals. One peak also likely corresponded to dehydration fragmentation, indicating an alcohol with neighbouring β -hydrogen atom, supporting suggested structures.

Mechanistic studies of \bullet OH-initiated thymine degradation using TART trapping had offered significant validation to the proposed mechanism (Figure 122). Standard MS had indicated existence of several trapped radicals corresponding to radicals produced during the reaction and offered some trapped radical quantification. HPLC-MS had allowed separation and detection of species, allowing isomers to be separately observed. D₂O exchange indicated number of labile hydrogen atoms for each species and tandem MS also provided further structural information. The success of this characterisation indicated that TART trapping could

be used for experimental mechanistic studies. To fully interpret the obtained data, kinetic modelling would be required. Improved MS quantification, through calibration using known trapped radical concentrations, would also likely be required. However, without any existing rate constants for this reaction, or a simple way of synthesising such trapped radicals, modelling and improved MS quantification would be complex and time consuming and hence, was not attempted.

TART trapping was similarly applied to $\bullet\text{OH}$ -initiated degradation of dipeptides as a proxy for proteins.

7.7. Dipeptides

Proteins are also highly vulnerable to damage by ROS such as $\bullet\text{OH}$. Studies indicate that ~70% $\bullet\text{OH}$ generated within cells reacts with proteins.³² Such damage may induce diseases.^{40–42} Therefore, $\bullet\text{OH}$ -initiated protein degradation is of significant interest in biochemistry and medicinal chemistry and therefore, was studied using TART trapping. Like nucleobases were studied as a proxy for key components of DNA (7.6), protected diglycines were studied as a simpler and model proxy for key components of proteins. TART trapping was used to investigate $\bullet\text{OH}$ -initiated diglycine degradation in collaboration with postgraduate Nikolas Vagkidis, who synthesised *N*-protected-diglycine starting materials, *N*-acetyl-diglycine (Ac-Gly-Gly-OH) and *N*-Boc-diglycine (Boc-Gly-Gly-OH). These dipeptides were *N*-protected to reduce amino group side reactions, which were irrelevant to degradation of glycine units in proteins. An $\bullet\text{OH}$ -initiated diglycine degradation mechanism was proposed, based upon literature and known general reaction pathways of $\bullet\text{OH}$ -initiated biochemical degradation (Figure 131).^{32,218,238}

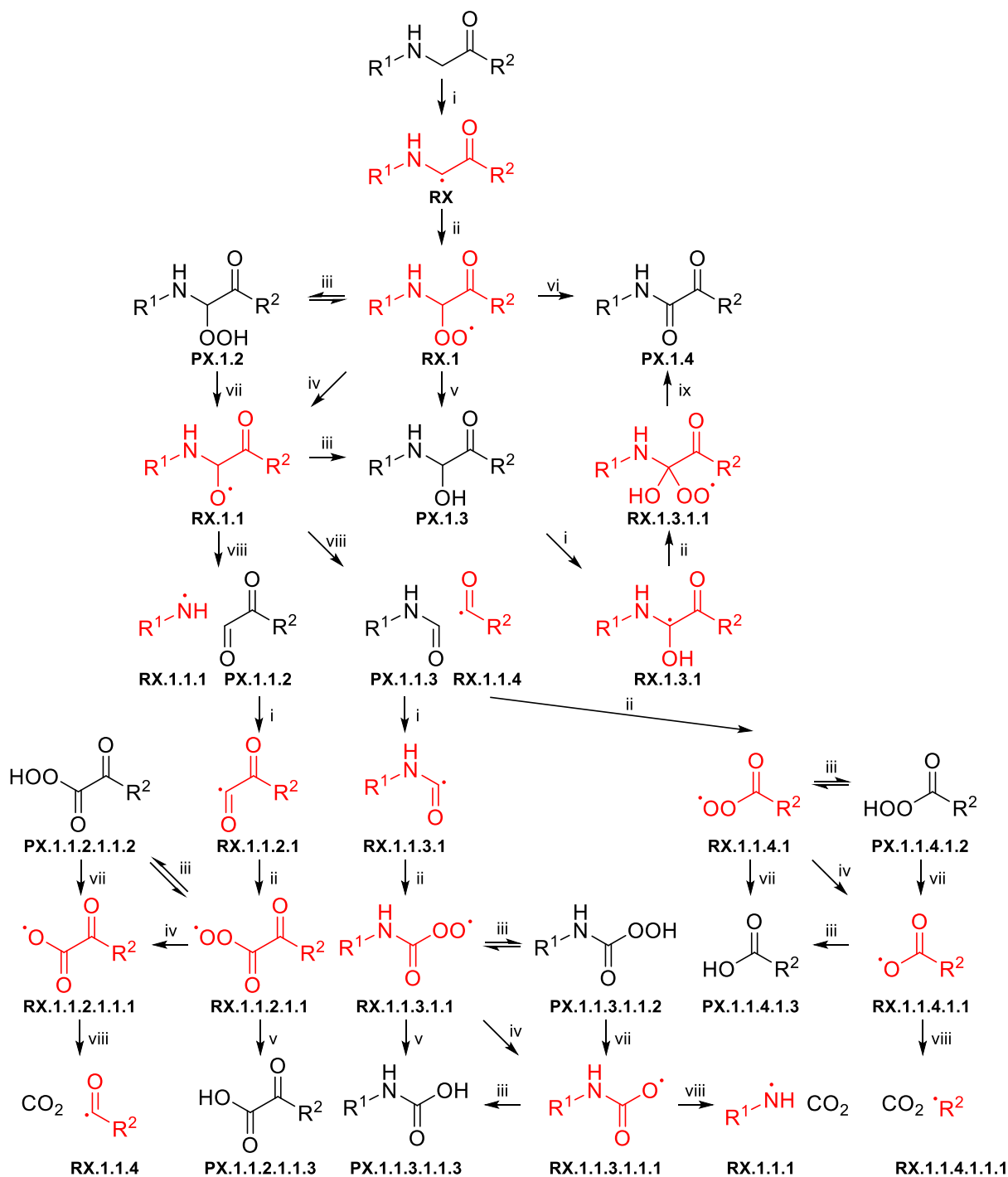


Figure 131: •OH-initiated diglycine degradation in aqueous solution. Structures and pathways were obtained or hypothesised using literature sources.^{32,218,238} X=1: R¹=Ac/Boc, R²=Gly-OH; X=2: R¹=Ac/Boc-Gly, R²=OH.
 i) + •OH, - H₂O. ii) + O₂. iii) + RH, - R•. iv) + RO₂•, - RO•. v) + RO₂•, - RCO. vi) + RO₂•, - ROH. vii) - •OH. viii) Fragmentation. ix) - HO₂•.

TART trapping was used to investigate •OH-initiated diglycine degradation for Ac-Gly-Gly-OH and Boc-Gly-Gly-OH, using DEADANT as TART (Figure 132, 11.6.4). Reaction mixtures were then characterised using MS (Table 34, 11.6.4).

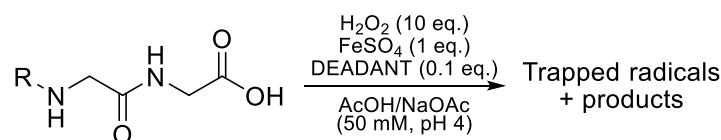


Figure 132: TART trapping of $\cdot\text{OH}$ -initiated dipeptide degradation, using Ac-Gly-Gly-OH and Boc-Gly-Gly-OH as substrates and DEADANT as TART (11.6.4).

Table 34: Species identified from TART trapping of $\cdot\text{OH}$ -initiated dipeptide degradation, using Ac-Gly-Gly-OH and Boc-Gly-Gly-OH as substrates, DEADANT as TART and MS for characterisation (11.6.4). Ac-Gly-Gly-OH: systematic m/z error = 0.0000; random m/z error = ± 0.0006 . Boc-Gly-Gly-OH: systematic m/z error = +0.0002; random m/z error = ± 0.0014 . 100% intensity = 1.09×10^9 absolute count.

Species		Ac-Gly-Gly-OH		Boc-Gly-Gly-OH	
		Predicted m/z	Intensity relative to TART standard / %	Predicted m/z	Intensity relative to TART standard / %
TART	[DEADANT+H] ⁺	312.2651	1.71	312.2651	1.50
Reactants	[Dipeptide+Na] ⁺	197.0538	4.86	255.0957	5.54
	[Dipeptide dimer+Na] ⁺	371.1179	61.3	487.2016	27.0
Trapped radicals	[R1:R3-ART+H] ⁺ ^a	329.1825	0.102	387.2243	4.64
	[R1:R3-TEMPO+H] ⁺ ^a	330.2029	3.35	388.2447	14.5
	[R1.1:R3.1-ART+H] ⁺ ^a	361.1723	0.934	419.2142	1.18
	[R1.1.1:R3.1.1-ART+H] ⁺ ^a	345.1774 ^b	1.20	403.2193	2.14
	[R1.1.1.1-ART+H] ⁺	214.1555	0	244.2025	0
	[R1.1.1.2.1-ART+H] ⁺	286.1403	0.007	314.1352	0
	[R1.1.1.2.1-TEMPO+H] ⁺	287.1607	0.026	315.1556	0
	[R1.1.1.2.1.1-ART+H] ⁺	318.1301	0.013	346.1251	0
	[R1.1.1.2.1.1.1-ART+H] ⁺	302.1352	0.013	330.1301	0
	[R1.1.1.3.1-ART+H] ⁺	242.1505	0	272.1974	0.003
	[R1.1.1.3.1-TEMPO+H] ⁺	243.1709	0.024	273.2178	0.010
	[R1.1.1.3.1.1-ART+H] ⁺	274.1403 ^b	0.075	304.1872	0.013
	[R1.1.1.3.1.1.1-ART+H] ⁺	258.1454 ^b	0.091	288.1923	0.012
	[R1.1.1.4-ART+H] ⁺	258.1454 ^b	0.091	288.1923	0.012
	[R1.1.1.4-TEMPO+H] ⁺	259.1658	0.044	289.2127	0.005
	[R1.1.1.4.1-ART+H] ⁺	290.1352	0.075	304.1872	0.013
	[R1.1.1.4.1.1-ART+H] ⁺	274.1403 ^b	0.061	290.1352	0.007
	[R1.1.1.4.1.1.1-ART+H] ⁺	230.1504	0.007	230.1504	0
	[R1.1.1.4.1.1.1-TEMPO+H] ⁺	231.1708	0.004	231.1708	0
	[R1.1.3.1:R3.1.3.1-ART+H] ⁺	345.1774 ^b	1.20	403.2193	2.14
	[R1.1.3.1:R3.1.3.1-TEMPO+H] ⁺	346.1978	0.387	404.2397	1.73
	[R1.1.3.1.1:R3.1.3.1.1-ART+H] ⁺	377.1672	0.192	435.2091	0.376
	[R2.1.1.1-ART+H] ⁺	271.1770	0	301.2240	0
	[R2.1.1.2.1-ART+H] ⁺	229.1188	0.018	229.1188	0
	[R2.1.1.2.1-TEMPO+H] ⁺	230.1392	0.041	230.1392	0
	[R2.1.1.2.1.1-ART+H] ⁺	261.1087	0	261.1087	0
[R2.1.1.2.1.1.1-ART+H] ⁺	245.1138	0.013	245.1138	0	
[R2.1.1.3.1-ART+H] ⁺	299.1719	0	357.2138	0.114	
[R2.1.1.3.1-TEMPO+H] ⁺	300.1923	0.107	358.2342	0.554	
[R2.1.1.3.1.1-ART+H] ⁺	331.1618	0.484	389.2036	3.83	
[R2.1.1.3.1.1.1-ART+H] ⁺	315.1668	0.158	373.2087	0.377	

Trapped radicals	[R2.1.1.4-ART+H] ⁺	201.1239	0	231.1709	0
	[R2.1.1.4-TEMPO+H] ⁺	202.1443	0	232.1913	0
	[R2.1.1.4.1-ART+H] ⁺	233.1137	0.041	233.1137	0.347
	[R2.1.1.4.1.1-ART+H] ⁺	217.1188	0.584	247.1658	0
	[OH-ART+H] ⁺	173.1290	0.009	173.1290	0.020
	[HO ₂ -ART+Na] ⁺	189.1239	0.006	189.1239	0
Products	[P1.2:P3.2+Na] ⁺	229.0437	0.167	287.0855	1.81
	[P1.3:P3.3+Na] ⁺	213.0487	0.202	271.0906	0.475
	[P1.4:P3.4+Na] ⁺	211.0331	0.043	269.0750	0.217
	[P1.1.1.2+Na] ⁺	154.0116	0	182.0066	0
	[P1.1.1.2.1.1.2+Na] ⁺	186.0015	0	213.9964	0
	[P1.1.1.2.1.1.3+Na] ⁺	170.0066	0	198.0015	0
	[P1.1.1.3+Na] ⁺	110.0218	0	140.0687	0
	[P1.1.1.3.1.1.2+Na] ⁺	142.0116	0	172.0586	0
	[P1.1.1.3.1.1.3+Na] ⁺	126.0167	0	156.0637	0
	[P1.1.1.4.1.2+Na] ⁺	156.9987	0	184.9936	0
	[P1.1.1.4.1.3+Na] ⁺	141.0038	0	168.9987	0
	[P2.1.1.2+Na] ⁺	96.9902	0	96.9902	0
	[P2.1.1.2.1.1.2+Na] ⁺	128.9800	0	128.9800	0
	[P2.1.1.2.1.1.3+Na] ⁺	112.9851	0	112.9851	0
	[P2.1.1.3+Na] ⁺	167.0433	0.071	197.0902	0.192
	[P2.1.1.3.1.1.2+Na] ⁺	199.0331	0	229.0800	0.021
	[P2.1.1.3.1.1.3+Na] ⁺	183.0382	0	213.0851	0.015
	[P2.1.1.4.1.2+Na] ⁺	100.9851	0	100.9851	0
[P2.1.1.4.1.3+Na] ⁺	84.9902	0	84.9902	0	

^aRadicals formed through HAA from C-H of protecting group forming R[•] (R3), O₂ addition to R[•] forming RO₂[•] (R3.1) and RO₂[•] degradation forming RO[•] (R3.1.1). ^bOther table entries have predicted species with identical *m/z*.

First observation of mass spectra revealed that these dipeptides mainly ionised as dimer complexes (Figure 133).²³⁹ This was believed to be exclusively an MS effect, as dipeptide NMR spectra indicated species were monomeric. Dipeptide propensity to dimerise during MS made quantification potentially challenging, as it would be difficult to predict how dipeptide side groups may affect propensity for dimerisation for other non-reactant species. However, manual searching for possible dipeptide-(R1:R3-ART, R1.1:R3.1-ART and R1.1.1:R3.1.1-ART) dimers yielded no matches, suggesting trapped radicals poorly dimerised. This suggested MS dimerisation could be ignored for non-reactant species.

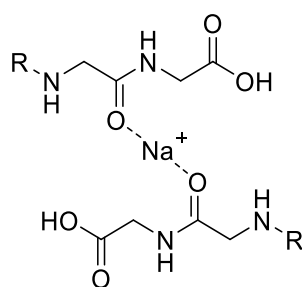


Figure 133: Possible R-Gly-Gly-OH dimer structure formed during MS.²³⁹

TART intensity was significantly lower than unreacted TART standard in both trapping reactions, indicating TART consumption. This likely meant that TART trapping had occurred.

MS peaks corresponding to Boc-Gly-Gly-OH were observed with relatively lower intensity than peaks corresponding to Ac-Gly-Gly-OH. This indicated that Boc-Gly-Gly-OH was consumed more rapidly than Ac-Gly-Gly-OH. This was surprising, since it was believed that HAA would primarily occur at diglycine C-H and therefore, both diglycines should have been consumed

at similar rates. Similarly, R1:R3, R1.1:R3.1 and R1.1.1:R3.1.1 corresponding peaks were observed more intensely for Boc-Gly-Gly-OH. In contrast, peaks corresponding to most other radicals were observed more intensely for Ac-Gly-Gly-OH than Boc-Gly-Gly-OH, including R1.1.1.2.1, R1.1.1.4 and R2.1.1.2.1. This indicated that HAA occurred more readily for Boc-Gly-Gly-OH whilst more fragmentation occurred during Ac-Gly-Gly-OH degradation. From this, it was hypothesised that HAA occurred more dominantly from the protecting group (R3) for Boc-Gly-Gly-OH than Ac-Gly-Gly-OH. For Boc-Gly-Gly-OH, it was believed that the HAA from one of nine unrestricted 1° C-H effectively competed with HAA from one of four relatively sterically shielded glycine 2° C-H. For Ac-Gly-Gly-OH however, HAA from one of three unrestricted 1° C-H would compete less effectively with HAA from one of four restricted glycine 2° C-H. HAA from the Boc group was proven to occur using tandem MS upon the [R1:R3-ART+H]⁺ corresponding peak (*m/z* 387.224, Figure 134). Two intense fragment peaks seemed to exclusively correspond to R3, indicating HAA occurred from the Boc group.

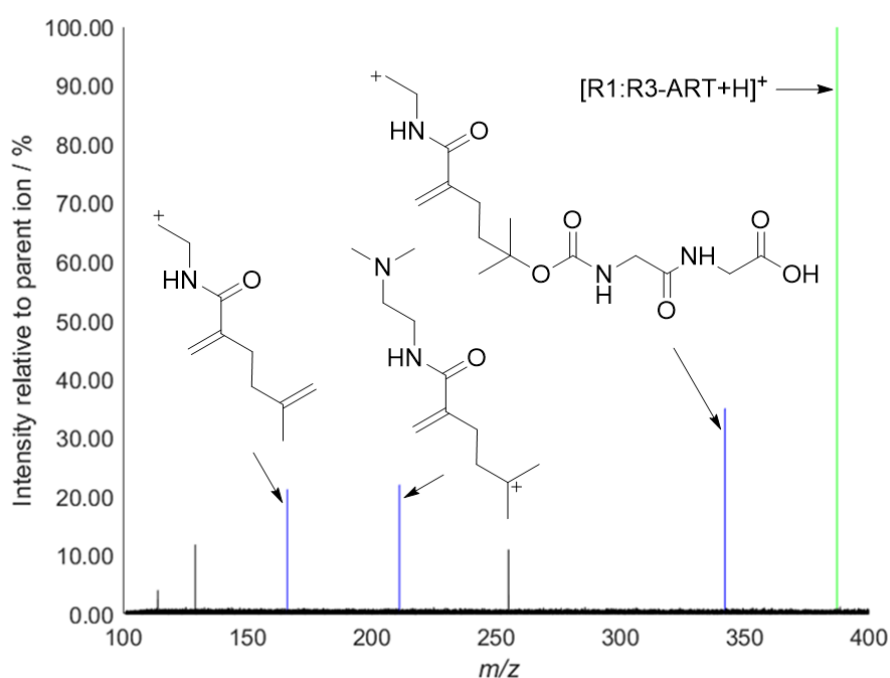


Figure 134: Tandem mass spectrum of [R1:R3-ART+H]⁺ corresponding peak for Boc-Gly-Gly-OH (*m/z* 387.224, green) with structures suggested for major fragment peaks (blue). These fragments indicated HAA from Boc-Gly-Gly-OH occurs readily upon the Boc group.

R3 formation was undesirable, as protecting group degradation was not relevant to protein degradation. Therefore, Boc-Gly-Gly-OH was not used for any subsequent investigations.

Whilst protecting group degradation probably also occurred for Ac-Gly-Gly-OH, over ten peaks corresponding to trapped radicals which could only be formed following HAA from a glycine C-H by •OH, indicated that Ac-Gly-Gly-OH could be used as a proxy for key components of proteins in their •OH-initiated degradation. D₂O exchange was used to further elucidate TART-trapped radicals and hence radical structures (SI5.3). Observation of peaks corresponding to TART-trapped radicals and additional D₂O data validated the mechanism proposed for •OH-initiated diglycine degradation, as supported by literature.^{32,218,238}

7.8. Saccharides

Saccharides, such as glucose, ribose, maltose and sucrose, are extremely vulnerable to degradation by $\bullet\text{OH}$. Saccharides contain many hydroxyl groups, which increase stability of α -carbon-centred radicals, increasing rate of HAA by $\bullet\text{OH}$. Whilst this makes saccharides very reactive, it also makes the exact site of initial HAA and radical formation much less certain, as all C–H are vulnerable to HAA (Figure 135). Furthermore, these radicals would likely progress through analogous steps in the early stage of the mechanism, leading to large numbers of isomeric intermediate radicals and products, which have identical m/z values and functionality.

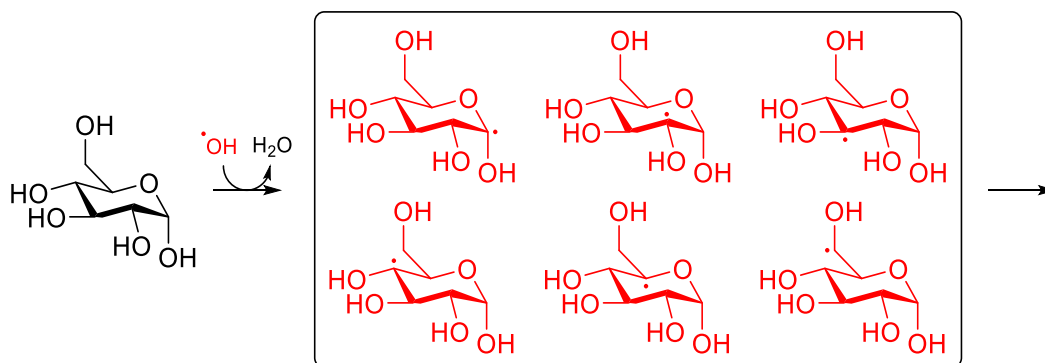


Figure 135: Plausible radicals formed after initial HAA in $\bullet\text{OH}$ -initiated glucose degradation.

This large number of possible radical intermediates and products makes mechanistic study of $\bullet\text{OH}$ -initiated saccharide degradation very difficult. Indeed, most literature surrounding $\bullet\text{OH}$ -initiated saccharide degradation tend to suggest many isomeric radical intermediates and products, without much indication of which are more prominent.^{240–242} As such, developing a comprehensive reaction scheme for $\bullet\text{OH}$ -initiated saccharide degradation was not attempted. Instead, functionality of radical intermediates and products was probed. TART trapping (Figure 136) and MS characterisation were undertaken similarly to as previously (11.6.4). However, MS analysis was conducted using the Formula Find programme (4.4.6). Formula limits and m/z limits were set as $\text{C}_{14}\text{H}_{0-28}\text{N}_2\text{O}_{1-12}$ and m/z 100-500 respectively, producing only non-fragmented TART-trapped radicals. Non-isomer specific radical structures were suggested that corresponded to the thirteen most intensely observed peaks (Table 35).

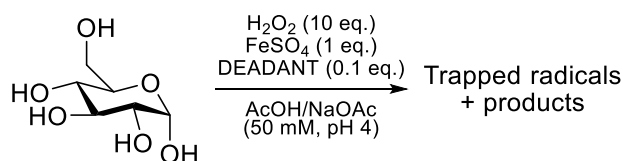


Figure 136: TART trapping of $\bullet\text{OH}$ -initiated glucose degradation, using DEADANT as TART (11.6.4).

Table 35: Identified radicals from the most intense MS peaks attributed to monomeric non-fragmented TART-trapped radicals from TART trapping of $\bullet\text{OH}$ -initiated glucose degradation, using DEADANT as TART and MS for characterisation (11.6.4). Molecular formula limits were set as $\text{C}_{14}\text{H}_{0-28}\text{N}_2\text{O}_{1-12}$ and m/z limits 100-500.

Unreasonable molecular formulae were eliminated. RCO represents formation of carbonyl from an existing alcohol group, i.e., $\text{R}\bullet$ and $\text{R}(\text{CO})\bullet$ differ by H_2 . Systematic m/z error = -0.0002; random m/z error = ± 0.0005 ; 100% intensity = 1.09×10^9 absolute count.

Entry	Observed m/z	Intensity relative to DEADANT standard / %	Corresponding radical molecular formula	Suggested radical functionality
1	365.1566	0.142	$\text{C}_6\text{H}_9\text{O}_8\bullet$	$\text{R}(\text{CO})\text{O}_2\bullet$ $\text{R}(\text{CO})(\text{OH})\text{O}\bullet$ $\text{R}(\text{CO})(\text{OOH})\bullet$ $\text{R}(\text{CO})(\text{OH})_2\bullet$
2	363.1410	0.140	$\text{C}_6\text{H}_7\text{O}_8\bullet$	$\text{R}(\text{CO})_2\text{O}_2\bullet$ $\text{R}(\text{CO})_2(\text{OH})\text{O}\bullet$ $\text{R}(\text{CO})_2(\text{OOH})\bullet$ $\text{R}(\text{CO})_2(\text{OH})_2\bullet$
3	381.1516	0.114	$\text{C}_6\text{H}_9\text{O}_9\bullet$	$\text{R}(\text{CO})(\text{OH})\text{O}_2\bullet$ $\text{R}(\text{CO})(\text{OOH})\text{O}\bullet$ $\text{R}(\text{CO})(\text{OH})_2\text{O}\bullet$ $\text{R}(\text{CO})(\text{OH})(\text{OOH})\bullet$ $\text{R}(\text{CO})(\text{OH})_3\bullet$
4	379.1361	0.081	$\text{C}_6\text{H}_7\text{O}_9\bullet$	$\text{R}(\text{CO})_2(\text{OH})\text{O}_2\bullet$ $\text{R}(\text{CO})_2(\text{OOH})\text{O}\bullet$ $\text{R}(\text{CO})_2(\text{OH})_2\text{O}\bullet$ $\text{R}(\text{CO})_2(\text{OH})(\text{OOH})\bullet$ $\text{R}(\text{CO})_2(\text{OH})_3\bullet$
5	347.1460	0.072	$\text{C}_6\text{H}_7\text{O}_7\bullet$	$\text{R}(\text{CO})_2\text{O}\bullet$ $\text{R}(\text{CO})_2(\text{OH})\bullet$
6	349.1617	0.049	$\text{C}_6\text{H}_9\text{O}_7\bullet$	$\text{R}(\text{CO})\text{O}\bullet$ $\text{R}(\text{CO})(\text{OH})\bullet$
7	397.1467	0.038	$\text{C}_6\text{H}_9\text{O}_{10}\bullet$	$\text{R}(\text{CO})(\text{OOH})\text{O}_2\bullet$ $\text{R}(\text{CO})(\text{OH})_2\text{O}_2\bullet$ $\text{R}(\text{CO})(\text{OH})(\text{OOH})\text{O}\bullet$ $\text{R}(\text{CO})(\text{OH})_3\text{O}\bullet$ $\text{R}(\text{CO})(\text{OOH})_2\bullet$ $\text{R}(\text{CO})(\text{OH})_2(\text{OOH})\bullet$ $\text{R}(\text{CO})(\text{OH})_4\bullet$
8	367.1722	0.034	$\text{C}_6\text{H}_{11}\text{O}_8\bullet$	$\text{RO}_2\bullet$ $\text{R}(\text{OH})\text{O}\bullet$ $\text{R}(\text{OOH})\bullet$ $\text{R}(\text{OH})_2\bullet$
9	383.1673	0.027	$\text{C}_6\text{H}_{11}\text{O}_9\bullet$	$\text{R}(\text{OH})\text{O}_2\bullet$ $\text{R}(\text{OOH})\text{O}\bullet$ $\text{R}(\text{OH})_2\text{O}\bullet$ $\text{R}(\text{OH})(\text{OOH})\bullet$ $\text{R}(\text{OH})_3\bullet$
10	331.1509	0.023	$\text{C}_6\text{H}_7\text{O}_6\bullet$	$\text{R}(\text{CO})_2\bullet$
11	333.1662	0.022	$\text{C}_6\text{H}_9\text{O}_6\bullet$	$\text{R}(\text{CO})\bullet$

12	361.1247	0.020	$C_6H_5O_8^\bullet$	$R(CO)_3O_2^\bullet$ $R(CO)_3(OH)O^\bullet$ $R(CO)_3(OOH)^\bullet$ $R(CO)_3(OH)_2^\bullet$
13	345.1298	0.017	$C_6H_5O_7^\bullet$	$R(CO)_3O^\bullet$ $R(CO)_3(OH)^\bullet$

All these peaks could correspond to at least one likely TART-trapped radical functionality and hence radical functionality (Table 35). Some examples of radical structures corresponding to these radical functionalities are indicated (Figure 137). This indicated TART was successfully used to trap radicals in $^\bullet OH$ -initiated glucose degradation. However, most peaks could correspond to multiple radical structures. Whilst these radical structures could all be sensibly produced during $^\bullet OH$ -initiated glucose degradation, due to the large number of pathways and possible structures, making certain structure assignment was impossible without further analysis. Due to the complex nature of these results, further MS characterisation was not undertaken. This meant that radical structures could not be specified in greater detail. However, many of these structures were previously suggested in literature.^{240–242}

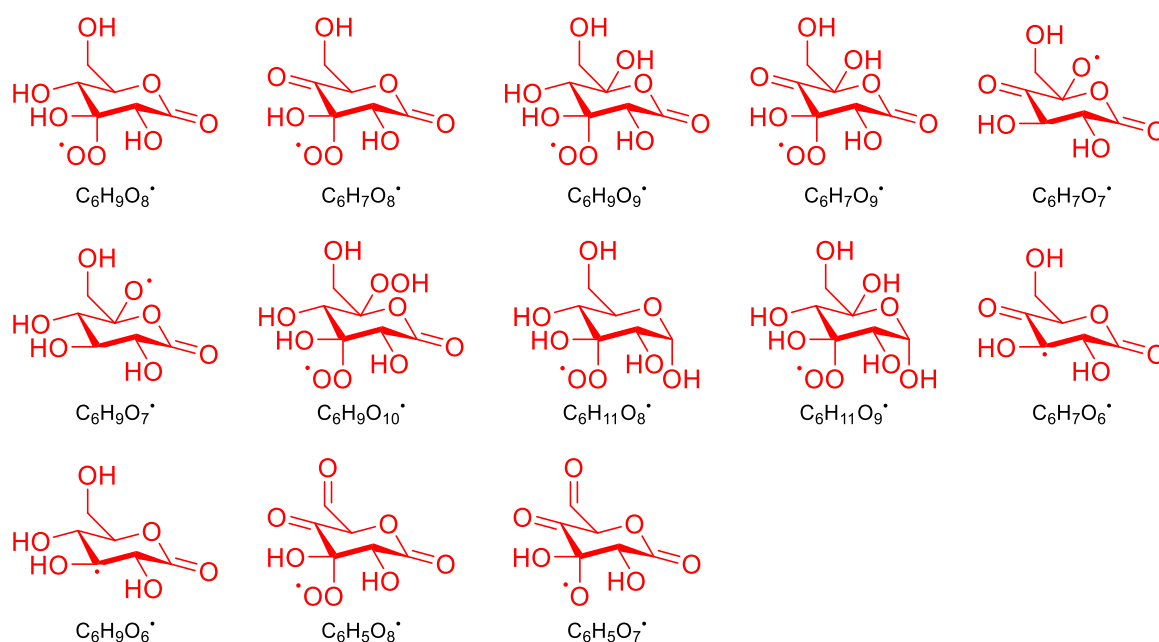


Figure 137: Example structures possibly produced during from $^\bullet OH$ -initiated glucose degradation.

7.9. Antioxidants

Antioxidants, such as ascorbic acid (vitamin C) and glutathione, play an important role in reducing and preventing oxidative damage to cellular components, such as DNA.^{33,34} As such, antioxidants and their role in reduction and prevention of oxidative damage and disease, have been widely researched (1.2.2). Therefore, TART trapping was used to investigate $^\bullet OH$ -initiated ascorbic acid degradation, for which a mechanism was proposed, based upon literature and known general reaction pathways of $^\bullet OH$ -initiated biochemical degradation (Figure 138).³³

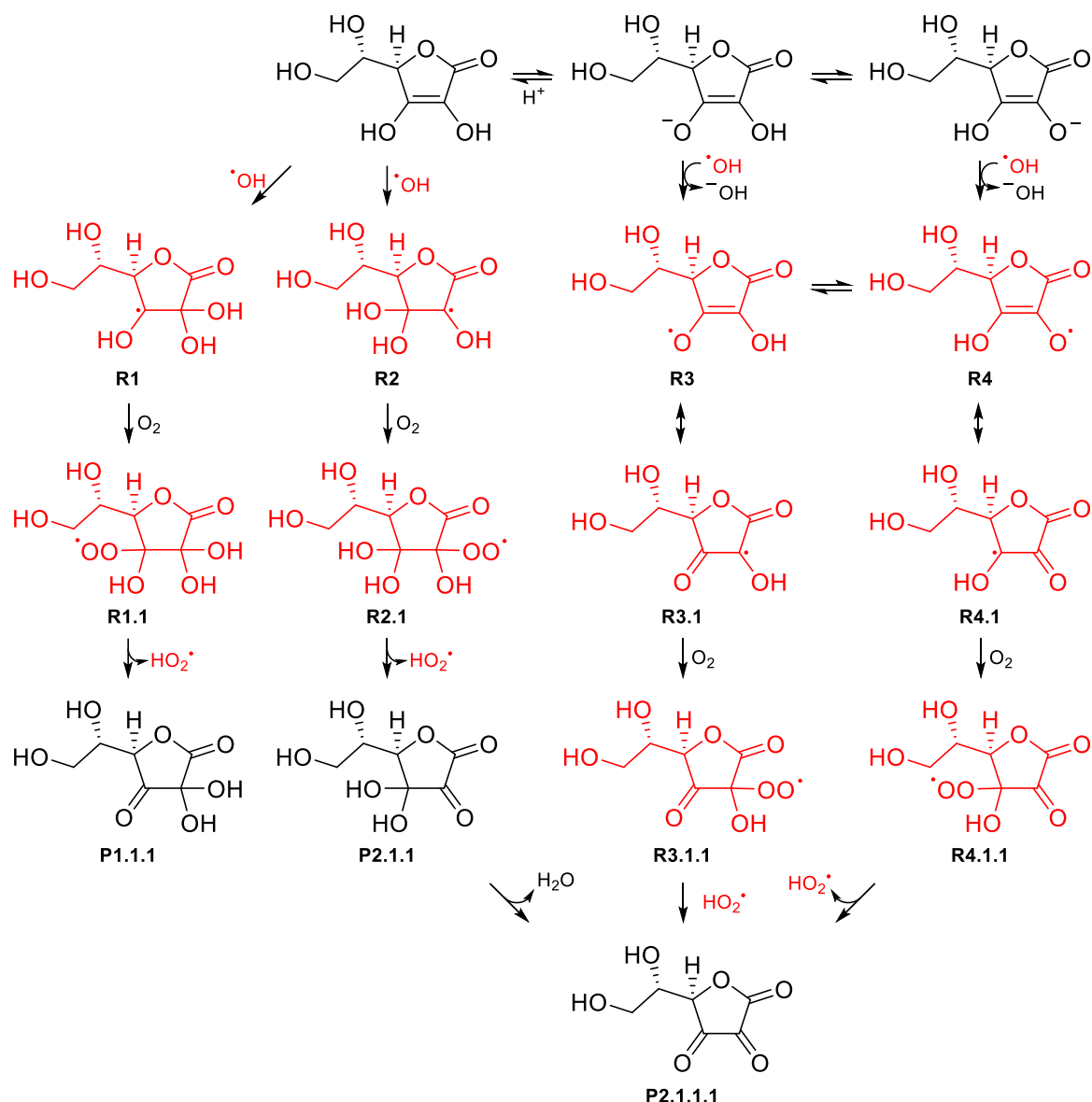


Figure 138: $\cdot\text{OH}$ -initiated ascorbic acid degradation in aqueous solution. Ascorbate and ascorbic acid dominate at physiological pH (typically pH 7.0-7.4)²³ and under somewhat acidic conditions (pH 4) respectively. Structures and pathways were obtained or hypothesised using literature sources.³³ Other reaction pathways, such as HAA from allylic C-H and alcohol O-H, were also possible.

TART trapping was then used to investigate $\cdot\text{OH}$ -initiated ascorbic acid degradation (Figure 139, 11.6.4). A trapless control was also undertaken. Reaction mixtures and TART standard were then MS characterised (Table 36). Ascorbic acid has first pKa 4.12 (~296 K).²⁴³ Therefore, at physiological pH (typically pH 7.0-7.4)²³, the ascorbate form dominates. However, under reaction conditions (pH 4), the ratio of ascorbic acid:ascorbate is ~4:3, meaning both forms are of significant concentration. Mass spectra were originally analysed by project student Dan Gugan but subsequently reanalysed in greater detail by the author.

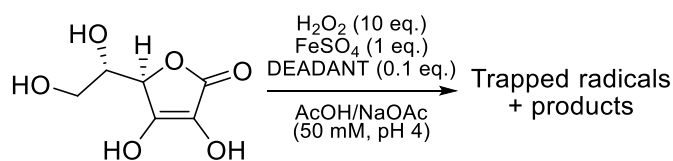


Figure 139: TART trapping of $\cdot\text{OH}$ -initiated ascorbic acid degradation, using DEADANT as TART (11.6.4).

Table 36: Species identified from TART trapping of •OH-initiated ascorbic acid degradation, using DEADANT as TART and MS for characterisation (11.6.4). Systematic m/z error = -0.0005; random m/z error = ± 0.0008 ; 100% intensity = 1.09×10^{10} absolute count^a.

	Species	Predicted m/z	Intensity relative to unreacted TART standard ^a / %		
			Trapless control	Standard ^a	Trapping reaction
TART	[DEADANT+H] ⁺	312.2651	0	100	0
Reactants	[Ascorbic acid+Na] ⁺	199.0219	0.0004	0	0
Trapped radicals	[R1/R2-ART+H] ⁺	349.1611	0	0	0.0021
	[R1/R2-TEMPO+H] ⁺	350.1815	0	0	0.0008
	[R1.1/R2.1-ART+H] ⁺	381.1509	0	0	0.0039
	[R3/R4-ART+H] ⁺	331.1505 ^b	0	0	0.0050
	[R3.1/R4.1-ART+H] ⁺	331.1505 ^b	0	0	0.0050
	[R3.1/R4.1-TEMPO+H] ⁺	332.1709 ^b	0	0	0.0466
	[R3.1.1/R4.1.1-ART+H] ⁺	363.1404	0	0	0.0315
	[OH-ART+H] ⁺	173.1290	0	0	0
Products	[HO ₂ -ART+H] ⁺	189.1239	0	0	0
	[P1.1.1/P2.1.1+Na] ⁺	215.0168	0.0241	0	0.0461
	[P2.1.1.1+Na] ⁺	197.0062	0.0007	0	0.0017

^aStandard scaled $\times 10$ to match dilution of samples. ^bOther table entries have predicted species with same m/z .

TART corresponding peak had ~50% compared to unreacted TART standard, post-trapping reaction. This indicated around half of TART was consumed, suggesting TART trapping had occurred.

Radicals formed during •OH-initiated ascorbic acid degradation had been successfully TART-trapped and MS characterised. These results indicated that ascorbic acid reacted with •OH and therefore, acted as an antioxidant, as expected. It was theorised that this antioxidant could reduce or prevent •OH-initiated biochemical degradation, such as for nucleobases. This would reduce concentration of radicals formed during degradation of these biochemicals.

TART trapping was used to investigate •OH-initiated degradation of a nucleobase-antioxidant system. It was theorised that antioxidant would reduce or prevent nucleobase degradation, resulting in reduced intensity of TART-trapped radicals. For this, TART trapping of •OH-initiated degradation of thymine, ascorbic acid or thymine and ascorbic acid were undertaken (Figure 140). These reaction mixtures were then MS characterised (Table 37, 11.6.5).

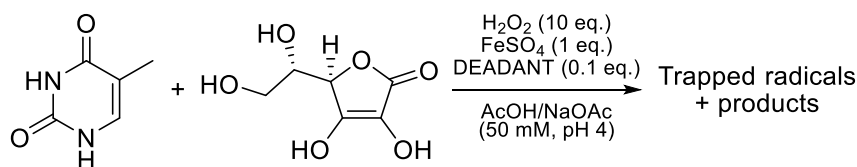


Figure 140: TART trapping of •OH-initiated thymine and ascorbic acid degradation, using DEADANT as TART (11.6.5).

Table 37: Trapped radicals from •OH-initiated thymine, ascorbic acid and simultaneous thymine and ascorbic acid degradation, using DEADANT as TART and MS for characterisation (11.6.5). T and A species are thymine- (Figure 122) and ascorbic acid-derived (Figure 138) respectively. Systematic m/z error = -0.0005; random m/z error = ± 0.0007 ; 100% intensity = 1.09×10^{10} absolute count^a.

	Species	Predicted m/z	Intensity relative to unreacted TART standard ^a / %		
			Thymine	Ascorbic acid	Both species
TART	[DEADANT+H] ⁺	312.2651	6.17	0	0.0014
Reactants	[Thymine+Na] ⁺	149.0327	0.0186	0	0
	[Ascorbic acid+Na] ⁺	199.0219	0	0	0
Thymine-derived trapped radicals	[TR1/TR2-ART+H] ⁺	299.1719	0.260	0	0.0002
	[TR1/TR2-TEMPO+H] ⁺	300.1923	0.196	0.0001	0.0184
	[TR1.1/TR2.1-ART+H] ⁺	331.1618	0.101	0	0.106
	[TR1.1.1/TR2.1.1-ART+H] ⁺	315.1668 ^b	0.311	0	0.0489
	[TR1.1.1.1/TR1.1.1.2-ART+H] ⁺	315.1668 ^b	0.311	0	0.0489
	[TR1.1.1.2-TEMPO+H] ⁺	316.1872 ^b	0.113	0.0017	0.0230
	[TR1.1.3.1-ART+H] ⁺	315.1668 ^b	0.311	0	0.0489
	[TR1.1.3.1-TEMPO+H] ⁺	316.1872 ^b	0.113	0.0017	0.0230
	[TR1.1.3.1.1-ART+H] ⁺	347.1567	0.0296	0	0.0521
	[TR2.1.1.1/TR 2.1.1.2-ART+H] ⁺	315.1668 ^b	0.311	0	0.0489
	[TR2.1.1.1/TR 2.1.1.2-TEMPO+H] ⁺	316.1872 ^b	0.113	0.0017	0.0230
	[TR3-ART+H] ⁺	281.1614	0.0058	0	0
	[TR3-TEMPO+H] ⁺	282.1818	0.245	0	0.0064
	[TR3.1-ART+H] ⁺	313.1512	0.0173	0	0.0102
	[TR3.1.1-ART+H] ⁺	297.1563	0.0061	0	0.0008
Ascorbic acid-derived trapped radicals	[AR1/AR2-ART+H] ⁺	349.1611	0.0004	0.0021	0.0031
	[AR1/AR2-TEMPO+H] ⁺	350.1815	0	0.0008	0
	[AR1.1/AR2.1-ART+H] ⁺	381.1509	0	0.0039	0.0034
	[AR3/AR4-ART+H] ⁺	331.1505 ^b	0	0.0050	0.0045
	[AR3.1/AR4.1-ART+H] ⁺	331.1505 ^b	0	0.0050	0.0045
	[AR3.1/AR4.1-TEMPO+H] ⁺	332.1709 ^b	0	0.0466	0.0255
Other trapped radicals	[OH-ART+H] ⁺	173.1290	0.0016	0	0
	[HO ₂ -ART+H] ⁺	189.1239	0	0	0
Thymine-derived products	[T1.1.2/T2.1.2+Na] ⁺	199.0331	0.0186	0	0.0022
	[TP1.1.3+Na] ⁺	183.0382	0.0280	0	0.0165
	[TP1.1.4+Na] ⁺	181.0225 ^a	0.0098	0	0.0438
	[TP3.1.2+Na] ⁺	181.0225 ^a	0.0098	0	0.0438
	[TP3.1.3+Na] ⁺	165.0276	0.0058	0	0
	[TP3.1.4+Na] ⁺	163.0120	0.0016	0	0
Ascorbic acid-derived products	[AP1.1.1/AP2.1.1+Na] ⁺	215.0168	0	0.0461	0.0252
	[AP2.1.1.1+Na] ⁺	197.0062	0	0.0017	0

^aStandard scaled $\times 10$ to match dilution of samples. ^bOther table entries have predicted species with same m/z .

Averaging the relative intensities of TART-trapped radicals between the simultaneous reaction to the substrate or antioxidant reactions yielded $50 \pm 20\%$ and $95 \pm 13\%$ respectively. This suggested that thymine-derived TART-trapped radicals decreased by $\sim 50\%$ in ascorbic acid presence, whilst ascorbic acid-derived TART-trapped radicals decreased by only $\sim 5\%$ in thymine presence. Assuming TART trapping occurred at similar rates for thymine- and

ascorbic acid-derived radicals, this indicated that ascorbic acid presence decreased thymine radical concentrations, and therefore thymine consumption, by around half and therefore acted as an antioxidant.

In this system, $\bullet\text{OH}$ are continuously generated and hence substrates continuously react with $\bullet\text{OH}$. In reality, antioxidants cause radical oxidation chains to break, preventing further radical reactions. Nevertheless, these results indicate that ascorbic acid is more reactive to $\bullet\text{OH}$ than thymine and therefore, would break radical oxidation chains more efficiently, implying that ascorbic acid is a better antioxidant than thymine. This showed that TART trapping could be used to investigate the effect of antioxidants on $\bullet\text{OH}$ -initiated biochemical degradation.

7.10. Conclusions and future work

TART trapping was successfully used for preliminary investigations of aqueous iron-catalysed $\bullet\text{OH}$ -initiated biochemical degradation. Biochemicals investigated included nucleobases (thymine), dipeptides (protected diglycine), saccharides (glucose) and antioxidants (ascorbic acid). $\bullet\text{OH}$ -initiated degradations of these biochemicals were believed to be relevant to oxidative stress and development of many diseases including cancers.^{40–42} Observations of TART-trapped radicals provided mechanistic and kinetic insights into these degradation processes, providing validation to hypothesised mechanisms of $\bullet\text{OH}$ -initiated biochemical degradation. Spin traps, are easily degraded by trace metals and therefore, may be less suitable than TARTs for radical characterisation in these iron-catalysed systems (1.3.2.1).¹²⁸ Furthermore, $\bullet\text{OH}$ -initiated biochemical degradation generated many oxygen-centred radicals, which could not be trapped using nitroxyl radical recombination traps (1.3.2.2).

These investigations showed that DANT and DEADANT were soluble in acidic solution and able to trap biochemically relevant radicals. However, peaks corresponding to DEADANT-trapped radicals were observed as protonated MS adducts and with much greater intensity than peaks corresponding to DANT-trapped radicals, which were observed as sodiated MS adducts. This was believed to be due to DEADANT-trapped radicals having highly basic 3° amine character, which improved their ionisation efficiency. Furthermore, relative intensity of peaks corresponding to TART-trapped radicals were believed to be more reliable, as ionisation efficiency depended less on reactant radical functionality. Additionally, tandem MS was performed more successfully for DEADANT-trapped radicals than DANT-trapped radicals. This indicated that DEADANT was generally a superior TART for these reactions. However, it should be noted that in some systems, its basicity may cause side reactions and therefore, its suitability for TART trapping must be carefully considered for each trapping reaction.

In general, evidence gathered using MS results, reaction mechanisms and literature-sourced rate constants suggested that TART rapidly reacted with short-lived carbon-centred $\text{R}\bullet$ and $\text{RO}\bullet$ but slowly reacted with long-lived $\text{RO}_2\bullet$. This indicated that whilst TART trapping was an effective tool for characterisation of short-lived radicals, it was not as useful for characterisation of long-lived radicals. This was also true of other indirect radical characterisation techniques, such as spin trapping and recombination trapping (1.3.2). Nevertheless, since existing direct radical characterisation techniques were generally better at detecting long-lived radicals and poorer at detecting short-lived radicals (1.3), TART trapping was still a valuable tool for radical characterisation.

TART trapping and MS characterisation indicated that $\bullet\text{OH}$ -initiated thymine degradation occurred primarily through $\bullet\text{OH}$ addition rather than HAA by $\bullet\text{OH}$, as predicted in literature. D_2O exchange, tandem MS and HPLC-MS were used to further characterise TART-trapped radicals. These techniques showed that many isomers corresponded to a single peak. In

particular, HPLC-MS was used effectively to separate and detect species with the same m/z . With further characterisation or modelling, it was believed that HPLC-MS could be used to quantify concentration of radicals.

The Formula Find programme was used effectively to find peaks corresponding to TART-trapped radicals and suggest the molecular formulae of these radicals in \bullet OH-initiated glucose degradation. This allowed key radicals to be identified, without needing to predict a mechanism first. This also ensured that intensely observed TART-trapped radicals would not go unobserved.

TART trapping and MS characterisation of dual \bullet OH-initiated thymine and ascorbic acid degradation showed that ascorbic acid worked effectively as an antioxidant to reduce \bullet OH-initiated thymine degradation. This indicated that TART trapping could be used to evaluate antioxidant activity, similarly to how DPPH and UV-Vis spectroscopy are commonly used (1.3.2.2).¹⁰³ However, TART trapping and MS characterisation were far more diagnostic, offering a distinct advantage over DPPH and UV-Vis spectroscopy.

Although TART trapping and MS characterisation were successfully used to characterise radicals formed during \bullet OH-initiated biochemical degradation, these investigations were very preliminary. Therefore, there was a lot of scope for further probing the mechanisms and kinetics of these reactions. For all reactions this could include: effect of different substrates; substrate concentration; different TART concentration and functionality; experimental conditions and kinetics investigations. Kinetic modelling would also allow results to be more quantitatively analysed, possibly allowing relative concentrations of radicals to be estimated using intensity of peaks corresponding to TART-trapped radicals. In particular, kinetic investigations of these reactions would be interesting, as it was not known at what rate these reactions progressed.

For all reactions, \bullet OH was believed to far exceed the amount of substrate. This meant that non-radical products formed following substrate reaction with \bullet OH could be reinitiated by another \bullet OH. This did not well emulate biological systems. Reducing $[H_2O_2]$ would likely yield fewer later stage radicals and hence results of TART trapping would have greater biological relevance. Therefore, an interesting experiment would be to undertake TART trapping in the studied \bullet OH-initiated biochemical degradations and observe how relative intensities of TART-trapped radicals were affected for earlier and later stage radicals. Similarly, antioxidant capacity of ascorbic acid could be further probed by comparing intensities of peaks corresponding to TART-trapped radicals between reactions where $[thymine]$ and $[ascorbic\ acid]$ were altered.

For TART trapping of \bullet OH-initiated thymine degradation, further MS characterisation, such as D_2O exchange HPLC-MS or tandem MS HPLC-MS may indicate which HPLC-MS chromatogram peaks corresponded to which TART-trapped radicals isomers. Furthermore, kinetic modelling could be used to experimentally determine relative concentrations of the corresponding radical isomers from intensity of MS peaks corresponding to TART-trapped radicals.

All TART trapping investigations thus far had been performed upon liquid phase radical reactions. However, gaseous radical reactions play a key role the formation of secondary organic aerosol (SOA), photochemical smog and tropospheric ozone and therefore, were of greater interest.^{10,11} Therefore, TART trapping was used to investigate the mechanisms and kinetics of atmospherically relevant radical reactions, such as alkene ozonolysis (8).

8. Alkene ozonolysis

8.1. Introduction

Atmospheric alkene decomposition is predominantly caused by reaction with hydroxyl radicals ($\bullet\text{OH}$), nitrate radicals ($\bullet\text{NO}_3$) and ozone (1.2.3). $\bullet\text{OH}$ and $\bullet\text{NO}_3$ appear to be more significant in alkene decomposition. However, there is strong evidence to suggest significant quantities of $\bullet\text{OH}$ for alkene decomposition are produced as a product of alkene ozonolysis, a radical process. Furthermore, recent measurements predict that alkene ozonolysis provides missing $\bullet\text{OH}$ reactivity observed over forested areas.⁵⁸ Alkene ozonolysis is also believed to cause formation of highly oxidised multifunctional (HOM) products.⁶⁵⁻⁶⁷ The high atmospheric abundance of alkenes, coupled with their widespread use in flavourings and fragrances, makes them important species in atmospheric chemistry and indoor and outdoor air quality control. Therefore, understanding the mechanisms of radical alkene decomposition is of great interest. As such, gaseous alkene ozonolysis was investigated using TART trapping.

8.2. General mechanistic steps of alkene ozonolysis

8.2.1. Alkene reaction with ozone

Alkene ozonolysis is initiated when alkene reacts with ozone in a [3+2] cycloaddition to form a molozonide. This subsequently breaks down into a carbonyl species and an excited zwitterionic carbonyl oxide, known as a Criegee zwitterion. This excited Criegee zwitterion is one of two resonance structures, with the other being an excited α -alkyl-peroxyl biradical, known as a Criegee biradical. Collectively, these two resonance structures are called Criegee intermediates (1.2.3).^{68,69,71} Unsymmetrical alkenes can form two different sets of carbonyls and Criegee intermediates (Figure 141). Alkene reaction with ozone requires a relatively high activation energy, with typical rate constants being $\sim 10^{-15}$ - 10^{-18} molec.⁻¹ cm³ s⁻¹ ($\sim 10^2$ - 10^5 mol⁻¹ dm³ s⁻¹) at RTP.^{57,244} Subsequent reactions are usually much faster, with rate constants $> 10^{-14}$ molec.⁻¹ cm³ s⁻¹ ($> 10^6$ mol⁻¹ dm³ s⁻¹).⁵⁷ Alkene reaction with ozone is therefore the rate determining step.

Excited Criegee intermediates may either rearrange and rapidly decay into α -radical carbonyl $\text{R}\bullet$ species and $\bullet\text{OH}$, via a vinyl hydroperoxide intermediate, or relax to form stabilised Criegee zwitterions (Figure 141). $\bullet\text{OH}$ formed during Criegee intermediate decay can further react with other species. Criegee intermediate stabilisation is usually a minor pathway, whilst subsequent reactions are non-radical. Therefore, species formed following Criegee intermediate stabilisation were largely ignored during radical trapping investigations.

In presence of air and hence high $[\text{O}_2]$, α -carbonyl radical $\text{R}\bullet$ reacts rapidly with O_2 to form $\text{RO}_2\bullet$, with rate constants typically being $\sim 10^{-12}$ - 10^{-11} molec.⁻¹ cm³ s⁻¹ ($\sim 10^8$ - 10^9 M⁻¹ s⁻¹) at RTP.^{245,246} This differs to radical reactions in solution, where $[\text{O}_2]$ is significantly lower, meaning $\text{R}\bullet$ reaction occurs less rapidly (7). Unsymmetrical Criegee intermediates may form two different α -radical carbonyl $\text{R}\bullet$ isomers (Figure 141).

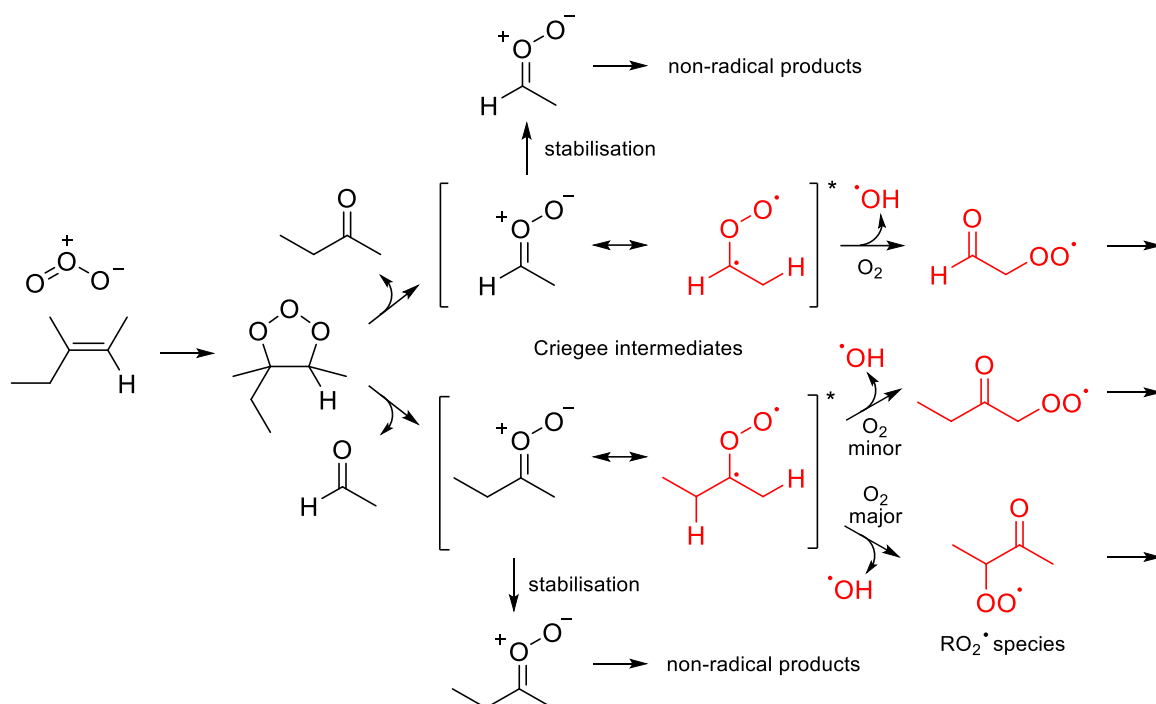


Figure 141: Example ozonolysis mechanism of 2-methylpent-2-ene in presence of O_2 , showing formation of Criegee intermediates and subsequent RO_2^\bullet formation.

Though faster than alkene reaction with ozone, rate of RO_2^\bullet consumption is relatively slow compared to rate of consumption of its subsequent products, resulting in another step which significantly affects overall rate of reaction. Consequently, detecting primary RO_2^\bullet species and elucidating their structures is fundamental for understanding alkene reaction with ozone, Criegee intermediate formation and degradation and the reaction mechanism for RO_2^\bullet and its subsequent species. Furthermore, comparing concentrations of primary RO_2^\bullet with other products and between different alkene ozonolysis reaction mechanisms, may offer insights into their kinetics. However, due to the relatively high stability of RO_2^\bullet , it was hypothesised to react slowly with TARTs compared to other radicals, as discussed previously (7.2). For example in solution, $(\text{CH}_3)_3\text{CO}_2^\bullet$ reacts with $\text{H}_2\text{C}=\text{C}(\text{CH}_3)\text{COOCH}_3$ with rate constant $\sim 0.1 \text{ M}^{-1} \text{ s}^{-1}$ (303 K).²²⁶

Further reactions which occur during alkene ozonolysis broadly progress through the same mechanistic steps as discussed previously in aqueous iron-catalysed $\cdot\text{OH}$ -initiated biochemical degradation (7.2).

8.2.2. Other mechanistic steps and differences from radical reactions in solution

Further reactions which occur during alkene ozonolysis include: HAA by $\cdot\text{OH}$ to form R^\bullet ; $\cdot\text{OH}$ addition to alkene to form R^\bullet ; subsequent RO_2^\bullet formation; $\text{RO}_2^\bullet + \text{RO}_2^\bullet$ reaction to form two RO^\bullet , ROH and RCO or ROOR ; HAA by RO_2^\bullet to form ROOH ; ROOR decay to form two RO^\bullet ; ROOH decay to form RO^\bullet and $\cdot\text{OH}$; HAA by RO^\bullet to form R^\bullet and ROH ; RO^\bullet fragmentation to form R^\bullet and RCO ; α -hydroperoxide- RO^\bullet decay to form HO_2^\bullet and RCO and carboxyl RO^\bullet decay to form R^\bullet and CO_2 (Figure 142, 7.2).

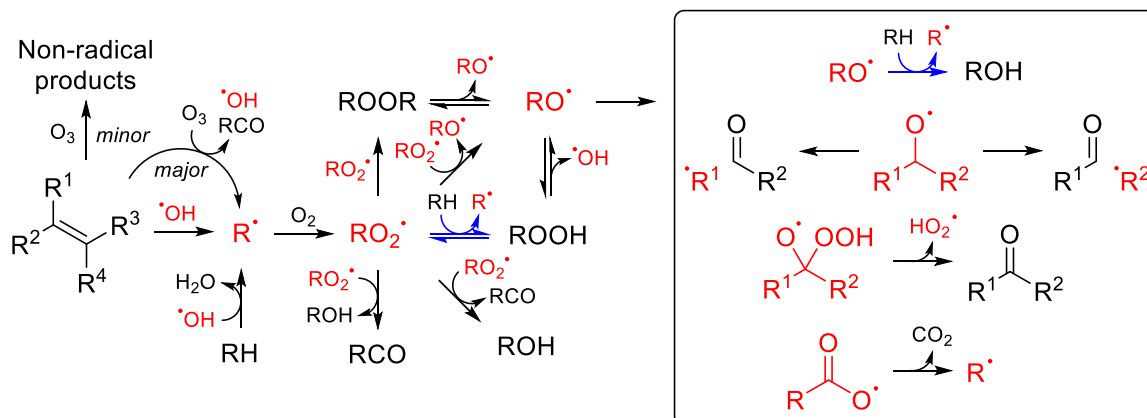


Figure 142: General reaction mechanism of alkene ozonolysis. Some reactions may occur either intermolecularly or intramolecularly (blue). O_2 release is not shown. RCO represents carbonyl species.

However, there are some key differences between aqueous biological systems and gaseous systems. Firstly, due to the high concentration of O_2 in air, R^\bullet react rapidly with O_2 to form RO_2^\bullet . Therefore, radical trapping of R^\bullet was not hypothesised to occur.

Furthermore, as previously stated, atmospheric alkene degradation principally occurs through reaction with $\bullet OH$ and $\bullet NO_3$. Alkene reaction with these radicals is much faster than alkene ozonolysis (typically $\sim 10^5$ - 10^7 times faster).⁵⁷ $\bullet OH$ radicals are formed as a by-product of alkene ozonolysis, as shown (Figure 141). Therefore, once alkene ozonolysis reactions had occurred and $\bullet OH$ radicals were produced, it was expected that alkenes would quickly react with $\bullet OH$ radicals. Compared to many other alkene ozonolysis species, $\bullet OH$ reaction rate was expected to be particularly high with unreacted alkene, due to its high abundance and reactive double bond. This contrasted with $\bullet OH$ -initiated biochemical degradation, in which $\bullet OH$ were in much greater excess than the biochemical (7.3).

To undertake TART trapping of alkene ozonolysis, a reaction set-up had to be devised.

8.3. Methodology

TART trapping of alkene ozonolysis was investigated using a standard set-up (Figure 143, 11.7.1). In this set-up, air was passed over a UV lamp, photolysing O_2 to generate ozone. The resulting ozone stream was mixed with a substrate vapour stream. Ozone and substrate reacted in the combined gas stream before being bubbled through TART trapping solution.

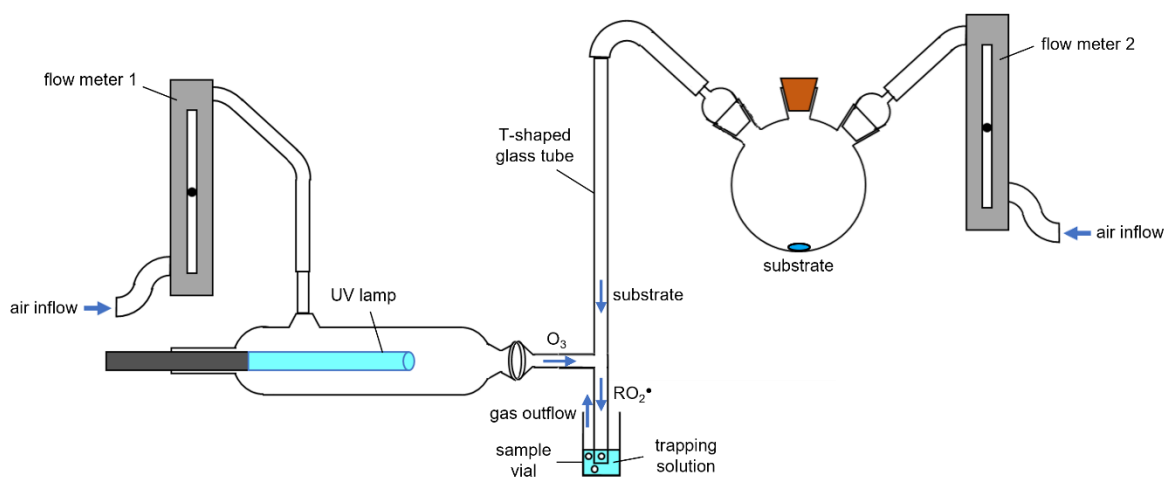


Figure 143: TART trapping of alkene ozonolysis set-up (11.7.1).

In this set-up, it was assumed that flow was laminar and mixing occurred instantly at the T-junction. Different length T-shaped glass tubes could be used to increase residence time for substrate reaction with ozone, with typical residence length set at 5.0 cm. TART functionality was chosen as required, however typically CHANT was used. [TART] was set between 50-5000 μM in MeCN but was typically 500 μM . Flow rate through trap solution was set at 1.5 L min^{-1} , to ensure rapid but controllable bubbling. Flow rate through each bubbler was adjusted as required, but was typically set at an equal 0.75 L min^{-1} through each flow meter. Under these standard conditions and in absence of substrate or trapping solution, [ozone] was measured to be $117.5 \pm 0.4 \text{ ppm}$ ($2.943 \pm 0.010 \times 10^{15} \text{ molec. cm}^{-3}$). Reaction time was varied as required, but was typically 10 min. Solvent was removed *in vacuo* upon reaction completion and the resultant MS characterised. These standard conditions had been optimised (8.6.2).

In this system, all studied alkenes were significantly in excess of ozone. For example in cyclohexene ozonolysis, gaseous [cyclohexene] was estimated to be $1.15 \times 10^{18} \text{ molec. cm}^{-3}$, >100 fold excess compared to ozone (11.7.1). This strongly contrasted to the $\bullet\text{OH}$ -initiated biochemical degradation system, in which $\bullet\text{OH}$ initiator was significantly in excess of the biochemical. Therefore, the vast majority of ozone and $\bullet\text{OH}$ was expected to react with unreacted alkene and not other species formed during alkene ozonolysis. Therefore, re-initiation of stable products formed during alkene ozonolysis such as ROH and RCO would be unlikely to occur and hence was largely ignored. It is important to note that this system does not reflect atmospheric concentrations of these species and hence, these species may not undergo typical atmospheric reactions.

Since all radicals were heteroatom-centred radicals, only TART-trapped radicals were hypothesised to be formed.

Before alkene ozonolysis radical trapping was undertaken, potential TART side reactions with ozone were explored.

8.4. TART ozonolysis

TARTs were themselves alkenes, which meant they may have undergone liquid phase ozonolysis in the TART trapping of alkene ozonolysis system. This would be undesirable. However, it was hoped that the large of excess of alkene to ozone would cause all ozone to be consumed before reaching the trapping solution, thereby minimising TART reaction with ozone. To ensure this, control reactions were undertaken. For these, CHANT was subjected to ozone both in presence and absence of cyclohexene and α -pinene (Figure 144, 11.7.2). Subsequent MS characterisation indicated three TART ozonolysis products were formed in solution (Table 38). Cyclohexene and α -pinene were later used as substrates in TART trapping of alkene ozonolysis studies (8.5 and 8.6).

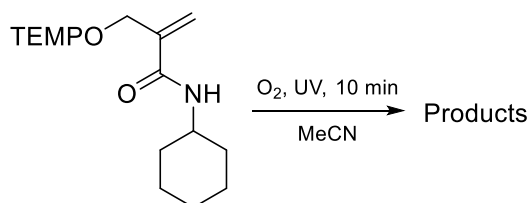


Figure 144: CHANT ozonolysis control experiment (11.7.2).

Table 38: Ozonolysis products identified in TART trapping of alkene ozonolysis, using MS for characterisation (11.7.2). Systematic m/z error = -0.0005; random m/z error = ± 0.0003 ; 100% intensity = 3.08×10^9 absolute count.

Species	Predicted m/z	Intensity relative to unreacted TART standard / %		
		No alkene	Cyclohexene	α -Pinene
[CHANT+H] ⁺	323.2698	0.164	48.4	18.3
 <chem>CC(=O)N(C1CCCCC1)O</chem> + H ⁺	325.2491	1.86	0	0.010
 <chem>CC(O)C(=O)N(C1CCCCC1)O</chem> + H ⁺	343.2597	6.52	0	0.036
 <chem>CC(O)C(=O)N(C1CCCCC1)O</chem> + H ⁺	341.2440	0.11	0	0

MS peaks corresponding to CHANT were significantly reduced compared to unreacted CHANT standard, for all three reactions. In substrate absence, CHANT was near totally consumed by ozonolysis, indicated by the peak corresponding to [CHANT+H]⁺ having ~0.2% intensity compared to unreacted CHANT standard. This was perhaps unsurprising since total ozone molarity was ~30 in excess of CHANT (1 eq.). However, ozone solubility in MeCN was low, implying TART reacted rapidly with ozone.²⁴⁷ In substrate presence, the peak corresponding to [CHANT+H]⁺ had relative intensity >15%, over two orders of magnitude less than in substrate absence. This indicated substrate consumed significant ozone before reaching CHANT solution, reducing CHANT ozonolysis.

Peaks corresponding to CHANT ozonolysis products were observed with significantly greater intensity in substrate absence than in substrate presence (<1% relatively). This suggested that in substrate presence, most ozone reacted with substrate prior to reaching CHANT solution. Furthermore, no CHANT ozonolysis products were detected in cyclohexene presence but were in α -pinene presence. Using estimated gaseous substrate concentrations and literature-sourced rate constants, cyclohexene and α -pinene were calculated to react with ozone with initial rates $\sim 3 \times 10^{17}$ and $\sim 2 \times 10^{16}$ molec. cm⁻³ s⁻¹ respectively (11.7.1).^{57,244} Therefore, ozone was consumed more rapidly by cyclohexene than α -pinene, meaning less ozone reached the trapping solution, reducing TART ozonolysis. Therefore, TART ozonolysis product intensities gave an indication of ozone consumption prior to reaching the trapping solution. Since rate of ozone consumption differed for each alkene, TART ozonolysis products were screened for in all alkene ozonolysis trapping reactions. However, from here onwards these TART ozonolysis products are not discussed.

TART ozonolysis was shown to be negligible in presence of substrate alkene. Therefore, the system should have been suitable for TART trapping of alkene ozonolysis investigations. First, TART trapping of cyclohexene ozonolysis was undertaken.

8.5. Cyclohexene ozonolysis

Alkene ozonolysis was initially studied using cyclohexene as substrate. Although not as atmospherically relevant as other alkenes, its simplicity, symmetry and cyclic nature reduced the number of possible reaction pathways, making it a model alkene for initial investigation. A cyclohexene ozonolysis mechanism was proposed, based upon literature and known general alkene ozonolysis reaction pathways (Figure 145).²⁴⁸

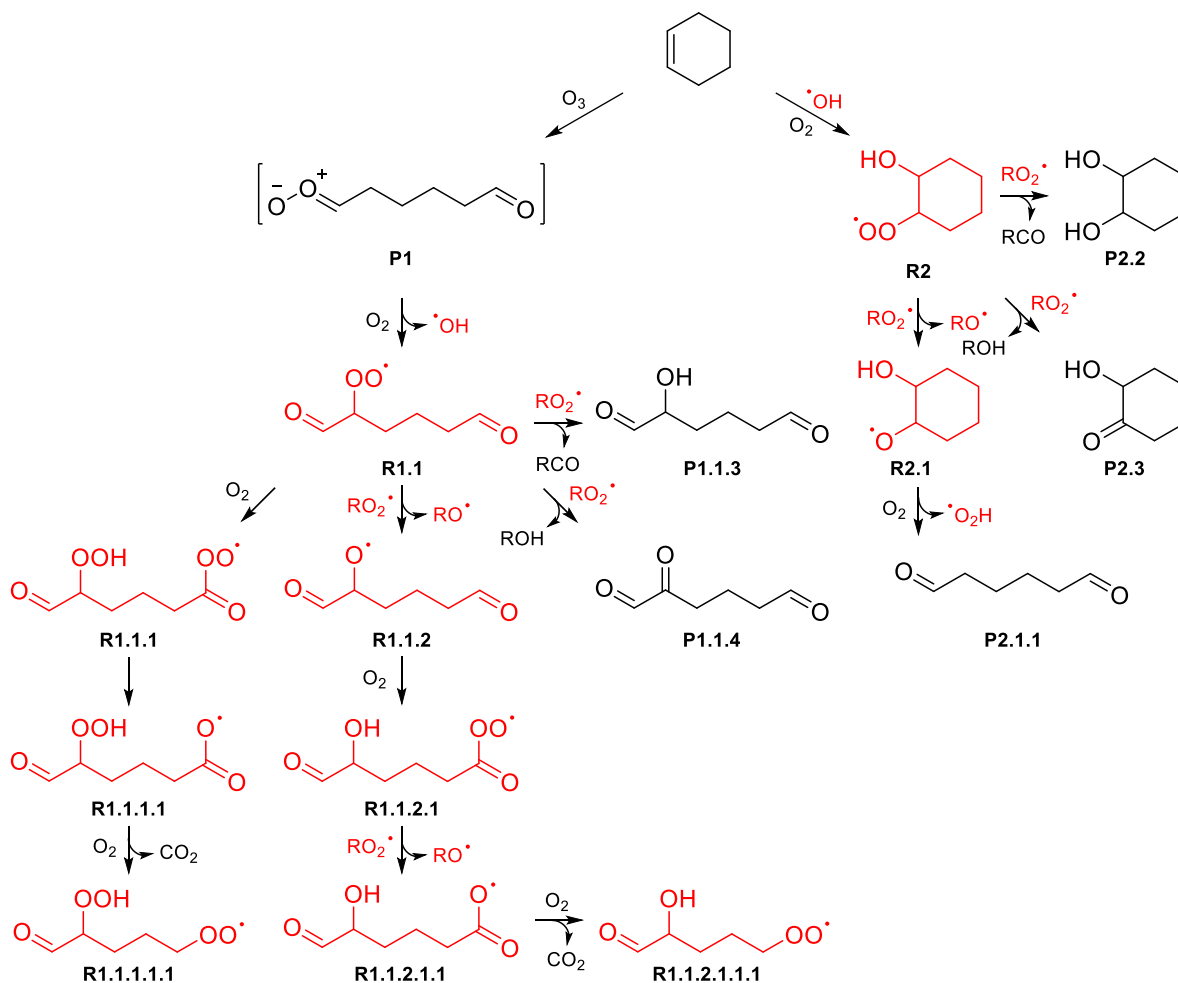


Figure 145: Non-comprehensive mechanism of cyclohexene ozonolysis. O₂ release is not shown. RCO represents carbonyl species. Structures and pathways were obtained or hypothesised using literature sources.²⁴⁸

TART trapping was then used to investigate cyclohexene ozonolysis (Figure 146, 11.7.2). A trapless control was also undertaken. Reaction mixtures and TART standard were then MS characterised (Figure 147). Under the experimental conditions, gaseous [cyclohexene] was estimated to be 1.2×10^{18} molec. cm⁻³, >100 fold excess compared to ozone, whilst total ozone passed was ~30 in excess of TART molarity.

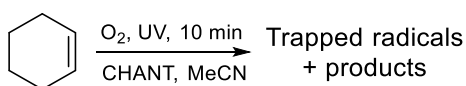


Figure 146: TART trapping of cyclohexene ozonolysis (11.7.2).

Table 39: Species identified from TART trapping of cyclohexene ozonolysis, using MS for characterisation (11.7.2). Systematic m/z error = -0.0005; random m/z error = ± 0.0005 ; 100% intensity = 3.08×10^9 absolute count.

	Species	Predicted m/z	Intensity relative to unreacted TART standard / %		
			Trapless control	Standard	Trapping reaction
TART	[CHANT+H] ⁺	323.2698	0	100	48.4
Reactant	[Cyclohexene+Na] ⁺	105.0680	0	0	0
Trapped radicals	[R1.1-ART+Na] ⁺	334.1630 ^a	0	0	0.031
	[R1.1.1-ART+Na] ⁺	366.1529	0	0	0
	[R1.1.1.1-ART+Na] ⁺	350.1580 ^a	0	0	0.004
	[R1.1.1.1.1-ART+Na] ⁺	338.1579	0	0	0.005
	[R1.1.2-ART+Na] ⁺	318.1681	0	0	0.032
	[R1.1.2.1-ART+Na] ⁺	350.1580 ^a	0	0	0.004
	[R1.1.2.1.1-ART+Na] ⁺	334.1630 ^a	0	0	0.031
	[R1.1.2.1.1.1-ART+Na] ⁺	322.1630	0	0	0
	[R2-ART+Na] ⁺	320.1838	0	0	0.009
	[R2.1-ART+Na] ⁺	304.1889	0	0	0
Products	[P1.1.3+Na] ⁺	153.0528 ^a	0.037	0	0.095
	[P1.1.4+Na] ⁺	151.0371	0.002	0	0.002
	[P2.1.1+Na] ⁺	137.0579 ^a	0.045	0	0.127
	[P2.2+Na] ⁺	139.0735	0	0	0
	[P2.3+Na] ⁺	137.0579 ^a	0.045	0	0.127

^aOther table entries have predicted species with identical m/z .

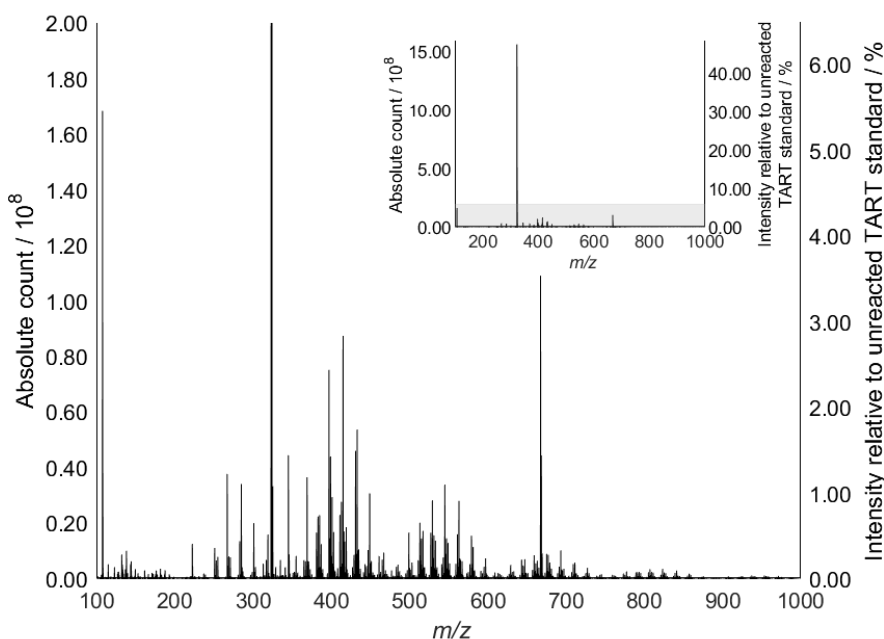


Figure 147: Background corrected mass spectrum from TART trapping of cyclohexene ozonolysis (11.7.2)

As previously observed for CHANT and other non-basic reactants (5.3), peaks corresponding to CHANT-trapped radicals, reactants and products were not observed or observed exclusively or much more intensely as sodiated MS adducts and hence, only these adducts are shown.

This mass spectrum (Figure 147) had “stegosaurus” character, i.e., it had several distinct regions of peaks, where each region formed an approximate bell curve of peaks. These regions were believed to corresponded to oligomeric products. Since TART trapping of cyclohexene ozonolysis was undertaken as a preliminary investigation to determine if gaseous radicals could be trapped and observed, the identities of these oligomeric products were not of interest.

MS peaks corresponding to CHANT in the trapping reaction had ~50% intensity compared to the unreacted CHANT standard, indicating approximately ~50% of CHANT was consumed. The CHANT-corresponding peak was significantly more intense than any other MS peak (Figure 147). Peaks corresponding to products were observed in both the trapless control and trapping reaction, as expected.

MS peaks corresponding to most TART-trapped radicals were observed exclusively in the trapping reaction. This showed that both TART-trapped radicals and products could be observed using TART trapping and MS characterisation. Peaks corresponding to R1.1-ART and R1.1.2-ART were observed with the greatest intensity of peaks corresponding to TART-trapped radicals and were clearly distinguishable from nearby peaks in the trapping reaction mass spectrum (Figure 148).

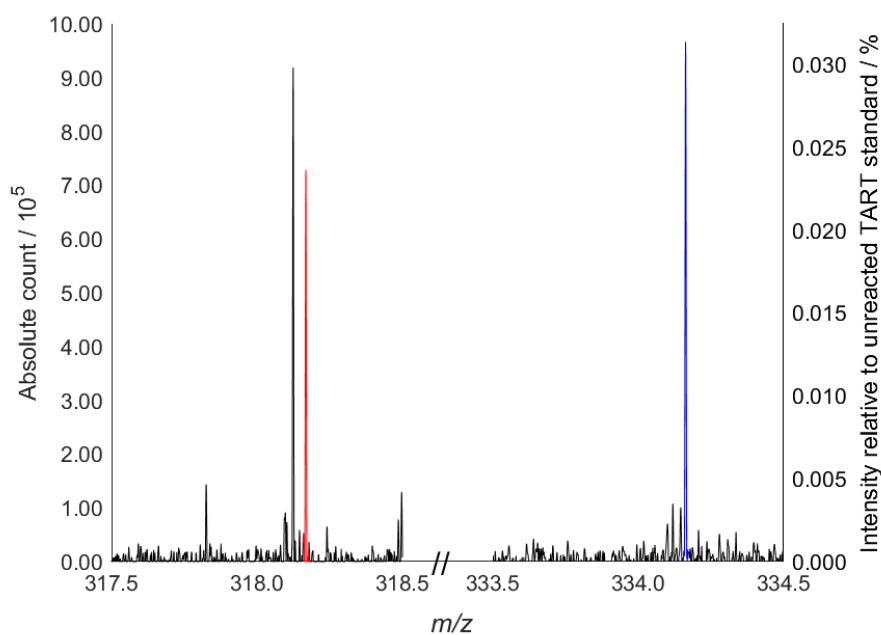


Figure 148: Background corrected mass spectrum from TART trapping of cyclohexene ozonolysis (11.7.2), showing peaks corresponding to R1.1-ART (m/z 334.163, blue) and R1.1.2-ART (m/z 318.168, red).

Peaks corresponding to R1.1-ART and R1.1.2-ART were of similar intensity. However, gaseous $[RO_2^\bullet]$ was predicted to be significantly greater than gaseous $[RO^\bullet]$. This was likely due to RO^\bullet reacting with TART more efficiently than RO_2^\bullet , as discussed previously (7.2). This was demonstrated through kinetic modelling (8.6.3.7).

Observation of MS peaks corresponding to R1.1-ART, R1.1.2-ART and R2-ART implied reactant radicals R1.1 (RO_2^\bullet formed following Criegee intermediate degradation), R1.1.2 (RO^\bullet formed from RO_2^\bullet degradation) and R2 (RO_2^\bullet formed from $\bullet OH$ addition to alkene) were formed during the reaction, trapped and MS observed. This showed that TART trapping could be used to investigate gaseous radical reactions, such as alkene ozonolysis.

Cyclohexene ozonolysis was investigated using TART trapping. Peaks corresponding to multiple TART-trapped radicals were successfully observed. Corresponding radicals observed included: RO_2^\bullet from Criegee intermediate decomposition; RO^\bullet from RO_2^\bullet decomposition and RO_2^\bullet from $\bullet\text{OH}$ -initiated cyclohexene decomposition. Study of this relatively simple alkene ozonolysis reaction provided a solid framework in which to investigate more complex alkene ozonolysis reactions, such as terpene ozonolysis.

8.6. α -Pinene ozonolysis

Terpene ozonolysis was of particular interest due to its significant atmospheric relevance (1.2.3). As α -pinene was the most atmospherically abundant monoterpene, TART trapping of α -pinene ozonolysis was undertaken. Furthermore, since α -pinene is a functionalised cyclohexene, it was hoped that previously successful TART trapping of cyclohexene ozonolysis experiments would aid TART trapping of α -pinene ozonolysis experimentation.

8.6.1. Initial results

Initial experiments were undertaken to prove that MS peaks corresponding to TART-trapped radicals could be observed from TART trapping of α -pinene ozonolysis. System optimisation would then be undertaken to maximise TART-trapped radical intensity. Therefore, initial experiments only considered early-stage radicals and products of α -pinene ozonolysis (Figure 149), obtained from the Master Chemical Mechanism (MCM).⁵⁷ These species are formed through mechanisms which are discussed later (Figure 153 and Figure 154).

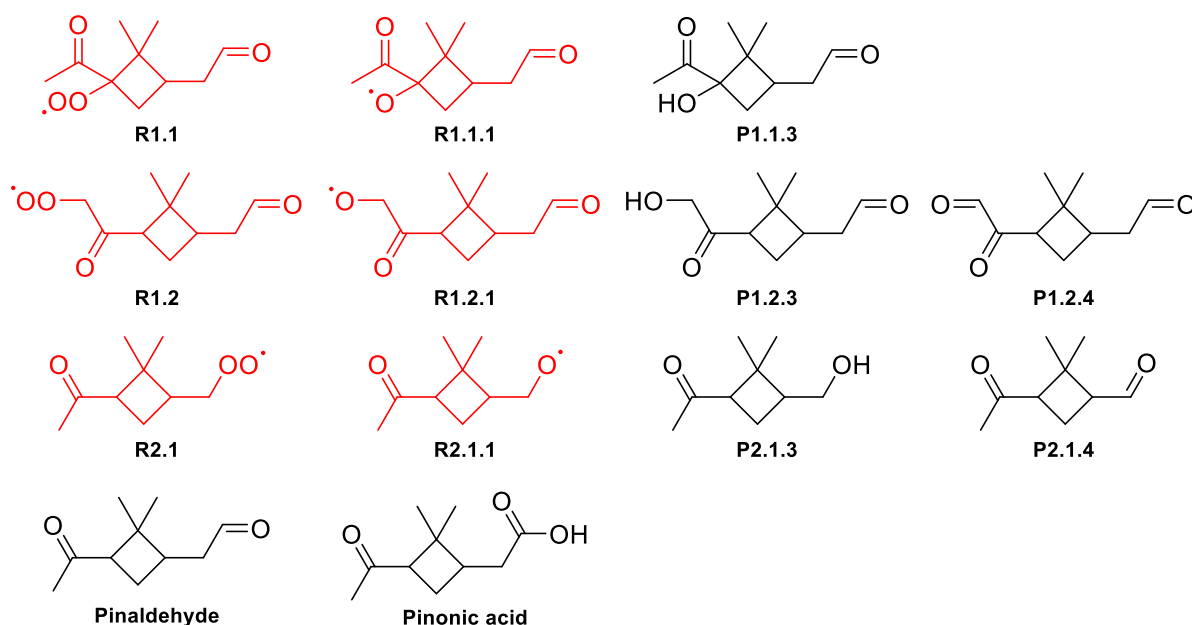


Figure 149: Radicals and products produced early in α -pinene ozonolysis (8.6.3.1).⁵⁷ These species are formed through mechanisms which are discussed later (Figure 153 and Figure 154).

TART trapping was used to investigate α -pinene ozonolysis, similarly as for cyclohexene previously (Figure 150, 11.7.2). A trapless control was also undertaken. Reaction mixtures and TART standard were then MS characterised (Table 40). Under the experimental conditions, gaseous $[\alpha\text{-pinene}]$ was estimated to be 5.2×10^{16} molec. cm^{-3} , >30 fold excess compared to ozone, whilst total ozone passed was ~ 30 in excess of TART molarity.

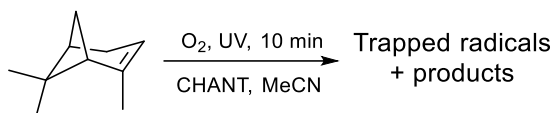


Figure 150: TART trapping of α -pinene ozonolysis (11.7.2).

Table 40: Species identified from TART trapping of α -pinene ozonolysis, using MS for characterisation (11.7.2). Systematic m/z error = -0.0005; random m/z error = ± 0.0013 ; 100% intensity = 2.01×10^9 absolute count.

	Species	Predicted m/z	Intensity relative to unreacted TART standard / %		
			Trapless control	Standard	Trapping reaction
TART	[CHANT+H] ⁺	323.2698	0	100	28.1
Trapped radicals	[R1.1/R1.2-ART+Na] ⁺	388.2100	0	0	0.035
	[R1.1.1/R1.2.1-ART+Na] ⁺	372.2151	0	0	0.020
	[R2.1-ART+Na] ⁺	360.2151	0.002	0	0.014
	[R2.1.1-ART+Na] ⁺	344.2202	0	0	0.005
Products	[Pinaldehyde+Na] ⁺	191.1048	0.676	0	1.11
	[Pinonic acid+Na] ⁺	207.0997 ^a	0.511	0	0.239
	[P1.1.3/P1.2.3+Na] ⁺	207.0997 ^a	0.511	0	0.239
	[P1.2.4+Na] ⁺	205.0841	0	0	0
	[P2.1.3+Na] ⁺	179.1048	0.011	0	0.008
	[P2.1.4+Na] ⁺	177.0891	0.010	0	0.008

^aOther table entries have predicted species with same m/z .

Peaks corresponding to products were observed in both the trapless control and trapping reaction, indicating these species did not require TART for formation, as expected. Peaks corresponding to TART-trapped radicals were observed exclusively or with much greater intensity in the trapping reaction, compared to other samples. These initial results indicated that radicals produced during α -pinene ozonolysis were successfully TART trapped and observed using MS. However, before more detailed investigations were undertaken, system optimisation was performed to maximise TART-trapped radical intensity.

8.6.2. Optimisation

Parameters were optimised to maximise intensity of peaks corresponding to TART-trapped radicals (11.7.3). These included: TART phase (8.6.2.1); functionality of TART, solvent and additives (8.6.2.2); TART concentration (8.6.2.3); flow rate and substrate concentration (8.6.2.4); residence time (8.6.2.5) and reaction time (8.6.2.6).

8.6.2.1. TART phase

Thus far, radicals formed during alkene ozonolysis were trapped by bubbling the reaction gas stream through trapping solution. However, it was theorised that TART immobilisation on a solid support might achieve cleaner mass spectra and greater intensity of MS peaks corresponding to TART-trapped radicals. Furthermore, radical dissolution would not need to be considered, simplifying the system. This would be particularly advantageous when undertaking kinetic modelling. This interaction between a reaction gas stream over immobilised TART was conceptually similar to gas chromatography. Therefore, TART trapping of α -pinene ozonolysis was attempted with TART immobilised on a solid support (11.7.3.2), rather than bubbling through trapping solution.

Hexadecyl-functionalised celite was synthesised and used as a solid support (11.7.3.2). Although peaks corresponding to TART-trapped radicals were successfully observed, they

were observed less intensely and with poorer reproducibility on this solid support, compared to in solution (SI6.1.1.1). This was hypothesised to be because totally redissolving and filtering samples was challenging, making amount of sample analysed inconsistent. It was theorised that intensity of peaks corresponding to TART-trapped radicals was reduced because poor interactions and short exposure times between gaseous radicals and solid TART reduced effective reactions, compared to gaseous radicals or dissolved radicals and dissolved TART, which had much longer exposure times. Therefore, additives were trialled, which were added to immobilised TART to try to improve fluidity. Additives trialled included low polarity oils, such as dodecamethylpentasiloxane, and ionic liquids, such as $[C_4mim]^+[Tf_2N]^-$. However, these additives did not improve TART-trapped radical intensity (SI6.1.1.1).

Since no improvement had been made upon bubbling gaseous radicals through trapping solution, this method was retained. However, it was still believed that optimised immobilised TART trapping could offer many benefits over dissolved TART trapping, such as a simpler trapping mechanism without radical dissolution, cleaner mass spectra and greater intensity of peaks corresponding to TART-trapped radicals.

8.6.2.2. Functionality of TART, solvent and additives

TART functionality was optimised for TART trapping of α -pinene ozonolysis (SI6.1.1.2). CHANT had thus far been used as TART, owing to its high stability in solution and relatively unreactive functionality. However, CHANT-trapped radicals generally had poor ionisation efficiency and hence low MS intensity, due to CHANT having a poorly basic ART group. Therefore, different TARTs were trialled in the reaction, to try to increase observed intensity of MS peaks corresponding to TART-trapped radicals. Additionally, different TART trapping solution solvents and additives were trialled during these investigations, to see if intensity of peaks corresponding to TART-trapped radicals could be increased. Otherwise, standard alkene ozonolysis conditions were used (11.7.3).

CHANT, DEADANT, TREADANT and Grantham TART were all trialled in MeCN. CHANT and DEADANT were also trialled in DMF and H₂O. Additionally, DEADANT was trialled in MeCN with trifluoroacetic acid and in H₂O with trifluoroacetic acid or AcOH/NaOAc (SI6.1.1.2). TART-trapped radical corresponding peaks were observed with greatest intensity when TART was dissolved in MeCN (SI6.1.1.2). CHANT produced consistently stronger and more reproducible intensities of peaks corresponding to TART-trapped radicals than the other trialled TARTs.

TART-trapped radicals were also observed in presence of DEADANT. However, DEADANT suffered from significant TART degradation. It was hypothesised that most DEADANT suffered from 3^o amine oxidation by ozone, even in presence of acids, which were used as additive to reduce N-oxidation. Whilst not affecting its trapping capability, this possible additional oxygen atom introduced greater uncertainty into the TART-trapped radical structure and therefore made it impractical for R[•], RO[•] and RO₂[•] differentiation. For example, in presence of trifluoroacetic acid peaks corresponding to RO-ART were observed with significantly greater intensity than RO₂-ART corresponding peaks, whilst in absence of trifluoroacetic acid, RO₂-ART corresponding peaks were observed significantly more intensely than RO-ART corresponding peaks. Therefore, in absence of trifluoroacetic acid, it was believed that peaks corresponding to RO₂-ART more likely corresponded to N-oxidised RO-ART (SI6.1.1.2). Furthermore, due to the weak basicity of N-oxides, DEADANT-oxide-trapped radicals likely had poorer basicity than DEADANT-trapped radicals. However, it was hypothesised that DEADANT may perform superiorly to CHANT in other systems with low ozone concentration.

Peaks corresponding to TREADANT-trapped radicals were scarcely observed. It was hypothesised that I⁻ oxidation by ozone produced radicals which were trapped by TREADANT,

thereby consuming it. This reduced TREADANT available for TART trapping of α -pinene ozonolysis and hence, decreased concentration of TART-trapped radicals.

Whilst Grantham TART appeared to produce very intense signals, these signals were detected with near equal intensity in both trapless controls and Grantham TART trapping reactions, indicating that these peaks did not come from Grantham TART-trapped species (SI6.1.1.2). It was likely that Grantham TART was trapping radicals, but other non-trapped species were dominating MS signal intensity. This meant that Grantham TART-trapped species could not be clearly identified and therefore Grantham TART was impractical for use. This also brought into question the validity of positive results obtained by Grantham for TART trapping of α -pinene ozonolysis, using Grantham TART (2.2).¹⁵²

CHANT was utilised for most subsequent alkene ozonolysis radical trapping, owing to its better reproducibility and greater trapped species intensity compared to other TARTs.

8.6.2.3. TART concentration

TART concentration was optimised to achieve maximum TART-trapped radical intensity compared to unreacted TART. Once appropriately diluted, this achieved maximum absolute TART-trapped radical signal intensity, increasing signal-to-noise ratio (S/N) and therefore making TART-trapped radicals as distinguishable as possible. In absence of TART-removing purification techniques, this was the best way to observe maximum TART-trapped radical intensity. 50-5000 μM concentrations of CHANT were trialled under otherwise standard alkene ozonolysis conditions (11.7.3). 500 μM CHANT solution was found to be optimal, achieving maximum TART-trapped radical signal intensity compared to unreacted TART (SI6.1.1.3).

8.6.2.4. Flow rate and substrate concentration

Alkene and ozone concentration could be altered by changing flow rate through each half of the system, delivering different concentrations of each reactant into the mixing tube. Different flow rates through each flow meter, totalling 1.5 L min^{-1} , were trialled under otherwise standard alkene ozonolysis conditions (Table 41, 11.7.3).

Table 41: Species identified from TART trapping of α -pinene ozonolysis, conducted at different substrate flow rates, using MS for characterisation (11.7.3). Systematic m/z error = -0.0005; random m/z error = ± 0.0013 ; 100% intensity = 2.01×10^9 absolute count.

	Species	Predicted m/z	Intensity relative to unreacted TART standard / %					
			Alkene:ozone flow / L min^{-1}					
			0.25: 1.25	0.50: 1.00	0.75: 0.75	1.00: 0.50	1.25: 0.25	
TART	[CHANT+H] ⁺	323.2698	32.3	26.6	29.3	33.5	47.1	
Trapped radicals	[R1.1/R1.2-ART+Na] ⁺	388.2100	0.025	0.060	0.072	0.056	0.062	
	[R1.1.1/R1.2.1-ART+Na] ⁺	372.2151	0.015	0.030	0.033	0.031	0.027	
	[R2.1-ART+Na] ⁺	360.2151	0.035	0.016	0.010	0.012	0.011	
	[R2.1.1-ART+Na] ⁺	344.2202	0.005	0.010	0.007	0.007	0.004	
Products	[Pinaldehyde+Na] ⁺	191.1048	1.30	1.62	1.64	1.47	1.31	
	[Pinonic acid+Na] ⁺	207.0997 ^a	0.590	0.325	0.260	0.268	0.164	
	[P1.1.3/P1.2.3+Na] ⁺	207.0997 ^a	0.590	0.325	0.260	0.268	0.164	
	[P1.2.4+Na] ⁺	205.0841	0.004	0.003	0.003	0.003	0.002	
	[P2.1.3+Na] ⁺	179.1048	0.028	0.011	0.007	0.006	0.003	
	[P2.1.4+Na] ⁺	177.0891	0.018	0.015	0.013	0.016	0.011	

^aOther table entries have predicted species with same m/z .

Peaks corresponding to R1.1/R1.2 and R1.1.1 were observed with greatest intensity at 0.75 L min⁻¹ flow rate through each flow meter. As such, 0.75 L min⁻¹ flow rate through each flow meter was deemed optimal. This may be different for other alkenes. At 0.75 L min⁻¹ flow rate through each flow meter and in alkene and trapping solution absence, ozone concentration was measured to be 117.5±0.4 ppm under other standard alkene ozonolysis conditions, using an ozonometer (11.7.2).

This corresponded to >30 fold excess of α-pinene to ozone. This should cause most ozone to react with α-pinene, rather than other species produced during α-pinene ozonolysis. Since each reaction of α-pinene with ozone produces one •OH, most •OH should likewise react with α-pinene. Furthermore, at 500 μM TART concentration, α-pinene:ozone:TART was ~1200:30:1, meaning substrates were in great excess in the liquid phase, compared to TART.

For α-pinene ozonolysis, these optimised features were expected to remain unchanged for the majority of further reactions. However, residence time and reaction time also required optimisation, but might later be changed for particular experiments.

8.6.2.5. Residence time

Residence time describes the time that substrates resided in the mixing tube and hence were able to react together in the gas phase, before reaching the trapping solution. Therefore, residence time is the time for which gaseous alkene ozonolysis occurs.

Residence time was optimised using kinetic modelling (8.6.3.7). Utilising the optimised flow rate and substrate concentrations, the residence time was altered to maximise [RO₂•] formed following Criegee intermediate degradation. The model predicted maximum RO₂• concentration at ~5 cm tube length or ~56.5 ms residence time, under standard alkene ozonolysis conditions (Figure 168, 11.7.2). This length and therefore residence time could be varied as required, for kinetic experiments. Modelling is discussed in greater detail below (8.6.3.7).

8.6.2.6. Reaction time

Reaction time describes the time that the experiment was run for. Reaction time was optimised to maximise intensity of peaks corresponding to TART-trapped radicals, both absolutely and relative to unreacted TART. Different reaction times were trialled under otherwise standard alkene ozonolysis conditions (Figure 151, 11.7.3).

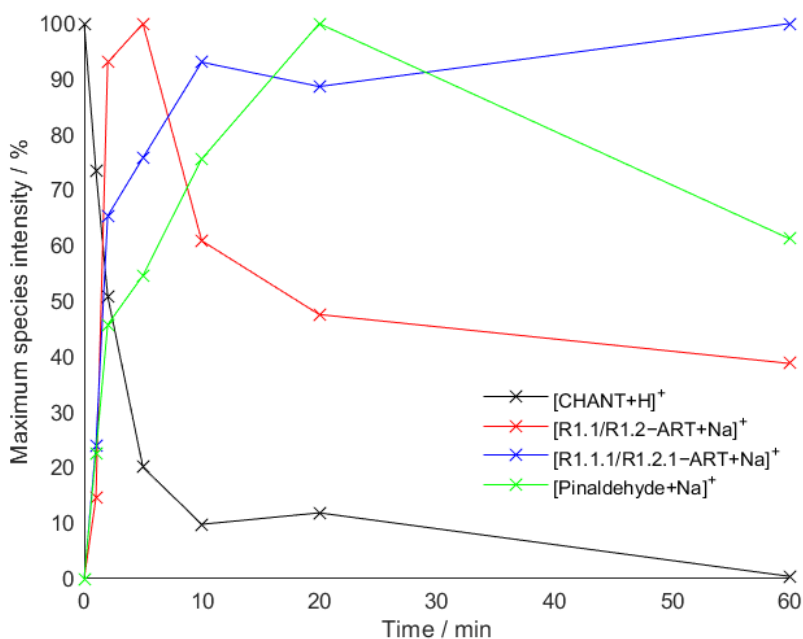


Figure 151: Species identified from TART trapping of α -pinene ozonolysis after different reaction times, using MS for characterisation (11.7.3). Species are scaled to show their maximum values at 100% intensity. Systematic m/z error = -0.0006; random m/z error = ± 0.0007 .

The peak corresponding to unreacted CHANT was observed to decrease exponentially with time. [CHANT] was estimated to have decreased to ~50% after 2 min and ~10% after 10 min. The peaks corresponding to R1.1/R1.2-ART was observed with greatest MS intensity after 5 min, but with a very marginal increase compared to 2 min (90% \rightarrow 100%). Maximum intensity was observed at 5 min, implying that after this time, R1.1/R1.2-ART formation was slower than its degradation. This was likely due to both increased TART consumption causing rate of R1.1/R1.2-ART formation to decrease and the peroxide R1.1/R1.2-ART having poor stability, causing it to degrade. Conversely, peaks corresponding to R1.1.1/R1.2.1-ART were observed most intensely after 60 min, but with a very marginal increase compared to 10 min (90% \rightarrow 100%). This was hypothesised to be because ethers are more stable than peroxides and hence R1.1.1/R1.2.1-ART underwent little degradation, whilst R1.1.1/R1.2.1-ART formation continued as time elapsed, albeit with decreasing rate due to TART consumption. Pinaldehyde appeared to behave similarly to R1.1.1/R1.2.1-ART.

From these data, it was decided that 10 min was the optimal reaction time, as peaks corresponding to TART-trapped radicals were observed most intensely around this time. Furthermore, greater reproducibility was observed as reaction time increased. However, for certain experiments, such as kinetics experiments, as [TART] significantly decreased, kinetics of TART trapping became increasingly dependent on [TART]. This meant that TART trapping kinetics decreasingly resembled the kinetics of gaseous alkene ozonolysis. Therefore, in kinetics experiments, reaction time was reduced to prevent TART consumption from significantly affecting TART trapping kinetics (8.6.3.7).

Following optimisation, TART trapping of α -pinene ozonolysis was repeated using these optimised conditions (11.7.2). Analysis was then undertaken in greater detail.

8.6.3. Detailed results

TART trapping of α -pinene ozonolysis (three repeats) and control reactions were carried out using optimised conditions (11.7.2). Each control omitted a single condition required for TART-

trapped radical formation: no substrate, no O₂ (replaced with N₂), no UV, no TART and an unreacted TART standard (set as 100% relative intensity). MS was then used to characterise these reaction mixtures (Figure 152).

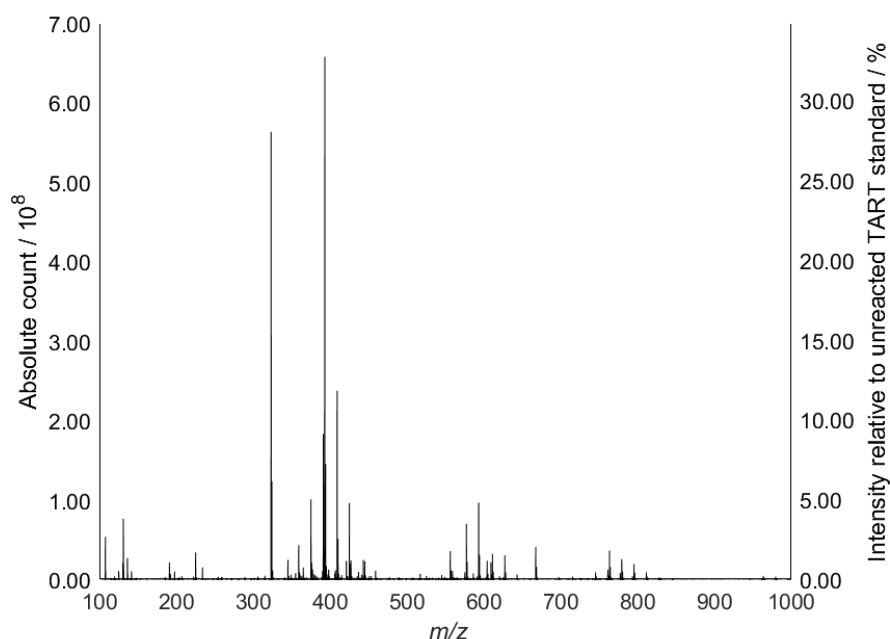


Figure 152: Background corrected mass spectrum from TART trapping of α -pinene ozonolysis (11.7.2). 100% intensity = 2.01×10^9 absolute count.

Peaks corresponding to unreacted TART were some of the most intense in the mass spectrum, indicating not all TART had reacted. This was desirable, since dominating TART concentration should have mitigated side reactions between TART-trapped radicals and incoming gaseous radicals. Furthermore, mass spectra had stegosaurus character, indicating presence of oligomeric products.

TART trapping of α -pinene ozonolysis was a very complex system. Therefore, the Formula Find programme was used for initial analysis of obtained mass spectra. This programme predicted molecular formulae of TART-trapped radicals, and hence reactant radicals, corresponding to peaks observed in mass spectra (8.6.3.1). These molecular formulae were then qualitatively assigned to structures, and their mechanism of formation, using literature. Peak Pick analysis was used to ensure peaks corresponding to TART-trapped radicals were only observed in presence of all reaction conditions necessary for TART-trapped radical formation before quantitative analysis was undertaken (8.6.3.2).

8.6.3.1. Formula Find analysis

The Formula Find programme was used to predict molecular formulae corresponding to peaks observed in mass spectra. Initially, molecular formula limits were set to only identify monomeric non-fragmented CHANT-trapped radicals. Molecular formulae limits were set as C₂₀H₀₋₃₈N₁O₁₋₁₀Na₀₋₁, corresponding to radicals of molecular formulae C₁₀H₀₋₂₂O₀₋₉Na₀₋₁[•], and *m/z* limits were set as *m/z* 100-500. These were limits such that only non-fragmented early-stage TART-trapped radicals should be found. Possible corresponding radical structures were successfully identified for seven of the ten most intense peaks corresponding to TART-trapped radicals (Table 42). These structures are discussed below.

Table 42: Ten most intense peaks believed to correspond to TART-trapped radicals from TART trapping of α -pinene ozonolysis, obtained using the Formula Find programme. Molecular formula limits were set as $C_{20}H_{0-38}N_{1}O_{1-10}Na_{0-1}$ and m/z limits 100-500. Illogical molecular formulae were eliminated.

Class	Observed m/z	Intensity relative to unreacted TART standard / %	Corresponding radical molecular formula	Radical structure identified
C	356.2198	0.097	$C_{10}H_{15}O_2^\bullet$	R6/R7
B	422.2153	0.070	$C_{10}H_{17}O_6^\bullet$	$C_{10}H_{17}O_6^\bullet$
B	406.2196	0.063	$C_{10}H_{17}O_5^\bullet$	R5.1/R5.2/ $C_{10}H_{17}O_5^\bullet$
D	440.2259	0.051	$C_{10}H_{19}O_7^\bullet$	Unknown
A	388.2097	0.035	$C_{10}H_{15}O_4^\bullet$	R1.1/R1.2
C	334.2378	0.024	$C_{10}H_{15}O_2^\bullet$	R6/R7
A/C	372.2147	0.020	$C_{10}H_{15}O_3^\bullet$	R1.1.1/R1.2.1
D	424.2311	0.016	$C_{10}H_{19}O_6^\bullet$	Unknown
A	404.2049	0.014	$C_{10}H_{15}O_5^\bullet$	R1.1.1.1/R1.2.1.2
D	408.2362	0.013	$C_{10}H_{19}O_5^\bullet$	Unknown

From the outputted radical molecular formulae, four distinct classes of TART-trapped radicals emerged. These classes indicated radicals of different character and formed through different mechanisms. Classes A-D had formulae: $C_{10}H_{15}O_{3-5}^\bullet$, $C_{10}H_{17}O_{5-6}^\bullet$, $C_{10}H_{15}O_{2-3}^\bullet$ and $C_{10}H_{19}O_{5-7}^\bullet$ respectively, with $C_{10}H_{15}O_3^\bullet$ belonging to classes A, C or both. These were principally separated based upon saturation degree. However, classes A and C were separated because peaks corresponding to TART-trapped $C_{10}H_{15}O_4^\bullet$ and $C_{10}H_{15}O_2^\bullet$ were more intense than the peak corresponding to TART-trapped $C_{10}H_{15}O_3^\bullet$. This indicated that $C_{10}H_{15}O_4^\bullet$ and $C_{10}H_{15}O_2^\bullet$ were formed through different mechanisms and hence $C_{10}H_{15}O_3^\bullet$ could belong to either or both classes.

These molecular formulae were then qualitatively assigned to structures, and their mechanism of formation, using literature. Class A radicals, $C_{10}H_{15}O_{3-5}^\bullet$, were assigned to structures formed following α -pinene reaction with ozone. Suggested structures of $C_{10}H_{15}O_{3-5}^\bullet$ were hypothesised to form through well established and widely accepted mechanistic steps, as described by the MCM (Figure 153 and Figure 154).⁵⁷

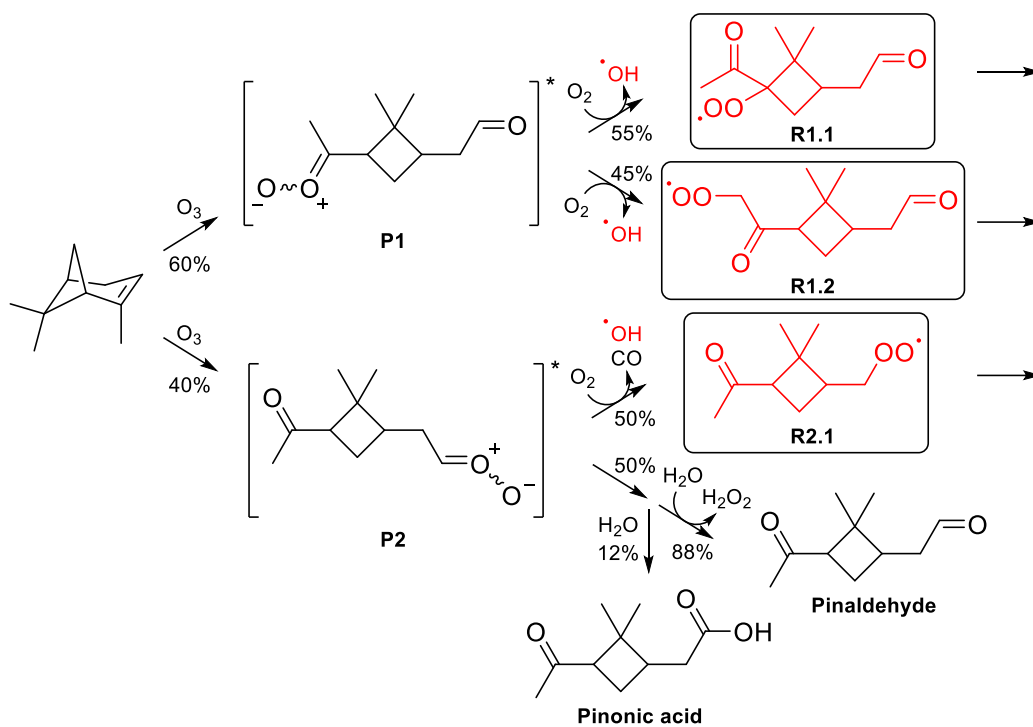


Figure 153: Mechanism of α -pinene reaction with ozone, showing formation of Criegee intermediates and subsequent degradation to form RO_2^{\bullet} . Radicals (red) have molecular formulae $C_{10}H_{15}O_4^{\bullet}$ and $C_9H_{15}O_3^{\bullet}$. Structures and pathway probabilities were obtained from the MCM.⁵⁷

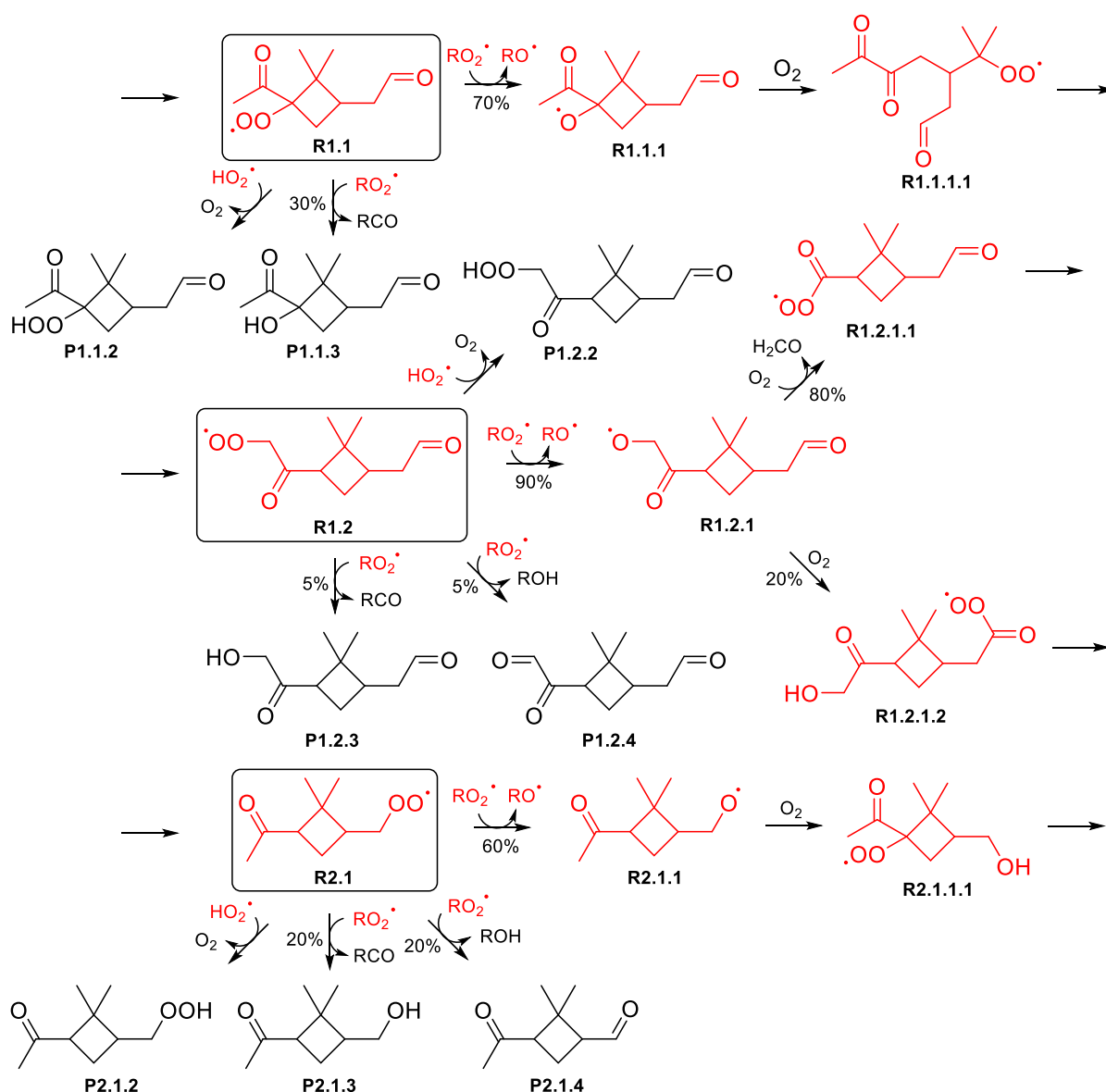


Figure 154: Mechanism of reaction of RO_2^\bullet formed following α -pinene reaction with ozone, forming RO^\bullet , and subsequent formation of other RO_2^\bullet . O_2 release is not shown. RCO represents carbonyl species. Radicals (red) have molecular formulae $\text{C}_{10}\text{H}_{15}\text{O}_{3-5}^\bullet$, $\text{C}_9\text{H}_{15}\text{O}_{2-4}^\bullet$, and $\text{C}_9\text{H}_{13}\text{O}_4^\bullet$. Structures and pathway probabilities were obtained from the MCM.⁵⁷

Many radicals including R1.1/R1.2 and R1.1.1/R1.2.1 had identical molecular formulae and therefore, their corresponding TART-trapped radicals had identical m/z . This meant that these species could not be distinguished using standard MS. However, peaks corresponding to R1.1/R1.2-ART and R1.1.1/R1.2.1-ART were clearly identifiable in the mass spectrum (Figure 155, 11.7.2).

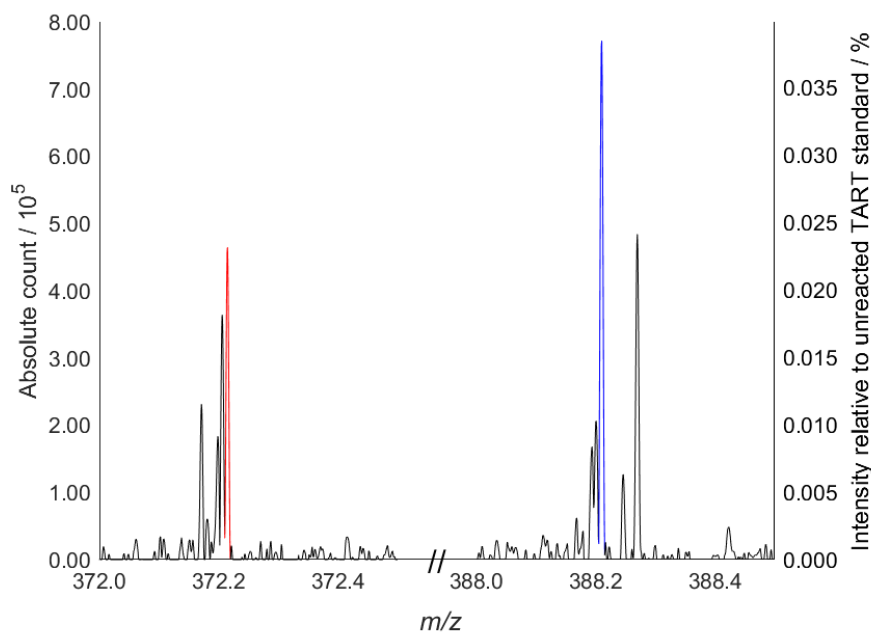


Figure 155: Background corrected mass spectrum from TART trapping of α -pinene ozonolysis (11.7.2), showing peaks corresponding to $[R1.1/R1.2-ART+Na]^+$ (m/z 388.210, blue) and $[R1.1.1/R1.2.1-ART+Na]^+$ (m/z 372.215, red). 100% intensity = 2.01×10^9 absolute count.

Qualitatively, observations of MS peaks corresponding to Class A radicals (Table 42) supported the widely accepted mechanistic steps of α -pinene reaction with ozone (Figure 153 and Figure 154). This included Criegee intermediate formation, Criegee intermediate degradation into RO_2^\bullet , $RO_2^\bullet + RO_2^\bullet$ reaction to form RO^\bullet and subsequent RO^\bullet degradation, as given in the MCM.⁵⁷

Another key mechanistic step believed to occur is $\bullet OH$ addition to α -pinene and subsequent O_2 addition, to form β -hydroxyl- RO_2^\bullet , with molecular formulae $C_{10}H_{17}O_3^\bullet$ (Figure 156). However, this molecular formula did not correspond to any of the ten most intense peaks corresponding to TART-trapped radicals (Table 42).

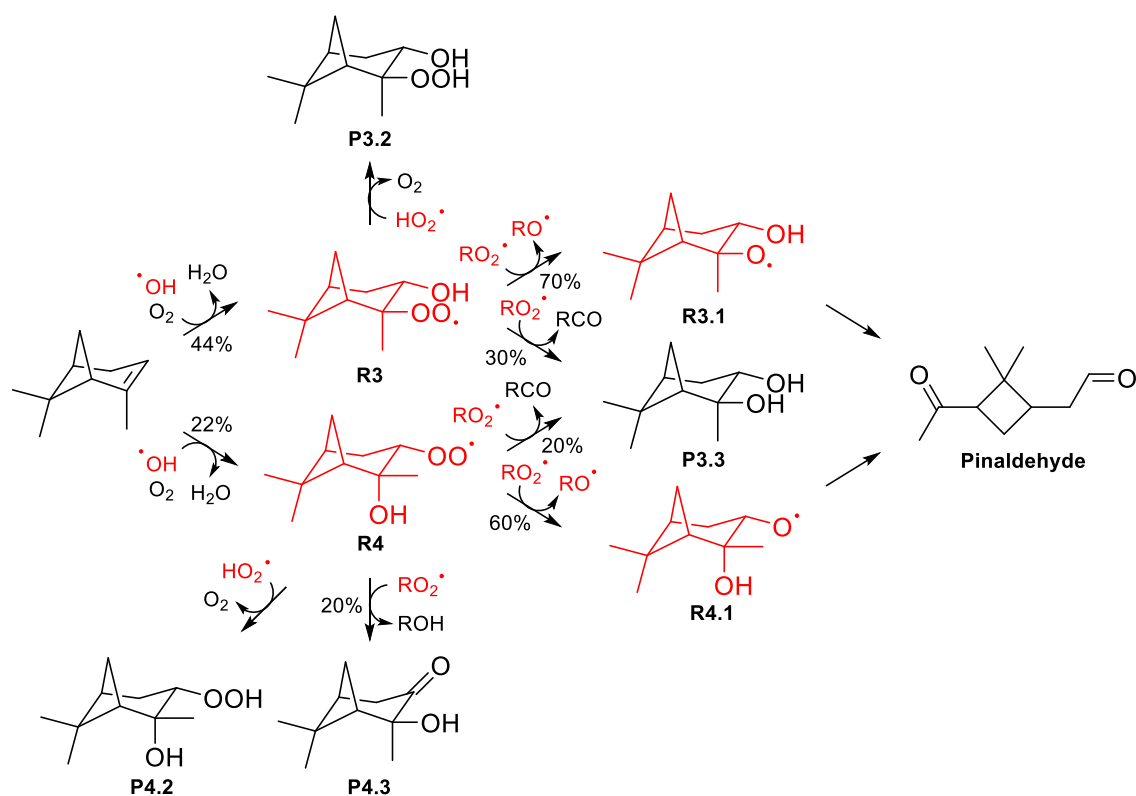


Figure 156: Mechanism of α -pinene reaction with $\cdot\text{OH}$, showing formation of β -hydroxyl- $\text{RO}_2\cdot$ and subsequent $\text{RO}\cdot$ formation. O_2 release is not shown. RCO represents carbonyl species. Radicals (red) have molecular formulae $\text{C}_{10}\text{H}_{15}\text{O}_{3-4}\cdot$. Structures and pathway probabilities were obtained from the MCM.⁵⁷

Peak Pick analysis indicated that peaks corresponding to R3/R4-ART and R3.1/R4.1-ART were weakly detected in both the no TART control and trapping reactions. This was a surprising result, since these peaks should only have been detectable in TART presence. Furthermore, modelling of the α -pinene ozonolysis gas stream indicated that gaseous [R3] and [R4] were similar to gaseous [R1.1] and [R1.2] (8.6.3.7). However, the peak corresponding to $[\text{R3/R4-ART+Na}]^+$ (observed m/z 374.2301) could be sensibly assigned to a species of molecular formula $\text{C}_{19}\text{H}_{34}\text{O}_7$ (Table 43).

Table 43: Possible molecular formulae calculated for observed m/z 374.2301, ordered with increasing difference from the observed m/z . Sensible molecular formula limits were set as $\text{C}_{0-40}\text{H}_{0-100}\text{N}_{0-2}\text{O}_{0-20}\text{Na}_{0-1}$. Only two molecular formulae had an acceptable difference between predicted and observed m/z (black).

Molecular formula		m/z	
Predicted	Corresponding radical	Predicted	Difference
$\text{C}_{19}\text{H}_{34}\text{O}_7$	$\text{C}_9\text{H}_{18}\text{N}_1\text{O}_6\cdot$	374.2305	-0.0004
$\text{C}_{20}\text{H}_{33}\text{NO}_4\text{Na}$	$\text{C}_{10}\text{H}_{17}\text{O}_3\cdot$	374.2307	-0.0006
$\text{C}_{22}\text{H}_{32}\text{NO}_4$	$\text{C}_{12}\text{H}_{16}\text{O}_3\cdot$	374.2280	0.0021

Therefore, formation of radicals R3 and R4 during α -pinene ozonolysis could not be confirmed. This appeared to contradict literature.⁵⁷ Furthermore, peaks corresponding to TART-trapped β -hydroxyl- $\text{RO}_2\cdot$ formed following $\cdot\text{OH}$ addition to alkene were previously observed during TART trapping of cyclohexene ozonolysis (8.5). These observations coupled with existing literature suggested that peaks corresponding to TART-trapped R3/R4 should have been observed. The reason that this was not the case was unknown.

However, peaks corresponding to TART-trapped Class B radicals, $C_{10}H_{17}O_5^\bullet$ and $C_{10}H_{17}O_6^\bullet$, were observed (Table 42). These radicals were hypothesised to be related to $C_{10}H_{17}O_3^\bullet$ but were more greatly oxygenated. The MCM did not describe formation of radicals with molecular formulae $C_{10}H_{17}O_5^\bullet$ and $C_{10}H_{17}O_6^\bullet$ during α -pinene ozonolysis.⁵⁷ However, these molecular formulae could correspond to cycloperoxide- RO_2^\bullet -derived radicals.

Computational chemistry experiments conducted by Vereecken *et al.* indicated that following $\bullet OH$ addition, ring opening of the α -pinene four-membered ring was competitive with RO_2^\bullet formation under atmospheric conditions (Figure 157).²⁴⁹ In this reaction, the carbon-centred R^\bullet formed following $\bullet OH$ addition to the α -pinene double bond, causes the four-membered ring to fragment, forming a new double bond, a stabilised 3° carbon-centred R^\bullet and releasing four-membered ring strain. Following O_2 addition, the new RO_2^\bullet (R5) adds to the double bond, forming a cycloperoxide- R^\bullet and following O_2 addition, a cycloperoxide- RO_2^\bullet (R5.1). This process has been computationally calculated to be significantly faster than RO_2^\bullet reaction into RO^\bullet (R5.3), though it was theorised that RO^\bullet formation may still occur, potentially leading to cycloether- RO_2^\bullet formation (R5.3.1) through the same ring closure mechanism (Figure 157).²⁴⁹ Radical addition to the double bond is conceptually similar to radical addition to TARTs, prior to TEMPO $^\bullet$ cleavage.

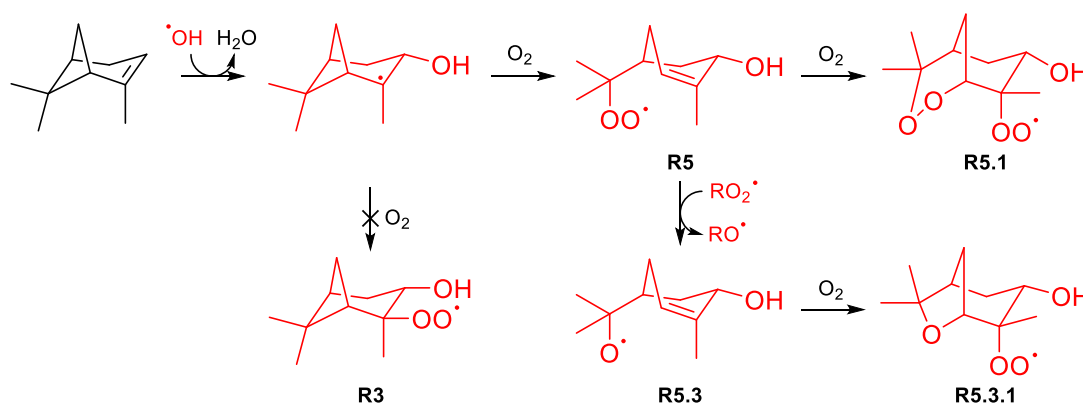


Figure 157: Mechanism of $\bullet OH$ addition to α -pinene and strained four-membered ring opening to form cycloperoxide- RO_2^\bullet and cycloether- RO_2^\bullet . O_2 release is not shown.

Likewise, many non-radical synthetic reactions involving α -pinene entail rearrangement to relieve four-membered ring strain, commonly via Wagner-Meerwein rearrangement. For example, for a literature reaction between α -pinene and acetyl chloride, 81% of identifiable products involved four-membered ring rearrangement (Figure 158).²⁵⁰

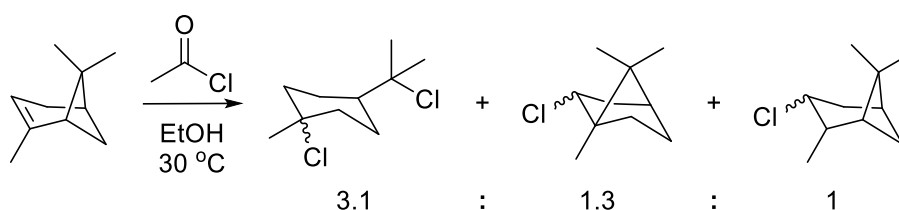


Figure 158: α -Pinene reaction with $AcCl$, showing formation of the majority of isolated products involved strained four-membered ring rearrangement.²⁵⁰

Though not yet totally accepted by the scientific community, much literature has since been published in agreement with the mechanism proposed by Vereecken *et al.*^{251,252} Berndt *et al.* suggested that ring opened RO_2^\bullet (R5) may undergo autoxidation prior to ring closure and that these species would be important in highly oxidised multifunctional (HOM) product formation

(Figure 160).²⁵² •OH reaction with α -pinene resulting in HOMs has been evidenced in literature.^{65,67,253,254}

Therefore, suggested structures of $C_{10}H_{17}O_{5-6}^{\bullet}$ were hypothesised to form through mechanistic steps involving ring opening following •OH addition and subsequent ring closure, as described by Vereecken *et al.* and Berndt *et al.* (Figure 159 and Figure 160).^{249,252} Due to the many possible locations of oxygen atoms in these species, exact structures of some radicals are not specified and are only described by their molecular formulae.

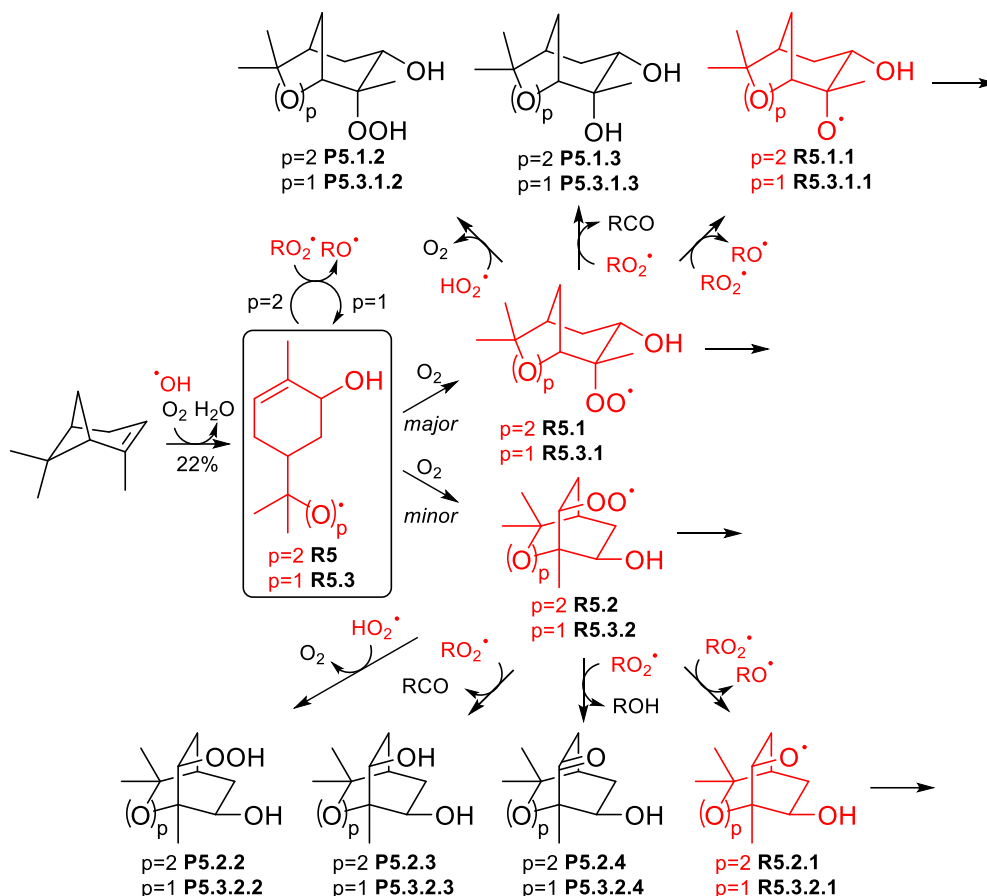


Figure 159: Mechanism of •OH addition to α -pinene, four-membered ring opening and subsequent ring closure to form species including cycloperoxide-RO₂[•] and cycloether-RO₂[•]. O₂ release is not shown. RCO represents carbonyl species. Radicals (red) have molecular formulae $C_{10}H_{17}O_{2-5}^{\bullet}$. Structures and pathway probabilities were obtained from Vereecken *et al.* and Berndt *et al.*^{249,252}

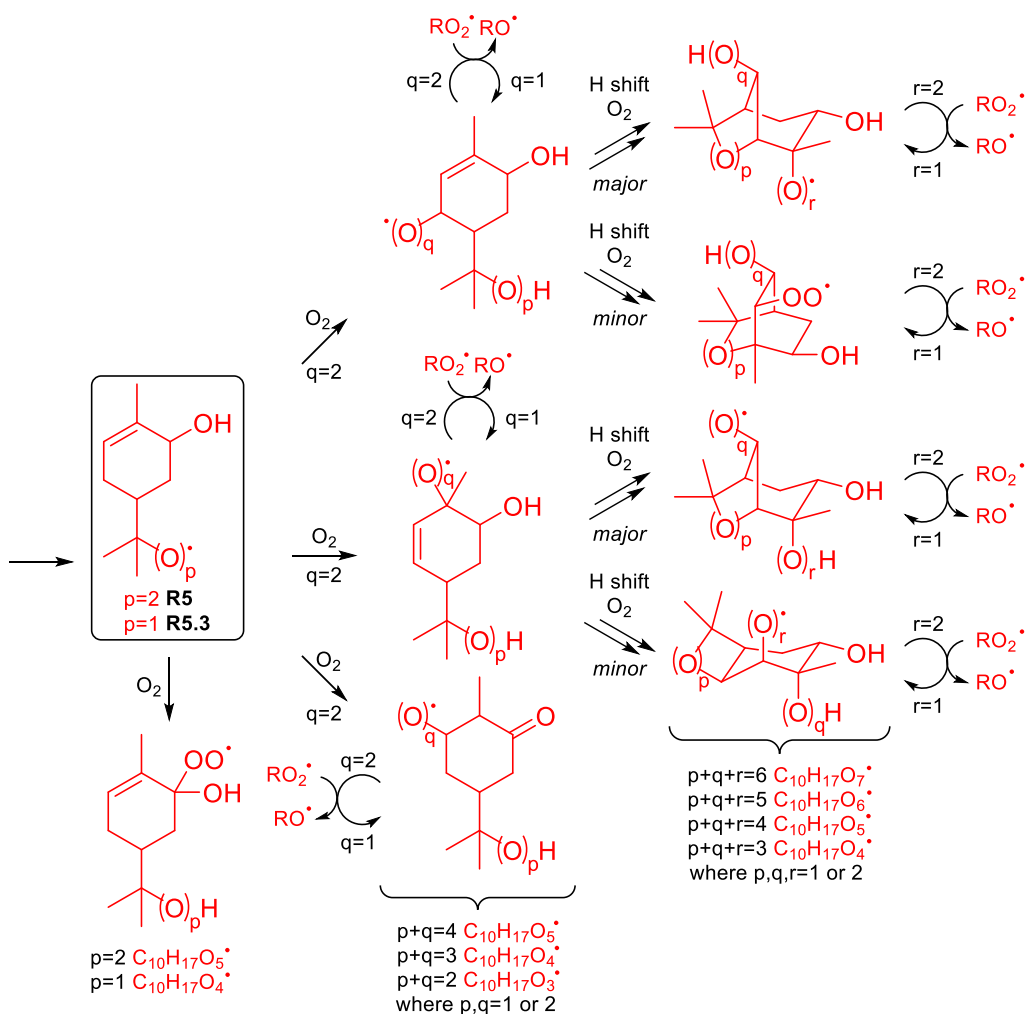


Figure 160: Mechanism of autooxidation and subsequent ring closure, following $\bullet OH$ addition to α -pinene and four-membered ring opening, to form species including oxygenated cycloperoxide- RO_2^\bullet and cycloether- RO_2^\bullet . O_2 release is not shown. Radicals (red) have molecular formulae $C_{10}H_{17}O_{2-7}^\bullet$. Structures and pathway probabilities were obtained from Vereecken *et al.* and Berndt *et al.*^{249,252}

Qualitatively, observations of MS peaks corresponding to Class B radicals (Table 42) supported the hypothesised mechanistic steps proposed by Vereecken *et al.* and Berndt *et al.*^{249,252} This included α -pinene ring opening following $\bullet OH$ addition and subsequent ring closure to form cycloperoxide- RO_2^\bullet or cycloether- RO_2^\bullet and their further oxygenated equivalents through intermediate autooxidation.

It was hypothesised that TART-trapped Class B radicals were observed, whilst TART-trapped radicals formed following $\bullet OH$ addition and immediate RO_2^\bullet formation were not, as strained four-membered ring opening ($R5$) was favoured over immediate RO_2^\bullet formation ($R3/R4$), which did not release four-membered ring strain (Figure 157). Though literature indicated that $\bullet OH$ addition and immediate RO_2^\bullet formation was competitive with strained four-membered ring opening under atmospheric conditions, this was not necessarily true in the α -pinene ozonolysis system used (8.3, 11.7.1). For example, α -pinene and ozone are more concentrated in this system than in the atmosphere, whilst O_2 has a similar concentration, potentially causing four-membered ring opening ($R5$) to outcompete O_2 addition ($R3/R4$).

Class C radicals were hypothesised to be formed following HAA abstraction from α -pinene by $\bullet OH$, mainly from the allylic C-H. Though not described in the MCM, nor widely accepted as a significant pathway by the scientific community, much literature has suggested such

mechanisms occur.^{57,251,255} Literature indicated that HAA from α -pinene by $\cdot\text{OH}$ accounts for ~12% of $\cdot\text{OH}$ reactions with α -pinene, of which ~8% (~67% total HAA) occurs from allylic C-H.²⁵¹ Therefore, suggested structures of $\text{C}_{10}\text{H}_{15}\text{O}_2\cdot$ were hypothesised to form through mechanistic steps involving HAA from α -pinene by $\cdot\text{OH}$, as described in literature (Figure 161).^{251,255}

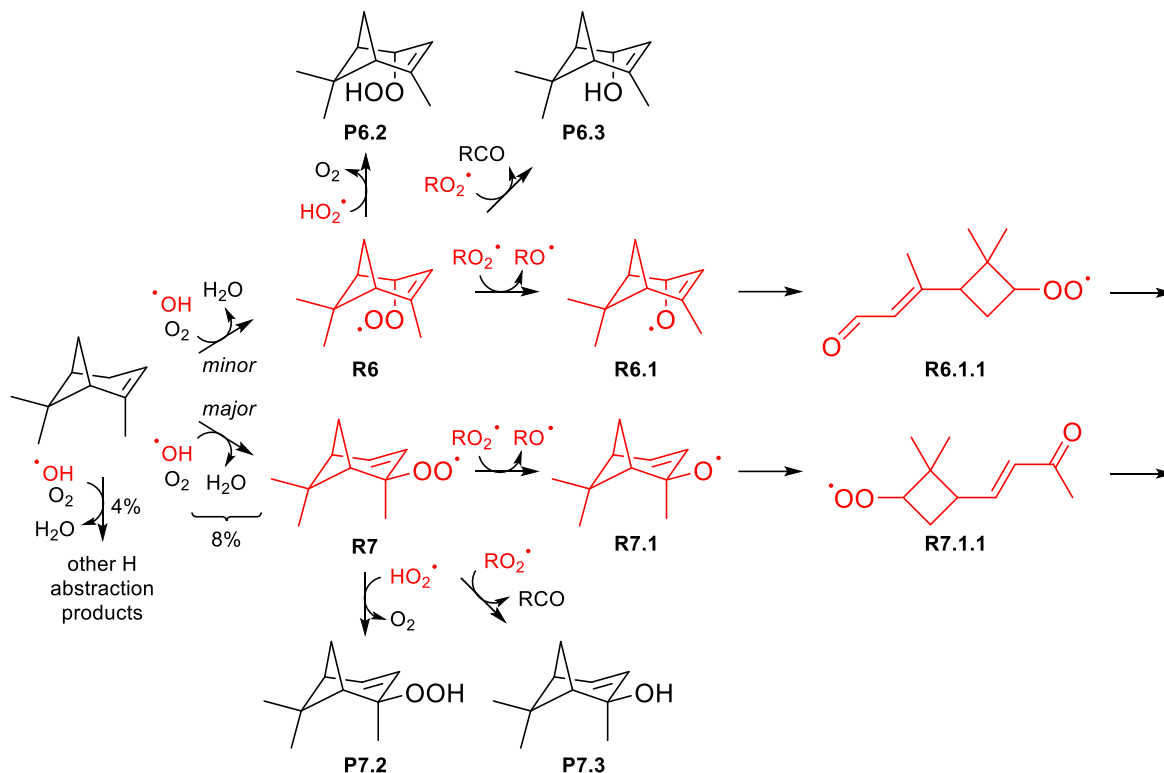


Figure 161: Mechanism of HAA from α -pinene by $\cdot\text{OH}$ forming $\text{RO}_2\cdot$ and subsequent reactions. O_2 release is not shown. RCO represents carbonyl species. Radicals (red) have molecular formulae $\text{C}_{10}\text{H}_{15}\text{O}_{1-2}\cdot$. Structures and pathways probabilities were obtained from literature or hypothesised using literature.^{251,255}

Peaks corresponding to R6/R7-ART were clearly visible in the mass spectrum (SI6.1.2.1). Qualitatively, observations of MS peaks corresponding to Class C radicals (Table 42) supported HAA from α -pinene by $\cdot\text{OH}$, as described in literature.^{251,255} The origin of Class D radicals was unknown.

Key radicals structures and their mechanisms of formation were successfully determined for α -pinene ozonolysis using TART trapping, MS characterisation and Formula Find analysis. Peak Pick analysis was then applied to further analyse TART trapping of α -pinene ozonolysis.

8.6.3.2. Peak Pick analysis

Peak Pick analysis was applied to ensure MS peaks corresponding to hypothesised TART-trapped radicals were only observed in presence of all reaction conditions necessary for TART-trapped radical formation and to obtain an average of three repeats of the trapping reaction (Table 44, 11.7.2). Quantitative analysis was then undertaken.

Table 44: Species identified from TART trapping of α -pinene ozonolysis, with three repeats and controls undertaken, using MS for characterisation (11.7.2). Systematic m/z error = -0.0005; random m/z error = ± 0.0013 ; 100% intensity = 2.01×10^9 absolute count.

Species	Predicted m/z	Intensity relative to control unreacted TART standard / %			Trapping reaction ^b
		No substrate	No O ₂ / No UV ^a	No TART	
[CHANT+H] ⁺	323.2698	0.019	98.1 / 92.5	0	29.5 \pm 1.2
[R1.1/R1.2-ART+Na] ⁺	388.2100	0	0	0	0.033 \pm 0.003
[R1.1.1/R1.2.1-ART+Na] ⁺	372.2151 ^c	0	0	0	0.023 \pm 0.002
[R1.1.1.1-ART+Na] ⁺	404.2049 ^c	0	0	0.002	0.015 \pm 0.001
[R1.2.1.1-ART+Na] ⁺	374.1943	0	0	0	0
[R1.2.1.2-ART+Na] ⁺	404.2049 ^c	0	0	0.002	0.015 \pm 0.001
[R2.1-ART+Na] ⁺	360.2151	0.005	0	0.002	0.015 \pm 0.001
[R2.1.1-ART+Na] ⁺	344.2202	0	0	0	0.006 \pm 0.001
[R2.1.1.1-ART+Na] ⁺	376.2100	0	0	0.007	0.007 \pm 0.001
[R3/R4-ART+Na] ⁺	374.2307 ^c	0	0	0.002	0.003 \pm 0.001
[R3.1/R4.1-ART+Na] ⁺	358.2358 ^c	0	0	0.005	0.006 \pm 0.001
[R5-ART+Na] ⁺	374.2307 ^c	0	0	0.002	0.003 \pm 0.001
[R5.1/R5.2-ART+Na] ⁺	406.2205 ^c	0	0	0.011	0.056 \pm 0.003
[R5.1.1/R5.2.1-ART+Na] ⁺	390.2256 ^c	0	0	0	0
[R5.3-ART+Na] ⁺	358.2358 ^c	0	0	0.005	0.005 \pm 0.001
[R5.3.1/R5.3.2-ART+Na] ⁺	390.2256 ^c	0	0	0	0
[R5.3.1.1/R5.3.2.1-ART+Na] ⁺	374.2307 ^c	0	0	0.002	0.003 \pm 0.001
[C ₁₀ H ₁₇ O ₄ -ART+Na] ⁺	390.2256 ^c	0	0	0	0
[C ₁₀ H ₁₇ O ₅ -ART+Na] ⁺	406.2205 ^c	0	0	0.011	0.056 \pm 0.003
[C ₁₀ H ₁₇ O ₆ -ART+Na] ⁺	422.2155	0	0	0.005	0.061 \pm 0.005
[C ₁₀ H ₁₇ O ₇ -ART+Na] ⁺	438.2104	0	0	0	0.011 \pm 0.001
[R6/R7-ART+Na] ⁺	356.2202	0	0	0	0.100 \pm 0.006
[R6.1/R7.1-ART+Na] ⁺	340.2252	0	0	0	0
[R6.1.1/R7.1.1-ART+Na] ⁺	372.2151 ^c	0	0	0	0.023 \pm 0.002
[Pinaldehyde+Na] ⁺	191.1048 ^c	0.023	0	0.676	1.14 \pm 0.03
[Pinonic acid+Na] ⁺	207.0997 ^c	0.003	0	0.511	0.247 \pm 0.007
[P1.1.2/P1.2.2+Na] ⁺	223.0946 ^c	0.005	0	0.070	0.068 \pm 0.002
[P1.1.3/P1.2.3+Na] ⁺	207.0997 ^c	0.003	0	0.511	0.247 \pm 0.007
[P1.2.4+Na] ⁺	205.0841	0	0	0	0
[P2.1.2+Na] ⁺	195.0997	0.003	0	0.015	0.002 \pm 0.001
[P2.1.3+Na] ⁺	179.1048	0	0	0.011	0.007 \pm 0.001
[P2.1.4+Na] ⁺	177.0891	0.002	0	0.010	0.009 \pm 0.001
[P3.2/P4.2+Na] ⁺	209.1154 ^c	0.009	0	0.080	0.104 \pm 0.009
[P3.3+Na] ⁺	193.1204	0	0	0.049	0.120 \pm 0.010
[P4.3+Na] ⁺	191.1048 ^c	0.023	0	0.676	1.14 \pm 0.03
[P5.1.2/P5.2.2+Na] ⁺	241.1052	0	0	0.048	0.077 \pm 0.003
[P5.1.3/P5.2.3+Na] ⁺	225.1103 ^c	0.001	0	0.918	1.64 \pm 0.05
[P5.2.4+Na] ⁺	223.0946 ^c	0.005	0	0.070	0.068 \pm 0.002
[P5.3.1.2/P5.3.2.2+Na] ⁺	225.1103 ^c	0.001	0	0.918	1.64 \pm 0.05
[P5.3.1.3/P5.3.2.3+Na] ⁺	209.1154 ^c	0.009	0	0.080	0.104 \pm 0.009
[P5.3.2.4+Na] ⁺	207.0997 ^c	0.003	0	0.511	0.247 \pm 0.007
[P6.2/P7.2+Na] ⁺	191.1048 ^c	0.023	0	0.676	1.14 \pm 0.03
[P6.3/P7.3+Na] ⁺	175.1099	0	0	0	0

^aNo UV and no N₂ controls combined into single column, with “/” used when values differ. ^bThree repeats undertaken and an average and associated error calculated. ^cOther table entries have predicted species with same m/z .

Peaks corresponding to TART were observed with similar intensity in the no O₂, no UV and unreacted TART standard controls, indicated ozone was not produced under these conditions (Table 44). Peaks corresponding to TART in the trapping reactions had around 30% intensity compared to unreacted TART standard, indicating ~70% TART was consumed during the trapping reactions.

Peaks corresponding to non-trapped products were observed in the trapping reactions and no TART control, as expected. Peaks corresponding to different products were observed more or less intensely in TART absence (Table 44). The reason for this was unclear. However, the relative difference in peak intensities corresponding to products in TART absence and presence was less than a factor of ~2 and therefore, was deemed insignificant.

All of the ten most intense MS peaks corresponding to monomeric non-fragmented TART-trapped radicals were observed exclusively or with significantly greater intensity in the trapping reactions than in control reactions (Table 44). Additionally, peaks corresponding to many other hypothesised TART-trapped radicals were observed exclusively or with significantly greater intensity in the trapping reactions than in control reactions (Table 44). This indicated that these species must have corresponded to TART-trapped radicals from α -pinene ozonolysis.

The reactant radicals corresponding to these TART-trapped radicals were formed through many different pathways including: α -pinene reaction with ozone, Criegee intermediate formation and Criegee intermediate degradation to form RO₂[•] (Figure 153); subsequent RO₂[•]+RO₂[•] reaction to form RO[•] (Figure 154); RO[•] fragmentation to form new RO₂[•] (Figure 154); [•]OH addition to α -pinene, subsequent ring opening and ring closure to form cycloperoxide-RO₂[•] (Figure 159); [•]OH addition to α -pinene, subsequent ring opening, autooxidation and ring closure to form oxygenated-cycloperoxide-RO₂[•] (Figure 160) and HAA from α -pinene by [•]OH to form RO₂[•] (Figure 161). These observations supported the literature which hypothesised such mechanisms.^{57,249,251,252,255} This was an excellent result, as it showed that TART trapping and MS characterisation could be used to trap, detect and characterise radicals in a mechanistically complex gaseous system, aiding mechanism elucidation and offering support to previously hypothesised mechanisms.

However, many species could not be separated due to their identical *m/z* including R1.1/R1.2-ART, R1.1.1/R1.2.1/R6.1.1/R7.1.1-ART, R5.1/R5.2/C₁₀H₁₇O₅-ART and R6/R7-ART, preventing existence of each species from being definitively proven, without further MS characterisation.

Furthermore, peaks corresponding to many TART-trapped radicals were not observed or observed with similar intensity in trapping and control reactions (Table 44). This suggested that the concentration of the radicals corresponding to these TART-trapped radicals was too low for detection. Such radicals included R3/R4, which are widely accepted to be formed through [•]OH addition to α -pinene and immediate RO₂[•] formation.⁵⁷ This was hypothesised to be due to strained four-membered ring opening being favourable to immediate RO₂[•] formation, following [•]OH addition to α -pinene. Though literature indicated that [•]OH addition and immediate RO₂[•] formation was competitive with four-membered ring opening under atmospheric conditions, this was not necessarily true in the utilised α -pinene ozonolysis system (8.3, 11.7.1), as discussed previously. Peaks corresponding to TART-trapped R5 were also not observed. It was therefore hypothesised that RO₂[•] reaction, either through autooxidation or addition to the double bond, was too rapid for R5 to be trapped.

Further conclusions could be drawn from quantitative analysis of the obtained MS results. However, quantitative conclusions were tentative, due to differences in trapping rates of different radicals and ionisation efficiencies of different TART-trapped radicals.

A peak corresponding to R6/R7 was the most intense peak corresponding to TART-trapped radicals (Table 44). Assuming RO_2^\bullet trapping rate constant was equal for all RO_2^\bullet , this indicated that R6/R7 had the highest gaseous concentration of RO_2^\bullet radicals. This was surprising, as literature indicated that R6/R7 formation was a minor pathway for $\bullet\text{OH}$ reaction with α -pinene (~8%). This potentially indicated that HAA from allylic C–H plays a more significant role in gaseous α -pinene ozonolysis than literature suggested or alternatively, that reactions of R6/R7 reaction were slow, resulting in relatively high [R6/R7].

RO_2^\bullet species R1.1/R1.2 were relatively stable and hence likely had relatively high gaseous concentration, whilst RO^\bullet species R1.1.1/R1.2.1 were poorly stable and hence likely had low gaseous concentration. However, peaks corresponding to R1.1/R2.1–ART and R1.1.1/R2.1.1–ART were observed with similar intensity (Table 44). This was likely due to RO^\bullet reacting with TART more efficiently than RO_2^\bullet , as discussed previously (7.2). Such conclusions would be better evidenced using kinetic modelling. Therefore, it was decided that kinetic modelling should be undertaken to allow more detailed quantitative interpretation of MS results. This was undertaken as detailed below (8.6.3.7).

TART-trapped radicals were successfully observed using standard MS. D_2O exchange (8.6.3.3) and tandem MS were utilised to further validate suggested structures (8.6.3.4), whilst HPLC-MS (8.6.3.5) was used to more cleanly isolate peaks and increase intensity of TART-trapped radicals.

8.6.3.3. D_2O

D_2O exchange was used to evaluate the labile hydrogen atom population of each species (Table 45). For species observed with low intensity corresponding MS peaks, D_2O exchange data were poor and hence these species are omitted from analysis. For TART-trapped radicals, –ART contained one labile hydrogen atom in the amide N–H.

Table 45: D exchanges observed for MS peaks corresponding to species from D_2O exchange of TART trapping of α -pinene ozonolysis, using MS for characterisation (11.7.2). Systematic m/z error = -0.0003; random m/z error = ± 0.0010 .

Species	Predicted m/z for 0D shift	Predicted D shift	Proportion of total intensity of all D-shifted peaks for each species / %				
			0D	1D	2D	3D	4D
[CHANT+D] ⁺	323.2698	1D	2.3	97.7	0	0	0
[R1.1/R1.2–ART+Na] ⁺	388.2100	1D	0	34.7	65.3	0	0
[R1.1.1/R1.2.1–ART+Na] ⁺	372.2151 ^a	1D	0	52.5	36.7	10.8	0
[R2.1–ART+Na] ⁺	360.2151	1D	0	82.3	17.7	0	0
[R2.1.1–ART+Na] ⁺	344.2202	1D	9.0	14.1	76.9	0	0
[R5.1/R5.2–ART+Na] ⁺	406.2205 ^a	2D	0	0	54.9	45.1	0
[C ₁₀ H ₁₇ O ₅ –ART+Na] ⁺	406.2205 ^a	3D	0	0	54.9	45.1	0
[C ₁₀ H ₁₇ O ₆ –ART+Na] ⁺	422.2155	3D	0	12.1	19.9	68.1	0
[R6/R7–ART+Na] ⁺	356.2202	1D	3.0	97.0	0	0	0
[R6.1.1/R7.1.1–ART+Na] ⁺	372.2151 ^a	1D	0	52.5	36.7	10.8	0
[Pinaldehyde+Na] ⁺	191.1048 ^a	0D	98.1	1.9	0	0	0
[Pinonic acid+Na] ⁺	207.0997 ^a	1D	10.8	89.1	0	0	0
[P1.1.2/P1.2.2+Na] ⁺	223.0946 ^a	1D	20.8	33.3	45.9	0	0
[P1.1.3/P1.2.3+Na] ⁺	207.0997 ^a	1D	10.8	89.1	0	0	0
[P2.1.2+Na] ⁺	195.0997	1D	16.5	63.5	20.0	0	0
[P2.1.3+Na] ⁺	179.1048	1D	10.7	89.3	0	0	0
[P2.1.4+Na] ⁺	177.0891	0D	83.2	16.8	0	0	0
[P3.2/P4.2+Na] ⁺	209.1154 ^a	2D	14.3	21.1	64.6	0	0
[P3.3+Na] ⁺	193.1204	2D	3.0	8.8	88.2	0	0

[P4.3+Na] ⁺	191.1048 ^a	1D	0.2	98.0	1.9	0	0
[P5.1.2/P5.2.2+Na] ⁺	241.1052	2D	0	0	54.5	36.5	8.9
[P5.1.3/P5.2.3+Na] ⁺	225.1103 ^a	2D	0.1	3.3	95.8	0.7	0
[P5.2.4+Na] ⁺	223.0946 ^a	1D	20.8	33.3	45.9	0	0
[P5.3.1.2/P5.3.2.2+Na] ⁺	225.1103 ^a	2D	0.1	3.3	95.8	0.7	0
[P5.3.1.3/P5.3.2.3+Na] ⁺	209.1154 ^a	2D	14.3	21.1	64.6	0	0
[P5.3.2.4+Na] ⁺	207.0997 ^a	1D	10.8	89.1	0	0	0
[P6.2/P7.2+Na] ⁺	191.1048 ^a	1D	98.1	1.9	0	0	0

^aOther table entries have predicted species with same *m/z*.

The predicted D shift was observed for peaks corresponding to most species, including for TART-trapped radicals. This offered validity to the suggested structures of these TART-trapped radicals. For example, a 1D shift was near exclusively observed for the peak corresponding to [R6/R7-ART+Na]⁺, matching the corresponding suggested structure of R6/R7 which contained no labile hydrogen atoms (Figure 162, 11.7.2).

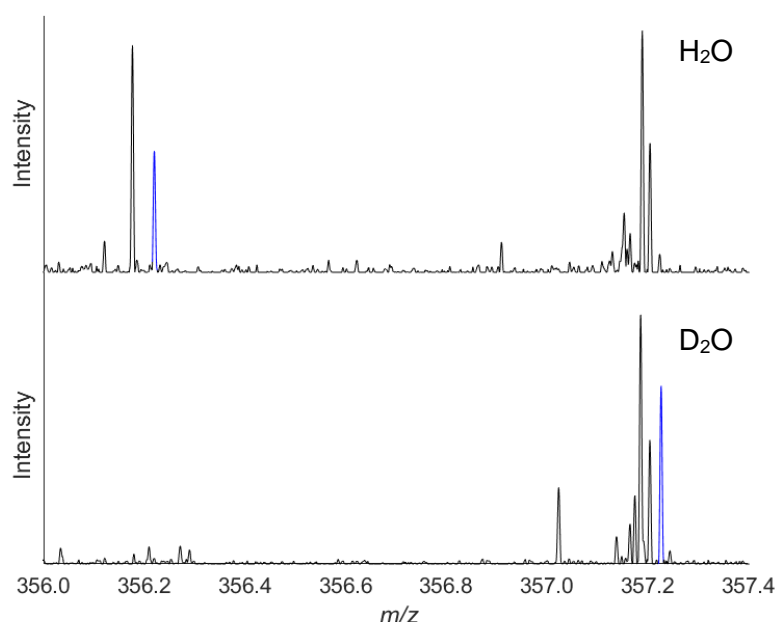


Figure 162: Background corrected mass spectra run in protonated (top) and deuterated (bottom) solvent, showing peaks corresponding to R6/R7-ART (blue) detected from D₂O exchange of TART trapping of α -pinene ozonolysis (11.7.2).

However, for many peaks other unexpected D shifts were additionally observed, often resulting in a range of D shifts for each species, as seen previously (7.6). This indicated that other unpredicted TART-trapped radicals contributed to the MS peaks intensities corresponding to TART-trapped radicals. For example, for the peak corresponding to R1.1/R1.2-ART, the predicted D shift (1D) only contributed ~35% to the total D shift, whilst ~65% originated from species with two labile hydrogen atoms. Therefore, in standard MS, R1.1/R1.2-ART only contributed ~35% to the R1.1/R1.2-ART corresponding peak intensity. This had significant ramifications for TART-trapped radical quantification. This 2D shifted peak could originate from a hydroxylated R1.1.1/R1.2.1-ART species, though this could not be confirmed. Additionally, for the peak corresponding to R5.1/R5.2/C₁₀H₁₇O₅-ART, D shifts observed were ~55% 2D and ~45% 3D. This indicated that relative proportion of [R5.1/R5.2-ART] to [C₁₀H₁₇O₅-ART] was ~55% to 45%. Therefore, D₂O exchange could be used to determine relative rates of mechanistic pathways. Nevertheless, for most TART-

trapped radicals and products, the predicted D shift was the most intensely observed D shift for the corresponding peaks, offering validation to their suggested structures.

8.6.3.4. Tandem MS

Tandem MS was employed to validate TART-trapped radical structures. This was challenging as peak intensities corresponding to TART-trapped radicals were very weak, whilst tandem MS produces less high-quality fragmentation upon sodiated MS adducts, which MS adducts of TART-trapped radicals predominantly were. However, some tandem mass spectra did offer validation to suggested structures of TART-trapped radicals. For example, tandem MS performed upon the peak corresponding to [R1.1/R1.2-ART+Na]⁺ (*m/z* 388.210) yielded a fragment corresponding to [C₁₀H₁₅NO₃Na]⁺ (*m/z* 220.095) which indicated [OO-ART+Na]⁺ and hence a peroxide bond (Figure 163). This added validation to the hypothesised TART-trapped RO₂[•] structure.

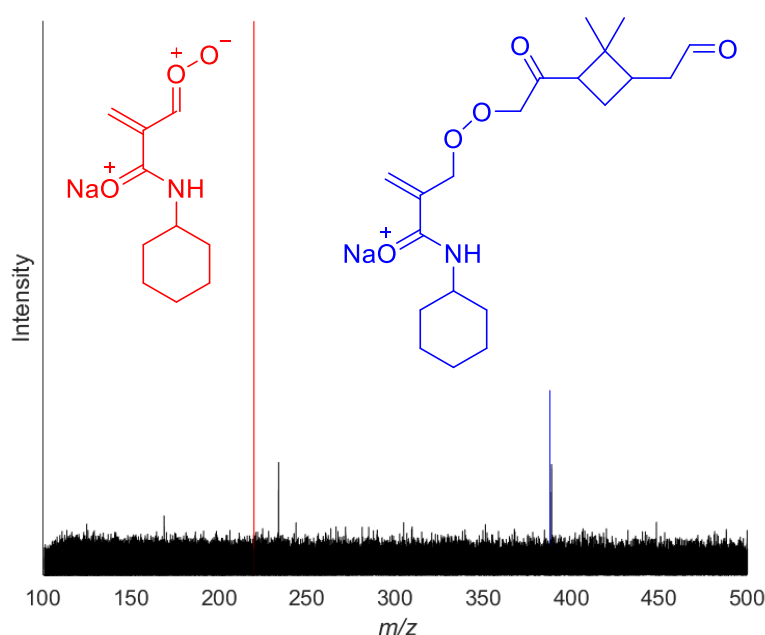


Figure 163: Tandem mass spectrum of the peak corresponding to R1.1/R1.2-ART (*m/z* 388.210, blue) from TART trapping of α -pinene ozonolysis, yielding suggested fragment (*m/z* 220.095, red). Structures are derived from R1.1-ART but could be equally attributed to R1.2-ART.

8.6.3.5. HPLC-MS

HPLC-MS was used to clean mass spectra, thus improving peak isolation and separate species with the same *m/z*, allowing different isomers to be separately detected. Furthermore, using the source-waste function, sample concentration could be increased, to maximise intensity of peaks corresponding to TART-trapped radicals (4.3.2.8). For example, the HPLC-MS chromatogram of peaks corresponding to R1.1/R1.2-ART (*m/z* 366.2280 \pm 0.0020 and *m/z* 388.2100 \pm 0.0020), revealed many isomers contributed to this peak (Figure 164, 11.7.2).

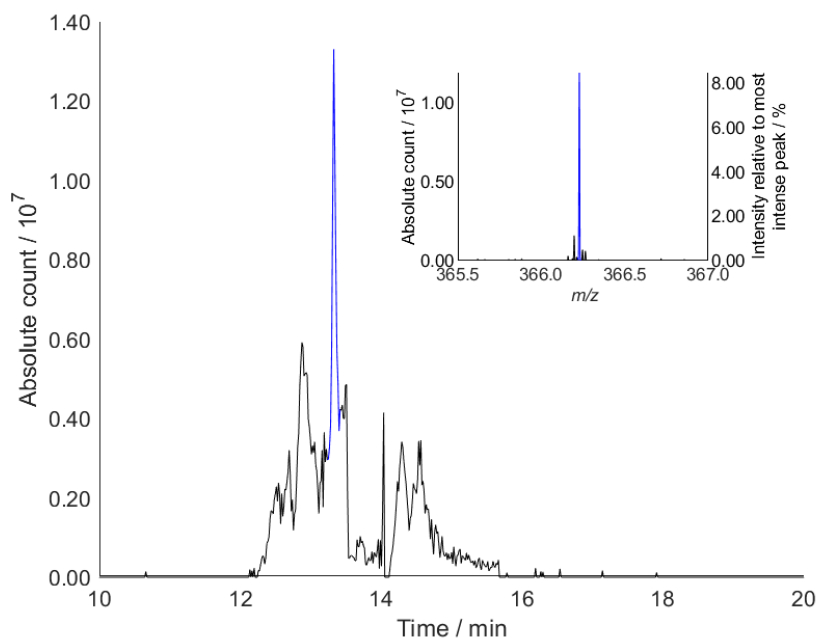


Figure 164: HPLC-MS chromatogram and mass spectrum (inset) of peaks corresponding to R1.1/R1.2-ART (m/z 366.228 \pm 0.002 and m/z 388.210 \pm 0.002) from TART trapping of α -pinene ozonolysis (11.7.2). MS source was sent to waste between 13.5-14.0 min, to prevent injection of unreacted TART. Mass spectrum of [R1.1/R1.2-ART+H]⁺ (blue) is at time of maximum intensity (blue).

MS cleanliness and peak isolation were significantly improved by HPLC-MS. However, TART-trapped RO₂[•] peak intensities could not be significantly improved. For example, maximum intensity of peaks corresponding to R1.1/R2.1-ART little increased from $\sim 1.1 \times 10^7$ to $\sim 1.3 \times 10^7$ absolute count. High MeCN concentration was required to elute most TART-trapped α -pinene ozonolysis radicals, even when using a weakly polar HPLC column. This caused low Na⁺ concentration compared to 1:1 MeCN:H₂O used for direct injections. This caused most HPLC-MS detected TART-trapped radicals to be observed predominantly as protonated adducts rather than sodiated adducts. It was therefore hypothesised that low Na⁺ concentration caused relatively poorer peak intensity than expected. It was also hypothesised that trace metals in the HPLC column could have catalysed peroxide bond degradation in TART-trapped RO₂[•].

Likewise, the HPLC-MS chromatogram of peaks corresponding to R1.1.1/R1.2.1-ART (m/z 350.2331 \pm 0.0020 and m/z 372.2151 \pm 0.0020), revealed many isomers contributed to this peak (SI6.1.2.2). However, contrary to RO₂[•], TART-trapped RO[•] peak intensities in HPLC-MS were significantly increased. For example, maximum intensity of the peak corresponding to R1.1.1/R1.2.1-ART increased around an order of magnitude from $\sim 0.7 \times 10^7$ to $\sim 5.3 \times 10^7$ absolute count (SI6.1.2.2). Therefore, HPLC-MS aided TART-trapped RO[•] peak isolation. This increased intensity obtained for TART-trapped RO[•] compared to RO₂[•] matched the hypothesis that relatively reactive TART-trapped RO₂[•] peroxides were decomposed by HPLC column, whereas stable TART-trapped RO[•] ethers were not, causing relatively greater increase in corresponding peak intensity.

Peaks corresponding to TART-trapped radicals had been thoroughly MS characterised through numerous techniques. However, the most intense product and TART-trapped radical corresponding peaks were not the most intense peaks in the mass spectrum (Figure 152). These peaks were instead believed to corresponding to oligomeric products.

8.6.3.6. Oligomeric products and trapped radicals

Whilst these peaks were not believed to correspond to trapped radicals, it was important to determine what these peaks corresponded to, as large unexplainable peaks may have invalidated TART trapping of α -pinene ozonolysis results. Therefore, the Formula Find programme was employed with wider search conditions, to try to identify molecular formulae for these peaks (Table 46). Molecular formulae limits were set to $C_{1-40}H_{0-100}N_{0-2}O_{0-15}Na_{0-1}$ and m/z limits 100-1000.

Table 46: Ten most intense peaks from TART trapping of α -pinene ozonolysis, obtained using the Formula Find programme. Molecular formula limits were set as $C_{1-40}H_{0-100}N_{0-2}O_{0-15}Na_{0-1}$ and m/z limits 100-1000. Illogical molecular formulae were eliminated.

Observed m/z	Intensity relative to unreacted TART standard / %	Corresponding molecular formula	Structure identified
393.2249	32.8	$C_{20}H_{34}O_6$	P5.1/5.2-Dim-3/PC ₁₀ H ₁₇ O ₆ -Dim-2
323.2694	28.3	$C_{19}H_{34}N_2O_2$	CHANT
409.2200	11.9	$C_{20}H_{34}O_7$	P5.1/5.2-Dim-4/PC ₁₀ H ₁₇ O ₆ -Dim-3
391.2094	9.16	$C_{20}H_{32}O_6$	P1.1/1.2-Dim-4/P6/7-Dim-6
375.2144	5.06	$C_{20}H_{32}O_5$	P1.1/1.2-Dim-3/P6/7-Dim-5
593.3301	4.87	$C_{30}H_{50}O_{10}$	P5.1/5.2-Trim-7/PC ₁₀ H ₁₇ O ₆ -Trim-6
425.2149	4.83	$C_{20}H_{34}O_8$	P5.1/5.2-Dim-5/PC ₁₀ H ₁₇ O ₆ -Dim-4
577.3352	3.54	$C_{30}H_{50}O_9$	P5.1/5.2-Trim-6/PC ₁₀ H ₁₇ O ₆ -Trim-5
359.2195	2.19	$C_{20}H_{32}O_4$	P1.1/1.2-Dim-2/P6/7-Dim-4
225.1098	1.74	$C_{10}H_{18}O_4$	P5.1.3/P5.2.3

Of the ten most intense peaks, only two had corresponding molecular formulae for which structures were previously identified. These were CHANT and P5.1.3/P5.2.3. All other species had 20 or 30 carbon atoms, implying dimeric or trimeric species respectively. Many of these species may be relevant to HOM product formation.¹⁰

Firstly, HPLC-MS was conducted to ensure oligomer peaks were not an MS effect, caused by multiple monomers forming a complex around a single Na^+ or monomers reacting together during MS. HPLC-MS showed presence of oligomers and significant chromatographic separation between oligomers and monomers required for MS clusters or oligomerisation (SI6.1.2.3). Therefore, oligomerisation was believed to occur during TART trapping of α -pinene ozonolysis.

It was first hypothesised that dimers formed during α -pinene ozonolysis would arise from $RO_2^{\bullet}+RO_2^{\bullet}$ coupling to form ROOR (Figure 142, 8.2). Therefore, the most concentrated ROOR were expected to be formed by $RO_2^{\bullet}+RO_2^{\bullet}$ coupling of the most concentrated RO_2^{\bullet} , which were identified from the most intense peaks corresponding to TART-trapped radicals. For example, R1.1/R1.2+R6/R7 coupling would form an R1.1/R1.2–R6/R7 dimer, termed P1.1/1.2–6/7. Therefore, ROOR structures were hypothesised and searched for (Table 47).

Table 47: ROOR species identified from TART trapping of α -pinene ozonolysis, using MS for characterisation (11.7.2). Systematic m/z error = -0.0005; random m/z error = ± 0.0010 ; 100% intensity = 2.01×10^9 absolute count. ROOR nomenclature is of the form PR-R', where R and R' are the indexes of the two reactant radicals.

Species	Predicted m/z	Intensity relative to unreacted TART standard / %			
		No substrate	No O ₂ /No UV ^a	No TART	Trapping reaction ^b
[CHANT+H] ⁺	323.2698	0.019	98.1/92.5	0	29.5 \pm 1.2
[P1.1/1.2-1.1/1.2+Na] ⁺	389.1940	0	0	0.112	0.099 \pm 0.004
[P1.1/1.2-5.1/5.2+Na] ⁺	407.2046 ^c	0	0	1.18	0.66 \pm 0.02
[P1.1/1.2-C ₁₀ H ₁₇ O ₆ +Na] ⁺	439.1944	0	0	0	0
[P1.1/1.2-6/7+Na] ⁺	373.1991	0	0	0.170	0.064 \pm 0.002
[P5.1/5.2-5.1/5.2+Na] ⁺	425.2151 ^c	0	0	3.46	4.77 \pm 0.13
[P5.1/5.2-C ₁₀ H ₁₇ O ₆ +Na] ⁺	441.2100 ^c	0	0	0.422	0.326 \pm 0.009
[P5.1/5.2-6/7+Na] ⁺	375.2147 ^c	0.005	0	3.92	5.6 \pm 0.3
[PC ₁₀ H ₁₇ O ₆ -C ₁₀ H ₁₇ O ₆ +Na] ⁺	457.2050 ^c	0	0	0.027	0.025 \pm 0.001
[PC ₁₀ H ₁₇ O ₆ -6/7+Na] ⁺	391.2096 ^c	0.009	0.001/0	6.67	9.7 \pm 0.3
[P6/7-6/7+Na] ⁺	325.2143	0	0	0	0

^aNo UV and no N₂ controls combined into single column, with “/” used when values differ. ^bThree repeats undertaken and an average and associated error calculated. ^cOther tables show entries that have predicted species with same m/z .

Peaks corresponding to these hypothesised ROOR were not the most intensely observed peaks corresponding to oligomers (Table 46). Therefore, it was hypothesised that the most intensely observed dimers were not formed through RO₂[•]+RO₂[•] coupling to form ROOR. It was hypothesised that dimerisation may instead be occurring by intermolecular radical addition across unreacted alkene by either RO₂[•] or RO[•] to an α -pinene unit, forming a radical-alkene dimer. This process would be similar to intramolecular radical addition to alkene, required for R5.1/5.2 formation and intermolecular radical addition to TARTs, prior to TEMPO[•] cleavage. The resultant radical dimer would rapidly form RO₂[•] and could subsequently form dimer products ROH or ROOH through previously described mechanistic steps (Figure 142, 8.2). Dimerisation through radical addition is not widely discussed in literature, as this reaction is slow in the atmosphere. However, in the TART trapping of α -pinene ozonolysis system, α -pinene is in significant excess of all other species. Therefore, it was hypothesised that this high alkene abundance made radical-alkene dimerisation competitive. However, radical addition to the α -pinene double bond can cause ring opening (Figure 157). Therefore, radical addition to α -pinene and immediate RO₂[•] formation or radical addition to α -pinene, ring opening and subsequent ring closure also needed to be considered. Therefore, oligomer structures were described by their number of oxygen atoms, rather than their exact structures (Figure 165).

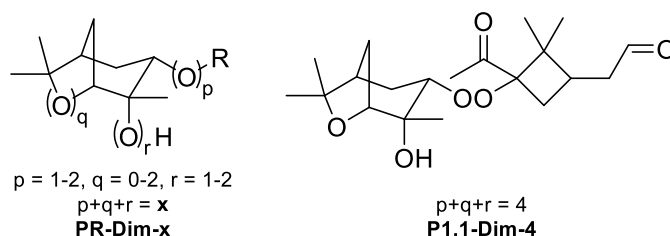


Figure 165: General radical-alkene dimer structure formed through radical addition to α -pinene and example dimer (P1.1-Dim-4) formed through radical (R1.1) addition to α -pinene, with the α -pinene unit containing four oxygen atoms (4). Radical-alkene dimer nomenclature is of the form PR-Dim-x, where R is the index of reactant radical species and x is the total oxygen count in the α -pinene unit, including the unit bridge (1-2), new alkene inner ring (0-2) and new alkene alcohol/hydroperoxide (1-2) functionalisation.

A key difference between the two discussed mechanisms of dimerisation is that radical-radical coupling is a terminal reaction whilst intramolecular radical addition to alkene is a propagation reaction. Therefore, the latter mechanism would allow other radical reactions to occur instead of ROH or ROOH formation, for example further oligomerisation or radical trapping. As previously, dimers formed through reaction of the most concentrated RO₂[•] and RO[•] with other α -pinene units were searched for (Table 48).

Table 48: Radical-alkene dimer species identified from TART trapping of α -pinene ozonolysis, using MS for characterisation (11.7.2). Systematic m/z error = -0.0005; random m/z error = ± 0.0010 ; 100% intensity = 2.01×10^9 absolute count. Radical-alkene dimer nomenclature is of the form PR-Dim-x, where R is the index of reactant radical species and x is the total oxygen count in the α -pinene unit, including the unit bridge (1-2), new alkene inner ring (0-2) and new alkene alcohol/hydroperoxide (1-2) functionalisation.

Species	Predicted m/z	Intensity relative to unreacted TART standard / %			
		No substrate	No O ₂ / No UV ^a	No TART	Trapping reaction ^b
[CHANT+H] ⁺	323.2698	0.019	98.1/ 92.5	0	29.5 \pm 1.2
[P1.1/1.2-Dim-2+Na] ⁺	359.2198 ^c	0.003	0.002/0	1.19	2.14 \pm 0.08
[P1.1/1.2-Dim-3+Na] ⁺	375.2147 ^{cd}	0.005	0	3.92	5.6 \pm 0.3
[P1.1/1.2-Dim-4+Na] ⁺	391.2096 ^{cd}	0.009	0	6.67	9.7 \pm 0.3
[P1.1/1.2-Dim-5+Na] ⁺	407.2046 ^d	0	0	1.18	0.66 \pm 0.02
[P1.1/1.2-Dim-6+Na] ⁺	423.1995	0	0	0	0
[P5.1/5.2-Dim-2+Na] ⁺	377.2304 ^c	0	0	0.913	0.65 \pm 0.02
[P5.1/5.2-Dim-3+Na] ⁺	393.2253 ^c	0.008	0	46.0	30.5 \pm 1.0
[P5.1/5.2-Dim-4+Na] ⁺	409.2202 ^c	0.002	0	11.2	11.5 \pm 0.2
[P5.1/5.2-Dim-5+Na] ⁺	425.2151 ^{cd}	0	0/0.001	3.46	4.77 \pm 0.13
[P5.1/5.2-Dim-6+Na] ⁺	441.2100 ^{cd}	0	0	0.422	0.326 \pm 0.009
[PC ₁₀ H ₁₇ O ₆ -Dim-2+Na] ⁺	393.2253 ^c	0.008	0	46.0	30.5 \pm 1.0
[PC ₁₀ H ₁₇ O ₆ -Dim-3+Na] ⁺	409.2202 ^c	0.002	0	11.2	11.5 \pm 0.2
[PC ₁₀ H ₁₇ O ₆ -Dim-4+Na] ⁺	425.2151 ^{cd}	0	0/0.001	3.46	4.77 \pm 0.13
[PC ₁₀ H ₁₇ O ₆ -Dim-5+Na] ⁺	441.2100 ^{cd}	0	0	0.422	0.326 \pm 0.009
[PC ₁₀ H ₁₇ O ₆ -Dim-6+Na] ⁺	457.2050 ^d	0	0	0.027	0.025 \pm 0.001
[P6/7-Dim-2+Na] ⁺	327.2300	0	0	0.005	0.007 \pm 0.001
[P6/7-Dim-3+Na] ⁺	343.2249	0	0	0.060	0.051 \pm 0.002
[P6/7-Dim-4+Na] ⁺	359.2198 ^c	0.003	0.002/0	1.19	2.14 \pm 0.08
[P6/7-Dim-5+Na] ⁺	375.2147 ^{cd}	0.005	0	3.92	5.6 \pm 0.3
[P6/7-Dim-6+Na] ⁺	391.2096 ^{cd}	0.009	0	6.67	9.7 \pm 0.3

^aNo UV and no N₂ controls combined into single column, with “/” used when values differ. ^bThree repeats undertaken and an average and associated error calculated. ^cOther table entries have predicted species with same m/z . ^dOther tables show entries that have predicted species with same m/z .

Peaks corresponding to these radical-alkene dimer products were observed with significant intensity. These species were likely to have low atmospheric relevance, due to alkene concentration being significantly lower than ozone concentration in the atmosphere. However, it did indicate that radical-alkene dimerisation was possible and could be significant under certain conditions. Peaks corresponding to radical-alkene dimer products are some of the most intense peaks observed in the mass spectrum (Figure 166).

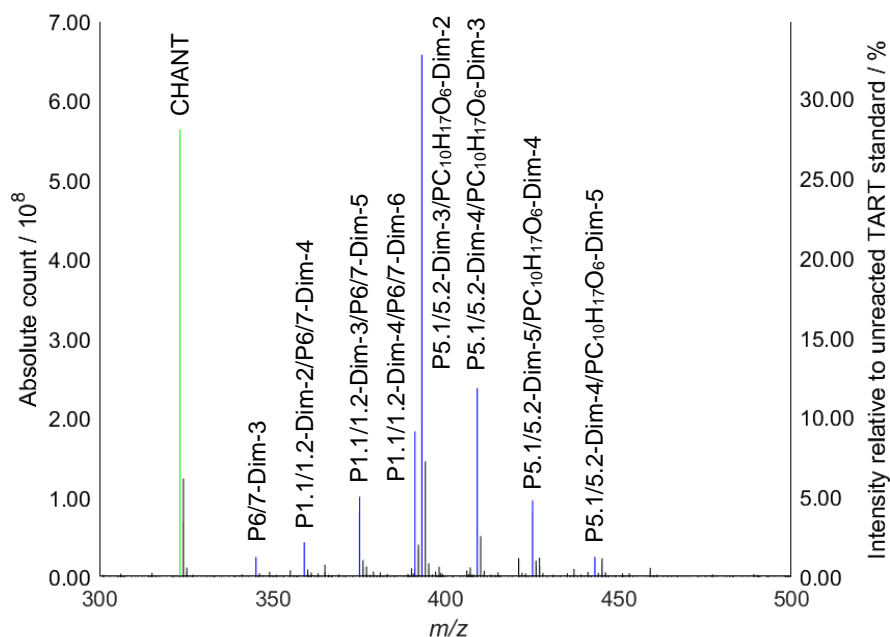


Figure 166: Background corrected mass spectrum from TART trapping of α -pinene ozonolysis (11.7.2), showing peaks corresponding to CHANT (green) and radical-alkene dimer products (blue).

Additionally, radical dimer RO_2^\bullet could form radical dimer RO^\bullet or dimer products ROH or ROOH . However, these RO_2^\bullet and RO^\bullet may instead be trapped by TARTs. This contrasted to $\text{RO}_2^\bullet + \text{RO}_2^\bullet$ coupling to form ROOR , as this process forms no radical dimers without further initiation, making TART trapping unlikely. Peaks corresponding to TART-trapped dimers were observed (Table 49, 11.7.2).

Table 49: TART-trapped dimer radicals identified from TART trapping of α -pinene ozonolysis, using MS for characterisation (11.7.2). Systematic m/z error = -0.0005 ; random m/z error = ± 0.0013 ; 100% intensity = 2.01×10^9 absolute count.

Species	Predicted m/z	Intensity relative to unreacted TART standard / %			
		No substrate	No O_2 / No UV	No TART	Trapping reaction ^a
$[\text{CHANT} + \text{H}]^+$	323.2698	0.019	98.1/ 92.5	0	29.5 ± 1.2
$[\text{R1.1/R1.2-Dim-4-ART} + \text{Na}]^+ / [\text{R6/R7-Dim-6-ART} + \text{Na}]^+$	556.3250	0	0	0	0.011 ± 0.001
$[\text{R1.1/R1.2-Dim-5-ART} + \text{Na}]^+$	572.3199	0	0	0	0
$[\text{R1.1/R1.2-Dim-6-ART} + \text{Na}]^+$	588.3148	0	0	0	0.010 ± 0.001
$[\text{R5.1/R5.2-Dim-3-ART} + \text{Na}]^+ / [\text{RC}_{10}\text{H}_{17}\text{O}_6\text{-Dim-2-ART} + \text{Na}]^+$	558.3407	0	0	0	0.014 ± 0.001
$[\text{R5.1/R5.2-Dim-6-ART} + \text{Na}]^+ / [\text{RC}_{10}\text{H}_{17}\text{O}_6\text{-Dim-5-ART} + \text{Na}]^+$	606.3254	0	0	0	0.009 ± 0.001

^aThree repeats undertaken and an average and associated error calculated.

These peaks corresponding to TART-trapped dimer radicals were observed exclusively in trapping reactions, validating that they were indeed TART-trapped radicals. These observations further supported the hypothesis that dimers were formed through radical addition to α -pinene. MS peaks corresponding to further oligomeric products, such as trimers, were also observed and assigned to structures (Figure 167, SI6.1.2.3). These species may be relevant to HOM product formation.¹⁰

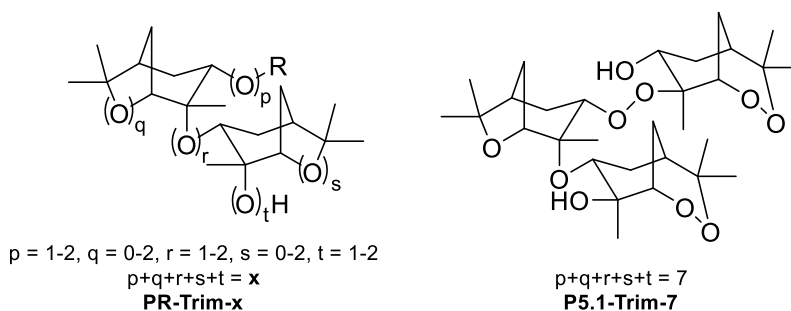


Figure 167: General trimer structure formed through radical addition to two α -pinene and example trimer (P5.1-Trim-7) formed through radical (R5.1) addition to α -pinene, with the two α -pinene units containing seven oxygen atoms (7). Radical-alkene-alkene trimer nomenclature is of the form PR-Trim-x, where R is the index of reactant radical species and x is the total oxygen count in the two α -pinene units, including the unit bridges (1-2), new alkene inner rings (0-2) and new alkene alcohol/hydroperoxide (1-2) functionalisation.

Observation and characterisation of peaks corresponding to both oligomeric products and TART-trapped radicals showed the advantages of being able to characterise both products and radicals simultaneously. This is a significant advantage of TART trapping and MS characterisation over other radical characterisation techniques.

The most intense peaks and peaks corresponding to TART-trapped radicals had been successfully characterised. Next, kinetic modelling was applied to further analyse results from TART trapping of α -pinene ozonolysis.

8.6.3.7. Kinetic modelling

To validate experimental observations and allow experimental results to be fully interpreted, kinetic modelling of TART trapping of α -pinene ozonolysis was undertaken (11.10.3). Initial simulations used the parameters of experimentally undertaken TART trapping of α -pinene ozonolysis (Figure 150, 11.7.2).

In all modelling, potential wall reactions were ignored, simulation conditions were set at RTP and trapping solution volume was assumed constant. These assumptions were made to significantly simplify modelling, though were unlikely to be true. This kinetic model required separate simulation of gaseous α -pinene ozonolysis, solution-gas interface trapping and solution phase trapping.

For gaseous α -pinene ozonolysis, atmospheric reactions of substrates were imported into the Kintecus chemical simulation programme from the MCM and truncated to remove late stage pathways.^{57,207} The MCM contained widely accepted mechanistic steps of α -pinene ozonolysis, such as α -pinene reaction with ozone (Figure 153 and Figure 157) and immediate RO_2^\bullet formation following $\bullet OH$ addition (Figure 156) but not other mechanistic steps, such as ring opening following $\bullet OH$ addition to α -pinene (Figure 159), HAA abstraction from α -pinene by $\bullet OH$ (Figure 161) or oligomer formation (8.6.3.6). Adding these less widely accepted reactions to the gaseous α -pinene ozonolysis model would be time consuming and hence was decided to be beyond the scope of this project. Furthermore, reliable rate constants for these reactions were not readily available. Simulation parameters were set to emulate experimental conditions immediately prior to bubbling through trapping solution, including residence time and initial substrate concentrations (11.10.3). The simulation results yielded final gaseous radical concentrations, immediately prior to bubbling (Figure 168, 11.10.3). These final gaseous radical concentrations were used to simulate TART trapping.

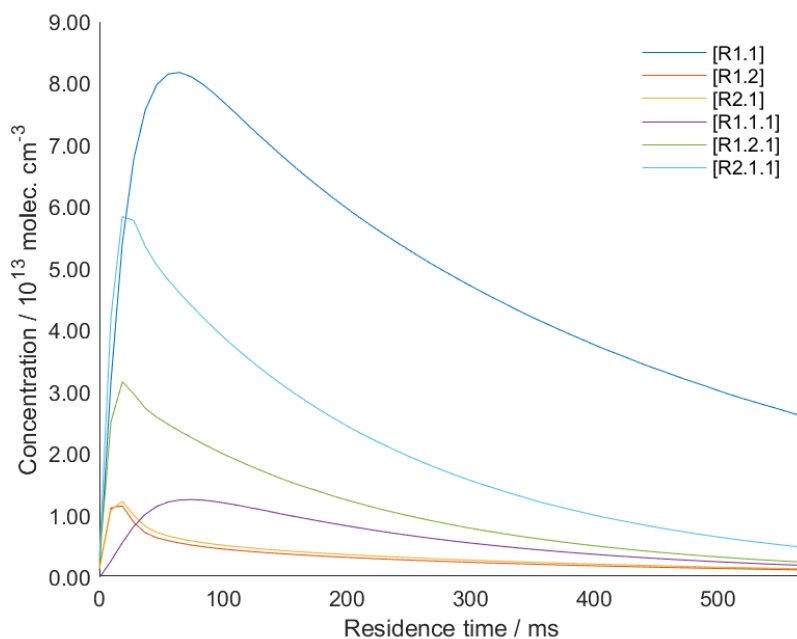


Figure 168: Simulation of gaseous α -pinene ozonolysis between 0-565 ms residence time (11.10.3). 56.5 ms was the typical residence time used in TART trapping of α -pinene ozonolysis.

~11% α -pinene species were estimated to dissolve in solution using experimental evidence (11.7.4). Therefore 11% of simulated gaseous radicals were entered into a liquid phase trapping model (dissolved), whilst the remaining 89% were entered into a gas-liquid interface trapping model (not dissolved). In both models, atmospheric reactions were assumed to stop immediately upon bubbling, whilst TART trapping could occur. Trapping rates of all RO_2^\bullet and all RO^\bullet were estimated to be 10^{-22} and 10^{-15} molec. $^{-1}$ cm 3 s $^{-1}$ respectively, based upon RO_2^\bullet addition to methyl methacrylate and assorted literature-sourced rate constants for RO^\bullet addition to alkenes respectively.^{226,228} In both models, initial trap concentration was set as its initial concentration in solution.

The liquid phase model was run for the total reaction time. During this time, 11% gaseous radicals were inputted at regular intervals to simulate incoming radicals, allowing trapping to occur. This yielded final trapped radical concentrations in solution for the liquid phase model.

In the gas-liquid interface model, the model was run for the estimated residence time of a gas bubble in solution. Initial gaseous radical concentrations were inputted using 89% final gaseous radical concentrations accumulated during this residence time, allowing trapping to occur. These results were then scaled to the total reaction time, yielding final trapped radical concentrations in solution for the gas-liquid interface model.

Results from these two models were summed together to yield final trapped radical concentrations in solution.

Initial modelling used the parameters of experimentally undertaken TART trapping of α -pinene ozonolysis (Figure 150, 11.10.3). This simulation indicated that most TART-trapped RO_2^\bullet were formed in solution, whilst most TART-trapped RO^\bullet were formed at the gas-liquid interface. Furthermore, it showed that dissolved $[\text{RO}_2^\bullet]$ increased steadily during the reaction time, due to its relatively slow trapping rate, whilst dissolved $[\text{RO}^\bullet]$ remained low throughout the reaction time, due to its very rapid trapping rate (SI6.1.2.4). Obtained solution phase concentrations of R1.1-ART, R1.2-ART, R2.1-ART, R1.1.1-ART, R1.2.1-ART and R2.1.1-ART were

2.37×10^{13} , 1.71×10^{12} , 1.93×10^{12} , 1.62×10^{12} , 3.27×10^{12} and 6.36×10^{12} molec. cm^{-3} respectively. Therefore, concentrations of R1.1/R1.2-ART and R1.1.1/R1.2.1-ART were 2.54×10^{13} and 4.90×10^{12} molec. cm^{-3} respectively.

These results could be used to draw quantitative conclusions from obtained MS results. However, these conclusions were tentative, due to modelling assumptions and limitations and differences in ionisation efficiencies of different TART-trapped radicals.

The peak corresponding to R1.1/R1.2-ART was more intense than the peak corresponding to R2.1-ART ($0.033 \pm 0.003\%$ compared to $0.015 \pm 0.001\%$), with a ratio of ~ 2.1 . Modelling indicated that the proportion of R1.1/R1.2-ART compared to R2.1-ART should be $\sim 9:1$. These relative proportions of R.1/R1.2-ART to R2.1-ART broadly matched, within an order of magnitude. Considering the assumptions required for modelling and MS quantification, this match was reasonable. Similarly to their RO_2^\bullet ancestors, the peak corresponding to R1.1.1/R1.2.1-ART was more intense than the peak corresponding to R2.1.1-ART ($0.023 \pm 0.002\%$ compared to $0.006 \pm 0.001\%$), with a ratio of $\sim 4:1$. Modelling indicated that the proportion of R1.1.1/R1.2.1-ART compared to R2.1.1-ART should be $\sim 5:1$.⁵⁷ Again, these data broadly matched. The peak corresponding to R1.1/R1.2-ART was more intense than the peak corresponding to R1.1.1/R1.2.1-ART ($0.033 \pm 0.003\%$ compared to $0.023 \pm 0.002\%$), with a ratio of $\sim 1.5:1$. Modelling indicated that the proportion of R1.1/R1.2-ART compared to R1.1.1/R1.2.1-ART should be $\sim 7:1$. These relative proportions of R.1/R1.2-ART to R1.1.1/R1.2.1-ART broadly matched, within an order of magnitude. This validated experimental results which showed that peaks corresponding to TART-trapped RO_2^\bullet and RO^\bullet were observed with similar intensities, due to low RO^\bullet concentration being counteracted by its fast trapping rate, as hypothesised previously. These observations offered validity to TART trapping and indicated that TART trapping could be used to inform reaction kinetics.

This kinetic model was used for comparison with results from kinetics experiments.

8.6.4. Kinetics experiments

The feasibility of quantitative radical detection was tested by comparing MS intensities of TART-trapped radicals from TART trapping of α -pinene ozonolysis at different residence times to the developed kinetic model (8.6.3.7, 11.7.5). The aim was to observe only an approximate match between simulated and experimental data, as many crude assumptions had to be made for this quantitative comparison. These kinetics experiments mostly used previously optimised conditions from TART trapping of α -pinene ozonolysis. However, multiple residence lengths were used (0-50 cm), resulting in residence times 0-565 ms. Furthermore, reaction time was reduced to 2 min (Figure 169, 11.7.5), to reduce the dependence of trapped radical concentration on TART concentration (8.6.2.6). Three repeats were undertaken for each residence time, allowing average MS intensities and associated errors to be obtained (11.7.5).

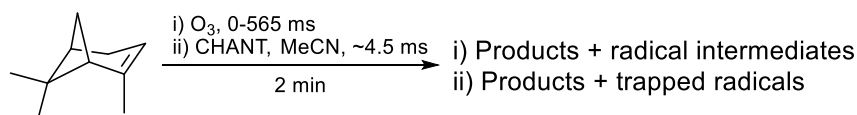


Figure 169: TART trapping of α -pinene ozonolysis kinetics experiments (11.7.5).

Experimental data were then scaled globally to minimise root-mean-square deviation (RMSD) between simulated and experimental data (Figure 170). This single scaling factor was the only optimised parameter.

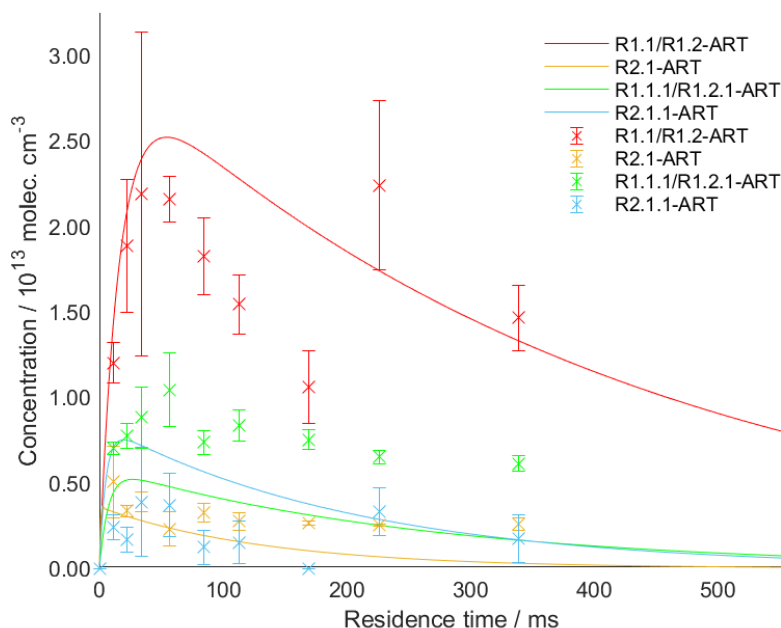


Figure 170: Simulation (line) of TART trapping of α -pinene ozonolysis kinetics experiment over different residence times (tube lengths) and corresponding average experimental MS intensities of corresponding peaks and associated errors (scatter and error bars, 11.7.5). Experimental results were globally scaled to minimise RMSD between simulated and experimental data.

Considering the crude approximations made in constructing the model and the complexity of the system, it was remarkable that the general shapes of simulated and experimental profiles were similar, including the time corresponding to maximum intensity and approximate relative concentrations of different radicals.

However, there were some discrepancies between experimental and simulated results. In particular, [R1.1.1/R1.2.1-ART] was indicated to be relatively larger by experimental results than simulated results. It was hypothesised that this could be due to accumulated solution phase RO_2^\bullet undergoing $\text{RO}_2^\bullet + \text{RO}_2^\bullet$ reaction to form RO^\bullet . Thus far, gaseous α -pinene ozonolysis reactions were assumed to stop upon reaching the trapping solution. However, whilst dissolved RO^\bullet were trapped very rapidly, RO_2^\bullet were not. This caused RO_2^\bullet accumulation in the trapping solution, potentially increasing the rate of solution phase $\text{RO}_2^\bullet + \text{RO}_2^\bullet$ to form RO^\bullet , meaning RO^\bullet were not exclusively generated in the gaseous phase. These RO^\bullet would be trapped rapidly, meaning that experimentally estimated relative [RO-ART], such as [R1.1.1/R1.2.1-ART], would be higher than modelling predicted. This complicated radical quantification and suggested that results from TART trapping of α -pinene may have less relevance to the gas phase than previously thought. However, this issue equally affects other techniques used for solution phase trapping of gaseous radicals, including conventional spin trapping.

These results suggest that with appropriate calibration, TART trapping and MS characterisation can be used to estimate approximate concentrations of radicals in complex systems. However, careful modelling would be required for more accurate quantification.

8.7. Conclusions and future work

Radicals formed during relatively complex gaseous alkene ozonolysis were successfully trapped and characterised using TART trapping and MS, by bubbling the radical gas stream through trapping solution. As previously observed in biochemistry (7), evidence suggested

that TART reacted rapidly with short-lived carbon-centred R^\bullet and RO^\bullet but slowly with long-lived RO_2^\bullet . This indicated that whilst TART trapping was an effective tool for characterisation of short-lived radicals, it was not as useful for characterisation of long-lived radicals.

TART trapping of cyclohexene ozonolysis indicated formation of RO_2^\bullet and RO^\bullet following cyclohexene reaction with ozone and Criegee intermediate degradation and RO_2^\bullet following $\bullet OH$ addition to cyclohexene, exclusively in presence of all necessary reaction conditions. In contrast, the very low concentrations of RO^\bullet were unlikely to be detectable using direct radical characterisation techniques, whilst recombination trapping using nitroxyl radicals would not be suitable for oxygen-centred radicals trapping (1.3).

TART trapping and MS characterisation were then used to study much more complex gaseous α -pinene ozonolysis. The Formula Find programme was used to obtain the most intensely observed peaks which could correspond to TART-trapped radicals. Of the ten most intense peaks, seven were assigned to six structures formed during the early stages of α -pinene ozonolysis. Three of these were formed through widely accepted mechanistic steps involving: α -pinene reaction with ozone, Criegee intermediate formation and Criegee intermediate degradation to form RO_2^\bullet ; subsequent $RO_2^\bullet + RO_2^\bullet$ reaction to form RO^\bullet ; RO^\bullet fragmentation to form new RO_2^\bullet .⁵⁷ Two were formed through widely discussed but not totally accepted mechanistic steps involving $\bullet OH$ addition to α -pinene, subsequent ring opening and ring closure to form cycloperoxide- RO_2^\bullet (R5.1/R5.2) and $\bullet OH$ addition to α -pinene, subsequent ring opening, autooxidation and ring closure to form oxygenated-cycloperoxide- RO_2^\bullet ($C_6H_{17}O_6$)^{249,252} One final structure (R6/R7) was formed through a hypothesised minor pathway involving allylic HAA from α -pinene by $\bullet OH$ to form RO_2^\bullet .^{251,255} However, its corresponding TART-trapped radical was observed with the greatest intensity, potentially indicating this radical had high gaseous concentration. This suggested that HAA from allylic C-H plays a more significant role in gaseous α -pinene ozonolysis than indicated in literature. The other three molecular formulae could not be assigned to structures. However, the corresponding radicals, $C_{10}H_{19}O_{5-7}^\bullet$, had similar molecular formulae to those above, suggesting these radicals were indeed formed.

In contrast, peaks corresponding to TART-trapped radicals formed following $\bullet OH$ addition to α -pinene and immediate RO_2^\bullet formation were not observed, contrary to literature.⁵⁷ It was therefore hypothesised that strained four-membered ring opening was preferable to immediate RO_2^\bullet formation, as evidenced by observation of peaks corresponding to R5.1/R5.2-ART and $C_6H_{17}O_6$ -ART.

These observations showed that TART trapping and MS characterisation could be used to trap, detect and characterise gaseous radicals, aiding mechanism elucidation and offering support to previously hypothesised mechanisms in complex gaseous systems. Additionally, peaks corresponding to oligomers were observed, which were hypothesised to be formed following intermolecular RO_2^\bullet addition to α -pinene. Such reactions were believed to be competitive in the system used, where substrate concentrations were greater than in the atmosphere. This showed that TART-trapped radicals and products could be characterised simultaneously, a potential advantage over spin trapping with EPR spectroscopy (1.3.2.1)

D_2O exchange, tandem MS and HPLC-MS were all used to further characterise TART-trapped radicals. For example, D_2O exchange indicated that R6/R7-ART had no labile hydrogen atoms, as hypothesised. Meanwhile, HPLC-MS showed that many species contributed to TART-trapped radical peaks.

An approximate match was observed between practical kinetic experiments and a literature-sourced kinetic model.⁵⁷ However, some discrepancies between the kinetic model and kinetic

experiments for [RO-ART] were attributed to dissolved RO_2^\bullet undergoing liquid phase $\text{RO}_2^\bullet + \text{RO}_2^\bullet$ reaction, forming RO^\bullet , which was then trapped. This indicated that some reactions believed to occur in the gas phase actually occurred in the liquid phase. However, this issue equally affects other indirect radical characterisation techniques including spin trapping. These results indicated that with appropriate calibration, TART trapping with MS characterisation can be used to estimate approximate concentrations of radicals in complex systems. However, careful modelling would be required for more accurate quantification.

Future TART trapping of gaseous radicals and MS characterisation would most benefit from improved quantification. In particular, development and use of ammonium TARTs would significantly benefit TART-trapped radical quantification, as their corresponding MS intensities would be less affected by ionisation efficiency of reactant radicals. Though previously attempted, TART isolation on a solid support would likely reduce non-gaseous reactions occurring prior to TART trapping, meaning intensities of peaks corresponding to TART-trapped radicals would more accurately reflect gaseous radical reactions.

Alternatively, TART trapping of alkene ozonolysis could be undertaken using a volatile TART, such as allyl-TEMPO, and evaporated into the gas stream before being detected using CI-MS. This would increase [TART] and residence time, potentially allowing RO_2^\bullet to be more efficiently trapped. Similar systems have been used for spin trapping of alkene ozonolysis.²⁵⁶

The literature-sourced kinetic model could also be improved by adding reactions observed to occur in this system.⁵⁷ Comparison with TART trapping of other atmospherically important alkene ozonolysis systems, such as ozonolysis of isoprene, β -pinene and limonene, would also be of great interest.

TART trapping was used to investigate another atmospherically relevant gaseous radical reaction, $^\bullet\text{OH}$ -initiated alkane degradation. This system was much simpler than alkene ozonolysis, meaning literature-sourced kinetic models were likely to be more accurate. Using this model, and accurately measured [$^\bullet\text{OH}$], it was hoped that detection limits could be estimated for TART trapping of $^\bullet\text{OH}$ -initiated alkane degradation (9).

9. •OH-initiated alkane degradation

9.1. Introduction

Radicals play a key role in the initiation and propagation of atmospheric oxidation cycles of emitted VOCs, which lead to formation of SOA, photochemical smog and tropospheric ozone (1.2.3). Since hydrocarbons are known to contribute to photochemical smog and tropospheric ozone production, their emissions need to be carefully monitored and controlled.⁵⁶

Emitted hydrocarbons are broken down through atmospheric radical propagated photochemical cycles, principally initiated by tropospheric hydroxyl radicals (•OH). •OH can be formed through multiple pathways including alkene ozonolysis (8.2.1) and photolysis of ozone with water.⁵¹ Radicals produced through •OH-initiated alkane degradation could be studied using TART trapping. This would confirm production of theorised radicals and therefore aid mechanistic understanding of these important atmospheric processes.

Therefore, TART trapping was used to study •OH-initiated alkane degradation. •OH-initiated alkane degradation was chosen for study because it is a relatively simple system, particularly compared to alkene ozonolysis (8). This simplicity made it a model system for kinetic modelling, with literature-sourced rate constants likely having high accuracy. Using these suitably accurate rate constants and accurate measurement of [•OH], concentrations of gaseous radicals were estimated. This allowed detection limits of gaseous radicals using TART trapping to be estimated. To accurately measure [•OH], a collaboration was sought with the University of Leeds, which had a set-up which cleanly generated and quantified [•OH] using water photolysis and fluorescence assay gas expansion (FAGE, 1.3.1.4) respectively (9.4). Furthermore, •OH-initiated alkane degradation is an atmospherically relevant process (1.2.3).⁵⁵ TART trapping with MS characterisation was used to trap and characterise radicals and therefore aid mechanistic understanding of this important atmospheric process.

However, before TART trapping of •OH-initiated alkane degradation was undertaken at the University of Leeds using water photolysis as an •OH source (9.4), TART trapping of •OH-initiated alkane degradation was undertaken at the University of York, using alkene ozonolysis as an •OH source (9.3). This was to ensure that TART trapping could be used to characterise radicals formed during •OH-initiated alkane degradation and to optimise aspects of TART trapping and MS characterisation methodology, that were relevant to both systems. Whilst alkene ozonolysis acted as a much less clean source of •OH than water photolysis, [•OH] was much greater and therefore, more •OH-initiated alkane degradations occurred. This meant that subsequent radicals formed were of higher concentration, allowing TART trapping to occur more readily. General mechanistic steps of •OH-initiated alkane degradation are described below.

9.2. General mechanistic steps of •OH-initiated alkane degradation

The mechanisms of individual steps of •OH-initiated alkane degradation have been discussed previously (7.2). These include: HAA by •OH to form R•; subsequent RO₂• formation; RO₂•+RO₂• reaction to form two RO•, ROH and RCO or ROOR; HAA by RO₂• to form ROOH; ROOR decay to form two RO•; ROOH decay to form RO• and •OH; HAA by RO• to form R• and ROH; RO• fragmentation to form R• and RCO; α-hydroperoxide-RO• decay to form HO₂• and RCO and carboxyl RO• decay to form R• and CO₂ (Figure 171, 7.2). However, as for biochemistry, besides ROOR formation through TART trapping, ROOR product formation was largely ignored, since many possible ROOR structures would significantly complicate analysis (7).

For longer chain *n*-alkanes, such as *n*-nonane, autoxidation can occur through intramolecular HAA by RO_2^\bullet and RO^\bullet , forming $\text{R}(\text{OOH})^\bullet$ and $\text{R}(\text{OH})^\bullet$ respectively. RO^\bullet fragmentation is not expected to occur earlier in the mechanism, due to the low stability of resulting radicals.

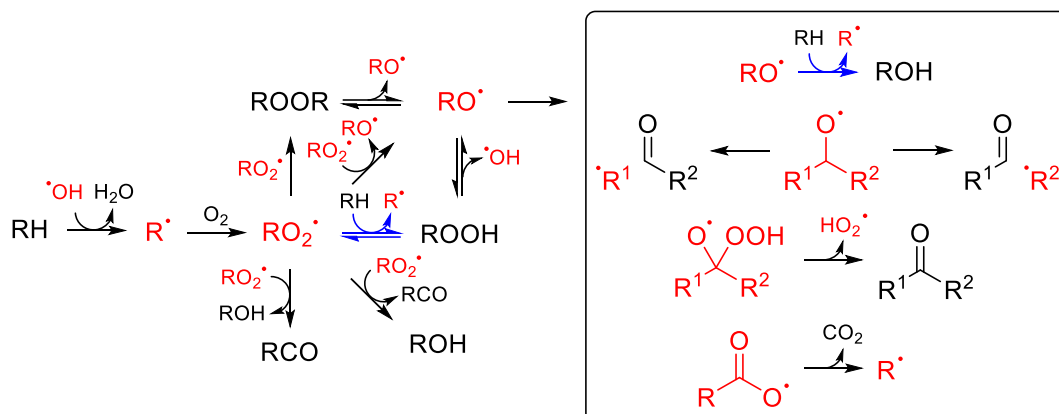


Figure 171: General reaction mechanism of $\bullet\text{OH}$ -initiated alkane degradation. For longer chain *n*-alkanes, some reactions may occur either intermolecularly or intramolecularly (blue), where reactants and products are a single species. O_2 release is not shown. RCO represents carbonyl species.

As previously in alkene ozonolysis (8.2.2), due to the high concentration of O_2 in air, R^\bullet were expected to react rapidly with O_2 to form RO_2^\bullet . Therefore, radical trapping of carbon-centred radicals was not hypothesised to occur.

For *n*-alkanes with molecular weight equal to and greater than propane, HAA from C–H can occur at multiple sites, resulting in structural isomers with identical *m/z*. *n*-Alkanes with even N_{C} atoms have N_{C} unique C–H = $0.5 \times N_{\text{C}}$ carbon atoms, whilst for odd N_{C} carbon atoms, *n*-alkanes have N_{C} unique C–H = $0.5(N_{\text{C}} \text{ carbon atoms} + 1)$. However, certain structural isomers will be formed more favourably than others, due to greater 2° radical stability formed after $\bullet\text{OH}$. This produces a range of structural isomers for subsequent species.

In the $\bullet\text{OH}$ -initiated alkane degradation system, using alkene ozonolysis for $\bullet\text{OH}$ production, a somewhat volatile liquid alkane was required. *n*-Alkanes with molecular weight equal to and between pentane and decane were suitably volatile for this purpose. *n*-Nonane and *n*-decane were deemed particularly valuable for study, since they were both predicted to undergo autoxidation and were atmospherically relevant (1.2.3). However, *n*-nonane had higher volatility. Therefore *n*-nonane was chosen as the main alkane for study. All other alkanes with molecular weight equal to and between pentane and decane were also trialled in TART trapping of $\bullet\text{OH}$ -initiated alkane degradation system, utilising alkene ozonolysis as an $\bullet\text{OH}$ source, but are not discussed.

For *n*-nonane, five structural isomers of R^\bullet were possible. The relative likelihood of formation of each isomer was estimated using a structure-reactivity relationship developed by Kwok *et al.* (Figure 172).²⁵⁷

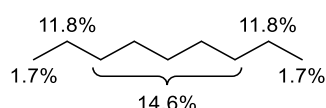


Figure 172: Percentage likelihood of HAA from each carbon environment, estimated using a structure-reactivity relationship by Kwok *et al.*²⁵⁷

$\bullet\text{OH}$ -initiated *n*-nonane degradation yields early-stage radicals RO_2^\bullet , RO^\bullet and $\text{R}(\text{OH})\text{O}_2^\bullet$ (Figure 173).

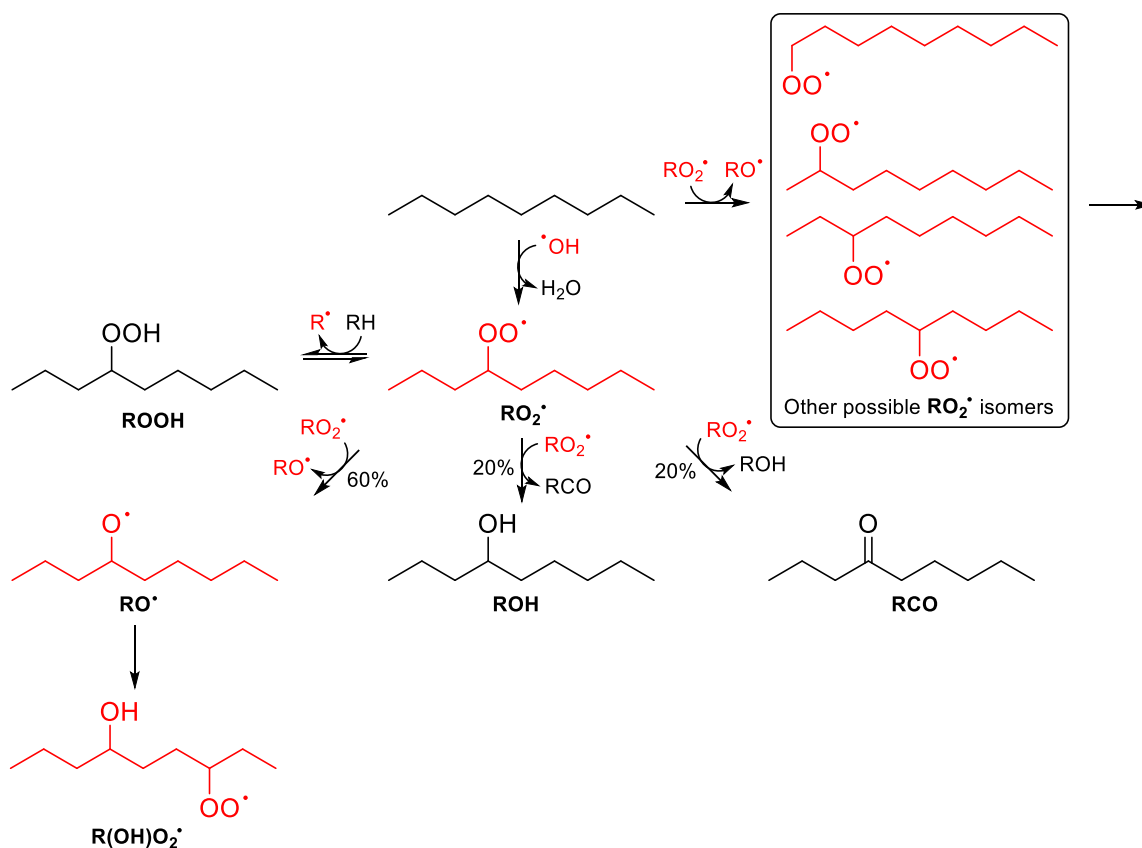


Figure 173: Early stages of $\bullet\text{OH}$ -initiated *n*-nonane degradation in absence of NO_x , showing formation of radical species $\text{RO}_2\bullet$, $\text{RO}\bullet$ and $\text{R(OH)O}_2\bullet$.^{50,57} RCO represents carbonyl species. Structures and pathway probabilities were obtained from the MCM.⁵⁷

9.3. $\bullet\text{OH}$ -initiated alkane degradation using alkene ozonolysis as an $\bullet\text{OH}$ source

$\bullet\text{OH}$ -initiated alkane degradation was investigated using alkene ozonolysis as an $\bullet\text{OH}$ source. As discussed and explored previously, decomposition of Criegee intermediates from alkene ozonolysis released $\bullet\text{OH}$. This $\bullet\text{OH}$ could be utilised for alkane degradation. An advantage of this method was that the system produced high $[\bullet\text{OH}]$, inducing much alkane degradation. However, the system was not particularly clean, as alkene ozonolysis radicals and products could react with $\bullet\text{OH}$ -initiated alkane degradation radicals and products, creating additional radicals and products. These additional radicals and alkene ozonolysis radicals could be TART trapped and, along with additional products and alkene ozonolysis products, significantly complicated mass spectra.

The set-up previously used for TART trapping of alkene ozonolysis was easily adapted for TART trapping of $\bullet\text{OH}$ -initiated alkane degradation.

9.3.1. Methodology

TART trapping of $\bullet\text{OH}$ -initiated alkane degradation, using alkene ozonolysis as an $\bullet\text{OH}$ source, was investigated using a standard set-up (Figure 143, 11.8.1.1). This system closely resembled the set-up used for TART trapping of alkene ozonolysis (8.3) but with alkane vapour being added into the air stream prior to being passed over the UV lamp.

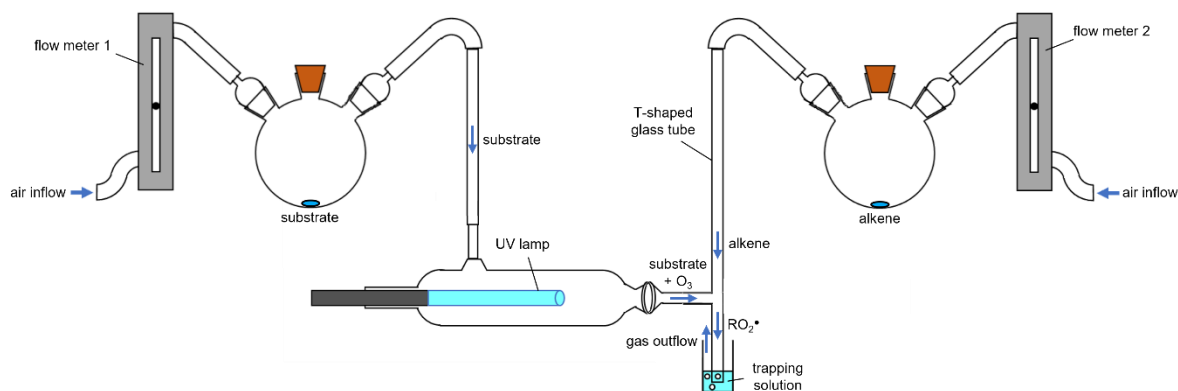


Figure 174: Set-up used for TART trapping of $\bullet\text{OH}$ -initiated alkane degradation, using alkene ozonolysis as an $\bullet\text{OH}$ source (11.8.1.1).

Most set-up parameters were the same as for TART trapping of alkene ozonolysis (8.3, 11.7.1). In this set-up, it was assumed that flow was laminar and mixing occurred instantly at the T-junction. Different length T-shaped glass tubes could be used to increase residence time for substrate reaction with ozone, with typical residence length set at 5.0 cm. TART functionality was chosen as required, however typically CHANT was used. [TART] was set between 5-500 μM in MeCN but was typically 50 μM . Flow rate through trap solution was set at 1.5 L min^{-1} , to ensure rapid but controllable bubbling. Flow rate through each bubbler was adjusted as required, but was typically set at 1.20 and 0.30 L min^{-1} through substrate and alkene flow meters respectively. These flow rates were selected to increase [alkane] to [alkene] ratio but were suitably high to accurately maintain each flow rate. Under these standard conditions and in absence of substrate, alkene or trapping solution, [ozone] was measured to be 106.3 ± 0.2 ppm ($2.663 \pm 0.005 \times 10^{15}$ molec. cm^{-3}). Reaction time was varied as required, but was typically 10 min. Solvent was removed *in vacuo* upon reaction completion and the resultant MS characterised. These standard conditions had been optimised (9.3.3).

Alkanes do not absorb light at the wavelengths emitted by the UV lamp and therefore alkane ozonolysis could not occur.²⁵⁸ Furthermore, literature indicated gaseous alkane ozonolysis would be negligible in this system. Therefore, alkane could be inputted through the UV lamp/ozone stream without compromising the experiment.

In all discussed reactions, *n*-nonane (C_9H_{20}) and tetramethylethylene (TME, C_6H_{12}) were used as substrate and alkene respectively. TME was used as alkene for several reasons. Firstly, at RTP, TME reacted with ozone very rapidly (1×10^{-10} molec. $^{-1}$ cm^3 s^{-1}) compared to other alkenes, for example α -pinene (5×10^{-11} molec. $^{-1}$ cm^3 s^{-1}).⁵⁷ This meant that $\bullet\text{OH}$ would be produced relatively rapidly and in high yields ($\sim 90\%$ from TME reaction with ozone).²⁵⁹ Secondly, all non-dimerised TME-derived radicals had fewer carbon atoms than non-fragmented *n*-nonane-derived radicals, meaning that peaks corresponding to TART-trapped non-fragmented *n*-nonane-derived radicals were unlikely to correspond to TME-derived radicals, reducing the risk of false positives. Based upon oligomerisation observed in alkene ozonolysis (8.6.3.6), it seemed likely than *n*-nonane would oligomerise with unreacted TME. However, these reactions were ignored.

In this system, all studied alkanes and alkenes were significantly in excess of ozone. For example, gaseous [TME] and [*n*-nonane] were estimated to be 9.07×10^{17} molec. cm^{-3} and 8.07×10^{16} molec. cm^{-3} respectively, a >100 and >30 fold excess compared to ozone respectively (11.8.1.1). Therefore, the vast majority of ozone was expected to react with unreacted alkene and not with other species formed in the system. Therefore, re-initiation of stable products formed in this system such as ROH and RCO would be unlikely to occur and

hence was largely ignored. It is important to note that this system does not reflect atmospheric concentrations of these species and hence, these species may not undergo typical atmospheric reactions.

With the set-up designed, TART trapping of •OH-initiated alkane degradation, using alkene ozonolysis as an •OH source, was undertaken (Figure 175).

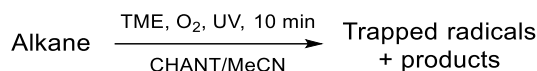


Figure 175: TART trapping of •OH-initiated alkane degradation, using alkene ozonolysis as an •OH source (11.8.1.2).

Initial experiments were conducted to ensure that early-stage •OH-initiated alkane degradation radicals could be successfully TART trapped, before optimisation, controls and detailed result analysis were undertaken.

9.3.2. Initial results

Species formed early in •OH-initiated *n*-nonane degradation were screened for (Figure 173, Table 50, 11.8.1.2).

Table 50: Species identified from initial TART trapping of •OH-initiated *n*-nonane degradation, using alkene ozonolysis as an •OH source and MS for characterisation (11.8.1.2). Systematic *m/z* error = -0.0005; random *m/z* error = ±0.0003; 100% intensity = 1.38×10⁹ absolute count.

Species	Predicted <i>m/z</i>	Intensity relative to unreacted TART standard / %			
		Trapless control	TART standard	Trapping reaction	
TART	[CHANT+H] ⁺	323.2698	0	100	27.9
Trapped radicals	[RO ₂ -ART+Na] ⁺	348.2515	0	0	0.041
	[RO-ART+Na] ⁺	332.2565	0	0	0.054
Products	[RH+Na] ⁺	151.1463	0	0	0
	[ROH+Na] ⁺	167.1412	0	0	0
	[RCO+Na] ⁺	165.1255	0.011	0	0.011
	[ROOH+Na] ⁺	183.1361	0.061	0	0.142

Intensity of peaks corresponding to TART was ~30% in the trapping reaction compared to the unreacted TART standard, indicating ~70% TART consumption.

Peaks corresponding to RCO and ROOH were observed in both the trapless control and trapping reaction. This was expected, as TART was not required for product formation. In contrast, peaks corresponding to RH and ROH were not detected in any sample. This was hypothesised to be due to poor ionisability of these species.

Peaks corresponding to TART-trapped radicals were detected exclusively in the trapping reaction, suggesting these species originated from TART trapping of radicals formed during •OH-initiated *n*-nonane degradation.

Therefore, initial results showed radicals produced during •OH-initiated *n*-nonane degradation, using alkene ozonolysis as an •OH source, were successfully TART trapped and observed using MS. However, before more detailed investigations were undertaken, system optimisation was required to maximise intensity of MS peaks corresponding to TART-trapped radicals. More importantly, these optimised conditions would initially be used for •OH-initiated *n*-nonane degradation, using water photolysis as an •OH source.

9.3.3. Optimisation

Many parameters and design aspects of •OH-initiated alkane degradation, using alkene ozonolysis as an •OH source, were based upon parameters and design aspects optimised for α -pinene ozonolysis (8.6.2), including TART phase, TART functionality, solvent and additives and residence time. However, other parameters required optimisation for this system. Hence these parameters were optimised to maximise intensity of MS peaks corresponding to TART-trapped radicals. These included TART concentration, reaction time and HPLC-MS conditions (9.3.4).

TART concentration was optimised to achieve maximum intensity of peaks corresponding to TART-trapped radicals compared to unreacted TART. Once appropriately diluted, this achieved maximum absolute TART-trapped radical signal intensity, increasing S/N and therefore making TART-trapped radicals as distinguishable as possible. In absence of TART-removing purification techniques, this was the best way to observe maximum TART-trapped radical intensity. Different concentrations of 5-500 μ M CHANT were trialled under otherwise standard conditions of •OH-initiated alkane degradation, using alkene ozonolysis as an •OH source (11.8.1.3).

Table 51: Species identified from TART trapping of •OH-initiated *n*-nonane degradation at different concentrations of TART, using alkene ozonolysis as an •OH source and MS for characterisation (11.8.1.3). Systematic *m/z* error = -0.0003; random *m/z* error = ± 0.0005 ; 100% intensity = 1.89×10^9 absolute count.

Species		Predicted <i>m/z</i>	Intensity relative to unreacted TART in 500 μ M sample / %		
			500 μ M	50 μ M	5 μ M
TART	[CHANT+H] ⁺	323.2698	100	36.1	10.7
Trapped radicals	[RO ₂ -ART+Na] ⁺	348.2515	0.005	0.041	0.006
	[RO-ART+Na] ⁺	332.2565	0.017	0.160	0.012
Products	[RH+Na] ⁺	151.1463	0	0	0
	[ROH+Na] ⁺	167.1412	0	0	0
	[RCO+Na] ⁺	165.1255	0	0	0.001
	[ROOH+Na] ⁺	183.1361	0.004	0.053	0.035

Peaks corresponding to TART-trapped radicals were observed with maximum intensity in presence of 50 μ M CHANT, Therefore, this TART concentration was deemed optimal.

Reaction time was optimised to maximise intensity of peaks corresponding to TART-trapped radicals, both absolutely and relative to unreacted TART. Different reaction times were trialled under otherwise standard conditions of TART trapping of •OH-initiated alkane degradation, using alkene ozonolysis as an •OH source (Figure 151, 11.8.1.3).

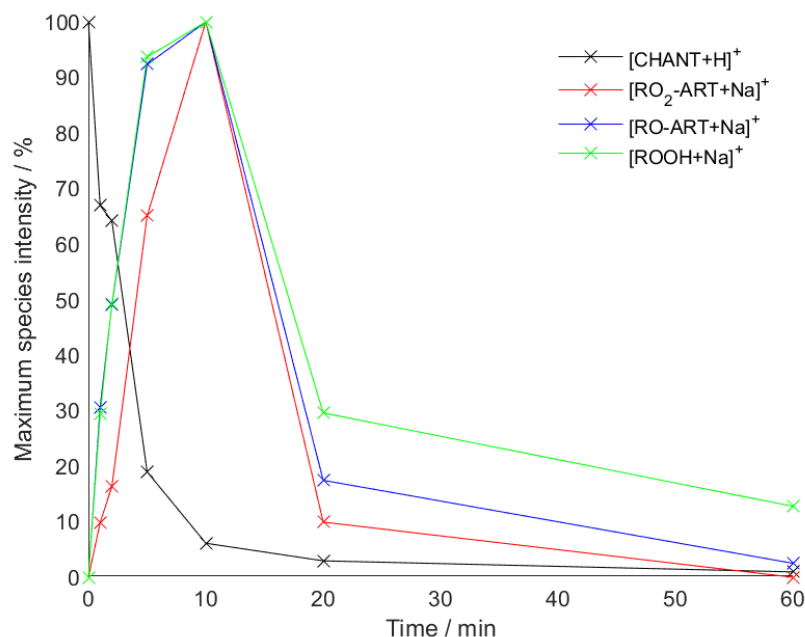


Figure 176: Species identified from TART trapping of $\bullet\text{OH}$ -initiated alkane degradation at different reaction times, using alkene ozonolysis as an $\bullet\text{OH}$ source and MS for characterisation (11.8.1.3). Species are scaled to show their maximum values at 100% intensity. Systematic m/z error = -0.0003 ; random m/z error = ± 0.0006 .

Intensity of the MS peak corresponding to CHANT, implying CHANT concentration, was observed to decrease exponentially with time. CHANT concentration was estimated to have decreased to $\sim 60\%$ after 2 min, $\sim 20\%$ after 5 min and $<10\%$ after 10 min.

Peaks corresponding to TART-trapped $\text{RO}_2\bullet$ and $\text{RO}\bullet$ were observed with greatest intensity after 10 min. Maximum intensity observed after 10 min indicated that, after this time, $\text{RO}_2\text{-ART}$ and RO-ART formation was slower than their consumption. This was likely due to slower TART trapping of $\text{RO}_2\bullet$ and $\text{RO}\bullet$ caused by decreased [TART], being outweighed by side reactions of TART-trapped radicals with incoming gaseous species.

From these data, it was decided that 10 min was the optimal reaction time. With these optimised conditions, TART trapping experiments were repeated along with control reactions. From these, more detailed analysis could be undertaken.

9.3.4. Detailed results and controls

TART trapping of $\bullet\text{OH}$ -initiated *n*-nonane degradation, using alkene ozonolysis as an $\bullet\text{OH}$ source (three repeats) and control reactions were carried out using optimised conditions (11.8.1.2). Each control omitted a single condition required for TART-trapped radical formation: no substrate, no alkene, no O_2 (replaced with N_2), no UV, no TART and an unreacted TART standard (set as 100% relative intensity). MS was then used to characterise these reaction mixtures.

Basic conclusions could be made by making observations on the overall MS spectrum of $\bullet\text{OH}$ -initiated *n*-nonane degradation CHANT TART trapping, utilising TME ozonolysis for $\bullet\text{OH}$ production (Figure 177).

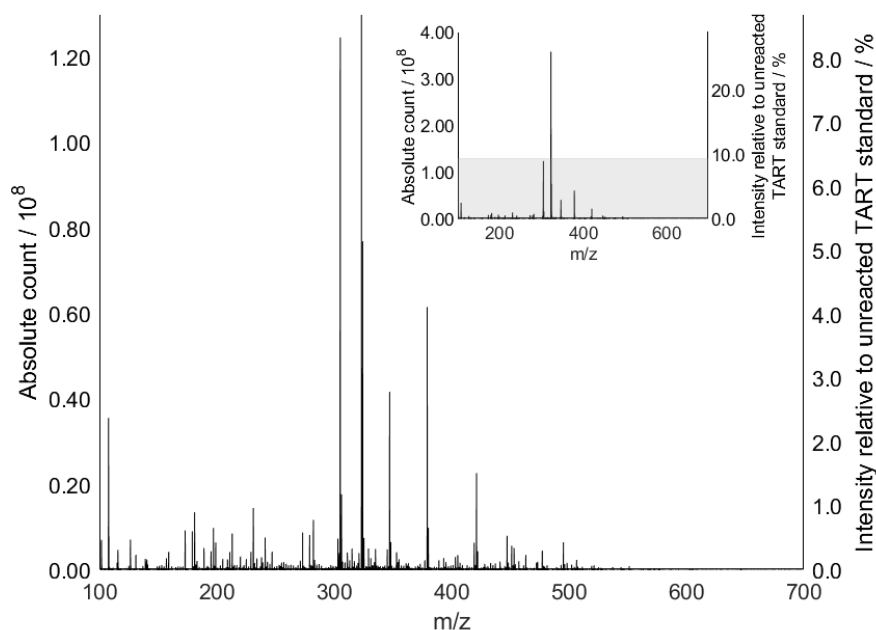


Figure 177: Background corrected mass spectrum from optimised TART trapping of •OH-initiated *n*-nonane degradation, using alkene ozonolysis as an •OH source (11.8.1.2).

Peaks corresponding to unreacted TART dominated the mass spectrum, indicating not all TART had reacted. This was desirable, since dominating TART concentration should have mitigated side reactions between TART-trapped radicals and incoming gaseous species. However, other species were within an order of magnitude intensity.

In this •OH-initiated *n*-nonane degradation system, all non-fragmented radicals were predicted to have molecular formula $C_9H_{19}O_y\bullet$, where y was degree of oxygenation, not expected to exceed four. This was because multiple initiations were unlikely and fragmentation was likely to occur before further oxygenation. Therefore, all iterations of TART-trapped radicals, based upon these criteria, were screened for (Table 52).

Table 52: Species identified from optimised TART trapping of •OH-initiated *n*-nonane degradation and controls, using alkene ozonolysis as an •OH source and MS for characterisation (11.8.1.2). No TART control showed no peaks corresponding to those in the table. Systematic m/z error = -0.0005; random m/z error = ± 0.0005 ; 100% intensity = 1.38×10^9 absolute count.

Species	Predicted m/z	Intensity relative to unreacted TART standard / %					Trapping reactions ^a
		No substrate	No alkene	No O ₂	No UV		
[CHANT+H] ⁺	323.2698	28.3	0	44.7	43.4	26.1±0.9	
[RO-ART+Na] ⁺	332.2565	0	0	0.008	0.004	0.044±0.004	
[RO ₂ -ART+Na] ⁺	348.2515	0	0	0.009	0	0.043±0.003	
[R(OH)O-ART+Na] ⁺							
[R(OH)O ₂ -ART+Na] ⁺	364.2464	0.002	0	0.008	0	0.064±0.009	
[R(OOH)O-ART+Na] ⁺							
[R(OH) ₂ O-ART+Na] ⁺							
[R(OOH)O ₂ -ART+Na] ⁺	380.2413	0.005	0.017	0.018	0	0.11±0.02	
[R(OH) ₂ O ₂ -ART+Na] ⁺							
[R(OH)(OOH)O-ART+Na] ⁺							
[R(OH) ₃ O-ART+Na] ⁺							

^aThree repeats undertaken and an average and associated error calculated.

TART corresponding peaks were observed with ~25% intensity in trapping reactions compared to the unreacted TART standard, indicating ~75% TART was consumed during the trapping reactions. Similar intensity was observed in the no substrate control, likely due to TART reaction with radicals formed during TME ozonolysis. Peaks indicated that All TART was consumed in absence of alkene, as was previously observed in alkene ozonolysis (8.4).

Peaks corresponding to all TART-trapped radicals were observed with significantly greater intensity in the trapping reactions than in any control reactions. TART-trapped RO₂• and RO• corresponding peaks were clearly distinguishable from neighbouring peaks (Figure 178).

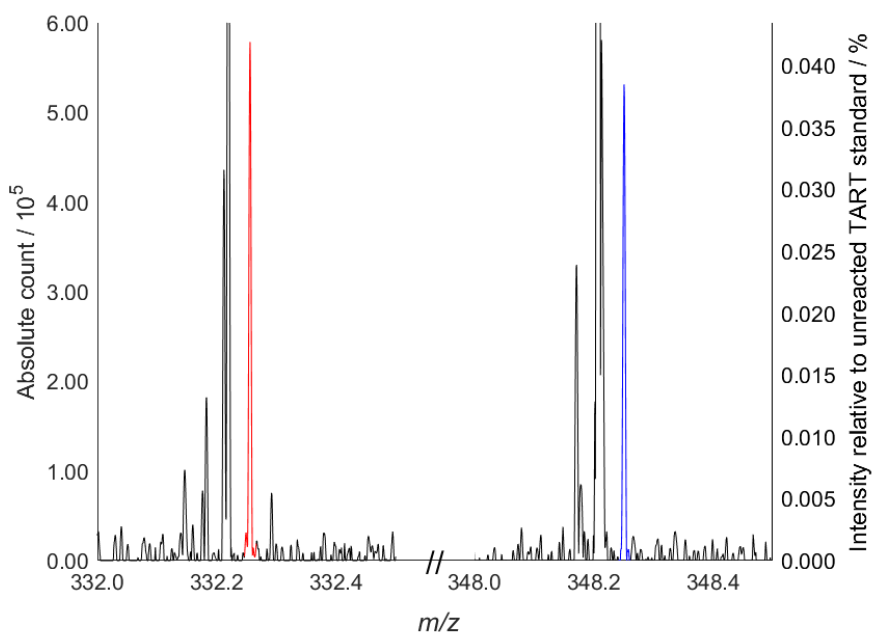


Figure 178: Background corrected mass spectrum from optimised TART trapping of •OH-initiated *n*-nonane degradation, using alkene ozonolysis as an •OH source (11.8.1.2), showing peaks corresponding to RO₂-ART (*m/z* 348.251, blue) and RO-ART (*m/z* 332.257, red). 100% intensity = 1.38×10⁹ absolute count.

These data positively indicated that •OH-initiated *n*-nonane degradation radicals could be TART trapped and MS characterised. Additionally, HPLC-MS was conducted to optimise HPLC-MS conditions for characterisation of TART trapping of •OH-initiated alkane degradation, using water photolysis as an •OH source. Optimised conditions were obtained which yielded relatively high intensity of peaks corresponding to TART-trapped radicals (Figure 179).

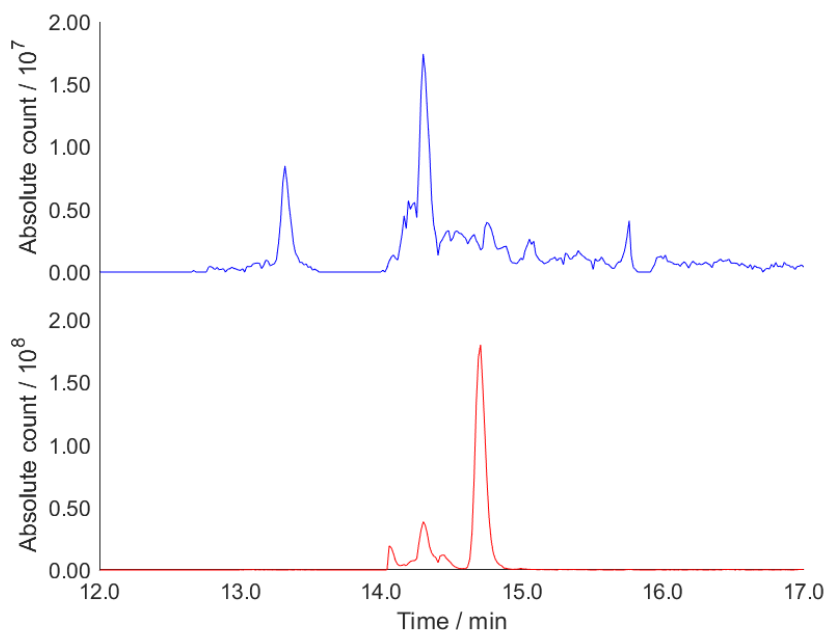


Figure 179: HPLC-MS chromatograms of peaks corresponding to RO₂-ART (m/z 326.270±0.002 and m/z 348.251±0.002, top, blue) and RO-ART (m/z 310.275±0.002 and m/z 332.257±0.002, bottom, red) from TART trapping of •OH-initiated *n*-nonane degradation, using alkene ozonolysis as an •OH source (11.8.1.2). HPLC output was sent to waste between 13.5-14.0 min, to prevent spectrometer contamination by unreacted TART.

As was previously observed for TART trapping of α -pinene ozonolysis, HPLC-MS yielded significantly greater intensity for peaks corresponding to RO-ART than RO₂-ART, despite these peaks being observed with similar intensity in standard MS (8.6.3.5). This was hypothesised to be due to trace metals in the HPLC column catalysing peroxide bond degradation in RO₂-ART.

TART trapping had been successfully used to investigate radicals produced during •OH-initiated *n*-nonane degradation. Furthermore, many conditions had been optimised to increase intensity of peaks corresponding to TART-trapped radicals, including for HPLC-MS characterisation. Therefore, it was decided that TART trapping of •OH-initiated *n*-nonane degradation, using water photolysis as an •OH source, could be undertaken in collaboration with the University of Leeds.

9.4. •OH-initiated *n*-nonane degradation, using water photolysis as an •OH source

TART trapping of •OH-initiated *n*-nonane degradation was investigated, using water photolysis as an •OH source. Water photolysis generates •OH and H•, with H• rapidly reacting with O₂ to form HO₂•.²⁶⁰ •OH could then react with *n*-nonane. An existing University of Leeds set-up for •OH-initiated alkane degradation was adapted to allow TART trapping.

9.4.1. Methodology

TART trapping of •OH-initiated *n*-nonane degradation, using water photolysis as an •OH source, was investigated using a standard set-up (Figure 180, 11.8.2). This set-up mixed water vapour and *n*-nonane vapour before being passed through a UV lamp, photolysing the water into •OH and HO₂• (collectively known as HO_x•). •OH and *n*-nonane then reacted before being bubbled through TART trapping solution.

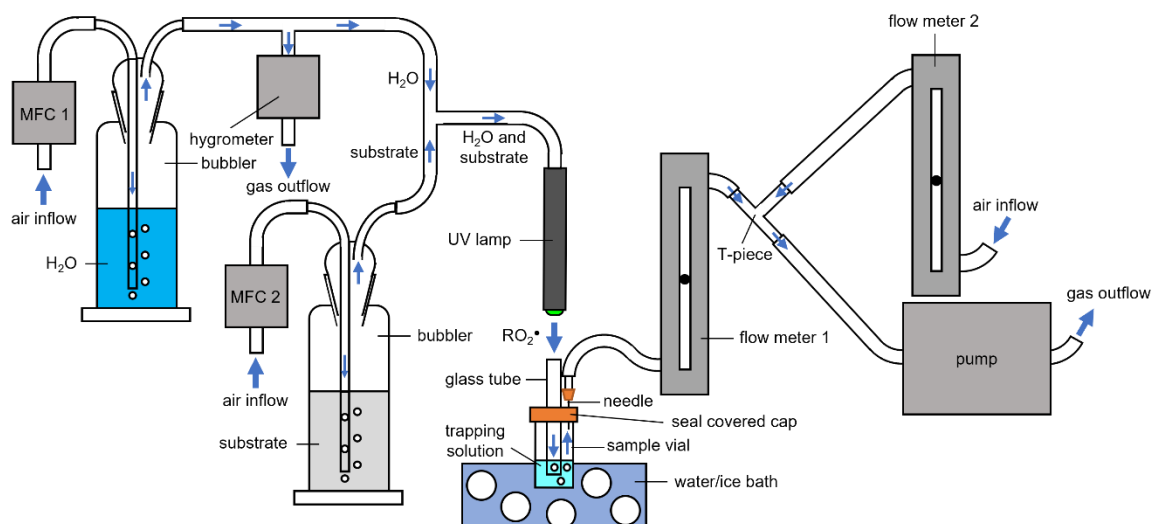


Figure 180: Set-up used for TART trapping of $\bullet\text{OH}$ -initiated alkane degradation, using water photolysis as an $\bullet\text{OH}$ source (11.8.2).

This set-up amalgamated two set-ups, the first designed by the University of Leeds for $\bullet\text{OH}$ -initiated alkane degradation (before and including the UV lamp) and the second self-designed for TART trapping (after and including the glass tube).

The water photolysis system (University of Leeds system, with no substrate) was calibrated offline. This involved using fluorescence assay gas expansion (FAGE) to measure a range of $[\text{HO}_x\bullet]$ ($\text{HO}_x\bullet = \bullet\text{OH} + \text{HO}_2\bullet$) produced depending on photon flux (measured using N_2O actinometry), irradiation time and $[\text{H}_2\text{O}]$ (measured using a hygrometer), as described by Onel *et al.*²⁶⁰ This calibration allowed accurate online $[\text{HO}_x\bullet]$ calculation.

In this set-up, it was assumed that flow was laminar. Different length T-shaped glass tubes could be used to increase residence time for substrate reaction with $\bullet\text{OH}$, with typical residence length set at 8.0 cm. TART functionality was chosen as required, however typically CHANT or DEADANT were used. $[\text{TART}]$ was set between 50-5000 μM in MeCN but was typically 50 μM . Flow rate through mass flow controller (MFC) 1 was set at 10 L min^{-1} , with 1 L min^{-1} being passed through the hygrometer to measure $[\text{H}_2\text{O}]$. Flow rate through MFC 2 was set at 1 L min^{-1} . Mixing these two flows created a flow rate through the UV lamp of 10 L min^{-1} . Glass tube was placed butt up to the UV lamp outflow. Flow rate through trap solution was set at 1.5 L min^{-1} , to ensure rapid but controllable bubbling. This meant that most UV lamp outflow was dispersed into the atmosphere. Under these standard conditions and in absence of substrate or trapping solution, gaseous $\bullet\text{OH}$ concentration was measured to be $\sim 3.4 \pm 0.5 \times 10^{11} \text{ molec. cm}^{-3}$ or $\sim 14 \pm 2 \text{ ppb}$. Reaction time was varied as required but was typically 10-100 min. Solvent was removed *in vacuo* upon reaction completion and the resultant MS characterised.

Alkanes do not absorb light at the wavelengths emitted by the UV lamp and therefore reaction was initiated exclusively by water photolysis.²⁵⁸ Therefore, alkane could be inputted through the UV lamp stream without compromising the experiment. Water photolysis generates $\bullet\text{OH}$ and $\text{HO}_2\bullet$. $\bullet\text{OH}$ can then react with alkane. Additional air (through flow meter 2) mixed with the set-up exhaust and a water/ice bath were used to ensure outputted gaseous $[\text{MeCN}]$ was below its explosion limit. Furthermore, this ensured that the trapping solution remained at constant temperature, improving the reproducibility of the experiment. However, the water/ice bath also likely reduced TART trapping rate.

In the set-up, gaseous [*n*-nonane] was estimated to be $\sim 1.0 \times 10^{16}$ molec. cm^{-3} , a $> 1 \times 10^4$ excess compared to $\bullet\text{OH}$, ensuring nearly all $\bullet\text{OH}$ was converted to $\text{RO}_2\bullet$ (11.8.2).

With the set-up designed, TART trapping of $\bullet\text{OH}$ -initiated *n*-nonane degradation, using water photolysis as an $\bullet\text{OH}$ source, was undertaken (Figure 181). Graham Boustead performed all trapping reactions and controls of $\bullet\text{OH}$ -initiated *n*-nonane degradation. MS characterisation and mass spectra analysis performed by the author.

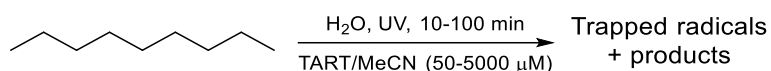


Figure 181: TART trapping of $\bullet\text{OH}$ -initiated *n*-nonane degradation, using water photolysis as an $\bullet\text{OH}$ source.

9.4.2. Experimental results

CHANT trapping of $\bullet\text{OH}$ -initiated *n*-nonane degradation and no TART controls, using water photolysis as an $\bullet\text{OH}$ source, were originally undertaken (11.8.2). [TART] used was 50-5000 μM and reaction times used were 10-100 min. Standard MS yielded TART-trapped radicals with unreliably weak intensity and therefore, HPLC-MS was conducted using highly concentrated samples and the source-waste function to remove unreacted TART.

However, when *n*-nonane was used as substrate, peaks corresponding to RO-ART were observed exclusively in the trapping reaction (Figure 182). Highest peak intensities were observed for 50 μM CHANT after 100 min, with the peak corresponding $[\text{RO-ART}+\text{H}]^+$ being significantly greater intensity than its neighbouring peaks (Figure 183). It was surprising that weaker intensities of peaks corresponding to RO-ART were observed using higher [TART]. This was later justified using kinetic modelling (9.4.3).

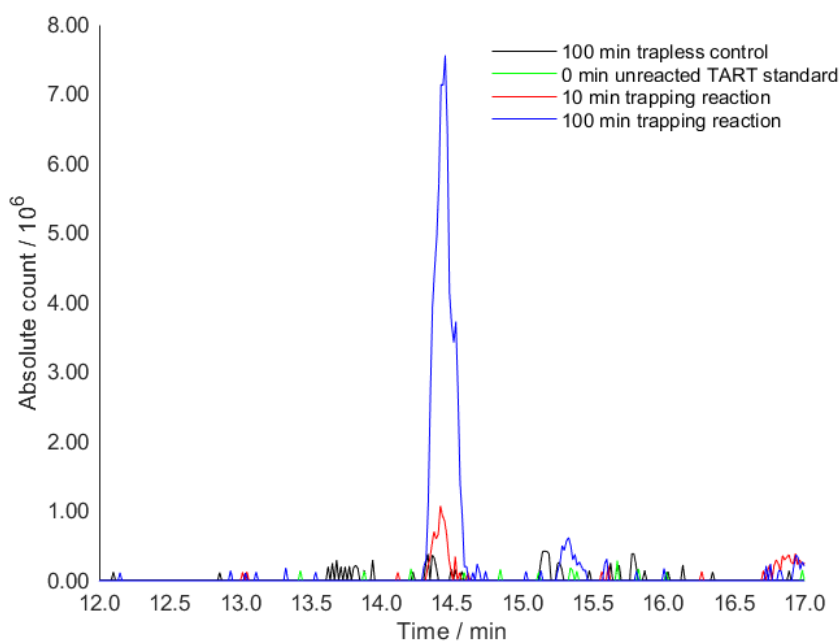


Figure 182: HPLC-MS chromatograms of peaks corresponding to RO-ART (m/z 310.275 \pm 0.002 and m/z 332.257 \pm 0.002) from TART trapping of $\bullet\text{OH}$ -initiated *n*-nonane degradation, using water photolysis as an $\bullet\text{OH}$ source and CHANT as TART, after 10 min, 100 min and with controls (11.8.2). HPLC output was sent to waste between 13.5-14.0 min, to prevent spectrometer contamination by unreacted TART.

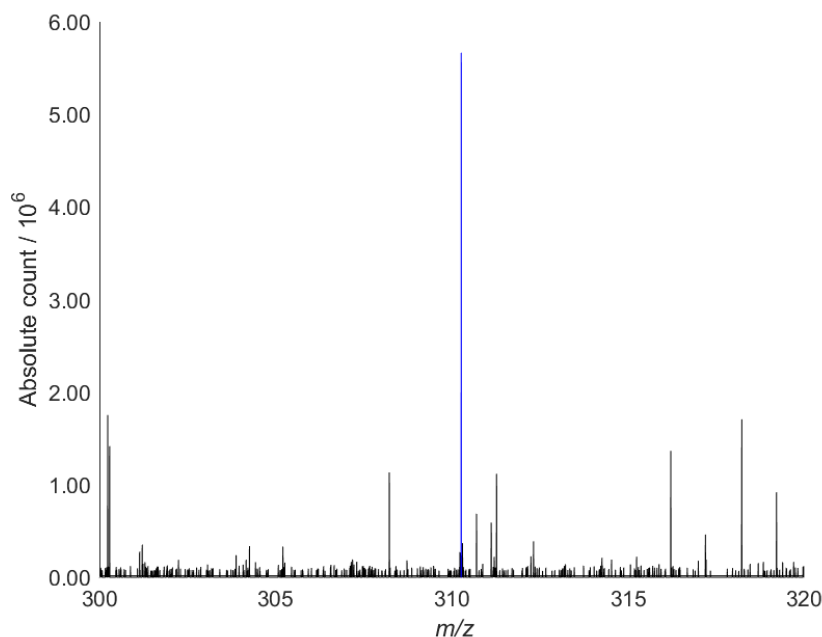


Figure 183: HPLC-MS mass spectrum at time of maximum intensity of peak corresponding to RO-ART (m/z 310.275 \pm 0.002, 14.4 min) corresponding peak (blue) from TART trapping of \bullet OH-initiated *n*-nonane degradation, using water photolysis as an \bullet OH source, using CHANT as TART, after 100 min (11.8.2).

This was a good result. However, peaks corresponding to RO₂-ART were observed with similar intensity across all samples, including controls (SI7.1). This meant that formation of RO₂-ART could not be confirmed. This was surprising, since TART trapping of \bullet OH-initiated *n*-nonane degradation, using alkene ozonolysis as an \bullet OH source, had yielded similar intensities of peaks corresponding to RO₂-ART and RO-ART (9.3.4). However, HPLC-MS of TART trapping of \bullet OH-initiated *n*-nonane degradation, using alkene ozonolysis as an \bullet OH source, had yielded significantly greater intensity for peaks corresponding to RO-ART than RO₂-ART (9.3.4). This was hypothesised to be due to trace metals in the HPLC column catalysing peroxide bond degradation in RO₂-ART. This was a disappointing result, as a detection limit for [RO₂ \bullet] was strongly desired. Since peaks corresponding to RO-ART were observed, it was theorised that RO₂ \bullet must have been formed, but [RO₂ \bullet] was below the detection limit. Therefore, strategies to increase intensity of peaks corresponding to RO₂-ART were considered.

For previous investigations involving TART trapping of gaseous radicals, ozone required for alkene ozonolysis had prevented use of DEADANT, as it quickly became oxidised, complicating mass spectra. However, in TART trapping of \bullet OH-initiated *n*-nonane degradation, using water photolysis as an \bullet OH source, very little ozone was generated. Therefore, DEADANT was trialled as TART in this system, as DEADANT-trapped radicals had 3^o amine functionality, making them highly ionisable in HPLC-MS. Minimal DEADANT oxidation occurred during TART trapping reactions (<2%, SI7.1).

DEADANT trapping of \bullet OH-initiated *n*-nonane degradation and no TART controls, using water photolysis as an \bullet OH source, were undertaken and characterised using HPLC-MS and the source-waste function (4.3.2.8). [TART] used was 50-500 μ M and reaction times used were 10-100 min. Five peaks corresponding to RO-ART were observed exclusively in the trapping reaction, believed to correspond to the five possible isomers of RO \bullet (Figure 184). Intensities of these peaks were observed an order of magnitude greater than when CHANT was used as TART, as desired. Highest peak intensities were observed for 50 μ M DEADANT after 10 min.

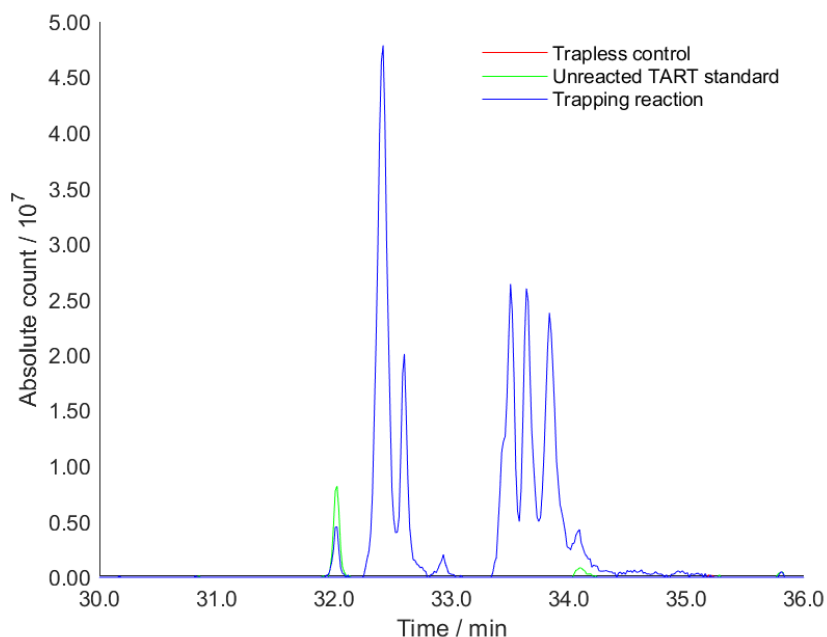


Figure 184: HPLC-MS chromatograms of the peak corresponding to RO-ART (m/z 299.270 \pm 0.002) from TART trapping of \bullet OH-initiated *n*-nonane degradation, using water photolysis as an \bullet OH source and DEADANT as TART, with controls (11.8.2). The five distinct peaks observed in the trapping reaction are believed to correspond to the five possible RO \bullet structural isomers.

However, as previously peaks corresponding to RO₂-ART were observed with similar intensity across all samples, including controls (SI7.1). This was again a disappointing result. No further optimisation was undertaken. However, there was sufficient evidence that RO-ART had been formed.

9.4.3. Kinetic modelling and detection limit estimation

Kinetic modelling was undertaken to estimate the detection limits of [RO \bullet] using TART trapping with MS characterisation (11.10.4). For gaseous \bullet OH-initiated *n*-nonane degradation, atmospheric reactions of substrates were imported into the Kintecus chemical simulation programme from the MCM and truncated to remove late stage pathways.^{57,207} Due to the relative simplicity of this reaction, the MCM was likely to be accurate. As for modelling of α -pinene ozonolysis, potential wall reactions were ignored and simulation conditions were set at RTP (8.6.3.7). These assumptions were made to significantly simplify modelling, though were unlikely to be true.

Simulation parameters were set to emulate experimental conditions immediately prior to bubbling through trapping solution, including residence time and initial substrate concentrations (11.10.4). The simulation results yielded final gaseous radical concentrations, immediately prior to bubbling (Figure 185).

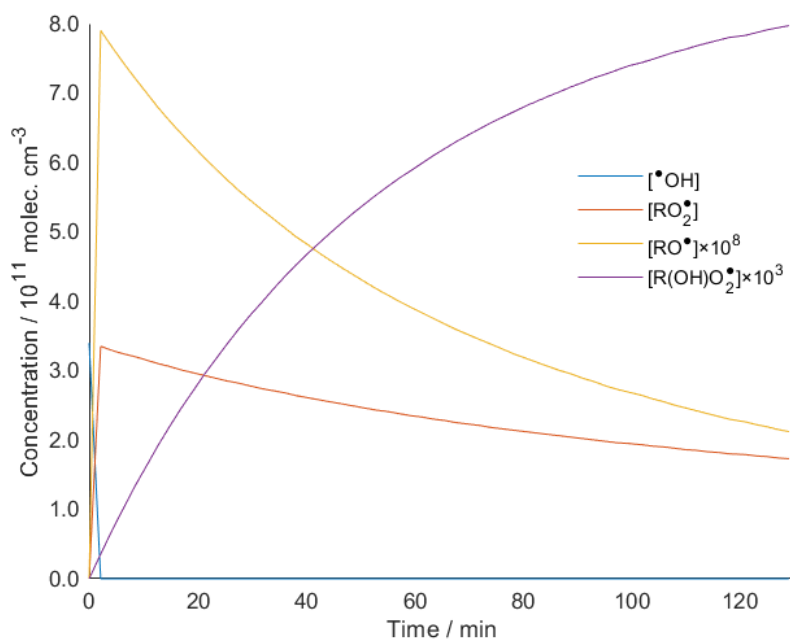


Figure 185: Modelling of $\bullet\text{OH}$ -initiated *n*-nonane degradation immediately prior to trapping, showing gaseous $[\bullet\text{OH}]$ (blue), $[\text{RO}_2\bullet]$ (orange), $[\text{RO}\bullet]\times 10^8$ (yellow) and $[\text{R(OH)O}_2\bullet]\times 10^3$ (purple).

This simulation indicated final gaseous $[\text{RO}_2\bullet]$ and $[\text{RO}\bullet]$ were $1.73\pm 0.14\times 10^{11}$ molec. cm^{-3} and $2.1\pm 0.3\times 10^3$ molec. cm^{-3} respectively. These errors were calculated through simulation using upper and lower $[\bullet\text{OH}]$ bounds. Therefore, this was the concentration of radicals at the gas-liquid interface. On face value, this seems to suggest that the detection limit of $[\text{RO}\bullet]$ using TART trapping with MS characterisation was $2.1\pm 0.3\times 10^3$ molec. cm^{-3} , which would be an astonishingly low detection limit. However, assuming that all $\text{RO}\bullet$ were trapped by TART, this would create a liquid-phase $[\text{RO-ART}]$ of $\sim 5\times 10^{-14}$ M. This was at the very lowest detection limits of ESI-MS (10^{-14} - 10^{-18}).¹⁵⁸ Therefore, it was deemed unlikely that this $\text{RO}\bullet$ was all formed in the gas phase.

As was discussed for TART trapping of α -pinene ozonolysis (8.6.4), it was theorised that during TART trapping of $\bullet\text{OH}$ -initiated *n*-nonane degradation, dissolved $[\text{RO}_2\bullet]$ steadily increased during the reaction time and that instead of radical reactions stopping upon reaching the trapping solution, dissolved $\text{RO}_2\bullet$ could undergo $\text{RO}_2\bullet + \text{RO}_2\bullet$ to form $\text{RO}\bullet$. Whilst dissolved $\text{RO}_2\bullet$ was trapped slowly, dissolved $\text{RO}\bullet$ was trapped immediately. This theory implied that most $\text{RO}\bullet$ were formed in solution.

Retrospectively, this offered an explanation as to why previously, greatest intensity was observed for peaks corresponding to RO-ART using least concentrated $[\text{TART}]$. Free $\text{TEMPO}\bullet$ in the trapping solution (measured as $\sim 0.05\%$ of TART, 3.5.2) reduced dissolved $\text{RO}_2\bullet$ to form TEMPO^+ oxoammonium cation and peroxide anion RO_2^- , competing with $\text{RO}_2\bullet + \text{RO}_2\bullet$ to form $\text{RO}\bullet$. $\text{RO}_2\bullet$ reduction by $\text{TEMPO}\bullet$ occurs rapidly with rate constant $\sim 10^7$ - 10^8 $\text{M}^{-1} \text{s}^{-1}$ ($\sim \text{RTP}$).²⁶¹ Using $[\text{RO}_2\bullet]$ obtained through modelling, at $50 \mu\text{M}$ $[\text{TART}]$, concentration of free $\text{TEMPO}\bullet$ to $\text{RO}_2\bullet$ was estimated to be $\sim 1:10$, indicating $\text{RO}_2\bullet$ was significantly in excess and therefore, available to undergo $\text{RO}_2\bullet + \text{RO}_2\bullet$ to form $\text{RO}\bullet$, which was subsequently trapped. However, at $5000 \mu\text{M}$ $[\text{TART}]$, concentration of free $\text{TEMPO}\bullet$ to $\text{RO}_2\bullet$ was estimated to be $\sim 10:1$, likely meaning reduction of $\text{RO}_2\bullet$ outcompeted $\text{RO}\bullet$ formation, preventing $\text{RO}\bullet$ trapping from occurring. TART trapping and its associated $\text{TEMPO}\bullet$ release would further contribute to free $\text{TEMPO}\bullet$ concentration. Therefore, maximum intensity of peaks corresponding to RO-ART were observed using $50 \mu\text{M}$ $[\text{TART}]$. Although higher

500 μM TART concentration was used for TART trapping of α -pinene ozonolysis (8.6.3.7), total $[\text{RO}_2^\bullet]$ was significantly higher ($>10^{13}$ molec. cm^{-3} compared to $\sim 10^{11}$ molec. cm^{-3}) and hence, concentration of free TEMPO $^\bullet$ to RO_2^\bullet was estimated to be $<1:100$, allowing $\text{RO}_2^\bullet + \text{RO}_2^\bullet$ to form RO^\bullet , and RO_2^\bullet and RO^\bullet to be trapped. Similarly, $[\text{RO}_2^\bullet]$ would be significantly higher in the $^\bullet\text{OH}$ -initiated *n*-nonane degradation system, using alkene ozonolysis as an $^\bullet\text{OH}$ source than in the system using water photolysis as an $^\bullet\text{OH}$ source, due to the large amount of $[\text{RO}_2^\bullet]$ generated through TME ozonolysis (9.3).

Since most RO^\bullet were believed to be formed in solution from $\text{RO}_2^\bullet + \text{RO}_2^\bullet$, detection limits of $[\text{RO}^\bullet]$ from TART trapping could not be reliably calculated. However, detection of RO-ART was therefore evidence that RO_2^\bullet radicals were formed. From this, detection limits of $[\text{RO}_2^\bullet]$ using TART trapping with MS characterisation could be estimated.

Maximum intensity of the $[\text{RO-ART+H}]^+$ corresponding peak (m/z 299.270 \pm 0.002) was $\sim 5 \times 10^7$ absolute count whilst noise was estimated to be $\sim 2.5 \times 10^5$, producing a S/N of ~ 200 . From this, detection limit of $[\text{RO}_2^\bullet]$ using TART trapping with MS characterisation was estimated to be $>1 \times 10^9$ molec. cm^{-3} (S/N = ~ 2 , 10 min) indirectly from RO-ART trapping. These limits were atmospherically relevant, with $[\text{RO}_2^\bullet]$ having previously been measured at $>1 \times 10^9$ molec. cm^{-3} in highly polluted cities.²⁶² Direct detection limits of $[\text{RO}_2^\bullet]$ using CI-MS of $>2 \times 10^5$ molec. cm^{-3} (S/N = 2, 10 min) has been achieved.²⁴⁸ Therefore, TART trapping with MS characterisation had significantly poorer detection limits than CI-MS. However, it was believed that for short-lived radicals, such as RO^\bullet , detection limits of TART trapping with MS characterisation would be much higher than for these other radical characterisation techniques. Additionally, gaseous spin trapping with CI-MS and measurement of $[\text{RO}^\bullet]$ with FAGE, formed through $[\text{RO}_2^\bullet]$ and $[\text{NO}^\bullet]$ reaction, have been used for indirect detection of $[\text{RO}_2^\bullet]$, with detection limits of $>1.6 \times 10^8$ molec. cm^{-3} (30 s)²⁵⁶ and $>3.8 \times 10^8$ molec. cm^{-3} (S/N = 2, 5 min) respectively.²⁶⁰ Therefore, TART trapping had a similar although poorer detection limit than spin trapping with CI-MS and FAGE. However, it should be noted that spin trapping can lead to false positives and therefore, could be considered less reliable than TART trapping.

9.5. Conclusions and future work

TART trapping was used to investigate radicals formed during $^\bullet\text{OH}$ -initiated alkane degradation. First, a University of York based test system, using alkene ozonolysis as an $^\bullet\text{OH}$ source and CHANT as TART, was employed. From this, peaks corresponding to TART-trapped RO_2^\bullet and RO^\bullet and other radicals formed through autoxidation, were observed. Optimisation of the trapping reaction and HPLC-MS conditions was then performed.

A University of Leeds based system was then adapted for TART trapping of $^\bullet\text{OH}$ -initiated alkane degradation, using water photolysis as an $^\bullet\text{OH}$ source, CHANT as TART and HPLC-MS for characterisation. This set-up accurately calculated $[\text{OH}^\bullet]$. Results were later improved using DEADANT as TART. This was hypothesised to be due to DEADANT-trapped radicals having 3 $^\circ$ amine functionality, increasing ionisation efficiency and hence MS intensity of corresponding peaks. This was especially beneficial for HPLC-MS. Peaks corresponding to TART-trapped RO^\bullet were observed, however, peaks corresponding to TART-trapped RO_2^\bullet were not observed. This was a disappointing result. Kinetic modelling indicated that during the reaction, formed $[\text{RO-ART}]$ would not be sufficiently high for MS detection. Therefore, as was discussed in alkene ozonolysis (8.6.4), formation of most RO-ART was attributed to dissolved RO_2^\bullet undergoing liquid phase $\text{RO}_2^\bullet + \text{RO}_2^\bullet$ reaction, forming RO^\bullet , which was then trapped. Therefore, detection limits of $[\text{RO}^\bullet]$ from TART trapping could not be reliably calculated. However, detection of RO-ART was therefore evidence that RO_2^\bullet radicals were formed. From

this, detection limits of $[\text{RO}_2^\bullet]$ using TART trapping with MS characterisation were estimated to be $>1 \times 10^9$ molec. cm^{-3} ($\text{S/N} = \sim 2$, 10 min), which would be suitable for some atmospheric field measurements. This compared to direct detection limits of $[\text{RO}_2^\bullet]$ using CI-MS and indirect detection limits using FAGE and spin trapping with CI-MS of $>2 \times 10^5$ molec. cm^{-3} ($\text{S/N} = 2$, 10 min)²⁴⁸, $>3.8 \times 10^8$ molec. cm^{-3} ($\text{S/N} = 2$, 5 min)²⁶⁰ and $>1.6 \times 10^8$ molec. cm^{-3} (30 s) respectively.²⁵⁶

This detection limit could be improved by reducing the amount of free TEMPO \bullet content associated with TART. This would reduce side reactions and hence increase TART-trapped radical formation. Furthermore, reducing free TEMPO \bullet content would allow greater [TART] to be used, which would further increase TART-trapped radical formation. Whilst it was believed that free TEMPO \bullet content was due to inherent TEMPO \bullet dissociation and reassociation associated with TARTs, if free TEMPO \bullet was instead an impurity, TARTs could potentially be purified. Alternatively, an additive which scavenged TEMPO \bullet but was inert to other radicals, could mitigate reduction of dissolved $[\text{RO}_2^\bullet]$ and hence increase TART-trapped radical formation. As discussed for alkene ozonolysis (8.7), lower detection limits could be obtained using ammonium TARTs, which would yield TART-trapped radicals with higher ionisation efficiencies. Alternatively, reaction time could be increased so that more RO_2^\bullet and RO^\bullet are trapped by TART. Additionally, non-gaseous reactions occurring prior to TART trapping, could be reduced by isolating TART on a solid support. This would mean that intensities of peaks corresponding to TART-trapped radicals would more accurately reflect gaseous radical reactions. Overall conclusions and suggestions for future work were then made (10).

10. Overall conclusions and future work

Radical intermediates play a key role in many chemical processes. However, existing methods for their characterisation have flaws that limit mechanistic and kinetic understanding of these processes. A new radical characterisation technique was used to isolate, detect, characterise and quantify radicals. This technique used novel radical traps, which consisted of an allyl group attached to a leaving group, which formed a stable radical upon cleavage. Reaction of a radical with novel radical trap formed a stable radical and non-radical product containing the reactant radical, which was then characterised by conventional techniques, such as NMR spectroscopy and MS. MS was used to characterise most novel radical trapping samples, due to its high sensitivity and suitability for studying complex mixtures. Novel radical trapping could be used to trap any radical, including radicals which were: short-lived; long-lived; carbon-centred or heteroatom-centred, including but not limited to nitrogen-centred, oxygen-centred and sulfur-centred radicals.

In general, novel radical trapping offered advantages over existing radical characterisation techniques, especially for short-lived radicals. Trapped radicals could be accumulated to concentrations suitable for study by conventional and highly diagnostic techniques, such as NMR spectroscopy and MS. This differed to direct radical characterisation techniques, which usually cannot detect the low concentrations typically observed for short-lived radicals and are often poorly diagnostic. Experiments showed that a significant advantage of novel radical trapping over spin trapping and recombination trapping, was that it did not produce false positives through side reactions. Novel radical traps also showed no degradation when stored neat and sealed under air over three months at RTP or six months when refrigerated (0-5 °C). Furthermore, novel radical traps had high stability under a range of reaction conditions, including in presence of: strong acid, strong base, high temperature, visible and ultraviolet light and metal catalysts. This contrasted to spin traps, which need to be refrigerated and are easily degraded by trace metals. Trapped radicals were also relatively stable, unlike spin trapped radicals, which typically have relatively short lifetimes.

All synthesised novel radical traps used TEMPO• as a leaving group (3). Additionally, most radical traps contained an α,β -unsaturated amide, where the α,β -unsaturated group was the allyl group. This increased rate of radical trapping through resonance stabilisation of the intermediate radical formed prior to TEMPO• cleavage and allowed easy functionalisation by tuning the amide group, for example to contain hydroxyl groups to aid water solubility. α,β -Unsaturated amide radical traps were first formed through a novel reaction involving heating methyl 2-(bromomethyl)acrylate with TEMPO• and subsequent deprotection to form 2-(TEMPOmethyl)acrylic acid in an 85% yield over two steps. Ten amide-functionalised novel radical traps were formed through coupling of amines with 2-(TEMPOmethyl)acrylic acid in 16-77% yields (14-65% overall). Two further novel radical traps were formed through additional transformations. Synthesised novel radical traps had a broad range of functionalities and properties, allowing them to be used in a wide variety of radical reactions. These properties included novel radical traps being: neutral, charged, weakly acidic, weakly basic, volatile, non-volatile, soluble in organic solvents and water soluble. Free TEMPO• concentration of novel radical traps was low (~0.05mol.%), meaning they could not initiate radical reactions, making them innocent components of reaction mixtures.

A general methodology was then developed for novel radical trapping, MS characterisation and mass spectra analysis (4). In particular, MS characterisation used a high-resolution FT-ICR mass spectrometer, to limit the number of species each peak could correspond to, and ESI-MS, to simplify mass spectra of the complex radical trapping samples. Mass spectra analysis was automated through self-written programmes.

Novel radical trapping was applied to a diverse array of radical reactions, including liquid phase synthetic reactions (5) and photochemical reactions (6), aqueous biochemical reactions (7) and gaseous alkene ozonolysis (8) and $\bullet\text{OH}$ -initiated alkane degradation (9). Trapped radicals were successfully observed in all systems.

Results from radical trapping offered validation to previously described mechanisms and experimentally determined kinetics of synthetic radical reactions. In the Hofmann-Löffler-Freytag (HLF) reaction, radical trapping indicated presence of structurally isomeric nitrogen-centred or subsequently formed carbon-centred radicals, through a 1,5-HAT. D_2O exchange, tandem MS and HPLC-MS techniques indicated that whilst both radicals were successfully trapped, there was a much higher concentration of trapped nitrogen-centred radicals than trapped carbon-centred radicals. This indicated that 1,5-HAT was the rate limiting step, as described in literature. This showed that novel radical trapping could provide mechanistic and kinetic insights.

Likewise, novel radical trapping was used to validate mechanisms of photochemical radical reactions. In Ru-photocatalysed radical thiol-ene addition, a trapped phenylthiyl radical was successfully isolated in a 63% yield and fully characterised, with NMR spectroscopy indicating the expected structure was formed, validating the novel radical trapping mechanism. Using this isolated trapped radical, calibration curves were obtained to relate its MS intensity to its concentration, allowing its concentration to be determined during kinetics experiments. This informed the development of a kinetic model, which was subsequently used to estimate the radical resting state for different radical thiol-ene additions, using different thiols and alkenes as substrates. The knowledge gained from studying this system was further applied to a niche catalyst-free photoinitiated radical dearomative spirocyclisation. In this reaction, observations from radical trapping allowed an initiation mechanism to be suggested. Improved knowledge of mechanisms and kinetics obtained through novel radical trapping could be used to optimise reaction conditions to improve product yields.

$\bullet\text{OH}$ -initiated degradation of biochemicals, such as thymine, was used to mimic oxidative stress of cellular components, such as DNA. Novel radical trapping supported the suggested mechanisms for these reactions and indicated trapped radical concentrations, offering mechanistic and kinetic insights. Additionally, radical trapping of $\bullet\text{OH}$ -initiated biochemical degradation indicated that thymine-derived radical formation markedly decreased in presence of antioxidant, whilst antioxidant-derived radical formation little decreased in presence of thymine. This indicated that novel radical trapping could be used to assess antioxidant activity.

Gaseous alkene ozonolysis, relevant to aerosol formation, was investigated using novel radical trapping. In α -pinene ozonolysis, radical trapping, MS characterisation and mass spectra analysis, in which molecular formulae were assigned to observed peaks, allowed structures to be suggested for the most intensely observed trapped radicals. The corresponding $\text{RO}_2\bullet$ and $\text{RO}\bullet$ radicals were assigned to: widely accepted steps of α -pinene reaction with ozone; widely discussed but not totally accepted $\bullet\text{OH}$ addition to α -pinene, ring opening and subsequent cycloperoxide formation, with and without autoxidation, and a hypothesised minor pathway of hydrogen atom abstraction from α -pinene. This showed that novel radical trapping could be used to trap and characterise gaseous radicals, aiding mechanism elucidation. Widely accepted $\bullet\text{OH}$ addition to α -pinene and immediate $\text{RO}_2\bullet$ formation was not indicated to occur. It was hypothesised that this reaction may be disfavoured over strained four-membered ring opening. Other MS peaks indicated that oligomers were formed through intermolecular $\text{RO}_2\bullet$ addition to α -pinene. This simultaneous observation of peaks corresponding to trapped radicals and products provided a thorough overview of the reaction. Comparison between experimental MS intensities of trapped radicals and modelling

of radical trapping of gaseous α -pinene ozonolysis, showed a reasonable fit for the overall trends of the reaction, suggesting that novel radical trapping was capable of offering mechanistic information to gaseous radical reactions.

Detection limits of $>1 \times 10^9$ molec. cm^{-3} (S/N = 2, 10 min) for RO_2^\bullet were estimated from novel radical trapping of $^\bullet\text{OH}$ -initiated *n*-nonane degradation, with known $^\bullet\text{OH}$ concentration, using kinetic modelling. These limits were atmospherically relevant and competitive with existing radical characterisation techniques. This detection limit was achieved by using trapped RO^\bullet detection as an indirect indicator for RO_2^\bullet , although the majority of RO^\bullet were likely formed through liquid phase $\text{RO}_2^\bullet + \text{RO}_2^\bullet$ reactions. Although novel radical trapping of gaseous radical reactions was not an accurate reflection of the gaseous radical reaction, it was suggested that with appropriate modelling, this deviation could be accounted for. This complication could potentially be solved using radical trap immobilised on a solid support.

Novel radical trapping methodology would most benefit from improved quantification. This could be achieved using inherently cationic traps, to make MS intensity of trapped radicals less dependent on reactant radical structure and available cations and reduce MS detection limits. HPLC-MS would also reduce dependency of MS intensity of trapped radicals, on the presence of other species. Calibration curves would further aid quantification by allowing trapped radical concentrations to be estimated from their MS intensities. These improvements would allow results to be more quantitatively interpreted, aiding kinetic understanding.

Potentially interesting applications of novel radical trapping include monitoring of radical reactions *in situ* using MS, to obtain high quality kinetic profiles, for example for radical thiol-ene addition. This could significantly improve obtained kinetic data and aid elucidation of radical reaction kinetics, potentially leading to reaction improvements. *In situ* reaction monitoring using MS has been used to study non-radical synthetic reactions, such as the Suzuki-Miyaura reaction.²⁶³ Accurately quantifying concentration of species, using MS intensities of their corresponding peaks, would likely be challenging, as discussed previously.

A fluorophore-functionalised TART could be used for fluorescence imaging. This could be used to detect areas of high radical reactivity, for example in cells, potentially having applications in biochemistry and medicinal chemistry. Fluorophore-functionalised recombination traps have previously been used to detect lipid radicals¹³⁴, whilst other fluorophore-functionalised trapping agents have been used for detection and kinetic monitoring of peroxide radical formation in cells *in vitro*.²⁶⁴ TART trapping would offer advantages over these techniques, in particular that it would not produce false positives, as discussed previously. However, using fluorescence spectroscopy to indicate TEMPO $^\bullet$ loss, to ensure TART trapping occurred, would be difficult.

Atmospherically relevant indirect detection limits were achieved for $[\text{RO}_2^\bullet]$ using TART trapping. Real world indoor and outdoor air sampling would be an interesting application of TART trapping, to characterise atmospheric radicals and monitor their concentrations, improving mechanistic and kinetic understanding of atmospheric processes. This would likely first require optimising radical trapping using solid supported TART, to ensure results reflected gaseous radical reactions. Since atmospheric radicals did not require laboratory equipment for production, significantly longer acquisition times could be used, lowering detection limits.

Novel radical trapping was used to isolate, detect, characterise and quantify a diverse array of radicals across a wide variety of systems, offering them mechanistic and kinetic insights. These studies demonstrated the viability of TART trapping, as a tool for all chemists, to investigate any radical reaction. It is hoped that chemists will widely adopt this technique to improve understanding and aid development of reactions involving radical intermediates.

11. Experimental

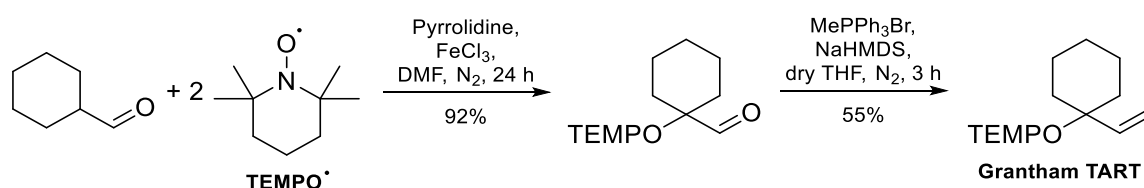
11.1. General

Except where stated, all reagents and solvents were purchased from commercial sources and used without further purification. A full list of chemicals used is available in the supporting information (SI1). Anhydrous solvents were obtained from an Innovative Technology Inc. PureSolv[®] solvent purification system.

All chemical reactions and analyses were acquired at room temperature and pressure (RTP, 293 K, 101325 Pa) unless stated otherwise. Thin layer chromatography was carried out on Merck silica gel 60F254 pre-coated aluminium foil sheets and were visualised using UV light (254 nm) or stained with basic aqueous potassium permanganate, as indicated. Flash column chromatography was carried out using slurry packed Fluka silica gel (SiO₂), 35–70 μm, 60 Å under a light positive pressure, eluting with the specified solvent system. Melting points were Stuart Scientific SMP3 apparatus and are uncorrected. CHN microanalysis was obtained using an Exeter Analytical Inc. CE-440 analyser. Infrared (IR) spectra were recorded on a PerkinElmer UATR 2 spectrometer, either as a compressed solid or neat oil. ¹H and ¹³C nuclear magnetic resonance (NMR) spectra were recorded in CDCl₃ on a JEOL ECX400 or JEOL ECS400 spectrometer, operating at 400 MHz and 100 MHz respectively. Chemical shifts (δ) are quoted in parts per million (ppm). The residual solvent peaks were used as references in ¹H and ¹³C{¹H} NMR spectroscopy were δH 7.26 ppm and δC 77.0 ppm respectively. Coupling constants (*J*) are reported in Hertz (Hz) to the nearest 0.1 Hz. The multiplicity abbreviations used are: s singlet, d doublet, t triplet, br broad, dd double doublet, dt double triplet, td triple doublet, ddd double double doublet and m multiplet. Signal assignment was achieved by analysis of DEPT, COSY and HMQC experiments where required. Mass spectra of TART synthesis products were recorded using positive electrospray ionisation (Pos ESI) on a Bruker compact QTOF MS (compact) mass spectrometer (±0.001 *m/z* precision, 30000 resolution), unless otherwise stated. Mass spectra of trapping reactions were recorded using positive electrospray ionisation (Pos ESI) on a high resolution solariX XR FTMS (solariX) mass spectrometer (±0.0001 *m/z* precision, >10⁷ maximum resolution, mass accuracy 600 ppb (internal)), unless stated otherwise.

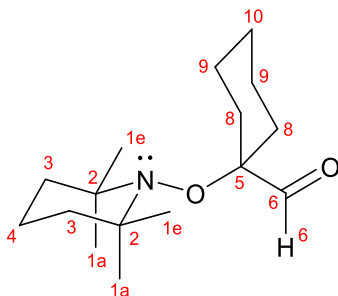
11.2. TART synthesis

11.2.1. Grantham TART



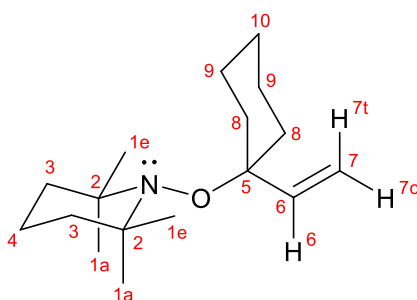
Grantham TART was synthesised as described in literature, with some minor modifications.¹⁵² (2,2,6,6-Tetramethylpiperidin-1-yl)oxyl (TEMPO•, 937 mg, 6.00 mmol, 2.0 eq.) was dissolved in *N,N*-dimethylformamide (DMF, 1.5 mL). This solution was sealed, sparged and placed under N₂. Cyclohexanecarboxaldehyde (337 mg, 3.00 mmol, 1.0 eq.) and pyrrolidine (64.0 mg, 0.74 mmol, 0.3 eq.) were added and the resultant solution stirred for 5 min. Anhydrous FeCl₃ (97.3 mg, 0.60 mmol, 0.2 eq.) dissolved in DMF (1.5 mL) was added and the solution stirred for 24 h. Saturated aqueous sodium ascorbate (10 mL) was then added and the upper organic layer extracted from the lower aqueous layer with Et₂O (3×20 mL). The combined organic layers were dried with MgSO₄, filtered and solvent removed *in vacuo*. The resultant orange/red

oil was purified using flash silica column chromatography (visualised using KMnO_4 stain) yielding pink 1-[(2,2,6,6-tetramethylpiperidin-1-yl)oxy]cyclohexane-1-carbaldehyde oil (741 mg, 92%). This was used in the next step without further purification.



R_f : 0.30 (30%DCM/PET ether). CHN: C, 71.5; H, 11.2; N, 5.3 (found); C, 71.9; H, 10.9; N, 5.2 (calc. for $\text{C}_{16}\text{H}_{29}\text{NO}_2$). IR: ν_{max} / cm^{-1} 2930 (CH), 1720 (C=O). ^1H , ^{13}C NMR (400, 100 MHz, CDCl_3): δ_{H} 9.92 (s, 1H, H_6), 1.95-1.83 (m, 2H, H_4), 1.80-1.66 (m, 4H, H_3), 1.59-1.36 (m, 8H, H_{8-9}), 1.35-1.25 (m, 2H, H_{10}), 1.14 (s, 6H, H_{1a}), 1.14 (s, 6H, H_{1e}); δ_{C} 204.3 (C_6), 82.7 (C_6), 60.2 (C_2), 40.7 (C_3), 34.3 (C_{1a}), 31.8 (C_8), 25.4 (C_{10}), 22.2 (C_9), 20.7 (C_{1e}), 17.1 (C_4). MS (Pos ESI): m/z 268.233 ($[\text{M}+\text{H}]^+$, 46%), 240.227 ($[\text{M}+\text{H}-\text{CO}]^+$, 100%), 158.156 ($[\text{TEMPOH}+\text{H}]^+$, 2%), 142.159 ($[\text{TMP}+\text{H}]^+$, 3%); 268.228 (calc. for $\text{C}_{16}\text{H}_{30}\text{NO}_2$, $[\text{M}+\text{H}]^+$). Obtained values were consistent with literature.¹⁵²

Methyltriphenylphosphonium bromide (714 mg, 2.00 mmol, 1.0 eq.) was dissolved in dry tetrahydrofuran (THF, 5.5 mL). This solution was sealed, sparged and placed under N_2 before being cooled in a dry ice/acetone bath ($-78\text{ }^\circ\text{C}$). Sodium bis(trimethylsilyl)amide (1.81 g, 1.0 M in dry THF, 2.00 mmol, 1.0 eq.) was added slowly and the solution stirred for 30 min. A solution of 1-[(2,2,6,6-tetramethylpiperidin-1-yl)oxy]cyclohexane-1-carbaldehyde (535 mg, 2.00 mmol, 1.0 eq.) in dry THF (5.5 mL) was added and the resultant solution allowed to warm to room temperature before being stirred for 3 h. Saturated aqueous NH_4Cl (10 mL) was then added and the upper organic layer extracted with EtOAc (3×10 mL). The combined organic layers were washed with saturated aqueous NaHCO_3 (10 mL) and brine (10 mL). The resultant solution was dried with MgSO_4 , filtered and solvent removed *in vacuo*. The oil obtained was purified using flash silica column chromatography (visualised using KMnO_4 stain) yielding peach 1-[(2,2,6,6-tetramethylpiperidin-1-yl)oxy]cyclohexane-1-ethenyl oil (Grantham TART, 287 mg, 54% or 50% overall).

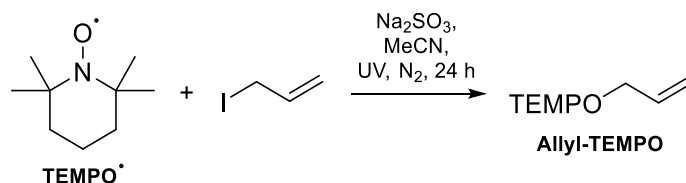


R_f : 0.28 (15%DCM/PET ether). CHN: C, 75.9; H, 11.6; N, 4.4 (found); C, 76.9; H, 11.8; N, 5.3 (calc. for $\text{C}_{17}\text{H}_{31}\text{NO}$). IR: ν_{max} / cm^{-1} 2930 (CH), 1680 (C=C). ^1H , ^{13}C NMR (400, 100 MHz, CDCl_3): δ_{H} 6.48 (dd, J 17.9, 11.4 Hz, 1H, H_6), 5.03 (dd, J 11.4, 1.5 Hz, 1H, H_{7c}), 4.98 (dd, J 17.9, 1.5 Hz, 1H, H_{7t}), 2.05-1.96 (m, 2H, H_4), 1.83-1.41 (m, 12H, H_3 , H_8 , H_9), 1.33-1.23 (m, 2H, H_{10}), 1.12 (s, 6H, H_{1a}), 1.09 (s, 6H, H_{1e}); δ_{C} 144.3 (C_6), 111.5 (C_7), 78.7 (C_5), 59.2 (C_2), 40.7 (C_3), 36.7 (C_8), 34.5 (C_{1a}), 25.8 (C_{10}), 22.4 (C_9), 20.9 (C_{1e}), 17.1 (C_4). MS (Pos ESI): m/z 266.248 ($[\text{M}+\text{H}]^+$, 100%), 282.243 ($[\text{M}+\text{Na}]^+$, 3%), 158.154 ($[\text{TEMPOH}+\text{H}]^+$, 8%), 142.159

([TMP+H]⁺, 3%); 266.248 (calc. for C₁₇H₃₂NO, [M+H]⁺). Obtained values were consistent with literature.¹⁵²

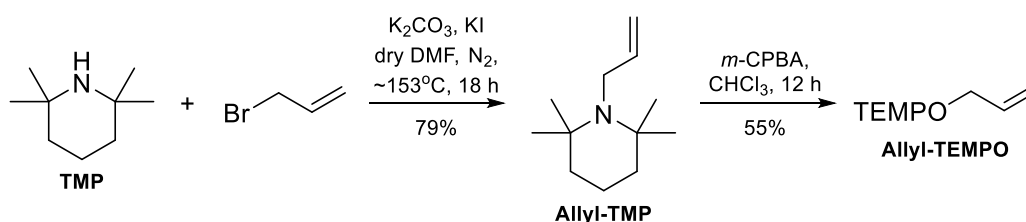
11.2.2. Allyl-TEMPO

11.2.2.1. Abandoned one-step synthesis

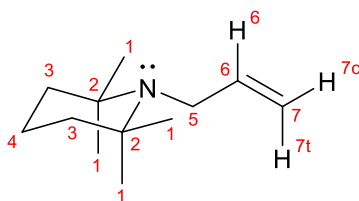


Allyl-TEMPO synthesis was attempted using a literature procedure.¹⁵⁴ (2,2,6,6-Tetramethylpiperidin-1-yl)oxyl (TEMPO•, 375 mg, 2.40 mmol, 1.2 eq.), allyl iodide (336 mg, 2.00 mmol, 1.0 eq.), Na₂SO₃ (504 mg, 4.00 mmol, 2.0 eq.) were placed in a polypropylene tube and dissolved in MeCN (20 mL). This solution was sealed, sparged and placed under N₂ before being irradiated with UV (100 W, 405 nm) for 24 h, whilst stirring. Water (40 mL) was then added and the upper organic layer extracted with Et₂O (4×10 mL). The combined organic layers were washed with water (10 mL) and brine (10 mL), dried with MgSO₄ and solvent removed *in vacuo* to yield an orange oil. Subsequent column chromatography was deemed impracticable due to identical retention factors found for TEMPO• and allyl-TEMPO in multiple solvent systems.

11.2.2.2. Two-step synthesis

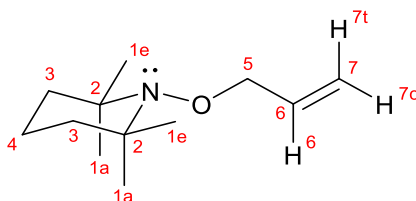


Allyl-TEMPO was synthesised in a two-step synthesis using literature procedures.^{155,156} 2,2,6,6-Tetramethylpiperidine (TMP, 1.13 g, 8.00 mmol, 1.0 eq.), allyl-bromide (2.13 g, 17.6 mmol, 2.2 eq.), K₂CO₃ (2.43 g, 17.6 mmol, 2.2 eq.) and KI (1.33 g, 8.00 mmol, 1.1 eq.) were dissolved in dry *N,N*-dimethylformamide (DMF, 20 mL), yielding a beige solution. This solution was sealed, sparged and placed under N₂ before being heated to reflux (~153 °C) and stirred for 18 h. The resultant orange solution was allowed to cool and filtered. Et₂O (30 mL) was added and the upper organic layer washed with water (4×10 mL). Et₂O (30 mL) was added to the first wash aqueous residue and the upper organic layer washed with water (3×10 mL). Et₂O (30 mL) was added to the second wash aqueous residue and the upper organic layer washed with water (2×10 mL). Combined organic layers were dried with MgSO₄, filtered and solvent removed *in vacuo*, yielding a yellow-brown oil. This was purified using flash silica column chromatography (visualised using KMnO₄ stain) yielding yellow-brown 1-allyl-2,2,6,6-tetramethylpiperidine oil (allyl-TMP, 1.15 g, 79%). This was used in the next step without further purification.



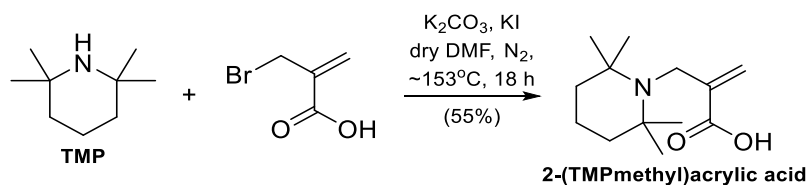
R_f: 0.33 (2%NH₄OH/5%MeOH/DCM). CHN: C, 79.3; H, 13.3; N, 7.3 (found); C, 79.5; H, 12.8; N, 7.7 (calc. for C₁₂H₂₃N). IR: ν_{\max} / cm⁻¹ 2970 (CH), 1650 (C=C). ¹H, ¹³C NMR (400, 100 MHz, CDCl₃): δ_{H} 5.86 (ddt, *J* 16.8, 9.9, 5.3 Hz, 1H, H₆), 5.13 (ddt, *J* 16.8, 2.1, 1.6 Hz, 1H, H_{7t}), 4.91 (dtd, *J* 9.9, 2.3, 2.1 Hz, 1H, H_{7c}), 3.11 (ddd, *J* 5.3, 2.3, 1.6 Hz, 2H, H₅), 1.59-1.51 (m, 2H, H₄), 1.46-1.40 (m, 4H, H₃) 1.00 (s, 12H, H₁); δ_{C} 143.6 (C₆), 112.6 (C₇), 54.6 (C₂), 46.9 (C₅), 41.3 (C₃), 27.5 (C₁), 17.9 (C₄). MS (Pos ESI): *m/z* 182.190 ([M+H]⁺, 100%); 182.191 (calc. for C₁₂H₂₄N, [M+H]⁺). Obtained values were consistent with literature.¹⁵⁵

1-Allyl-2,2,6,6-tetramethylpiperidine (1.09 g, 6.00 mmol, 1.0 eq.) was dissolved in CHCl₃ (30 mL) and cooled in a water/ice bath (~0 °C). *meta*-Chloroperoxybenzoic acid (*m*-CPBA, <77%, 1.34 g, 6.00 mmol, 1.0 eq.) in CHCl₃ (30 mL) was added slowly over 20 min. This solution was let warm to room temperature and stirred for 12 h. The resultant solution was washed with saturated aqueous K₂CO₃ (2x30 mL), dried with MgSO₄, filtered and solvent removed *in vacuo*. The resultant orange oil was purified using flash silica column chromatography (visualised using KMnO₄ stain) yielding mint green 1-allyloxy-2,2,6,6-tetramethylpiperidine oil (allyl-TEMPO, 651 mg, 55% or 43% overall).



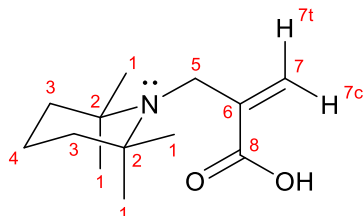
R_f: 0.34 (5%EtOAc/hexane). IR: ν_{\max} / cm⁻¹ 2930 (CH), 1640 (C=C). ¹H, ¹³C NMR (400, 100 MHz, CDCl₃): δ_{H} 5.90 (ddt, *J* 17.5, 10.7, 5.3 Hz, 1H, H₆), 5.28 (ddt, *J* 17.5, 2.0, 1.8 Hz, 1H, H_{7t}), 5.12 (dtd, *J* 10.7, 1.8, 1.3 Hz, 1H, H_{7c}), 4.28 (ddd, *J* 5.3, 1.8, 1.3 Hz, 2H, H₅), 1.57-1.40 (m, 4H, H₃), 1.35-1.21 (m, 2H, H₄) 1.15 (s, 6H, H_{1a}), 1.14 (s, 6H, H_{1e}); δ_{C} 134.3 (C₆), 116.2 (C₇), 78.4 (C₅), 59.9 (C₂), 39.8 (C₃), 33.1 (C_{1a}), 20.3 (C_{1e}), 17.3 (C₄). MS (Pos ESI): *m/z* 198.185 ([M+H]⁺, 100%); 198.186 (calc. for C₁₂H₂₄NO, [M+H]⁺). Obtained values were consistent with literature.¹⁵⁵

11.2.3. Abandoned 2-(bromomethyl)acrylic acid nucleophilic substitution by TMP and Meisenheimer rearrangement

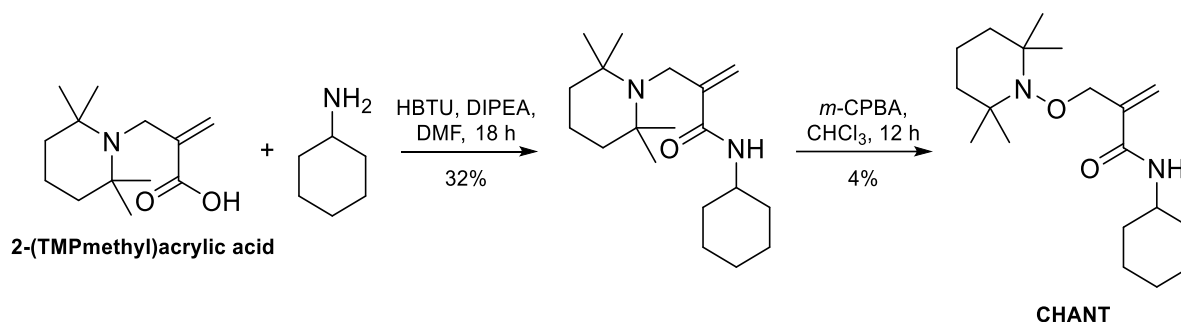


2-(TMPmethyl)acrylic acid synthesis was adapted from a literature procedure.³ 2-(Bromomethyl)acrylic acid (330 mg, 2.00 mmol, 1.0 eq.), K₂CO₃ (885 mg, 6.40 mmol, 3.2 eq.) and KI (365 mg, 2.20 mmol, 1.1 eq.) were dissolved in dry *N,N*-dimethylformamide (5 mL), yielding a yellow solution. This was sealed, sparged and placed under N₂. 2,2,6,6-Tetramethylpiperidine (TMP, 622 mg, 4.40 mmol, 2.2 eq.) was slowly injected, forming

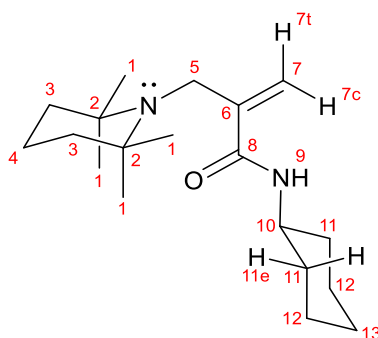
a beige solution. This was heated to reflux (~153 °C) and stirred for 18 h. The resultant dark orange solution was allowed to cool. Product collected at the condenser base was manually removed with a spatula and returned to the reaction mixture. The condenser was washed with DMF (2.5 mL) into the reaction mixture and the resultant reaction mixture filtered. The remaining solid was rewashed with DMF (2.5 mL) and the resulting solution filtered. The two filtrates were combined, yielding a golden liquid containing 2-([2,2,6,6-tetramethylpiperidine]methyl)acrylic acid (2-(TMPmethyl)acrylic acid, qNMR yield 55%). This solution was carried directly into the next step without purification.



MS (Pos ESI): m/z 226.183 ($[M+H]^+$, 100%), 248.165 ($[M+Na]^+$, 25%), 142.161 ($[TMP+H]^+$, 37%); 226.181 (calc. for $C_{13}H_{24}NO_2$, $[M+H]^+$).



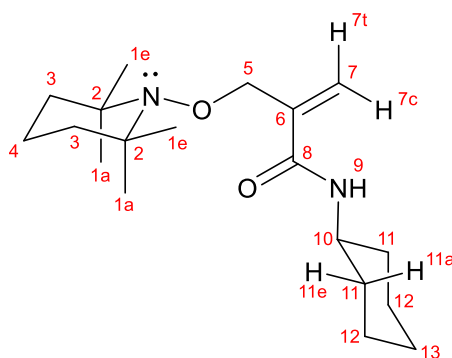
To crude 2-(TMPmethyl)acrylic acid solution (10 mL) was added *O*-(benzotriazol-1-yl)-*N,N,N,N*-tetramethyluronium hexafluorophosphate (HBTU, 910 mg, 2.40 mmol, 1.2 eq.), *N,N*-diisopropylethylamine (DIPEA, 517 mg, 4.00 mmol, 2.0 eq.) and cyclohexylamine (238 mg, 2.40 mmol, 1.2 eq.) and stirred for 18 h. Saturated aqueous $NaHCO_3$ (20 mL) was then added and product extracted with EtOAc (3×20 mL). The combined organic layers were washed with brine (3×20 mL). The organic phase was dried with $MgSO_4$, filtered and solvent removed *in vacuo*, yielding a brown oil. This was purified using flash silica column chromatography (visualised using $KMnO_4$ stain) yielding dirty white *N*-cyclohexyl-2-([2,2,6,6-tetramethylpiperidine]methyl)acrylamide (209 mg, 32% across the first two steps).



R_f : 0.37 (1% NH_4OH /3% $MeOH$ / DCM). 1H , ^{13}C NMR (400, 100 MHz, $CDCl_3$): δ_H 8.70 (br s, 1H, H_9), 5.91 (dt, J 2.0, 1.6 Hz, 1H, H_{7c}), 5.44 (dt, J 2.0, 1.6 Hz, 1H, H_{7t}), 3.90-3.79 (m, 1H, H_{10}), 3.53 (dd, J 1.9, 1.6 Hz, 2H, H_5), 2.05-1.97 (m, 2H, H_{11e}), 1.79-1.70 (m, 2H, H_{12e}), 1.70-1.53 (m,

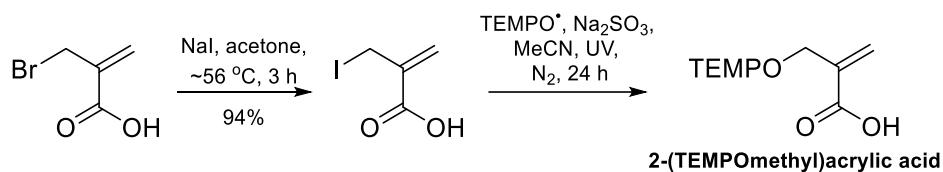
3H, H_{12a}, H_{13e}), 1.53-1.46 (m, 4H, H₃), 1.45-1.31 (m, 2H, H₄), 1.26-1.11 (m, 4H, H_{11a}, H_{13a}) 1.07 (s, 12H, H₁); δ_c 164.6 (C₈), 145.2 (C₆), 119.5 (C₇), 56.0 (C₂), 48.4 (C₁₀), 47.4 (C₅), 41.7 (C₃), 36.6 (C₁), 33.6 (C₁₁), 25.8 (C₁₂), 25.3 (C₁₃), 17.8 (C₄). MS (Pos ESI): m/z 307.274 ([M+H]⁺, 100%); 307.275 (calc. for C₁₉H₃₅N₂O, [M+H]⁺).

N-Cyclohexyl-2-([2,2,6,6-tetramethylpiperidine]methyl)acrylamide (153 mg, 0.50 mmol, 1.0 eq.) was dissolved in CHCl₃ (2.5 mL) and cooled in a water/ice bath (~0 °C). A solution of *meta*-chloroperoxybenzoic acid (*m*-CPBA, <77%, 112 mg, 1.0 eq.) in CHCl₃ (2.5 mL) was added slowly over 20 min. The resultant solution was let warm to room temperature and stirred for 12 h. This was then washed with saturated aqueous K₂CO₃ (2x5 mL), dried with MgSO₄, filtered and solvent removed *in vacuo* yielding an orange oil. This was purified using flash silica column chromatography (visualised using KMnO₄ stain) yielding dirty white crystalline *N*-cyclohexyl-2-[(2,2,6,6-tetramethylpiperidin-1-yl)oxy]methyl)acrylamide (6.8 mg, 4% or 1% overall).

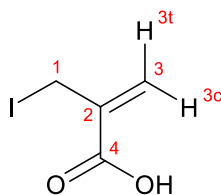


R_f: 0.32 (20%EtOAc/PET ether). ¹H, ¹³C NMR (400, 100 MHz, CDCl₃): δ_H 6.61 (br d, *J* 8.1 Hz, 1H, H₉), 6.08 (d, *J* 1.8 Hz, 1H, H_{7c}), 5.47 (dt, *J* 1.8, 1.1 Hz, 1H, H_{7t}), 4.47 (d, *J* 1.1 Hz, 2H, H₅), 3.88-3.76 (m, 1H, H₁₀), 2.02-1.95 (m, 2H, H_{11e}), 1.74-1.63 (m, 5H, H_{12e}, H_{12e}, H_{13e}), 1.57-1.44 (m, 4H, H₃), 1.48-1.32 (m, 2H, H₄), 1.19 (s, 6H, H_{1a}), 1.18-1.12 (m, 3H, H_{11a}, H_{13a}), 1.10 (s, 6H, H_{1e}); δ_c 166.0 (C₈), 140.0 (C₆), 124.0 (C₇), 77.8 (C₅), 60.1 (C₂), 48.3 (C₁₀), 39.8 (C₃), 33.5 (C_{1a}), 32.6 (C₁₁), 25.7 (C₁₂), 25.1 (C₁₃), 20.5 (C_{1e}), 17.1 (C₄). MS (Pos ESI): m/z 323.270 ([M+H]⁺, 100%); 323.270 (calc. for C₁₉H₃₅N₂O₂).

11.2.4. Unsuccessful 2-(bromomethyl)acrylic acid UV irradiation



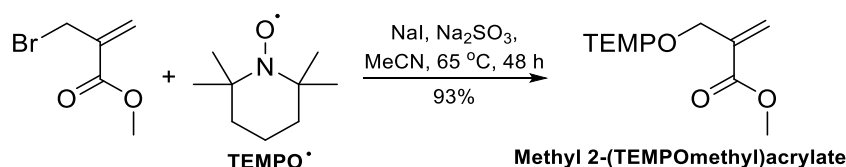
2-(Bromomethyl)acrylic acid (495 mg, 3.00 mmol, 1 eq.) and NaI (1350 mg, 9.00 mmol, 3.0 eq.) were dissolved in acetone (9.0 mL), heated to reflux (~56 °C) and stirred for 3 h. The resultant solution was washed with water (20 mL) and the lower organic layer extracted with CHCl₃ (3x20 mL). Combined organic layers were dried with MgSO₄, filtered and solvent removed *in vacuo*, yielding a brown oil. This was purified using flash silica column chromatography (visualised using KMnO₄ stain) yielding solid brown allyl 2-(iodomethyl)acrylic acid (598 mg, 94%).



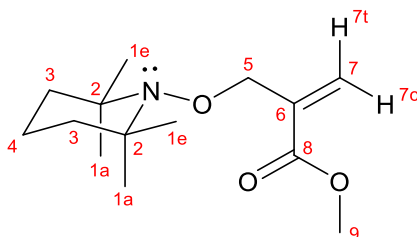
R_f: 0.20 (10%MeOH/DCM). ¹H, ¹³C NMR (400, 100 MHz, CDCl₃): δ_H 6.38 (s, 1H, H_{3c}), 6.08 (s, 1H, H_{3t}), 4.48 (s, 2H, H₁); δ_C 170.1 (C₄), 138.3 (C₂), 130.1 (C₃), -0.6 (C₅).

2-(Iodomethyl)acrylic acid (336 mg, 2.00 mmol, 1.0 eq.), (2,2,6,6-tetramethylpiperidin-1-yl)oxyl (TEMPO, 375 mg, 2.40 mmol, 1.2 eq.) and Na₂SO₃ (504 mg, 4.00 mmol, 2.0 eq.) were placed in a polypropylene tube and dissolved in MeCN (10.0 mL). This was sealed, sparged and placed under N₂ before being irradiated with UV (100 W, 405 nm) for 24 h, whilst stirring. The solution was then filtered and solvent removed *in vacuo*, yielding crude brown oil. This was purified using flash silica column chromatography (0.2%AcOH/40%hexane/EtOAc, R_f 0.41, visualised using KMnO₄ stain) yielding impure allyl 2-([(2,2,6,6-tetramethylpiperidin-1-yl)oxyl]methyl)acrylic acid oil (2-(TEMPOmethyl)acrylic acid, 62.1 mg). Further purification was deemed impractical.

11.2.5. Methyl 2-(TEMPOmethyl)acrylate

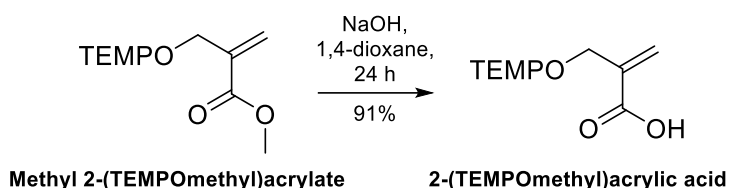


Methyl 2-(bromomethyl)acrylate (1.79 g, 10.0 mmol, 1.0 eq.), (2,2,6,6-tetramethylpiperidin-1-yl)oxyl (TEMPO, 1.88 g, 12.0 mmol, 1.2 eq.), NaI (3.00 g, 20.0 mmol, 2.0 eq.), Na₂SO₃ (3.78 g, 30.0 mmol, 3.0 eq.) were dissolved in MeCN (100 mL). This solution was sealed, sparged and placed under N₂ before being heated to 65 °C and stirred for 48 h. MeCN was then removed *in vacuo*. H₂O (100 mL) was added and product extracted with EtOAc (3×100 mL). The organic phase was dried with MgSO₄, filtered and solvent removed *in vacuo*, yielding crude orange oil. This was purified using flash silica column chromatography (visualised using KMnO₄ stain) yielding methyl 2-([(2,2,6,6-tetramethylpiperidin-1-yl)oxyl]methyl)acrylate yellow oil (methyl 2-(TEMPOmethyl)acrylate, 2.37 g, 93%).

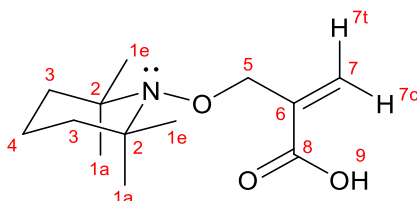


R_f: 0.33 (2%Et₂O/DCM). CHN: C, 65.4; H, 9.9; N, 5.1 (found); C, 65.9; H, 9.9; N, 5.5 (calc. for C₁₄H₂₅NO₃). IR: ν_{max} / cm⁻¹ 2980 (CH), 2900 br (OH), 1720 (C=O), 1630 (C=C), 1150 (C-O), 1060 (C-O). ¹H, ¹³C NMR (400, 100 MHz, CDCl₃): δ_H 6.28 (dt, *J* 1.8, 1.6 Hz, 1H, H_{7c}), 5.91 (td, *J* 1.9, 1.8 Hz, 1H, H_{7t}), 4.49 (dd, *J* 1.9, 1.6 Hz, 2H, H₅), 3.75 (s, 3H, H₉), 1.55-1.48 (m, 1H, H₄), 1.47-1.42 (m, 4H, H₃) 1.35-1.28 (m, 1H, H₄), 1.15 (s, 6H, H_{1a}), 1.10 (s, 6H, H_{1e}); δ_C 166.5 (C₈), 137.0 (C₆), 125.4 (C₇), 74.7 (C₅), 60.1 (C₂), 51.9 (C₉), 39.8 (C₃), 32.9 (C_{1a}), 20.4 (C_{1e}), 17.2 (C₄). MS (Pos ESI): *m/z* 256.191 ([M+H]⁺, 100%); 256.191 (calc. for C₁₄H₂₆NO₃, [M+H]⁺).

11.2.6. 2-(TEMPOmethyl)acrylic acid

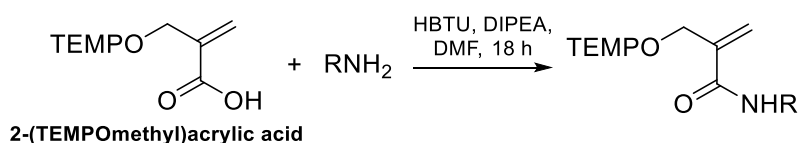


2-[[2,2,6,6-Tetramethylpiperidin-1-yl]oxy]methyl)acrylate (1.58 g, 6.20 mmol, 1.0 eq.) was placed in 1,4-dioxane (40 mL), aqueous NaOH (1.0 M, 40 mL, 40 mmol, 6.5 eq.) added and the solution stirred for 24 h. The resultant solution was acidified (pH 5) with aqueous HCl (2.0 M, 20 mL, 40 mmol, 6.5 eq.) and product extracted with EtOAc (3×40 mL). The organic phase was washed with brine (40 mL), dried with MgSO₄, filtered and solvent removed *in vacuo*, yielding crude golden oil. This was purified using flash silica column chromatography (visualised using KMnO₄ stain) yielding white crystalline 2-[[2,2,6,6-tetramethylpiperidin-1-yl]oxy]methyl)acrylic acid (2-(TEMPOmethyl)acrylic acid, 1.36 g, 91% or 85% overall).



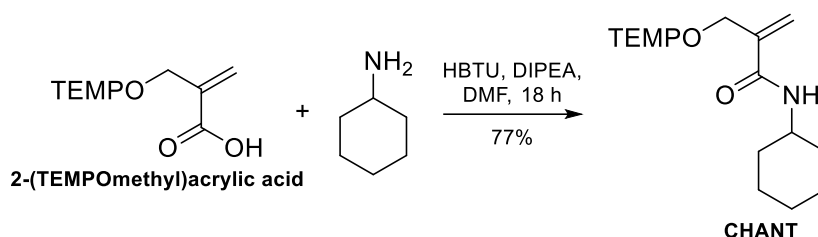
R_f: 0.32 (0.1%AcOH/5%MeOH/DCM). Mp: 94.7-96.1 °C. CHN: C, 64.3; H, 9.8; N, 5.8 (found); C, 64.7; H, 9.6; N, 5.8 (calc. for C₁₃H₂₃NO₃). IR: ν_{max} / cm⁻¹ 2980 (CH), 1700 (C=O), 1640 (C=C), 1360 (C-O); ¹H, ¹³C NMR (400, 100 MHz, CDCl₃): δ_H 6.40 (dt, *J* 3.3, 1.8 Hz, 1H, H_{7c}), 5.96 (dt, *J* 3.3, 1.6 Hz, 1H, H_{7t}), 4.53 (dd, *J* 1.8, 1.6 Hz, 2H, H₅), 1.61-1.55 (m, 1H, H₄), 1.53-1.48 (m, 4H, H₃) 1.38-1.34 (m, 1H, H₄), 1.19 (s, 6H, H_{1a}), 1.14 (s, 6H, H_{1e}); δ_C 173.3 (C₈), 137.5 (C₆), 128.1 (C₇), 74.6 (C₅), 60.6 (C₂), 39.6 (C₃), 32.6 (C_{1a}), 20.6 (C_{1e}), 17.1 (C₄). MS (Pos ESI): *m/z* 242.175 ([M+H]⁺, 100%), 264.157 ([M+Na]⁺, 16%); 242.176 (calc. for C₁₃H₂₄NO₃, [M+H]⁺); (Neg ESI): *m/z* 240.160 ([M-H]⁻, 100%); 240.160 (calc. for C₁₃H₂₂NO₃, [M-H]⁻).

11.2.7. Standard amide coupling procedure

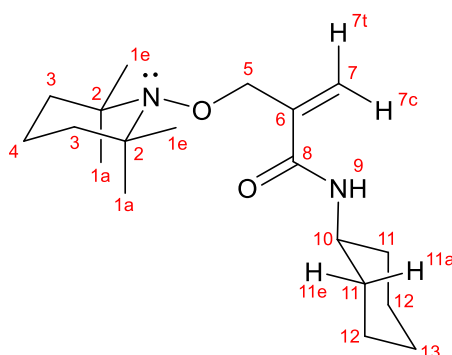


2-[[2,2,6,6-Tetramethylpiperidin-1-yl]oxy]methyl)acrylic acid (2-(TEMPOmethyl)acrylic acid, 1.0 eq.), O-(benzotriazol-1-yl)-*N,N,N',N'*-tetramethyluronium hexafluorophosphate (HBTU, 1.1 eq.), *N,N*-diisopropylethylamine (DIPEA, 2.0 eq.) and amine (1.0 eq.) were dissolved in *N,N*-dimethylformamide (DMF, 5.0 L mol⁻¹) and stirred for 18 h. Solvent was then removed *in vacuo*. Saturated aqueous NaHCO₃ (10 L mol⁻¹) was added and product extracted with EtOAc (3×10 L mol⁻¹). The combined organic layers were washed with brine (3×10 L mol⁻¹). The organic phase was dried with MgSO₄, filtered and solvent removed *in vacuo* yielding crude product. This was purified using flash silica column chromatography (visualised using KMnO₄ stain) yielding pure product.

11.2.8. CHANT

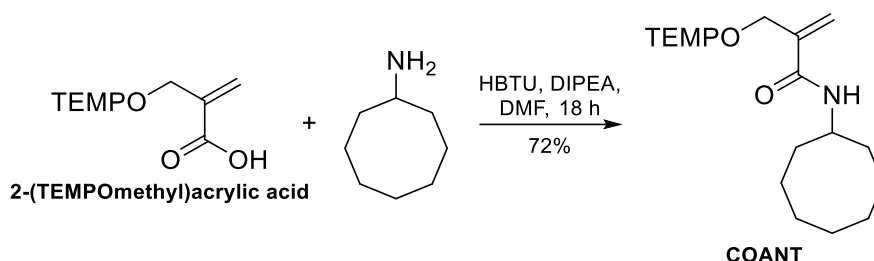


Standard amide coupling procedure (11.2.7) was performed with 2-(TEMPOmethyl)acrylic acid (483 mg, 2.00 mmol, 1.0 eq.), HBTU (834 mg, 2.20 mmol, 1.1 eq.), DIPEA (517 mg, 4.00 mmol, 2.0 eq.), cyclohexylamine (198 mg, 2.00 mmol, 1.0 eq.) and DMF (10.0 mL) yielding white *N*-cyclohexyl-2-[(2,2,6,6-tetramethylpiperidin-1-yl)oxy]methylacrylamide needles (CHANT, 497 mg, 77% or 65% overall).



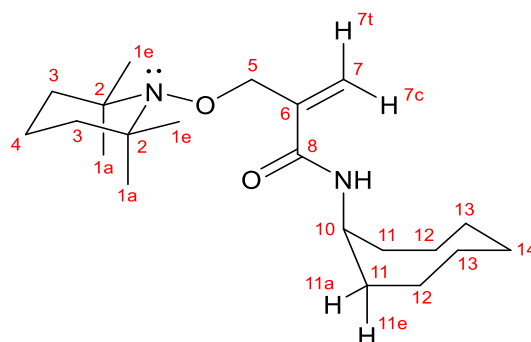
R_f: 0.32 (20%EtOAc/PET ether). Mp: 99.0-100.1 °C. CHN: C, 70.6; H, 10.7; N, 8.4 (found); C, 70.8; H, 10.6; N, 8.7 (calc. for C₁₉H₃₄N₂O₂). IR: ν_{\max} / cm⁻¹ 3340 (NH), 2930 (CH), 1650 (C=O), 1610 (C=C), 1540 (NH). ¹H, ¹³C NMR (400, 100 MHz, CDCl₃): δ_{H} 6.62 (br d, *J* 6.9 Hz, 1H, H₉), 6.09 (d, *J* 1.8 Hz, 1H, H_{7c}), 5.48 (dt, *J* 1.8, 1.0 Hz, 1H, H_{7t}), 4.48 (d, *J* 1.0 Hz, 2H, H₅), 3.90-3.79 (m, *J* 7.2, 6.9 Hz, 1H, H₁₀), 2.00 (ddd, *J* 12.4, 7.2, 3.7 Hz, 2H, H_{11e}), 1.74 (dt, *J* 13.7, 3.7 Hz, 2H, H_{12e}), 1.60-1.53 (m, 1H, H_{13e}), 1.52-1.48 (m, 4H, H₃), 1.48-1.44 (m, 1H, H₄), 1.39 (dt, *J* 13.7, 3.7 Hz, 2H, H_{12a}), 1.38-1.32 (m, 1H, H₄), 1.20 (s, 6H, H_{1a}), 1.16-1.13 (m, 1H, H_{13a}), 1.13 (m, *J* 12.4, 7.2 Hz, 2H, H_{11a}) 1.11 (s, 6H, H_{1e}); δ_{C} 165.7 (C₈), 139.7 (C₆), 123.7 (C₇), 77.5 (C₅), 59.8 (C₂), 48.0 (C₁₀), 39.5 (C₃), 33.2 (C_{1a}), 32.9 (C₁₁), 25.4 (C₁₂), 24.8 (C₁₃), 20.1 (C_{1e}), 16.8 (C₄). MS (Pos ESI): *m/z* 323.270 ([M+H]⁺, 100%), 345.252 ([M+Na]⁺, 4%); 323.270 (calc. for C₁₉H₃₅N₂O₂, [M+H]⁺).

11.2.9. COANT



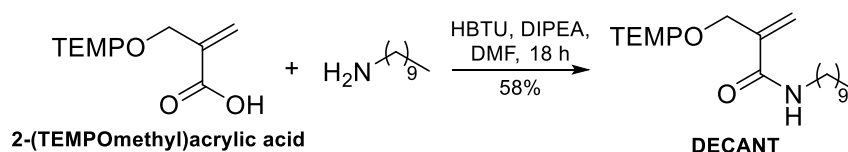
Standard amide coupling procedure (11.2.7) was performed with 2-(TEMPOmethyl)acrylic acid (241 mg, 1.00 mmol, 1.0 eq.), HBTU (417 mg, 1.10 mmol, 1.1 eq.), DIPEA (260 mg, 2.00 mmol, 2.0 eq.), cyclooctylamine (198 mg, 2.00 mmol, 1.0 eq.) and DMF (5.0 mL) yielding

white *N*-cyclooctyl-2-[[2,2,6,6-tetramethylpiperidin-1-yl]oxy]methyl]acrylamide needles (COANT, 252 mg, 72% or 61% overall).

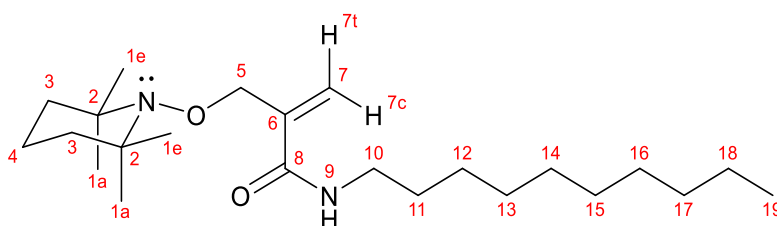


R_f: 0.33 (20%EtOAc/PET ether). Mp: 90.5-92.3 °C. CHN: C, 72.0; H, 11.1; N, 7.9 (found); C, 72.0; H, 10.9; N, 8.0 (calc. for C₂₁H₃₈N₂O₂). IR: ν_{max} / cm⁻¹ 3319 (NH), 2922 (CH), 1654 (C=O), 1608 (C=C), 1531 (NH). ¹H, ¹³C NMR (400, 100 MHz, CDCl₃): δ_H 6.66 (br d, *J* 7.0 Hz, 1H, H₉), 6.08 (d, *J* 1.5 Hz, 1H, H_{7c}), 5.47 (dt, *J* 1.5, 1.0 Hz, 1H, H_{7t}), 4.48 (d, *J* 1.0 Hz, 2H, H₅), 4.12-4.02 (m, *J* 7.0 Hz, 1H, H₁₀), 1.91-1.82 (m, 2H, H_{11e}), 1.38-1.31 (m, 1H, H₄), 1.19 (s, 6H, H_{1a}), 1.19 (m, 18H, H₃, H₄, H_{11a}, H₁₂₋₁₄), 1.10 (s, 6H, H_{1e}); δ_C 165.7 (C₈), 140.0 (C₆), 124.0 (C₇), 77.9 (C₅), 60.1 (C₂), 49.4 (C₁₀), 39.8 (C₃), 33.2 (C_{1a}), 32.4 (C₁₁), 27.4 (C₁₂), 25.6 (C₁₃), 23.9 (C₁₄), 20.5 (C_{1e}), 17.1 (C₄). MS (Pos ESI): *m/z* 351.300 ([M+H]⁺, 100%), 373.283 ([M+Na]⁺, 6%); 351.301 (calc. for C₂₁H₃₉N₂O₂, [M+H]⁺).

11.2.10. DECANT

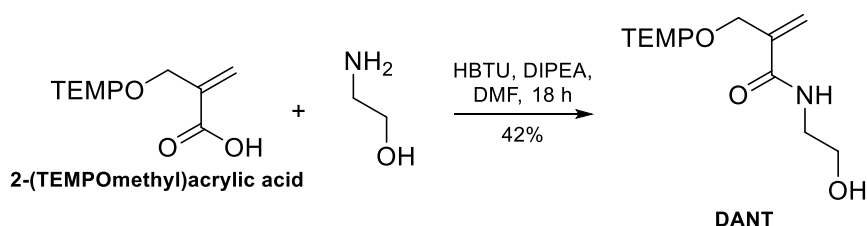


Standard amide coupling procedure (11.2.7) was performed with 2-(TEMPOmethyl)acrylic acid (60.3 mg, 0.250 mmol, 1.0 eq.), HBTU (104 mg, 0.275 mmol, 1.1 eq.), DIPEA (65.0 mg, 0.500 mmol, 2.0 eq.), 1-decanamine (39.3 mg, 0.250 mmol, 1.0 eq.) and DMF (1.25 mL) yielding white *N*-decyl-2-[[2,2,6,6-tetramethylpiperidin-1-yl]oxy]methyl]acrylamide needles (DECANT, 54.8 mg, 58% or 49% overall).

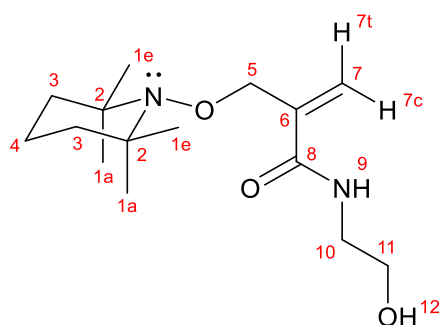


R_f: 0.30 (15%EtOAc/PET ether). ¹H, ¹³C NMR (400, 100 MHz, CDCl₃): δ_H 6.70 (br t, *J* 5.5 Hz, 1H, H₉), 6.07 (d, *J* 1.8 Hz, 1H, H_{7c}), 5.48 (dt, *J* 1.8, 1.2 Hz, 1H, H_{7t}), 4.48 (d, *J* 1.2 Hz, 2H, H₅), 3.32 (td, *J* 7.0, 5.5 Hz, 2H, H₁₀), 1.54 (tt, *J* 7.0, 7.0 Hz, 2H, H₁₁), 1.50-1.21 (m, 20H, H₁₂₋₁₈, H₃, H₄), 1.18 (s, 6H, H_{1a}), 1.09 (s, 6H, H_{1e}), (t, *J* 6.9 Hz, 3H, H₁₉); δ_C 167.0 (C₈), 139.8 (C₆), 123.8 (C₇), 77.7 (C₅), 60.1 (C₂), 39.8 (C₃), 33.2 (C_{1a}), 32.0 (C₁₀), 29.7 (C₁₁), 29.4-22.8 (C₁₂₋₁₈), 20.4 (C_{1e}), 11.0 (C₄), 14.3 (C₁₉). MS (Pos ESI): *m/z* 381.348 ([M+H]⁺, 100%), 403.323 ([M+Na]⁺, 7%); 381.348 (calc. for C₂₃H₄₅N₂O₂, [M+H]⁺).

11.2.11. DANT

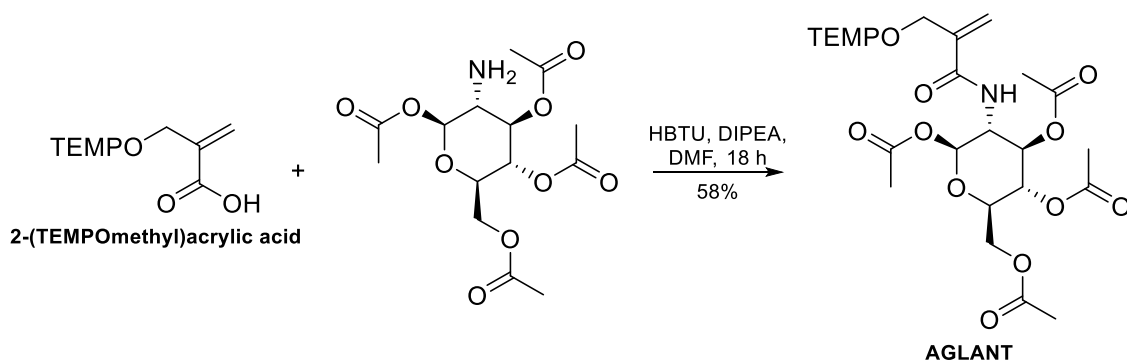


Standard amide coupling procedure (11.2.7) was performed with 2-(TEMPOmethyl)acrylic acid (481 mg, 2.00 mmol, 1.0 eq.), HBTU (831 mg, 2.20 mmol, 1.1 eq.), DIPEA (517 mg, 4.00 mmol, 2.0 eq.), ethanolamine (122 mg, 2.00 mmol, 1.0 eq.) and DMF (10.0 mL) yielding white crystalline *N*-2-hydroxyethyl-2-[(2,2,6,6-tetramethylpiperidin-1-yl)oxy]meth]acrylamide (DANT, 238 mg, 42% or 36% overall).



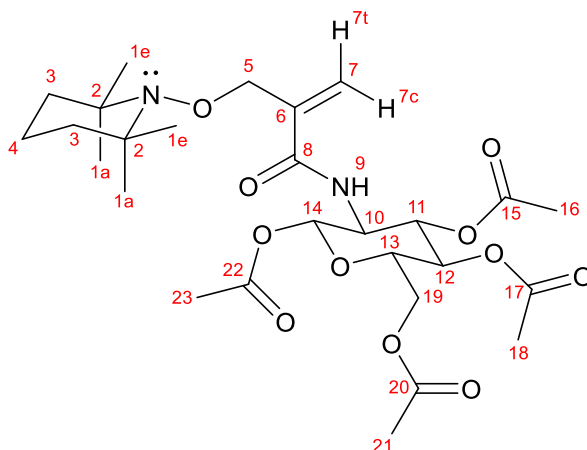
R_f: 0.36 (7%MeOH/DCM). Mp: 91.8-93.6 °C. CHN: C, 63.0; H, 9.9; N, 9.6 (found); C, 63.4; H, 9.9; N, 9.9 (calc. for C₁₅H₂₈N₂O₃). IR: ν_{\max} / cm⁻¹ 3371 (NH), 2936 (CH), 1660 (C=O), 1611 (C=C), 1551 (NH). ¹H, ¹³C NMR (400, 100 MHz, CDCl₃): δ_{H} 7.14 (br t, *J* 5.5 Hz, 1H, H₉), 6.07 (d, *J* 1.1 Hz, 1H, H_{7c}), 5.55 (dt, *J* 1.1, 0.9 Hz, 1H, H_{7t}), 4.51 (d, *J* 0.9 Hz, 2H, H₅), 3.77 (t, *J* 5.0 Hz, 2H, H₁₀), 3.51 (dt, *J* 5.5, 5.0 Hz, 2H, H₁₁), 2.88 (br s, 1H, H₁₂), 1.61-1.50 (m, 4H, H₃), 1.50-1.43 (m, 1H, H₄), 1.38-1.30 (m, 1H, H₄), 1.18 (s, 6H, H_{1a}), 1.10 (s, 6H, H_{1e}); δ_{C} 168.3 (C₈), 139.5 (C₆), 124.0 (C₇), 77.3 (C₅), 60.1 (C₂), 62.7 (C₁₀), 42.8 (C₁₁), 39.8 (C₃), 33.1 (C_{1a}), 20.4 (C_{1e}), 17.1 (C₄). MS (Pos ESI): *m/z* 285.217 ([M+H]⁺, 100%), 307.198 ([M+Na]⁺, 2%); 285.218 (calc. for C₁₅H₂₉N₂O₃, [M+H]⁺).

11.2.12. AGLANT



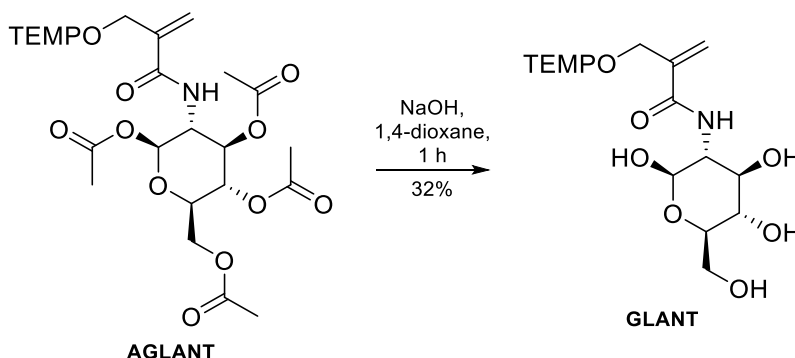
Standard amide coupling procedure (11.2.7) was performed with 2-(TEMPOmethyl)acrylic acid (60.3 mg, 0.250 mmol, 1.0 eq.), HBTU (104 mg, 0.275 mmol, 1.1 eq.), DIPEA (65.0 mg, 0.500 mmol, 2.0 eq.), 1,3,4,6-tetra-O-acetyl-2-amino-2-deoxy- β -D-glucopyranose hydrochloride (95.9 mg, 0.250 mmol, 1.0 eq.) and DMF (1.25 mL) yielding white crystalline

N-1,3,4,6-tetra-*O*-acetyl-2-aminoglucosyl-2-[[2,2,6,6-tetramethylpiperidin-1-yl]oxy]methyl]acrylamide (AGLANT, 54.8 mg, 58% or 49% overall).

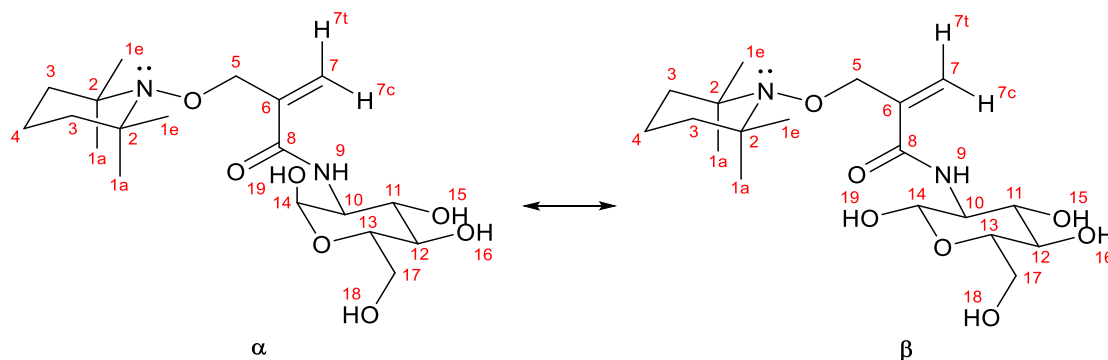


R_f: 0.42 (50%EtOAc/PET ether). Mp: 121.7-123.1 °C. ¹H, ¹³C NMR (400, 100 MHz, CD₃OD): δ_H 5.85 (d, *J* 8.9 Hz, 1H, H₁₄), 5.69 (s, 1H, H_{7c}), 5.63 (s, 1H, H_{7t}), 5.35 (dd, *J* 10.5, 9.6, 1H, H₁₁), 5.06 (dd, *J* 10.1, 9.2, 1H, H₁₂), 4.48 (ddd, *J* 12.8, 1.6, 1.3 Hz, 1H, H₅), 4.44 (ddd, *J* 12.8, 1.6, 1.3 Hz, 1H, H₅), 4.30 (dd, *J* 12.8, 4.3 Hz, 1H, H₁₉), 4.17 (dd, *J* 10.5, 9.2 Hz, 1H, H₁₀), 4.11 (dd, *J* 12.8, 2.3 Hz, 2H, H₁₉), 3.93 (ddd, *J* 10.1, 4.3, 2.3 Hz, 1H, H₁₃), 2.06 (s, 3H, H₁₆), 2.06 (s, 3H, H₁₈), 2.02 (s, 3H, H₂₃), 1.96 (s, 3H, H₂₁), 1.70-1.55 (m, 1H, H₄), 1.50-1.43 (m, 4H, H₃), 1.38-1.28 (m, 1H, H₄), 1.17 (s, 6H, H_{1a}), 1.12 (s, 6H, H_{1e}); δ_C 172.3-170.1 (C₂₂, C₂₀, C₁₇, C₁₅, C₈), 142.5 (C₆), 120.4 (C₇), 93.3 (C₁₄), 76.6 (C₅), 73.8 (C₁₃), 73.8 (C₁₁), 69.6 (C₁₂), 62.9 (C₁₉), 61.1 (C₂), 54.2 (C₁₀), 40.7 (C₃), 33.3 (C_{1a}), 20.7-20.5 (C₂₃, C₂₁, C₁₈, C₁₆, C_{1e}), 18.0 (C₄). MS (Pos ESI): *m/z* 571.286 ([M+H]⁺, 100%), 593.268 ([M+Na]⁺, 6%), 529.267 ([M-CH₂O+H]⁺, 75%), 551.246 ([M-CH₂O+Na]⁺, 4%); 571.287 (calc. for C₂₇H₄₃N₂O₁₁, [M+H]⁺).

11.2.13. GLANT



N-1,3,4,6-tetra-*O*-acetyl-2-aminoglucosyl-2-[[2,2,6,6-tetramethylpiperidin-1-yl]oxy]methyl]acrylamide (65.1 g, 0.11 mmol, 1.0 eq.) was dissolved in 1,4-dioxane (0.77 mL), aqueous NaOH (1.0 M, 0.77 mL, 0.77 mmol, 7.0 eq.) added and the solution stirred for 1 h. This was neutralised (pH 7) with aqueous HCl (2.0 M, 0.34 mL, 0.77 mmol, 7.0 eq.) and solvent removed *in vacuo*. The resultant solid was dissolved in a 1:1 MeOH:MeCN mixture and MeOH evaporated *in vacuo*. The resultant solution was dried with MgSO₄ and filtered, yielding crude pale yellow oil. This was purified using flash silica column chromatography (15%MeOH/DCM, R_f 0.36, visualised using KMnO₄ stain) yielding white crystalline *N*-glucosyl-2-[[2,2,6,6-tetramethylpiperidin-1-yl]oxy]methyl]acrylamide (GLANT, 14.8 mg, 32% or 16% overall).



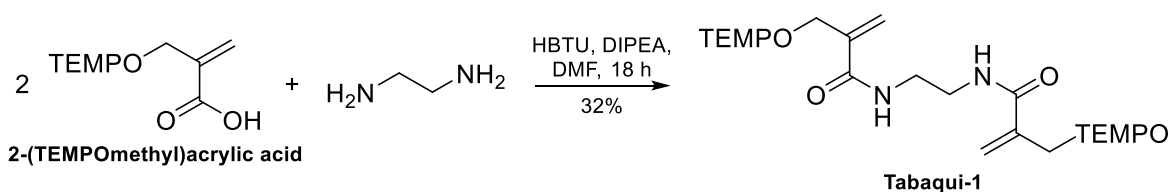
α : 65%: $^1\text{H NMR}$ (400 MHz, CD_3OD): δ_{H} 5.98 (d, J 0.9 Hz, 1H, $\text{H}_{7\text{c}}$), 5.62 (td, J 2.7, 0.9 Hz, 1H, $\text{H}_{7\text{t}}$), 5.14 (d, J 3.2 Hz, 1H, H_{14}), 4.58-4.47 (m, 2H, H_5), 3.94 (dd, J 10.2, 3.7 Hz, 1H, H_{10}), 3.83-3.33 (m, 5H, H_{11} , H_{12} , H_{13} , H_{17}), 1.68-1.55 (m, 1H, H_4), 1.52-1.43 (m, 4H, H_3) 1.38-1.28 (m, 1H, H_4), 1.22-1.09 (m, 12H, H_1);

β : 21%: $^1\text{H NMR}$ (400 MHz, CD_3OD): δ_{H} 5.87 (d, J 0.9 Hz, 1H, $\text{H}_{7\text{c}}$), 5.65 (td, J 2.7, 0.9 Hz, 1H, $\text{H}_{7\text{t}}$), 4.66 (d, J 8.2 Hz, 1H, H_{14}), 4.58-4.47 (m, 2H, H_5), 3.86 (dd, J 11.9, 1.8 Hz, 1H, H_{10}), 3.83-3.33 (m, 5H, H_{11} , H_{12} , H_{13} , H_{17}), 1.68-1.55 (m, 1H, H_4), 1.52-1.43 (m, 4H, H_3) 1.38-1.28 (m, 1H, H_4), 1.22-1.09 (m, 12H, H_1); MS (Pos ESI): m/z 403.243 ($[\text{M}+\text{H}]^+$, 100%), 425.225 ($[\text{M}+\text{Na}]^+$, 9%); 402.237 (calc. for $\text{C}_{19}\text{H}_{34}\text{N}_2\text{O}_7$).

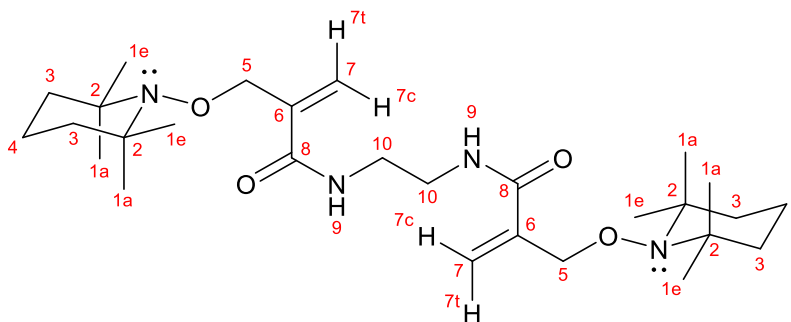
Unknown: 14%: $^1\text{H NMR}$ (400 MHz, CD_3OD): δ_{H} 5.88 (d, J 0.9 Hz, 1H, $\text{H}_{7\text{c}}$), 5.63 (td, J 2.7, 0.9 Hz, 1H, $\text{H}_{7\text{t}}$), 5.08 (d, J 1.4 Hz, 1H, H_{14}), 4.58-4.47 (m, 2H, H_5), 4.04 (dd, J 9.6, 4.6 Hz, 1H, H_{10}), 3.83-3.33 (m, 5H, H_{11} , H_{12} , H_{13} , H_{17}), 1.68-1.55 (m, 1H, H_4), 1.52-1.43 (m, 4H, H_3) 1.38-1.28 (m, 1H, H_4), 1.22-1.09 (m, 12H, H_1); MS (Pos ESI): m/z 403.243 ($[\text{M}+\text{H}]^+$, 100%), 425.225 ($[\text{M}+\text{Na}]^+$, 9%); 402.237 (calc. for $\text{C}_{19}\text{H}_{34}\text{N}_2\text{O}_7$).

All: $^{13}\text{C NMR}$ (100 MHz, CD_3OD): δ_{C} 169.8 (C_8), 141.7 (C_6), 122.8 (C_7), 92.5 (C_{14}), 77.7 (C_5), 73.1 (C_{13}), 72.8 (C_{11}), 72.5 (C_{12}), 62.8 (C_{19}), 61.2 (C_2), 55.9 (C_{10}), 40.8 (C_{17}), 40.7 (C_3), 33.4 ($\text{C}_{1\text{a}}$), 20.8 ($\text{C}_{1\text{e}}$), 18.0 (C_4). MS (Pos ESI): m/z 403.243 ($[\text{M}+\text{H}]^+$, 100%), 425.225 ($[\text{M}+\text{Na}]^+$, 6%); 403.244 (calc. for $\text{C}_{19}\text{H}_{35}\text{N}_2\text{O}_7$, $[\text{M}+\text{H}]^+$).

11.2.14. Tabaqui-1

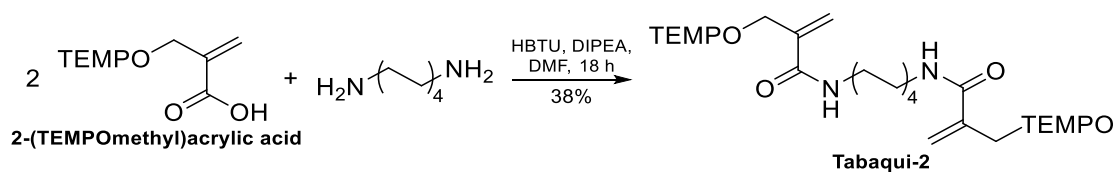


Standard amide coupling procedure (11.2.7) was performed with 2-(TEMPOmethyl)acrylic acid (121 mg, 0.500 mmol, 2.0 eq.), HBTU (208 mg, 0.550 mmol, 2.2 eq.), DIPEA (130 mg, 1.00 mmol, 4.0 eq.), ethylenediamine (15.0 mg, 0.250 mmol, 1.0 eq.) and DMF (1.25 mL) yielding white crystalline N,N' -ethylene-bis(2-((2,2,6,6-tetramethylpiperidin-1-yl)oxy)methyl)acrylamide) (Tabaqui-1, 43.2 mg, 32% or 27% overall).

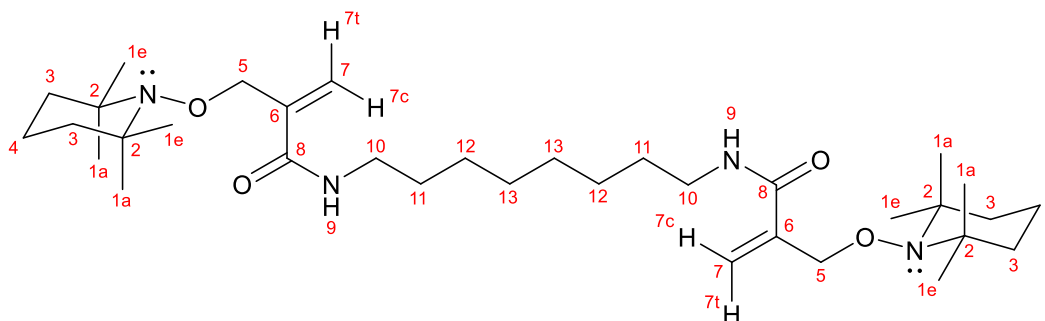


R_f: 0.37 (70%EtOAc/DCM). ¹H, ¹³C NMR (400, 100 MHz, CD₃OD): δ_H 5.78 (s, 2H, H_{7c}), 5.62 (s, 2H, H_{7t}), 4.49 (s, 4H, H₅), 3.39 (s, 4H, H₁₀), 1.67-1.53 (m, 2H, H₄), 1.49-1.42 (m, 8H, H₃) 1.36-1.29 (m, 2H, H₄), 1.16 (s, 12H, H_{1a}), 1.11 (s, 12H, H_{1e}); δ_C 170.4 (C₈), 142.5 (C₆), 119.9 (C₇), 76.7 (C₅), 61.1 (C₂), 40.7 (C₃), 40.3 (C₁₀), 33.3 (C_{1a}), 20.7 (C_{1e}), 18.0 (C₄). MS (Pos ESI): *m/z* 507.391 ([M+H]⁺, 100%), 529.373 ([M+Na]⁺, 5%), 254.210 ([M+2H]²⁺, 34%); 507.391 (calc. for C₂₈H₅₁N₄O₄, [M+H]⁺).

11.2.15. Tabaqui-2

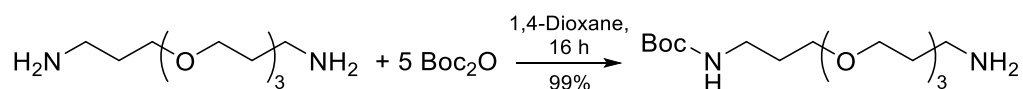


Standard amide coupling procedure (11.2.7) was performed with 2-(TEMPOmethyl)acrylic acid (121 mg, 0.500 mmol, 2.0 eq.), HBTU (209 mg, 0.550 mmol, 2.2 eq.), DIPEA (130 mg, 1.00 mmol, 4.0 eq.), 1,8-diaminooctane (36.1 mg, 0.250 mmol, 1.0 eq.) and DMF (1.25 mL) yielding white crystalline *N,N'*-octyl-1,8-diamino-bis(2-[[2,2,6,6-tetramethylpiperidin-1-yl]oxy]methyl)acrylamide (Tabaqui-4, 55.4 mg, 38% or 32% overall).

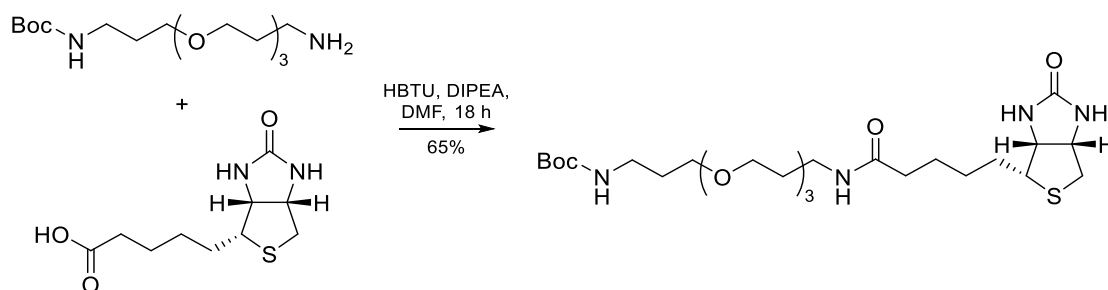


R_f: 0.31 (40%EtOAc/PET ether). Mp: 134.2-135.3 °C. CHN: C, 68.9; H, 10.4; N, 9.3 (found); C, 69.1; H, 10.6; N, 9.5 (calc. for C₃₄H₆₂N₄O₄). ¹H, ¹³C NMR (400, 100 MHz, CD₃OD): δ_H 5.74 (s, 2H, H_{7c}), 5.58 (s, 2H, H_{7t}), 4.50 (s, 4H, H₅), 3.24 (t, *J* 7.0 Hz, 4H, H₁₀), 1.67-1.59 (m, 2H, H₄), 1.55 (t, *J* 7.0 Hz, 4H, H₁₁), 1.51-1.45 (m, 8H, H₃) 1.40-1.30 (m, 2H, H₁₃), 1.40-1.30 (m, 2H, H₁₂), 1.40-1.30 (m, 2H, H₄), 1.18 (s, 12H, H_{1a}), 1.13 (s, 12H, H_{1e}); δ_C 170.1 (C₈), 140.9 (C₆), 120.0 (C₇), 77.3 (C₅), 61.2 (C₂), 40.7 (C₃), 40.7 (C₁₀), 40.5 (C₁₁), 33.3 (C_{1a}), 30.4 (C₁₂), 30.4 (C₁₃), 20.7 (C_{1e}), 18.0 (C₄). MS (Pos ESI): *m/z* 591.495 ([M+H]⁺, 100%), 613.480 ([M+Na]⁺, 11%), 296.260 ([M+2H]²⁺, 53%); 591.485 (calc. for C₃₄H₆₃N₄O₄, [M+H]⁺).

11.2.16. BIOANT

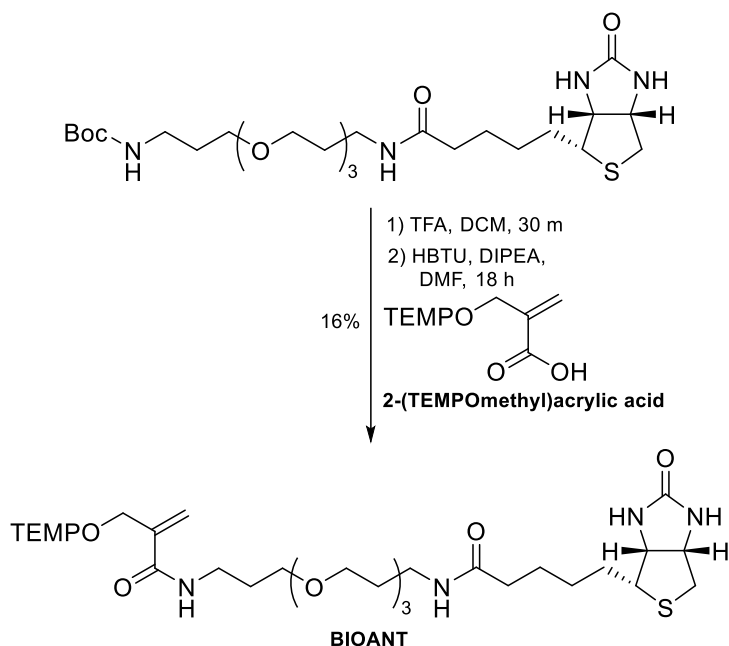


N-biotin-*N'*-Boc-4,7,10-trioxatridecane-1,13-diamine was synthesised as described in literature.²⁶⁵ 4,7,10-trioxa-1,13-diaminotridecane (22.0 g, mL, 100 mmol, 5.0 eq.) was dissolved in 1,4-dioxane (50 mL) and a solution of Boc anhydride (4.37 g, 20.0 mmol, 1.0 eq.) in dioxane (30 mL) was added dropwise over 3 h, whilst stirring and further stirred for 16 h. Solvent was removed *in vacuo*, resulting in a yellow oil. H₂O (50 mL) was added and product extracted with DCM (3×50 mL). The combined organic layers were washed with brine (3×50 mL). The extraction procedure and the subsequent washing were repeated. The resulting organic solution was dried (MgSO₄), filtered, and solvent removed *in vacuo*, producing almost colourless mono-Boc-4,7,10-trioxatridecane-1,13-diamine oil (7.48 g, 99%). ¹H and ¹³C NMR spectroscopy and mass spectrometry confirmed product identity and showed product was suitably pure for use in next step without further purification. Obtained values were consistent with literature.²⁶⁵



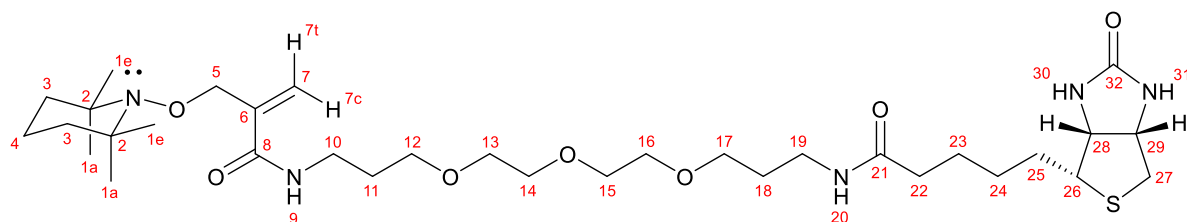
Standard amide coupling reaction procedure (11.2.7) was followed using D-biotin (883 mg, 3.60 mmol, 1.2 eq.), HBTU (1530 mg, 4.00 mmol, 1.4 eq.), DIPEA (939 mg, 7.27 mmol, 2.4 eq.), mono-Boc-4,7,10-trioxatridecane-1,13-diamine (960 mg, 3.00 mmol, 1.0 eq.) and DMF (15 mL). Crude product was purified using flash silica column chromatography (10%MeOH/DCM, R_f 0.39) yielding *N*-biotin-*N'*-Boc-4,7,10-trioxatridecane-1,13-diamine (1070 mg, 65%). ¹H and ¹³C NMR spectroscopy and mass spectrometry confirmed product identity and showed product was suitably pure for use in next step. Obtained values were consistent with literature.²⁶⁵

Mono-biotin-4,7,10-trioxatridecane-1,13-diamine was synthesised from *N*-biotin-*N'*-Boc-4,7,10-trioxatridecane-1,13-diamine as described in literature.²⁶⁶



N-biotin-*N'*-Boc-4,7,10-trioxatridecane-1,13-diamine (541 mg, 1.00 mmol, 1.0 eq.) was dissolved in DCM (10.0 mL) and cooled using an ice-water bath (0 °C). Trifluoroacetic acid (TFA, 5.0 mL) was added and the solution stirred for 15 min. The solution was stirred at room temperature for a further 15 min. Solvent was removed *in vacuo* yielding crude yellow oil. This was purified by silica gel flash chromatography (2%NH₄OH/20%MeOH/DCM, R_f 0.35, visualised using KMnO₄ stain) to afford light yellow sticky mono-biotin-4,7,10-trioxatridecane-1,13-diamine solid (442 mg, ~100%). ¹H NMR spectroscopy and mass spectrometry confirmed product identity and showed product was suitably pure for use in next step without further purification.

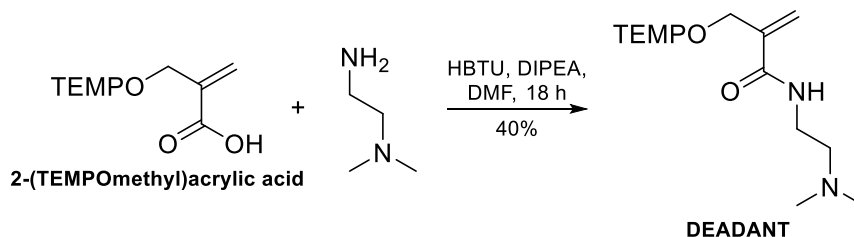
Standard amide coupling procedure (11.2.7) was performed with 2-(TEMPOmethyl)acrylic acid (242 mg, 1.00 mmol, 1.0 eq.), HBTU (418 mg, 1.10 mmol, 1.1 eq.), DIPEA (261 mg, 2.00 mmol, 2.0 eq.), mono-boc-4,7,10-trioxatridecane-1,13-diamine (442 mg, 1.00 mmol, 1.0 eq.) and DMF (5.0 mL) yielding yellow *N*-biotin-*N'*-boc-4,7,10-trioxatridecane-1,13-diamine oil (105 mg, 16% or 14% overall).



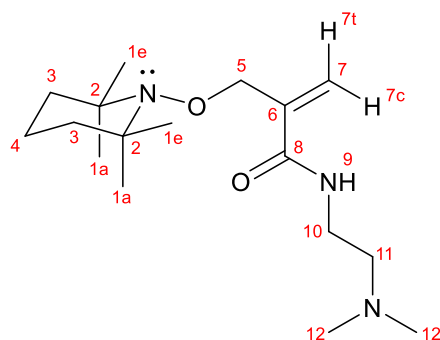
R_f: 0.39 (12%MeOH/DCM). IR: ν_{\max} / cm⁻¹ 3318 (NH), 2930 (CH), 1656 (C=O), 1617 (C=C), 1530 (NH), 841 (big sharp peak). ¹H, ¹³C NMR (400, 100 MHz, CDCl₃): δ_{H} 6.99 (t, *J* 5.9 Hz, 1H, H₉), 6.73 (t, *J* 5.9 Hz 1H, H₂₀), 5.96 (br m, 1H, H₃₁), 5.96 (m, 1H, H_{7c}), 5.54 (d, *J* 1.0 Hz, 1H, H_{7t}), 5.42 (br m, 1H, H₃₀), 4.52 (dt, *J* 6.5, 4.0 Hz, 1H, H₂₉), 4.48 (*app s*, 2H, H₅), 4.32 (dd, *J* 6.5 5.0 Hz 1H, H₂₈), 3.73-3.51 (m, 14 H, H₁₀, H₁₂₋₁₇), 3.40 (td, *J* 6.8, 5.9 Hz 1H, H₁₀), 3.30 (td, *J* 6.8, 5.9 Hz 1H, H₁₉), 3.14 (m, 1H, H₂₆), 2.89 (dd, *J* 12.9, 4.7 Hz, 1H, H₂₇), 2.73 (d, *J* 12.9 Hz, 1H, H₂₇), 2.18 (t, *J* 7.2 Hz, 1H, H₂₂), 1.82 (m, 2H, H₂₅), 1.76 (tt, *J* 7.2 Hz, 2H, H₂₄), 1.64 (t, *J* 7.2 Hz, 2H, H₂₃), 1.60-1.30 (m, 10H, H₃, H₄, H₁₁, H₁₈), 1.16 (s, 6H, H_{1a}), 1.09 (s, 6H, H_{1e}). δ_{C} 173.9 (C₃₂), 167.4 (C₈), 164.1 (C₂₁), 140.0 (C₆), 122.2 (C₇), 76.8 (C₅), 70.4, 70.3, 70.1, 69.9, 69.6, 69.2 (C₁₂₋₁₇), 61.9 (C₂₉), 60.4 (C₂₈), 60.1 (C₂), 55.6 (C₂₆), 55.0, 48.0, 43.1, 40.6 (C₂₇), 39.7

(C₃), 38.0 (C₁₀), 37.3 (C₁₉), 35.8 (C₂₂) 33.0 (C_{1a}), 29.4, 29.0, 28.1, 27.9, 25.7 (C₁₁, C₁₈, C₂₃, C₂₄, C₂₅), 20.4 (C_{1e}), 19.0, 17.1 (C₄), 12.5. MS (Pos ESI): *m/z* 692.417 ([M+Na]⁺, 100%), 670.438 ([M+H]⁺, 73%), 346.719 ([M+H+Na]²⁺, 11%); 692.403 (calc. for C₃₃H₅₉N₅O₇SNa, [M+Na]⁺).

11.2.17. DEADANT

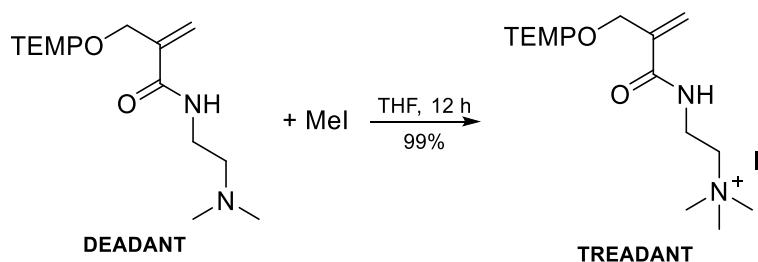


Standard amide coupling procedure (11.2.7) was performed with 2-(TEMPOmethyl)acrylic acid (482 mg, 2.00 mmol, 1.0 eq.), HBTU (835 mg, 2.20 mmol, 1.1 eq.), DIPEA (517 mg, 4.00 mmol, 2.0 eq.) *N,N*-dimethylethylenediamine (177 mg, 2.00 mmol, 1.0 eq.) and DMF (10.0 mL) yielding colourless *N',N,N*-dimethylethyleneamino-2-[(2,2,6,6-tetramethylpiperidin-1-yl)oxy]methyl}acrylamide oil (DEADANT, 251 mg, 40% or 34% overall).



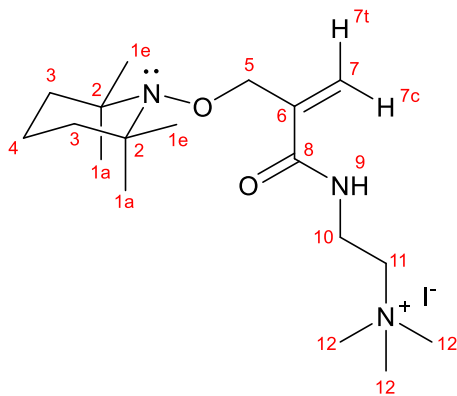
R_f: 0.29 (2%NH₄OH/5%MeOH/DCM). CHN: C, 65.7; H, 11.0; N, 13.5 (found); C, 65.6; H, 10.7; N, 13.5 (calc. for C₁₇H₃₃N₃O₂). IR: ν_{\max} / cm⁻¹ 3345 (NH), 2932 (CH), 1660 (C=O), 1616 (C=C), 1532 (NH), 1056 (CN), 1043 (CN). ¹H, ¹³C NMR (400, 100 MHz, CDCl₃): δ_{H} 7.01 (br s, 1H, H₉), 6.07 (dt, *J* 1.5, 1.1 Hz, 1H, H_{7c}), 5.51 (dt, *J* 1.5, 0.6 Hz, 1H, H_{7t}), 4.50 (dd, *J* 1.1, 0.6 Hz, 2H, H₅), 3.42 (td, *J* 6.0, 5.2 Hz, 2H, H₁₀), 2.45 (t, *J* 6.0 Hz, 2H, H₁₁), 2.20 (s, 6H, H₁₂), 1.65-1.50 (m, 1Hf, H₄), 1.50-1.43 (m, 4H, H₃), 1.37-1.30 (m, 1H, H₄), 1.18 (s, 6H, H_{1a}), 1.10 (s, 6H, H_{1e}); δ_{C} 167.0 (C₈), 139.9 (C₆), 123.4 (C₇), 77.5 (C₅), 60.0 (C₂), 57.8 (C₁₁), 45.2 (C₁₂), 39.8 (C₃), 37.1 (C₁₀), 33.1 (C_{1a}), 20.2 (C_{1e}), 17.2 (C₄). MS (Pos ESI): *m/z* 312.266 ([M+H]⁺, 100%), 334.247 ([M+Na]⁺, 4%); 312.265 (calc. for C₁₇H₃₄N₃O₂, [M+H]⁺).

11.2.18. TREADANT



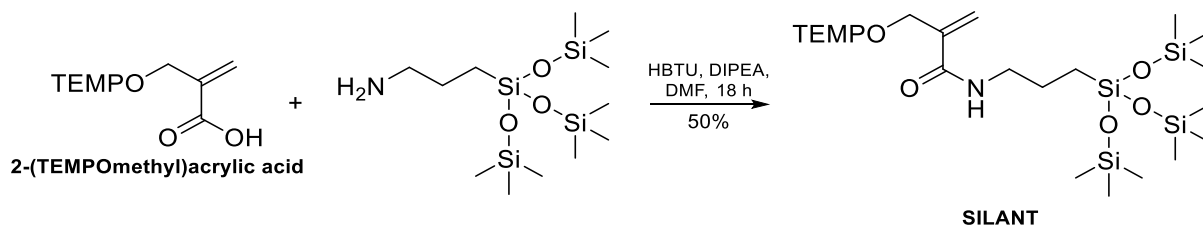
N',N,N-Dimethylethyleneamino-2-[(2,2,6,6-tetramethylpiperidin-1-yl)oxy]methyl}acrylamide (DEADANT, 155 mg, 0.500 mmol, 1.0 eq.) was dissolved in dry tetrahydrofuran (THF),

0.50 mL), MeI (81.6 mg, 0.575 mmol, 1.15 eq.) added and the reaction mixture stirred for 12 h. The precipitated white solid was washed with dry THF (2x0.50 mL). Residual solvent was removed *in vacuo*, yielding white solid *N,N,N,N*-trimethylethyleneammonium-2-[[2,2,6,6-tetramethylpiperidin-1-yl)oxy]methyl]acrylamide iodide (TREADANT, 224 mg, 99% or 34% overall).

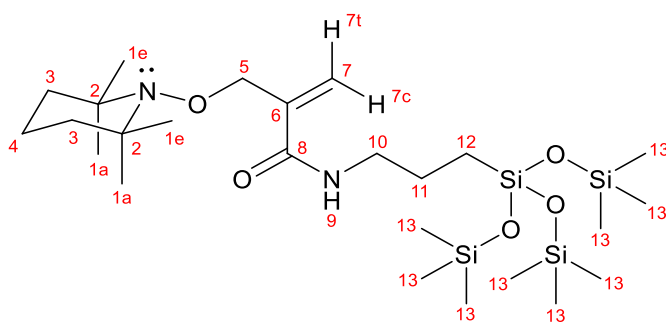


IR: ν_{\max} / cm^{-1} 3345 (NH), 2928 (CH), 1660 (C=O), 1615 (C=C), 1526 (NH), 1037 (CN). ^1H , ^{13}C NMR (400, 100 MHz, CD_3CN): δ_{H} 7.39 (br s, 1H, H_9), 5.90 (td, J 1.1, 0.9 Hz, 1H, $\text{H}_{7\text{c}}$), 5.67 (td, J 1.7, 0.9 Hz, 1H, $\text{H}_{7\text{t}}$), 4.47 (dd, J 1.7, 1.1 Hz, 2H, H_5), 3.68 (td, J 6.3, 5.2 Hz, 2H, H_{10}), 3.48 (t, J 6.3 Hz, 2H, H_{11}), 3.13 (s, 9H, H_{12}), 1.64-1.52 (m, 1H, H_4), 1.50-1.38 (m, 4H, H_3), 1.35-1.27 (m, 1H, H_4), 1.15 (s, 6H, $\text{H}_{1\text{a}}$), 1.09 (s, 6H, $\text{H}_{1\text{e}}$); δ_{C} 168.3 (C_8), 141.6 (C_6), 120.7 (C_7), 76.4 (C_5), 65.9 (C_{11}), 60.5 (C_2), 54.3 (C_{12}), 40.4 (C_3), 34.4 (C_{10}), 33.3 ($\text{C}_{1\text{a}}$), 20.4 ($\text{C}_{1\text{e}}$), 17.7 (C_4). MS (Pos ESI): m/z 326.276 ($[\text{M}-\text{I}]^+$, 100%); 326.281 (calc. for $\text{C}_{18}\text{H}_{36}\text{N}_3\text{O}_2$, $[\text{M}-\text{I}]^+$).

11.2.19. SILANT



Standard amide coupling procedure (11.2.7) was performed with 2-(TEMPOmethyl)acrylic acid (217 mg, 0.900 mmol, 1.0 eq.), HBTU (379 mg, 1.00 mmol, 1.1 eq.), DIPEA (233 mg, 1.80 mmol, 2.0 eq.), (3-aminopropyl)tris(trimethylsiloxy)silane (318 mg, 1.00 mmol, 1.0 eq.) and DMF (4.5 mL) yielding white *N,N'*-(3-(tris(trimethylsiloxy)silane)propylamino)-2-[[2,2,6,6-tetramethylpiperidin-1-yl)oxy]methyl]acrylamide needles (S4P4.7 or SILANT, 258 mg, 50% or 42% overall).



R_f: 0.37 (15%EtOAc/PET ether). Mp: 52.6-54.3 °C. CHN: C, 52.0; H, 9.6; N, 4.7 (found); C, 52.0; H, 9.8; N, 4.9 (calc. for C₂₅H₅₆N₂O₅Si₄). IR: ν_{max} / cm⁻¹ 3343 (NH), 2958 (CH), 1654 (C=O), 1606 (C=C), 1532 (NH), 1250 (CSi), 1040 (SiOSi). ¹H, ¹³C NMR (400, 100 MHz, CDCl₃): δ_H 6.74 (t, *J* 5.5 Hz, 1H, H₉), 6.07 (d, *J* 1.8 Hz, 1H, H_{7c}), 5.49 (dt, *J* 1.8, 0.9 Hz, 1H, H_{7t}), 4.50 (d, *J* 0.9 Hz, 2H, H₅), 3.31 (td, *J* 7.3, 5.5 Hz, 2H, H₁₀), 1.57 (tt, *J* 8.2, 7.3 Hz, 2H, H₁₁), 1.19 (s, 6H, H_{1a}), 1.10 (s, 6H, H_{1e}), 0.48 (t, *J* 8.2 Hz, 2H, H₁₂), 0.09 (s, 27H, H₁₃); δ_C 166.9 (C₈), 139.8 (C₆), 123.8 (C₇), 77.7 (C₅), 60.1 (C₂), 42.5 (C₁₀), 39.8 (C₃), 33.2 (C_{1a}), 23.8 (C₁₁), 20.5 (C_{1e}), 17.1 (C₄), 12.0 (C₁₂), 1.9 (C₁₃). MS (Pos ESI): *m/z* 577.336 ([M+H]⁺, 100%), 599.316 ([M+Na]⁺, 5%); 577.334 (calc. for C₂₅H₅₇N₂O₅Si₄, [M+H]⁺).

11.3. TART properties and stability studies

11.3.1. Free TEMPO• concentration

Free TEMPO• concentration in pure CHANT was quantified using electron paramagnetic resonance (EPR) spectroscopy. Double integrals of EPR spectra of CHANT solution (1.00 mM) and standard TEMPO• solution (0.100 mM) in MeCN were used to determine radical concentration. EPR spectra were recorded at X-band on a JEOL X320 spectrometer using 1 G modulation width and 1 mW power. EPR spectra indicated ~0.05mol.% free TEMPO• relative to CHANT.

11.3.2. Oxidation and reduction

Oxidation and reduction processes of CHANT were investigated using cyclic voltammetry (CV). Cyclic voltammetry was performed using a 5 mL electrochemical cell containing platinum wire working and counter electrodes and a Ag/AgCl reference electrode. CHANT analyte (1.00 mM) and Bu₄NPF₆ electrolyte (100 mM) in MeCN (2.5 mL total volume) was added to the cell and a cyclic voltammogram was recorded over a range of -1 V to +2 V at a scan rate of 100 mV s⁻¹. Spectra showed that CHANT did not undergo any significant oxidative or reductive processes under these conditions (Figure 186).

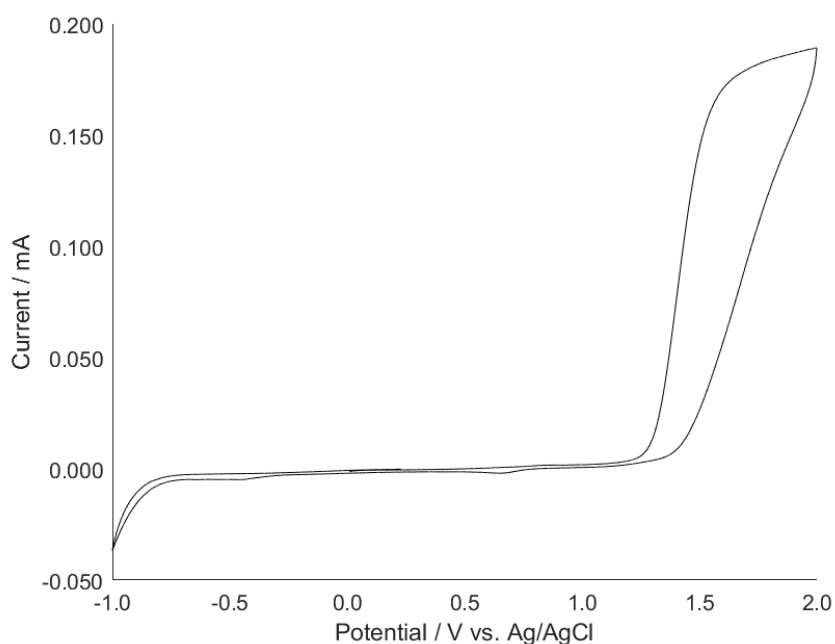


Figure 186: Cyclic voltammogram of CHANT (1.00 mM), using MeCN as solvent and Bu₄NPF₆ (100 mM) as electrolyte and Pt wire working and counter electrodes and a Ag/AgCl reference electrode.

11.3.3. Michael addition

CHANT susceptibility to Michael addition by polar solvents and weak bases was explored. For this, CHANT subjected to polar solvents and weak bases was routinely monitored using ^1H NMR spectroscopy over three weeks. During this time, CHANT (~ 10 mM) dissolved in CD_3OD showed no detectable decay. CHANT (~ 10 mM) in presence of diisopropylamine ($\sim 1:5$ molar ratio) and dissolved in CD_3OD , showed no detectable decay after 24 h but some decay after three weeks (Figure 52). From NMR spectra observations (Figure 188), it was believed that diisopropylamine added across the CHANT double bond, without the loss of TEMPO^\bullet (Figure 51). New peaks were assigned as follows: ^1H NMR (400 MHz, CD_3OD): δ_{H} 3.92 (d, J 8.2 Hz, 1H, $\text{H}_{5\text{p}}$), 3.82 (d, J 8.2 Hz, 1H, $\text{H}_{5\text{p}}$), 2.90-2.74 (m, 1H, H_6), 2.82 (d, J 11.9 Hz, 1H, $\text{H}_{7\text{p}}$), 2.68 (d, J 11.9 Hz, 1H, $\text{H}_{7\text{p}}$).

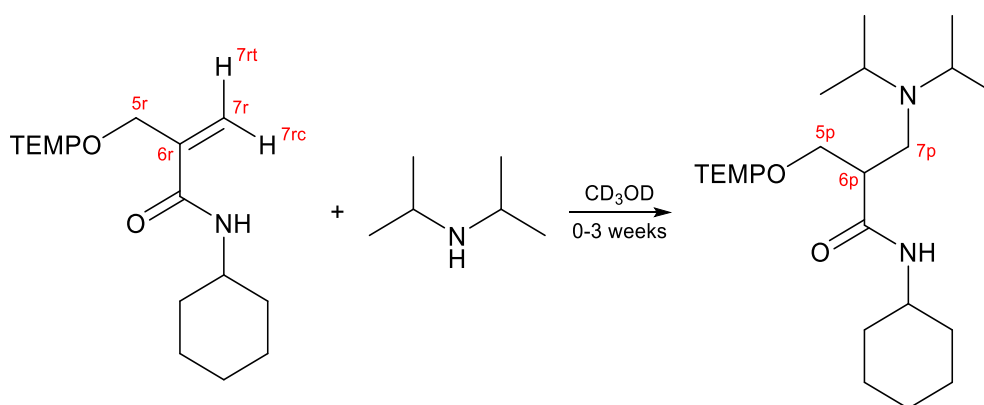


Figure 187: Michael addition of diisopropylamine to CHANT, forming a decay product.

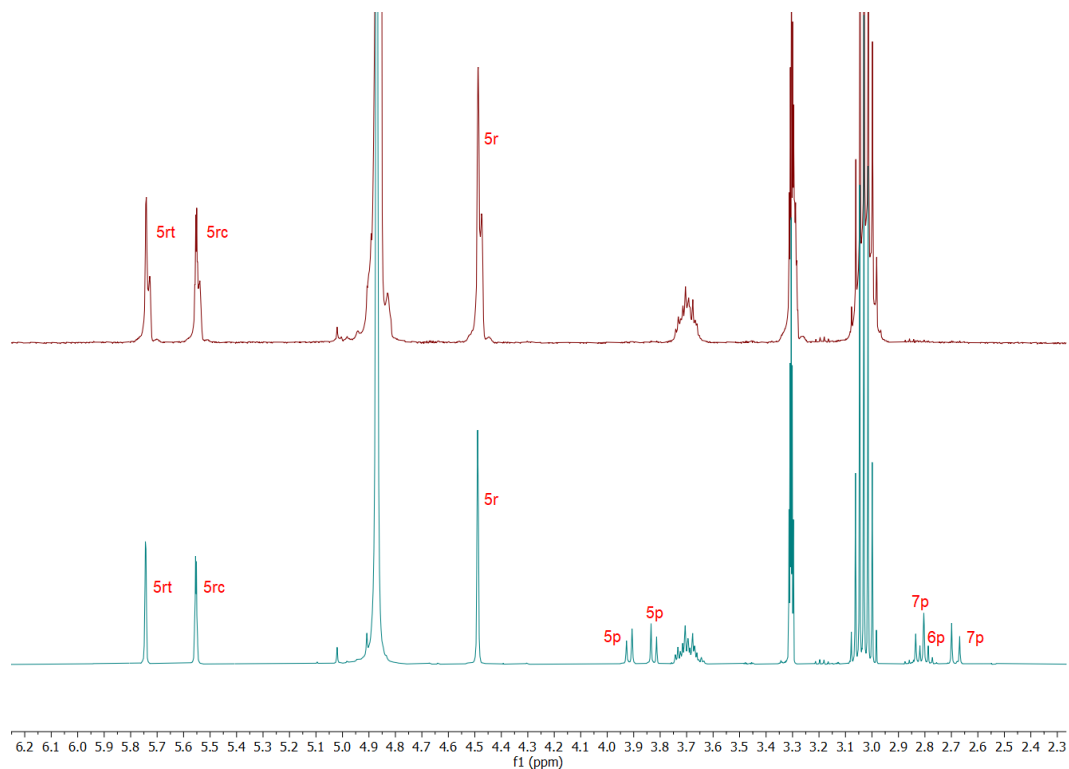


Figure 188: Stacked ^1H NMR spectra of CHANT in presence of diisopropylamine after 0 h (top) and 3 weeks (bottom), showing peaks which decrease in intensity (5r - 7r) and new signals corresponding to the decay product (5p - 7p).

11.3.4. Absorbance of blue LED light (455 nm)

Absorbance of ultraviolet-visible light (250-800 nm) by CHANT (10.0 mM) in MeCN was measured using ultraviolet-visible (UV-Vis) spectroscopy (Figure 82). UV-Vis spectra were recorded using a Shimadzu UV-Vis Spectrophotometer UV-2600 system.

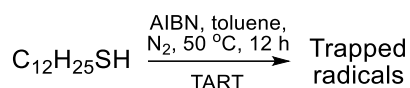
11.3.5. MS calibration curves

MS calibration curves were obtained for CHANT (Figure 53) and TART-trapped PhS• (Figure 95). For this, standard MS was undertaken at concentrations of 0.01-100 μM for CHANT and 0.01-10.0 μM for TART-trapped PhS•.

11.4. Synthetic radical reactions

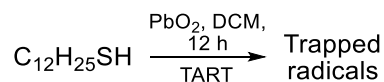
11.4.1. Thiyl radicals

11.4.1.1. AIBN initiated



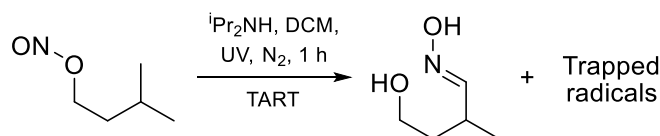
The procedure for trapping of the thiyl radicals, using azobisisobutyronitrile (AIBN) as initiator, was adapted from literature.¹⁵² Allyl-TEMPO or Grantham TART (19.7 mg or 26.7 mg respectively, 0.100 mmol, 0.5 eq.) was dissolved in toluene (0.40 mL). This solution was sealed, sparged and placed under N_2 . 1-Dodecanethiol (40.5 mg, 0.200 mmol, 1.0 eq.) was added and the resultant solution heated to 50 $^\circ\text{C}$. AIBN (3.5 mg, 0.020 mmol, 0.10 eq.) dissolved in dry toluene (0.10 mL) was added dropwise. The reaction solution was stirred for 12 h, yielding a yellow solution. This was let cool, solvent removed *in vacuo* and MS characterised.

11.4.1.2. PbO₂ initiated



The procedure for trapping of the thiyl radicals, using PbO_2 as initiator, was adapted from literature.¹⁵² Allyl-TEMPO (19.7 mg, 0.100 mmol, 0.1 eq.) was dissolved in DCM (2.0 mL) before 1-dodecanethiol (202 mg, 1.00 mmol, 1.0 eq.) and PbO_2 (478 mg, 1.00 mmol, 1.5 eq.) were added. The reaction solution was stirred for 12 h, yielding a grey solution. This was filtered, solvent removed *in vacuo* and MS characterised.

11.4.2. Barton reaction

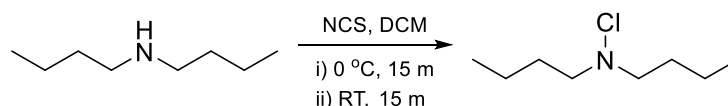


The procedure for TART trapping of the Barton reaction was adapted from a trapless literature procedure.¹⁷⁹ Isopentyl nitrite (58.6 mg, 0.500 mmol, 1.0 eq.) was placed in a UV transparent polypropylene centrifuge tube and dissolved in DCM (30 mL). If undertaking radical trapping, allyl-TEMPO or CHANT (19.7 mg and 32.2 mg, 0.100 mmol, 0.2 eq.) was added. This solution was sealed, sparged and placed under N_2 before diisopropylamine (202 mg, 2.00 mmol, 4.0 eq.) was added. For all reaction mixtures, an aliquot was removed (6 mL) before being

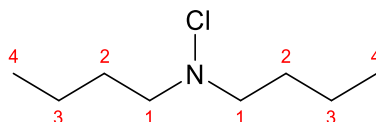
irradiated using a UV lamp (100 W, 405 nm) for 1 h, whilst stirring. Another aliquot was removed (6 mL) and all aliquots had solvent removed *in vacuo* and were MS characterised.

11.4.3. Hoffman-Löffler-Freytag (HLF) reaction

11.4.3.1. Precursor synthesis

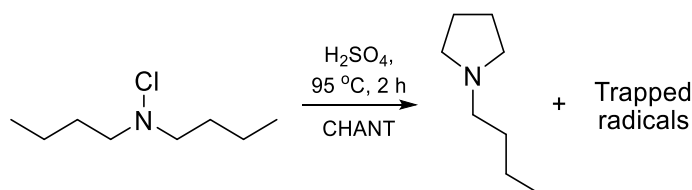


The procedure for *N*-chlorodibutylamine synthesis was adapted from literature.^{267,268} Dibutylamine (1.29 g, 10.0 mmol, 1.0 eq.) was sparged in dry degassed DCM (25 mL) and placed under N₂. *N*-Chlorosuccinimide (NCS, 1.47 g, 11.0 mmol, 1.1 eq.) was added and the reaction stirred at 0 °C for 15 min and room temperature for 15 min. Solvent was removed *in vacuo* and the resultant washed in *n*-pentane (2×25 mL) and filtered, yielding colourless *N*-chlorodibutylamine oil (1.48 g, 90%).



¹H, ¹³C NMR (400, 100 MHz, CDCl₃): δ_H 2.94-2.88 (m, *J* 7.3 Hz, 4H, H₁), 1.69-1.59 (m, *J* 7.3, 7.3 Hz, 4H, H₂), 1.36 (dt, *J* 7.3, 7.3 Hz, 4H, H₃), 0.93 (t, *J* 7.3 Hz, 6H, H₄); δ_C 64.2 (C₁), 30.2 (C₂), 20.2 (C₃), 14.1 (C₄). Obtained values were consistent with literature.²⁶⁹

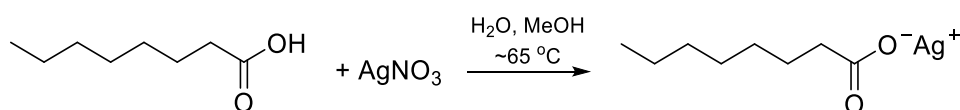
11.4.3.2. Trapping reaction



The procedure for TART trapping of the HLF reaction was adapted from a trapless literature procedure.²⁷⁰ *N*-Chlorodibutylamine (81.8 mg, 0.500 mmol, 1.0 eq.) was dissolved in H₂SO₄ solution (0.25 M, 0.50 mL, 0.125 mmol, 0.25 eq.). If undertaking radical trapping, CHANT (16.1 mg, 0.050 mmol, 0.10 eq.) was added. For all reaction mixtures, an aliquot was removed (50 μL) and the remaining solution heated at 95 °C for 2 h, whilst stirring. This was let cool and an aliquot removed (50 μL). All aliquots were diluted with water (0.5 mL) and neutralised (pH 7) with NaOH (1.0 M, 13 μL, 0.125 mmol, 0.25 eq.), extracted with Et₂O (2×0.5 mL), solvent removed *in vacuo* and MS characterised.

11.4.4. Hunsdiecker reaction

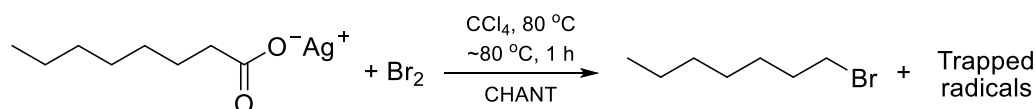
11.4.4.1. Precursor synthesis



The procedure for silver octanoate synthesis was adapted from literature.²⁷¹ Octanoic acid (288 mg, 2.0 mmol, 1.0 eq.) and AgNO₃ (340 mg, 2.0 mmol, 1.0 eq.) dissolved in MeOH (5.0 mL) and NaOH (2.0 M, 1.0 mL) were heated to reflux (~65 °C) to aid dissolution and

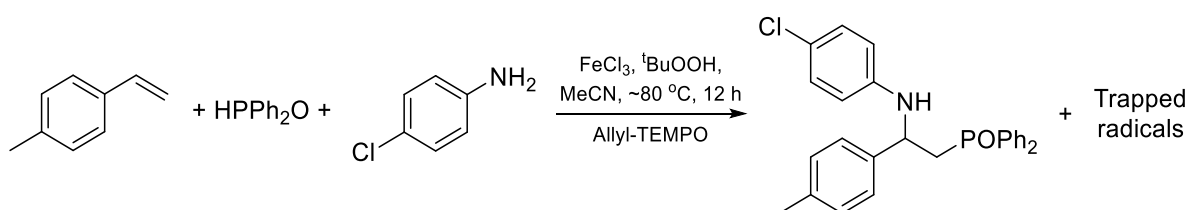
allowed to cool. Silver octanoate precipitated and was filtered, before being washed with water (5 mL) and MeOH (5 mL). Residual solvent was removed *in vacuo* overnight, yielding grey silver octanoate flakes (407 mg, 81%). Product was used in trapping reactions without characterisation or further purification.

11.4.4.2. Trapping reaction



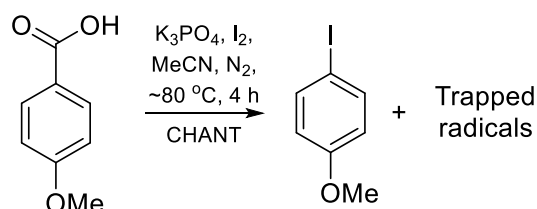
The procedure for TART trapping of the Hunsdiecker reaction was adapted from a trapless literature procedure.²⁷² Silver octanoate (126 mg, 0.500 mmol, 1.0 eq.) was dissolved in CCl₄ (1.5 mL). If undertaking radical trapping, CHANT (32.2 mg, 0.100 mmol, 0.2 eq.) was added. This solution was then cooled in an ice bath (~0 °C) and Br₂ (2.0 M in CCl₄, 0.25 mL, 1.0 eq.) added dropwise over 15 min. For all reaction mixtures, an aliquot was removed (0.35 mL) and the remaining solution heated to reflux (~80 °C) for 1 h, whilst stirring. This was let cool and filtered before another aliquot was removed (0.35 mL). All aliquots had solvent removed *in vacuo* and were MS characterised.

11.4.5. Radical aromatic aminophosphinoylation



The procedure for TART trapping of radical aromatic aminophosphinoylation was adapted from a trapless literature procedure.²⁰⁰ 4-Methylstyrene (59.1 mg, 0.500 mmol, 1.0 eq.), diphenylphosphine oxide (162 mg, 0.800 mmol, 1.6 eq.) and 4-chloroaniline (128 mg, 1.00 mmol, 2.0 eq.) were dissolved in MeCN (3.0 mL). If undertaking radical trapping, allyl-TEMPO (19.7 mg, 0.100 mmol, 0.2 eq.) was added. For all reactions, this solution was sealed, sparged and placed under N₂. FeCl₃ (16.2 mg, 0.100 mmol, 0.2 eq.) and tBuOOH (70% in H₂O, 129 mg, 1.00 mmol, 2.0 eq.) were added and the solution resealed. An aliquot was removed (0.60 mL) and the remaining solution heated to reflux (~80 °C) and stirred for 12 h. This was let cool and an aliquot removed (0.60 mL). All aliquots were filtered and MS characterised.

11.4.6. Radical decarboxylative aromatic iodination

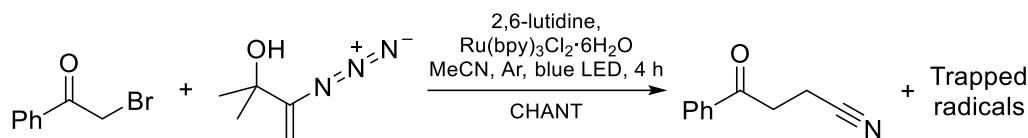


The procedure for TART trapping of radical decarboxylate aromatic iodination was adapted from a trapless literature procedure.²⁰¹ I₂ (508 mg, 2.00 mmol, 4.0 eq.) was placed under N₂ and *p*-anisic acid (76.1 mg, 0.500 mmol, 1.0 eq.), K₃PO₄ (106 mg, 0.500 mmol, 1.0 eq.) and MeCN (2.5 mL) were added. If undertaking radical trapping, CHANT (32.2 mg, 0.100 mmol, 0.2 eq.) was added. For all reaction mixtures, this solution was resealed and an aliquot

removed (0.50 mL). The remaining solution was heated to reflux (~80 °C) and stirred for 4 h. This was let cool before another aliquot was removed (0.50 mL). All aliquots had solvent removed *in vacuo* and were MS characterised.

11.5. Photochemistry

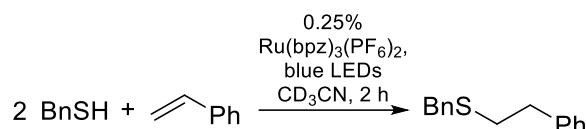
11.5.1. Radical cyanomethylation



3-Azido-2-methylbut-3-en-2-ol was synthesised as described in literature.²⁰³ The procedure for TART trapping of radical cyanomethylation was adapted from a trapless literature procedure.²⁰³ 2-bromoacetophenone (40.0 mg, 200 μmol, 1.00 eq.), 3-azido-2-methylbut-3-en-2-ol (38.1 mg, 300 μmol, 1.50 eq.), 2,6-lutidine (32 mg, 35 μL, 300 μmol, 1.50 eq.) and Ru(bpz)₃Cl₂·6H₂O (1.5 mg, 2.0 μmol, 0.01 eq.) were placed in a transparent 2 mL vial and dissolved in MeCN (1.0 mL). If undertaking radical trapping, CHANT (12.9 mg, 40 μmol, 0.20 eq.) was also added. For all reaction mixtures, an aliquot was removed (0.10 mL) and the remaining solution sparged with argon for 10 min, whilst stirring. This reaction mixture was irradiated with blue LEDs (60 W, 455 nm) for 4 h, whilst stirring. Another aliquot was then removed (0.10 mL) and all aliquots had solvent removed *in vacuo* and were MS characterised.

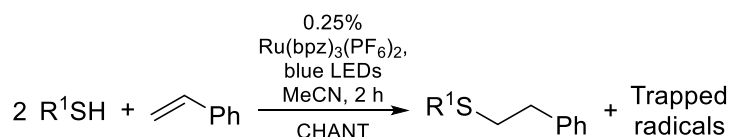
11.5.2. Radical thiol-ene addition

11.5.2.1. Literature replication



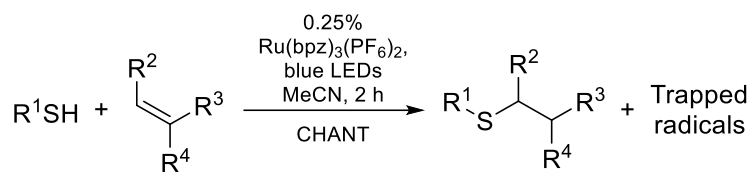
The procedure for radical thiol-ene addition was adapted from a literature procedure.²⁰⁵ Styrene (115 μL, 1.00 mmol, 1.00 eq.) and Ru(bpz)₃(PF₆)₂ (2.2 mg, 2.5 μmol, 0.0025 eq.) were placed in a transparent 2 mL vial and dissolved in CD₃CN (0.50 mL, 0.20 M). Benzyl mercaptan 235 μL, 2.00 mmol, 2.00 eq.) was added and the resultant solution irradiated with blue LEDs (60 W, 455 nm) for 2 h, before being characterised by NMR spectroscopy.

11.5.2.2. Initial reactions



The procedure for TART trapping of radical thiol-ene addition was adapted from a trapless literature procedure.²⁰⁵ Styrene (115 μL, 1.00 mmol, 1.00 eq.) and Ru(bpz)₃(PF₆)₂ (2.2 mg, 2.5 μmol, 0.0025 eq.) were placed in a transparent 2 mL vial and dissolved in dry MeCN (0.50 mL, 0.20 M). If undertaking radical trapping, CHANT (32.2 mg, 0.100 mmol, 0.10 eq.) was also added. For all reaction mixtures, benzyl mercaptan or thiophenol (235 μL or 205 μL respectively, 2.00 mmol, 2.00 eq.) was added and an aliquot removed (5.0 μL). The remaining solution was irradiated with blue LEDs (60 W, 455 nm) for 1-2 h. Another aliquot was removed (5.0 μL) and all aliquots MS characterised.

11.5.2.3. Standard procedure



The procedure for TART trapping of radical thiol-ene addition was adapted from a trapless literature procedure.²⁰⁵ Alkene (100 μ mol, 1.0 eq.) was placed in a transparent 2 mL vial and dissolved in $Ru(bpz)_3(PF_6)_2$ solution (0.50 mM in dry MeCN, 0.50 mL, 0.25 μ mol, 0.0025 eq.). If undertaking radical trapping, CHANT (3.22 mg, 10 μ mol, 0.10 eq.) was also added. For all reaction mixtures, thiol (200 μ mol, 2.0 eq.) was added and an aliquot removed (5.0 μ L). The remaining solution was irradiated with blue LEDs (60 W, 455 nm) for 1-72 h. Another aliquot was removed (5.0 μ L) and all aliquots MS characterised.

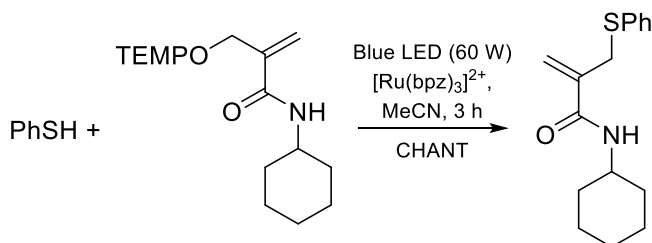
11.5.2.4. Optimised reaction

Two standard reactions (11.5.2.3) were performed with CHANT, styrene (11.5 μ L, 100 μ mol, 1.0 eq.) and benzyl mercaptan (S2.1, 23.5 μ L, 200 μ mol, 2.0 eq.) or thiophenol (S2.2, 20.5 μ L, 200 μ mol, 2.0 eq.) for 2 h.

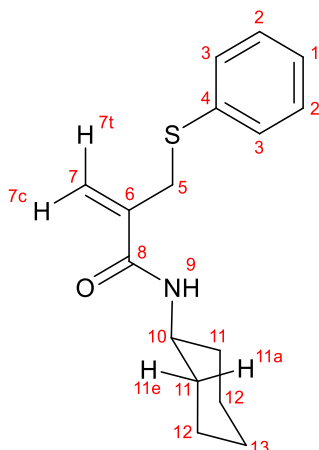
11.5.2.5. Controls

Six standard reactions (11.5.2.3) were performed with benzyl mercaptan (23.5 μ L, 200 μ mol, 2.0 eq.), styrene (11.5 μ L, 100 μ mol, 1.0 eq.) and CHANT for 2 h. A trapping reaction and five controls were performed, where each control omitted a single condition required for TART-trapped radical formation: no thiol, no alkene, no catalyst, no light or no TART.

11.5.2.6. TART-trapped radical isolation



The procedure for CHANT-trapped PhS-ART synthesis was adapted from literature.²⁰⁵ Thiophenol (41 μ L, 400 μ mol, 4.0 eq.), CHANT (32.2 mg, 100 μ mol, 1.0 eq.) and $Ru(bpz)_3(PF_6)_2$ (2.22 mg, 2.50 μ mol, 0.0025 eq.) were placed in a transparent 2 mL sample vial and dissolved in dry MeCN (0.50 mL, 0.20 M). The resultant solution was irradiated with blue LEDs (60 W, 455 nm). Aliquots (5.0 μ L) were removed regularly to monitor the reaction using MS, with eight aliquots having been removed in total (40.0 μ L) when the reaction was stopped after 3 h. Solvent was removed *in vacuo* and the resultant purified using flash silica column chromatography (visualised using UV light or $KMnO_4$ stain) yielding white *N*-cyclohexyl-2-[(phenylsulfanyl)methyl]acrylamide semi-solid (17.3 mg, 63%).



R_f: 0.23 (2%Et₂O/DCM). ¹H, ¹³C NMR (400, 100 MHz, CDCl₃): δ_H 7.35-7.23 (m, 4H, H₂, H₃), 7.22-7.16 (m, 1H, H₁), 6.00 (br d, *J* 6.4 Hz, 1H, H₉), 5.58 (s, 1H, H_{7c}), 5.23 (s, 1H, H_{7t}), 3.77 (s, 2H, H₅), 3.87-3.78 (m, *J* 7.2, 6.4 Hz, 1H, H₁₀), 1.92 (ddd, *J* 12.4, 7.2, 3.7 Hz, 2H, H_{11e}), 1.69 (dt, *J* 13.7, 3.8 Hz, 2H, H_{12e}), 1.59 (dt, *J* 12.8, 3.8 Hz, 1H, H_{13e}), 1.37 (dt, *J* 13.7, 3.8 Hz, 2H, H_{12a}), 1.25-1.09 (m, 3H, H_{11a}, H_{13a}); δ_C 166.7 (C₈), 140.7 (C₆), 131.0 (C₂), 129.0 (C₃), 127.1 (C₁), 120.7 (C₇), 48.4 (C₁₀), 36.7 (C₅), 33.1 (C₁₁), 25.6 (C₁₃), 24.9 (C₁₂), 134.9 (C₄). MS (Pos ESI): *m/z* 298.125 ([M+Na]⁺, 100%), 276.145 ([M+H]⁺, 33%), 573.261 ([2M+Na]⁺, 8%); 298.124 (calc. for C₁₆H₂₁NOSNa, [M+Na]⁺).

11.5.2.7. Kinetics experiments

Two standard reactions (11.5.2.3) were performed with CHANT, styrene (11.5 μL, 100 μmol, 1.0 eq.) and thiols: thiophenol (20.5 μL, 200 μmol, 2.0 eq.) or methyl thiosalicylate (27.5 μL, 200 μmol, 2.0 eq.). Aliquots (5.0 μL) were removed periodically over 24 h and MS characterised.

11.5.2.8. Effect of different thiols on reaction mechanism and kinetics

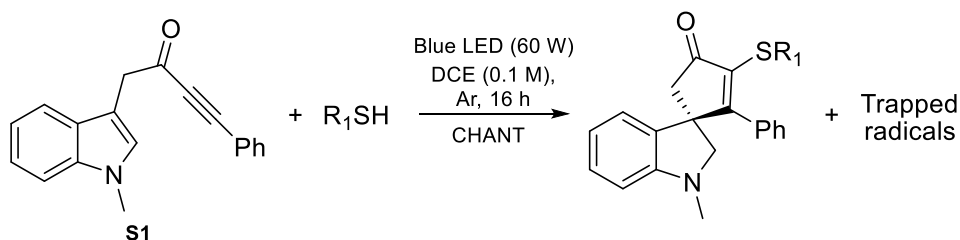
Six standard reactions (11.5.2.3) were performed with CHANT, styrene (11.5 μL, 100 μmol, 1.0 eq.) and different thiols: benzyl mercaptan (S2.1, 23.5 μL, 200 μmol, 2.0 eq.), thiophenol (S2.2, 20.5 μL, 200 μmol, 2.0 eq.), 3-methoxythiophenol (S2.3, 25.0 μL, 200 μmol, 2.0 eq.), cyclohexanethiol (S2.4, 24.5 μL, 200 μmol, 2.0 eq.), methyl thiosalicylate (S2.5, 27.5 μL, 200 μmol, 2.0 eq.) or *tert*-butylthiol (S2.6, 22.5 μL, 200 μmol, 2.0 eq.). Aliquots (5.0 μL) were removed periodically over 72 h and MS characterised.

11.5.2.9. Effect of different alkenes on reaction mechanism and kinetics

Six standard reactions (11.5.2.3) were performed with CHANT, benzyl mercaptan (23.5 μL, 200 μmol, 2.0 eq.) and different alkenes: styrene (S3.1, 11.5 μL, 100 μmol, 1.0 eq.), methylenecyclohexane (S3.2, 12.0 μL, 100 μmol, 1.0 eq.), 1-methylcyclohexene (S3.3, 12.0 μL, 100 μmol, 1.0 eq.), allyl chloride (S3.4, 8.0 μL, 100 μmol, 1.0 eq.), phenylacetylene (S3.5, 11.0 μL, 100 μmol, 1.0 eq.) or ethyl *trans*-cinnamate (S3.6, 17.0 μL, 100 μmol, 1.0 eq.). Aliquots (5.0 μL) were removed periodically over 72 h and MS characterised.

11.5.3. Radical dearomative spirocyclisation

11.5.3.1. Standard procedure



Indole-tethered ynone (S1) was synthesised as described in literature.²¹² The procedure for TART trapping of radical dearomative spirocyclisation was adapted from a trapless literature procedure.²¹² Indole-tethered ynone (27.3 mg, 100 μ mol, 1.0 eq.) was placed in a transparent 2 mL vial and dissolved in degassed dichloroethylene (DCE, 1.0 mL, 0.10 M). If undertaking radical trapping, CHANT (3.22 mg, 10 μ mol, 0.1 eq.) was also added. For all reaction mixtures, the solution was sparged with argon for 5 min, whilst stirring. Thiol was added and an aliquot removed (0.10 mL). The remaining solution was irradiated with blue LEDs (60 W, 455 nm) for 16 h, whilst stirring. Another aliquot was removed (0.10 mL) and all aliquots had solvent removed *in vacuo* and were MS characterised.

11.5.3.2. Main radical cycle mechanism

Two standard reactions (11.5.3.1) were performed with 3-methoxythiophenol (S2.3, 19.8 μ L, 160 μ mol, 1.6 eq.) and CHANT (trapping reaction) or no CHANT (trapless control).

11.5.3.3. Initiation mechanism

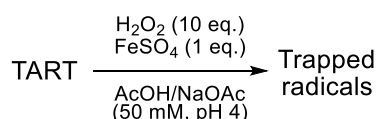
Three standard reactions (11.5.3.1) were performed with CHANT and 3-methoxythiophenol (S2.3, 19.8 μ L, 160 μ mol, 1.6 eq.), a reduced amount of 3-methoxythiophenol (S2.3, 6.2 μ L, 50 μ mol, 0.5 eq.) or no 3-methoxythiophenol.

11.5.3.4. Effects of different thiols on reaction mechanism and kinetics

Four standard reactions (11.5.3.1) were performed with CHANT and thiols: 3-methoxythiophenol (S2.3, 19.8 μ L, 160 μ mol, 1.6 eq.), cyclohexanethiol (S2.4, 19.6 μ L, 160 μ mol, 1.6 eq.), methyl thiosalicylate (S2.5, 22.0 μ L, 160 μ mol, 1.6 eq.) or *tert*-butylthiol (S2.6, 18.0 μ L, 160 μ mol, 1.6 eq.).

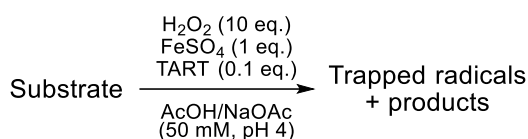
11.6. Biochemistry

11.6.1. \bullet OH and HO₂ \bullet trapping



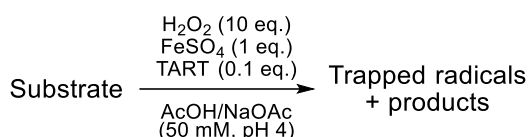
The procedure for trapping in aqueous \bullet OH-initiated biochemical degradation was adapted from trapless literature procedures.^{232–234} GLANT or DANT (3.66 mg or 2.84 mg respectively, 10.0 μ mol, 1.0 eq.) was dissolved in AcOH/NaOAc buffer (50 mM, pH 4, 1780 μ L) and stirred. Fe₂SO₄·7H₂O solution (500 mM in AcOH/NaOAc buffer, 20 μ L, 10.0 μ mol, 1.0 eq.) was added. For all reaction mixtures, H₂O₂ solution (500 mM in AcOH/NaOAc buffer, 200 μ L, 100 μ mol, 10 eq.) was added slowly over 5 min and the solution stirred overnight unsealed. This was MS characterised.

11.6.2. •OH-initiated alcohol degradation



The procedure for trapping in aqueous •OH-initiated biochemical degradation was adapted from trapless literature procedures.^{232–234} AcOH/NaOAc buffer (50 mM, pH 4, 580 µL) and methanol or *tert*-butanol (10.0 mM in AcOH/NaOAc buffer, 1.0 mL, 10.0 µmol, 1.0 eq.) were mixed and stirred. Fe₂SO₄·7H₂O solution (500 mM in AcOH/NaOAc buffer, 20 µL, 10.0 µmol, 1.0 eq.) was added. If undertaking radical trapping, DEADANT solution (5.0 mM in AcOH/NaOAc buffer, 200 µL, 1.0 µmol, 0.10 eq.) was added but otherwise, AcOH/NaOAc buffer (200 µL) was added. For all reaction mixtures, H₂O₂ solution (500 mM in AcOH/NaOAc buffer, 200 µL, 100 µmol, 10 eq.) was added slowly over 5 min and the solution stirred overnight unsealed. This was MS characterised.

11.6.3. Standard procedure



The procedure for trapping in aqueous •OH-initiated biochemical degradation was adapted from trapless literature procedures.^{232–234} Biochemical (10.0 µmol, 1.0 eq.) was dissolved in AcOH/NaOAc buffer (50 mM, pH 4, 1580 µL) and stirred. Fe₂SO₄·7H₂O solution (500 mM in AcOH/NaOAc buffer, 20 µL, 10.0 µmol, 1.0 eq.) was added. If undertaking radical trapping, TART solution (5.0 mM in AcOH/NaOAc buffer, 200 µL, 1.0 µmol, 0.10 eq.) was added but otherwise, AcOH/NaOAc buffer (200 µL) was added. For all reaction mixtures, H₂O₂ solution (500 mM in AcOH/NaOAc buffer, 200 µL, 100 µmol, 10 eq.) was added slowly over 5 min and the solution stirred overnight unsealed. This was MS characterised.

11.6.4. •OH-initiated biochemical degradations

Two standard reactions (11.6.3) were performed with thymine (1.26 mg, 10.0 µmol, 1.0 eq.) and DANT (trapping reaction) or no DANT (trapless control).

Two standard reactions (11.6.3) were performed with DEADANT (trapping reaction) or no DEADANT (trapless control) for each biochemical: thymine (1.26 mg, 10.0 µmol, 1.0 eq.), *N*-acetyl-diglycine (Ac-Gly-Gly-OH, 1.74 mg, 10.0 µmol, 1.0 eq.), *N*-Boc-diglycine (Boc-Gly-Gly-OH, 2.32 mg, 10.0 µmol, 1.0 eq.), D(+)-glucose (1.80 mg, 10.0 µmol, 1.0 eq.) and ascorbic acid (1.76 mg, 10.0 µmol, 1.0 eq.).

11.6.5. Antioxidant activity of ascorbic acid

Six standard reactions (11.6.3) were performed with DEADANT (trapping reaction) or no DEADANT (trapless control) and thymine (1.26 mg, 10.0 µmol, 1.0 eq.), ascorbic acid (1.76 mg, 10.0 µmol, 1.0 eq.) or thymine (1.26 mg, 10.0 µmol, 1.0 eq.) and ascorbic acid (1.76 mg, 10.0 µmol, 1.0 eq.).

11.7. Alkene ozonolysis

11.7.1. Set-up

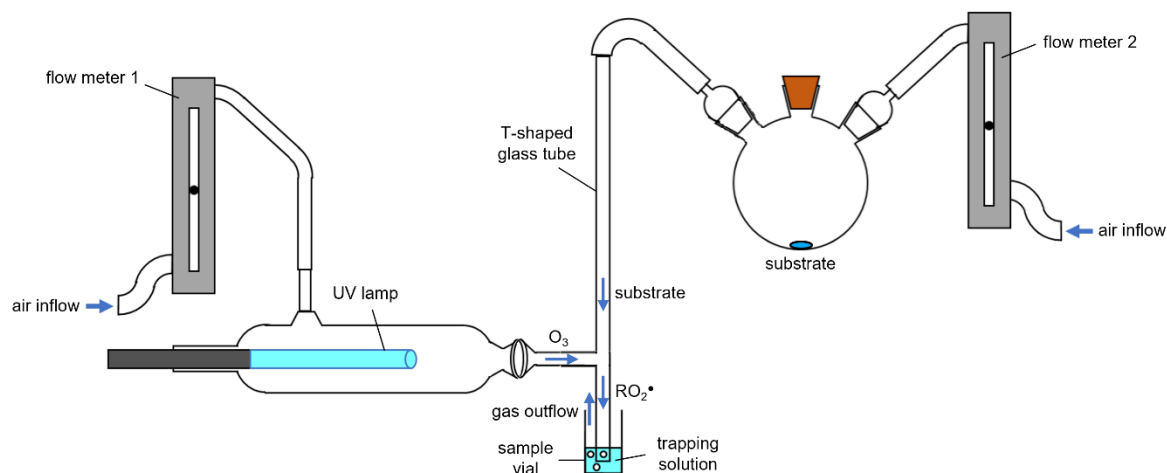
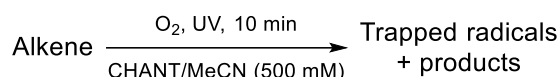


Figure 189: Set-up used for TART trapping of alkene ozonolysis.

A set-up was designed for radical trapping in alkene ozonolysis (Figure 143). The system was used at RTP. T-shaped glass tube had 0.60 cm internal diameter and sample vial had 2.0 cm internal diameter. Different length T-shaped glass tubes could be used to increase residence time for substrate reaction with O₃, with typical residence length set at 5.0 cm, resulting in residence volume 1.41 cm³. Liquid substrate was placed as shown, with a sufficient volume to avoid complete evaporation. TART functionality was chosen as required, however typically CHANT was used. [TART] was set between 50-5000 μM in 2.0 mL MeCN but was typically 500 μM. T-shaped glass tube outlet was placed at the bottom of the trapping solution, meaning the outlet lay 6 mm below the trapping solution surface. Pen-Ray UV lamp (maximum emission at 254 nm, with significant emission at 185 nm) current and power output were kept constant for all experiments. Flow rate through the trapping solution was set at 1.5 L min⁻¹, to ensure rapid but controllable bubbling. This typically resulted in residence time 56.5 ms. Flow rate through each bubbler was adjusted as required, but was typically set at an equal 0.75 L min⁻¹ through each flow meter. Under these standard conditions and in absence of substrate or trapping solution, [O₃] was measured to be 118 ppm (2.96×10¹⁵ molec. cm⁻³), using a pre-calibrated Thermo Scientific model 49i ozonometer. Reaction time was varied as required, but was typically 10 min. After trapping completion, trapping solution solvent was carefully removed *in vacuo* (30 °C, 100 mbar, ~10 min) and the resultant MS characterised. These standard alkene ozonolysis conditions had been optimised.

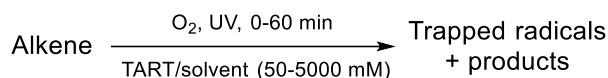
11.7.2. Standard procedure



The standard alkene ozonolysis set-up was used with cyclohexene (3 mL) and α-pinene (1 mL) for cyclohexene and α-pinene ozonolyses respectively. For control experiments, one required component for trapped radical generation was omitted at a time: substrate, air (replaced with N₂), UV and TART.

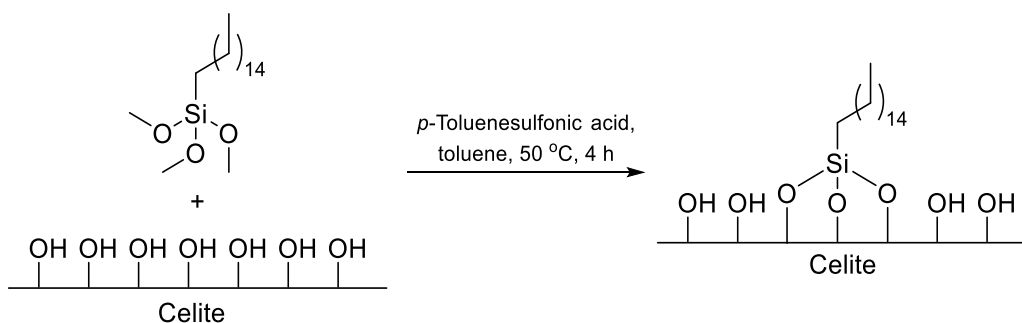
11.7.3. Optimisation

11.7.3.1. General

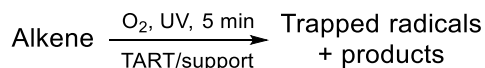


The standard set-up of TART trapping of alkene ozonolysis was used for optimisation unless stated otherwise. Deviations included: TART phase (11.7.3.2); functionality of TART, solvent and additives; flow rate; [TART] = 50-5000 μM and reaction time = 0-60 min.

11.7.3.2. Solid support synthesis and use in TART trapping of alkene ozonolysis



Hexadecylsilane functionalised celite was synthesised as described in literature.²⁷³ Celite (1.00 g) was placed in toluene (15 mL) and rotated for 30 min. *p*-Toluenesulfonic acid monohydrate (20.0 mg, 0.105 mmol) and hexadecyltrimethoxysilane (0.065 mmol) were then added and the solution rotated at 50 °C for 4 h. This was then let cool and centrifuged for 10 min, before the supernatant was removed. The remaining mixture washed with DCM (15 mL), centrifuged and supernatant removed three times. Remaining solvent was removed *in vacuo* and the resultant functionalised celite dried in a vacuum oven (50 °C, 24 h).



TART (20.0 μmol), additive (if applicable, 20.0 μmol) and DCM (1.0 mL) were mixed and functionalised celite (200 mg) added. DCM was then removed *in vacuo*. A glass wool plug was inserted into a T-shaped glass tube and immobilised TART (20.0 mg) added. The immobilised TART was then squashed into a flat disc using a PTFE tape covered rod and placed the required distance from the T-joint. This T-shaped glass tube was then incorporated into a similar system, as used for TART trapping of alkene ozonolysis, where the gas stream was bubbled through solution (Figure 190).

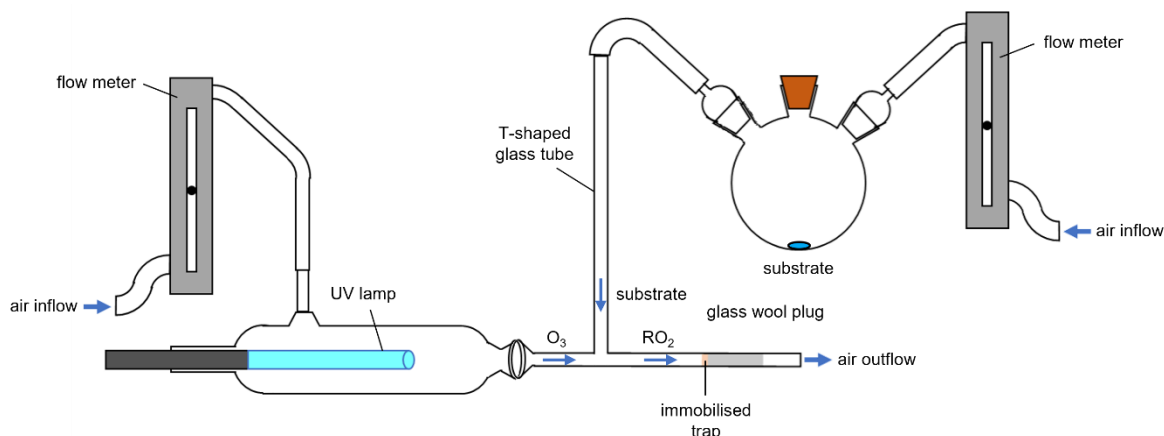


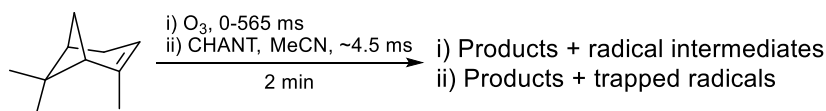
Figure 190: Set-up used for TART trapping of alkene ozonolysis, using solid supported TART.

A set-up was designed for radical trapping in alkene ozonolysis (Figure 143). The system was used at RTP. T-shaped glass tube had 0.60 cm internal diameter. Different length T-shaped glass tubes could be used to increase residence time for substrate reaction with O_3 , with typical residence length set at 10.0 cm, resulting in residence volume 2.83 cm³. Liquid substrate was placed as shown, with a sufficient volume to avoid complete evaporation. Pen-Ray UV lamp (maximum emission at 254 nm, with significant emission at 185 nm) current and power output were kept constant for all experiments. Flow rate through the trapping solution was set at 3.0 L min⁻¹, to ensure rapid but controllable bubbling. This typically resulted in residence time 56.5 ms. Flow rate through each bubbler was adjusted as required, but was typically set at an equal 1.5 L min⁻¹ through each flow meter. Reaction time was varied as required, but was typically 5 min. After trapping completion, immobilised TART was removed and washed with DCM (1 mL). The glass wool was also washed with DCM (4 mL) and the two solutions combined, filtered, solvent removed *in vacuo* and the resultant MS characterised.

11.7.4. Estimation of α -pinene dissolution

The standard alkene ozonolysis set-up was used with α -pinene (1 mL) as substrate, no UV (no ozone generation) and the output bubbled through “trap solution” containing only CD₃CN. Mass difference of α -pinene before and after the experiment was used to calculate amount of α -pinene evaporated. Using a dibromomethane standard, qNMR spectroscopy was undertaken on the resulting “trap solution” to calculate mass of α -pinene in solution. MS characterisation was not undertaken. From these data, α -pinene dissolution was estimated to be ~11%.

11.7.5. α -Pinene kinetics experiment



Standard alkene ozonolysis set-up was used with α -pinene (1 mL) as substrate but with reaction time reduced (2 min). Multiple residence lengths were used (0-50 cm), resulting in residence times 0-565 ms, with three repeats undertaken for each residence time.

11.8. •OH-initiated alkane degradation

11.8.1. Using alkene ozonolysis as an •OH source

11.8.1.1. Set-up

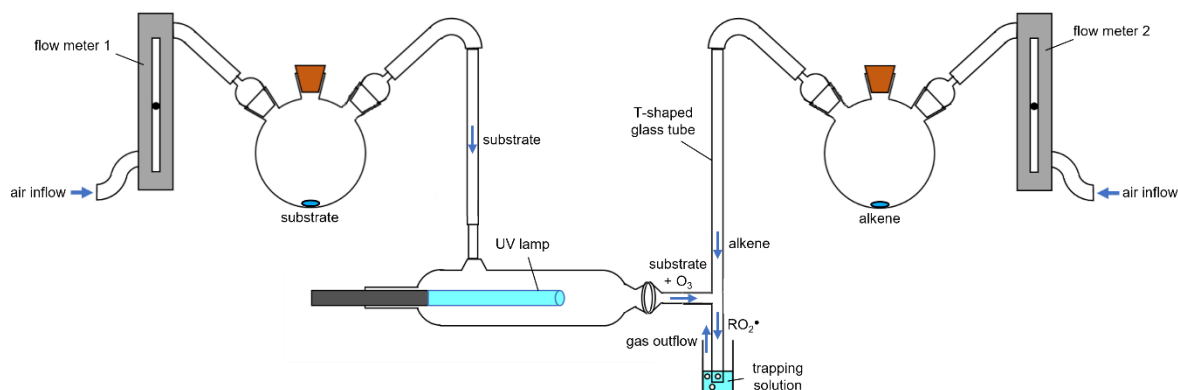
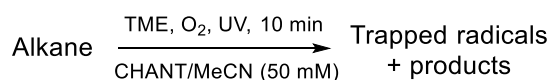


Figure 191: Set-up used for TART trapping of •OH-initiated alkane degradation, using alkene ozonolysis as an •OH source.

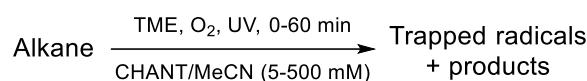
A set-up was designed for radical trapping in alkene ozonolysis (Figure 191). The system was used at RTP. T-shaped glass tube had 0.60 cm internal diameter and sample vial had 2.0 cm internal diameter. Different length T-shaped glass tubes could be used to increase residence time for substrate reaction with O₃, with typical residence length set at 5.0 cm, resulting in residence volume 1.41 cm³. Liquid substrate was placed as shown, with a sufficient volume to avoid complete evaporation. TART functionality was chosen as required, however typically CHANT was used. [TART] was set between 5-500 μM in 2.0 mL MeCN but was typically 50 μM. T-shaped glass tube outlet was placed at the bottom of the trapping solution, meaning the outlet lay 6 mm below the trapping solution surface. Pen-Ray UV lamp (maximum emission at 254 nm, with significant emission at 185 nm) current and power output were kept constant for all experiments. Flow rate through the trapping solution was set at 1.5 L min⁻¹, to ensure rapid but controllable bubbling. This typically resulted in residence time 56.5 ms. Flow rate through each bubbler was adjusted as required, but was typically set at 1.20 and 0.30 L min⁻¹ through substrate and alkene flow meters respectively. Under these standard conditions and in absence of substrate or trapping solution, [O₃] was measured to be 106.3±0.2 ppm (2.663±0.005×10¹⁵ molec. cm⁻³), using a pre-calibrated Thermo Scientific model 49i ozonometer. Reaction time was varied as required, but was typically 10 min. After trapping completion, trapping solution solvent was carefully removed *in vacuo* (30 °C, 100 mbar, ~10 min) and the resultant MS characterised. These standard alkene ozonolysis conditions had been optimised.

11.8.1.2. Initial results, detailed results and controls



The standard set-up and typical conditions of •OH-initiated alkane degradation, using alkene ozonolysis as an •OH source, was used for all experiments unless stated otherwise. For control experiments, TART was omitted.

11.8.1.3. Optimisation



The standard set-up of TART trapping of $\bullet\text{OH}$ -initiated alkane degradation, using alkene ozonolysis as an $\bullet\text{OH}$ source, was used for optimisation unless stated otherwise. Deviations included: [CHANT] = 5-500 μM and reaction time = 0-60 min.

11.8.2. Using water photolysis as an $\bullet\text{OH}$ source

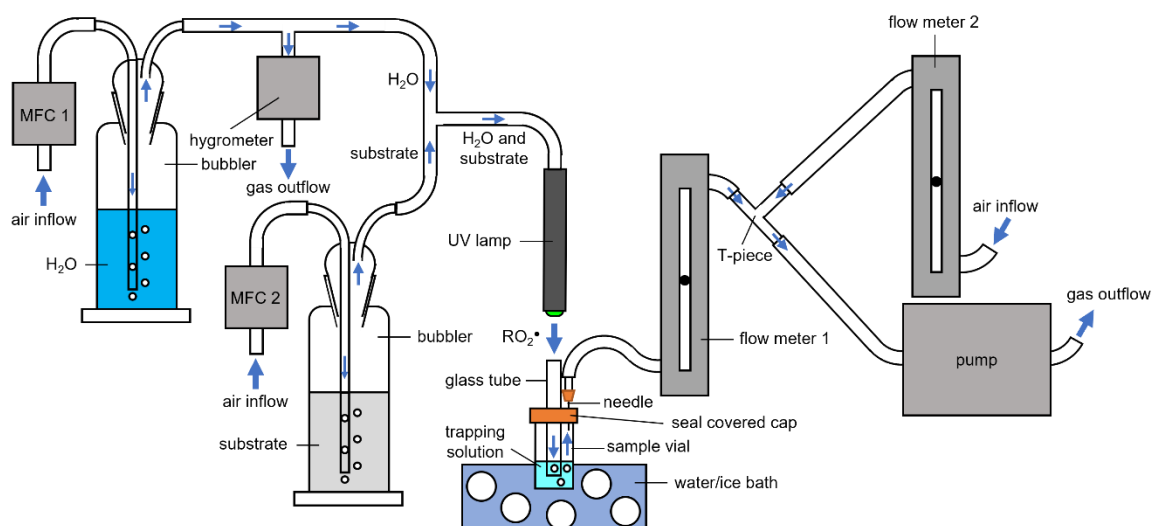
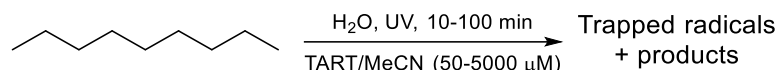


Figure 192: Set-up used for TART trapping of $\bullet\text{OH}$ -initiated alkane degradation, using water photolysis as an $\bullet\text{OH}$ source.

A set-up was designed for TART trapping of $\bullet\text{OH}$ -initiated *n*-nonane degradation (Figure 192). The water photolysis system (UV lamp output and prior, with no substrate) was calibrated offline. This involved using fluorescence assay gas expansion (FAGE) to measure a range of $[\text{HO}_x\bullet]$ ($\text{HO}_x\bullet = \bullet\text{OH} + \text{HO}_2\bullet$) produced depending on photon flux (measured using N_2O actinometry), irradiation time and $[\text{H}_2\text{O}]$ (measured using a hygrometer), as described by Onel *et al.*²⁶⁰ This calibration allowed accurate online $[\text{HO}_x\bullet]$ calculation.

The system was used at RTP. Hg Pen-Ray UV lamp (184.9 nm) had 1.6 cm^2 cross-sectional area, glass tube had 0.60 cm internal diameter and sample vial had 2.0 cm internal diameter. Length between UV lamp centre and outflow was 3.8 cm, resulting in 6.1 cm^3 average residence volume for $[\text{HO}_x\bullet]$ inside the UV lamp. Different length glass tubes could be used to increase residence time for $\bullet\text{OH}$ reaction with substrate, with typical residence length set at 8.0 cm, resulting in residence volume 2.3 cm^3 . TART functionality was chosen as required, however typically CHANT or DEADANT were used. [TART] was set between 50-5000 μM in 2.0 mL MeCN, but was typically 50 μM . Glass tube outlet was placed at the bottom of the trapping solution, meaning the outlet lay 6 mm below the trapping solution surface. UV lamp current was set at 20 mA for all experiments. Flow rate through mass flow controller (MFC) 1 was set at 10 L min^{-1} , with 1 L min^{-1} being passed through the hygrometer to measure $[\text{H}_2\text{O}]$. Flow rate through MFC 2 was set at 1 L min^{-1} . Mixing these two flows created a flow rate through the UV lamp of 10 L min^{-1} . This resulted in 37 ms lamp residence time. Under these standard conditions, in the total flow $[\text{H}_2\text{O}]$ was measured to be $\sim 3 \times 10^{17}$ molec. cm^{-3} and [*n*-nonane] was calculated to be $\sim 1.0 \times 10^{16}$ molec. cm^{-3} , using its partial volume, vapour pressure (408 Pa, 293 K)²⁷⁴ and the ideal gas law. Pump suction rate was set at 6.0 L min^{-1} , with gas intake through flow meters 1 and 2 set at 1.5 and 4.5 L min^{-1} respectively. This

1.5 L min⁻¹ flow rate through the trapping solution ensured rapid but controllable bubbling. This resulted in residence time 92 ms and therefore total residence time 129 ms. Under these standard conditions, initial gaseous [HO_x•] was calculated to be ~6.8±1.0×10¹¹ (~28±4 ppb) and therefore, [•OH] and [HO₂•] were each calculated to be ~3.4±0.5×10¹¹ (~14±2 ppb). This was orders of magnitude lower than [*n*-nonane], ensuring nearly all •OH was converted into RO₂•. Reaction time was varied as required, but was typically 10-100 min. After trapping completion, trapping solution solvent was carefully removed *in vacuo* (30 °C, 100 mbar, ~10 min) and the resultant MS characterised.



The standard set-up and typical conditions of TART trapping of •OH-initiated alkane degradation, using water photolysis as an •OH source, was used for all experiments unless stated otherwise. For control experiments, TART was omitted.

11.9. MS procedures for TART trapping

11.9.1. Characterisation

A high resolution solariX XR FTMS (solariX) mass spectrometer ($m/z \pm 0.0001$ precision, $>10^7$ maximum resolution, mass accuracy 600 ppb (internal)) using positive ion mode electrospray ionisation (Pos ESI-MS) was used for MS characterisation of radical trapping samples, unless stated otherwise. This characterisation and analysis are described below. Elsewhere, negative ion mode (Neg) ESI-MS may have been conducted using the solariX or Pos ESI-MS may have been recorded using a Bruker HCT ultra ETD II mass spectrometer (HCT, $m/z \pm 0.1$ precision, m/z 0.3 mass resolution, m/z 26,000 s⁻¹ scan speed) or Bruker compact QTOF mass spectrometer (compact, $m/z \pm 0.001$ precision, 30000 resolution, 1-50 Hz scan speed).

Dissolution solvent (1:1 CH₃CN:H₂O), MS solvent (0.1%/1:1 HCOOH/CH₃CN:H₂O), deuterated dissolution solvent (1:1 CH₃CN:D₂O) and deuterated MS solvent (0.1%/1:1 DCOOH/CH₃CN:D₂O) were prepared when required. Samples not in solution were dissolved in dissolution solvent (0.0-2.0 mL). An appropriate aliquot was then extracted from samples in solution using a Hamilton syringe and diluted with MS solvent to form a solution of ~10 μM TART concentration, assuming moles of TART were equal before reaction and after reaction. Dilution of trapping reaction samples and control samples were scaled to ensure equivalent concentrations between samples, assuming no reaction had taken place. The m/z of the mass spectrometer was calibrated using observed and known peaks for sodium trifluoroacetate in MS solvent.

Standard direct injection MS was the first MS characterisation recorded for most samples. Parameters were initially optimised and then kept constant for all experiments, including m/z recording range of m/z 100-1000 (11.9.3). MS solvent was injected (2 μL min⁻¹) and once signal stabilised, an average background spectrum was recorded (typically 16 scans). The same process was then performed for diluted sample and an average sample spectrum recorded. The system was then flushed clean with MS solvent. D₂O exchange MS was performed similarly, however deuterated equivalents of solvents were used instead. Samples were let equilibrate in deuterated solvent for at least 1 h prior to MS characterisation. Tandem MS was also performed similarly to standard MS, but sometimes required parameter adjustments, such as ion acquisition time (11.9.3). Tandem MS involved using source CID isolation to isolate a peak of interest. Subsequent source CID fragmentation was used to fragment the peak. If source CID isolation could not obtain clean peak isolation then additional in-cell SORI-CID was used to remove nearby offending peaks. Fragmentation was then

similarly carried out as before but utilising in-cell SORI-CID fragmentation instead of source CID fragmentation.

HPLC-MS used an Agilent-1200 HPLC instrument equipped with a reverse phase column was connected to the mass spectrometer. Columns used were reverse phase columns: Waters Symmetry C18 3.5 μm , 4.6 \times 75 mm (Waters Symmetry) column, for synthetic and photochemical radical reactions; Eclipse Plus Phenyl-Hexyl 1.8 μm , 4.6 \times 50 mm (Eclipse Plus Phenyl-Hexyl) column, for samples related to gaseous CHANT trapping and Atlantis C18 3 μm , 4.6 \times 150 mm (Atlantis) column, for samples related to DEADANT. MS method parameters were optimised for HPLC-MS conditions (11.9.3) and single sequential scans were recorded. HPLC combined 0.1% HCOOH/H₂O and 0.1% HCOOH/MeCN into a mobile phase injected at 300 $\mu\text{L min}^{-1}$, for the Waters Symmetry and Eclipse Plus Phenyl-Hexyl columns or 500 $\mu\text{L min}^{-1}$ for the Atlantis column. Solvent gradient varied from high H₂O to high MeCN content as required (11.9.3). During the run, column output was sometimes sent to waste, to prevent permanent contamination of the mass spectrometer by overly concentrated species (11.9.3).

11.9.2. Analysis

Standard MS analysis involved either screening mass spectra for MS peaks corresponding to predicted structures (Peak Pick) or predicting structures corresponding to observed MS peaks (Formula Find). For both methods, molecular formula assignments were formulated on the accurate mass of pseudomolecular ions $[\text{M}+\text{H}]^+$, $[\text{M}+\text{Na}]^+$ or $[\text{M}+\text{K}]^+$. Both analysis methods were usually processed automatically. Typically, background spectra were subtracted from sample spectra during automated processing. Minor fluctuations in m/z accuracy required alignment of background and sample peaks with the same predicted m/z but different measured m/z , within set acceptance limits. Background peak intensities were then subtracted from sample peak intensities. If no background peak was observed within the accepted m/z range of the sample peak, intensity of the nearest background m/z value was subtracted instead. Both analysis methods used acceptance limits to prevent false positives. These included random m/z error (typically $m/z < 0.0000-0.0015$), systematic m/z error (typically $m/z -0.0006-0.0003$) and minimum acceptable intensity. Formula Find used additional acceptance limits to increase method speed. These were intensity of background peak compared to sample peak (typically $< 50\%$), m/z search range (e.g., $m/z 100-500$), species molecular formulae range (e.g., C₀₋₂₀H₀₋₁₀₀N₀₋₂O₀₋₁₀) and unsaturation range. Both methods outputted observed peak m/z , difference from predicted m/z and intensity. Formula Find additionally outputted predicted m/z and molecular formulae. D₂O exchange MS and tandem MS analysis were usually performed using Peak Pick and Formula Find respectively. HPLC-MS analysis was usually performed manually. Peak Pick and Formula Find programmes are available upon request.

11.9.3. Parameters

MS characterisation was recorded using a solariX XR FTMS mass spectrometer in positive-ion mode ESI, unless stated otherwise. Mass spectra were recorded over an m/z range of $m/z 100-1000$. If multiple scans were used, these were averaged. Ion transfer time (TOF) was set to 1.0 ms. In general, ESI settings were as follows: drying gas flow = 4.0 L min^{-1} ; nebulizer pressure: 2.0 bar; capillary voltage = 4500 V; spray shield voltage = -500 V; skimmer voltage = 15 V. Additional parameters are available upon request.

For standard MS (including D₂O exchange), other settings used were: injection speed = 2 $\mu\text{L min}^{-1}$; scans = 16; ion accumulation time = 0.2 s; drying gas temperature = 160 °C.

For tandem MS, other settings used were: scans = 16-64; ion accumulation time = 0.2-5.0 s; drying gas temperature = 160 °C; octupole tandem MS CID energy = 0-20 V and in-source collision energy = 0-20 V. Number of scans and amount of ion accumulation time was set depending on the intensity of the desired MS peak. Octupole tandem MS CID energy and in-source collision energy were set to cause an appropriate amount of fragmentation.

For HPLC-MS, other settings used were: injection speed = 300 or 500 $\mu\text{L min}^{-1}$ for samples relating to CHANT and DEADANT respectively; scans = single sequential; ion accumulation time = 0.2 s; drying gas temperature = 180 °C. HPLC conditions used in HPLC-MS characterisation are shown for samples related to: CHANT trapping of radical decarboxylative aromatic iodination (Table 53, 11.4.6); CHANT trapping of radical thiol-ene addition (Table 54, 11.5.2.5); TART trapping of aqueous $\bullet\text{OH}$ -initiated biochemical degradation (Table 55, 11.6); CHANT trapping of gaseous α -pinene ozonolysis and $\bullet\text{OH}$ -initiated *n*-nonane degradation (Table 56, 11.7, 11.8.1) and DEADANT trapping of gaseous $\bullet\text{OH}$ -initiated *n*-nonane degradation, using water photolysis as an $\bullet\text{OH}$ source (Table 57, 11.8.2).

Table 53: HPLC conditions of sample analysis from TART trapping of radical decarboxylative aromatic iodination, using *p*-anisic acid as substrate, CHANT as TART and HPLC-MS for characterisation (11.4.6). Column = Waters Symmetry. Injection speed = 300 $\mu\text{L min}^{-1}$.

Time / m	0.1%HCOOH/ H ₂ O / %	0.1%HCOOH/ MeCN / %
0.0	95	5
1.0	95	5
2.0	50	50
8.0	5	95
22.0	5	95
24.0	95	5
25.0	95	5

Table 54: HPLC conditions of sample analysis from TART trapping of radical thiol-ene addition, using benzyl mercaptan and styrene as substrates, CHANT as TART and HPLC-MS for characterisation (11.5.2.5). Column = Waters Symmetry. Injection speed = 300 $\mu\text{L min}^{-1}$.

Time / m	0.1%HCOOH/ H ₂ O / %	0.1%HCOOH/ MeCN / %
0.0	95	5
5.0	95	5
10.0	50	50
25.0	5	95
35.0	5	95
39.0	95	5
40.0	95	5

Table 55: HPLC conditions of sample analysis from TART trapping of aqueous •OH-initiated biochemical degradation, using DEADANT as TART and HPLC-MS for characterisation (11.6). Column = Atlantis. Injection speed = 500 $\mu\text{L min}^{-1}$.

Time / m	0.1%HCOOH/ H ₂ O / %	0.1%HCOOH/ MeCN / %
0.0	100	0
5.0	100	0
15.0	90	10
25.0	70	30
30.0	30	70
31.0	5	95
35.0	5	95
39.0	100	0
40.0	100	0

Table 56: HPLC conditions of sample analysis from TART trapping of gaseous α -pinene ozonolysis and •OH-initiated *n*-nonane degradation, using CHANT as TART and HPLC-MS for characterisation (11.7, 11.8.1). Column = Eclipse Plus Phenyl-Hexyl. Injection speed = 300 $\mu\text{L min}^{-1}$.

Time / m	0.1%HCOOH/ H ₂ O / %	0.1%HCOOH/ MeCN / %	MS or waste
0.0	95	5	MS
5.0	95	5	MS
10.0	20	80	MS
13.5	↓	↓	Waste
14.0	↓	↓	MS
25.0	5	95	MS
35.0	5	95	MS
39.0	95	5	MS
40.0	95	5	MS

Table 57: HPLC conditions of sample analysis from TART trapping of gaseous α -pinene ozonolysis and •OH-initiated *n*-nonane degradation, using water photolysis as an •OH source, DEADANT as TART and HPLC-MS for characterisation (11.8.2). Column = Atlantis. Injection speed = 500 $\mu\text{L min}^{-1}$.

Time / m	0.1%HCOOH/ H ₂ O / %	0.1%HCOOH/ MeCN / %	MS or waste
0.0	100	0	MS
1.0	↓	↓	Waste
5.0	100	0	Waste
15.0	90	10	MS
25.0	70	30	MS
30.0	30	70	MS
31.0	5	95	MS
35.0	5	95	MS
39.0	100	0	MS
40.0	100	0	MS

11.10. Modelling procedures

11.10.1. General

Parameters, reactions and their rate constants used in modelling are described in full in the supporting information (SI7). All model files are available upon request.

Potential wall reactions were ignored and simulation conditions were set at RTP. Rate constants were calculated using the Arrhenius equation $k = Ae^{-\frac{E_a}{RT}}$, where A was the pre-exponential factor, E_a was activation energy, R was the universal gas constant (8.314 J K⁻¹ mol⁻¹) and T was absolute temperature (K). Key parameters: E_a units = K; temperature = 293 K; accuracy = 10⁻¹⁰.

11.10.2. Radical thiol-ene addition

A kinetic model was designed based upon previous DFT-informed kinetic modelling of radical thiol-ene addition undertaken by Northrop *et al.*²⁰⁴ and Findik *et al.*²⁰⁸ with trapping reactions added (Figure 97).

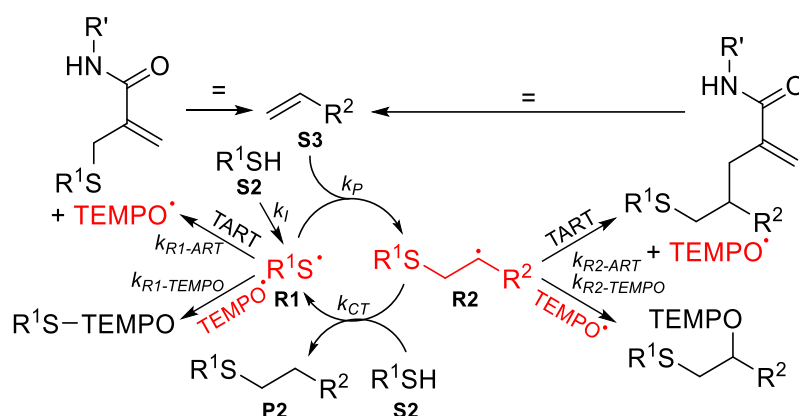


Figure 193: Kinetic model of TART trapping of radical thiol-ene addition. Arrows are included to indicate that trapped radicals R1-ART and R2-ART could undergo subsequent radical thiol-ene addition.

Rate constants were obtained from assorted literature sources.^{204,208–210} Parameters, reactions and their rate constants are described in full in the supporting information (SI8.1). Concentration units were M. Initiation rate constant was initially set as 10⁻⁵ s⁻¹, estimated by Northrop *et al.*²⁰⁴ and Findik *et al.*²⁰⁸ but later estimated to be 5.39×10⁻⁶ s⁻¹ for TART trapping of radical thiophenol-styrene using kinetics experiments. Forward and backward rate constants of propagation (k_P and k_{-P}) and chain transfer (k_{CT} and k_{-CT}) were obtained from Northrop *et al.* and Findik *et al.* for each substrate or estimated from similar substrates.^{204,208} Forward rate constant of TART trapping of R1 (k_{R1-ART}) was set equal to forward R1 reaction with methyl methacrylate obtained from Northrop *et al.* and Findik *et al.* for each substrate or estimated from similar substrates.^{204,208} Forward TEMPO• trapping of R1 and all reverse trapping rates were estimated to be arbitrarily slow 1.00 s⁻¹. Forward rate constants of TART and TEMPO• trapping of R2 (k_{R2-ART} and $k_{R2-TEMPO}$) were estimated from similar literature reactions.^{209,210} For TART-trapped radicals, rate constants of forward and backward propagation and chain transfer were estimated to be equal to R1 reaction with methyl methacrylate obtained from Northrop *et al.* and Findik *et al.* for each substrate or estimated from similar substrates.^{204,208} The radicals formed could be trapped, for which the same rate constants were assigned as previously. Radical-radical termination rate constants were set as 10⁸ mol⁻¹ dm³ s⁻¹, as estimated by Northrop *et al.*²⁰⁴ Each model was run for 24 h.

Kinetic modelling was used to predict the resting states in for different substrates based upon experimental observations. For each substrate combination, rate constants were assigned as previously. After this, reverse rate constants were kept constant and hence, $k_p/k_{p,r}$ and $k_{CT}/k_{CT,r}$ defined the propagation cycle rate constants. Each model was run for 24 h. Initiation and forward propagation rate constants were then reasonably altered by hand until $[R1-ART]/[R2-ART]$ broadly matched the ratio of experimental intensities of MS peaks corresponding to $[R1-ART+X]^+/[R2-ART+X]^+$. The obtained rate constants are available in the supporting information (SI8.1). TART was then removed from the simulation, to determine $[R1]/[R2]$ and hence estimate the radical resting state. For different thiols, all rate constants were kept the same except for rates in which R1 was involved. For different alkenes, all rate constants were kept the same except for rates in which R2 was involved.

11.10.3. α -Pinene ozonolysis

Atmospheric reactions of α -pinene were imported into the Kintecus chemical simulation programme²⁰⁷ from the MCM⁵⁷ and truncated to remove late stage pathways (SI8.2). Simulation parameters were set to emulate experimental conditions immediately prior to bubbling through trap solution. Simulation time was set as calculated residence time (56.5 ms). Concentration units were molec. cm⁻³. As measured or calculated, initial $[O_3]$ and $[\alpha\text{-pinene}]$ were set as 2.96×10^{15} and 5.20×10^{16} molec. cm⁻³ respectively. Simulation results yielded final gaseous radical concentrations, immediately prior to bubbling.

These final gaseous radical concentrations were used to simulate radical trapping. Using measured 11% α -pinene dissolution (11.7.4), 11% of these gaseous radicals were entered into a liquid phase model (dissolved), whilst the remaining 89% were entered into a gas-liquid interface model (not dissolved). In both models, atmospheric reactions were assumed to stop immediately upon bubbling, whilst trapping reactions could occur. These reactions involved reaction of trap with radicals to form a trapped radical and TEMPO \cdot . Trapping rate of RO₂ \cdot and RO \cdot was estimated to be 10^{-22} and 10^{-15} molec.⁻¹ cm³ s⁻¹ respectively, based upon RO₂ \cdot addition to methyl methacrylate²²⁶ and assorted literature-sourced rate constants for RO \cdot addition to alkenes²²⁸ respectively. In both models, initial trap concentration was set as its initial concentration in solution, 3.01×10^{17} molec. cm⁻³.

The liquid phase model was run for total reaction time (2 min). During this time, 11% gaseous radicals were inputted at regular intervals to simulate incoming radicals, allowing trapping to occur. This yielded final trapped radical concentrations in solution for the liquid phase model.

In the gas-liquid interface model, the model was run for the estimated residence time of a gas bubble in solution (6.79 ms). Initial gaseous radical concentrations were inputted using 89% final gaseous radical concentrations accumulated during this residence time, allowing trapping to occur. These results were then scaled to the total reaction time (2 min), yielding final trapped radical concentrations in solution for the gas-liquid interface model.

Results from these two models were summed together to yield final trapped radical concentrations in solution.

11.10.4. \cdot OH-initiated *n*-nonane degradation

Atmospheric reactions of *n*-nonane were imported into the Kintecus chemical simulation programme²⁰⁷ from the MCM⁵⁷ and truncated to remove late stage pathways (SI8.3). Simulation parameters were set to emulate experimental conditions immediately prior to bubbling through the trapping solution. Simulation time was set as calculated residence time (129 ms). Concentration units were molec. cm⁻³. As measured or calculated, initial $[\cdot\text{OH}]$, $[\text{HO}_2\cdot]$ and $[n\text{-nonane}]$ were set as $3.4 \pm 0.5 \times 10^{11}$ molec. cm⁻³, $3.4 \pm 0.5 \times 10^{11}$ molec. cm⁻³ and

1.0×10^{16} molec. cm^{-3} respectively. Simulation results yielded final gaseous $[\text{C}_9\text{H}_{19}\text{O}_2^*]$ and $[\text{C}_9\text{H}_{19}\text{O}^*]$ to be $1.73 \pm 0.14 \times 10^{11}$ molec. cm^{-3} and $2.1 \pm 0.3 \times 10^3$ molec. cm^{-3} respectively, allowing detection limits to be estimated (Figure 185).

Commonly used abbreviations

Ac	acetyl
ART	allyl radically trapped
Boc	<i>tert</i> -butyloxycarbonyl
br	broad (in NMR spectroscopy and IR spectroscopy)
CHANT	<i>N</i> -cyclohexyl-2-[[[(2,2,6,6-tetramethylpiperidin-1-yl)oxy]methyl]acrylamide
CI	chemical ionisation
CID	collision-induced dissociation
d	doublet (in NMR spectroscopy)
DANT	<i>N</i> -2-hydroxyethyl-2-[[[(2,2,6,6-tetramethylpiperidin-1-yl)oxy]methyl]acrylamide
DCM	dichloromethane
DEADANT	<i>N'</i> - <i>N,N</i> -dimethylethyleneamino-2-[[[(2,2,6,6-tetramethylpiperidin-1-yl)oxy]methyl]acrylamide
DIPEA	<i>N,N</i> -diisopropylethylamine
DMF	dimethylformamide
DNA	deoxyribonucleic acid
EPR	electron paramagnetic resonance
eq.	equivalents
ESI	electrospray ionisation
FAGE	fluorescence assay gas expansion
FT-ICR	Fourier transform ion cyclotron resonance
HAA	hydrogen atom abstraction
HBTU	<i>O</i> -(benzotriazol-1-yl)- <i>N,N,N',N'</i> -tetramethyluronium hexafluorophosphate
HLF	Hofmann-Löffler-Freytag
HOM	highly oxidised multifunctional
HPLC	high-performance liquid chromatography
IR	infrared
<i>J</i>	coupling constant (Hz)
LC	liquid chromatography
M	unfragmented molecule
<i>m/z</i>	mass to charge ratio
<i>m</i> -CPBA	<i>meta</i> -chloroperbenzoic acid
MCM	Master Chemical Mechanism
MS	mass spectrometry
NMR	nuclear magnetic resonance
Neg	negative ion mode
PET ether	petroleum ether
Pos	positive ion mode
ppb	parts per billion
ppm	parts per million
qNMR	quantitative nuclear magnetic resonance
q	quartet (in NMR spectroscopy)
<i>R_f</i>	retention factor
ROS	reactive oxygen species
RTP	room temperature (293 K) and pressure (101325 Pa)
s	singlet (in NMR spectroscopy); strong (in IR spectroscopy)
SOA	secondary organic aerosol
SORI	sustained off-residence irradiation (in MS)

t	triplet (in NMR spectroscopy)
TART	TEMPO-allyl radical trap
TEMPO	(2,2,6,6-tetramethylpiperidin-1-yl)oxyl
THF	tetrahydrofuran
TMP	2,2,6,6-tetramethylpiperidine
TOF	time-of-flight
UV	ultraviolet
Vis	visible
VOC	volatile organic compound

References

- 1 J. Fossey, D. Lefort and J. Sorba, *Free Radicals in Organic Chemistry*, Wiley, New York, 1995.
- 2 A. F. Parsons, *An Introduction to Free Radical Chemistry*, Blackwell Science, Oxford, 2000.
- 3 W. A. Braunecker and K. Matyjaszewski, *Prog. Polym. Sci.*, 2007, **32**, 93–146.
- 4 K. Matyjaszewski and J. Xia, *Chem. Rev.*, 2001, **101**, 2921–2990.
- 5 C. K. Prier, D. A. Rankic and D. W. C. MacMillan, *Chem. Rev.*, 2013, **113**, 5322–5363.
- 6 M. H. Shaw, J. Twilton and D. W. C. MacMillan, *J. Org. Chem.*, 2016, **81**, 6898–6926.
- 7 N. A. Romero and D. A. Nicewicz, *Chem. Rev.*, 2016, **116**, 10075–10166.
- 8 K. Apel and H. Hirt, *Annu. Rev. Plant Biol.*, 2004, **55**, 373–399.
- 9 M. Valko, D. Leibfritz, J. Moncol, M. T. D. Cronin, M. Mazur and J. Telser, *Int. J. Biochem. Cell Biol.*, 2007, **39**, 44–84.
- 10 M. Hallquist, J. C. Wenger, U. Baltensperger, Y. Rudich, D. Simpson, M. Claeys, J. Dommen, N. M. Donahue, C. George, A. H. Goldstein, J. F. Hamilton, H. Herrmann, T. Hoffmann, Y. Iinuma, M. Jang, M. E. Jenkin, J. L. Jimenez, A. Kiendler-Scharr, W. Maenhaut, G. McFiggans, T. F. Mentel, A. Monod, A. S. H. Prévôt, J. H. Seinfeld, J. D. Surratt, R. Szmigielski and J. Wildt, *Atmos. Chem. Phys.*, 2009, **9**, 5155–5236.
- 11 B. Nozière, M. Kalberer, M. Claeys, J. Allan, B. D’Anna, S. Decesari, E. Finessi, M. Glasius, I. Grgić, J. F. Hamilton, T. Hoffmann, Y. Iinuma, M. Jaoui, A. Kahnt, C. J. Kampf, I. Kourtchev, W. Maenhaut, N. Marsden, S. Saarikoski, J. Schnelle-Kreis, J. D. Surratt, S. Szidat, R. Szmigielski and A. Wisthaler, *Chem. Rev.*, 2015, **115**, 3919–3983.
- 12 A. L. Zanocco, A. Cañete M. and M. X. Melendez, *Bol. Soc. Chil. Quím.*, 2000, **45**, 123–129.
- 13 H. Togo, *Advanced Free Radical Reactions for Organic Synthesis*, Elsevier B.V., 2004.
- 14 K. J. Romero, M. S. Galliher, D. A. Pratt and C. R. J. Stephenson, *Chem. Soc. Rev.*, 2018, **47**, 7851–7866.
- 15 P. Nesvadba, in *Encyclopedia of Radicals in Chemistry, Biology and Materials*, John Wiley & Sons Ltd., 2012.
- 16 K. C. Berger, P. C. Deb and G. Meyerhoff, *Macromolecules*, 1977, **10**, 1075–1080.
- 17 T. Posner, *Berichte der Dtsch. Chem. Gesellschaft*, 1905, **1**, 646–657.
- 18 N. B. Cramer and C. N. Bowman, *J. Polym. Sci. Part A Polym. Chem.*, 2001, **39**, 3311–3319.
- 19 O. Okay and C. N. Bowman, *Macromol. Theory Simul.*, 2005, **14**, 267–277.
- 20 A. B. Lowe, *Polym. Chem.*, 2010, **1**, 17–36.
- 21 C. E. Hoyle and C. N. Bowman, *Angew. Chem. Int. Ed.*, 2010, **49**, 1540–1573.
- 22 B. H. J. Bielski, D. E. Cabelli, R. L. Arudi and A. B. Ross, *J. Phys. Chem. Ref. Data*, 1985, **14**, 1041–1100.
- 23 L. Gaohua, X. Miao and L. Dou, *Expert Opin. Drug Metab. Toxicol.*, 2021, **17**, 1103–1124.

- 24 S. Yoshikawa, K. Muramoto, K. Shinzawa-ito and H. Aoyama, *Biochim. Biophys. Acta*, 2006, **1757**, 1110–1116.
- 25 K. Schmidt-Rohr, *ACS Omega*, 2020, **5**, 2221–2233.
- 26 X. Li, P. Fang, J. Mai, E. T. Choi, H. Wang and X. F. Yang, *J. Hematol. Oncol.*, 2013, **6**, 1–19.
- 27 A. W. Segal, *Annu. Rev. Immunol.*, 2005, **23**, 197–223.
- 28 M. Herb and M. Schramm, *Antioxidants*, 2021, **10**, 1–39.
- 29 J. F. Curtin, M. Donovan and T. G. Cotter, *J. Immunol. Methods*, 2002, **265**, 49–72.
- 30 T. Ozben, *J. Pharm. Sci.*, 2007, **96**, 2181–2196.
- 31 M. Hayyan, M. A. Hashim and I. M. Alnashef, *Chem. Rev.*, 2016, **116**, 3029–3085.
- 32 M. J. Davies, *Biochim. Biophys. Acta - Proteins Proteomics*, 2005, **1703**, 93–109.
- 33 S. B. Nimse and D. Pal, *RSC Adv.*, 2015, **5**, 27986–28006.
- 34 P. Sharma, A. B. Jha, R. S. Dubey and M. Pessarakli, *J. Bot.*, 2012, **2012**, 1–26.
- 35 P. Chelikani, I. Fita and P. C. Loewen, *Cell. Mol. Life Sci.*, 2004, **61**, 192–208.
- 36 A. Meister and M. E. Anderson, *Ann. Rev. Biochem.*, 1983, **52**, 711–760.
- 37 F. Q. Schafer and G. R. Buettner, *Free Radic. Biol. Med.*, 2001, **30**, 1191–1212.
- 38 N. Couto, N. Malys, S. J. Gaskell and J. Barber, *J. Proteome Res.*, 2013, **12**, 2885–2894.
- 39 C. E. Ofoedu, L. You, C. M. Osuji, J. O. Iwouno, N. O. Kabuo, M. Ojukwu, I. M. Agunwah, J. S. Chacha, O. P. Muobike, A. O. Agunbiade, G. Sardo, G. Bono, C. O. R. Okpala and M. Korzeniowska, *Foods*, 2021, **10**, 699.
- 40 Y. P. A. de Oliveira, L. C. Pontes-de-Carvalho, R. D. Couto and A. A. Noronha-Dutra, *Brazilian J. Infect. Dis.*, 2017, **21**, 19–26.
- 41 F. Ahmadinejad, S. Geir Møller, M. Hashemzadeh-Chaleshtori, G. Bidkhorji and M.-S. Jami, *Antioxidants*, 2017, **6**, 51.
- 42 Y. Liu, Q. Jia, Q. Guo, A. Jiang and J. Zhou, *Anal. Chem.*, 2017, **89**, 12299–12305.
- 43 D. Harman, *J. Gerontol.*, 1956, **11**, 298–300.
- 44 H. C. Birnboim, *Carcinogenesis*, 1986, **7**, 1511–1517.
- 45 J. Cadet, T. Delatour, T. Douki, D. Gasparutto, J. P. Pouget, J. L. Ravanat and S. Sauvaigo, *Mutat. Res.*, 1999, **424**, 9–21.
- 46 L. C. Colis, P. Raychaudhury and A. K. Basu, *Biochemistry*, 2008, **47**, 8070–8079.
- 47 H. C. Box, E. E. Budzinski, J. D. Dawidzik, J. C. Wallace, S. Marianne, J. S. Gobey, H. C. Box, E. E. Budzinski, D. Dawidzik, C. Wallace, S. Evans and S. Gobey, *Radiat. Res.*, 2014, **145**, 641–643.
- 48 A. Parent, A. Benjdia, A. Guillot, X. Kubiak, C. Balty, B. Lefranc, J. Leprince and O. Berteau, *J. Am. Chem. Soc.*, 2017, **140**, 2469–2477.
- 49 C. N. Hewitt and R. M. Harrison, *Atmos. Environ.*, 1985, **19**, 545–554.
- 50 S. Gligorovski, R. Strekowski, S. Barbati and D. Vione, *Chem. Rev.*, 2015, **115**, 13051–

- 13092.
- 51 C. M. Spivakovsky, J. A. Logan, S. A. Montzka, Y. J. Balkanski, M. Foreman-Fowler, D. B. A. Jones, L. W. Horowitz, A. C. Fusco, C. A. M. Brenninkmeijer, M. J. Prather, S. C. Wofsy and M. B. McElroy, *J. Geophys. Res. Atmos.*, 2000, **105**, 8931–8980.
- 52 R. P. Adamsa and J. W. Wrightb, *J. Essent. Oil Res.*, 2012, **24**, 435–440.
- 53 H. J. Kim, K. Kim, N. S. Kim and D. S. Lee, *J. Chromatogr. A*, 2000, **902**, 389–404.
- 54 H. Wittcoff and B. Reuben, *Industrial Organic Chemicals*, John Wiley, New York, NY, 1996.
- 55 R. E. Dunmore, J. R. Hopkins, R. T. Lidster, J. D. Lee, M. J. Evans, A. R. Rickard, A. C. Lewis and J. F. Hamilton, *Atmos. Chem. Phys.*, 2015, **15**, 9983–9996.
- 56 P. Ciccioli, E. Brancaleoni, R. Mabilia and A. Cecinato, *J. Chromatogr. A*, 1997, **777**, 267–274.
- 57 Master Chemical Mechanism, MCM v3.3.1 (Jenkin *et al.*, *Atmos. Environ.*, 1997, **31**, 81; Saunders *et al.*, *Atmos. Chem. Phys.*, 2003, **3**, 161; Jenkin *et al.*, *Atmos. Chem. Phys.*, 2015, **15**, 11433), <http://mcm.york.ac.uk>.
- 58 D. Zhang and R. Zhang, *J. Chem. Phys.*, 2005, **122**, 114308.
- 59 M. Camredon, J. F. Hamilton, M. S. Alam, K. P. Wyche, T. Carr, I. R. White, P. S. Monks, A. R. Rickard and W. J. Bloss, *Atmos. Chem. Phys.*, 2010, **10**, 2893–2917.
- 60 S. D. Tetali, *Planta*, 2019, **249**, 1–8.
- 61 K. Sindelarova, C. Granier, I. Bouarar, A. Guenther, S. Tilmes, T. Stavrou, J. F. Müller, U. Kuhn, P. Stefani and W. Knorr, *Atmos. Chem. Phys.*, 2014, **14**, 9317–9341.
- 62 A. Guenther, C. Nicholas Hewitt, E. David, R. Fall, G. Chris, G. Tom, H. Peter, L. Klinger, L. Manuel, W. A. McKay, P. Tom, B. Scholes, R. Steinbrecher, R. Tallamraju, J. Taylor and P. Zimmerman, *J. Geophys. Res.*, 1995, **100**, 8873–8892.
- 63 G. I. Gkatzelis, M. M. Coggon, B. C. McDonald, J. Peischl, J. B. Gilman, K. C. Aikin, M. A. Robinson, F. Canonaco, A. S. H. Prevot, M. Trainer and C. Warneke, *Environ. Sci. Technol.*, 2021, **55**, 4332–4343.
- 64 C. Stöner, A. Edtbauer and J. Williams, *Indoor Air*, 2018, **28**, 164–172.
- 65 M. Ehn, J. A. Thornton, E. Kleist, M. Sipilä, H. Junninen, I. Pullinen, M. Springer, F. Rubach, R. Tillmann, B. Lee, F. Lopez-Hilfiker, S. Andres, I. H. Acir, M. Rissanen, T. Jokinen, S. Schobesberger, J. Kangasluoma, J. Kontkanen, T. Nieminen, T. Kurtén, L. B. Nielsen, S. Jørgensen, H. G. Kjaergaard, M. Canagaratna, M. D. Maso, T. Berndt, T. Petäjä, A. Wahner, V. M. Kerminen, M. Kulmala, D. R. Worsnop, J. Wildt and T. F. Mentel, *Nature*, 2014, **506**, 476–479.
- 66 A. Mutzel, L. Poulain, T. Berndt, Y. Iinuma, M. Rodigast, O. Böge, S. Richters, G. Spindler, M. Sipilä, T. Jokinen, M. Kulmala and H. Herrmann, *Environ. Sci. Technol.*, 2015, **49**, 7754–7761.
- 67 F. Bianchi, T. Kurtén, M. Riva, C. Mohr, M. P. Rissanen, P. Roldin, T. Berndt, J. D. Crouse, P. O. Wennberg, T. F. Mentel, J. Wildt, H. Junninen, T. Jokinen, M. Kulmala, D. R. Worsnop, J. A. Thornton, N. Donahue, H. G. Kjaergaard and M. Ehn, *Chem. Rev.*, 2019, **119**, 3472–3509.
- 68 D. Johnson and G. Marston, *Chem. Soc. Rev.*, 2008, **37**, 699–716.
- 69 R. Criegee, *Angew. Chem. Int. Ed.*, 1975, **14**, 745–752.

- 70 C. A. Taatjes, G. Meloni, T. M. Selby, A. J. Trevitt, D. L. Osborn, C. J. Percival and D. E. Shallcross, *J. Am. Chem. Soc.*, 2008, **130**, 11883–11885.
- 71 O. Welz, J. D. Savee, D. L. Osborn, S. S. Vasu, C. J. Percival, D. E. Shallcross and C. A. Taatjes, *Science*, 2012, **335**, 204–207.
- 72 Y. Te Su, Y. H. Huang, H. A. Witek and Y. P. Lee, *Science*, 2013, **340**, 174–176.
- 73 M. J. Newland, A. R. Rickard, M. S. Alam, L. Vereecken, A. Muñoz, M. Ródenas and W. J. Bloss, *Phys. Chem. Chem. Phys.*, 2015, **17**, 4076–4088.
- 74 E. Zavoisky, *J. Phys. USSR*, 1945, **9**, 211–245.
- 75 V. Parish, *NMR, NQR, EPR and Mössbauer Spectroscopy in Inorganic Chemistry*, Ellis Horwood Limited, Chichester, UK, 1990.
- 76 C. A. Rice-Evans, A. T. Diplock and M. C. R. Symons, in *Techniques in Free Radical Research*, Elsevier Science Publishers B.V., Amsterdam, 1991, pp. 51–100.
- 77 V. Chechik, E. Carter and D. Murphy, *Electron Paramagnetic Resonance*, Oxford University Press, Oxford, UK, 2016.
- 78 A. Yamada, M. Abe, Y. Nishimura, S. Ishizaka, M. Namba, T. Nakashima, K. Shimoji and N. Hattori, *Beilstein J. Org. Chem.*, 2019, **15**, 863–873.
- 79 A. C. Eslami, W. Pasanphan, B. A. Wagner and G. R. Buettner, *Chem. Cent. J.*, 2010, **4**, 1–4.
- 80 D. Mihelcic, D. H. Ehhalt, G. F. Kulesa, J. Klomfass, M. Trainer, U. Schmidt and H. Röhrs, *Pure Appl. Geophys.*, 1978, **116**, 530–536.
- 81 D. Mihelcic, P. Müsgen and D. H. Ehhalt, *J. Atmos. Chem.*, 1985, **3**, 341–361.
- 82 D. Mihelcic, D. Klemp, P. Müsgen, H. W. Pätz and A. Volz-Thomas, *J. Atmos. Ocean. Technol.*, 1993, **16**, 313–335.
- 83 E. G. Janzen, *Acc. Chem. Res.*, 1971, **4**, 31–40.
- 84 D. F. Church, *Anal. Chem.*, 1994, **66**, 419–427.
- 85 R. Kaptein and J. L. Oosterhoff, *Chem. Phys. Lett.*, 1969, **4**, 195–197.
- 86 M. Goetz, in *Annual Reports on NMR Spectroscopy*, Elsevier Ltd., 2009, vol. 66, pp. 77–147.
- 87 C. Karunakaran, P. Santharaman and M. Balamurugan, *¹H and ¹³C nuclear magnetic resonance spectroscopy*, Elsevier Inc., 2018.
- 88 O. A. Krumkacheva, V. R. Gorelik, E. G. Bagryanskaya, N. V. Lebedeva and M. D. E. Forbes, *Langmuir*, 2010, **26**, 8971–8980.
- 89 J. A. McCloskey, *Mass Spectrometry*, Academic Press, San Diego, 1990.
- 90 J. R. Chapman, *Practical Organic Mass Spectrometry: A Guide for Chemical and Biological Analysis*, John Wiley, Chichester, UK, 1993.
- 91 E. de Hoffmann and V. Stroobant, *Mass Spectrometry: Principles and Applications*, John Wiley & Sons Ltd., Chichester, UK, 2007.
- 92 G. L. Glish and R. W. Vachet, *Nat. Rev. Drug Discov.*, 2003, **2**, 140–150.
- 93 F. W. McLafferty, *Annu. Rev. Anal. Chem.*, 2011, **4**, 1–22.

- 94 H. Awad, M. M. Khamis and A. El-Aneed, *Appl. Spectrosc. Rev.*, 2015, **50**, 158–175.
- 95 A. Gaudel-Siri, C. Marchal, V. Ledentu, D. Gignes, D. Siri and L. Charles, *Eur. J. Mass Spectrom.*, 2019, **25**, 229–238.
- 96 M. J. Eirod, *J. Phys. Chem. A*, 1999, **103**, 4378–4384.
- 97 D. Hanson, J. Orlando, B. Nozière and E. Kosciuch, *Int. J. Mass Spectrom.*, 2004, **239**, 147–159.
- 98 B. Nozière and D. R. Hanson, *J. Phys. Chem. A*, 2017, **121**, 8453–8464.
- 99 B. Nozière and L. Vereecken, *Angew. Chem. Int. Ed.*, 2019, **58**, 13976–13982.
- 100 C. Zhu, K. Kawamura and B. Kunwar, *Atmos. Chem. Phys.*, 2015, **15**, 1959–1973.
- 101 H.-H. Perkampus, *UV-Vis Spectroscopy and Its Applications*, Springer-Verlag, New York, 1992.
- 102 J. R. Lakowicz, *Principles of Fluorescence Spectroscopy*, Springer, New York, 2006.
- 103 A. Celebioglu and T. Uyar, *J. Agric. Food Chem.*, 2017, **65**, 5404–5412.
- 104 Y. Beldjoudi, M. A. Nascimento, Y. J. Cho, H. Yu, H. Aziz, D. Tonouchi, K. Eguchi, M. M. Matsushita, K. Awaga, I. Osorio-Roman, C. P. Constantinides and J. M. Rawson, *J. Am. Chem. Soc.*, 2018, **140**, 6260–6270.
- 105 V. Sick and N. Wermuth, *Appl. Phys. B Lasers Opt.*, 2004, **79**, 139–143.
- 106 X. Ren, H. Harder, M. Martinez, I. C. Faloon, D. Tan, R. L. Lesher, P. Di Carlo, J. B. Simpas and W. H. Brune, *J. Atmos. Chem.*, 2004, **47**, 169–190.
- 107 D. E. Heard, *Annu. Rev. Phys. Chem.*, 2006, **57**, 191–216.
- 108 D. Stone, L. K. Whalley and D. E. Heard, *Chem. Soc. Rev.*, 2012, **41**, 6348–6404.
- 109 Y. Gong and L. Andrews, *J. Phys. Chem. A*, 2011, **115**, 3029–3033.
- 110 H. Li, Y. Cheng, H. Tang, Y. Bi, Y. Chen, G. Yang, S. Guo, S. Tian, J. Liao, X. Lv, S. Zeng, M. Zhu, C. Xu, J. X. Cheng and P. Wang, *Adv. Sci.*, 2020, **7**, 1903644.
- 111 A. Saiz-Lopez, A. S. Mahajan, R. A. Salmon, S. J. B. Bauguitte, A. E. Jones, H. K. Roscoe and J. M. C. Plane, *Science*, 2007, **317**, 348–351.
- 112 M. Sangwan and L. Zhu, *J. Phys. Chem. A*, 2018, **122**, 1861–1872.
- 113 N. Wei, B. Fang, W. Zhao, C. Wang, N. Yang, W. Zhang, W. Chen and C. Fittschen, *Anal. Chem.*, 2020, **92**, 4334–4339.
- 114 P. L. Zamora and F. A. Villamena, *J. Phys. Chem. A*, 2012, **116**, 7210–7218.
- 115 M. Pelletier, V. Lavastre and D. Girard, *Toxicol. Sci.*, 2002, **69**, 210–216.
- 116 F. Poulhès, E. Rizzato, P. Bernasconi, R. Rosas, S. Viel, L. Jicsinszky, A. Rockenbauer, D. Bardelang, D. Siri, A. Gaudel-Siri, H. Karoui, M. Hardy and O. Ouari, *Org. Biomol. Chem.*, 2017, **15**, 6358–6366.
- 117 M. Cassien, C. Petrocchi, S. Thétiot-Laurent, M. Robin, E. Ricquebourg, C. Kandouli, A. Asteian, A. Rockenbauer, A. Mercier, M. Culcasi and S. Pietri, *Eur. J. Med. Chem.*, 2016, **119**, 197–217.
- 118 K. Abbas, M. Hardy, F. Poulhès, H. Karoui, P. Tordo, O. Ouari and F. Peyrot, *Free Radic. Biol. Med.*, 2014, **71**, 281–290.

- 119 M. A. Rudat and C. N. McEwen, *J. Am. Chem. Soc.*, 1981, **103**, 4349–4354.
- 120 H. Iwahashi, C. E. Parker, R. P. Mason and K. B. Tomer, *Rapid Commun. Mass Spectrom.*, 1990, **4**, 352–354.
- 121 C. E. Parker, H. Iwahashi and K. B. Tomer, *J. Am. Soc. Mass Spectrom.*, 1991, **2**, 413–418.
- 122 Q. Guo, S. Y. Qian and R. P. Mason, *J. Am. Soc. Mass Spectrom.*, 2003, **14**, 862–871.
- 123 P. Domingues, C. Fonseca, A. Reis and M. R. M. Domingues, *Biomed. Chromatogr.*, 2012, **26**, 51–60.
- 124 Y. Wang, M. Liu, Y. Zhu, K. Cheng, W. Da, B. Liu and F. Li, *Talanta*, 2016, **160**, 106–112.
- 125 C. Giorio, S. J. Campbell, M. Bruschi, F. Tampieri, A. Barbon, A. Toffoletti, A. Tapparo, C. Paijens, A. J. Wedlake, P. Grice, D. J. Howe and M. Kalberer, *J. Am. Chem. Soc.*, 2017, **139**, 3999–4008.
- 126 A. Zaytsev, M. Breitenlechner, A. Novelli, H. Fuchs, D. Knopf, J. Kroll and F. Keutsch, *Atmos. Meas. Tech. Discuss.*, 2020, **14**, 1–20.
- 127 F. Leinisch, J. Jiang, E. F. Derose, V. V. Khramtsov and R. P. Mason, *Free Radic. Biol. Med.*, 2013, **65**, 1497–1505.
- 128 S. Pou, D. J. Hassett, B. E. Britigan, M. S. Cohen and G. M. Rosen, *Anal. Biochem.*, 1989, **177**, 1–6.
- 129 G. R. Buettner and L. W. Oberley, *Biochem. Biophys. Res. Commun.*, 1978, **83**, 69–74.
- 130 N. Sankuratri, Y. Kotake and E. G. Janzen, *Free Radic. Biol. Med.*, 1996, **21**, 889–894.
- 131 N. Khan, C. M. Wilmot, G. M. Rosen, E. Demidenko, J. Sun, J. Joseph, J. O'Hara, B. Kalyanaraman and H. M. Swartz, *Free Radic. Biol. Med.*, 2003, **34**, 1473–1481.
- 132 K. Stolze, N. Udilova, T. Rosenau, A. Hofinger and H. Nohl, *Biochem. Pharmacol.*, 2003, **66**, 1717–1726.
- 133 T. Vogler and A. Studer, *Synthesis*, 2008, **13**, 1979–1993.
- 134 Y. Matsuoka, Y. Izumi, M. Takahashi, T. Bamba and K. Yamada, *Anal. Chem.*, 2020, **92**, 6993–7002.
- 135 X. F. Xia, S. L. Zhu, Y. N. Niu, D. Zhang, X. Liu and H. Wang, *Tetrahedron*, 2016, **72**, 3068–3072.
- 136 H. Yan, G. Rong, D. Liu, Y. Zheng, J. Chen and J. Mao, *Org. Lett.*, 2014, **16**, 6306–6309.
- 137 A. P. Dobbs, P. Jones, M. J. Penny and S. E. Rigby, *Tetrahedron*, 2009, **65**, 5271–5277.
- 138 P. J. Wright and A. M. English, *J. Am. Chem. Soc.*, 2003, **125**, 8655–8665.
- 139 Y. R. Luo, *Comprehensive Handbook of Chemical Bond Energies*, CRC Press, Boca Raton, FL, 2007.
- 140 D. H. R. Barton, V. N. Le Gloahec and J. Smith, *Tetrahedron Lett.*, 1998, **39**, 7483–7486.
- 141 C. D. Cook and R. C. Woodworth, *J. Am. Chem. Soc.*, 1953, **75**, 6242–6244.

- 142 V. A. Khizhnyi and G. A. Goloverda, *Teor Eksperim Khim*, 1988, **24**, 154–159.
- 143 P. Griva and E. T. Dexisov, *Int. J. Chem. Kinet.*, 1973, **5**, 869–877.
- 144 M. A. DaRooge and L. R. Mahoney, *J. Org. Chem.*, 1967, **32**, 1–6.
- 145 M. Tomita, T. Okuyama, S. Watanabe and H. Watanabe, *Arch. Toxicol.*, 1994, **68**, 428–433.
- 146 X. Yang, M. Zhan, L. Kong and L. Wang, *J. Environ. Sci.*, 2004, **16**, 687–689.
- 147 H. Jian, *Chinese J. Chem.*, 2005, **23**, 1273–1274.
- 148 H. Karoui, F. Le Moigne, O. Ouari and P. Tordo, in *Stable Radicals: Fundamentals and Applied Aspects of Odd-Electron Compounds*, ed. R. G. Hicks, John Wiley & Sons, Inc., 2010, vol. 12, pp. 173–229.
- 149 E. G. Bagryanskaya and S. R. A. Marque, *Chem. Rev.*, 2014, **114**, 5011–5056.
- 150 Y.-M. Dang and X.-Q. Guo, *Appl. Spectrosc.*, 2006, **60**, 203–207.
- 151 R. Toba, H. Gotoh and K. Sakakibara, *Org. Lett.*, 2014, **16**, 3868–3871.
- 152 A. Grantham, PhD thesis, University of York, 2017.
- 153 J. F. Van Humbeck, S. P. Simonovich, R. R. Knowles and D. W. C. Macmillan, *J. Am. Chem. Soc. Commun.*, 2010, **132**, 10012–10014.
- 154 M. E. Jenkin, T. P. Murrells, S. J. Shalliker and G. D. Hayman, *J. Chem. Soc. Faraday Trans.*, 1993, **89**, 433–446.
- 155 T. Wang, G. Kehr, L. Liu, S. Grimme, C. G. Daniliuc and G. Erker, *J. Am. Chem. Soc.*, 2016, **138**, 4302–4305.
- 156 D. E. Bergbreiter and B. Walchuk, *Macromolecules*, 1998, **31**, 6380–6382.
- 157 O. Ito, Y. Arito and M. Matsuda, *J. Chem. Soc. Perkin Trans. 2*, 1988, 869–873.
- 158 A. M. Tsedilin, A. N. Fakhruddinov, D. B. Eremin, S. S. Zalesskiy, A. O. Chizhov, N. G. Kolotyrykina and V. P. Ananikov, *Mendeleev Commun.*, 2015, **25**, 454–456.
- 159 S. J. Gaskell, *J. Mass Spectrom.*, 1997, **32**, 677–688.
- 160 S. Banerjee and S. Mazumdar, *Int. J. Anal. Chem.*, 2012, **2012**, 1–40.
- 161 P. Liigand, J. Liigand, K. Kaupmees and A. Kruve, *Anal. Chim. Acta*, 2021, **1152**, 238117.
- 162 S. Indelicato, D. Bongiorno and L. Ceraulo, *Front. Chem.*, 2021, **8**, 1–6.
- 163 F. W. McLafferty, *Acc. Chem. Res.*, 1980, **13**, 33–39.
- 164 J. J. Coon, J. E. P. Syka, J. Shabanowitz and D. F. Hunt, *Biotechniques*, 2005, **38**, 519–523.
- 165 A. R. Johnson and E. E. Carlson, *Anal. Chem.*, 2015, **87**, 10668–10678.
- 166 J. F. Parcher, M. Wang, A. G. Chittiboyina and I. A. Khan, *Drug Test. Anal.*, 2018, **10**, 28–36.
- 167 J. W. Flora, J. C. Hannis and D. C. Muddiman, *Anal. Chem.*, 2001, **73**, 1247–1251.
- 168 K. A. Herrmann, A. Somogyi, V. H. Wysocki, L. Drahos and K. Vekey, *Anal. Chem.*, 2005, **77**, 7626–7638.

- 169 W. A. Korfmacher, *Drug Discov. Today*, 2005, **10**, 1357–1367.
- 170 J. J. Pitt, *Clin. Biochem. Rev.*, 2009, **30**, 19–34.
- 171 N. A. Pratima, *Arch. Org. Inorg. Chem. Sci.*, 2018, **1**, 26–34.
- 172 I. M. Klotz and B. H. Frank, *J. Am. Chem. Soc.*, 1965, **87**, 2721–2728.
- 173 N. Hogg, *J. Biol. Chem.*, 1996, **271**, 6000–6009.
- 174 L. Engman, J. Lind and G. Merényi, *J. Phys. Chem.*, 1994, **98**, 3174–3182.
- 175 P. Carloni, E. Damiani, M. Iacussi, L. Greci, P. Stipa, D. Cauzi, C. Rizzoli and P. Sgarabotto, *Tetrahedron*, 1995, **51**, 12445–12452.
- 176 M. Méndez, J. S. Francisco and D. A. Dixon, *Chem. Eur. J.*, 2014, **20**, 10231–10235.
- 177 D. H. R. Barton and J. M. Beaton, *J. Am. Chem. Soc.*, 1961, **83**, 4083–4089.
- 178 D. R. Barton, J. M. Beaton, L. E. Geller and M. M. Pechet, *J. Am. Chem. Soc.*, 1961, **83**, 4076–4083.
- 179 D. H. R. Barton, R. H. Hesse, M. M. Pechet and L. C. Smith, *J. Chem. Soc., Perkin Trans. 1*, 1979, 1159–1165.
- 180 M. Akhtar and M. M. Pechet, *J. Am. Chem. Soc.*, 1964, **86**, 265–268.
- 181 A. W. Hofmann, *Chem. Ber.*, 1885, **18**, 109–131.
- 182 K. Löffler and C. Freytag, *Chem. Ber.*, 1909, **42**, 3427–3431.
- 183 E. J. Corey and W. R. Hertler, *J. Am. Chem. Soc.*, 1960, **82**, 1657–1668.
- 184 C. Martínez and K. Muñoz, *Angew. Chem. Int. Ed.*, 2015, **54**, 8287–8291.
- 185 P. Becker, T. Duhamel, C. J. Stein, M. Reiher and K. Muñoz, *Angew. Chem. Int. Ed.*, 2017, **56**, 8004–8008.
- 186 P. Becker, T. Duhamel, C. Martínez and K. Muñoz, *Angew. Chem. Int. Ed.*, 2018, **57**, 5166–5170.
- 187 S. Shkunnikova, H. Zipse and D. Šakić, *Org. Biomol. Chem.*, 2021, **19**, 854–865.
- 188 A. Artaryan, A. Mardyukov, K. Kulbitski, I. Avigdori, G. A. Nisnevich, P. R. Schreiner and M. Gandelman, *J. Org. Chem.*, 2017, **82**, 7093–7100.
- 189 A. E. Bosnidou, T. Duhamel and K. Muñoz, *European J. Org. Chem.*, 2020, 6361–6365.
- 190 S. Wawzonek and P. J. Thelen, *J. Am. Chem. Soc.*, 1950, **72**, 2118–2120.
- 191 A. Borodine, *Justus Liebigs Ann. Chem.*, 1861, **119**, 121–123.
- 192 H. Hunsdiecker and C. Hunsdiecker, *Berichte der Dtsch. Chem. Gesellschaft*, 1942, **75**, 291–297.
- 193 R. G. Johnson and R. K. Ingham, *Chem. Rev.*, 1956, **56**, 219–269.
- 194 J. A. den Hollander and J. P. M. van der Ploeg, *Tetrahedron*, 1976, **32**, 2433–2436.
- 195 J. W. Hilborn and J. A. Pincock, *J. Am. Chem. Soc.*, 1991, **113**, 2683–2686.
- 196 A. Bhattacharjee, M. Sneha, L. Lewis-Borrell, O. Tau, I. P. Clark and A. J. Orr-Ewing, *Nat. Commun.*, 2019, **10**, 1–7.
- 197 J. C. Bevington and J. Leech, *Eur. Polym. J.*, 1980, **16**, 917–920.

- 198 J. Chateaufeuf, J. Luszyk and K. U. Ingold, *J. Am. Chem. Soc.*, 1987, **109**, 897–899.
- 199 J. Chateaufeuf, J. Luszyk and K. U. Ingold, *J. Am. Chem. Soc.*, 1988, **110**, 2886–2893.
- 200 Y. Wang, W. Wang, R. Tang, Z. Liu, W. Tao and Z. Fang, *Org. Biomol. Chem.*, 2018, **16**, 7782–7786.
- 201 G. J. P. Perry, J. M. Quibell, A. Panigrahi and I. Larrosa, *J. Am. Chem. Soc.*, 2017, **139**, 11527–11536.
- 202 L. Buzzetti, G. E. M. Crisenza and P. Melchiorre, *Angew. Chem. Int. Ed.*, 2019, **58**, 3730–3747.
- 203 J. R. Donald and S. L. Berrell, *Chem. Sci.*, 2019, **10**, 5832–5836.
- 204 B. H. Northrop and R. N. Coffey, *J. Am. Chem. Soc.*, 2012, **134**, 13804–13817.
- 205 E. L. Tyson, M. S. Ament and T. P. Yoon, *J. Org. Chem.*, 2013, **78**, 2046–2050.
- 206 C. M. Q. Le, F. Morlet-Savary and A. Chemtob, *Polym. Chem.*, 2021, **12**, 6594–6605.
- 207 J. C. Ianni, Kintecus, Windows Version 6.50, www.kintecus.com.
- 208 V. Findık, I. Degirmenci, Ş. Çatak and V. Aviyente, *Eur. Polym. J.*, 2019, **110**, 211–220.
- 209 G. S. Prementine and D. A. Tirrell, *Macromolecules*, 1989, **22**, 52–55.
- 210 J. Chateaufeuf, J. Luszyk and K. U. Ingold, *J. Org. Chem.*, 1988, **53**, 1629–1632.
- 211 I. Degirmenci and M. L. Coote, *J. Phys. Chem. A*, 2016, **120**, 7398–7403.
- 212 H. E. Ho, A. Pagano, J. A. Rossi-Ashton, J. R. Donald, R. G. Epton, J. C. Churchill, M. J. James, P. O'Brien, R. J. K. Taylor and W. P. Unsworth, *Chem. Sci.*, 2020, **11**, 1353–1360.
- 213 M. S. Cooke, M. D. Evans, M. Dizdaroglu and J. Lunec, *FASEB J.*, 2003, **17**, 1195–1214.
- 214 B. Halliwell, *Biochem. J.*, 2007, **401**, 1–11.
- 215 M. Dizdaroglu and P. Jaruga, *Free Radic. Res.*, 2012, **46**, 382–419.
- 216 J. Cadet and J. Richard Wagner, *Cold Spring Harb. Perspect. Biol.*, 2013, **5**, 1–18.
- 217 G. V. Buxton, C. L. Greenstock, W. P. Helman and A. B. Ross, *J. Phys. Chem. Ref. Data*, 1988, **17**, 513–886.
- 218 L. M. Smith, H. M. Aitken and M. L. Coote, *Acc. Chem. Res.*, 2018, **51**, 2006–2013.
- 219 M. Dorfman L. and E. Adams G., *Reactivity of the Hydroxyl Radical in Aqueous Solutions*, Columbus, OH, 1973.
- 220 B. Maillard, K. U. Ingold and J. C. Scaiano, *J. Am. Chem. Soc.*, 1983, **105**, 5095–5099.
- 221 P. Neta, R. E. Huie and A. B. Ross, *J. Phys. Chem. Ref. Data*, 1988, **17**, 1027–1284.
- 222 S. Korcek, J. H. B. Chenier, J. A. Howard and K. U. Ingold, *Can. J. Chem.*, 1972, **50**, 2285–2297.
- 223 J. K. Thomas, *J. Phys. Chem.*, 1967, **71**, 1919–1925.
- 224 K. Münger and H. Fischer, *Int. J. Chem. Kinet.*, 1985, **17**, 809–829.
- 225 H. Rubin, PhD Thesis, University of Zurich, 1993.

- 226 J. A. Howard, *Can. J. Chem.*, 1972, **50**, 2298–2304.
- 227 P. Koelewijn, *Recl. des Trav. Chim. des Pays-Bas*, 1972, **91**, 759–779.
- 228 P. C. Wong, D. Griller and J. C. Scaiano, *J. Am. Chem. Soc.*, 1982, **104**, 5106–5108.
- 229 C. Wang, Z. Wang, B. Zeng, M. Zheng, N. Xiao and Z. Zhao, *Chem. Commun.*, 2021, **57**, 12293–12296.
- 230 I. H. Madshus, *Biochem. J.*, 1988, **250**, 1–8.
- 231 A. Fischbacher, C. von Sonntag and T. C. Schmidt, *Chemosphere*, 2017, **182**, 738–744.
- 232 M. Kimura, M. Tohma and T. Tomita, *Chem. Pharm. Bull.*, 1972, **20**, 2185–2190.
- 233 J. Woodward, K. W. Lennon, G. Zanin, M. Wagner and M. A. Scott, *Biotechnol. Lett.*, 1985, **7**, 197–202.
- 234 S.-S. Liang, Y.-L. Shiue, C.-J. Kuo, S.-E. Guo, W.-T. Liao and E.-M. Tsai, *Sci. World J.*, 2013, 189162.
- 235 C. P. Rao and K. Geetha, *BioMetals*, 1994, **7**, 25–29.
- 236 Y. S.H., Y. H. and J. P., *Handbook of Aqueous Solubility Data*, CRC Press, 2010.
- 237 J. Cadet and J. R. Wagner, *Cold Spring Harb. Perspect. Biol.*, 2013, **5**, 1–18.
- 238 C. L. Hawkins and M. J. Davies, *Biochim. Biophys. Acta - Bioenerg.*, 2001, **1504**, 196–219.
- 239 A. E. Counterman, A. E. Hilderbrand, C. A. Srebalus Barnes and D. E. Clemmer, *J. Am. Soc. Mass Spectrom.*, 2001, **12**, 1020–1035.
- 240 M. N. Schuchmann and C. Von Sonntag, *J. Chem. Soc. Perkin Trans. 2*, 1977, 1958–1963.
- 241 R. A. M. Vreeburg, O. B. Airianah and S. C. Fry, *Biochem. J.*, 2014, **463**, 225–237.
- 242 A. Matros, D. Peshev, M. Peukert, H. P. Mock and W. Van Den Ende, *Plant J.*, 2015, **82**, 822–839.
- 243 W. D. Kumler and T. C. Daniels, *J. Am. Chem. Soc.*, 1935, **57**, 1929–1930.
- 244 D. J. Stewart, S. H. Almabrok, J. P. Lockhart, O. M. Mohamed, D. R. Nutt, C. Pfrang and G. Marston, *Atmos. Environ.*, 2013, **70**, 227–235.
- 245 D. L. Baulch, C. T. Bowman, C. J. Cobos, R. A. Cox, T. Just, J. A. Kerr, M. J. Pilling, D. Stocker, J. Troe, W. Tsang, R. W. Walker and J. Warnatz, *J. Phys. Chem. Ref. Data*, 2005, **34**, 757–1397.
- 246 R. X. Fernandes, K. Luther and J. Troe, *J. Phys. Chem. A*, 2006, **110**, 4442–4449.
- 247 N. M. Panich and B. G. Ershov, *J. Mol. Liq.*, 2021, **340**, 117318.
- 248 A. Hansel, W. Scholz, B. Mentler, L. Fischer and T. Berndt, *Atmos. Environ.*, 2018, **186**, 248–255.
- 249 L. Vereecken and J. Peeters, *J. Phys. Chem. A*, 2004, **108**, 5197–5204.
- 250 V. K. Yadav and K. G. Babu, *European J. Org. Chem.*, 2005, 452–456.
- 251 L. Vereecken, J. F. Müller and J. Peeters, *Phys. Chem. Chem. Phys.*, 2007, **9**, 5241–5248.

- 252 T. Berndt, S. Richters, T. Jokinen, N. Hyttinen, T. Kurtén, R. V. Otkjær, H. G. Kjaergaard, F. Stratmann, H. Herrmann, M. Sipilä, M. Kulmala and M. Ehn, *Nat. Commun.*, 2016, **7**, 1–8.
- 253 T. Jokinen, T. Berndt, R. Makkonen, V. M. Kerminen, H. Junninen, P. Paasonen, F. Stratmann, H. Herrmann, A. B. Guenther, D. R. Worsnop, M. Kulmala, M. Ehn and M. Sipilä, *Proc. Natl. Acad. Sci. U. S. A.*, 2015, **112**, 7123–7128.
- 254 J. Kirkby, J. Duplissy, K. Sengupta, C. Frege, H. Gordon, C. Williamson, M. Heinritzi, M. Simon, C. Yan, J. Almeida, J. Trostl, T. Nieminen, I. K. Ortega, R. Wagner, A. Adamov, A. Amorim, A. K. Bernhammer, F. Bianchi, M. Breitenlechner, S. Brilke, X. Chen, J. Craven, A. Dias, S. Ehrhart, R. C. Flagan, A. Franchin, C. Fuchs, R. Guida, J. Hakala, C. R. Hoyle, T. Jokinen, H. Junninen, J. Kangasluoma, J. Kim, M. Krapf, A. Kurten, A. Laaksonen, K. Lehtipalo, V. Makhmutov, S. Mathot, U. Molteni, A. Onnela, O. Perakyla, F. Piel, T. Petaja, A. P. Praplan, K. Pringle, A. Rap, N. A. D. Richards, I. Riipinen, M. P. Rissanen, L. Rondo, N. Sarnela, S. Schobesberger, C. E. Scott, J. H. Seinfeld, M. Sipilä, G. Steiner, Y. Stozhkov, F. Stratmann, A. Tomé, A. Virtanen, A. L. Vogel, A. C. Wagner, P. E. Wagner, E. Weingartner, D. Wimmer, P. M. Winkler, P. Ye, X. Zhang, A. Hansel, J. Dommen, N. M. Donahue, D. R. Worsnop, U. Baltensperger, M. Kulmala, K. S. Carslaw and J. Curtius, *Nature*, 2016, **533**, 521–526.
- 255 J. Peeters, L. Vereecken and G. Fantechi, *Phys. Chem. Chem. Phys.*, 2001, **3**, 5489–5504.
- 256 A. Zaytsev, M. Breitenlechner, A. Novelli, H. Fuchs, D. A. Knopf, J. H. Kroll and F. N. Keutsch, *Atmos. Meas. Tech.*, 2021, **14**, 2501–2513.
- 257 E. S. C. Kwok and Atkinson, *Science*, 1995, **29**, 1685–1695.
- 258 J. W. Raymond and W. T. Simpson, *J. Chem. Phys.*, 1967, **47**, 430–448.
- 259 M. S. Alam, A. R. Rickard, M. Camredon, K. P. Wyche, T. Carr, K. E. Hornsby, P. S. Monks and W. J. Bloss, *J. Phys. Chem. A*, 2013, **117**, 12468–12483.
- 260 L. Onel, A. Brennan, P. W. Seakins, L. Whalley and D. E. Heard, *Atmos. Meas. Tech.*, 2017, **10**, 3985–4000.
- 261 S. Goldstein and A. Samuni, *J. Phys. Chem. A*, 2007, **111**, 1066–1072.
- 262 L. Whalley, E. Slater, C. Ye, R. Woodward-Massey, J. Lee, F. Squires, J. Hopkins, R. Dunmore, J. Hamilton, A. Lewis, L. Crilley, L. Kramer, W. Bloss and D. Heard, *Geophys. Res. Abstr.*, 2018, **20**, 7409.
- 263 L. P. E. Yunker, Z. Ahmadi, J. R. Logan, W. Wu, T. Li, A. Martindale, A. G. Oliver and J. S. McIndoe, *Organometallics*, 2018, **37**, 4297–4308.
- 264 L. E. Greene, R. Lincoln and G. Cosa, *J. Am. Chem. Soc.*, 2017, **139**, 15801–15811.
- 265 M. Braun, U. Hartnagel, E. Ravanelli, B. Schade, C. Böttcher, O. Vostrowsky and A. Hirsch, *European J. Org. Chem.*, 2004, 1983–2001.
- 266 X. Chen, L. Henschke, Q. Wu, K. Muthoosamy, B. Neumann and T. Weil, *Org. Biomol. Chem.*, 2013, **11**, 353–361.
- 267 R. Göttlich, *Synthesis*, 2000, **11**, 1561–1564.
- 268 S. Pandiancherri and D. W. Lupton, *Tetrahedron Lett.*, 2011, **52**, 671–674.
- 269 Y. Xie, M. Sun, H. Zhou, Q. Cao, K. Gao, C. Niu and H. Yang, *J. Org. Chem.*, 2013, **78**, 10251–10263.

- 270 S. L. Titouani, J.-P. Lavergne, P. Viallefont and R. Jacquier, *Tetrahedron*, 1980, **36**, 2961–2965.
- 271 J. Cason, M. J. Kalm and R. H. Mills, *J. Org. Chem.*, 1953, **18**, 1670–1674.
- 272 H. Merten and H. Gilman, *J. Am. Chem. Soc.*, 1954, **76**, 5798–5799.
- 273 H. J. Perera, H. Mortazavian and F. D. Blum, *Langmuir*, 2017, **33**, 2799–2809.
- 274 J. Ortega, C. González and S. Galván, *J. Chem. Eng. Data*, 2001, **46**, 904–912.